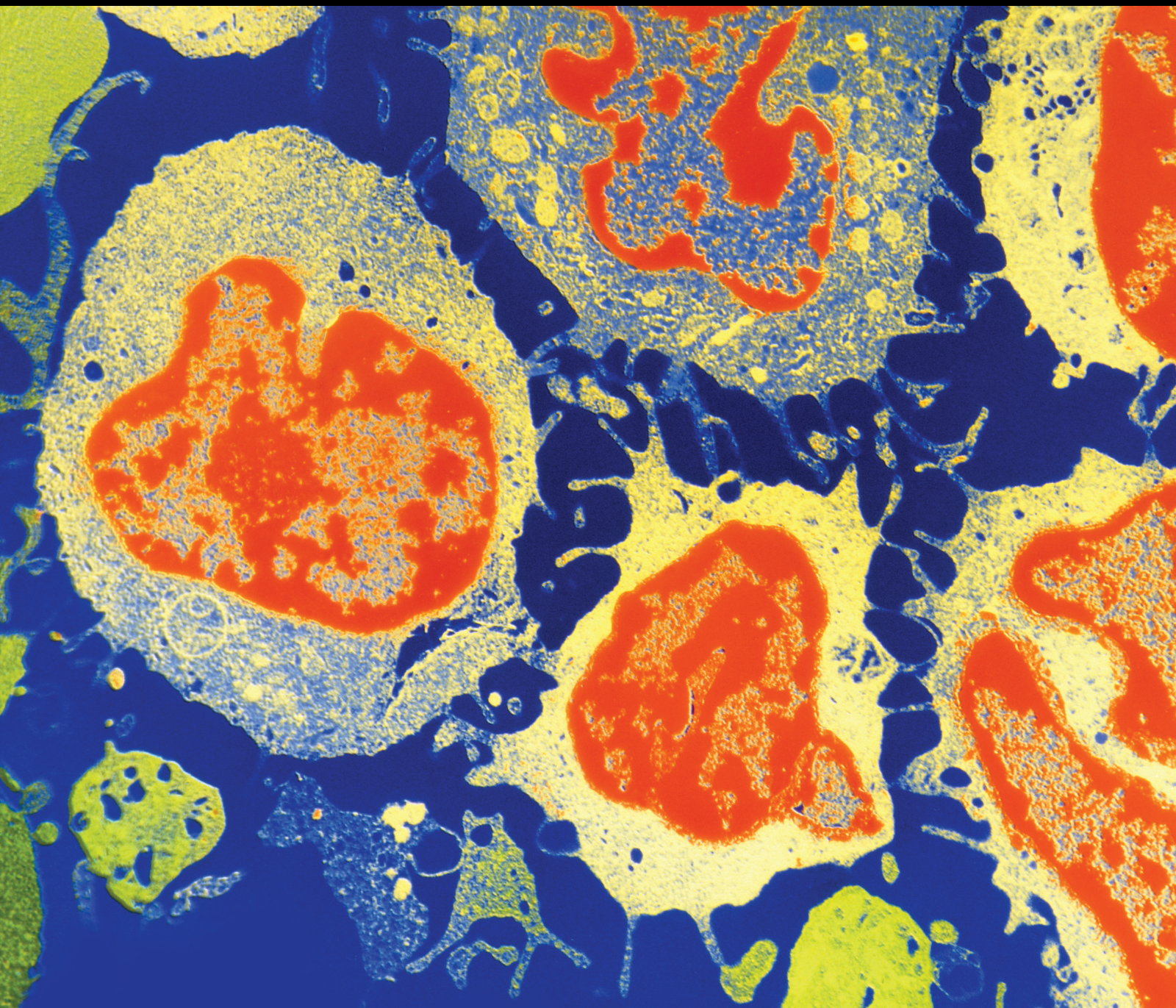# The Involvement of RNA Interference in Cancer

Lead Guest Editor: Zhongjie Shi
Guest Editors: Dong Pan and Ioannis Kosmas

The Involvement of RNA Interference in Cancer

The Involvement of RNA Interference in Cancer

Lead Guest Editor: Zhongjie Shi
Guest Editors: Dong Pan and Ioannis Kosmas

Contents

Contents

Retraction

Retracted: PRR15 Is a Novel Diagnostic and Prognostic Biomarker in Papillary Thyroid Cancer and Modulates the Tumor Microenvironment

Journal of Oncology

This article has been retracted by Hindawi following an investigation undertaken by the publisher [1]. This investigation has uncovered evidence of one or more of the following indicators of systematic manipulation of the publication process:

(1) Discrepancies in scope

(2) Discrepancies in the description of the research reported

(3) Discrepancies between the availability of data and the research described

(4) Inappropriate citations

(5) Incoherent, meaningless and/or irrelevant content included in the article

(6) Peer-review manipulation

The presence of these indicators undermines our confidence in the integrity of the article's content and we cannot, therefore, vouch for its reliability. Please note that this notice is intended solely to alert readers that the content of this article is unreliable. We have not investigated whether authors were aware of or involved in the systematic manipulation of the publication process.

Wiley and Hindawi regrets that the usual quality checks did not identify these issues before publication and have since put additional measures in place to safeguard research integrity.

We wish to credit our own Research Integrity and Research Publishing teams and anonymous and named external researchers and research integrity experts for contributing to this investigation.

The corresponding author, as the representative of all authors, has been given the opportunity to register their agreement or disagreement to this retraction. We have kept a record of any response received.

References

[1] L. Wang, X. Deng, Y. Chen, Y. Zhao, and Z. Li, "PRR15 Is a Novel Diagnostic and Prognostic Biomarker in Papillary Thyroid Cancer and Modulates the Tumor Microenvironment," *Journal of Oncology*, vol. 2022, Article ID 3290479, 11 pages, 2022.

Retraction

Retracted: Efficacy Evaluation of Inflammatory Mediators in the Treatment of Multiple Myeloma with Daratumumab

Journal of Oncology

This article has been retracted by Hindawi following an investigation undertaken by the publisher [1]. This investigation has uncovered evidence of one or more of the following indicators of systematic manipulation of the publication process:

(1) Discrepancies in scope

(2) Discrepancies in the description of the research reported

(3) Discrepancies between the availability of data and the research described

(4) Inappropriate citations

(5) Incoherent, meaningless and/or irrelevant content included in the article

(6) Peer-review manipulation

The presence of these indicators undermines our confidence in the integrity of the article's content and we cannot, therefore, vouch for its reliability. Please note that this notice is intended solely to alert readers that the content of this article is unreliable. We have not investigated whether authors were aware of or involved in the systematic manipulation of the publication process.

In addition, our investigation has also shown that one or more of the following human-subject reporting requirements has not been met in this article: ethical approval by an Institutional Review Board (IRB) committee or equivalent, patient/participant consent to participate, and/or agreement to publish patient/participant details (where relevant).

Wiley and Hindawi regrets that the usual quality checks did not identify these issues before publication and have since put additional measures in place to safeguard research integrity.

We wish to credit our own Research Integrity and Research Publishing teams and anonymous and named external researchers and research integrity experts for contributing to this investigation.

The corresponding author, as the representative of all authors, has been given the opportunity to register their agreement or disagreement to this retraction. We have kept a record of any response received.

References

[1] J. Meng, X. Zhao, D. Jiang, C. Liang, X. Ji, and M. Dong, "Efficacy Evaluation of Inflammatory Mediators in the Treatment of Multiple Myeloma with Daratumumab," *Journal of Oncology*, vol. 2022, Article ID 9350211, 6 pages, 2022.

Retraction

Retracted: SFRP2 is a Novel Diagnostic Biomarker and Suppresses the Proliferation of Pituitary Adenoma

Journal of Oncology

This article has been retracted by Hindawi following an investigation undertaken by the publisher [1]. This investigation has uncovered evidence of one or more of the following indicators of systematic manipulation of the publication process:

(1) Discrepancies in scope

(2) Discrepancies in the description of the research reported

(3) Discrepancies between the availability of data and the research described

(4) Inappropriate citations

(5) Incoherent, meaningless and/or irrelevant content included in the article

(6) Peer-review manipulation

The presence of these indicators undermines our confidence in the integrity of the article's content and we cannot, therefore, vouch for its reliability. Please note that this notice is intended solely to alert readers that the content of this article is unreliable. We have not investigated whether authors were aware of or involved in the systematic manipulation of the publication process.

Wiley and Hindawi regrets that the usual quality checks did not identify these issues before publication and have since put additional measures in place to safeguard research integrity.

We wish to credit our own Research Integrity and Research Publishing teams and anonymous and named external researchers and research integrity experts for contributing to this investigation.

The corresponding author, as the representative of all authors, has been given the opportunity to register their agreement or disagreement to this retraction. We have kept a record of any response received.

References

[1] R. Huang, D. Chen, H. Wang, B. Zhang, Y. Zhang, and W. Ren, "SFRP2 is a Novel Diagnostic Biomarker and Suppresses the Proliferation of Pituitary Adenoma," *Journal of Oncology*, vol. 2022, Article ID 4272525, 8 pages, 2022.

Hindawi

Research Article

HKDC1 Silencing Inhibits Proliferation and Glycolysis of Gastric Cancer Cells

Chen Yu ,[1] Ting-ting Bao,[1] Li Jin,[2,3] Jian-wei Lu ,[4] and Ji-feng Feng [4]

[1]Department of Integrated TCM & Western Medicine, Jiangsu Cancer Hospital & Jiangsu Institute of Cancer Research & the
 Affiliated Cancer Hospital of Nanjing Medical University, 42 Baiziting Road, Nanjing 210009, China
[2]State Key Laboratory of Quality Research in Chinese Medicine & School of Pharmacy, Macau University of Science
 and Technology, Taipa, China
[3]Department of Radiotherapy, Sichuan Cancer Hospital & Institute, Sichuan Cancer Center, School of Medicine, University of
 Electronic Science and Technology of China, 55 Renmin South Road, 610041 Chengdu, Sichuan, China
[4]Department of Medical Oncology, Jiangsu Cancer Hospital & Jiangsu Institute of Cancer Research & The Affiliated Cancer Hospital
 of Nanjing Medical University, 42 Baiziting Road, Nanjing 210009, China

Correspondence should be addressed to Jian-wei Lu; lujw@medmail.com.cn and Ji-feng Feng; jifeng_feng@163.com

Gastric cancer (GC) is the third most lethal and fifth most common cancer in the world. In a variety of cancers, the hexokinase domain component 1 (HKDC1) is carcinogenic. This study was to investigate into how HKDC1 contributes to the development and progression of GC. Three different datasets (GSE103236, GSE13861, and GSE55696) were extracted from the Gene Expression Omnibus (GEO) database and then analyzed using the sva package. The R software was used to identify 411 differentially expressed genes (DEGs) in the pooled dataset. We discovered 326 glycolysis-related genes (glyGenes) in the cancer genome atlas-stomach adenocarcinoma (TCGA-STAD) cohort using gene set enrichment analysis set (GSEA). HKDC1 is one of the most prevalent glyGenes in GC tumor tissues and cells, as seen in the Venn diagram. According to the results of the Cell Count Kit-8 assay, the proliferation of AGS and MKN-45 cells decreased when HKDC1 was knocked down. Lack of HKDC1 in cells enhanced oxygen consumption and decreased glycolytic protein expression while suppressing glucose absorption, lactate production, ATP level, and extracellular acidification ratio. As an oncogene in gastric cancer development, HKDC1 influences cell proliferation and glycolysis.

1. Introduction

As one of the most common types of cancer, gastric cancer has the fifth-highest incidence rate (5.7%) [1]. Both the incidence and mortality rate of gastric cancer are the highest in China [2, 3]. The overall survival rate for gastric cancer is still around 30 percent, despite the finding that smoking and alcohol consumption are the principal drivers of gastric cancer. In contrast to the respiratory metabolism of the vast majority of normal cells, cancer cells prefer glycolysis as the source of energy even when nutrients are present [4]. This is a phenomenon known as the Warburg effect, and it is characterized by an increase in glucose uptake and lactate generation. The intermediate products produced during glycolysis

not only offer nutrition for the expansion of tumor cells but also shield tumor cells, which increases the rate of malignant tumor cell proliferation and spread [5]. According to several studies, glycolysis results in the production of a variety of metabolites, including pyruvate, lactate, and ketone bodies, which are found in increased concentrations in the tissues and cells of gastric cancer [6–8]. Lowering glucose consumption while maintaining normal energy requirements significantly suppresses the Warburg effect on tumor cells [9], which slows down the growth of tumors.

The aerobic glycolysis and glycolysis pathways are both controlled by more than ten genes that encode key glycolysis enzymes and glucose transporters [10, 11]. As a consequence of this, transcription factors including HIF1, c-Myc, NF-B,

and SIX1 that can directly influence the gene expression and protein activity of glucose transporters and key glycolysis enzymes play a significant role in the regulation of malignant tumor metabolism. In this study, the use of bioinformatics allowed for the identification of hexokinase domain component 1 (HKDC1) as a gene linked to gastric cancer, which was found to be closely associated with glycolysis. HKDC1 was found to potentially act as a fifth hexokinase and plays an essential role in preserving glucose homeostasis throughout the body [12]. On the other hand, abnormal expression of HKDC1 has been linked to the development of a wide variety of diseases and cancers. An example of this would be the overexpression of the gene HKDC1, which has been associated with metabolic inefficiency in hepatocytes, which in turn has been linked to nonalcoholic fatty liver disease [13]. In addition, there is accumulating evidence that HKDC1 may play an oncogenic function in cancers such as lymphoma, liver, breast, and colorectal cancers [14]. However, very little is known about the role that HKDC1 plays in the development of gastric cancer or the metabolic processes of tumors.

2. Materials and Methods

2.1. Gene Expression Microarray Datasets from the GEO Database and TCGA Database. For the purpose of obtaining GC-associated RNA expression patterns, the GEO database was employed. The GSE13861 dataset, the GSE55696 dataset, and the GSE103236 dataset were utilized in subsequent research. The GSE13861 dataset contained 71 GC tumor samples (65 primary gastric adenocarcinoma and 6 gastrointestinal stromal tumors) and 19 adjacent non-tumor samples derived from the GPL6884 platform. The GSE55696 dataset comprised 58 GC cancer samples (19 high-grade intraepithelial neoplasia, 20 low-grade intraepithelial neoplasia, and 19 gastric early-stage carcinoma) and 19 chronic gastritis tissue samples derived from the GPL6480 platform. GSE103236 dataset included 10 GC tumor samples and 9 adjacent non-tumor samples from the GPL4133 platform.

Raw gene mRNA data for 375 GC tissue samples and 32 adjacent non-tumor tissue samples were obtained through the TCGA database (https://portal.gdc.cancer.gov). These samples were taken from patients with a range of stages of the disease.

Due to the fact that the data originated from TCGA and GEO databases, authorization from an ethical committee was not required.

2.2. Differentially Expressed Genes (DEGs). We created one single dataset by combining the previous three, each of which contained 139 GC cancer samples and 47 control samples. We batch standardized the combined datasets using the sva tool in R in order to eliminate any bias that may have existed among the three datasets (version 4.1.3). After that, the limma tool was used to extract DEG information from the GEO and TCGA databases. The criteria for selection were an adjusted *p*-value of 0.05 or lower and a log fold change (FC) of greater than 1. Those DEGs that we are able to meet the threshold were considered to have

statistical significance. When attempting to visualize the data, the R software was utilized to generate volcano plots as well as heat maps.

2.3. Cell Culture and Transfection. The human gastric cancer cells (MKN-45, AGS, and MGC-803), as well as the normal GES-1 gastric mucosal cells, were generously provided by the American Type Culture Collection (ATCC). These cells were grown in a RPMI-1640 media from Gibco (Grand Island, New York), which included 10% fetal bovine serum (FBS), 100 units per milliliter of penicillin, and 100 milligrams per milliliter of streptomycin (Gibco). All cells were grown at a temperature of 37 degree Celsius in an atmosphere that was 95 percent humidity and 5 percent carbon dioxide. GenePharma (Shanghai, China) developed two shRNAs (sh-HKDC1#1 and sh-HKDC1#2) to target HKDC1, as well as one sh-NC for negative control. These plasmids were transfected into AGS and MKN-45 cells with the use of Lipofectamine 3000 (Invitrogen, Carlsbad, CA).

2.4. RNA Extraction and Quantitative RT-PCR (qRT-PCR). Total RNA was extracted from GC cell lines by using TRIzol (Invitrogen, located in Grand Island, New York), and it was then processed in accordance with the technique that was provided by the manufacturer. cDNA was synthesized by following the instructions given by the manufacturer of the PrimeScript RT Reagent Kit and carrying out the procedure in accordance with those instructions (TaKaRa Bio, Shiga, Japan). In order to carry out real-time PCR, a Roche Light Cycler 480 (Roche) was coupled with an SYBR Green PCR Master Mix. Both of these components were manufactured by Roche (TaKaRa Bio, Shiga, Japan). The calculation was carried out by 2Ct to find the fold change about the mean value. Each experiment yielded three distinct data sets, which were collected separately. The primer sequences are presented down below.

HKDC1:
5′-GCAAGAGACAATCCTGGTACG-3′ (forward).
5′-GTTGCCCTCTGAACGCAATC-3′ (reverse);
Ki67:
5′-ATGCTTGTCGTGTTTTACGGC-3′ (forward).
5′-CGTGGTAATGTAAAGTCCCATGTGTAA-3′ (reverse);
PCNA:
5′-CTGTTAGTAGATGAAACATGGGGG-3′ (forward).
5′-CATCGTGTACGTGCCCAGTGAATGTGTGTG-3′ (reverse);
GAPDH:
5′-GAAAAGATCCCTCCGGAGCAT-3′ (forward).
5′-CTGTGGTGTTTCTCATGCATACG-3′ (reverse);

2.5. Cell Count Kit-8 Assay. After the HKDC1 was knocked down, the amount of cell proliferation was measured using the CCK-8 assay, which was created by Dojindo Laboratories in Kumamoto, Japan. We examine the outcomes after just planting four times 10^3 transfected cells in each well of 96-well plates and leaving them there for 24 hours at a
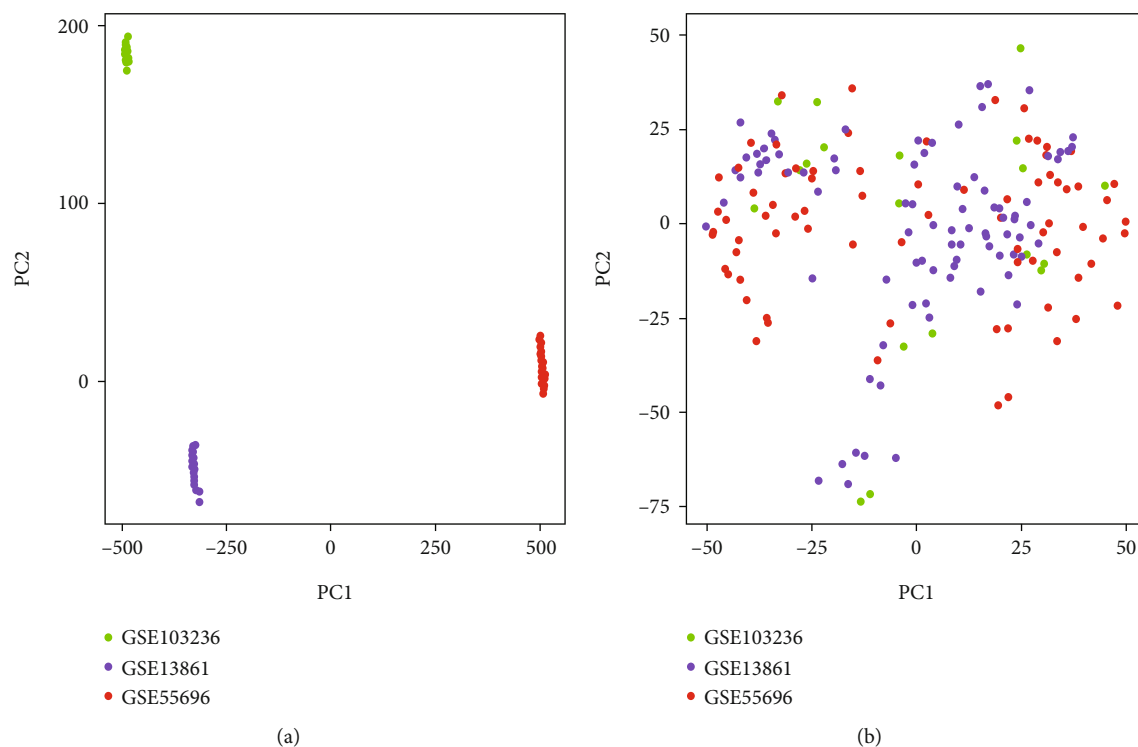
Figure 1: Validation of data. (a, b) PCA showed that the repeatability of the data in GSE103236, GSE13861, and GSE55696 was acceptable.

temperature of 37 degrees Celsius with 5 percent carbon dioxide. Following this step, a $10\,\mu l$ solution of CCK-8 was given to each well, and the cells were cultured for a total of two hours at each of the periods that were stated (0, 24, 48, 72, and 96 h). A spectrophotometer microplate reader (Bio-Rad, California) was utilized for the measurement of cell viability at 450 nm.

2.6. Glycolysis Measurement. The levels of glucose uptake, lactate, and ATP generation were each determined in accordance with the instructions that were provided by the respective manufacturers by using the Glucose Uptake Colorimetric Assay Kit (BioVision, Milpitas, CA), the Lactate Assay Kit II (BioVision), and the ATP Colorimetric Assay Kit (BioVision). We used the Seahorse Extracellular Flux Analyzer XF96 (Seahorse Bioscience, North Billerica, MA) to determine the extracellular acidification ratio (ECAR) and oxygen consumption ratio (OCR) of gastric cancer cells. In brief, 2x 10^4 of the transfected cells were plated into each well of the XF96-well plate and incubated overnight. In order to calculate the ECAR (in mpH/min), glucose, oligomycin (an inhibitor of oxidative phosphorylation), and 2-DG (an inhibitor of glycolysis) were sequentially added to the wells. In order to determine the OCR (in pmol/min), oligomycin, p-trifluoromethoxy carbonyl cyanide phenylhydrazone (FCCP, the reversible inhibitor of oxidative phosphorylation), rotenone (the inhibitor of mitochondrial complex I), and antimycin A (mitochondrial complex III inhibitor) were sequentially added to the wells. The Seahorse XF-96 analysis tool was applied in order to check the results.

2.7. Gene Set Enrichment Analysis (GSEA). In order to evaluate any potential differences, linked pathways, and molecular processes that were discovered in the TCGA cohort, a GSEA was carried out. This was done for the purpose of determining whether or not there were any underlying molecular mechanisms of the glycolysis signature that might be attained. Java SE version 4.1.0 was used to carry out the GSEA, and the following gene sets were included in the analysis: "c5.go.bp.v7.4," "c5.go.cc.v7.4," "c5.go.mf.v7.4," and "c2.cp.kegg.v7.4." It was determined that a result was statistically significant if it had a |NES| value that was greater than 1 and a p-value that was lower than 0.05.

2.8. Repeatability Test for Data. The principal component analysis (PCA) is a well-respected statistical method that was used to simplify the data by lowering the degree of interdependence that existed between the variables. In order to determine whether or not the data could be reproduced accurately, PCA was applied.

2.9. Statistical Analysis. We analyzed the data with the IBM's SPSS version 21.0 software (Armonk, New York) and presented the findings in the form of the mean and standard deviation. In order to perform comparisons between the groups, we utilized either the Student's t-test or a one-way analysis of variance. The value of $p < 0.05$ (2-sided) was used to denote statistical significance.

3. Results

3.1. Validation of Data. After using PCA, it was determined that the repeatability of the data in GSE103236, GSE13861,
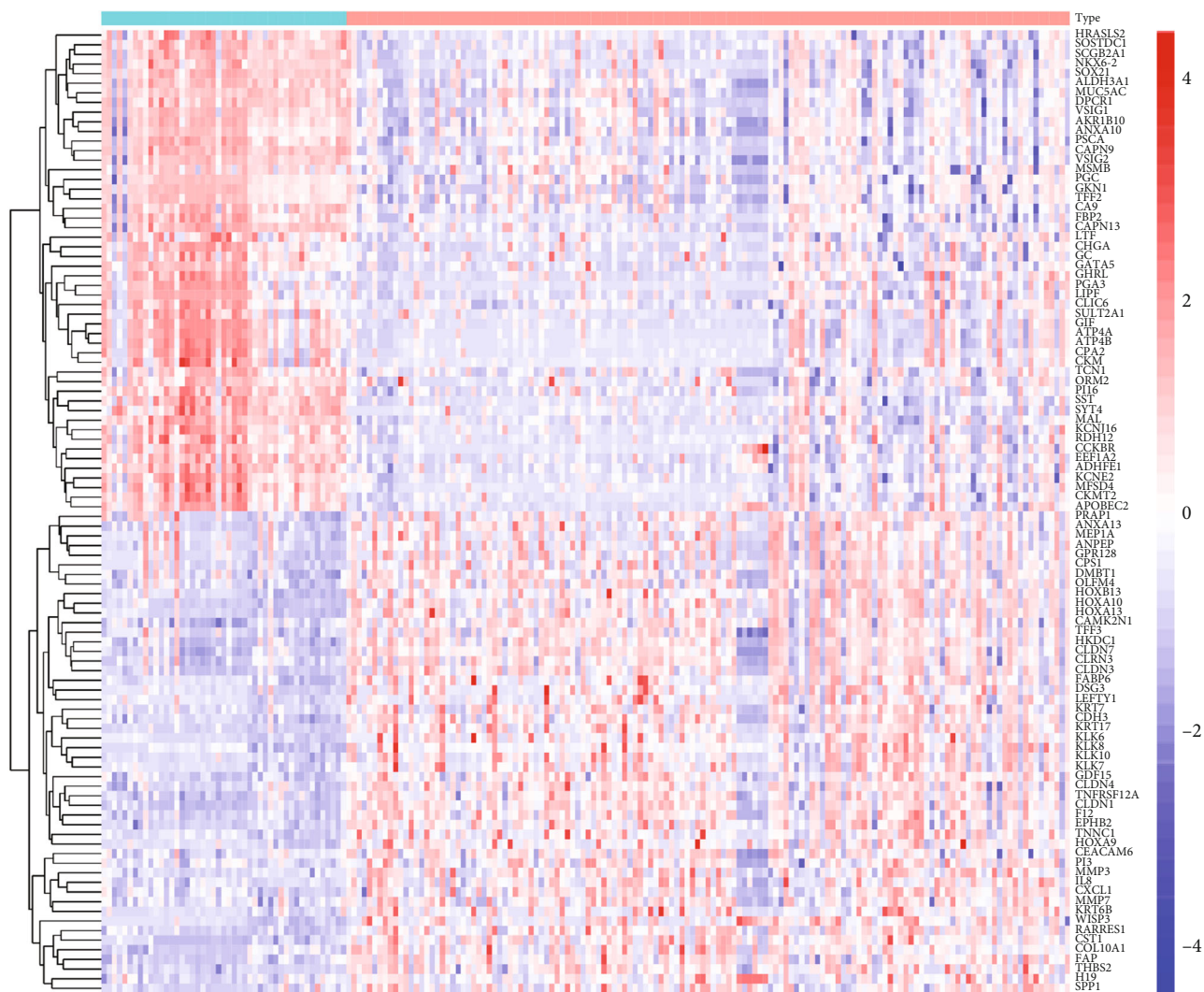
(a)

Figure 2: Continued.

(b)
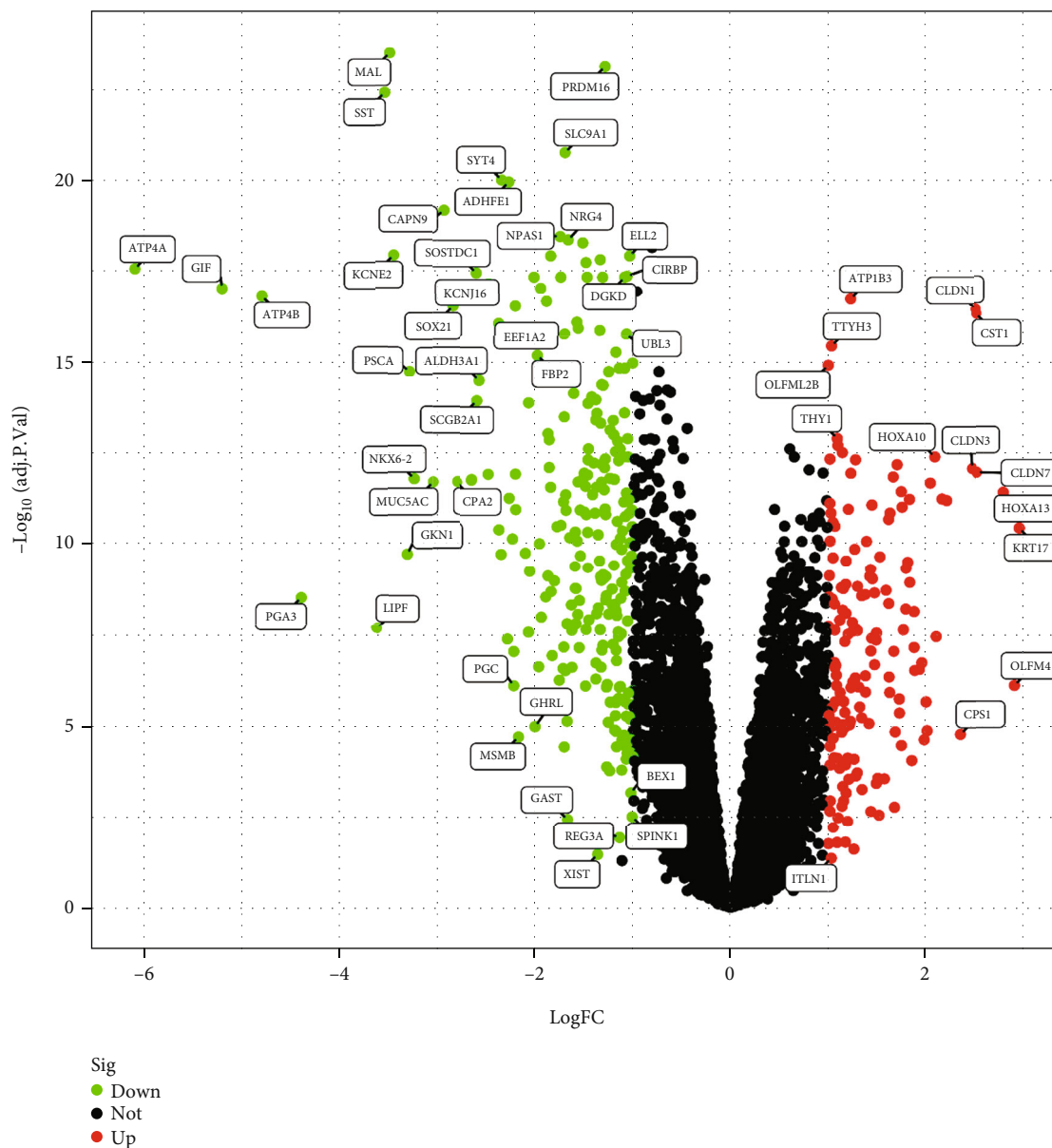
FIGURE 2: The identification of differentially expressed genes from the GEO database. (a) Heat map presenting DEGs from the merged dataset consisted of GSE103236, GSE13861, and GSE55696. (b) Volcano map presenting DEGs from the merged dataset.

TABLE 1: Gene sets enriched in GC.

GS follow link to MSigDB	SIZE	ES	NES	NOM p-val	FDR q-val
BIOCARTA_GLYCOLYSIS_PATHWAY	3	0.35	0.58	0.9409	0.9409
GO_GLYCOLYTIC_PROCESS	106	0.57	1.91	0.0056	0.0056
HALLMARK_GLYCOLYSIS	200	0.42	1.36	0.1439	0.1439
KEGG_GLYCOLYSIS_GLUCONEOGENESIS	62	-0.41	-1.28	0.1821	0.1821
REACTOME_GLYCOLYSIS	72	0.68	1.97	0.0040	0.0040

and GSE55696 was adequate (Figure 1(a)). Both the distances between samples in the control group and the distances between samples in the GC group were quite close in the first dimension of the PC analysis.

3.2. The Identification of Differentially Expressed Genes from the GEO Database. In order to determine which genes are associated with GC using the GEO database, we first combined three datasets, namely, GSE103236, GSE13861, and

Enrichment plot: BIOCARTA_GLYCOLYSIS_PATHWAY

(a)

Enrichment plot: GO_GLYCOLYTIC_PROCESS

(b)

Figure 3: Continued.

Enrichment plot: HALLMARK_GLYCOLYSIS

(c)

Enrichment plot:
KEGG_GLYCOLYSIS_GLUCONEOGENESIS
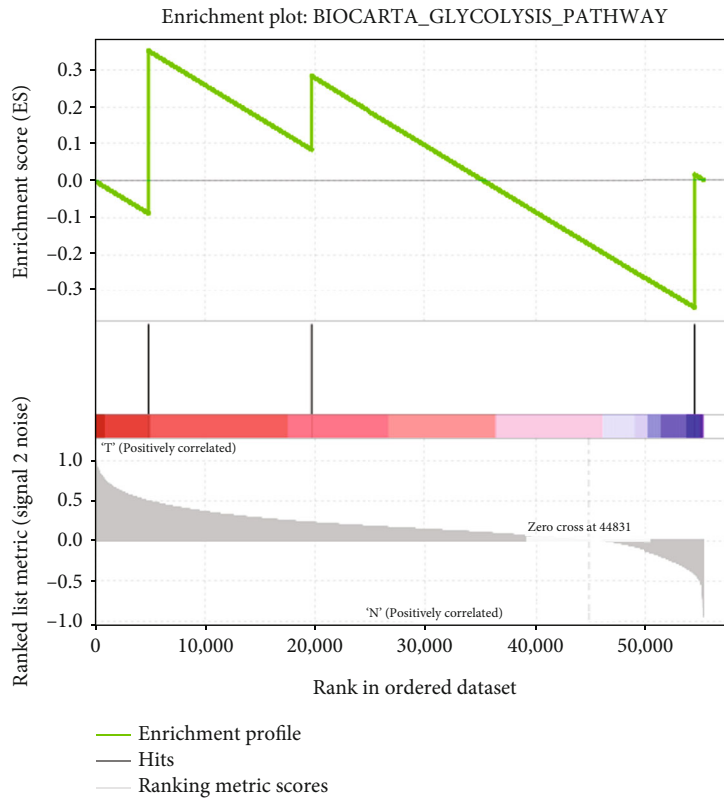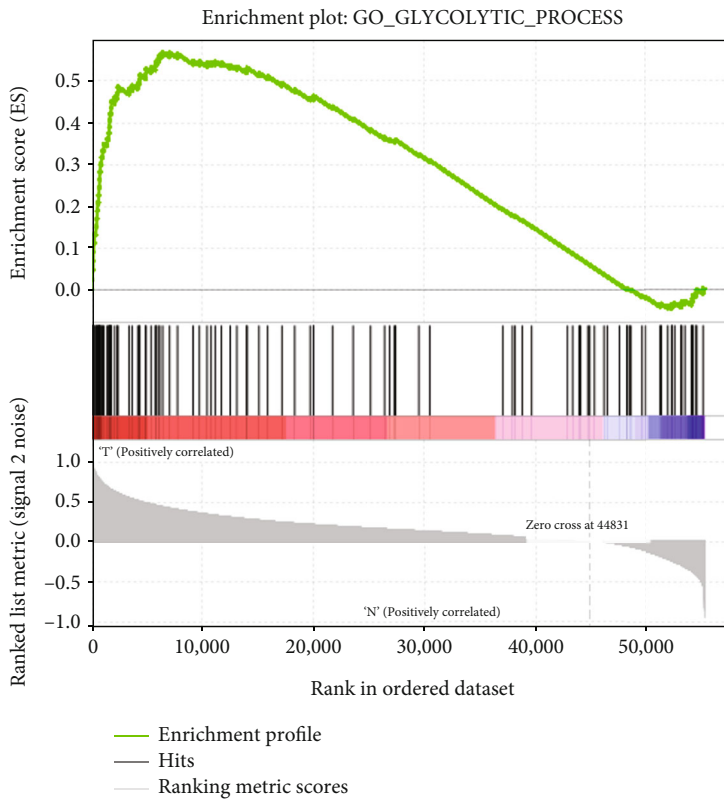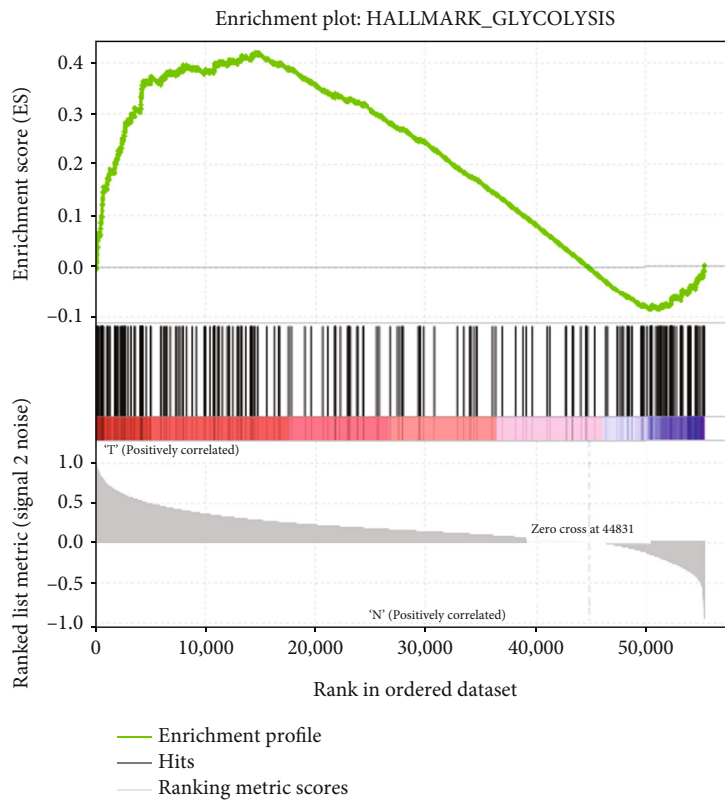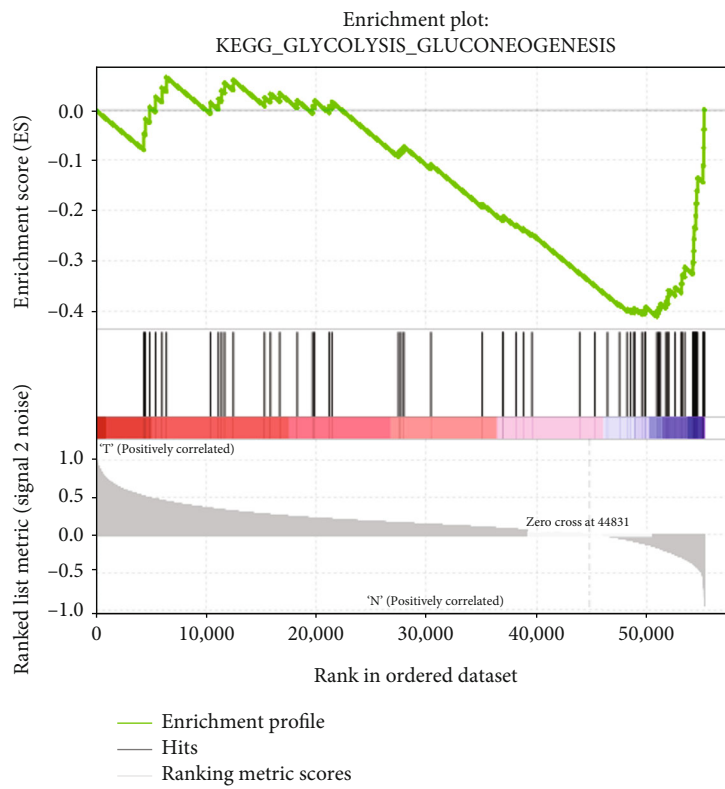
(d)

Figure 3: Continued.
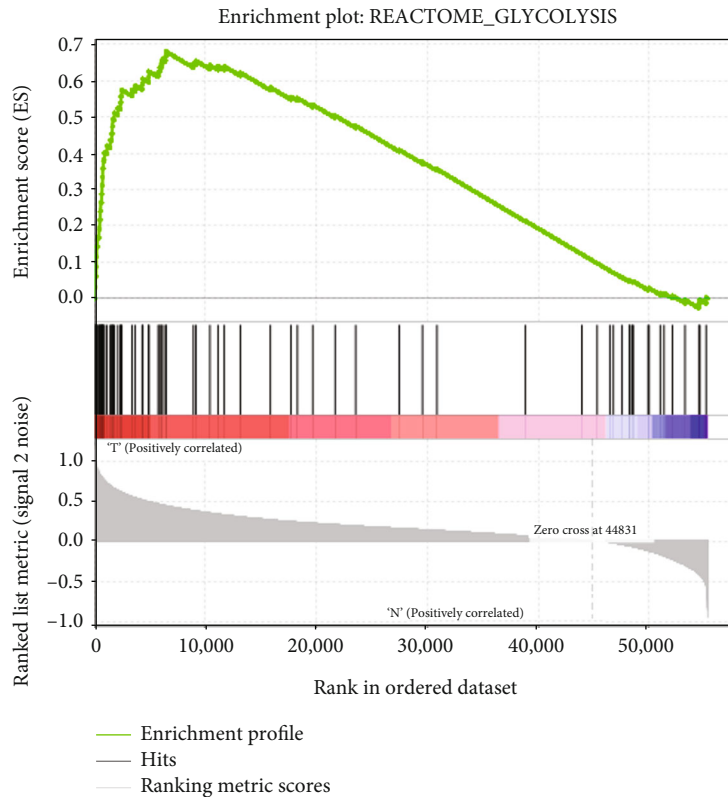
(e)

FIGURE 3: Initial screening of genes using gene set enrichment analysis.Enrichment plots of five gene sets that had significant differences between normal tissues and GC tissues by performing GSEA.

GSE55696, in order to increase the total number of samples to 139 tumor samples and 47 control samples. After that, the pooled dataset was processed to remove 411 genes that had a p-value of less than 0.05 and a logFC of either 1 or −1. (Figure 2(a)). Overall, 253 DEGs saw upregulation, while 158 DEGs experienced downregulation (Figure 2(b); Suppl 1).

3.3. Initial Screening of Genes Using Gene Set Enrichment Analysis. The TCGA provided us with information regarding the levels of expression for 56,753 different mRNAs. Downloading five different glycolysis-related gene sets from MSigDB version 6.2 resulted in a total of 443 genes being found (Suppl 2). With the help of the aforementioned data and GSEA, we were able to establish which gene sets displayed significant differences between GC tissues and the normal tissues that surrounded them. With adjusted p values of 0.05, it was shown that four gene sets were significantly enriched from the following pathways: BIOCARTA GLYCOLYSIS PATHWAY, GO GLYCOLYTIC PROCESS, HALLMARK GLYCOLYSIS, KEGG GLYCOLYSIS GLUCONEOGENESIS, and REACTOME_GLYCOLYSIS (Table 1; Figure 3). For the sake of this subsequent research, the 326 genes that belong to these four gene sets were selected.

3.4. The Expression Level of Glycolysis-Related Genes in the TCGA Database. Figure 4(a) depicts a heat map of gene expression from the TCGA-STAD dataset. The TCGA data-base was used to identify the expression levels of 326 glycolysis-related genes (Figure 4(b)).

3.5. The Identification of the Hub Gene Associated with Glycolysis. The results of a Venn analysis showed that thirteen DEGs taken from the TCGA and GEO datasets were linked to the process of glycolysis (Figure 5(a)). According to the findings of our study, the expression of 13 genes in an integrated dataset and TCGA dataset is shown in Figure 5(b). HKDC1 expression was shown to have significantly increased expression levels in GC tumor tissues from two datasets. Following this, GC cell lines exhibited increased levels of HKDC1 mRNA expression (Figure 5(c)). In addition, HKDC1 expression in MKN-45 and AGS cells was higher than that in GES-1, SGC-7901, and MGC-803 cells. Therefore, MKN-45 and AGS cells were used to carry out the experiment of HKDC1 knockdown.

3.6. Downregulation of HKDC1 Inhibits the Growth of Gastric Cancer Cells. In order to investigate the role that HKDC1 plays in the progression of gastric cancer, AGS and MKN-45 cells were transfected with two different shRNAs directed against HKDC1. Validation of the efficiency of transfection was achieved by the use of a quantitative real-time polymerase chain reaction (qRT-PCR) assay. As can be shown in Figure 6(a), each shRNA was successful in suppressing the expression of HKDC1 (Figure 6(b)). Compared to the sh-NC group, the sh-HKDC1#2 group

(a)

(b)
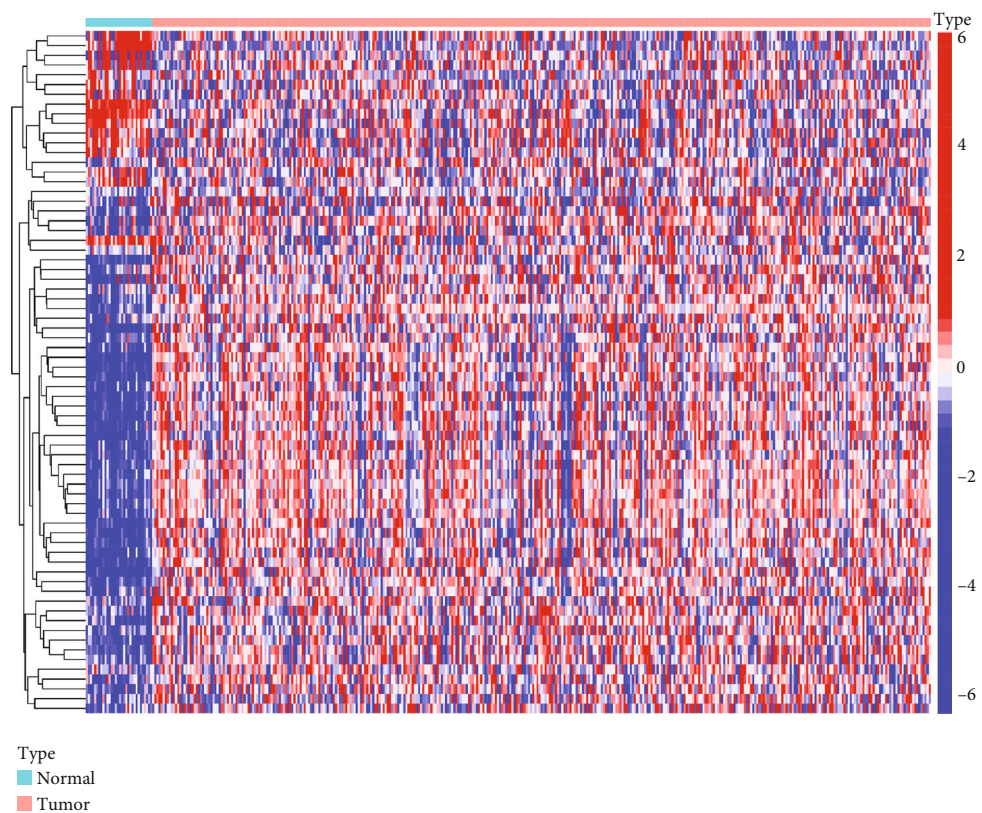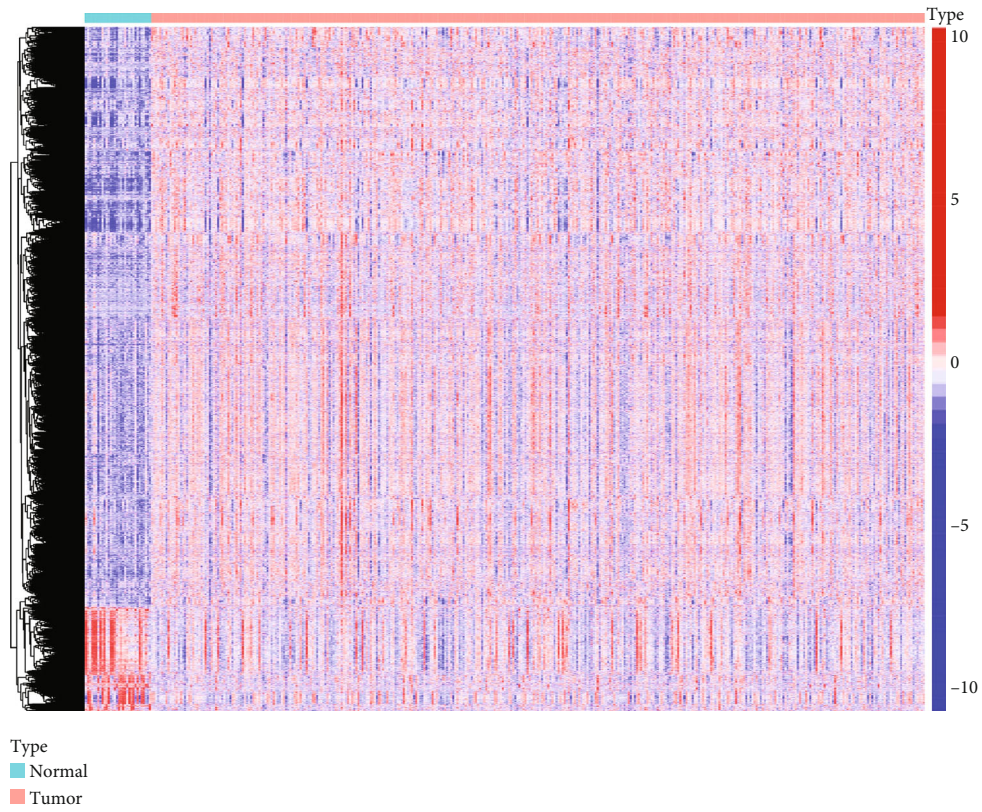
FIGURE 4: The expression level of glycolysis-related genes in the TCGA database. (a) Heat map of TCGA-derived DEGs with logFC > 1 and p − value < 0.05. (b) Heat map of glycolysis-related genes.

(a)

GEO data	
Genesymbol	LogFC
CLDN3	2.472841538
ADH4	1.090017791
HKDC1	2.161330984
TFF3	1.727609435
XYLT2	−1.003008985
ENTPD5	−1.015153282
GCKR	−1.055164896
ANG	−1.289102425
ALDOC	−1.369774366
B3GAT1	−1.568111844
ADH1A	−1.621607418
FBP2	−1.972130857
ALDH3A1	−2.566147276

TCGA data	
Genesymbol	LogFC
ADH1A	NA
XYLT2	NA
CLDN3	1.344664141
HKDC1	0.620627539
TFF3	0.105920089
GCKR	−0.393422669
ANG	−0.65777008
ENTPD5	−0.988057178
ALDOC	−1.11129069
B3GAT1	−1.58905384
ADH4	−2.047038821
ALDH3A1	−2.559788333
FBP2	−2.642621687

(b)

(c)

FIGURE 5: The identification of the hub gene associated with glycolysis. (a) Venn diagram showing 13 DEGs found in both datasets. (b) The expression of glycolysis-related genes in the merged dataset and TCGA database. (c) qRT-PCR analysis of HKDC1 expression in GC cell lines. Data are shown as mean $\pm$ SD; $^*p < 0.05$.

had lower amounts of mRNA in AGS and MKN-45 cells (Figures 6(a) and 6(b)). Throughout the entirety of this trial, sh-HKDC1#2 was utilized due to the higher knock effectiveness it exhibited. The results of the CCK-8 experiment showed that inhibiting HKDC1 resulted in a considerable and prolonged slowdown in the development of AGS and MKN-45 cells (Figures 6(c) and 6(d)). The expression of proliferation-related proteins, such as Ki67 and PCNA, was consistently decreased after HKDC1 was knocked down (Figures 6(e) and 6(f)).

3.7. Downregulation of HKDC1 Inhibits the Glycolysis of Gastric Cancer Cells. The process of glycolysis has been linked to the development of gastric cancer in several studies. As a consequence of our research, we looked into whether or not HKDC1 had any effect on the glycolysis process in gastric cancer cells. The effects of HKDC1 knockdown may be seen in Figures 7(a)–7(f), where it can be

seen that glucose absorption, lactate production, and ATP synthesis are all reduced. The electron carrier anion pair (ECAR) and oxygen consumption rate (OCR), which both measure the total flux of glycolysis and mitochondrial oxidative respiration, were also indicators of glycolysis. The results of HKDC1 knockdown are shown in (Figures 7(g)–7(j)), which demonstrate a significant reduction in ECAR and an increase in OCR in AGS and MKN-45 cells, respectively. Our findings indicate that glycolytic activity is hindered in gastric cancer cells when HKDC1 expression is reduced due to downregulation.

4. Discussion

More than one million people throughout the world are given a diagnosis of gastric cancer each year, making it a major public health concern [5]. In spite of the fact that both the incidence rate and the mortality rate of gastric cancer
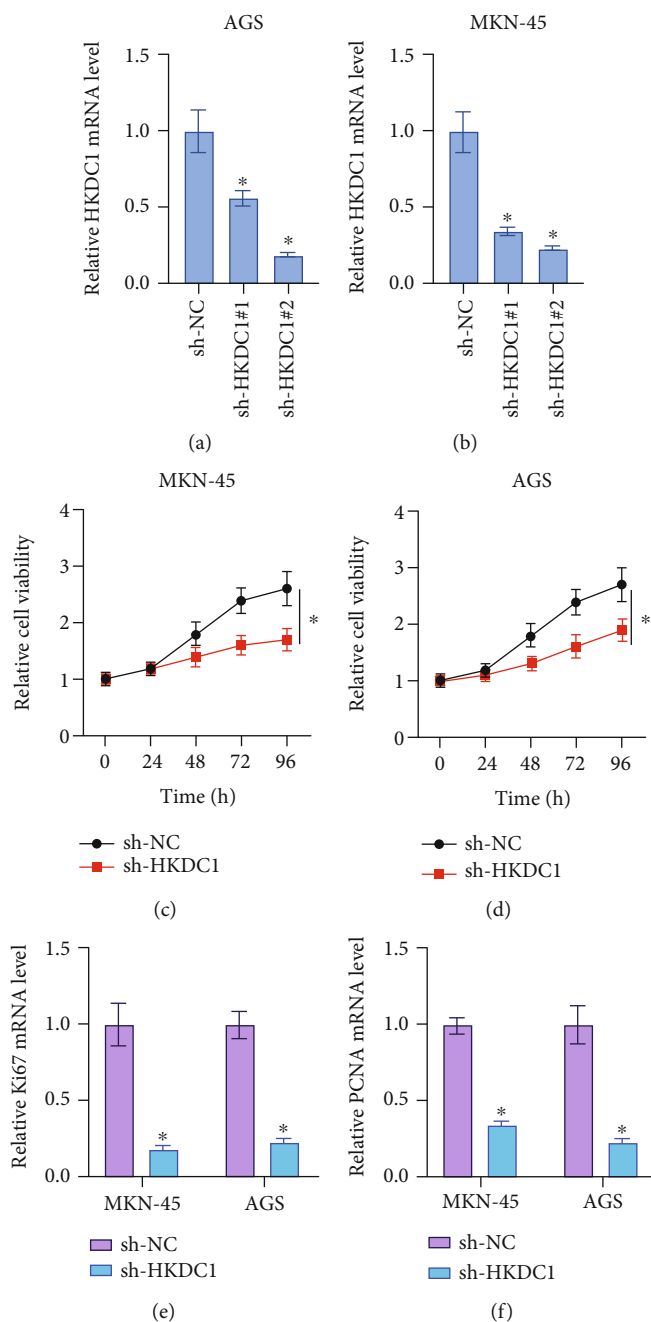
FIGURE 6: Downregulation of HKDC1 inhibits the growth of gastric cancer cells. (a and b) The qRT-PCR assay was used to evaluate the mRNA level of HKDC1 in AGS and MKN-45 cells. (c and d) CCK-8 assay was used to determine the cell viabilities of AGS and MKN-45 cells. (e and f) The qRT-PCR assay was used to evaluate the mRNA level of Ki67 and PCNA in AGS and MKN-45 cells. Data are shown as mean $\pm$ SD; $^*p < 0.05$.

have been steadily declining over the course of the past five years, it continues to be the most common and deadly tumor in the world [15]. As a consequence of this, it is of the utmost importance to get a deeper comprehension of the molecular processes that underlie the development of gastric cancer, as well as to locate innovative clinical screening and diagnostic targets.

The study of glycolysis using bioinformatics led to the discovery of 13 genes related to the process. There was a discernible uptick in the levels of expression for CLDN3,

ADH4, HKDC1, and TFF3. The genes CLDN3 [16], ADH4 [17], and TFF3 [18] have all been implicated in the development of gastric cancer. Next, HKDC1 expression was significantly increased in the GEO and TCGA databases. Our investigation into the role of HKDC1 in gastric cancer was highly exciting because no one had ever reported on its significance before.

In addition, the oncogenic effect of HKDC1 in hepatocellular [19] and colorectal cancers [20] served as a driving force behind our decision to investigate the functional

(a)

(b)

(c)

(d)

(e)

(f)

(g)

Figure 7: Continued.

(h)

(i)

(j)
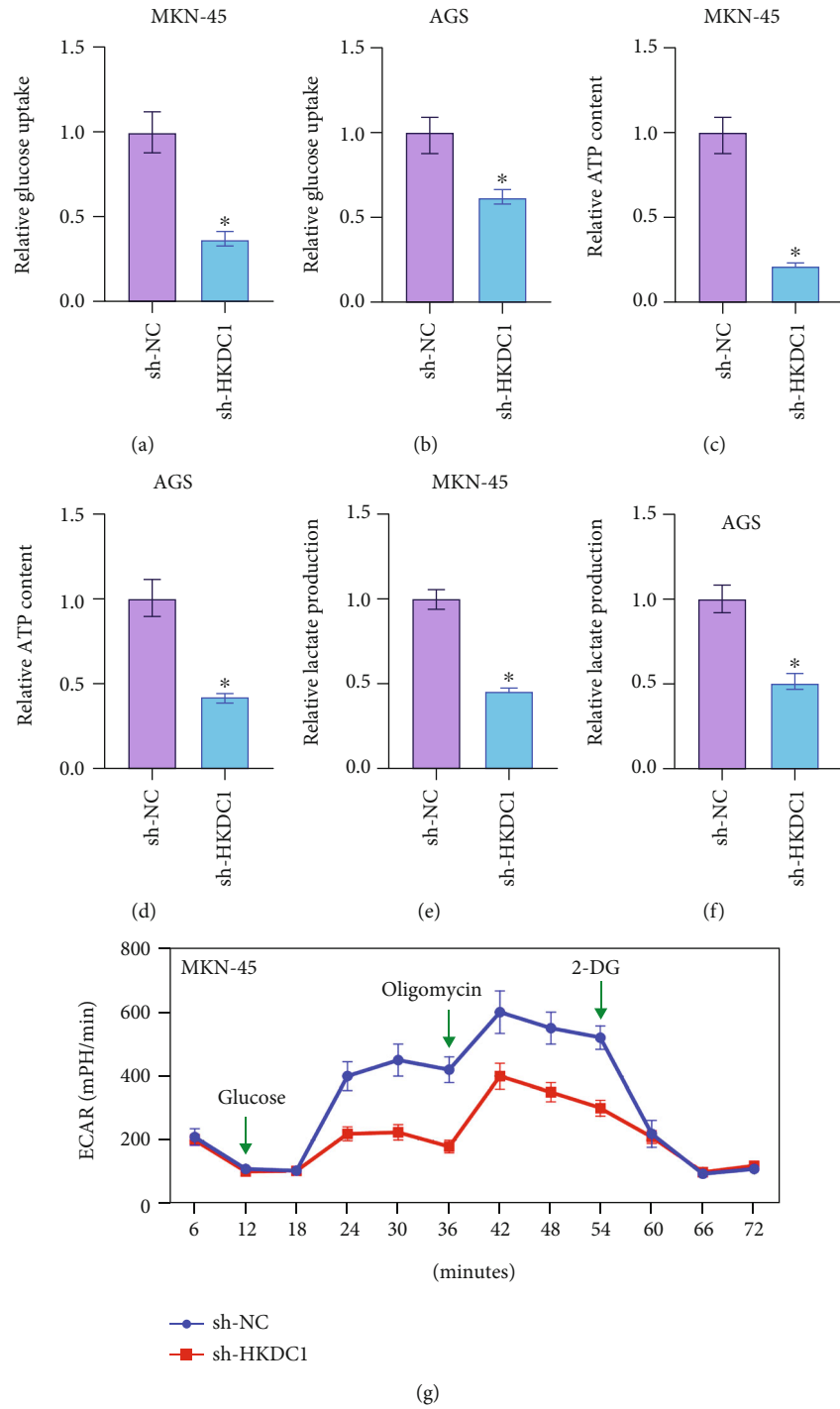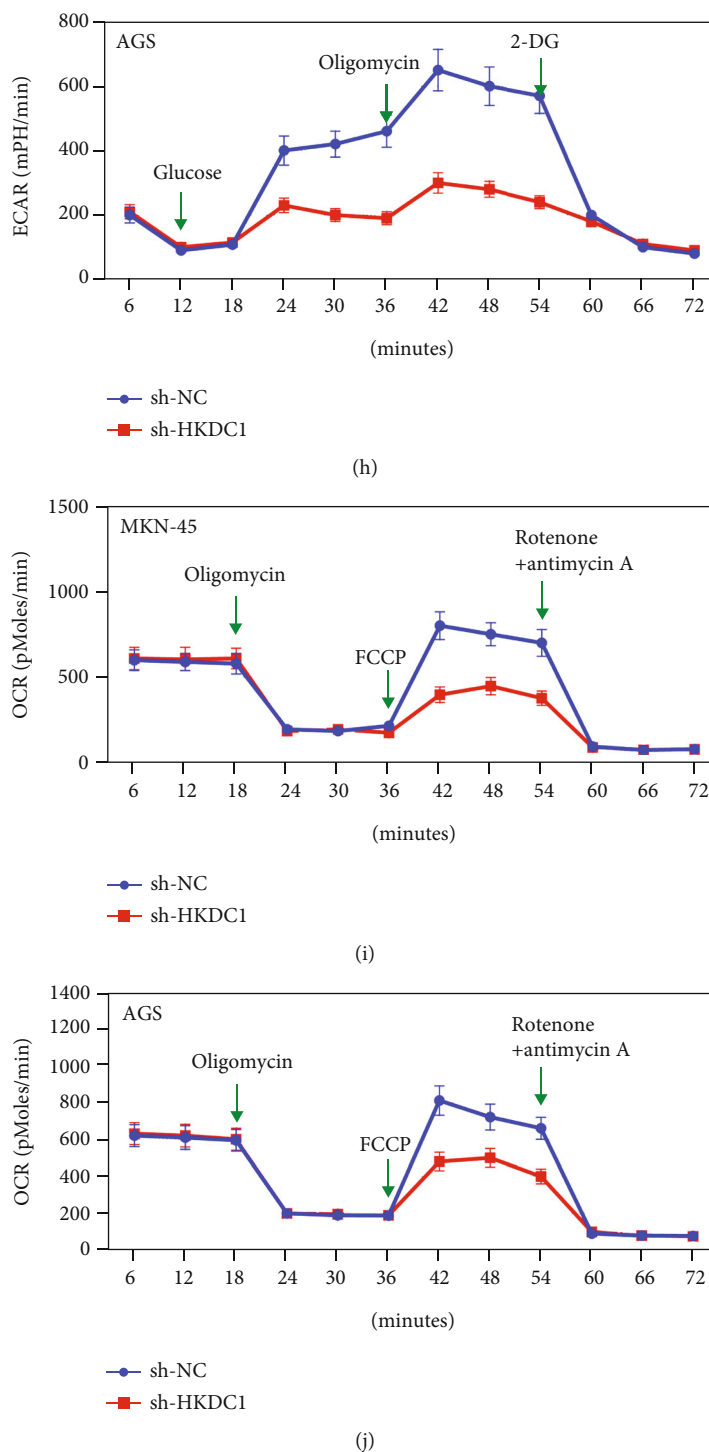
FIGURE 7: Downregulation of HKDC1 inhibits the glycolysis of gastric cancer cells. (a and b) Glucose uptake of AGS and MKN-45 cells was determined by a glucose uptake colorimetric assay kit. (c and d) ATP synthesis of AGS and MKN-45 cells was determined by ATP colorimetric assay kit. (e and f) Lactate production of AGS and MKN-45 cells was determined by lactate assay kit II. (g and h) The ECAR values of AGS and MKN-45 cells were measured using the Seahorse XF96 analyzer. (i and j) The OCR values of AGS and MKN-45 cells were measured using the Seahorse XF96 analyzer. Data are shown as mean ± SD; $*p < 0.05$.

importance of HKDC1 in gastric cancer. During this examination, we found that the gene HKDC1 was highly expressed in the tissues and cell lines of GC, although its expression was relatively low in the normal tissues that were located in the vicinity. These preliminary data suggest that the gene HKDC1 plays an oncogenic role in gastric cancer. Furthermore, due to its distinctive properties, HKDC1 is ideally suited to serve as a therapeutic target for gastric cancer. It is generally accepted that metabolic reprogramming, such as glycolysis in aerobic circumstances, is an indication

of tumor growth in a wide variety of cancers. This is because glycolysis is an aerobic process. The increased glycolysis that occurs in cancer cells leads to increased glucose intake and lactate formation [7]. This alters the metabolic requirements of the cancer cells, which in turn leads to increased invasion and metastasis. According to the findings of a recent analysis, HKDC1 is responsible for catalyzing glucose phosphorylation and the metabolism of cellular energy, both of which are critical in the development and spread of cancer [12]. According to the findings of the current research, HKDC1 is associated with both the process of proliferation and glycolysis in gastric cancer. As a result, HKDC1 may serve as a potential research target for the detection and treatment of gastric cancer, an area that calls for additional investigation.

There is mounting evidence to support the hypothesis that aerobic glycolysis plays a key part in the carcinogenic process, most notably in the development of gastric cancer. Glycolysis reprogramming is predominately glycolytic even when there is a significant amount of oxygen present in cancer cells [21]. It has been proven that oncogenic drive is the primary cause of the cleavage of aerobic glycolysis. This increases cancer cell proliferation and survival by delivering more intermediates for particular biosynthetic pathways and adaptability to hypoxic settings [22, 23]. Cancer cells have a distinctive metabolic phenotype that allows them to maintain the malignant biological processes for that they are responsible. This phenotype includes increased glucose uptake, lactate release, ATP production, and ECAR [4]. We demonstrate in this study that removing HKDC1 has an effect on the proliferation of cells in vitro. In addition, the downregulation of HKDC1 in gastric cancer cells resulted in a significant reduction in glucose uptake, lactate production, ATP synthesis, and ECAR, as well as an increase in OCR and modest inhibition of glycolysis. The initial indication that HKDC1 is a tumorigenic gene in gastric cancer comes from these studies.

5. Conclusion

Taken as a whole, the inhibition of cell proliferation and glycolysis brought about by the downregulation of HKDC1 provided a potential new avenue for the investigation of gastric cancer as a research target.

Data Availability

The data used to support the findings of this study are available from the corresponding authors upon request.

Disclosure

Chen Yu and Ting-ting Bao are co-first authors.

Conflicts of Interest

The authors declare that they have no conflicts of interest.

Supplementary Materials

Suppl 1: list of significantly changed DEGs from the GEO database ($p < 0.05$). Suppl 2. List of significantly changed DEGs after screened using Gene Set Enrichment Analysis ($p < 0.05$). (Supplementary Materials)

References

[1] E. C. Smyth, M. Nilsson, H. I. Grabsch, N. C. T. van Grieken, and F. Lordick, "Gastric cancer," *The Lancet*, vol. 396, no. 10251, pp. 635–648, 2020.

[2] L. Yang, C. Kartsonaki, P. Yao et al., "The relative and attributable risks of cardia and non-cardia gastric cancer associated with Helicobacter pylori infection in China: a case-cohort study," *The Lancet Public Health*, vol. 6, no. 12, pp. e888–e896, 2021.

[3] M. Abbas, A. Faggian, D. N. Sintali et al., "Current and future biomarkers in gastric cancer," *Biomedicine & Pharmacotherapy*, vol. 103, pp. 1688–1700, 2018.

[4] S. Ganapathy-Kanniappan and J. F. Geschwind, "Tumor glycolysis as a target for cancer therapy: progress and prospects," *Molecular Cancer*, vol. 12, no. 1, p. 152, 2013.

[5] Z. Abbaszadeh, S. Çeşmeli, and Ç. Biray Avcı, "Crucial players in glycolysis: cancer progress," *Gene*, vol. 726, article 144158, 2020.

[6] N. S. Akins, T. C. Nielson, and H. V. Le, "Inhibition of glycolysis and glutaminolysis: an emerging drug discovery approach to combat cancer," *Current Topics in Medicinal Chemistry*, vol. 18, no. 6, pp. 494–504, 2018.

[7] Y. Cao, "Adipocyte and lipid metabolism in cancer drug resistance," *The Journal of Clinical Investigation*, vol. 129, no. 8, pp. 3006–3017, 2019.

[8] Z. Wu, J. Wu, Q. Zhao, S. Fu, and J. Jin, "Emerging roles of aerobic glycolysis in breast cancer," *Clinical & Translational Oncology*, vol. 22, no. 5, pp. 631–646, 2020.

[9] W. Li, M. Xu, Y. Li et al., "Comprehensive analysis of the association between tumor glycolysis and immune/inflammation function in breast cancer," *Journal of Translational Medicine*, vol. 18, no. 1, p. 92, 2020.

[10] Q. Yang, J. Xu, Q. Ma et al., "PRKAA1/AMPKα1-driven glycolysis in endothelial cells exposed to disturbed flow protects against atherosclerosis," *Nature Communications*, vol. 9, no. 1, p. 4667, 2018.

[11] Y. Zhang, L. Zhao, S. Yang et al., "CircCDKN2B-AS1 interacts with IMP3 to stabilize hexokinase 2 mRNA and facilitate cervical squamous cell carcinoma aerobic glycolysis progression," *Journal of Experimental & Clinical Cancer Research*, vol. 39, no. 1, p. 281, 2020.

[12] X. Wang, B. Shi, Y. Zhao et al., "HKDC1 promotes the tumorigenesis and glycolysis in lung adenocarcinoma via regulating AMPK/mTOR signaling pathway," *Cancer Cell International*, vol. 20, no. 1, p. 450, 2020.

[13] C. M. Pusec, A. de Jesus, M. W. Khan et al., "Hepatic HKDC1 expression contributes to liver metabolism," *Endocrinology*, vol. 160, no. 2, pp. 313–330, 2019.

[14] X. Chen, Y. Lv, Y. Sun et al., "PGC1β regulates breast tumor growth and metastasis by SREBP1-mediated HKDC1 expression," *Frontiers in Oncology*, vol. 9, p. 290, 2019.

[15] A. F. Milano, "20-year comparative survival and mortality of cancer of the stomach by age, sex, race, stage, grade, cohort entry time-period, disease duration & selected ICD-O-3 oncologic phenotypes: *A systematic review of 157,258 cases for diagnosis years 1973–2014: (SEER*stat 8 3 4)," Journal of Insurance Medicine*, vol. 48, no. 1, pp. 5–23, 2019.

[16] N. V. Danilova, K. A. Anikina, N. A. Oleynikova, D. V. Vychuzhanin, and P. G. Malkov, "Claudin-3 expression in gastric cancer," *Arkhiv Patologii*, vol. 82, no. 2, pp. 5–11, 2020.

[17] H. M. Yin, Q. He, J. Chen, Z. Li, W. Yang, and X. Hu, "Drug metabolism-related eight-gene signature can predict the prognosis of gastric adenocarcinoma," *Journal of Clinical Laboratory Analysis*, vol. 35, no. 12, article e24085, 2021.

[18] J. R. Meng, H. Z. Tang, K. Z. Zhou, W. H. Shen, and H. Y. Guo, "TFF3 and survivin expressions associate with a lower survival rate in gastric cancer," *Clinical and Experimental Medicine*, vol. 13, no. 4, pp. 297–303, 2013.

[19] H. Jiang, Q. Yao, Y. An, L. Fan, J. Wang, and H. Li, "Baicalin suppresses the progression of Type 2 diabetes-induced liver tumor through regulating METTL3/m^{6}A/HKDC1_ axis and downstream p-JAK2/STAT1/clevaged Capase3 pathway," *Phytomedicine*, vol. 94, article 153823, 2022.

[20] H. Lian, A. Wang, Y. Shen et al., "Identification of novel alternative splicing isoform biomarkers and their association with overall survival in colorectal cancer," *BMC Gastroenterology*, vol. 20, no. 1, p. 171, 2020.

[21] Y. Jiang, Q. Han, H. Zhao, and J. Zhang, "Promotion of epithelial-mesenchymal transformation by hepatocellular carcinoma-educated macrophages through Wnt2b/β-catenin/c-Myc signaling and reprogramming glycolysis," *Journal of Experimental & Clinical Cancer Research*, vol. 40, no. 1, p. 13, 2021.

[22] E. Enzo, G. Santinon, A. Pocaterra et al., "Aerobic glycolysis tunes YAP/TAZ transcriptional activity," *The EMBO Journal*, vol. 34, no. 10, pp. 1349–1370, 2015.

[23] N. Xie, Z. Tan, S. Banerjee et al., "Glycolytic reprogramming in myofibroblast differentiation and lung fibrosis," *American Journal of Respiratory and Critical Care Medicine*, vol. 192, no. 12, pp. 1462–1474, 2015.

Research Article

Integrated Analyses of the Expression and Prognostic Value of EPHB6 in Cervical Cancer and Its Correlation with Immune Infiltrates

Siyang Xiang,[1,2] **Mei Wei,**[1,2] **Limei Zhao** ![ORCID],[2] **Anping Lin** ![ORCID],[1] **and Zhengai Xiong** ![ORCID][1]

[1]*Department of Obstetrics and Gynecology, Chongqing Medical University, Chongqing, China*
[2]*Department of Gynaecology, The First People's Hospital of Chongqing Liangjiang New District, Chongqing, China*

Correspondence should be addressed to Limei Zhao; zhaolimei_gynaec@163.com, Anping Lin; anpinglin2022@163.com, and Zhengai Xiong; xiongzhengai2008@163.com

Among women, cervical cancer (CC) ranks as the third most frequent form of carcinoma and the fourth greatest cancer-related cause of deaths. There is increasing evidence that points to the dysregulation of EPH receptor B6 (EPHB6) in various cancers. On the other hand, neither the expression nor the function of EPHB6 in CC has been researched. In the first part of this investigation, we analyzed the data from the TCGA and discovered that the level of EPHB6 was much lower in CC tissues than in normal cervical tissues. ROC assays revealed that high EPHB6 expression had an AUC value of 0.835 for CC. The survival study revealed that both the overall and disease-specific survivals in this condition were considerably lower among patients who had a low EPHB6 level compared to those who had a high EPHB6 level. It is important to note that the multivariate COX regression analysis indicated that the expression of EPHB6 was an independent predictive factor. In addition to this, the C-indexes and calibration plots of a nomogram derived from multivariate assays revealed an accurate prediction performance among patients with CC. Immune infiltration analysis indicated that the expression of EPHB6 was positively associated with the levels of Tcm, TReg, B cells, T cells, iDC, T helper cells, cytotoxic cells, and DC, while negatively associated with NK CD56bright cells and neutrophils. In summary, the downregulation of EPHB6 was strongly linked to a more aggressive clinical development of CC, suggesting its potential utility as a diagnostic and therapeutic target in CC.

1. Introduction

Cervical cancer (CC) is one of the most common gynecological malignant tumors worldwide, which has become a prominent public health issue [1]. It is observed that the incidence of CC ranks second among gynecological malignant tumors, but its mortality rate ranks first among female malignant tumors in the genital tract [2]. As a result, CC has evolved into a condition that poses a risk to the wellbeing of women [3]. The average age at which CC develops is getting younger, which poses a significant risk to women's health and even life, particularly in less-developed nations [4, 5]. Adenocarcinoma, squamous cell carcinoma, and adenosquamous carcinoma are three subtypes of CC that may be identified histologically, which are results of the

heterogeneity that characterizes CC [6, 7]. Chemotherapy, radiation, and surgery are the primary treatment options available to people who have colon cancer at the present time [8]. However, the prognosis of patients continues to be dismal as a result of the spread of metastases and the resistance of the cancer to chemotherapy [9, 10]. Oncotherapy is still faced with significant obstacles despite the progress that has been made in the field of health care. These obstacles include a delayed diagnosis, recurrence or metastasis, and cancer-associated mutations [11, 12]. As a result, the investigation of sensitive biomarkers is of utmost importance.

In the human genome, the erythropoietin-producing hepatocytes, Ephs, or receptors make up the biggest family of tyrosine kinase receptors. EphA1-A10 and EphB1-B6 are the names of the two sets of members that make up the

Eph receptor subfamily at this point [13]. There are a total of 16 members making up this subfamily. During embryonic development, Eph receptors play a mediating role in the processes of cell compartmentalization and directional cell migration [14]. Ephs are thought to play crucial roles in the invasiveness of cancers due to their ability to govern cell adhesion and migration [15]. Despite the fact that the functions of various EphB receptors in cancers appear to be in conflict with one another, the Eph receptors have been linked to a number of other malignancies. EPHB6 is considered to be a kinase-dead receptor tyrosine kinase due to the fact that its kinase domain is catalytically inactive, which exhibits many changes in amino acids that are normally conserved [16]. The protein EPHB6 is deleted in more aggressive breast cancers, melanomas, and neuroblastomas [17–19]. It has been demonstrated in the past that the epigenetic silencing of the EPHB6 gene caused by promoter methylation is connected to the downregulation of the EPHB6 gene. Additionally, reports on the predictive significance of EPHB6 in tongue squamous cell carcinoma have also been made [20]. However, very little information is available for the expression and function of EPHB6 in CC.

Because it is intimately connected to the investigation of tumor etiology and the responsiveness of immunotherapy, the interaction between tumor microenvironment (TME) and tumors has become an essential element of studies on tumor biology in recent years [21]. The efficacy of immunotherapy in the treatment of several forms of cancer sheds information on the critical function of TME [22]. However, as CC is a heterogeneous illness, it poses a significant obstacle to the development of customized treatments due to the wide variety of phenotypes it exhibits and its poor outlook. Through complex, two-way, and dynamical interactions between tumors and the stroma, CC tumor cells gain a heightened capacity to penetrate and spread into surrounding tissues, according to a growing body of research [23, 24]. In recent years, bioinformatics assays have played a highly significant role in improving both our understanding of various diseases and our abilities to treat them. One of these diseases is cancer. The expression level of certain markers may be used as a reflection of the invasion of particular cell types in tumor tissues by employing algorithms such as ssGSEA [25, 26]. It is possible to assess the significance of the correlations between the infiltration levels of various cell types and the survival rates of patients by analyzing the follow-up information of numerous cohorts in their entirety. As a result, we wanted to investigate the expression of EPHB6 in patients with CC and its predictive relevance. In addition, we investigated whether or not there was a connection between the expression of EPHB6 and TME.

2. Materials and Methods

2.1. TCGA Data Acquisition.
The TCGA database was accessed to get the survival data of patients with CC, together with the RNA transcriptome data presented in the format of FPKM. The TCGA publishing standards were adhered to throughout the entirety of the analysis process. A total of 306

CC specimens and 3 nontumor specimens were enlisted for later studies when duplicate samples from the same individuals were determined to be disregarded. The studies on CC of the TCGA were consulted to get fundamental clinical information pertaining to patients with CC. Following the application of the aforementioned filters, a total of 306 individuals diagnosed with CC in the TCGA dataset were included in this analysis.

2.2. Differential Expression of EPHB6 in CC Tissues in the TCGA Database.
In order to calculate the differential expression of EPHB6, boxplots and scatter plots were produced using the illness state as a variable. The disease state was either tumorigenic or normal. How well EPHB6 performed as a diagnostic tool was determined through the use of receiver operating characteristic (ROC) curves. It was determined that a statistical ranking of EPHB6 expression that was either higher or lower than the median value was designated as EPHB6-high or EPHB6-low, respectively.

2.3. Clinical Statistical Analysis on Prognosis, Model Construction, and Evaluation.
The Wilcoxon signed-rank sum test and logistic regression were utilized to delve into the nature of the connection existing between clinical pathologic characteristics and EPHB6. Using Cox regression and the Kaplan–Meier technique, patients with TCGA were analyzed to determine the clinicopathological features that were linked with 10-year overall survival (OS) and disease-specific survival (DSS). In order to evaluate the impact of EPHB6 expression on survivals in conjunction with other clinical parameters, a multivariate Cox regression model was utilized (stage, myometrial invasion, lymph node status, distant metastasis status, histological grade, and subtype). The median value of EPHB6 expression was used to establish the value that served as the cut-off point. In every experiment, a p value of less than 0.05 was deemed to indicate statistical significance. Using the Kaplan–Meier technique and a two-sided log-rank test, we were able to determine the difference between the 10-year OS and DSS of groups with a high and low level of EPHB6.

The independent prognostic indicators acquired from a multivariate analysis were utilized to build nomograms, through which the expected survival probability for one 1, 3, and 5 years was individualized. These nomograms were established on the basis of Cox regression models. The RMS software was decidedly used to create nomograms containing important clinical features and calibration plots. The calibration curves were visually evaluated by mapping the nomogram-predicted probability against the occurrences observed; the 45° line represented the best predictive value among all the lines in the assessment. To evaluate the accuracy of discrimination based on the nomogram, a concordance index, abbreviated as C-index, was utilized, whose value was determined using the bootstrap method with a total of 1,000 resamples. The C-index was utilized to make a comparison between the prediction accuracy of the nomogram and that of individual prognostic parameters. In this particular research

endeavor, all statistical tests were conducted using two different sets of data, and the threshold of statistical significance was established as 0.05.

2.4. Immune Infiltration Analysis. We calculated the infiltration extent of 28 immune cell types using the single-sample gene set enrichment analysis (ssGSEA) method included in the GSVA R package [27]. Our calculations were based on the expression levels of genes included in 28 published gene sets that were associated with immune cells.

2.5. Statistical Analysis. All statistical analyses were conducted with R Studio (4.0.2, Boston, USA). All hypothetical tests were two-sided, and a p value < 0.05 was considered significant.

3. Results

3.1. EPHB6 is Downregulated in Human CC Specimens. In order to evaluate the relevance of the expression of EPHB6 in CC, we began by examining its expression in patients with CC based on TCGA datasets. This allowed us to analyze both the expression of EPHB6 and its significance in CC. The expression of EPHB6 was dramatically downregulated in CC tissues compared to normal cervical tissues, as is illustrated in Figure 1. This difference was statistically significant ($p < 0.01$).

3.2. The Diagnostic Significance of EPHB6 Expression in CC. Previous research has demonstrated that a number of functional genes have diagnostic significance for patients with CC. After that, we carried out ROC tests, which demonstrated that a high EPHB6 expression possessed an AUC value of 0.835 for CC (Figure 2).

3.3. Association of EPHB6 with the Clinicopathological Parameters of CC. Further investigations into the relationships between EPHB6 and the clinicopathological factors of CC were carried out so that we could examine the clinical significance of EPHB6 in CC. According to what is presented in Table 1, our team did not identify a discernible distinction between the expression of EPHB6 and a number of clinical variables, including age and clinical stage.

3.4. Prognostic Values of EPHB6 Expression in Patients with CC. The Kaplan–Meier survival curves indicated that the overall survival (Figure 3, $p = 0.001$) and illness-specific survival (Figure 4, $p = 0.008$) of patients with a low EPHB6 level were considerably lower than those of patients with a high EPHB6 level. An investigation using univariate Cox regression revealed that clinical stages and EPHB6 expression had a significant impact on both the overall survival rate and the survival rate specific to the illness (Tables 2 and 3). Additionally, a multivariate COX regression analysis demonstrated that the expression of EPHB6 was an independent predictive predictor for both overall and disease-specific survivals (Tables 2 and 3).
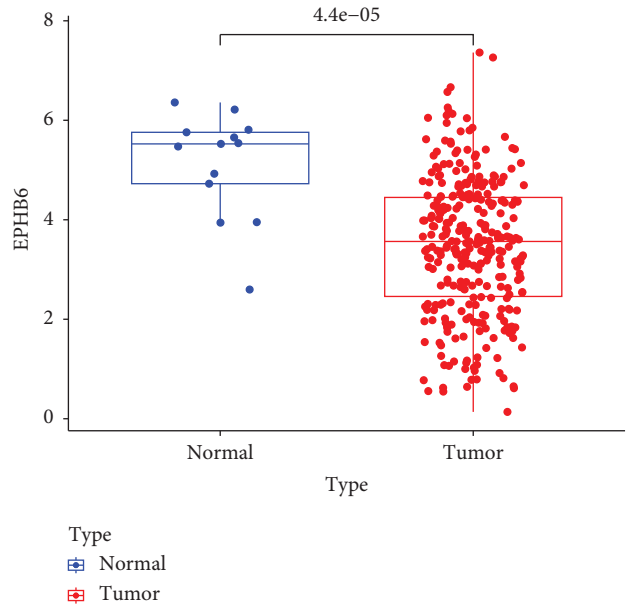
Figure 1: The expression of EPHB6 was analyzed based on TCGA datasets for both CC and non-tumor samples.
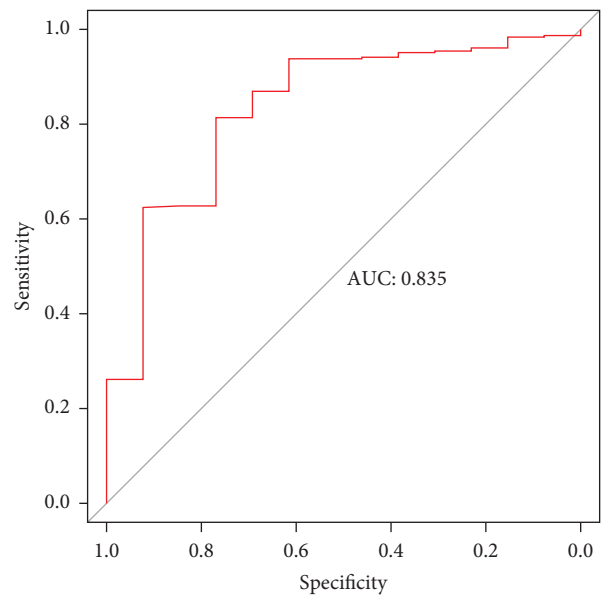
Figure 2: Diagnostic utility of EPHB6 expression in screening CC and non-tumor tissues, as is measured by receiver operating characteristic curves.

3.5. The Construction and Validation of a Nomogram Based on EPHB6. In order to give a quantitative method for predicting the outcome of patients with GC, a nomogram was constructed using EPHB6 in conjunction with other clinical risk indicators that are independent of one another (Figure 5(a)). A point scale was utilized in the construction of a nomogram based on a multivariate Cox analysis. Each variable was given a certain number of points depending on the scale. The total number of points given to each variable was recalculated to fall within the range of 1 to 100. The number of points earned across all

TABLE 1: Correlation of clinicopathological features of CC with the expression level of EPHB6.

Characteristic	Low expression of EPHB6	High expression of EPHB6	p
n	153	153	
Age, n (%)			0.127
≤50	101 (33%)	87 (28.4%)	
>50	52 (17%)	66 (21.6%)	
Clinical stage, n (%)			0.449
Stage I	85 (28.4%)	77 (25.8%)	
Stage II	29 (9.7%)	40 (13.4%)	
Stage III	25 (8.4%)	21 (7%)	
Stage IV	12 (4%)	10 (3.3%)	
Histologic grade, n (%)			1.000
G1	9 (3.3%)	10 (3.6%)	
G2	67 (24.5%)	68 (24.8%)	
G3	60 (21.9%)	59 (21.5%)	
G4	0 (0%)	1 (0.4%)	
Age, median (IQR)	45 (37, 55)	47 (40, 59)	0.071
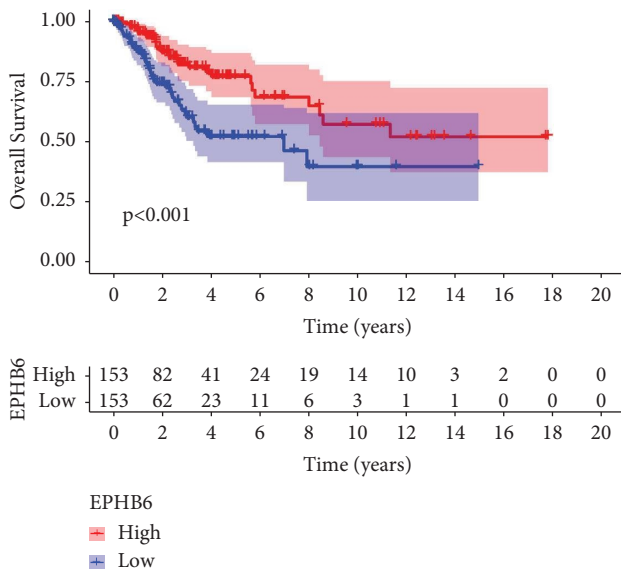
FIGURE 3: Overall curves of two groups defined by a low and high expression of EPHB6 in patients with CC.

FIGURE 4: Disease-specific survivals in the two groups defined by a low and high expression of EPHB6 in patients with CC.

the factors was then used as the basis for the final score. A vertical line was drawn immediately downwards from the total point axis to the outcome axis, where the chance of survivals was calculated for patients with CC 1, 3, and 5 years after their diagnosis (Figure 5(a)). We also performed an analysis on the ability of the nomogram to accurately forecast the future, and the findings showed that the C-index of the model was greater than 0.7, which indicated that the ability of the nomogram to accurately predict the future was only moderate. The bias-corrected line in the calibration plot was utilized to be close to the ideal curve, which was the line at 45°, showing that the prediction and the observation were in close agreement with one another (Figure 5(b)). These findings revealed that the nomogram was a more accurate model than individual prognostic indicators for predicting the short- or long-term survival of patients who had CC.

3.6. Comparison of Immune Infiltration. We carried out ssGSEA tests so that we could investigate the relationship between the level of EPHB6 and the immune microenvironment. The expression of EPHB6 was shown to be favorably linked with the levels of TCM, TReg, B cells, T cells, iDC, T helper cells, cytotoxic cells, and DC, as is shown in Figure 6. On the other hand, it was found to be negatively associated with NK CD56bright cells and neutrophils. Based on our findings, it seems likely that EPHB6 is involved in the intricate workings of the immunological microenvironment.

4. Discussion

In recent years, the technology of microarrays has been used in conjunction with integrated bioinformatic analyses to find new genes associated with a variety of disorders [28, 29]. These genes have the potential to operate as biological markers for diagnosis and prognosis. For instance, Yang

Table 2: Univariate and multivariate analyses on the overall survival based on the cox regression model.

Characteristics	Total (N)	Univariate analysis		Multivariate analysis	
		Hazard ratio (95% CI)	p value	Hazard ratio (95% CI)	p value
Age	306				
≤50	188	Reference			
>50	118	1.289 (0.810–2.050)	0.284		
Clinical stage	299				
Stage I and Stage II	231	Reference			
Stage III and Stage IV	68	2.369 (1.457–3.854)	**<0.001**	2.529 (1.551–4.123)	**<0.001**
Histologic grade	274				
G1 and G2	154	Reference			
G3 and G4	120	0.866 (0.514–1.459)	0.589		
EPHB6	306				
Low	153	Reference			
High	153	0.439 (0.272–0.709)	**<0.001**	0.420 (0.259–0.680)	**<0.001**

The bold values mean statistically significant.

Table 3: Univariate and multivariate analyses on disease-specific survivals based on the cox regression model.

Characteristics	Total (N)	Univariate analysis		Multivariate analysis	
		Hazard ratio (95% CI)	p value	Hazard ratio (95% CI)	p value
Age	302				
≤50	186	Reference			
>50	116	1.295 (0.761–2.204)	0.340		
Clinical stage	295				
Stage I and Stage II	227	Reference			
Stage III and Stage IV	68	2.675 (1.550–4.615)	**<0.001**	2.800 (1.620–4.839)	**<0.001**
Histologic grade	271				
G1 and G2	152	Reference			
G3 and G4	119	0.922 (0.514–1.654)	0.785		
EPHB6	302				
Low	149	Reference			
High	153	0.473 (0.275–0.813)	**0.007**	0.454 (0.263–0.783)	**0.005**

The bold values mean statistically significant.

(a)

(b)
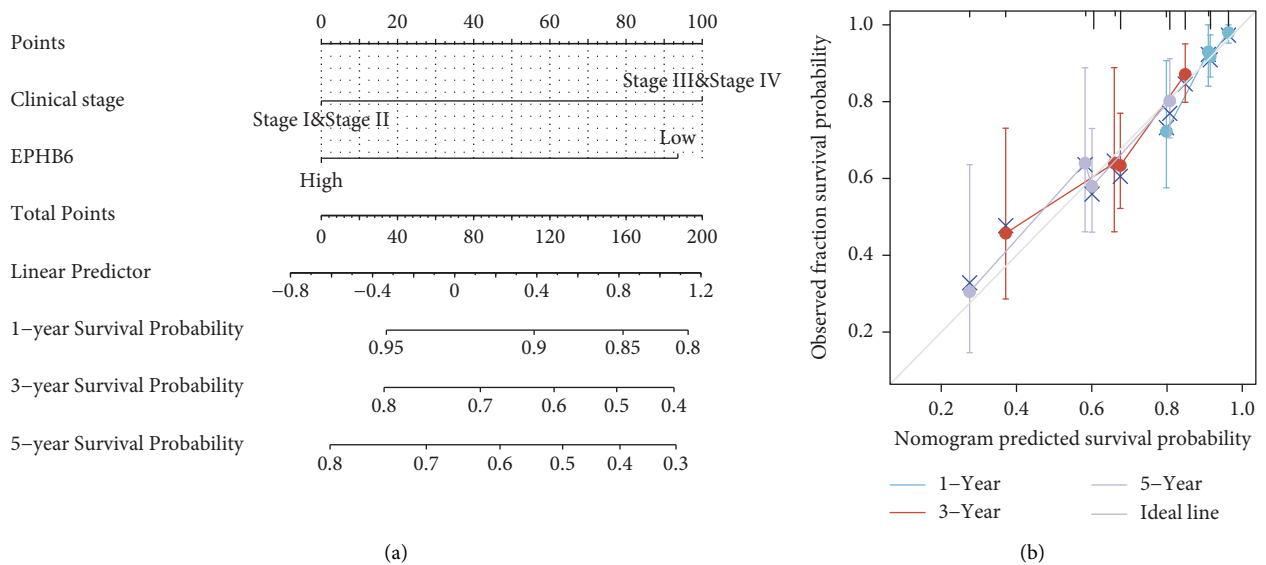
Figure 5: A quantitative approach that can be used to forecast the likelihood of a cancerous patient's overall survival after 1, 3 and 5 years. (a) A nomogram used to estimate the likelihood of 1-year, 3-year and 5-year overall survival of patients with cancers. (b) Plots of calibration based on the nomogram used to forecast the chance of overall survival after 1, 3 and 5 years.
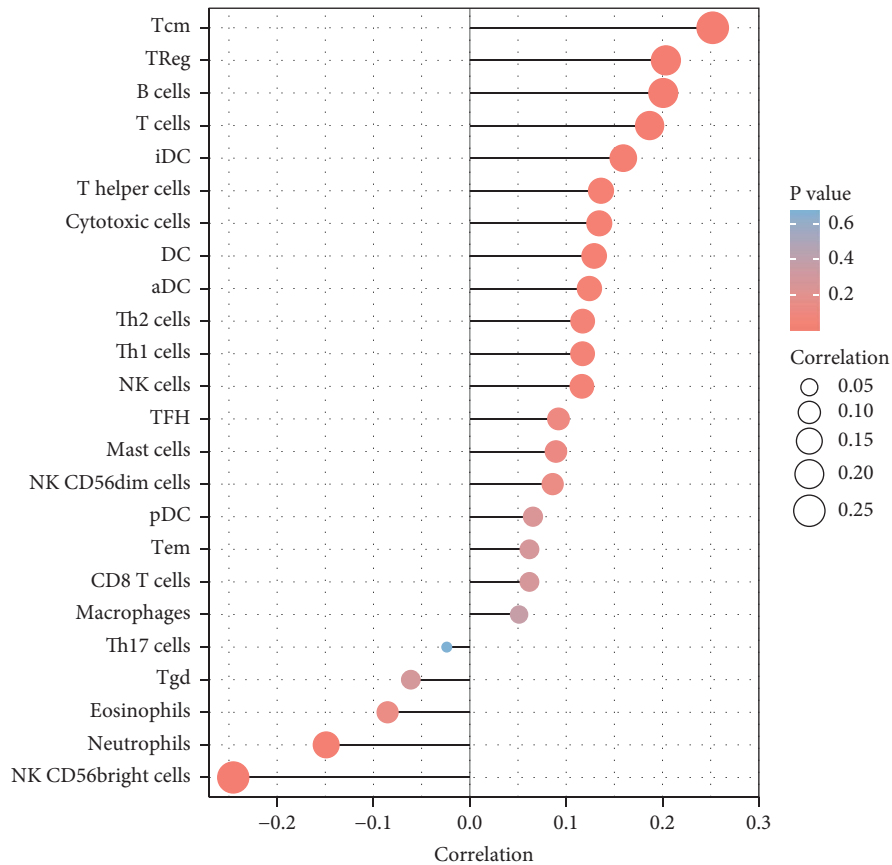
Figure 6: Relationships between EPHB6 and infiltrating immune cells in CC.

et al. reported that the expression level of PAMR1 in cervical cancer tissues was lower than that in normal cervix tissues, which was negatively associated with clinicopathologic characteristics. This is the case for all cervical cancer tissues. A positive prognosis was also predicted for individuals with CC who had a high expression level of PAMR1. The results of the CCK8, transwell, and wound-healing experiments revealed that CC cells were allowed to proliferate, migrate, and invade into surrounding tissues more easily through inhibiting PAMR1 [30]. He et al. showed that the expression of MYO10 was shown to be higher in cancerous cervical tissues and cells compared to normal controls. Furthermore, studies on survivals revealed that patients with a high MYO10 expression had a worse chance to survive the disease overall. In addition, by rewiring the PI3K/Akt signaling pathway of CC caused by the knockdown or overexpression of MYO10, the capability of cervical cells in terms of proliferation, invasion, and migration was dramatically hindered or improved [31]. These findings showed that some tumor-related genes might have the potential to be employed as new biomarkers for the diagnosis and prognosis of individuals suffering from CC.

In the past, a number of studies have revealed the deregulation of EPHB6 in a variety of malignancies, including breast cancers, colorectal cancers and pediatric T-cell acute lymphoblastic leukemia, among others [32–34]. However, whether EPHB6 was operating in an aberrant manner in CC has not been determined. After doing an

analysis of TCGA and GTEx data, the first thing that we did in this study was to report that the expression of EPHB6 was significantly lower in CC specimens compared with nontumor samples. According to our findings, EPHB6 might act as a positive regulator in the evolution of CC. The findings of the ROC tests verified the diagnostic utility of EPHB6 expression in screening CC specimens from non-tumor ones, which highlighted its potential as a diagnostic biomarker for CC. In addition, a survival study showed that a decreased expression of EPHB6 was connected to a bad outcome of individuals who had CC. It is important to note that the multivariate Cox regression analysis indicated that the expression of EPHB6 was an independent predictive factor for both overall and illness-specific survivals. After that, an exhaustive review was carried out on a nomogram, in which EPHB6 was combined with other significant clinical patterns (clinical stage and EPHB6 specifically), so as to produce a more accurate diagnosis. According to the calibration plot, there was a satisfactory concordance between the observed values and those expected for 1, 3, and 5 years of OS. Our approach was built on a complimentary perspective for each different tumor, which supplied an individualized score for each individual patient. As a consequence of this, our nomogram has the potential to become a very helpful new prognostic tool in the near future.

TME is a multilayered intricate system created when cancer cells interact with the stromal and immune cells in their surroundings [35], which are involved throughout the

whole process, from the beginning of the tumor growth to its response to treatment. Patients with colorectal cancers have a highly-immunosuppressive TME, which is one of the primary factors that contributes to their immunotherapy resistance in CC [36, 37]. The accumulation of lactate as a byproduct of aerobic glycolysis results in the formation of an acidic environment that makes tumor penetration easier, which plays a crucial role in the formation of an immunosuppressive TME. The primary components of this immunosuppressive TME are known as tumor-associated macrophages (TAMs), regulatory T cells (Tregs), and myeloid-derived suppressor cells (MDSCs), respectively. It has been shown that these cells can enhance systemic T cell failure, which avoids immune detection and the spread of CC. The results of an examination of immune infiltration indicated that the expression of EPHB6 was favorably linked with the level of TCM, TReg, B cells, T cells, iDC, T helper cells, cytotoxic cells, and DC, but was negatively associated with NK CD56bright cells and neutrophils. As a result, the relationship that exists between EPHB6 and the immune cells may be partially responsible for the anti-cancer impact that it has.

Nonetheless, there are certain limitations. Because the tests took place in different labs, first of all, there was a lack of standardized treatments and a dearth of clinical data in public databases. Secondly, research into the molecular pathways through which EPHB6 might contribute to carcinogenesis was lacking. Future wet lab work is planned to investigate the potential role of EPHB6 in CC signaling pathways.

5. Conclusion

Together, our findings suggest that EPHB6 may improve our ability to predict the outcomes of people with CC, encourage the creation of cutting-edge immune-based treatments, and maximize clinical effectiveness. Overall, the possible impact and mechanism of EPHB6 in CC need more investigations.

Data Availability

The original data can be obtained from the corresponding authors upon reasonable requests.

Conflicts of Interest

The authors declare that they have no potential competing conflicts of interest.

Authors' Contributions

Siyang Xiang and Mei Wei contributed equally to this work.

References

[1] R. L. Siegel, K. D. Miller, and A. Jemal, "Cancer statistics, 2019," *CA: A Cancer Journal for Clinicians*, vol. 69, no. 1, pp. 7–34, 2019.

[2] S. E. Waggoner, "Cervical cancer," *The Lancet*, vol. 361, no. 9376, pp. 2217–2225, 2003.

[3] K. Kim and H. R. Han, "Potential links between health literacy and cervical cancer screening behaviors: a systematic review," *Psycho-Oncology*, vol. 25, no. 2, pp. 122–130, 2016.

[4] G. Menderes, J. Black, C. L. Schwab, and A. D. Santin, "Immunotherapy and targeted therapy for cervical cancer: an update," *Expert Review of Anticancer Therapy*, vol. 16, no. 1, pp. 83–98, 2016.

[5] C. A. Johnson, D. James, A. Marzan, and M. Armaos, "Cervical cancer: an overview of pathophysiology and management," *Seminars in Oncology Nursing*, vol. 35, no. 2, pp. 166–174, 2019.

[6] S. Weyers, S. M. Garland, M. Cruickshank, M. Kyrgiou, and M. Arbyn, "Cervical cancer prevention in transgender men: a review," *BJOG: An International Journal of Obstetrics and Gynaecology*, vol. 128, no. 5, pp. 822–826, 2021.

[7] S. Revathidevi, A. K. Murugan, H. Nakaoka, I. Inoue, and A. K. Munirajan, "APOBEC: a molecular driver in cervical cancer pathogenesis," *Cancer Letters*, vol. 496, pp. 104–116, 2021.

[8] A. Buskwofie, G. David-West, and C. A. Clare, "A review of cervical cancer: incidence and disparities," *Journal of the National Medical Association*, vol. 112, no. 2, pp. 229–232, 2020.

[9] E. M. Burd, "Human papillomavirus and cervical cancer," *Clinical Microbiology Reviews*, vol. 16, no. 1, pp. 1–17, 2003.

[10] P. Olusola, H. N. Banerjee, J. V. Philley, and S. Dasgupta, "Human papilloma virus-associated cervical cancer and health disparities," *Cells*, vol. 8, no. 6, p. 622, 2019.

[11] D. Mauricio, B. Zeybek, J. Tymon-Rosario, J. Harold, and A. D. Santin, "Immunotherapy in cervical cancer," *Current Oncology Reports*, vol. 23, no. 6, p. 61, 2021.

[12] A. Gadducci and S. Cosio, "Neoadjuvant chemotherapy in locally advanced cervical cancer: review of the literature and perspectives of clinical research," *Anticancer Research*, vol. 40, no. 9, pp. 4819–4828, 2020.

[13] S. Feduniw, D. Warzecha, I. Szymusik, and M. Wielgos, "Epidemiology, prevention and management of early postpartum hemorrhage - a systematic review," *Ginekologia Polska*, vol. 91, no. 1, pp. 38–44, 2020.

[14] L. Y. Liang, O. Patel, P. W. Janes, J. M. Murphy, and I. S. Lucet, "Eph receptor signalling: from catalytic to non-catalytic functions," *Oncogene*, vol. 38, no. 39, pp. 6567–6584, 2019.

[15] E. Shiuan and J. Chen, "Eph receptor tyrosine kinases in tumor immunity," *Cancer Research*, vol. 76, no. 22, pp. 6452–6457, 2016.

[16] E. O. Mason, Y. Goldgur, D. Robev, A. Freywald, D. B. Nikolov, and J. P. Himanen, "Structure of the EphB6 receptor ectodomain," *PLoS One*, vol. 16, no. 3, Article ID e0247335, 2021.

[17] M. Zangrossi, P. Romani, P. Chakravarty et al., "EphB6 regulates TFEB-lysosomal pathway and survival of disseminated indolent breast cancer cells," *Cancers*, vol. 13, no. 5, p. 1079, 2021.

[18] C. Hafner, F. Bataille, S. Meyer et al., "Loss of EphB6 expression in metastatic melanoma," *International Journal of Oncology*, vol. 23, no. 6, pp. 1553–1559, 2003.

[19] X. X. Tang, A. E. Evans, H. Zhao et al., "High-level expression of EPHB6, EFNB2, and EFNB3 is associated with low tumor stage and high TrkA expression in human neuroblastomas," *Clinical Cancer Research: An Official Journal of the American Association for Cancer Research*, vol. 5, no. 6, pp. 1491–1496, 1999.

[20] Y. Dong, J. Pan, Y. Ni, X. Huang, X. Chen, and J. Wang, "High expression of EphB6 protein in tongue squamous cell

carcinoma is associated with a poor outcome," *International Journal of Clinical and Experimental Pathology*, vol. 8, no. 9, pp. 11428–11433, 2015.

[21] B. Arneth, "Tumor microenvironment," *Medicina*, vol. 56, no. 1, p. 15, 2019.

[22] M. Jarosz-Biej, R. Smolarczyk, T. Cichoń, and N. Kułach, "Tumor microenvironment as A "game changer" in cancer radiotherapy," *International Journal of Molecular Sciences*, vol. 20, no. 13, p. 3212, 2019.

[23] E. Butturini, A. Carcereri de Prati, D. Boriero, and S. Mariotto, "Tumor dormancy and interplay with hypoxic tumor microenvironment," *International Journal of Molecular Sciences*, vol. 20, no. 17, p. 4305, 2019.

[24] I. Lodewijk, S. P. Nunes, R. Henrique, C. Jerónimo, M. Dueñas, and J. M. Paramio, "Tackling tumor microenvironment through epigenetic tools to improve cancer immunotherapy," *Clinical Epigenetics*, vol. 13, no. 1, p. 63, 2021.

[25] T. Le, R. A. Aronow, A. Kirshtein, and L. Shahriyari, "A review of digital cytometry methods: estimating the relative abundance of cell types in a bulk of cells," *Briefings in Bioinformatics*, vol. 22, no. 4, Article ID bbaa219, 2021.

[26] X. Li, Y. Cheng, Y. Cheng, and H. Shi, "Transcriptome analysis reveals the immune infiltration profiles in cervical cancer and identifies KRT23 as an immunotherapeutic target," *Frontiers in Oncology*, vol. 12, Article ID 779356, 2022.

[27] S. Hänzelmann, R. Castelo, and J. Guinney, "GSVA: gene set variation analysis for microarray and RNA-seq data," *BMC Bioinformatics*, vol. 14, no. 1, p. 7, 2013.

[28] V. C. Kok and C. C. Yu, "Cancer-Derived exosomes: their role in cancer biology and biomarker development," *International Journal of Nanomedicine*, vol. 15, pp. 8019–8036, 2020.

[29] L. S. Pessoa, M. Heringer, and V. P. Ferrer, "ctDNA as a cancer biomarker: a broad overview," *Critical Reviews In Oncology-Hematology*, vol. 155, Article ID 103109, 2020.

[30] R. Yang, M. Ma, S. Yu, X. Li, J. Zhang, and S. Wu, "High expression of PAMR1 predicts favorable prognosis and inhibits proliferation, invasion, and migration in cervical cancer," *Frontiers in Oncology*, vol. 11, Article ID 742017, 2021.

[31] J. H. He, J. G. Chen, B. Zhang et al., "Elevated MYO10 predicts poor prognosis and its deletion hampers proliferation and migration potentials of cells through rewiring PI3K/akt signaling in cervical cancer," *Technology in Cancer Research and Treatment*, vol. 19, Article ID 153303382093677, 2020.

[32] R. P. Kandpal, "Tyrosine kinase-deficient EphB6 receptor-dependent alterations in proteomic profiles of invasive breast carcinoma cells as determined by difference gel electrophoresis," *Cancer Genomics and Proteomics*, vol. 7, no. 5, pp. 253–260, 2010.

[33] J. Wang, Y. Zhang, J. Ma et al., "Determining the effects of Ephrin Type B Receptor 6 and Type A Receptor 3 on facilitating colorectal epithelial cell malignant transformation," *Neoplasma*, vol. 68, no. 05, pp. 955–964, 2021.

[34] A. El Zawily, E. McEwen, B. Toosi et al., "The EphB6 receptor is overexpressed in pediatric T cell acute lymphoblastic leukemia and increases its sensitivity to doxorubicin treatment," *Scientific Reports*, vol. 7, no. 1, p. 14767, 2017.

[35] L. Bejarano, M. J. C. Jordão, and J. A. Joyce, "Therapeutic targeting of the tumor microenvironment," *Cancer Discovery*, vol. 11, no. 4, pp. 933–959, 2021.

[36] L. Laplane, D. Duluc, A. Bikfalvi, N. Larmonier, and T. Pradeu, "Beyond the tumour microenvironment," *International Journal of Cancer*, vol. 145, no. 10, pp. 2611–2618, 2019.

[37] S. Cao, C. Lin, X. Li, Y. Liang, and P. E. Saw, "TME-responsive multistage nanoplatform for siRNA delivery and effective cancer therapy," *International Journal of Nanomedicine*, vol. 16, pp. 5909–5921, 2021.

Research Article

LncRNA LINC01207 Could Positively Regulate the Development of Colorectal Cancer

Gaowu Hu,[1] Wenquan Chen,[1] Wei Peng,[1] and Yongqing Cao [ID][2]

[1]*Department of Anorectal Medicine, Shanghai Traditional Chinese and Western Medicine Integrated Hospital
 Affiliated to Shanghai University of Traditional Chinese Medicine, Floor 9, Building 5, No. 303, Changyang Road,
 Hongkou District, Shanghai, China*
[2]*Department of Anorectal Medicine, Longhua Hospital Affiliated to Shanghai University of Traditional Chinese Medicine,
 725 Wanping South Road, Shanghai, China*

Correspondence should be addressed to Yongqing Cao; 18221133607@shutcm.edu.cn

Background. LINC01207 expression is associated with colorectal cancer progression. However, the exact role of LINC01207 in colorectal cancer (CRC) is not clear, and further exploration is needed. *Methods*. Gene expression data of the GSE34053 database were used to explore the differential expressed genes (DEGs) between colon cancer cells and normal cells. The gene expression profiling interactive analysis (GEPIA) was used to determine the differential expression of LINC01207 between CRC and normal tissues and the association between the expression of LINC01207 and survival in patients with CRC. The Kyoto Encyclopedia of Genes and Genomes (KEGG) and Gene Ontology (GO) analysis were performed to obtain the biological processes and pathways associated with DEGs and LINC01207 coexpressed genes in CRC. The qRT-PCR was used to determine the LINC01207 level in CRC cell lines and tissue samples. CCK-8 assay was employed to measure cell viability and Transwell assay to assess cell invasion and migration. *Results*. In this study, a total of 954 DEGs were identified, including 282 upregulated and 672 downregulated genes. LINC01207 was significantly upregulated in CRC samples with a poor prognosis. LINC01207 was also associated with pathways such as ECM-receptor interaction, O-glycan processing, and TNF signaling pathway in CRC. Knockdown of LINC01207 inhibited the migration, invasion, and proliferation of CRC cells. *Conclusion*. LINC01207 might act as an oncogene and promote the progression of CRC. Our study suggested that LINC01207 had the potential to be a novel biomarker for CRC detection and a therapeutic target for CRC treatment.

1. Introduction

Colorectal cancer (CRC) is one of the most common malignant tumors worldwide [1]. Approximately 900,000 people die from CRC each year, and the incidence is higher in the more economic regions [2]. In China, there are approximately 521,000 new cases and 248,000 deaths each year. The incidence rate ranks third among malignant tumors, and the mortality rate ranks fifth [3]. With the improvement of medical technology, some patients can be cured by surgery, adjuvant radiotherapy, and chemotherapy [4]. The 5-year survival rate of early-stage patients is about 80%–90%, but the survival rate is only 10% for advanced-stage patients [5]. To improve the overall survival rate of patients, early diagnosis and treatment are necessary.

As a special class of RNA molecule, long noncoding RNA (lncRNA) does not encode proteins. The length of lncRNA is more than 200 nucleotides [6]. Previous study indicated that abnormal expression of lncRNA was associated with human disease occurrence, including cancer, cardiovascular diseases, and degenerative neurological diseases [7]. It has been reported that the dysregulation of lncRNA expression can regulate various types of cancer progression, such as prostate cancer, bladder cancer, breast cancer, lung cancer, gastric cancer, and colorectal cancer. lncRNAs can lead to tumor metastasis, promote tumorigenesis, and increase chromosomal instability [8]. Therefore, it is necessary to further identify the function of lncRNAs in CRC.

Long noncoding RNA 1207 (LINC01207), located at 4q32, contains three exons and two introns. LINC01207 regulates gene transcription and protein translation [9]. LINC01207 is positively regulated in lung cancer [10] and pancreatic cancer [9], and its downregulation inhibits tumor growth and promotes apoptosis. LINC01207 could predict poor prognosis and inhibit cell metastasis by regulating the GSK-3 β/β-catenin signaling pathway in malignant glioma [11]. According to the data in the TCGA database [12], LINC01207 is associated with the prognosis of patients with CRC, indicating that LINC01207 may be an independent biomarker for CRC. Nevertheless, the present research on LINC01207's role in CRC is still limited, and the molecular mechanism remains unclear.

This study aimed to explore the biological effects and mechanisms of LINC01207 on CRC cell growth and invasion through bioinformatics and experimental analysis. LINC01207 expression was specifically increased in CRC tissues and cell lines. This may suggest LINC01207 as a new factor in CRC detection as a biomarker or therapeutic target.

2. Methods and Materials

2.1. Microarray Data. The GSE34053 mRNA expression data were obtained from the Gene Expression Omnibus (GEO) [13] database in the National Center of Biotechnology Information (NCBI) (https://www.ncbi.nlm.nih.gov/geo). GPL570 [HG-U133_Plus_2] Affymetrix Human Genome U133 Plus 2.0 Array was used in this study. Both the carcinoma cells and carcinoma-associated fibroblasts (CAF) from the same patient tumor were isolated and separately cultured. The CD133-positive colorectal cancer cells were set as the experimental group. CAF samples were used for the control group.

2.2. PPI Network Construction and Analysis. The Retrieval of Interacting Genes (STRING; string-db.org) database was used to perform the construction of the protein-protein interaction (PPI) network between DEGs. The confidence of threshold value for PPIs was set as (combined score) >0.7.

2.3. GEPIA Database. As a public online tool, gene expression profiling interactive analysis (GEPIA; https://gepia.cancer-pku.cn/) provides customizable functionalities based on data from The Cancer Genome Atlas (TCGA) and the Genotype-Tissue Expression project (GTEx). In the present study, through GEPIA, differential expression of LINC01207 graphically between colon cancer and normal tissues and the association between the expression of LINC01207 and survival in patients with CRC were determined.

2.4. GO and KEGG Pathway Enrichment Analyses. The Kyoto Encyclopedia of Genes and Genomes (KEGG) and Gene Ontology (GO) analyses both for DEGs and LINC01207 coexpressed genes were performed by The Database for Annotation, Visualization, and Integrated Discovery (DAVID, https://David.ncifcrf.gov/tools.jsp). The number of enriched genes >2 and $P < 0.05$ were set as cut-off criteria.

2.5. Clinical Tissue Samples. A total of 30 pairs of tumor tissue and adjacent normal tissue samples were collected from the Longhua Hospital Affiliated to Shanghai University of Traditional Chinese Medicine and stored in liquid nitrogen for subsequent experiments. This study was approved by the Ethics Committee of Longhua Hospital Affiliated to Shanghai University of Traditional Chinese Medicine, and all patients signed the informed consent.

2.6. Cell Lines and Cell Culture. The CRC cell lines (HRT-18, HCT-15, SW480, HCT-116, and RKO) and colorectal cell line FHC were obtained from the American Type Culture Bank (ATCC, Manassas, USA). Cells were maintained in RPMI-1640 (Gibco BRL, Karlsruhe, Germany) containing 10% fetal bovine serum (Gibco FBS, USA), 100 IU/mL penicillin, and 100 μg/mL streptomycin (Baishitong, Chongqing, China).

2.7. Cell Transfection Assay. The si-LINC01207 #1, si-LINC01207 #2, and negative control (NC) were synthesized from GenePharma (Shanghai, China). Cells seeded in 6-well plates. The transfection was performed using Lipofectamine 2000 reagent (Invitrogen, USA) according to the manufacturer's instructions.

2.8. Cell Proliferation Assay (CCK-8). The cell proliferation was assessed using a CCK-8 kit (Takara, Dalian, China). After 24 hours of transfection, HCT-116 and RKO $(1 \times 10^3$ cells per well) cells were seeded into 96-well plates. 10 μl of CCK-8 reagent was added to each well at 0, 24, 48, and 72 hours, respectively. After incubation at 37°C for 1.5 h, the OD value of each well at 450 nm was measured with a microplate reader (BioRad, USA).

2.9. Quantitative Reverse Transcription-Polymerase Chain Reaction (qRT-PCR). The total RNA from cells and tissues was isolated by Trizol reagent (Invitrogen). The cDNA was synthesized by a reverse transcription kit (Byotime, China). The qRT-PCR was performed using the SYBR Green Master Mix (Biosharp, China) on the ABI 7500 qPCR system (ABI, USA) with GAPDH as the internal reference gene. The primer mix was ordered from Kumei (Kumei, China). The reaction conditions were as follows: predenaturation at 95°C for 3 minutes, denaturation at 95°C for 2 hours, annealing at 60°C for 20 seconds, and extension at 72°C for 1 minute, a total of 40 steps. The relative expression was determined by $2^{-\Delta\Delta Ct}$ method.

2.10. Migration and Invasion Assays. The cell migration and invasion were determined by the Transwell method. Cells were plated into a 24-well plate with a serum-free medium at a density of 8×10^4 cells per well. Subsequently, cells were washed and fixed in anhydrous methanol for

(a)

(b)
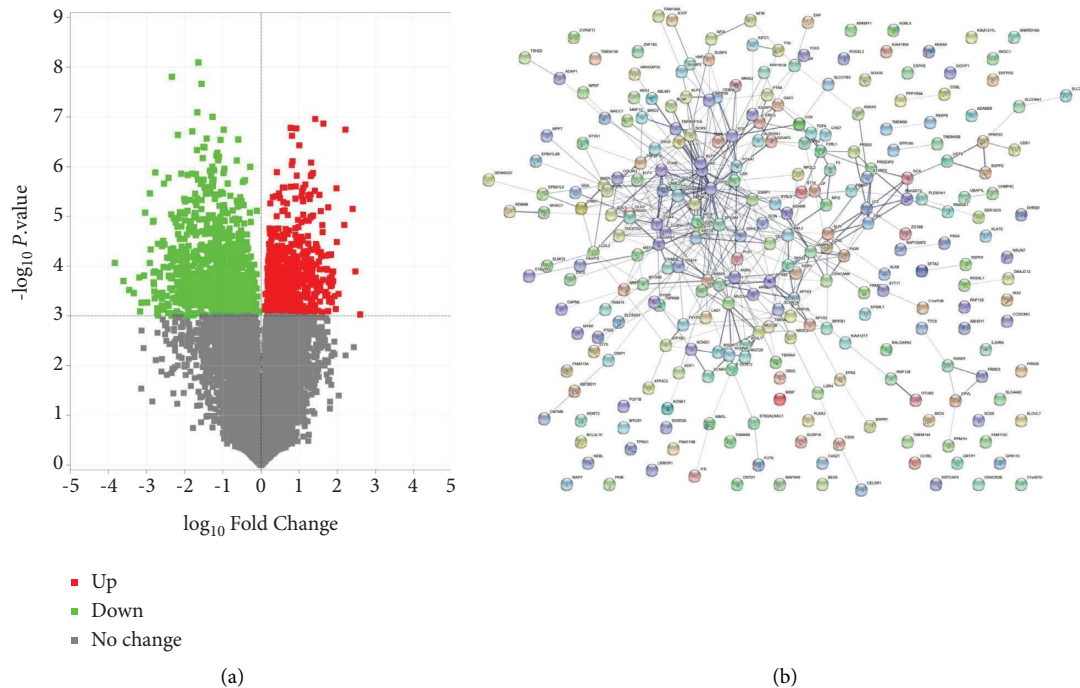
Figure 1: Analysis of DEGs between patients with colon cancer and controls. (a) Volcano plots of the aberrantly expressed genes between CD133-positive colorectal cancer cells and CAF according to GEO dataset GSE34053. Red dots represent upregulated genes defined as lgFC>1.0 and $P < 0.001$. Green dots indicate downregulated genes based on lgFC<-1.0 and $P < 0.001$. Gray dots represent mRNA expression with |lgFC|<1.0 and $P > 0.001$. FC, fold change. (b) Protein-protein interaction network analysis of DEGs.

10 minutes and stained with DAPI for 10 minutes. Five different fields were randomly selected for observation.

2.11. Statistical Analysis. The statistical analysis was performed by using SPSS 18.0 software (SPSS Corporation, Chicago, Illinois, USA). The differences between two groups were determined by paired Student's *t*-test, and one-way analysis of variance (ANOVA) was used to determine differences between multiple groups. $P < 0.05$ indicated statistical significance.

3. Results

3.1. Analysis of DEGs. To determine the DEGs between colon cancer cells and controls, the publicly available microarray dataset GSE34053 was obtained from the GEO database and the Limma package was analyzed. A total of 954 DEGs with the threshold of $P < 0.001$ and |Fold Change| >10 were identified, including 282 upregulated and 672 downregulated DEGs (Figure 1(a)). LINC01207 was identified as one of the upregulated genes. Subsequently, the PPI network was generated by using the STRING database. As shown in Figure 1(b), 271 nodes and 453 interaction pairs were determined (Figure 1(b)).

3.2. Association between High Expression of LINC01207 and Poor Prognosis. The molecular mechanism and prognostic value of LINC01207 in CRC were further investigated. As shown in Figure 2(a), LINC0120 was significantly

upregulated in CRC tumor tissues ($n = 275$) compared with adjacent normal tissues ($n = 349$) based on the publicly available GEPIA dataset. To further evaluate the role of LINC01207 in prognosis, 270 patients with CRC from GEPIA were analyzed. As shown in Figures 2(b) and 2(c), both the overall survival and disease-free survival curve revealed that high LINC01207 expression was associated with an increased risk of mortality in patients with CRC compared to those with low LINC01207 expression. These results indicated that LINC01207 expression may serve as a prognostic biomarker in CRC.

3.3. Biological Processes and Pathway Enrichment Analyses. To evaluate the molecular mechanisms in CRC initiation and progression, the GO and KEGG enrichment analyses for DEGs and LINC01207 coexpressed genes were performed. The results showed that the DEGs were significantly abundant in 193 GO biological processes and 13 KEGG pathways including epithelial cell development, ERBB signaling pathway, epidermal growth factor receptor signaling pathway, epithelial cell morphogenesis, ECM-receptor interaction, Cell adhesion molecules (CAMs), Human papillomavirus infection and Focal adhesion (Figures 3(a) and 3(b)). The coexpressed genes were abundant in 190 biological processes 26 KEGG pathways, such as O-glycan processing, protein O-linked glycosylation and oligosaccharide biosynthetic process, Mucin type O-glycan biosynthesis, Glycosphingolipid biosynthesis, GnRH signaling pathway, Ether lipid metabolism and TNF signaling pathway (Figures 4(a) and 4(b)).

(a)

(b)

(c)
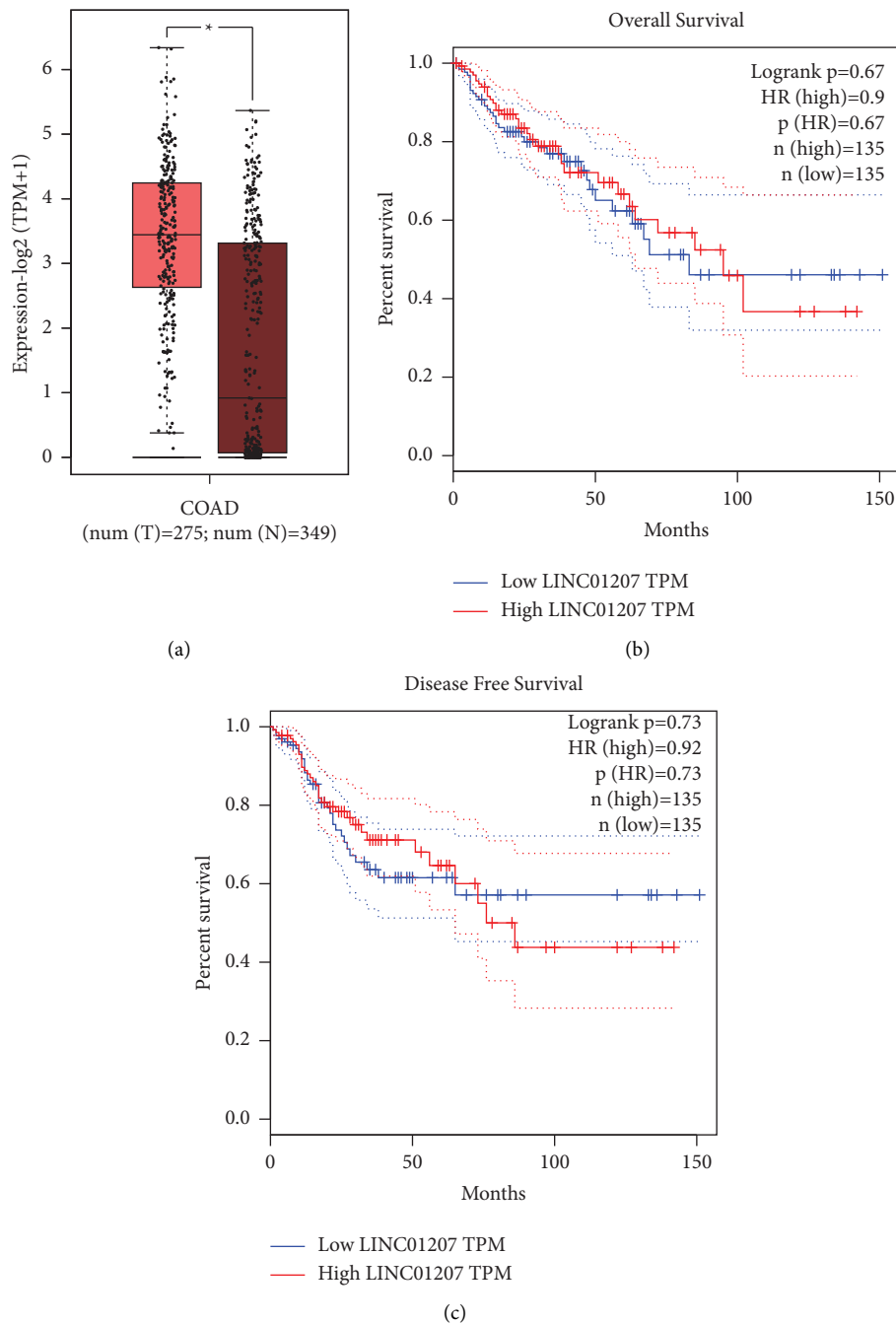
Figure 2: Association between high expression of LINC01207 and poor prognosis. (a) LINC01207 expression was significantly regulated positively in 275 CRC tissues in comparison with 349 normal colon tissues according to the GEPIA dataset. $P < 0.05$. (b) Association between LINC01207 expression level and overall survival of patients with CRC according to the GEPIA dataset. (c) Association between LINC01207 expression level and disease-free survival of patients with CRC based on the GEPIA dataset.

3.4. The LINC01207 Level in CRC Samples and Cell Lines. To explore the role of LINC01207 in CRC occurrence and development, the LINC01207 expression levels in CRC samples and cell lines were determined. As shown in Figure 5(a), the LINC01207 level in tumor tissues ($n = 30$) was significantly higher than that in normal samples ($n = 30$). Furthermore, LINC01207 levels in FHC, HRT-18, HCT-15, SW480, RKO, and HCT-116 cells were determined. The results indicated that LINC01207 was highly

expressed in CRC cell lines (Figure 5(b)). These results suggested that LINC01207 may participate in CRC occurrence and development.

3.5. Silencing LINC01207 Inhibited CRC Cell Proliferation, Migration, and Invasion. To further determine the biological function of LINC01207 in CRC, expression of LINC01207 was inhibited by si-LINC01207 #1 and si-LINC01207 #2 in HCT-116 and RKO cells (Figure 5(c)).

(a)

(b)
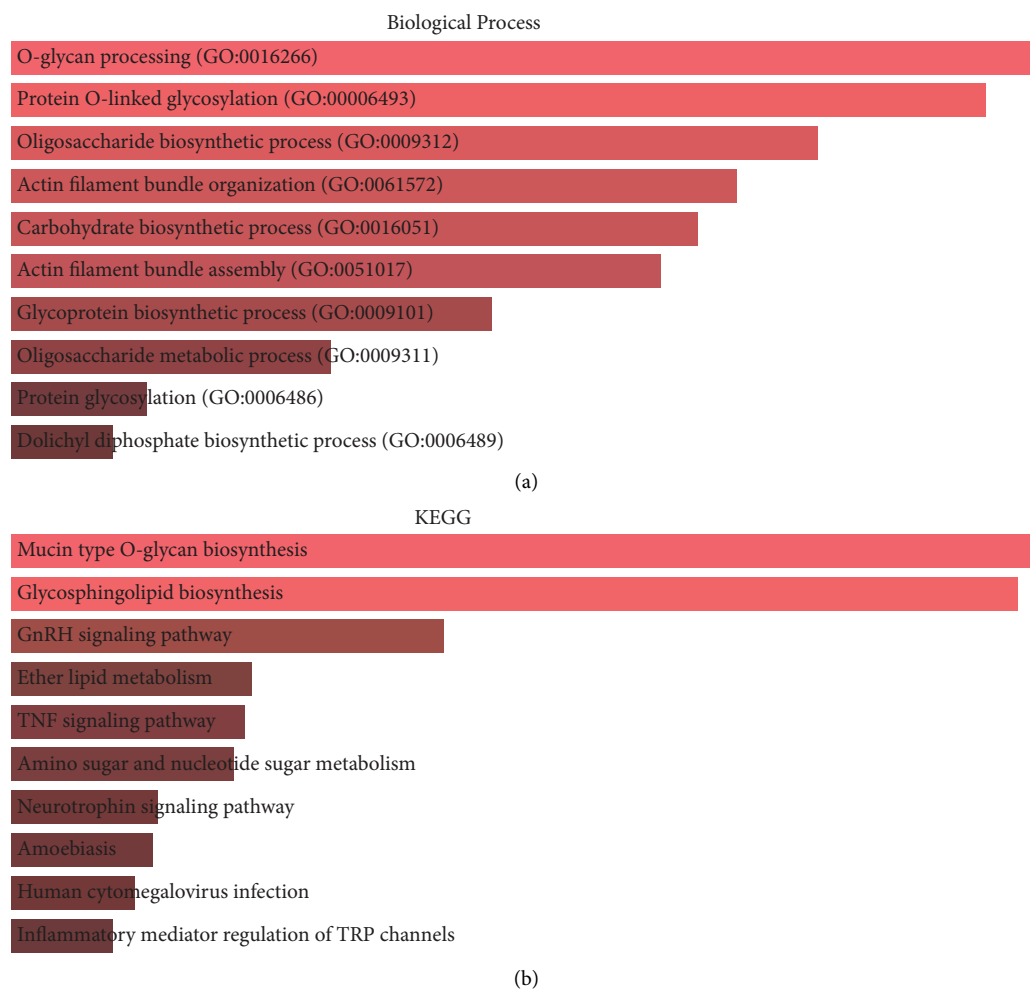
FIGURE 3: Enrichment analysis of differentially expressed genes. (a) Top 10 obviously enriched biological processes by GO analysis. (b) Top 10 enriched pathways by KEGG analysis.

The CCK-8 analysis demonstrated that the knockdown of LINC01207 significantly inhibited cell proliferation of RKO (Figure 5(d)) and HCT-116 cells (Figure 5(e)). Additionally, Transwell migration and invasion assays indicated that LINC01207 knockdown also inhibited CRC cell migration and invasion (Figures 6(a)–6(d)). These results demonstrated LINC01207 was critical for CRC cell progression.

4. Discussion

CRC is a malignant tumor that occurs in the epithelium of the large intestine, most commonly in elderly patients [14]. Therefore, the disease is difficult to diagnose but easy to distant metastasis. The prognosis for patients with recurrent or metastatic disease is not ideal. For advanced colorectal cancer patients with liver or lung metastasis, the five-year survival rate is only about 5%–10% [15]. Therefore, it is very important to explore the molecular biological mechanism of CRC.

Bioinformatics analysis can identify candidate genes and help understand the genetic basis of diseases [16]. In the present study, mRNA expression data of GSE34053 obtained from GEO was analyzed by bioinformatics analysis. A total of 954 DEGs were screened, including 282 upregulated and 672 downregulated genes. Additionally, the PPI network of 282 upregulated DEGs was constructed to determine the close association of these genes in CRC. The LINC01207 was obviously upregulated in CRC and closed related to prognosis as determined by the online database GEPIA. The patients with high LINC01207 expression had shorter survival time. Therefore, LINC01207 has the potential to be a novel and valuable treatment and prognosis target in CRC.

Furthermore, GO and KEGG enrichment analyses both for DEGs and LINC01207 coexpressed genes were performed to evaluate the molecular mechanisms in CRC initiation and progression. The results revealed multiple biological processes and pathways associated with DEGs and LINC01207 coexpressed genes in CRC, such as epidermal growth factor receptor signaling pathway, ECM-receptor interaction, O-glycan processing, and TNF signaling pathway. These pathways were also reported to be critical for various cancers. For example, the ECM-receptor interaction signal pathway possibly participates in breast cancer development through transcriptome profiling [17]. O-glycan truncation in gastric

Biological Process

Bicellular tight junction assembly (GO:0070830)

Epithelial cell development (GO:0002064)

Apical junction assembly (GO:0043297)

Cell-cell junction assembly (GO:0007043)

ERBB signaling pathway (GO:0038127)

Epidermal growth factor receptor signaling pathway (GO:0007173)

Myelination (GO:0042552)

Epithelial cell morphogenesis (GO:0003382)

Digestive tract development (GO:0048565)

Skin development (GO:0043588)

(a)

KEGG

ECM-receptor interaction

Protein digestion and absorption

Tight junction

Cell adhesion molecules (CAMs)

Regulation of actin cytoskeleton

Aldosterone-regulated sodium reabsorption

Arrhythmogenic right ventricular cardiomyopathy (ARVC)

Human papillomavirus infection

Focal adhesion

Salivary secretion

(b)

Figure 4: Enrichment analysis of LINC01207 coexpressed genes. (a) Top 10 obviously enriched biological processes by GO analysis. (b) Top 10 significantly enriched pathways by KEGG analysis.

(a)

(b)

(c)

Figure 5: Continued.

(d)

(e)
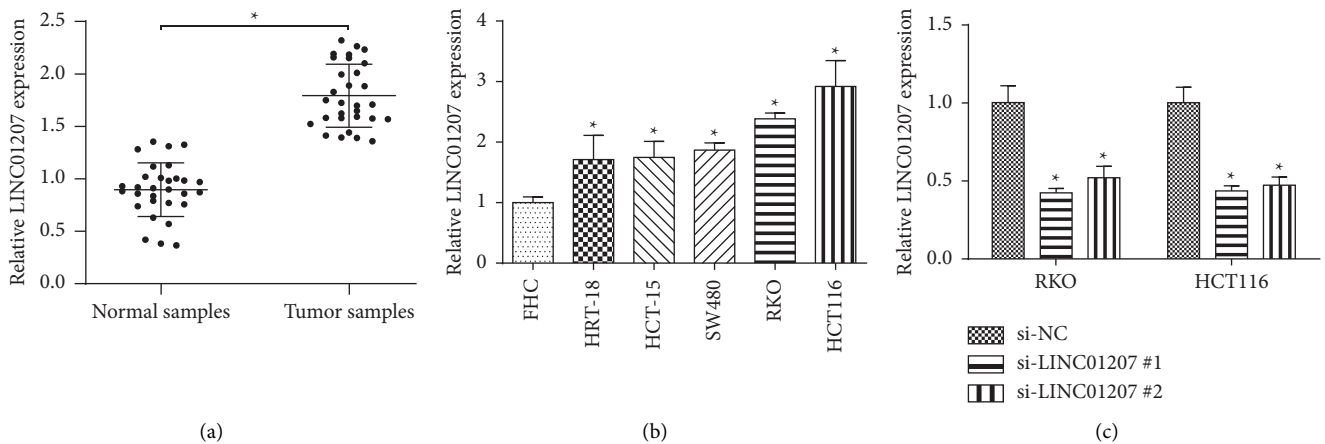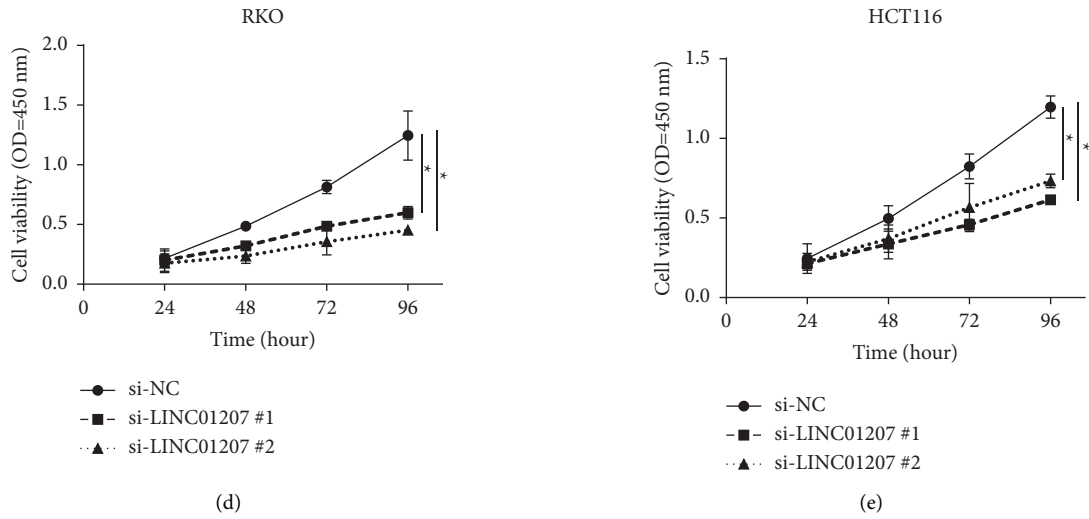
FIGURE 5: Increased expression of LINC01207 in CRC samples and cell lines. (a) Relative LINC01207 expression in CRC tumors and normal tissues. (b) Relative LINC01207 expression in CRC cell lines and normal cells. (c) LINC01207 was knocked down by si-LINC01207 #1 and si-LINC01207 #2 in HCT-116 and RKO cells. (d) The effect of LINC01207 knockdown on cell growth in RKO cells. (e) The effect of LINC01207 knockdown on cell growth in HCT-116 cells, $*P < 0.05$.

(a)

(b)
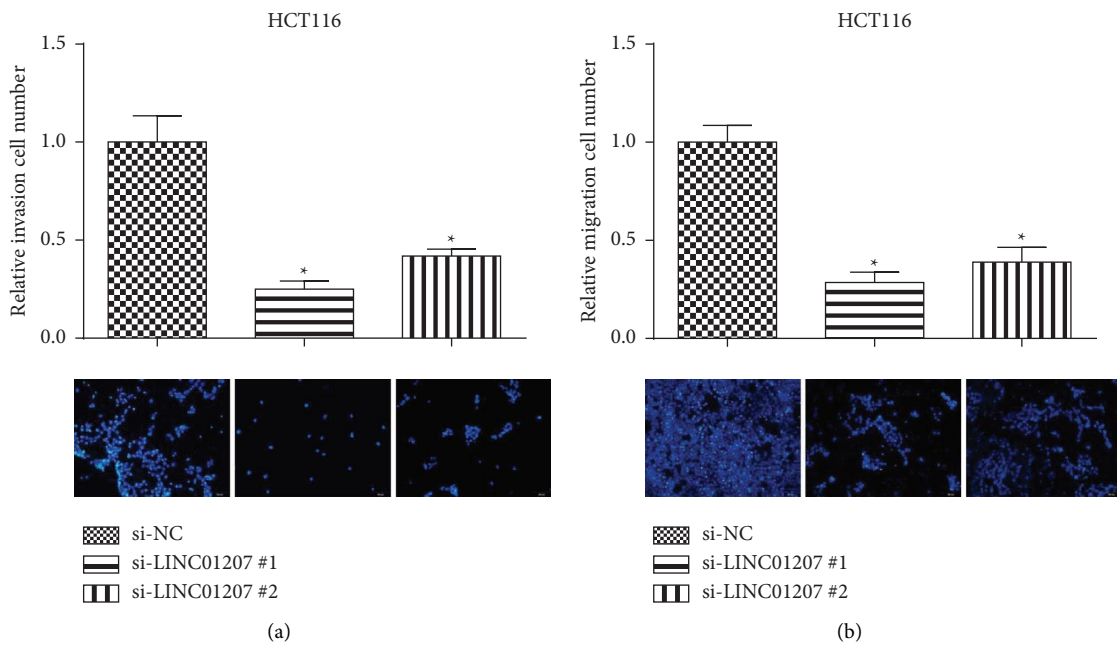
FIGURE 6: Continued.

(c)   (d)
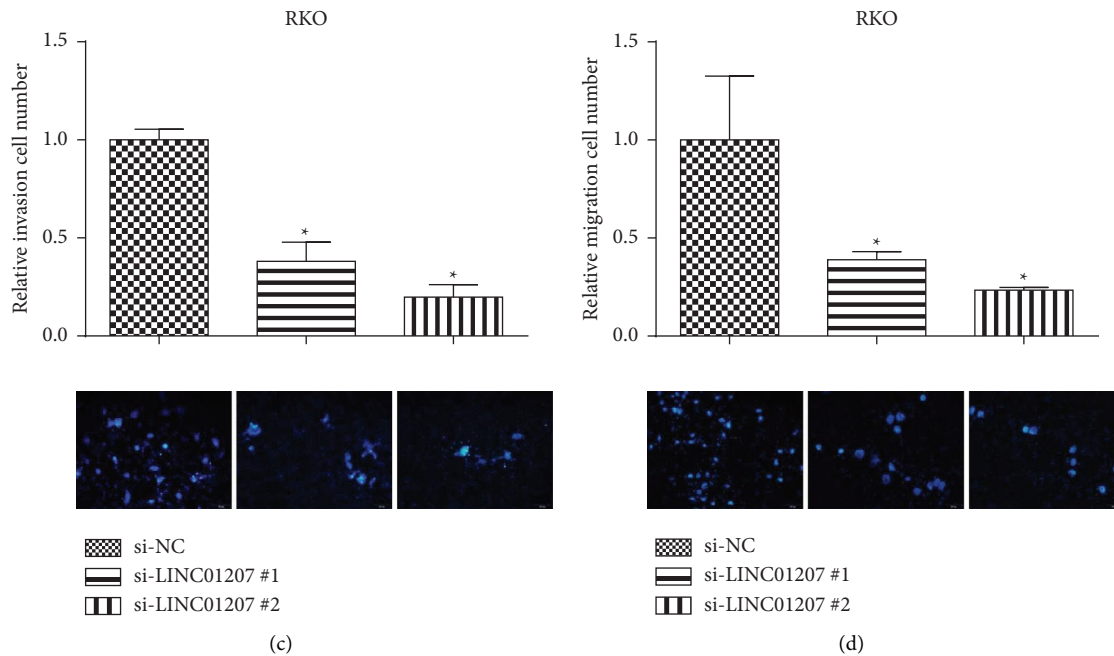
FIGURE 6: Silencing LINC01207 inhibited CRC cell migration and invasion. (a) Relative invasion cell number in HCT-116 cells transfected with si-LINC01207 #1 and si-LINC01207 #2. (b) Relative migration cell number in HCT-116 cells transfected with si-LINC01207 #1 and si-LINC01207 #2. (c) Relative invasion cell number in RKO cells transfected with si-LINC01207 #1 and si-LINC01207 #2. (d) Relative migration cell number in RKO cells transfected with si-LINC01207 #1 and si-LINC01207 #2, $^*P < 0.05$.

cancer can enhance cancer-related functions of CD44 [18]. O-glycan-altered extracellular vesicles can act as a specific serum marker in pancreatic cancer [19, 20].

LINC01207 has been shown to be involved in various signaling pathways to regulate cancer development. In this study, the expression of LINC01207 in CRC clinical tissues and cells was high. CCK-8 and Transwell assays confirmed that LINC01207 could promote CRC cell proliferation, migration, and invasion. In summary, this study improves our understanding of the role of LINC01207 in CRC.

5. Conclusion

In conclusion, the bioinformatic analysis demonstrated that lncRNA LINC01207 may act as an oncogene that is highly expressed in CRC samples and associated with pathways such as ECM-receptor interaction, O-glycan processing, TNF signaling pathway in tumor growth, and metastasis. Moreover, our data demonstrated that LINC01207 can promote CRC cell migration, proliferation, and invasion. These findings suggested that LINC01207 had the potential to be a novel biomarker and target for CRC diagnosis and treatment.

Data Availability

Data are available from the corresponding author upon request.

Conflicts of Interest

All authors declare that they have no conflicts of interest.

Acknowledgments

References

[1] I. Marmol, C. Sanchez-de-Diego, A. Pradilla Dieste, E. Cerrada, and M. J. Rodriguez Yoldi, "Colorectal carcinoma: a general overview and future perspectives in colorectal cancer," *International Journal of Molecular Sciences*, vol. 18, no. 1, p. 197, 2017.

[2] M. Zorzi, J. Battagello, A. R. Fiore, L. Memo, C. Senore, and M. Rugge, "Colorectal cancer incidence and mortality after negative fecal immunochemical tests by age 70: a prospective observational study," *International Journal of Cancer*, vol. 149, no. 6, pp. 1257–1265, 2021.

[3] W. F. Yu, J. Wang, C. Li, M. Xuan, and Z. Zhao, "miR-17-5p Promotes the Invasion and Migration of Colorectal Cancer by Regulating HSPB2," *Journal of Cancer*, vol. 13, no. 3, pp. 918–931, 2020.

[4] D. Kerr, "Clinical development of gene therapy for colorectal cancer," *Nature Reviews Cancer*, vol. 3, no. 8, pp. 615–622, 2003.

[5] K. Hase, C. Shatney, D. Johnson, M. Trollope, and M. Vierra, "Prognostic value of tumor "budding" in patients with colorectal cancer," *Diseases of the Colon & Rectum*, vol. 36, no. 7, pp. 627–635, 1993.

[6] J. J. Quinn and H. Y. Chang, "Unique features of long noncoding RNA biogenesis and function," *Nature Reviews Genetics*, vol. 17, no. 1, pp. 47–62, 2016.

[7] G. Yang, X. Lu, and L. Yuan, "LncRNA: a link between RNA and cancer," *Biochimica et Biophysica Acta (BBA) - Gene*

Regulatory Mechanisms, vol. 1839, no. 11, pp. 1097–1109, 2014.

[8] S. Dhamija and S. Diederichs, "From junk to master regulators of invasion: lncRNA functions in migration, EMT and metastasis," *International Journal of Cancer*, vol. 139, no. 2, pp. 269–280, 2016.

[9] C. Liu, J. O. Wang, W. Y. Zhou et al., "Long non-coding RNA LINC01207 silencing suppresses AGR2 expression to facilitate autophagy and apoptosis of pancreatic cancer cells by sponging miR-143-5p," *Molecular and Cellular Endocrinology*, vol. 493, Article ID 110424, 2019.

[10] G. Wang, H. Chen, and J. Liu, "The long noncoding RNA LINC01207 promotes proliferation of lung adenocarcinoma," *American Journal of Cancer Research*, vol. 5, no. 10, pp. 3162–3173, 2015.

[11] D. Chi, W. Zhang, Y. Jia, D. Cong, K. Yu, and S. Hu, "LINC01207 predicts poor prognosis and suppresses cell growth and metastasis via regulating GSK-3β/β-catenin signaling pathway in malignant glioma," *Medical Science Monitor: International Medical Journal of Experimental and Clinical Research*, vol. 26, Article ID e923189, 2020.

[12] K. Tomczak, P. Czerwinska, and M. Wiznerowicz, "Review the cancer Genome Atlas (TCGA): an immeasurable source of knowledge," *Współczesna Onkologia*, vol. 19, no. 1A, pp. A68–A77, 2015.

[13] E. Clough and T. Barrett, "The gene expression Omnibus database," *Methods in Molecular Biology*, vol. 1418, pp. 93–110, 2016.

[14] T. A. Ullman and S. H. Itzkowitz, "Intestinal inflammation and cancer," *Gastroenterology*, vol. 140, no. 6, pp. 1807–1816.e1, 2011.

[15] T. Goya, N. Miyazawa, H. Kondo, R. Tsuchiya, T. Naruke, and K. Suemasu, "Surgical resection of pulmonary metastases from colorectal cancer. 10-year follow-up," *Cancer*, vol. 64, no. 7, pp. 1418–1421, 1989.

[16] D. Benton, "Bioinformatics--principles and potential of a new multidisciplinary tool," *Trends in Biotechnology*, vol. 14, no. 8, pp. 261–272, 1996.

[17] Y. Bao, L. Wang, L. Shi et al., "Transcriptome profiling revealed multiple genes and ECM-receptor interaction pathways that may be associated with breast cancer," *Cellular and Molecular Biology Letters*, vol. 24, no. 1, p. 38, 2019.

[18] S. Mereiter, A. M. Martins, C. Gomes et al., "O-glycan truncation enhances cancer-related functions of CD44 in gastric cancer," *FEBS Letters*, vol. 593, no. 13, pp. 1675–1689, 2019.

[19] T. Yokose, Y. Kabe, A. Matsuda et al., "O-Glycan-Altered extracellular vesicles: a specific serum marker elevated in pancreatic cancer," *Cancers*, vol. 12, no. 9, p. 2469, 2020.

[20] Z. Li, G. Wu, J. Li, Y. Wang, X. Ju, and W. Jiang, "lncRNA CRNDE promotes the proliferation and metastasis by acting as sponge miR-539-5p to regulate POU2F1 expression in HCC," *BMC Cancer*, vol. 20, no. 1, p. 282, 2020.

Research Article

Construction of a Novel Diagnostic Model Based on Ferroptosis-Related Genes for Hepatocellular Carcinoma Using Machine and Deep Learning Methods

Shiming Yi,[1] Chunlei Zhang,[2] Ming Li,[3] and Jiafeng Wang [4]

[1]*Department of Hepatobiliary Surgery, Yantai Affiliated Hospital of Binzhou Medical University, Yantai, China*
[2]*Department of Anus and Colorectal Surgery, Yantai Affiliated Hospital of Binzhou Medical University, Yantai, China*
[3]*Department of Gastroenterology, Yantai Affiliated Hospital of Binzhou Medical University, Yantai, China*
[4]*Department of Hepatobiliary Surgery, The Affiliated Taian City Central Hospital of Qingdao University, Taian, China*

Correspondence should be addressed to Jiafeng Wang; doctorwangjf@126.com

Hepatocellular carcinoma (HCC) is one of the most general malignant tumors. Ferroptosis, a type of necrotic cell death that is oxidative and iron-dependent, has a strong correlation with the development of tumors and the progression of cancer. The present study was designed to identify potential diagnostic Ferroptosis-related genes (FRGs) using machine learning. From GEO datasets, two publicly available gene expression profiles (GSE65372 and GSE84402) from HCC and nontumor tissues were retrieved. The GSE65372 database was used to screen for FRGs with differential expression between HCC cases and nontumor specimens. Following this, a pathway enrichment analysis of FRGs was carried out. In order to locate potential biomarkers, an analysis using the support vector machine recursive feature elimination (SVM-RFE) model and the LASSO regression model were carried out. The levels of the novel biomarkers were validated further using data from the GSE84402 dataset and the TCGA datasets. In this study, 40 of 237 FRGs exhibited a dysregulated level between HCC specimens and nontumor specimens from GSE65372, including 27 increased and 13 decreased genes. The results of KEGG assays indicated that the 40 differential expressed FRGs were mainly enriched in the longevity regulating pathway, AMPK signaling pathway, the mTOR signaling pathway, and hepatocellular carcinoma. Subsequently, HSPB1, CDKN2A, LPIN1, MTDH, DCAF7, TRIM26, PIR, BCAT2, EZH2, and ADAMTS13 were identified as potential diagnostic biomarkers. ROC assays confirmed the diagnostic value of the new model. The expression of some FRGs among 11 FRGs was further confirmed by the GSE84402 dataset and TCGA datasets. Overall, our findings provided a novel diagnostic model using FRGs. Prior to its application in a clinical context, there is a need for additional research to evaluate the diagnostic value for HCC.

1. Introduction

According to the findings of the Global Cancer Statistics 2018, there were around 841,000 newly diagnosed cases of liver cancer and 782,000 deaths caused by liver cancer around the world, with China alone accounting for about 50% of the total number of cases and deaths [1–3]. It is estimated that between 75 and 80 percent of all occurrences of liver cancer are caused by hepatocellular carcinoma (HCC), which is an aggressive kind of malignant tumor that is typically discovered at a later stage when treatment is no longer effective [4, 5]. Although there have been significant progresses and advancements in the treatment of HCC in recent years, in terms of surgical procedures, chemotherapeutic medications, and targeted drugs, HCC continues to have a very high incidence and mortality rate, which poses a serious threat to human health [6, 7]. The most popular blood biomarker for HCC, alpha-fetoprotein (AFP), demonstrates subpar performance as a serological test in HCC surveillance due to its low sensitivity being only 10%–20% in early-stage HCC and its labile levels during hepatitis flares [8, 9]. It is due to the fact that AFP levels fluctuate during

hepatitis flares. Therefore, patients diagnosed with HCC at an early stage who have a high chance of experiencing recurrence need to be identified as quickly as possible so that tailored therapeutic options can be optimized and patient survival can be improved.

In recent years, the technology of microarrays has been employed in conjunction with integrated bioinformatics analysis in order to locate novel genes that have been linked to a range of diseases [10, 11]. These genes have the potential to function as diagnostic and prognostic biological markers. For instance, Lan et al. reported that the expressions of KIAA1429 were distinctly increased in HCC specimens. In individuals with HCC, having a high expression of KIAA1429 was related with having a bad prognosis. The knockdown of KIAA1429 resulted in a reduction in cell proliferation and metastasis both in vitro and in vivo. This was accomplished through a post-transcriptional alteration of GATA3 that was dependent on N6-methyladenosine [12]. Zhang et al. showed that DDX39 expression was positively connected with advanced clinical stages, and survival assays confirmed that patients with high-DDX39 levels exhibited a poor outcome. DDX39 was increased in HCC tissues and cells. According to the findings of a functional analysis, increased levels of DDX39 in HCC cells facilitated motility, migration, growth, and invasion via regulating the Wnt/-catenin pathway [13]. In addition, several genes in the blood of HCC patients were also reported to show important diagnostic values, such as serum IL27, HMMR, NXPH4, PITX1, and THBS4 [14, 15].

Ferroptosis is a sort of regulated cell death (RCD) that is triggered by the accumulation of harmful lipid peroxidation and is dependent on the presence of iron [16]. In recent years, the induction of ferroptosis has emerged as a promising therapeutic alternative to suppress tumor proliferation and growth, especially for advanced tumors that are resistant to surgical treatment, radiotherapy, and chemotherapy [17, 18]. It has been shown that ferroptosis plays an important role in the regulation of metabolism and redox biology, which has implications for the development of cancer and its treatment, including HCC [19–21]. Shan et al. showed that UBA1 contributed to the progression of HCC by elevating the activity of the Nrf2 signaling pathway and lowering the concentration of ferric ions, which triggered ferroptosis-inhibiting bioactivities [22]. In addition, several studies have reported the prognostic value of many ferroptosis-related genes (FRGs). However, the diagnostic model based on ferroptosis-related genes has not been investigated. In this study, we aimed to develop a diagnostic model based on ferroptosis-related genes using machine and deep learning methods.

2. Materials and Methods

2.1. Microarray Data Source.
The GEO database was searched using the following keywords in order to retrieve the mRNA expression datasets of HCC: "hepatocellular carcinoma," "homo sapiens" (porgn: txid9606)," and "expression profiling by array." Following an in-depth analysis, two GSE profiles (GSE65372 and GSE84402) were chosen,

and their respective downloads were initiated. GSE65372 and GSE84402 were based on GPL14951 and GPL570, respectively. The array data for GSE65372 were composed of 39 HCC specimens and 15 nontumor specimens, respectively. For GSE84402, the array data also included 14 HCC specimens and 14 nontumor specimens. All data were freely accessible, and the present study did not involve any human or animal experimentation.

2.2. Differential Expression Analysis.
We began by retrieving the expression data of 237 FRGs from the GSE65372 database. Within this dataset, only 237 FRGs were found to be expressed. These data were then applied to normal samples and HCC samples. Following that, the Student's t-test was carried out in R in order to identify the FRGs that exhibited different levels of expression in the two distinct samples. Genes that had a p value of less than 0.001 were determined to be significant.

2.3. Pathway Analysis.
The "clusterProfiler," "enrichplot," and "ggplot2" programs were used to conduct GO and KEGG pathway enrichment analyses in order to determine the biological characteristics of differently expressed genes (DEGs) linked to ferroptosis. These analyses were carried out in order to identify the biological features of DEGs. Enrichment results with an FDR (false discovery rate) of <0.05 were recognized as significant functional categories.

2.4. Candidate Diagnostic Biomarker Screening.
Two different machine learning methods were employed to make predictions about the disease's progression in order to find meaningful prognostic variables. The least absolute shrinkage and selection operator (LASSO) is an approach for regression analysis that makes use of regularization in order to increase the accuracy of prediction. In order to determine the genes that are significantly connected with the differentiation of HCC samples from normal samples, the LASSO regression algorithm was implemented in R and carried out with the "glmnet" package. Support vector machine (SVM) is a popular type of supervised machine learning approach that may be used for both classification and regression. As a result, support vector machine recursive feature elimination (SVM-RFE) was utilized in order to choose the pertinent characteristics in order to find the group of genes that had the capacity to differentiate across groups the most effectively.

2.5. Diagnostic Value of Feature Biomarkers in HCC.
An ROC curve was constructed by using the mRNA expression data of 39 HCC samples and 15 nontumor samples. It was done so that the predictive value of the selected biomarkers could be evaluated. The value of the area under the ROC curve was used to measure the diagnostic efficiency in distinguishing HCC samples from nontumor specimens, which was further confirmed using the GSE65372 dataset. Assessing AUC, sensitivity, and specificity were all parts of the process that were used to evaluate the diagnostic

(a)

(b)
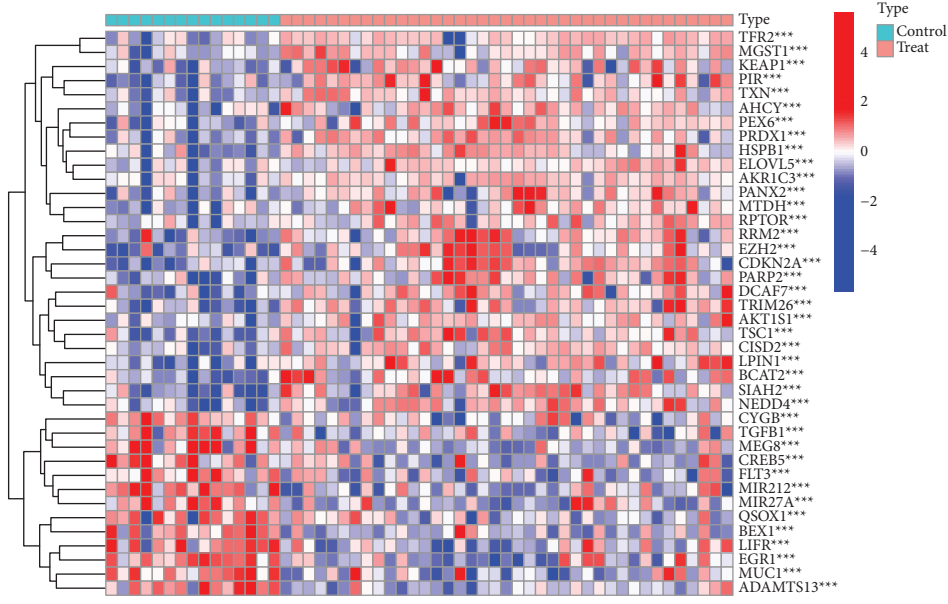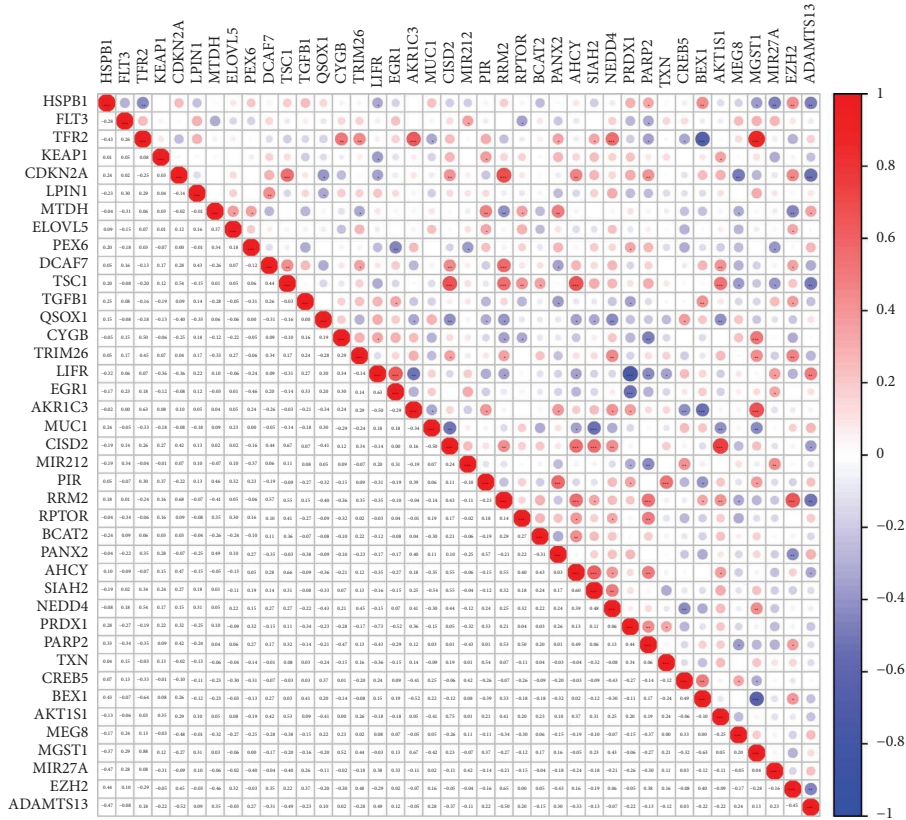
Figure 1: Identification of differential expressed FRGs in HCC. (a) The expressing pattern of 44 differential expressed FRGs was shown in heatmap. (b) The correlation of these genes.

(a)

(b)

(c)
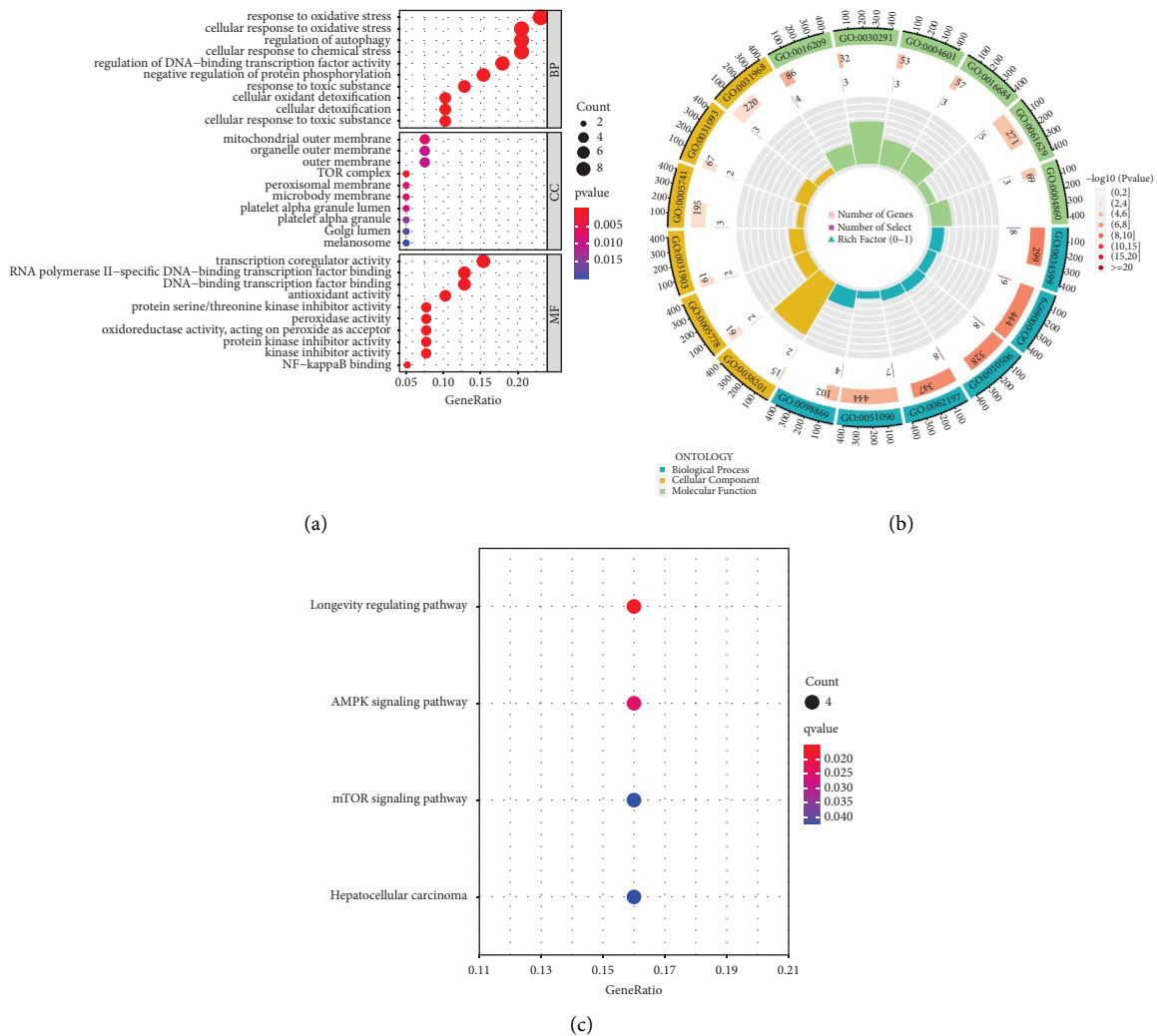
Figure 2: Functional analysis based on 44 differential expressed FRGs. (a and b) Significantly enriched GO terms of DEGs in HCC. (c) Significant KEGG pathway terms of DEGs in HCC.

potential of the best gene biomarkers. In addition, the predict function included within the "glm" package of the R programming language was utilized to build a logistic regression model that was based on 11 novel genes. Our model was then used to make predictions regarding the sample types found within the GSE65372 dataset. In a similar manner, ROC curves were utilized in order to assess the diagnostic capability of the logistic regression model. In addition to this, the expressions of the essential genes were verified even further using the GSE84402 and TCGA datasets.

2.6. Statistical Analysis. All statistical analyses were conducted using R (version 3.6.3). $p < 0.05$ was considered as statistically significant.

3. Results

3.1. Identification of Differential Expressed FRGs in the GSE65372 Datasets. 40 of the 237 FRGs exhibited

a dysregulated level between HCC specimens and nontumor specimens, including 27 increased and 13 decreased genes, which were identified from the GSE65372 dataset. The clustering heatmap displayed the expression pattern of FRGs that were differentially expressed between the samples (Figure 1(a)). Figure 1(b) illustrates the correlation between these genes.

3.2. Functional Analyses for the Differential Expressed FRGs. To explore the functional effects of differential expressed FRGs, we performed GO and KEGG assays. As shown in Figures 2(a) and 2(b), we found that the 40 differential expressed FRGs were mainly associated with responses to oxidative stress, cellular response to oxidative stress, regulation of autophagy, cellular response to chemical stress, mitochondrial outer membrane, organelle outer membrane, outer membrane, TOR complex, transcription coregulator activity, DNA-binding transcription factor bindin, and antioxidant activity. The results of KEGG assays indicated that the 40 differential expressed FRGs were mainly enriched

in the longevity regulating pathway, AMPK signaling pathway, the mTOR signaling pathway, and hepatocellular carcinoma (Figure 2(c)).

3.3. Differential Expressed FRGs Were Identified as Diagnostic Genes for HCC.

Estimating the diagnostic capability of differentially expressed FRGs was our goal in order to take into account the differences that exist between patients with HCC and healthy individuals. Subsequently, we carried out two separate machine learning algorithms in the GSE65372 datasets for the identification of the distinct differentially expressed FRGs in order to differentiate HCC from normal specimens. These algorithms were used to identify the FRGs that was significantly different between the two groups. In order to choose HCC-related features, the LASSO logistic regression algorithm was utilized, and the penalty parameter tuning process was carried out using 10-foldcross-validation (Figures 3(a) and 3(b)). After that, we sorted through the 17 differentially expressed FRGs using the SVM-RFE algorithm in order to locate the best possible combination of feature genes. In the end, seven genes were selected as the best candidates for feature genes (Figures 3(c) and 3(d)). Following the intersection of the marker genes generated from the LASSO and SVM-RFE models, 11 new markers (HSPB1, CDKN2A, LPIN1, MTDH, DCAF7, TRIM26, PIR, BCAT2, EZH2, and ADAMTS13) were identified for further investigation (Figure 3(e)).

3.4. The Identification of the Diagnostic Value of the New Model for HCC.

With the use of the glm R package, we developed a logistic regression model. Subsequent ROC curves demonstrated that the 11 marker gene-based logistic regression model correctly differentiated normal samples from HCC samples with an area under the curve (AUC) value of 1.000. This model was based on the 11 marker genes mentioned earlier (Figure 4(a)). In addition, ROC curves were constructed for each of the 11 marker genes in order to provide light on the ability of individual genes to differentiate normal samples from those containing HCC. AUC was higher than 0.7 for every gene, as shown in Figure 4(b). Based on the information shown above, it appears that the logistic regression model provides a higher level of accuracy and specificity when compared to the individual marker genes when it comes to discriminating HCC samples from normal samples.

3.5. Expressions of Novel Diagnostic Genes in the GSE84402 and TCGA Datasets.

In the final step of this process, we checked the expression of marker genes using the GSE84402 dataset. We found that the GSE20680 dataset was consistent with the patterns of expression for ADAMTS13, DCAF7, EZH2, HSPB1, and CDKN2A (Figure 5). Among them, the expressions of DCAF7, EZH2, HSPB1, and CDKN2A in HCC specimens were distinctly increased compared with normal specimens, while the expressions of ADAMTS13 were distinctly decreased in HCC samples. In addition, in TCGA datasets, we found that the expression of 10 genes showed a dysregulated level in HCC (Figure 6).

4. Discussion

HCC is the most prevalent primary malignancy of the liver, accounting for about 90% of all malignant cases. It is also the most curable form of primary liver cancer [23, 24]. The fact that the formation of HCC is a multistep process, as well as a multigene alteration-induced malignancy with a high level of heterogeneity, has been established via extensive research and documentation [25, 26]. It has been determined that hepatitis B, hepatitis C, alcoholism, steatohepatitis, and obesity are all etiologic factors that contribute to the disease [27, 28]. Recent studies at the molecular levels have indicated that specific gene mutations play an important part in the progression of HCC. By controlling iron metabolism, amino acid and glutathione metabolism, and reactive oxygen species (ROS) metabolism, ferroptosis has shown promising results in inducing cancer cell death in recent years, especially in the elimination of aggressive malignancies that are resistant to conventional therapies [29, 30]. Therefore, ferroptosis can be a potential and powerful target for cancer therapy. However, the relationship between ferroptosis-related genes and HCC progression is still vastly unknown, making it a challenge to develop ferroptosis therapy for HCC.

Thanks to the development of high-throughput technologies, gene microarray analysis has emerged as a powerful tool for detecting DEGs and, by extension, putative biomarkers in a wide range of disorders. Gene microarray analysis has been used in a number of studies to discover crucial genes in the etiology of HCC. There is hope that integrated multiple gene microarray analysis will help find more reliable gene biomarkers. Machine learning algorithms have been shown to offer great potential for screening sensitive diagnostic biomarkers in a variety of diseases, and this research has only increased in the last few years [31, 32]. In this study, we screened differential expressed FRGs, and 40 of 237 FRGs exhibited a dysregulated level between HCC specimens and nontumor samples, including 27 increased and 13 decreased genes. By eliminating cells from the environment that lack vital nutrients, ferroptosis has been shown to play a crucial role in suppressing carcinogenesis, as demonstrated by recent scientific studies. Functional studies of FRGs as tumor promoters or inhibitors have increased in the field of HCC. The results of KEGG indicated that the 40 differential expressed FRGs were manly enriched in the longevity regulating pathway, AMPK signaling pathway, the mTOR signaling pathway, and hepatocellular carcinoma, highlighting their roles in HCC progression. Our finding suggested the 44 differential expressed FRGs may play an important role in the progression of HCC.

Based on the 40 differential expressed FRGs, we carried out LASSO and SVM and confirmed 11 novel marker genes (HSPB1, CDKN2A, LPIN1, MTDH, DCAF7, TRIM26, PIR, BCAT2, EZH2, and ADAMTS13). The AUC for all 11 genes

(a)

(b)

(c)

(d)

(e)
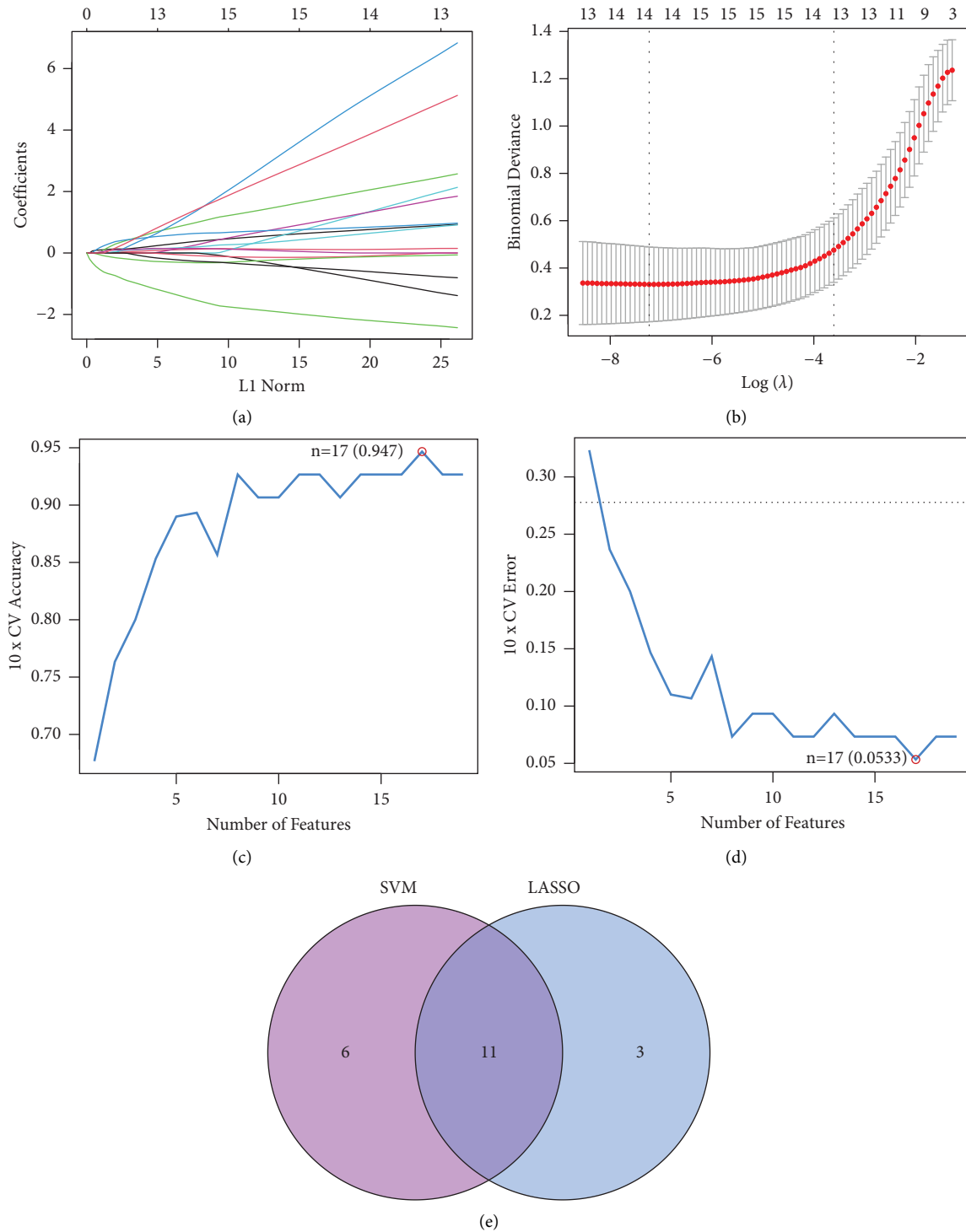
FIGURE 3: Screening processes of diagnostic biomarker candidates for HCC. (a and b) Tuning feature selection in the LASSO. (c and d) SVM-RFE algorithm was applied to screen the 17 differential expressed FRGs. (e) Venn diagram demonstrating 11 critical genes(HSPB1, CDKN2A, LPIN1, MTDH, DCAF7, TRIM26, PIR, BCAT2, EZH2, and ADAMTS13) shared by LASSO and SVM-RFE algorithms.

are more than 0.75, indicating that they can reliably and accurately separate HCC specimens from nontumor specimens. Among the 11 genes, some genes have been functionally studied in HCC. For instance, He et al. reported that the expressions of MTDH were found to be distinctly elevated in HCC specimens. In HCC patients, the expressions

of MTDH were predictive of a short overall survival without any heterogeneity. In addition, high-grade histological differentiation, nonvascular invasion, and HCC metastases were all found to be linked with MTDH expression. The results of in vitro investigations showed that MTDH has the ability to limit cell growth in all four HCC cell lines, in

(a)

(b)
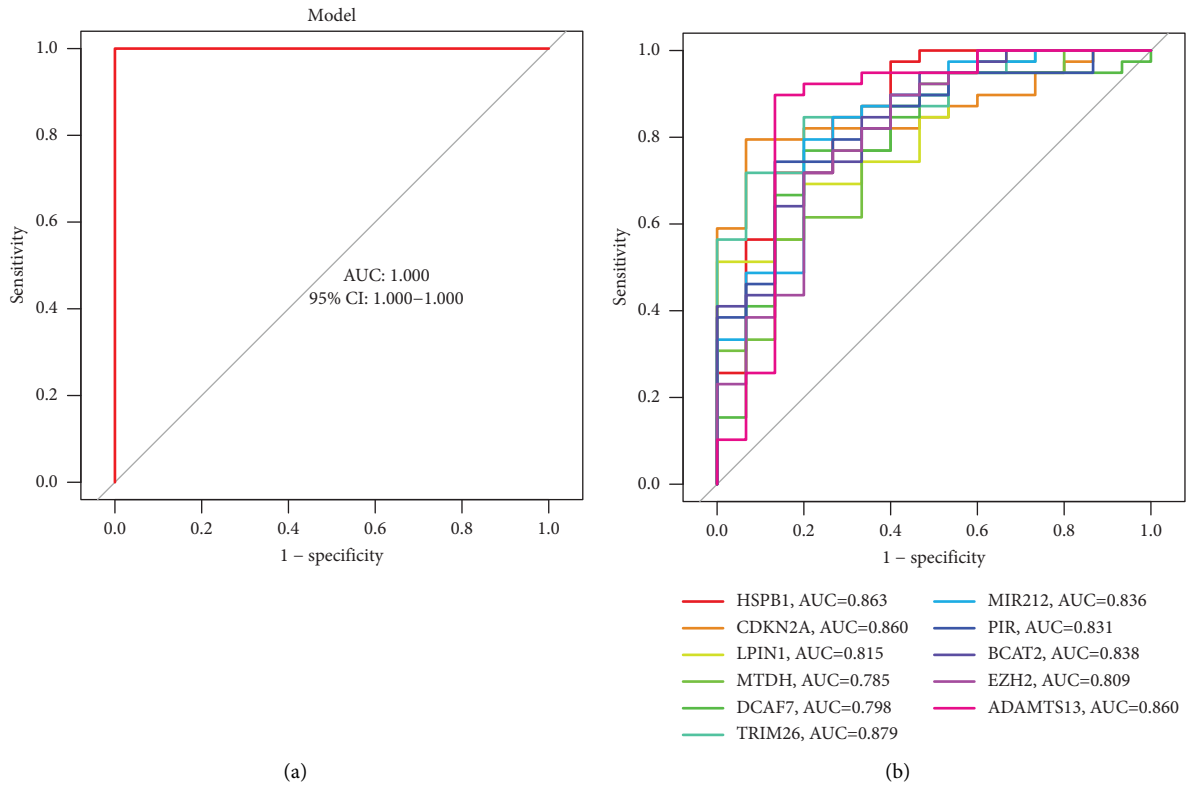
FIGURE 4: The diagnostic value of new mode for HCC patients. (a) Logistic regression model to identify the AUC of all samples. (b) ROC curves for the 11 marker genes.
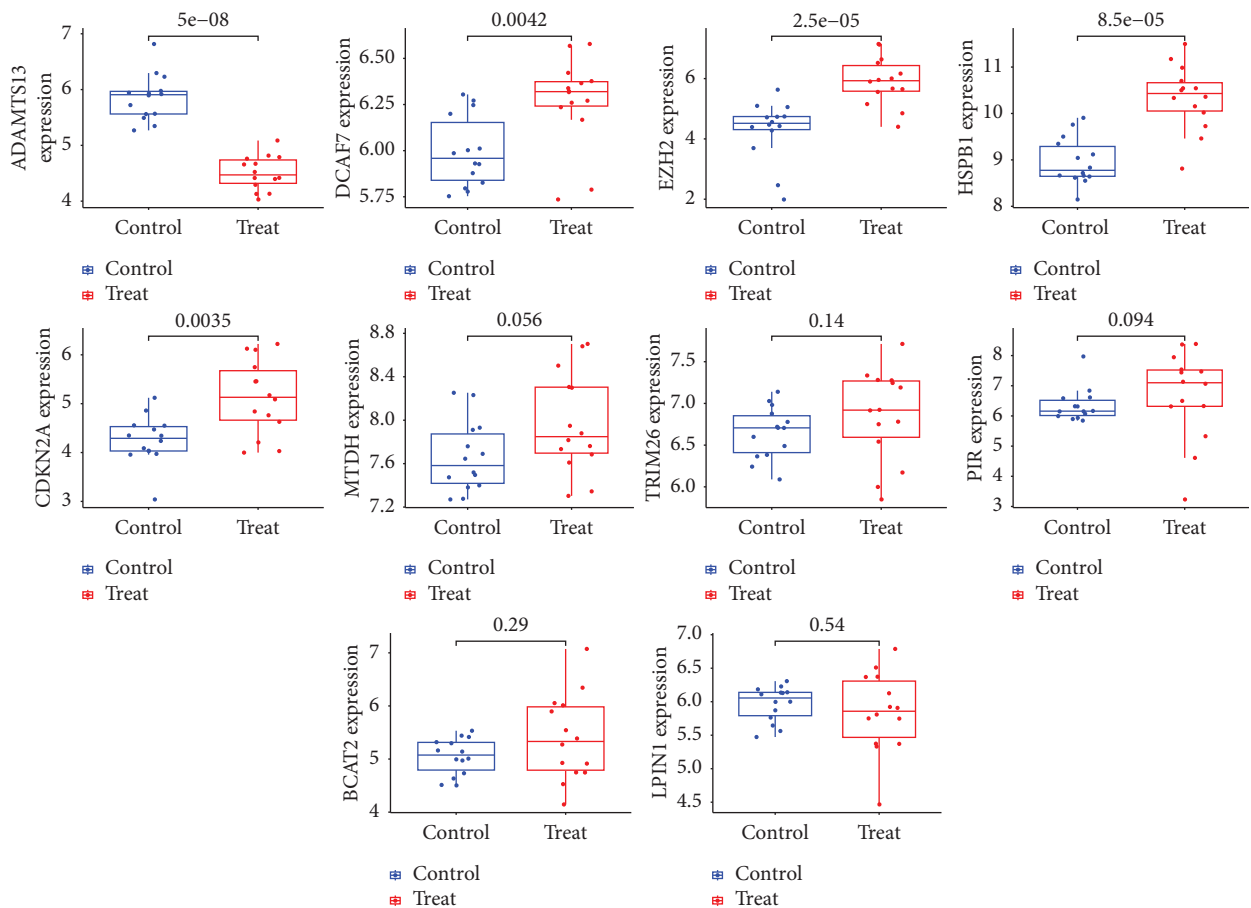
FIGURE 5: The expressions of the diagnostic genes in GSE84402 dataset.
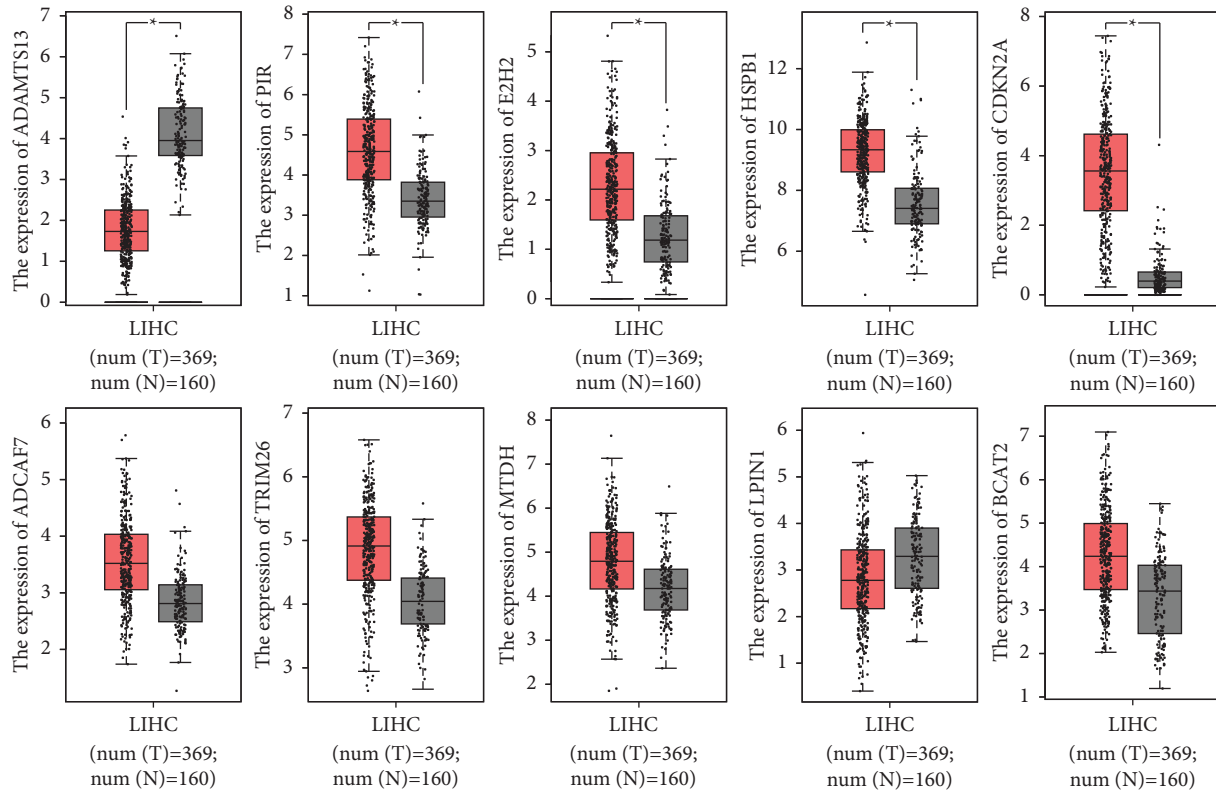
FIGURE 6: The expressions of the diagnostic genes in TCGA dataset.

addition to activating caspase-3/7 activity and death [33]. Wang et al. showed that, when compared with normal liver tissue, the level of TRIM26 expression was much lower in HCC tissue; this was found to be associated with an advanced T stage and a bad prognosis. In vitro studies with HCC cells showed that inhibiting TRIM26 led to increased cancer cell proliferation and metastasis [34]. These findings were consistent with our findings. Our ROC curves showed that the logistic regression model based on these 11 marker genes successfully distinguished between normal and HCC samples (AUC = 1.000) using the R package glm. Our findings suggested the novel diagnostic model based on 11 marker genes had great clinical reference values. Finally, we demonstrated the expression of 11 marker genes in other GSE84402 and TCGA datasets. The expression of several genes was on track. However, more samples were needed to further confirm our findings.

Several limitations could also be found in our study. First, the sample size was low; despite the fact that our findings were constructed using and validated using two separate datasets. Validation of this model in larger prospective clinical studies is required in the future. Second, to further understand the molecular functions of the 11 critical genes, additional biological research is required.

5. Conclusion

We developed a novel diagnostic model based on 11 FRGs for HCC. These efforts may also serve to further promote patient compliance, assist healthcare providers in better managing patients, and eventually improve their overall health status and quality of life.

Data Availability

The data used to support this study are available from the corresponding author upon request.

Conflicts of Interest

The authors declare that they have no conflicts of interest.

Authors' Contributions

Shiming Yi and Jiafeng Wang designed the study and supervised the data collection. Shiming Yi and Chunlei Zhang analyzed the data and interpreted the data. Chunlei Zhang and Ming Li prepared the manuscript for publication and reviewed the draft of the manuscript. All authors have read and approved the manuscript.

References

[1] H. Sung, J. Ferlay, R. L. Siegel et al., "Global cancer Statistics 2020: GLOBOCAN estimates of incidence and mortality worldwide for 36 cancers in 185 countries," *CA: A Cancer Journal for Clinicians*, vol. 71, no. 3, pp. 209–249, 2021.

[2] R. M. Feng, Y. N. Zong, S. M. Cao, and R. H. Xu, "Current cancer situation in China: good or bad news from the 2018 Global Cancer Statistics?" *Cancer Communications*, vol. 39, no. 1, p. 22, 2019.

[3] A. Villanueva and H. Carcinoma, "Hepatocellular carcinoma," *New England Journal of Medicine*, vol. 380, no. 15, pp. 1450–1462, 2019.

[4] J. Hartke, M. Johnson, and M. Ghabril, "The diagnosis and treatment of hepatocellular carcinoma," *Seminars in Diagnostic Pathology*, vol. 34, no. 2, pp. 153–159, 2017.

[5] I. E. Dika and G. K. Abou-Alfa, "Treatment options after sorafenib failure in patients with hepatocellular carcinoma," *Clinical and Molecular Hepatology*, vol. 23, no. 4, pp. 273–279, 2017.

[6] E. Juárez-Hernández, D. Motola-Kuba, N. C. Chávez-Tapia, M. Uribe, and V. Barbero Becerra, "Biomarkers in hepatocellular carcinoma: an overview," *Expert Review of Gastroenterology & Hepatology*, vol. 11, no. 6, pp. 549–558, 2017.

[7] A. Schlachterman, W. W. Craft, E. Hilgenfeldt, A. Mitra, and R. Cabrera, "Current and future treatments for hepatocellular carcinoma," *World Journal of Gastroenterology*, vol. 21, no. 28, pp. 8478–8491, 2015.

[8] R. Lencioni, "Loco-regional treatment of hepatocellular carcinoma in the era of molecular targeted therapies," *Oncology*, vol. 78, no. 1, pp. 107–112, 2010.

[9] E. K. Nakakura and M. A. Choti, "Management of hepatocellular carcinoma," *Oncology*, vol. 14, no. 7, pp. 1085–1098, 2000.

[10] S. Krizkova, M. Kepinska, G. Emri et al., "Microarray analysis of metallothioneins in human diseases--A review," *Journal of Pharmaceutical and Biomedical Analysis*, vol. 117, pp. 464–473, 2016.

[11] F. Stahl, B. Hitzmann, K. Mutz et al., "Transcriptome analysis," *Advances in biochemical engineering/biotechnology*, vol. 127, pp. 1–25, 2012.

[12] T. Lan, H. Li, D. Zhang et al., "KIAA1429 contributes to liver cancer progression through N6-methyladenosine-dependentpost-transcriptional modification of GATA3," *Molecular Cancer*, vol. 18, no. 1, p. 186, 2019.

[13] T. Zhang, Z. Ma, L. Liu et al., "DDX39 promotes hepatocellular carcinoma growth and metastasis through activating Wnt/β-catenin pathway," *Cell Death & Disease*, vol. 9, no. 6, p. 675, 2018.

[14] J. W. Eun, J. W. Jang, H. D. Yang et al., "Serum proteins, HMMR, NXPH4, PITX1 and THBS4; A panel of biomarkers for early diagnosis of hepatocellular carcinoma," *Journal of Clinical Medicine*, vol. 11, no. 8, p. 2128, 2022.

[15] J. T. Kao, C. L. Feng, C. J. Yu et al., "IL-6, through p-STAT3 rather than p-STAT1, activates hepatocarcinogenesis and affects survival of hepatocellular carcinoma patients: a cohort study," *BMC Gastroenterology*, vol. 15, no. 1, p. 50, 2015.

[16] X. Chen, J. Li, R. Kang, D. J. Klionsky, and D. Tang, "Ferroptosis: machinery and regulation," *Autophagy*, vol. 17, no. 9, pp. 2054–2081, 2021.

[17] X. Jiang, B. R. Stockwell, and M. Conrad, "Ferroptosis: mechanisms, biology and role in disease," *Nature Reviews Molecular Cell Biology*, vol. 22, no. 4, pp. 266–282, 2021.

[18] T. Xu, W. Ding, X. Ji et al., "Molecular mechanisms of ferroptosis and its role in cancer therapy," *Journal of Cellular and Molecular Medicine*, vol. 23, no. 8, pp. 4900–4912, 2019.

[19] M. M. Capelletti, H. Manceau, H. Puy, and K. Peoc'h, "Ferroptosis in liver diseases: an overview," *International Journal of Molecular Sciences*, vol. 21, no. 14, p. 4908, 2020.

[20] B. Gan, "Mitochondrial regulation of ferroptosis," *Journal of Cell Biology*, vol. 220, no. 9, Article ID e202105043, 2021.

[21] Y. Mou, J. Wang, J. Wu et al., "Ferroptosis, a new form of cell death: opportunities and challenges in cancer," *Journal of Hematology & Oncology*, vol. 12, no. 1, p. 34, 2019.

[22] Y. Shan, G. Yang, H. Huang et al., "Ubiquitin-like modifier activating enzyme 1 as a novel diagnostic and prognostic indicator that correlates with ferroptosis and the malignant phenotypes of liver cancer cells," *Frontiers in Oncology*, vol. 10, Article ID 592413, 2020.

[23] D. W. Kim, C. Talati, and R. Kim, "Hepatocellular carcinoma (HCC): beyond sorafenib-chemotherapy," *Journal of Gastrointestinal Oncology*, vol. 8, no. 2, pp. 256–265, 2017.

[24] T. E. Jabbour, S. M. Lagana, and H. Lee, "Update on hepatocellular carcinoma: pathologists' review," *World Journal of Gastroenterology*, vol. 25, no. 14, pp. 1653–1665, 2019.

[25] Y. Zhang, C. Wang, H. Xu, P. Xiao, and Y. Gao, "Hepatocellular carcinoma in the noncirrhotic liver: a literature review," *European Journal of Gastroenterology and Hepatology*, vol. 31, no. 7, pp. 743–748, 2019.

[26] F. Foerster and P. R. Galle, "The current landscape of clinical trials for systemic treatment of HCC," *Cancers*, vol. 13, no. 8, p. 1962, 2021.

[27] T. T. Cheung, K. W. Ma, and W. H. She, "A review on radiofrequency, microwave and high-intensity focused ultrasound ablations for hepatocellular carcinoma with cirrhosis," *Hepatobiliary Surgery and Nutrition*, vol. 10, no. 2, pp. 193–209, 2021.

[28] W. T. Wang, W. L. Jin, and X. Li, "Intercellular communication in the tumour microecosystem: mediators and therapeutic approaches for hepatocellular carcinoma," *Biochimica et Biophysica Acta, Molecular Basis of Disease*, vol. 1868, no. 12, Article ID 166528, 2022.

[29] C. Liang, X. Zhang, M. Yang, and X. Dong, "Recent progress in ferroptosis inducers for cancer therapy," *Advanced Materials*, vol. 31, no. 51, Article ID e1904197, 2019.

[30] H. Mao, Y. Zhao, H. Li, and L. Lei, "Ferroptosis as an emerging target in inflammatory diseases," *Progress in Biophysics and Molecular Biology*, vol. 155, pp. 20–28, 2020.

[31] K. W. DeGregory, P. Kuiper, T. DeSilvio et al., "A review of machine learning in obesity," *Obesity Reviews*, vol. 19, no. 5, pp. 668–685, 2018.

[32] R. C. Deo, "Machine learning in medicine," *Circulation*, vol. 132, no. 20, pp. 1920–1930, 2015.

[33] R. He, L. Gao, J. Ma et al., "The essential role of MTDH in the progression of HCC: a study with immunohistochemistry, TCGA, meta-analysis and in vitro investigation," *American Journal of Tourism Research*, vol. 9, no. 4, pp. 1561–1579, 2017.

[34] Y. Wang, D. He, L. Yang et al., "TRIM26 functions as a novel tumor suppressor of hepatocellular carcinoma and its downregulation contributes to worse prognosis," *Biochemical and Biophysical Research Communications*, vol. 463, no. 3, pp. 458–465, 2015.

Research Article

miR-4757-3p Inhibited the Migration and Invasion of Lung Cancer Cell via Targeting Wnt Signaling Pathway

Pei Zhao [1] **, Qian Zhao,**[1] **Chen Chen,**[1] **Song Lu,**[1] **and Li Jin** [2]

[1]*Department of Intensive Care Unit, Sichuan Cancer Hospital & Institute, Sichuan Cancer Center, School of Medicine, University of Electronic Science and Technology of China, 55# Renmin South Road, Wuhou District, Chengdu 610041, Sichuan, China*
[2]*State Key Laboratory of Quality Research in Chinese Medicine and School of Pharmacy, Macau University of Science and Technology, Taipa, China*

Correspondence should be addressed to Pei Zhao; icuzhaopei@scszlyy.org.cn and Li Jin; lee247487642king@163.com

Lung cancer accounts for the vast majority of cancer-related deaths worldwide, and aberrant miRNA expression is commonly observed as the disease progresses. The current study aimed to determine the role of miR-4757-3p in the development of lung cancer. The real-time PCR test was performed to determine the expression of miR-4757-3p in lung cancer cell lines. miR-4757-3p was downregulated in A549 cells. CCK8 and transwell assays demonstrated that overexpression of miR-4757-3p significantly reduced A549 cell invasion and migration. Bioinformatic analysis by the TargetScan database predicted the possible targets of miR-4757-3p. A luciferase activity test was used to determine the direct relationship between miR-4757-3p, Wnt5a, and Wnt8b. The overexpression of miR-4757-3p drastically inhibited the expression of Wnt5a and Wnt8b. Furthermore, we discovered that silencing Wnt5a and Wnt8b significantly lowered β-catenin expression and hampered invasion and migration. Finally, miR-4757-3p inhibited lung cancer cell migration and invasion by inhibiting the activation of the Wnt signaling pathway. Our study provided evidence that miR-4757-3p could be developed as an indicator or an anticancer target in the clinical application.

1. Introduction

Over the past few decades, the incidence of lung cancer in both men and women has shown a clear upward trend [1]. In 2020, lung cancer caused 1.8 million deaths worldwide. Lung cancer remains the most common cancer and the leading cause of cancer death in China. The overall 5year survival rate of lung cancer is between 10% and 20% in most countries [2]. The final stage of progression of lung cancer is the unrestrained development and division of abnormal cells [3]. The development of lung cancer is attributable to a variety of factors, including genetic and environmental factors [4]. Lung cancer treatment depends on an in-depth understanding of the cause. The exploration of possible targets to halt the growth and progression of lung cancer aids in the development of lung cancer treatment strategies.

MicroRNAs, also known as miRNAs, are small, noncoding RNAs that are produced in the body and range in length from 21 to 25 nucleotides. miRNAs inhibit protein translation by binding to mismatched sequences in the $3'$ untranslated regions of messenger RNAs [5]. After transcription occurs, miRNAs regulate the amount of gene expression produced. Inflammation, viral infection, cancer development, cell division, and apoptosis are all regulated by miRNAs [6]. The abnormal expression of miRNAs in lung cancer may be closely related to the development of cancer and play a role in the pathogenesis of cancer. miRNAs are attractive therapeutic targets, either as oncogenes or as repressors. Previous studies have shown that miR-4757-3p is a target miRNA of Wnt5a or Wnt8b in some tumors [7, 8]. The marker molecules of the Wnt signaling pathway, Wnt5a, and Wnt8b are required for progression of cancer [9]. In this study, we aimed to investigate the function of miR-4757-3p in lung cancer.

2. Materials and Methods

2.1. Cell Lines and Cell Transfection. The BEAS-2B and A549 cell lines were obtained from the Shanghai Institute of Cell Biology, the China Academy of Sciences (Shanghai, China). Cells were grown in Dulbecco's modified Eagle's medium (DMEM; Sigma, MO, USA) containing 10% fetal bovine serum (FBS) and 1% penicillin-streptomycin solution (Invitrogen, USA). The cells were maintained at 37°C in an incubator. The Lipofectamine 3000 reagent (Invitrogen, USA) was used for transfection with miR-4757-3p mimics (5′-CAUGACGUCACAGAGGCUUCGC-3′), inhibitors (HSTUD1826, Sigma, USA), or miR-NC(5′-CAGUACUUU UGUGUAGUACAA-3′). The media used to cultivate the cells the day before transfection did not include any antibiotics. For siRNA transfection, the cells were transfected with WNT5A-siRNA(5′-GTGGATCAGTTCGTGTGC AAA-3′; Sigma, USA), Wnt8b-siRNA(5′-GCATGGCAG CCTAAACTGCAC-3′; Sigma, USA) or a negative control by using the Lipofectamine 3000 reagent (Invitrogen, USA). After incubation for 48 hours, the cells were collected for further analysis.

2.2. Cell Grouping and the CCK-8 Assay. Cell were divided into the following groups: control group (cell transfection with miR-4757-3p mimics/inhibitor NC), miR-4757-3p mimic group (cell transfection with miR-4757-3p mimics), miR-4757-3p inhibitor group (cell transfection with miR-4757-3p inhibitors), siNC group (cell transfection with NC), siWnt5a (cell transfection with Wnt5a-siRNA), siWnt8b (cell transfection with Wnt8b-siRNA), miR-4757-3p inhibitors + siNC (cell cotransfection with miR-4757-3p inhibitors and NC), miR-4757-3p inhibitors + siWnt8b (cell cotransfection with miR-4757-3p inhibitors and Wnt8b-siRNA), and miR-4757-3p inhibitors + Rspo1 (cell transfection with miR-4757-3p inhibitors, while cell incubation with 0.1% Rspo1). The cells were plated into a 96-well plate at a density of 1×10^5 cells per well. The cells were permitted to continue growing for additional 12, 24, or 48 hours. Subsequently, $10 \, \mu l$ of CCK-8 solution was added into cells and incubated for 2 h. The OD_{450} values were determined by using an iMark microplate absorbance reader (BioRad Laboratories, Inc., Hercules, CA, USA).

2.3. Transwell Assay. For the migration assay, cells in a serum-free medium were seeded into each well in the upper transwell chamber (Corning USA), and the complete medium was added to the lower chamber. After incubation for 24 h, the cells that were collected using cotton swabs from the upper surface of the membrane migrated to the bottom surface of the membrane. The cells were fixed in 4% paraformaldehyde and stained with 0.1% crystal violet solution. The cells were observed under a microscope (Leica, Germany).

The transwell invasion experiment was performed in the same way as the migration assay, except that 100 mL of Matrigel (BD, USA) diluted 1 : 8 in DMEM was added to each well and incubated at 37°C for 6 hours.

2.4. Real-time PCR. Total cellular RNA was extracted by using the TRIzol reagent (Invitrogen, USA). Real-time PCR was performed by utilizing an ABI 7500 fast real-time detection system (Applied Biosystems, Foster City, CA, USA) with SYBR Green I Master Mix (Molecular Probes, Invitrogen) according to the manufacturer's instructions. The relative fold changes were quantified using the delta-delta Ct method with U6 or GAPDH as the endogenous control for normalization. The primers used in real-time PCR are summarized in Table 1.

2.5. Western Blot. The proteins in cells were isolated by using the ProteoPrep® total extraction sample kit (Sigma, USA). After centrifuging the cells at a speed of 12,000 g for ten minutes at 4°C, the supernatant was subjected to SDS gel electrophoresis. The proteins were transferred to polyvinylidene fluoride membranes (Millipore, Shanghai, China) and blocked for 1 h at room temperature. The membranes were incubated with antibodies against Wnt5a (#2392, CST, USA), Wnt8b (bs-6245R, Invitrogen, USA), and GAPDH (AG109, Beyotime, China). Subsequently, the membranes were incubated with an anti-mouse IgG HRP-linked antibody (#7076, CST, USA), and the bands were developed by using the ECL detection reagent (Sigma, USA).

2.6. Statistical Analysis. Statistical analysis was performed by using SPSS 22.0 software (IBM SPSS Statistics, USA). The data were presented as a mean ± standard deviation (SD). The differences were determined by Student's *t*-test or one-way ANOVA analysis. $P < 0.05$ was considered statistically significant.

3. Results

3.1. miR-4757-3p Regulated the Migration and Invasion in a549 Cells. The real-time PCR results indicated that miR-4757-3p was downregulated in lung cancer cells (Figure 1(a)). The miR-4757-3p inhibitor and mimic significantly decreased and increased miR-4757-3p levels in A549 cells, respectively (Figure 1(b)). The results of the CCK-8 assay showed that the ability of A549 cells was enhanced after transfection with the miR-4757-3p inhibitor and inhibited after transfection with the miR-4757-3p mimic (Figure 1(c)). Invasion and migration of cells were further determined by the transwell assay. The cell migration and invasion abilities of the miR-4757-3p mimic group were significantly lower than those of the control group, and the cell migration and invasion abilities of the miR-4757-3p inhibitor group were significantly higher than those of the control group (Figure 1(e)). Meanwhile, downregulation of miR-4757-3p increased the expression of Ki67, MMP2, MMP9, and N-cadherin and decreased the expression of E-cadherin (Figures 2(a)–2(e)).

3.2. miR-4757-3p Regulated Wnt5a and Wnt8b Expressions and the Activation of the Wnt Signaling Pathway. Based on the results of the miRNA target gene prediction database

TABLE 1: Primer sequences used in this study.

Gene	Forward primer sequence	Reverse primer sequence
miR-4757-3p	AUAGGCCGCUAACGGGC	CCATGACTTGGGGTTACTTAGG
U6	CTGGCCAAAAAGCTTGAAATGGAT	TCGTCCCTAACGCTAGGTCCCT
Ki67	GTGTTAGAGACAAGCGGGGA	TGAAAAGTCGAAGGCGTAGC
MMP2	CAACATACTTTGCATCCTGCAT	AGAGCAGGCAAGCTGGATCTGTG
MMP9	GGCCTTTGGGATCCAGAACGAG	TGTATCCCTGTACACTCTCCAC
E-cadherin	CCACGGCCGACAAATCATCAGCC	GAGCTTCATTGGGTCTCCCTGT
N-cadherin	GTTGCCTATCTCAAATCAAGCCG	TGACGGACTGTCTTGTTTTCACCT
GAPDH	CCCAGGGAGCATTTCGACTGAT	TCACTCGCTCCACAACCCTGT

(TargetScan, https://www.targetscan.org/vert_72/), Wnt5a and Wnt8b were identified as target genes of miR-4757-3p (Figures 3(a) and 3(b)). The luciferase reporter assay was employed to validate the above results. The expression of Wnt5a and Wnt8b was significantly decreased in the miR-4757-3p group (Figure 3(c)). Subsequently, the real-time PCR results showed that the expressions of Wnt5a and Wnt8b in the miR-4757-3p mimic group were significantly lower than those in the control group (Figure 3(d)). In contrast, the expression of Wnt5a and Wnt8b in the miR-4757-3p inhibitor group was significantly higher than those in the control group (Figure 3(e)). In addition, compared with the control group, the expression of β-catenin was significantly decreased in the miR-4757-3p mimic group, while it was increased in the miR-4757-3p inhibitor group (Figure 3(f)).

3.3. Knockdown of Wnt5a or Wnt8b Regulated the Migration and Invasion in A459 Cells and Mediated the Activation of the Wnt Signaling Pathway. Initially, the expressions of Wnt5a and Wnt8b in the BEAS-2B and A549 cells were compared. As shown in Figures 4(a) and 4(b), both Wnt5a and Wnt8b were highly expressed in A549 cells. The knockdown of two genes by RNA interference on A459 cells was validated by real-time PCR and Western blot. After transfection of Wnt5a-siRNA or Wnt8b-siRNA, the expression of both Wnt5a and Wnt8b in cells was significantly reduced (Figure 4(c)). Furthermore, siWnt5a and siWnt8b significantly reduced cell viability (Figure 4(d)). In addition, knockdown of Wnt5a or Wnt8b was able to inhibit cell migration and invasion (Figure 4(e)) and suppress expression of β-catenin (Figure 4(f)).

3.4. miR-4757-3p Promoted Cell Migration and Invasion by Targeting Wnt5a and Wnt8b in A549 Cells to Activate the Wnt Signaling Pathway. As shown in Figure 5, compared with the inhibitor group, cell survival and invasion abilities were improved after cotransfection with the miR-4757-3p inhibitor. The cell viability and invasive capacity of the miR-4757-3p inhibitor group were reduced after cotransfection with Wnt8b-siRNA/or Wnt5a-siRNA (Figures 5(a) and 5(b)). Compared with the miR-4757-3p inhibitor group, cell viability and invasive ability were inhibited. Furthermore, Wnt5a-siRNA, Wnt8b-siRNA, or Rspo1 treatment inhibited the expression of Ki67, MMP-2, MMP-9, and N-cadherin, while they increased E-cadherin expression (Figures 5(c)–5(g)).

4. Discussion

Abnormally high proliferation rates, lack of differentiation, and apoptosis are hallmarks of malignancies such as lung cancer, one of the most common types of cancerous tumors [10]. Aberrant expression of miRNAs has the potential to tip the balance in an organism toward the development of cancer [5]. miRNAs can promote the production of oncogenes and reduce the expression of anticancer genes. The expression of target genes has been regulated by miRNA regulatory networks during carcinogenesis and tumor development [11]. No studies indicated that miR-4757-3p was related to cancer, but it was found to be associated with type 1 diabetes. We first examined the expression level of miR-4757-3p, and the results showed that its expression level was relatively low in lung cancer cell lines. Transfection of A549 cells with miR-4757-3p mimics or inhibitors indicated that increasing the levels of miR-4757-3p greatly reduced the ability of cells to migrate and invade. On the other hand, the expression of miR-4757-3p was decreased, resulting in easier migration and invasion of cells. miR-4757-3p may play a role in cell motility and invasion.

To predict the genes targeted by miR-4757-3p, bioinformatic analysis was carried out. The TargetScan database predicted that Wnt5a and Wnt8b genes could bind to miR-4757-3p. The results of the luciferase reporter experiments confirmed their binding. Wnt5a and Wnt8b have been shown to promote cancer progression [12, 13]. Wnt5a and Wnt8b maintain the viability of cancer cells by accelerating the cell cycle, promoting cell proliferation, promoting cell differentiation and senescence, and preventing apoptosis within cells. Wnt5a and Wnt8b are involved in the process of repairing damaged DNA [14]. The Wnt/catenin signaling pathway is often referred to as the canonical Wnt pathway. The Wnt signaling pathway is activated by overexpression of Wnt5a and Wnt8b. It is possible that the Wnt/catenin signaling pathway is persistently activated in an aberrant manner, leading to excessive cell proliferation and transformation into a malignant state [15, 16]. In some cases, this can ultimately result in the development of cancer. A steady low level of catenin is kept in the cells of a healthy organism, and any excess catenin is eliminated by a complex that is made up of proteins, namely, Axin, APC, GSK3, and CK1. Within the degradation complex, the proteins (APC and Axin) serve the function of scaffold proteins, while phosphorylated serine/threonine kinases, GSK3 and CK1, have the ability to phosphorylate catenin [17]. The creation of

(a)

(b)

(c)

(d)

(e)
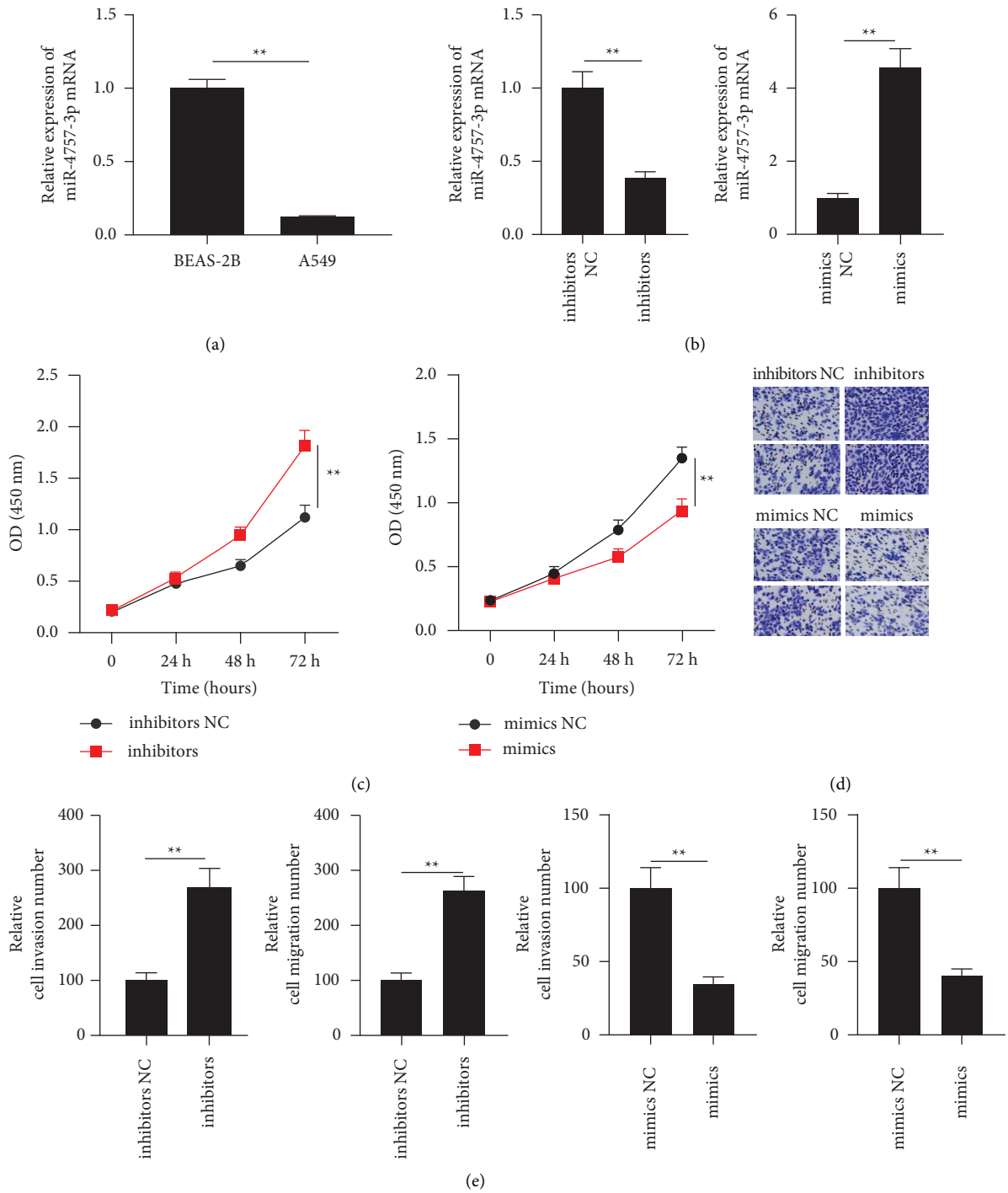
FIGURE 1: miR-4757-3p regulated the migration and invasion in A549 cells. (a) Real-time PCR analysis of miR-4757-3p expression in A549 cells. (b) Real-time PCR analysis of miR-4757-3p expression in A549 cell transfection with inhibitors or mimics. (c) CCK8 analysis of cell viability in A549 cell transfection with inhibitors or mimics. (d, e) Transwell analysis of cell invasion and migration in A549 cell transfection with inhibitors or mimics. $**P < 0.01$.

(a)

(b)

(c)

(d)

(e)
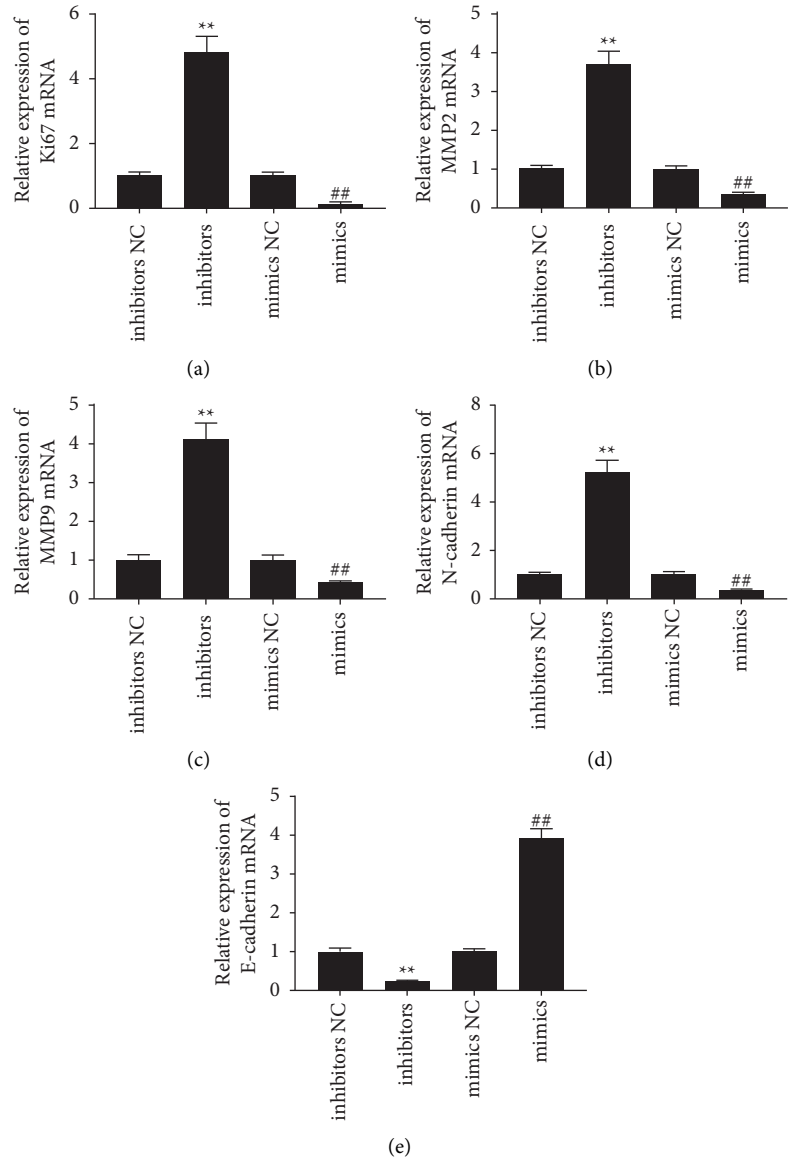
Figure 2: miR-4757-3p regulated gene expression. Real-time PCR analysis of mRNA levels of Ki67 (a), MMP2 (b), MMP9 (c), N-cadherin (d), and E-cadherin (e). $^{**}P < 0.01$ and $^{\#\#}P < 0$.

	Predicted consequential pairing of target region (top) and miRNA (bottom)
Position 652-658 of WNT5A 3′ UTR	5′ ...CAUUUGCAGACAGACCGUCAUAU... ‖‖‖‖‖‖
hsa-miR-4757-3p	3′ CGCUUCGGAGACACUGCAGUAC

(a)

	Predicted consequential pairing of target region (top) and miRNA (bottom)
Position 2088-2094 of WNT8B 3′ UTR	5′ ...GUCAGCACUCUAAAUACGUCAUG... ‖‖‖ ‖‖‖‖‖
hsa-miR-4757-3p	3′ CGCUUCGGAGACAC-UGCAGUAC

(b)

Figure 3: Continued.

(c)

(d)

(e)

(f)
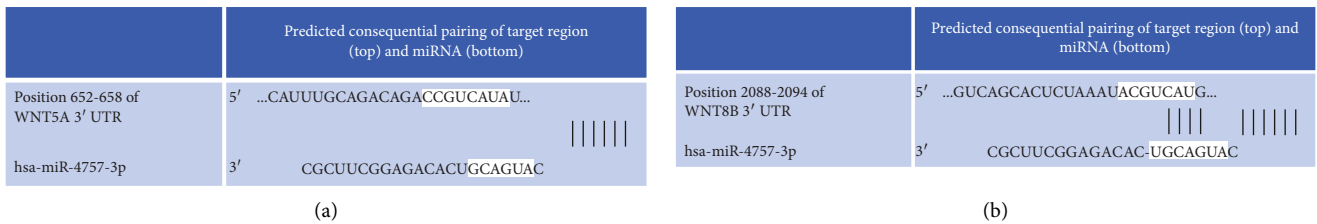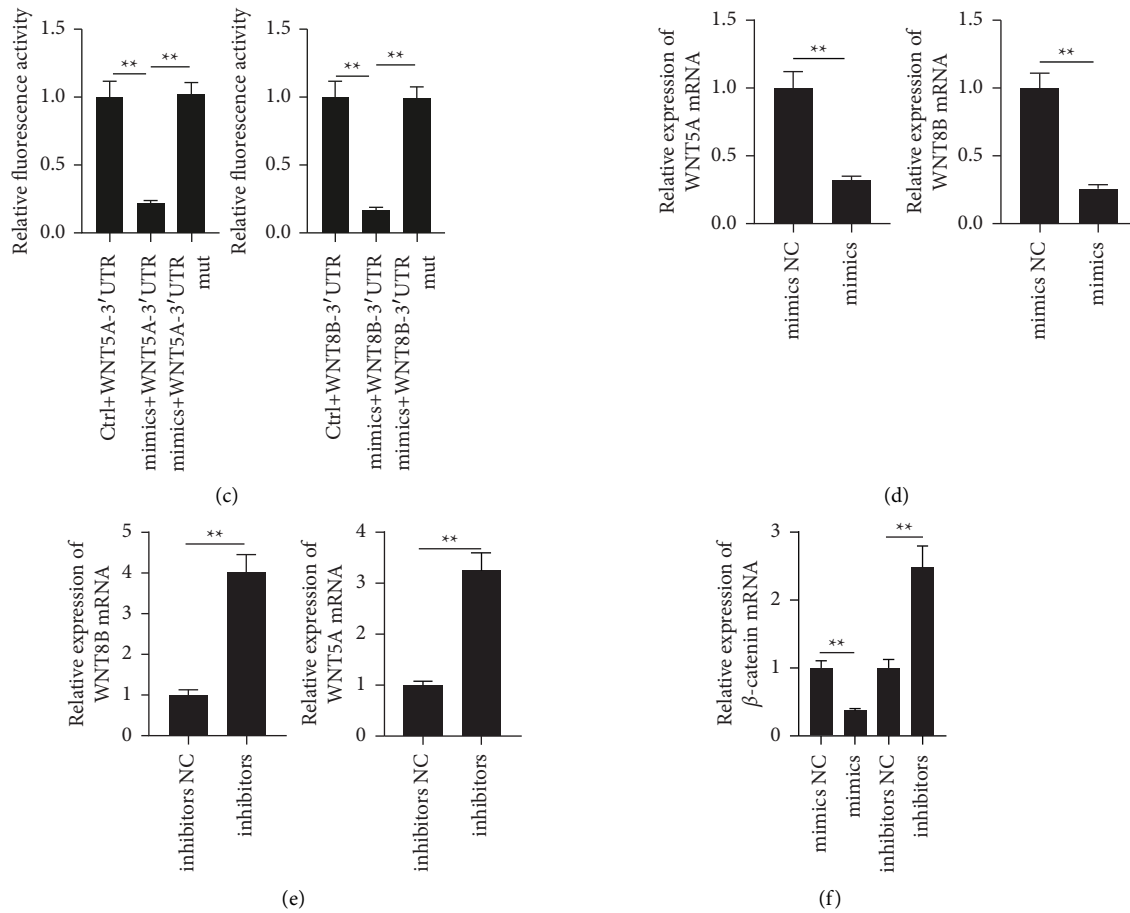
Figure 3: miR-4757-3p regulated Wnt5a and Wnt8b expressions and activated the Wnt signaling pathway. (a) Predicting binding sequences of miR-4757-3p and Wnt5a. (b) Predicting binding sequences of miR-4757-3p and WNT8B. (c) The luciferase reporter assay demonstrated that Wnt5a or Wnt8b 3′ untranslated region-WT was targeted by miR-4757-3p. (d) Real-time PCR analysis of mRNA levels of Wnt5a and Wnt8b in A549 cell transfection with mimics. (e) Real-time PCR analysis of mRNA levels of Wnt5a and Wnt8b in A549 cell transfection with inhibitors. (f) Real-time PCR analysis of β-catenin expression in A549 cell transfection with mimics or inhibitors. $^{**}P < 0.01$.

a complex that includes seven FZD transmembrane protein receptors is the consequence of a connection between factor extracellular Wnt protein and low-density lipoprotein receptor-associated proteins (LRP-5 and LRP-6). It is possible for a Wnt-FZD-LRP5/6 complex to form, and this can lead to the phosphorylation of LRP-6, localization of Axin to the cell membrane, dissociation of GSK3 from Axin and APC, inhibition of catenin degradation, accumulation of catenin, and infiltration of catenin into the cytoplasm and the nucleus of the cell [18–20]. Target genes that are associated with proliferation, invasion, and migration are activated as a result of this continuing connection between nuclear catenin and T lymphocytes/limb-like enhancer and other transcriptional activators [21], leading to abnormally high rates of cell proliferation and metastasis, which, in turn, cause tumors to develop and progress further [22–24]. It was discovered that inhibitors of miR-4757-3p led to a considerable increase in the expression of Wnt5a and Wnt8b. These findings provided evidence that an elevated level of

expression of miR-4757-3p can suppress Wnt signaling. In addition, we found that inhibiting Wnt5a and/or Wnt8b activity reduced the amount of cell invasion and migration. A459 cells transfected with miR-4757-3p inhibitors exhibited higher cell migration and invasion in comparison to the control group. However, this effect was reversed when WNT8B expression was reduced by Wnt8b-siRNA/BML-286. Next, the results showed that Wnt8b expression was reduced by Wnt8b-siRNA/Rspo1. Because of targeting Wnt5a and Wnt8b, miR-4757-3p can regulate cell migration and invasion in addition to affecting cell survival.

In conclusion, miR-4757-3p was able to limit the migration and invasion of cells. In addition, the Wnt5a/or Wnt8b interference phenotype was very comparable to the miR-4757-3p phenotype, which was observed in A549 cells. Inhibition of Wnt signaling pathway activation enables miR-4757-3p to regulate Wnt5a and Wnt8b genes to stimulate cell invasion and migration in lung cancer.

(a)

(b)

(c)

(d)

(e)

Figure 4: Continued.

(f)

(g)
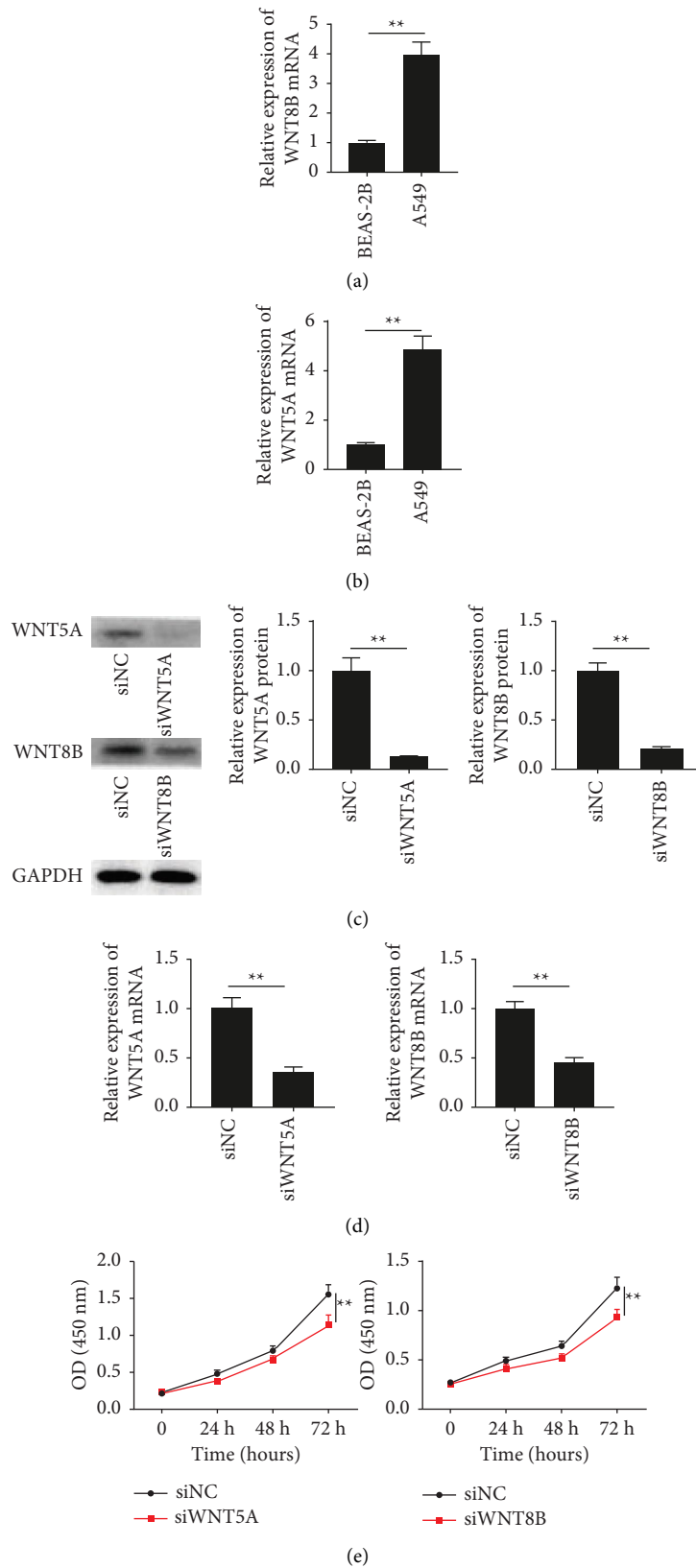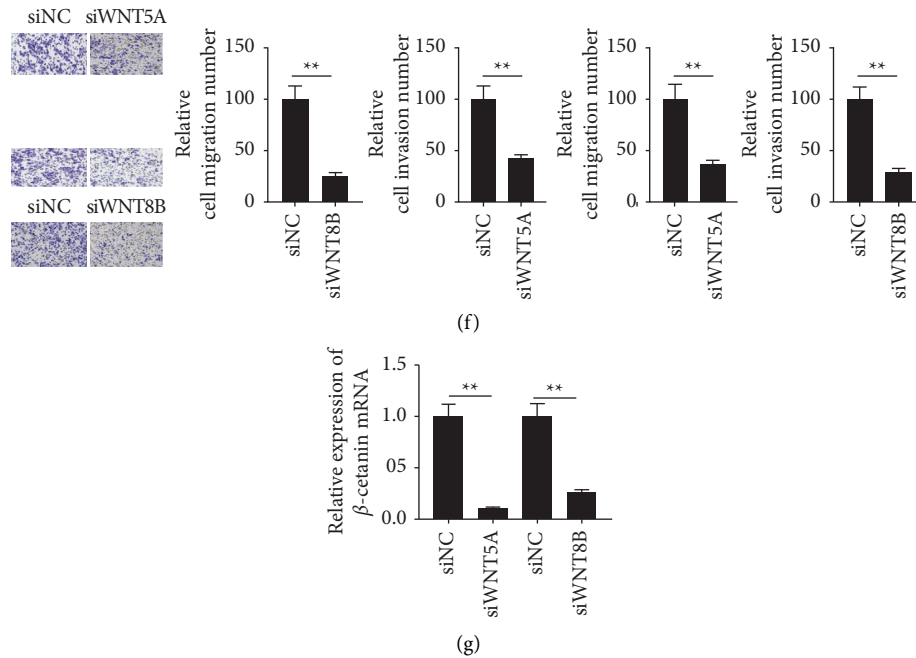
Figure 4: Wnt5a or Wnt8b silencing regulated the migration and invasion in. A459 cells and mediated the activation of the Wnt signaling pathway. (a, b) Real-time PCR analysis of Wnt5a and Wnt8b expressions in A549 cells. (c, d) Western blot and real-time PCR analysis of Wnt5a and Wnt8b expressions in A549 cell transfection with Wnt5a-siRNA or Wnt8b-siRNA. (e) CCK8 analysis of cell viability in A549 cell transfection with Wnt5a-siRNA or Wnt8b-siRNA. (f) Transwell analysis of cell invasion and migration in A549 cell transfection with Wnt5a-siRNA or Wnt8b-siRNA. (g) Real-time PCR analysis of β-catenin expression in A549 cell transfection with Wnt5a-siRNA or Wnt8b-siRNA. $^{**}P < 0.01$.

(a)

(b)

(c)

(d)

Figure 5: Continued.

(e)

(f)

(g)
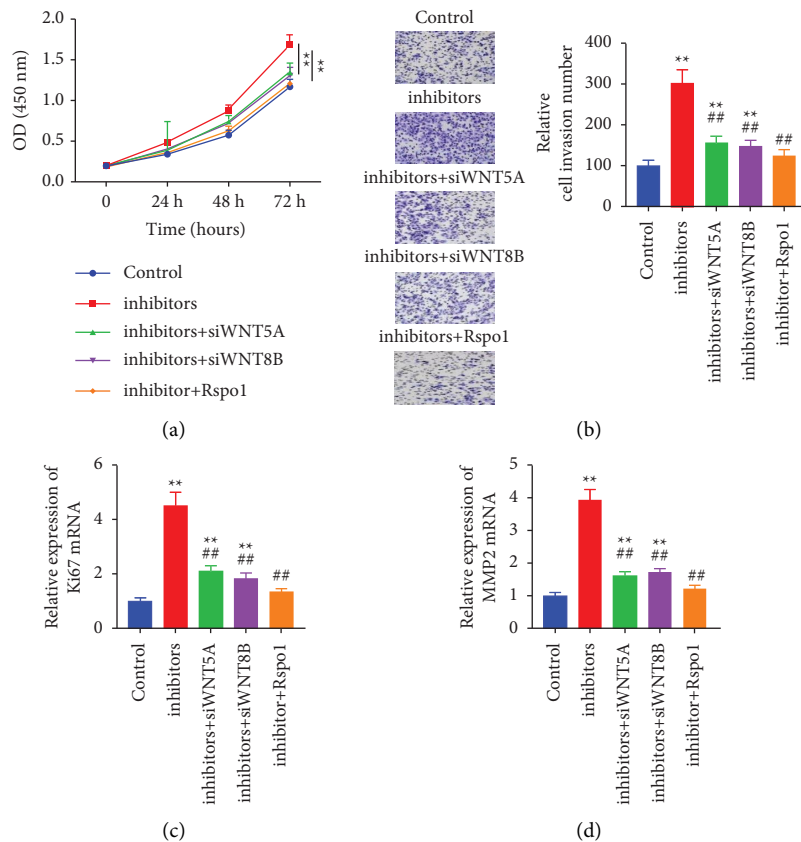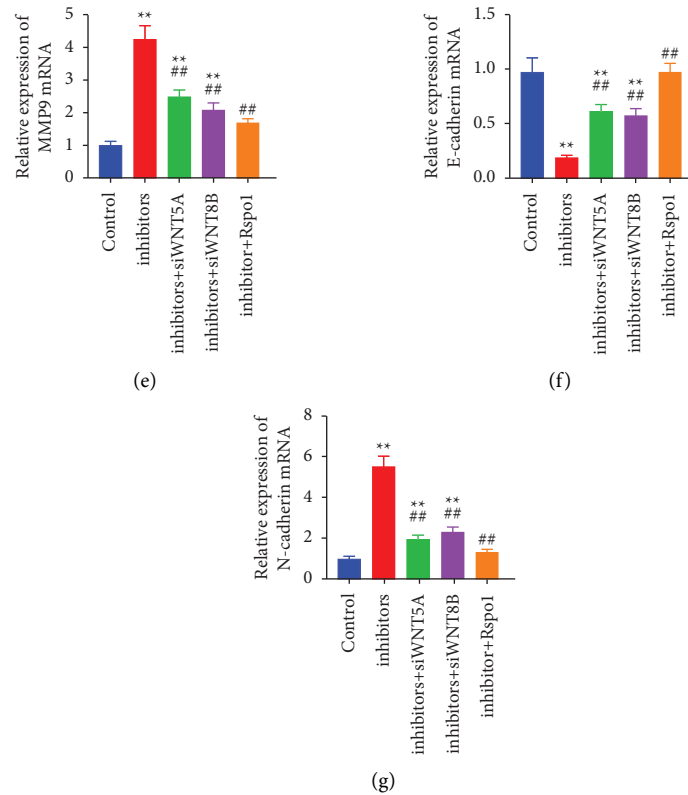
FIGURE 5: miR-4757-3p promoted cell migration and invasion by targeting Wnt5a and Wnt8b in A549 cells to activate the Wnt signaling pathway. (a) CCK8, (b) transwell analysis of cell viability and invasion, and (c–g) the expression of Ki67, MMP-2/-9, E-cadherin, and N-cadherin in different groups. $^{**}P < 0.01$; $^{##}P < 0.01$.

Data Availability

Data are available upon request from the corresponding author.

Conflicts of Interest

The authors declare that they have no conflicts of interest.

References

[1] F. Wu, L. Wang, and C. Zhou, "Lung cancer in China: current and prospect," *Current Opinion in Oncology*, vol. 33, no. 1, pp. 40–46, 2021.

[2] Z. Wu, F. Wang, W. Cao et al., "Lung cancer risk prediction models based on pulmonary nodules: a systematic review," *Thoracic Cancer*, vol. 13, no. 5, pp. 664–677, 2022.

[3] R. Nooreldeen and H. Bach, "Current and future development in lung cancer diagnosis," *International Journal of Molecular Sciences*, vol. 22, no. 16, p. 8661, 2021.

[4] H. Hoy, T. Lynch, and M. Beck, "Surgical treatment of lung cancer," *Critical Care Nursing Clinics of North America*, vol. 31, no. 3, pp. 303–313, 2019.

[5] M. Hill and N. Tran, "miRNA interplay: mechanisms and consequences in cancer," *Disease Models & Mechanisms*, vol. 14, no. 4, Article ID dmm047662, 2021.

[6] M. Correia de Sousa, M. Gjorgjieva, D. Dolicka, C. Sobolewski, and M. Foti, "Deciphering miRNAs' action through miRNA editing," *International Journal of Molecular Sciences*, vol. 20, no. 24, p. 6249, 2019.

[7] Y. Zhao, Q. Dai, X. Fu et al., "CircVAPA exerts oncogenic property in non-small cell lung cancer by the miR-876-5p/WNT5A axis," *The Journal of Gene Medicine*, vol. 23, no. 6, Article ID e3325, 2021.

[8] C. Ngernsombat, P. Prattapong, N. Larbcharoensub, K. Khotthong, and T. Janvilisri, "WNT8B as an independent prognostic marker for nasopharyngeal carcinoma," *Current Oncology*, vol. 28, no. 4, pp. 2529–2539, 2021.

[9] X. Nie, H. Liu, L. Liu, Y. D. Wang, and W. D. Chen, "Emerging roles of wnt ligands in human colorectal cancer," *Frontiers Oncology*, vol. 10, p. 1341, 2020.

[10] K. J. Radomska, F. Coulpier, A. Gresset et al., "Cellular origin, tumor progression, and pathogenic mechanisms of cutaneous neurofibromas revealed by mice with Nf1 knockout in boundary cap cells," *Cancer Discovery*, vol. 9, no. 1, pp. 130–147, 2019.

[11] B. He, Z. Zhao, Q. Cai et al., "miRNA-based biomarkers, therapies, and resistance in Cancer," *International Journal of Biological Sciences*, vol. 16, no. 14, pp. 2628–2647, 2020.

[12] Q. Liu, C. Yang, S. Wang et al., "Wnt5a-induced M2 polarization of tumor-associated macrophages via IL-10 promotes colorectal cancer progression," *Cell Communication and Signaling*, vol. 18, no. 1, p. 51, 2020.

[13] Y. Liu, D. Wu, H. Cheng et al., "Wnt8B, transcriptionally regulated by ZNF191, promotes cell proliferation of hepatocellular carcinoma via Wnt signaling," *Cancer Science*, vol. 112, no. 2, pp. 629–640, 2021.

[14] T. Zhan, N. Rindtorff, and M. Boutros, "Wnt signaling in cancer," *Oncogene*, vol. 36, no. 11, pp. 1461–1473, 2017.

[15] S. Patel, A. Alam, R. Pant, and S. Chattopadhyay, "Wnt signaling and its significance within the tumor microenvironment: novel therapeutic insights," *Frontiers in Immunology*, vol. 10, p. 2872, 2019.

[16] V. Murillo-Garzón and R. Kypta, "WNT signalling in prostate cancer," *Nature Reviews Urology*, vol. 14, no. 11, pp. 683–696, 2017.

[17] S. He and S. Tang, "WNT/β-catenin signaling in the development of liver cancers," *Biomedicine & Pharmacotherapy*, vol. 132, Article ID 110851, 2020.

[18] J. M. Bugter, N. Fenderico, and M. M. Maurice, "Mutations and mechanisms of WNT pathway tumour suppressors in cancer," *Nature Reviews Cancer*, vol. 21, no. 1, pp. 5–21, 2021.

[19] M. Koni, V. Pinnarò, and M. F. Brizzi, "The wnt signalling pathway: a tailored target in cancer," *International Journal of Molecular Sciences*, vol. 21, no. 20, p. 7697, 2020.

[20] P. Polakis, "Wnt signaling in cancer," *Cold Spring Harbor Perspectives in Biology*, vol. 4, no. 5, Article ID a008052, 2012.

[21] W. Hankey, W. L. Frankel, and J. Groden, "Functions of the APC tumor suppressor protein dependent and independent of canonical WNT signaling: implications for therapeutic targeting," *Cancer & Metastasis Reviews*, vol. 37, no. 1, pp. 159–172, 2018.

[22] F. Carreira-Barbosa and S. C. Nunes, "Wnt signaling: paths for cancer progression," *Advances in Experimental Medicine & Biology*, vol. 1219, pp. 189–202, 2020.

[23] G. Maric, M. G. Annis, P. A. MacDonald et al., "GPNMB augments Wnt-1 mediated breast tumor initiation and growth by enhancing PI3K/AKT/mTOR pathway signaling and β-catenin activity," *Oncogene*, vol. 38, no. 26, pp. 5294–5307, 2019.

[24] E. Martin-Orozco, A. Sanchez-Fernandez, I. Ortiz-Parra, and M. Ayala-San Nicolas, "WNT signaling in tumors: the way to evade drugs and immunity," *Frontiers in Immunology*, vol. 10, p. 2854, 2019.

Hindawi

Research Article

Comprehensive Analysis of Transcriptomic Profiles Identified the Prediction of Prognosis and Drug Sensitivity of Aminopeptidase-Like 1 (NPEPL1) for Clear Cell Renal Cell Carcinoma

Xiaoyu Wei,[1] Zhongbao Zhou [ORCID],[2] Guikai Ma [ORCID],[3] and Fengze Sun [ORCID][4]

[1]*Department of Oncology, Tianjin Binhai New Area Hospital of Traditional Chinese Medicine, Tianjin, China*
[2]*Department of Urology, Beijing Tiantan Hospital, Capital Medical University, Beijing, China*
[3]*Department of Medical Oncology, Weifang People's Hospital, Weifang, Shandong, China*
[4]*Department of Urology, Yantai Yuhuangding Hospital, Qingdao University, Yantai, Shandong, China*

Correspondence should be addressed to Guikai Ma; 2397136581@qq.com and Fengze Sun; doctorsunfz@163.com

Aminopeptidase-like 1 (NPEPL1) is a member of the aminopeptidase group that plays a role in the development and progression of various diseases. Expression of NPEPL1 has been reported to be involved in prostate, breast, and colorectal cancers. However, the role and mechanism of NPEPL1 in clear cell renal cell carcinoma (ccRCC) are unclear. The Cancer Genome Atlas (TCGA) and Human Protein Atlas (HPA) databases were used to predict the relationship between clinicopathological features and NPEPL1 expression. Changes in immune status and drug sensitivity with NPEPL1 expression were analyzed by the "CIBERSORT" function in R software. The results found that NPEPL1 expression was upregulated in ccRCC tissues, with expression progressively increasing with ccRCC stage and grade. Patients with high NPEPL1 expression presented with a poor prognosis across different clinicopathological features. Univariate and multivariate Cox regression analyses indicated that aberrant NPEPL1 expression was an independent risk factor for ccRCC. The nomogram showed that NPEPL1 expression improved the accuracy of predicting the prognosis of ccRCC patients. The Gene Ontology (GO) term enrichment analysis and the Kyoto Encyclopedia of Genes and Genomes (KEGG) pathway analysis revealed that NPEPL1 may be involved in the development of ccRCC through the voltage-gated calcium channel complex, channel activity, cAMP signaling pathway, and oxytocin signaling pathway. The coexpression analysis found that NPEPL1 altered tumor characteristics by interacting with related genes. The "CIBERSORT" analysis showed that elevated NPEPL1 expression was followed by an enrichment of regulatory T cells and follicular helper T cells in the microenvironment. The drug sensitivity analysis found patients with high NPEPL1 expression had a higher benefit from axitinib, cisplatin, and GSK429286A. In conclusion, upregulation of NPEPL1 expression was involved in ccRCC prognosis and treatment. NPEPL1 could be used as a therapeutic target to guide clinical dosing.

1. Introduction

Renal cell carcinoma (RCC) is one of the most common malignancies among urological carcinomas, representing 80% of renal malignancies [1]. The main pathological types include clear cell RCC (ccRCC), collecting duct RCC, chromophobe RCC, and papillary RCC [2, 3]. ccRCC, as the most common subtype, accounts for approximately 70% of all RCC [4]. Patients are generally found by examination and diagnosed at an advanced stage, with a 5-year survival rate of about 11.7% due to a lack of specific inspection methods [5]. Patients treated with conventional chemoradiotherapy always had poor outcomes. For targeted therapy, some patients may have drug resistance, resulting in poor long-term prognosis, which poses a new challenge for the treatment of renal cancer [6]. With the development of tumor therapy, immune therapy, including immune checkpoint inhibitors (ICIs), has been the most promising choice for ccRCC. The therapeutic mechanism of ICIs is briefly considered to be blocking the abnormal pathways that maintain immune self-tolerance to

prevent immune escape. Since antibody-mediated programmed cell death protein 1 (PD-1) blockade was approved by the American Food and Drug Administration (FDA), ICIs have emerged as the new first- and second-line standard of care for patients with intermediate to advanced disease as monotherapy or combination therapy [7, 8]. Despite these therapies being widely used in clinical practice, most RCC patients do not derive lasting benefit from ICI treatment. Thus, understanding the pathogenesis associated with progression and finding new therapeutic markers are important for predicting outcomes and prognosis.

Exogenous amino acids are essential for the survival of tumor cells. The stable state of amino acids and proteins essential for cells depends on the catalytic cleavage of amino acids at the amino terminus of proteins by aminopeptidases [9]. Clinical studies have also shown that cancer patients with high aminopeptidase expression tend to have a poor prognosis [10, 11]. Proliferating active tumor cells may be inhibited by low expression of aminopeptidase. This provides the rationale that aminopeptidase can be used as a new therapeutic approach [12, 13].

Aminopeptidase-like 1 (NPEPL1), a member of the aminopeptidase family, has functions such as manganese ion binding and metalloexopeptidase activity. It plays a role in proteolysis and also takes part in the development and progression of various diseases. NPEPL1 has been reported as one of the prognostic markers of destructive resistance prostate cancer and appeared to be useful in predicting the recurrence-free survival of patients [14]. It can bind directly to miR-19a and take part in the development and progression of breast and colorectal cancers [15–17]. Abnormalities in NPEPL1 may also be closely associated with the development of Alzheimer's disease [18]. Moreover, elevated expression of NPEPL1 and adjacent STX16 could promote the probability of gastrointestinal tumorigenesis [19]. Long-range deletion spanning NPEPL1 and adjacent STX16 is related to rare pseudohypoparathyroidism [20]. However, the relation between NPEPL1 and ccRCC in terms of prognosis and treatments has not yet been completely elucidated.

In this study, we assessed the relationship between NPEPL1 expression and the clinical characteristics of ccRCC patients using the TCGA and Human Protein Atlas (HPA) databases. We found that high expression of NPEPL1 suggested a poor prognosis for patients. The "CIBERSORT" analysis was then used to validate the correlation between NPEPL1 expression and immune status. We found that NPEPL1 might affect a variety of immune cells. Finally, we also predicted drug sensitivity in patients with high NPEPL1 expression, who were especially sensitive to cisplatin, axitinib, and GSK429286A. Therefore, upregulation of NPEPL1 expression was involved in ccRCC prognosis and treatment and guided the application of therapeutic drugs.

2. Method

2.1. The Expression of NPEPL1 in TCGA and HPA Databases.
This study was conducted according to the method of Dr. Zhou et al. [21]. The TCGA database was used to collect clinical data (containing 539 KIRC cases), including gender, age, grade, TNM stage, pathological stage, survival status, and survival time. Protein expression of NPEPL1 in renal tissue and KIRC was obtained from the HPA database.

2.2. Survival Analysis.
The R package "survival" was used to analyze survival data. Patients were graded into high and low expression groups according to the median value set for NPEPL1 expression in the tumor. The relationship between NPEPL1 expression and clinical outcomes was detected.

2.3. Univariate and Multivariate Logistic Regression Analyses.
The association between NPEPL1 expression and clinicopathological characteristics and overall survival (OS) can be assessed using univariate Cox regression. Multivariate Cox regression clarified the importance of NPEPL1 in the survival of ccRCC patients. When the P value was less than 0.05, we considered that the factor showed significance in the OS of the patients.

2.4. Evaluation and Construction of Prognostic Nomogram.
We drew a prognostic nomogram to visually show the prognostic predictors of ccRCC patients (age, T, N, M, histological grade, and NPEPL1 expression level) on OS. The reliability and accuracy of the nomogram were evaluated by the calibration curve.

2.5. Analysis of Differentially Expressed Genes and Their Functions.
Differential expression genes (DEGs) were analyzed by the R package "limma" between high and low NPEPL1 expression. The false discovery rate (FDR) was performed to correct P value for multiple test correction. When |log2FC| value was set at more than 1 and FDR less than 0.05, DEGs were selected and included in the Gene Ontology (GO) term enrichment analysis and the Kyoto Encyclopedia of Genes and Genomes (KEGG) pathway analysis.

2.6. Immune Landscape Assessment.
To describe the link between the immune microenvironment and NPEPL1 expression, "CIBERSORT" analysis was used to collect data on immune cell infiltration in ccRCC patients and was evaluated by R software. "Spearman" analysis was used to clarify the correlation between NPEPL1 and the immune microenvironment in tumor development. Comparison of differentially expressed immune checkpoints between NPEPL1 high and low expressing groups was performed to clarify immune mechanisms by which NPEPL1 mediates tumorigenesis development.

2.7. Sensitivity to Drugs of NPEPL1.
The R package "pRRophetic" was employed to identify the half-maximal inhibitory concentrations (IC_{50}s) of commonly used drugs, including cisplatin, axitinib, ICIs, and others, in order to estimate the sensitivity of high and low NPEPL1 expression to different drugs. The difference in IC_{50} values between high- and low-expression groups was estimated by the Wilcoxon signed rank test.

2.8. Statistics Analysis. All statistical analyses were calculated using R software (version 4.0.2). The Kaplan–Meier analysis was used to assess the impact of NPEPL1 on patients' survival. Univariate Cox regression was performed to evaluate the relationship between clinicopathological characteristics and OS, and multivariate Cox regression was used to clarify that NPEPL1 was an important factor for patients' survival. The Wilcoxon rank-sum test was used to evaluate the relation between NPEPL1 and molecular functions. The results were deemed statistically significant when the P value was less than 0.05.

3. Result

3.1. NPEPL1 Expression in Pan-Cancer Analysis. NPEPL1 expression was detected in 32 cancers, as shown in Figure 1. Compared to normal tissues, NPEPL1 expression was higher in 13 types of cancer, including KIRC, and lower in thyroid carcinoma and kidney chromophobe. The data suggested that NPEPL1 was differentially expressed in different tissues and in different types of cancer in the same tissue.

3.2. The Expression Characteristics of NPEPL1 in KIRC. The patients were divided into various groups according to their clinicopathological features, including age (less than 65 years old and more than 65 years old), gender (male and female), grade (grade 1, grade 2, grade 3, and grade 4), stage (stage I, stage II, stage III, and stage IV), and TNM stages (T1, T2, T3, T4, N0, N1, M0, and M1). The expression of NPEPL1 in different features was detected to clarify its role in ccRCC, in which the expression was higher in tumor tissues (Figures 2(a) and 2(b)). The gender and age of tumor patients were not affected by expression (Figures 2(c) and 2(d)). With the increase in tumor stage and grade, the expression level of NPEPL1 increased significantly (Figures 2(e)–2(i)). The expression affected the metastasis of the tumor, rather than lymph node metastasis. This result identified that the high NPEPL1 expression was related to the advanced stage of ccRCC. The HPA database was also applied to suggest that NPEPL1 protein overexpression was correlated with the development and progression of ccRCC (Figures 2(j) and 2(k)).

3.3. Relationship between NPEPL1 Expression and ccRCC Prognosis. We classified the 539 patients in the TCGA-KIRC cohort into high and low NPEPL1 groups according to the median expression of NPEPL1 in tumor tissue as the cutoff. The details of the patients are shown in Table 1. The significant difference was presented in OS ($P < 0.001$), progression-free survival (PFS, $P < 0.001$), and disease-specific survival (DSS, $P < 0.001$) (Figures 2(l)–2(n)). The area under the curve (AUC) at 1 year, 3 years, and 5 years were 0.659, 0.672, and 0.709, respectively, which were better than 0.6, implying good predictive value (Figure 2(o)). Next, the correlation between survival and NPEPL1 expression was performed according to subgroups of clinicopathological features. The high expression of NPEPL1 indicated poor survival in clinical features including age (less than

60 years old and more than 60 years old) and gender (male and female) (Figures 3(a)–3(d)). For the pathologic stage, the patients with high NPEPL1 expression presented poorer outcomes in stages II, III, and IV ($P < 0.001$), whereas the difference was not significant in stage I ($P = 0.152$). (Figures 3(e) and 3(f)). For the histologic grade, the high NPEPL1 expression meant worse survival in both grades I and II ($P = 0.038$) and grades III and IV ($P < 0.001$). (Figures 3(g) and 3(h)). The NPEPL1 expression was not correlated with survival in early T stage ($P = 0.066$); however, the high NPEPL1 expression implied worse survival in T2, T3, and T4 ($P < 0.001$) (Figures 3(i) and 3(j)). Whether distant metastasis occurred or not, high NPEPL1 expression indicated poor survival (Figures 3(k) and 3(l)). These results indicate that the higher NPEPL1 expression meant poor prognosis for ccRCC patients in different clinical features.

3.4. Construction and Evaluation of Nomogram. The univariate and multivariate analyses identified that M stage, age, and NPEPL1 expression were all independent risk factors for the prognosis of ccRCC (Table 2). Furthermore, the bar plot and table presented that T stage ($P < 0.001$), M stage ($P < 0.01$), pathologic stage ($P < 0.001$), and histologic grade ($P < 0.01$) were notably associated with NPEPL1 expression (Figure 4(a) and Table 3). NPEPL1 expression and clinicopathological features were used to build a nomogram to predict OS at 1, 3, and 5 years in ccRCC patients (Figure 4(b)). High expression of NPEPL1 predicted a poor prognosis. Calibration curves showed the predictive value of the nomogram was consistent with actual results, which demonstrated that the nomogram was robust and precise (Figure 4(c)).

3.5. DEGs and Enrichment Analysis of Low and High NPEPL1 Expression. Finally, about 5,679 DEGs were determined, of which 5,635 genes were upregulated and 44 genes were downregulated. The top 50 DEGs were mapped by heatmap in Figure 5(a). The GO analysis was used to predict the enrichment analysis of low and high NPEPL1 expression by applied biological process (BP), molecular function (MF), and cellular component (CC) groups. The main enrichment items were detection of external stimulus, detection of abiotic stimulus, immunoglobulin complex, voltage-gated calcium channel complex, channel activity, and passive transmembrane transporter activity (Figures 5(b) and 5(c)). The main KEGG enrichment pathways were neuroactive ligand-receptor interaction, pancreatic secretion, the cAMP signaling pathway, and the oxytocin signaling pathway (Figure 5(d)).

3.6. Coexpression Network Construction. The DEGs that interacted directly with NPEPL1 were selected to draw an interaction network using the "limma" R package. The top 11 genes interacted with NPEPL1 closely were performed, including CHTF18, AL139349.1, ARFGAP1, PIDD1, AL591845.1, KMT5C, SERINC1, PPP6C, RBM18, ITGA6, and COPS4 (Figure 6(a)). The NPEPL1 presented high
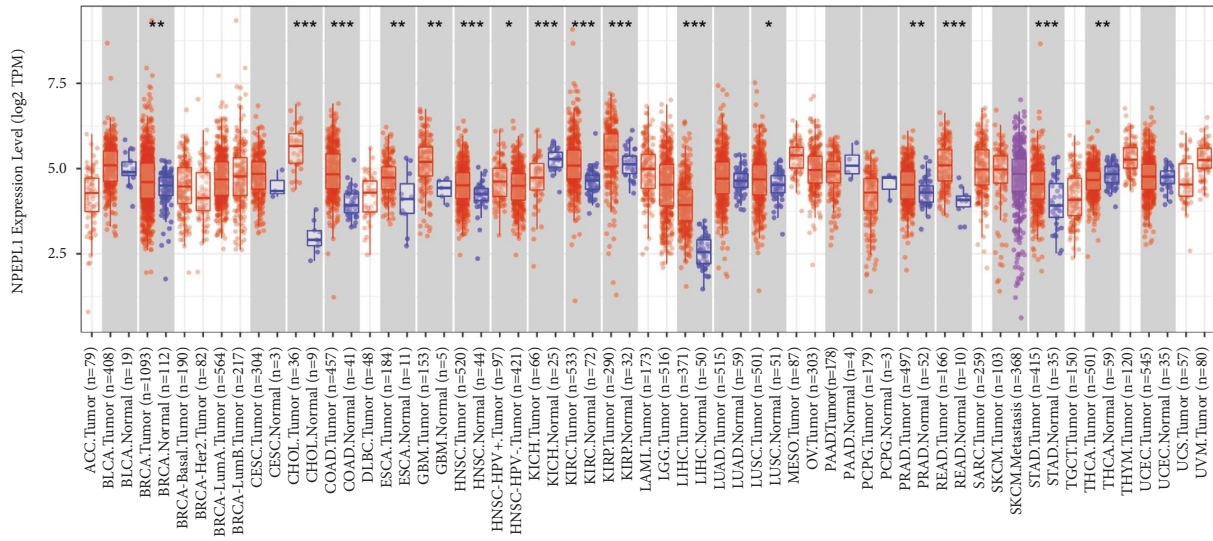
Figure 1: Pan-cancer-related expression pattern of NPEPL1. (*: $P < 0.05$, **: $P < 0.01$, ***: $P < 0.0001$).

(a)

(b)

(c)

(d)

(e)

(f)

(g)

(h)
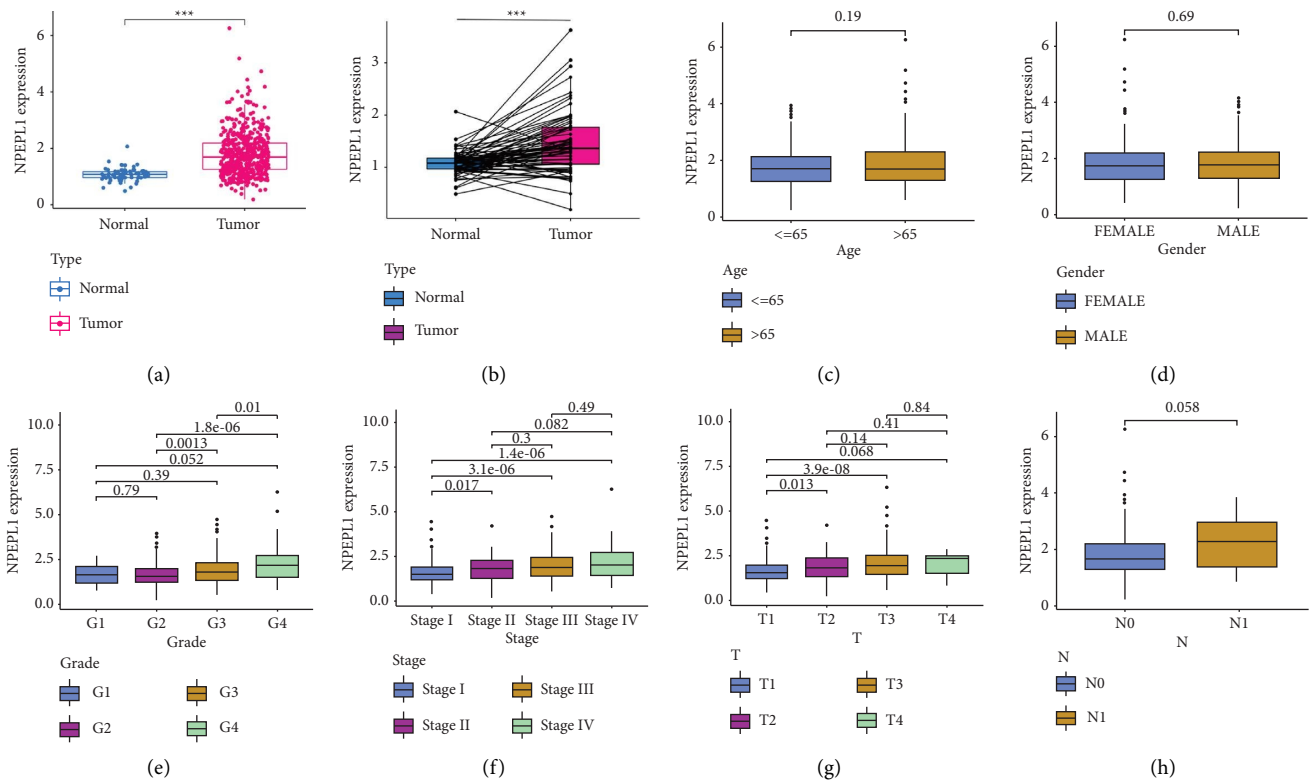
Figure 2: Continued.
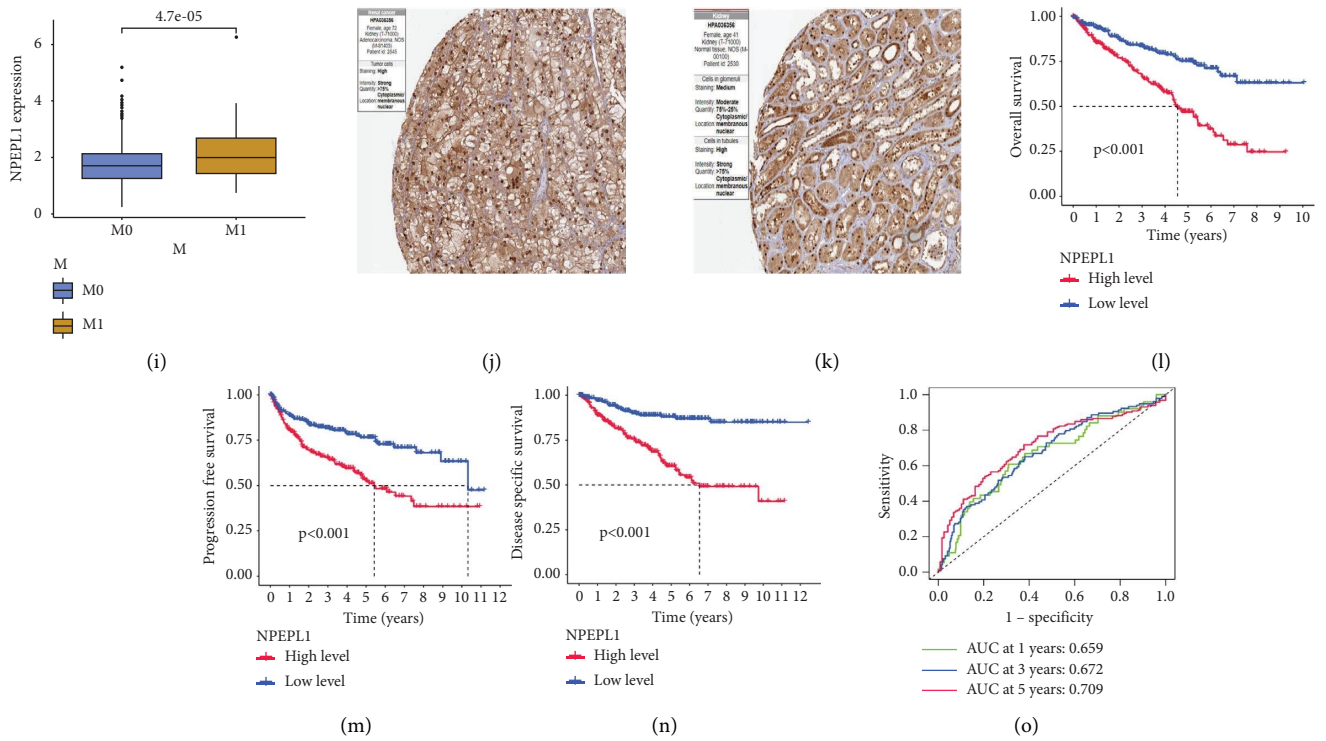
FIGURE 2: The expression of NPEPL1 and related clinical features in ccRCC. The NPEPL1 expression between normal and tumor tissues. (a, b) The NPEPL1 expression according to different clinical features, including age (c); gender (d); grade (e); stage in stages I II, III, and IV (f); T stage in T1, T2, and T3 (g); N stage in N0 and N1 (h); M stage in M0 and M1. (i) The protein expression of NPEPL1 between normal and tumor tissue. (j, k) The overall survival, progression-free survival, and disease-specific survival between low and high NPEPL1 expression. (l, m, n) AUC curve related to OS (o).

TABLE 1: Association between NPEPL1 expression and various clinicopathological characteristics in the TCGA database.

Characteristic		Low expression of NPEPL1 $N = 269$	High expression of NPEPL1 $N = 270$
Age, mean ± SD		61.09 ± 12.04	60.16 ± 12.15
Gender, n (%)	Female	91 (16.9%)	95 (17.6%)
	Male	178 (33%)	175 (32.5%)
Histologic grade, n (%)	G1	7 (1.3%)	7 (1.3%)
	G2	135 (25.4%)	100 (18.8%)
	G3	97 (18.3%)	110 (20.7%)
	G4	24 (4.5%)	51 (9.6%)
Pathologic stage, n (%)	Stage I	164 (30.6%)	108 (20.1%)
	Stage II	28 (5.2%)	31 (5.8%)
	Stage III	46 (8.6%)	77 (14.4%)
	Stage IV	30 (5.6%)	52 (9.7%)
T stage, n (%)	T1	166 (30.8%)	112 (20.8%)
	T2	34 (6.3%)	37 (6.9%)
	T3	66 (12.2%)	113 (21%)
	T4	3 (0.6%)	8 (1.5%)
N stage, n (%)	N0	126 (49%)	115 (44.7%)
	N1	6 (2.3%)	10 (3.9%)
M stage, n (%)	M0	236 (46.6%)	192 (37.9%)
	M1	28 (5.5%)	50 (9.9%)
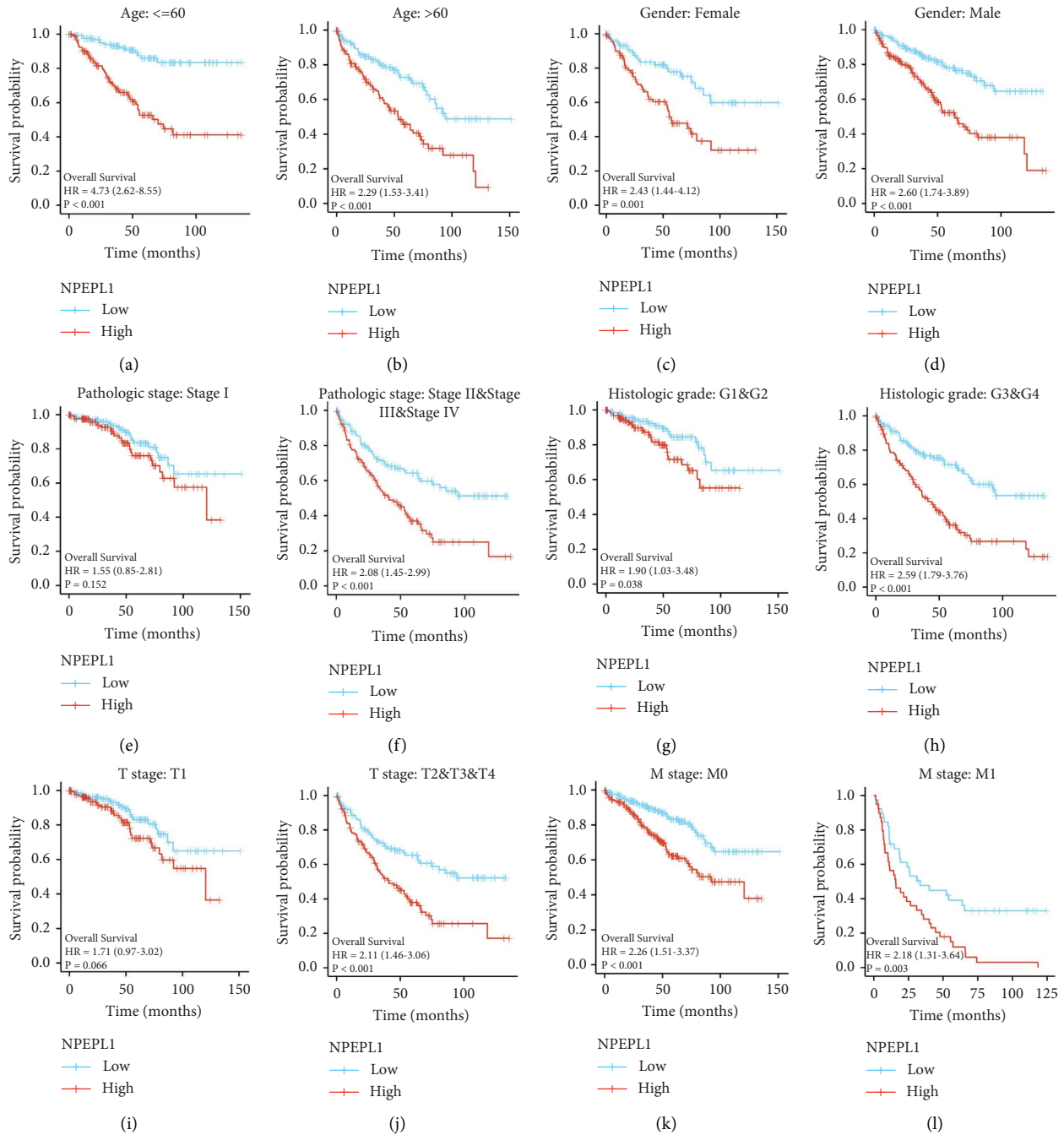
FIGURE 3: The OS between low and high NPEPL1 expressions according to clinicopathological features, including age between lower than 60 years old and higher than 60 years old (a, b); gender between male and female (c, d); stage between stage I and stage II, III, and IV (e, f); grade between grade 1 and 2 and grade 3 and 4 (g, h); T stage between T1 and T2, 3 and 4 (i, j); M stage between M0 and M1 (k, l).

coexpression relationship with CHTF18 ($R = 0.75$), AL139349.1 ($R = 0.75$), ARFGAP1 ($R = 0.77$), PIDD1 ($R = 0.76$), AL591845.1 ($R = 0.78$), KMT5C ($R = 0.77$), SER-INC1 ($R = -0.63$), PPP6C ($R = -0.64$), RBM18 ($R = -0.61$), ITGA6 ($R = -0.66$), and COPS4 ($R = -0.61$).

3.7. Relation between NPEPL1 and Infiltrating Immune Cells.
The occurrence and development of tumor were closely linked to immune cell infiltration. We analyzed the difference of immune cell infiltration between high and low NPEPL1 expression groups, and some infiltrating immune cell subtypes presented significant correlation with NPEPL1, including regulatory T cell, follicular helper T cell, memory B cell, CD8 T cell, activated NK cell, plasma cell, M0 macrophage, CD4 memory resting T cell, monocytes, gamma delta T cell, naïve B cell, eosinophiles, M2 macrophage, resting dendritic cell, activated dendritic cell, and resting mast cell (Figure 7(a)). By analyzing three immune cell subtypes with obvious differences, it was found that

TABLE 2: Univariate Cox regression analysis and multivariate Cox regression analysis of NPEPL1 and clinicopathologic parameters with OS in ccRCC.

Characteristics		Total (N)	Univariate analysis		Multivariate analysis	
			Hazard ratio (95% CI)	P value	Hazard ratio (95% CI)	P value
T stage N = 539	T1 and T2	349	3.228 (2.382–4.374)	**<0.001**	1.388 (0.610–3.158)	0.434
	T3 and T4	190				
N stage N = 257	N0	241	3.453 (1.832–6.508)	**<0.001**	1.258 (0.616–2.569)	0.529
	N1	16				
M stage N = 506	M0	428	4.389 (3.212–5.999)	**<0.001**	3.090 (1.804–5.291)	**<0.001**
	M1	78				
Gender N = 539	Female	186	0.930 (0.682–1.268)	0.648	NA	NA
	Male	353				
Age N = 539	≤60	269	1.765 (1.298–2.398)	**<0.001**	1.859 (1.211–2.852)	**0.005**
	>60	270				
NPEPL1 N = 539	Low	269	2.621 (1.900–3.615)	**<0.001**	2.401 (1.509–3.821)	**<0.001**
	High	270				
Pathologic stage N = 536	Stage I and stage II	331	3.946 (2.872–5.423)	**<0.001**	1.348 (0.532–3.415)	0.529
	Stage III and stage IV	205				
Histologic grade N = 531	G1 and G2	249	2.702 (1.918–3.807)	**<0.001**	1.508 (0.905–2.513)	0.115
	G3 and G4	282				

The indicators in bold are meaningful. Due to the limitation of prognostic statistics, we choose to retain 3 decimal places and use < 0.001 to represent meaningful indicators.
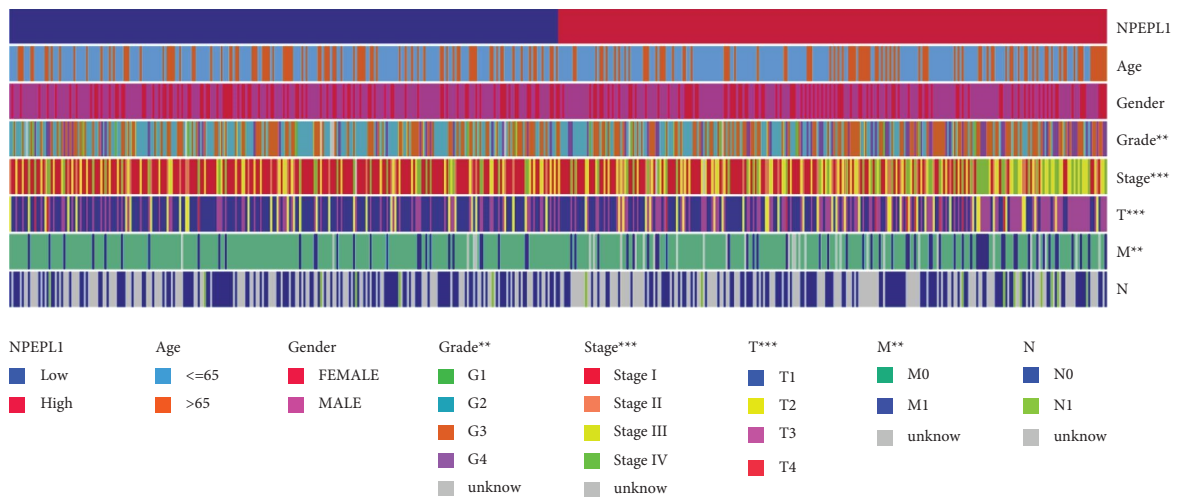
(a)

(b)

FIGURE 4: Continued.

(c)
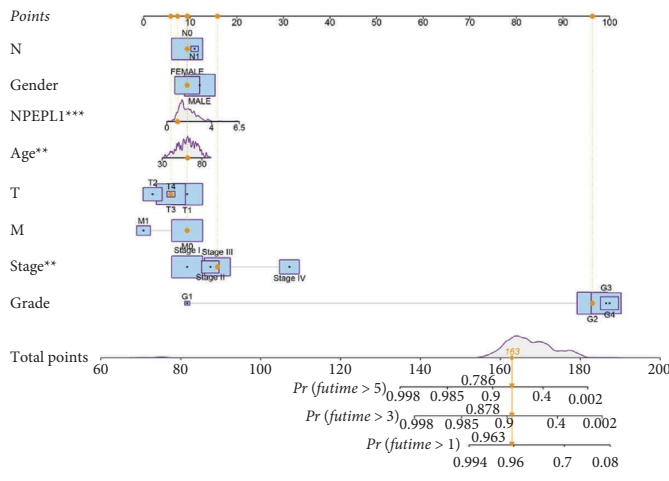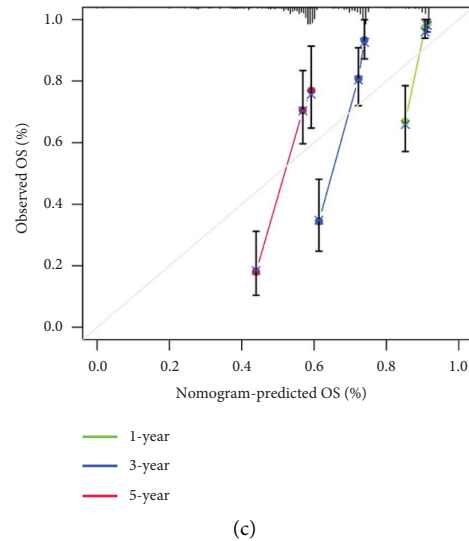
Figure 4: (a) Heatmap showed a significant histologic grade, pathologic stage, and T and M stage between high- and low-expression NPEPL1. (b) Nomogram predicting the probability of patients with OS at 1, 3, and 5 years. (c) The calibration curve shows the actual and predicted survival rates.

Table 3: The impact of high and low NPEPL1 expression for clinicopathologic parameters.

Characteristics	Total (N)	Odds ratio (OR)	P value
T stage (T3&T4 vs. T1&T2)	539	2.354 (1.640–3.398)	<0.001
N stage (N1 vs. N0)	257	1.826 (0.657–5.515)	0.258
M stage (M1 vs. M0)	506	2.195 (1.340–3.658)	0.002
Age (>60 vs. ≤60)	539	0.737 (0.525–1.034)	0.078
Gender (male vs. female)	539	0.942 (0.660–1.344)	0.741
Pathologic stage (stage III and stage IV vs. stage I and stage II)	536	2.345 (1.643–3.363)	<0.001
Histologic grade (G3&G4 vs. G1&G2)	531	1.766 (1.253–2.496)	0.001

regulatory T cells and follicular helper T cells were significantly positively associated with the expression of NPEPL1, while resting mast cells were associated with a significant negative correlation with NPEPL1 expression (Figures 7(b)–7(d)).

3.8. Immune Microenvironment and Checkpoints Related with NPEPL1. The analysis of the immune microenvironment identified that high NPEPL1 expression correlated with a high immune score in violin plots, which implied that NPEPL1 could increase immune activity rather than stromal activity to promote the progression of ccRCC (Figure 7(e)). Furthermore, the immune checkpoints related to NPEPL1 were also drawn in a heatmap, in which red meant positive correlation and blue meant negative correlation (Figure 7(f)). The TNFRSF25 and TNFSF14 presented a positive correlation with NPEPL1, while the NRP1 and TNFSF15 had a negative correlation with NPEPL1. These results identified that high NPEPL1 may affect the progression of ccRCC by changing the immune microenvironment.

3.9. Drugs Sensitivity of NPEPL1. Checkpoint inhibitors monotherapy and combination therapy with target drugs,

and chemotherapy have been the main therapy methods for ccRCC. We also tried to predict whether the NPEPL1 expression was related to sensitivity of ccRCC patients to checkpoint inhibitors, chemotherapeutic agents and common targeted drugs. We found that two groups had a significant difference in response to ctla-4_pos_pd1_neg and ctla-4_pos_pd1_pos, which powerfully predicted that patients with different NPEPL1 expression had a significantly different immunotherapy response (Figures 8(a) and 8(b)). Patients with high NPEPL1 expression had lower IC50 for axitinib ($P < 0.001$, Figure 8(c)), cisplatin ($P < 0.0001$, Figure 8(d)), and GSK429286A ($P < 0.001$, Figure 8(e)), which implied that patients were more sensitive to these drugs. However, the patients with high NPEPL1 expression were not sensitive for rapamycin, sunitinib, and pazopanib, whose IC_{50} was lower in low NPEPL1 expression (Figures 8(f)–8(h)).

4. Discussion

Clear cell RCC is the common type of RCC, which is highly malignant with poor prognosis and remains difficult to predict and treat. Monotherapy or combination therapy based on immunotherapy has become the standard

(a)
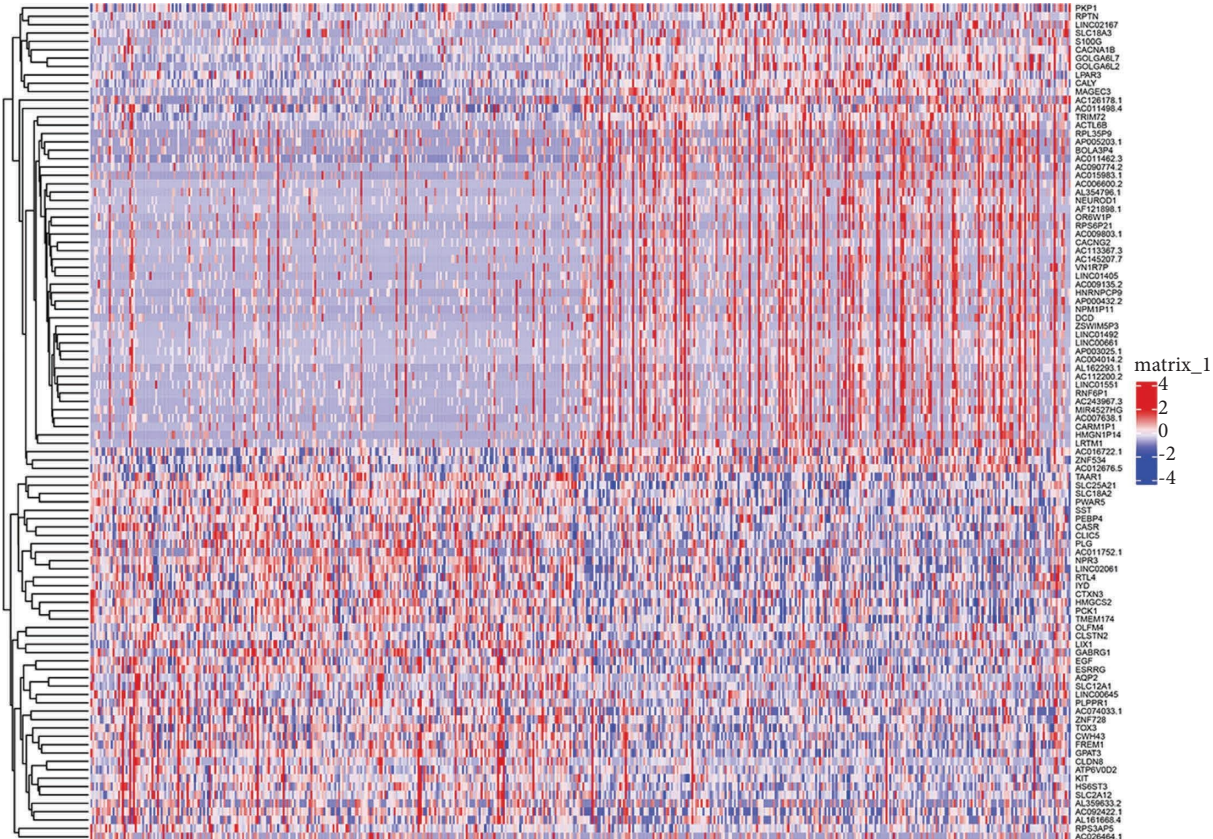
Figure 5: Continued.

(b)

FIGURE 5: Continued.

(c)
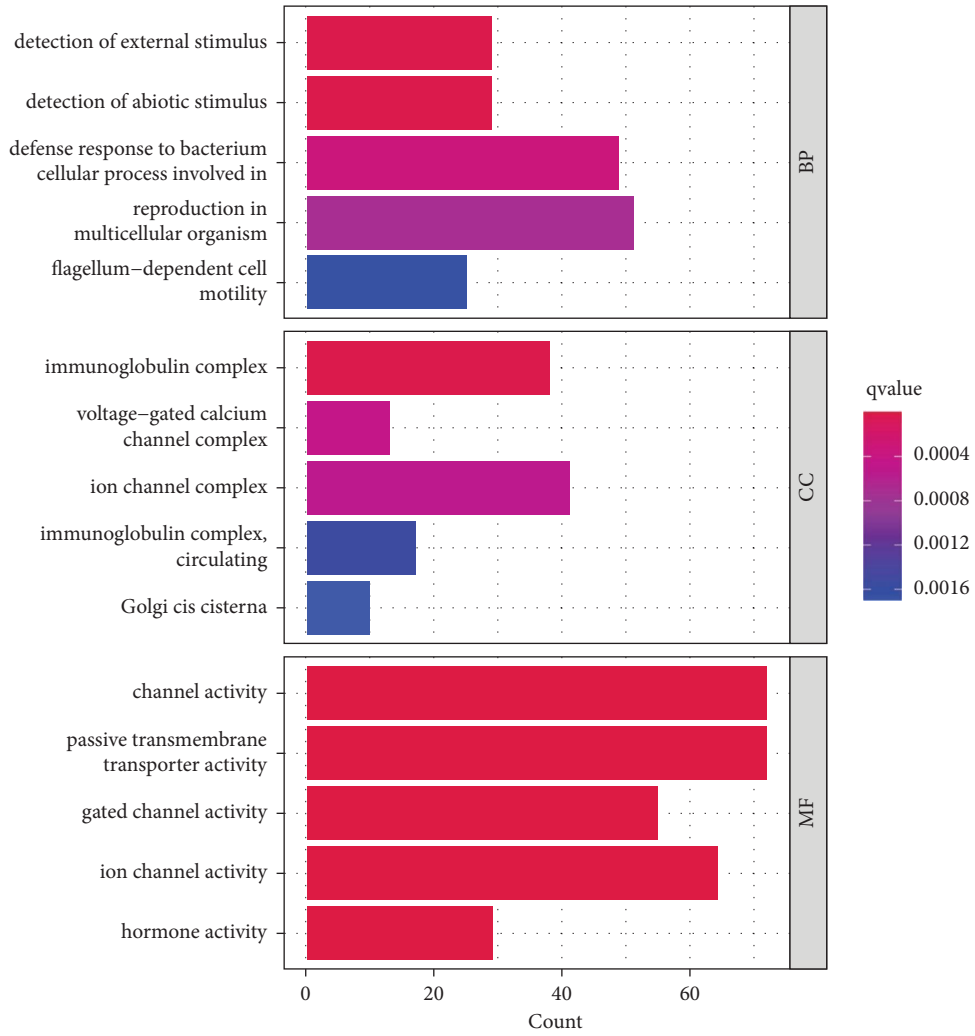
FIGURE 5: Continued.

(d)
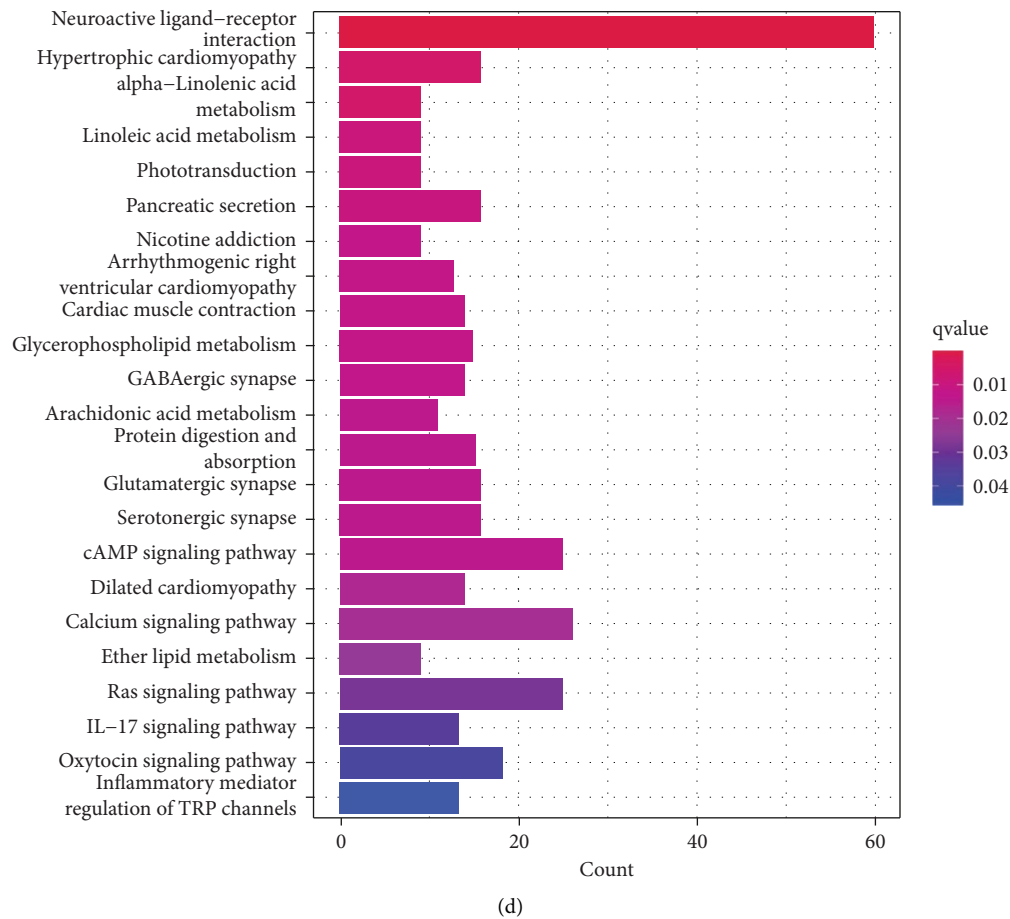
Figure 5: (a) Heatmap of differential expression genes between high- and low-expression NPEPL1. (b, c) Enrichment of DEG for biological processes (BP), cellular components (CC), and molecular functions (MF). (d) KEGG enrichment pathway of DEGs.

treatment strategy for ccRCC, and patients with similar clinical features and the same treatment may have different prognoses [22–24]. Individualized treatment approaches based on the patient's characteristics are important in improving the patient's prognosis. Therefore, it is essential to look for relevant markers to predict prognosis and clarify clinical outcomes after systematic treatment.

The mRNA NPEPL1 is located on chromosome 20q13.32 and encodes probable aminopeptidase-1, whose main function includes manganese ion binding and metalloexopeptidase activity. In the previous study, NPEPL1 had functions in the development and progression of prostate cancer and breast cancer [14–17]. Moreover, NPEPL1 is adjacent to STX16, and the transcript STX16-NPEPL1 is allowed to emerge. The read-through transcript is related to gastrointestinal tumorigenesis and rare pseudohypoparathyroidism [19, 20]. However, the functions of NPEPL1 in the prognosis and treatment of ccRCC were not clear. This study sought to elucidate the character of NPRPL1 in ccRCC.

First, we found that mRNA NPEPL1 was differentially expressed between normal tissues and tumor tissues in different organs via pan-cancer analysis. We also used the TCGA database to analyze the relation between NPEPL1

expression and the clinicopathological features of ccRCC. NPEPL1 expression was higher in ccRCC tissues, and the expression increased gradually with the increase in tumor grade and stage. The HPA database also confirmed that the protein of NPEPL1 was more detectable in tumor tissue. Kaplan–Meier curves were applied to predict the prognosis of ccRCC patients between low and high NPEPL1 expression groups and indicated that the high NPEPL1 expression group had a poor prognosis. The multivariate logistic regression analysis indicated that high NPEPL1 expression was an independent prognostic factor.

Next, the GO analysis was mostly abundant in "detection of external stimulus," "voltage-gated calcium channel complex," "ion channel complex," and "channel activity." The abnormal activity of channels in a cell member may cause the occurrence of renal cell carcinoma, especially in calcium channels and transient receptor potential (TRP) channels [25–27]. The calcium channel and TRP channels activity broke the balance of proangiogenic and antiangiogenic factors, which could shift towards proangiogenic function [28]. The calcium entry across the plasma membrane accelerated the angiogenesis process by stimulating mature ECs, and TRP channels provided the pathway for the calcium entry signal. The related channel activity also played

(a)

(b)

(c)

(d)

(e)

(f)

(g)

(h)

(i)

(j)

(k)

(l)
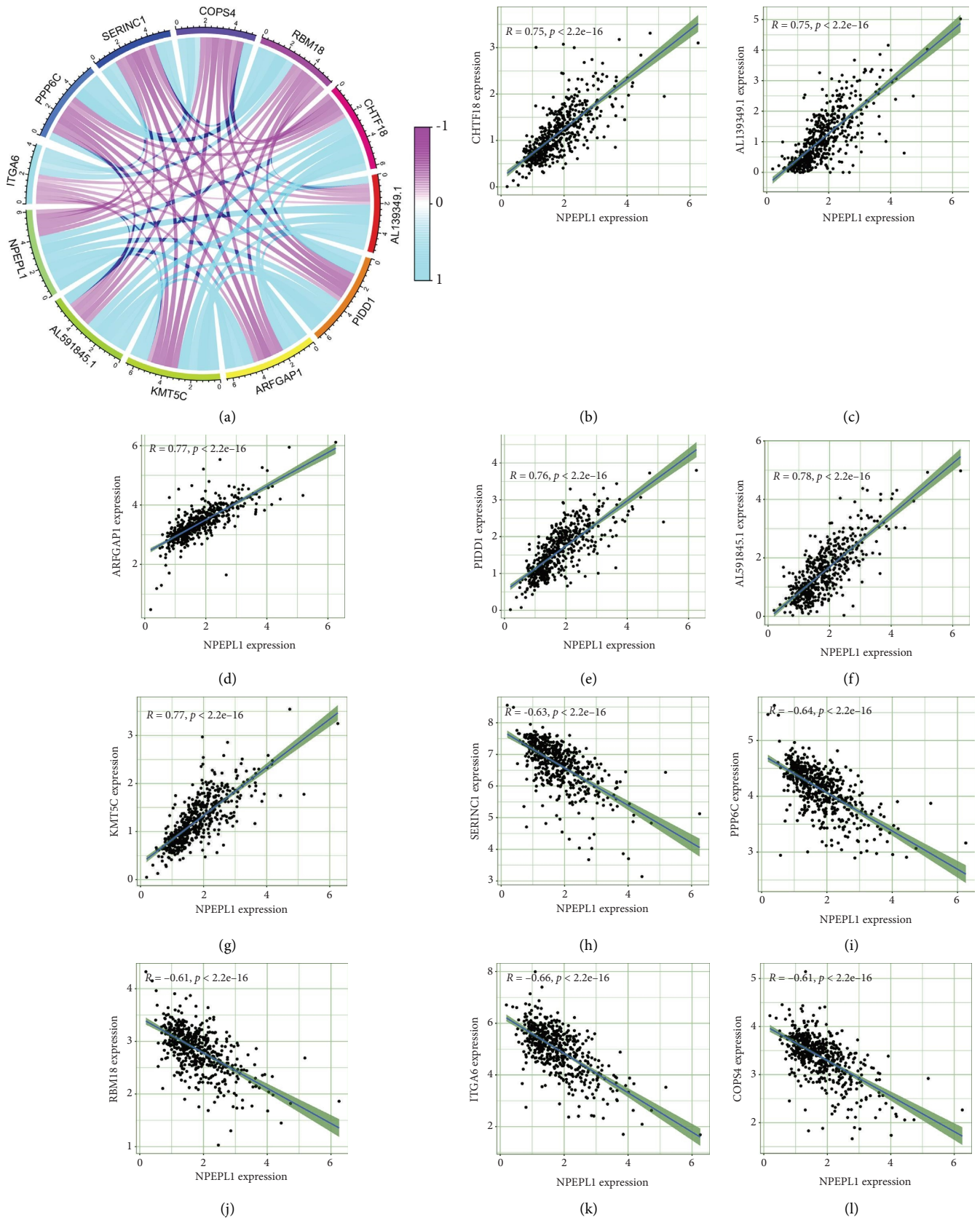
FIGURE 6: (a) Correlation analysis of NPEPL1 expression. The association of NPEPL1 with the top eleven core genes includes CHTF18 (b), AL139349.1 (c), ARFGAP1 (d), PIDD1 (e), AL591845.1 (f), KMT5C (g), SERINC1 (h), PPP6C (i), RBM18 (j), ITGA6 (k), and COPS4 (l).
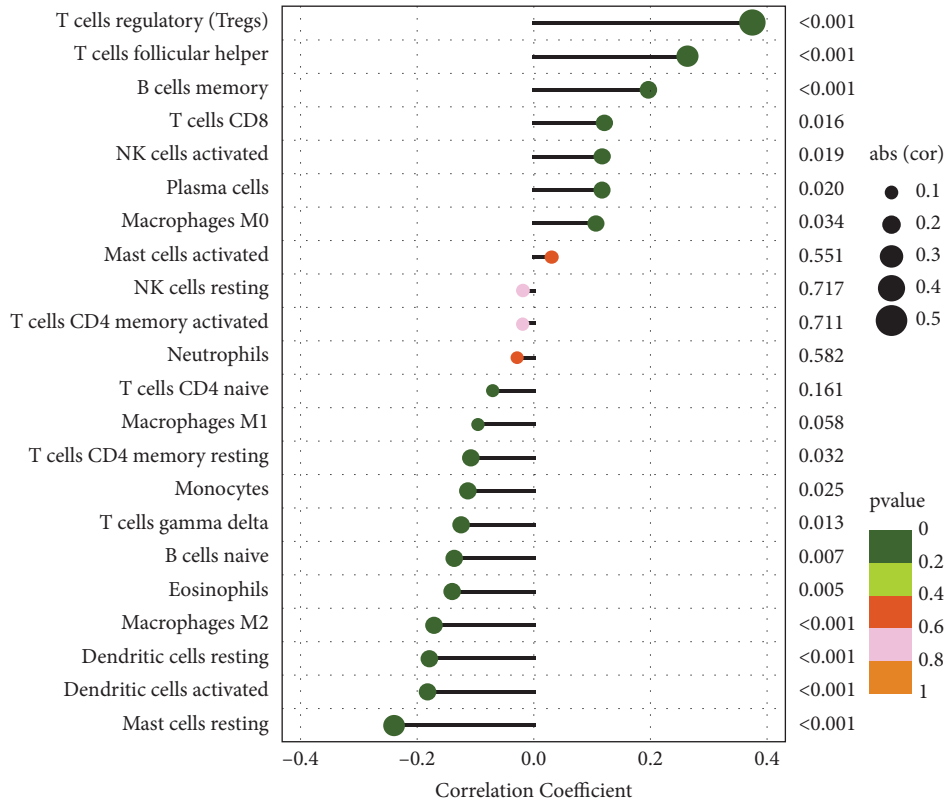
(a)
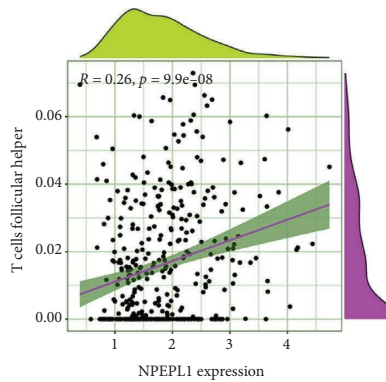
(b)
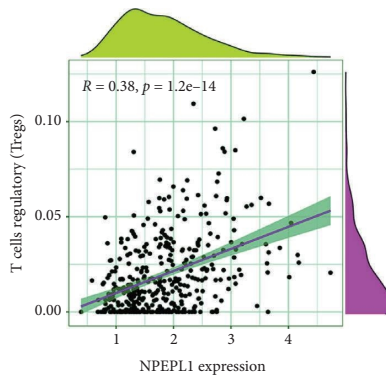
(c)

Figure 7: Continued.

(d)

(e)

(f)
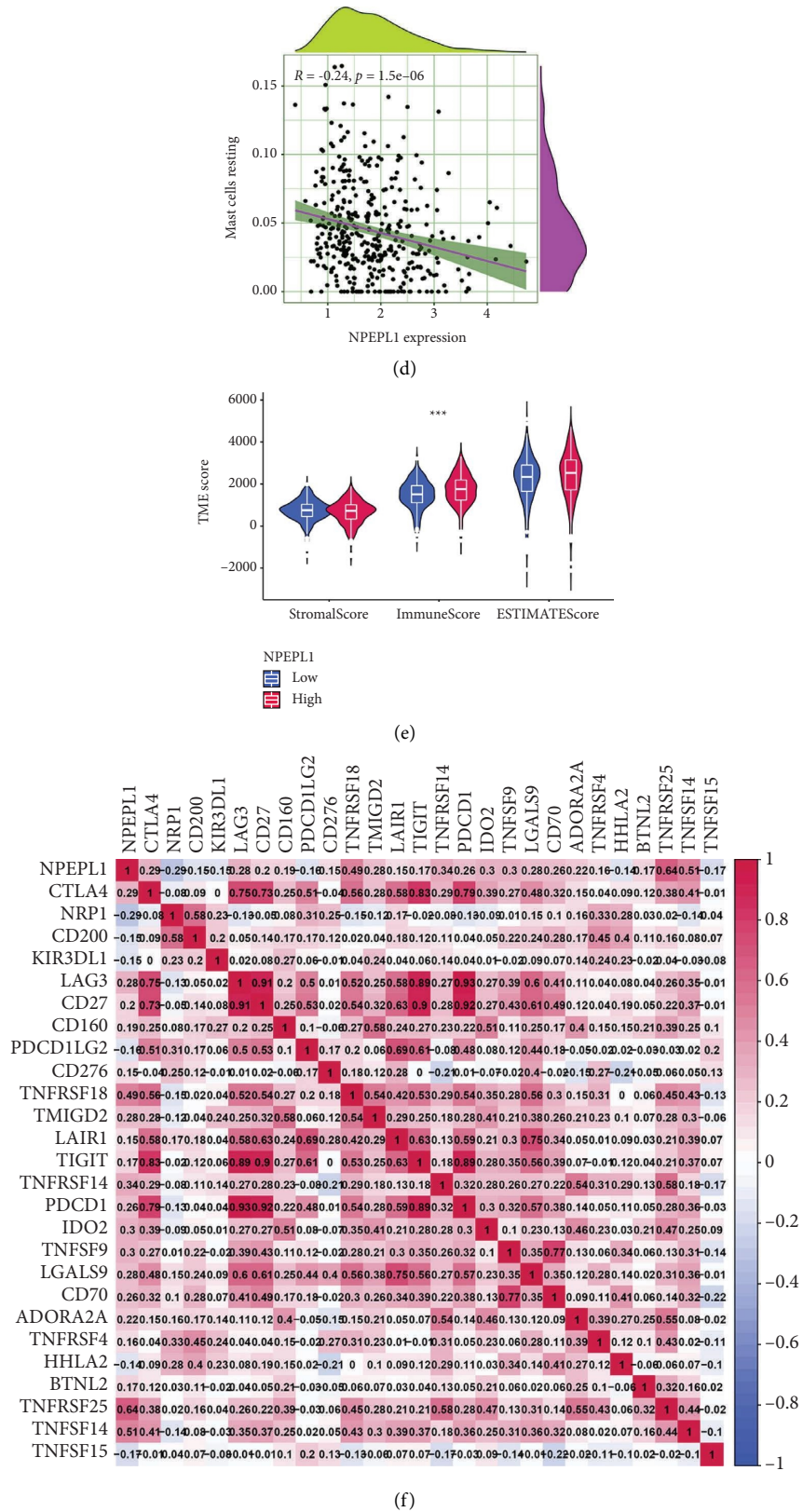
Figure 7: (a) Forest plot of NPEPL1 expression correlation with 24 immune cells. The scatter plot of the correction between NPEPL1 expression and immune cell regulation includes regulatory T cells (b), follicular helper T cells (c), and resting mast cells (d). The pink line in each scatter plot is a fitting linear model, suggesting a significant correlation between immune cells and NPEPL1 expression. (e) The immune microenvironment between high and low expression of NPEPL1, including stromal score, immune score, and ESTIMATE score. (f) Heatmap of immune checkpoints related with NPEPL1.
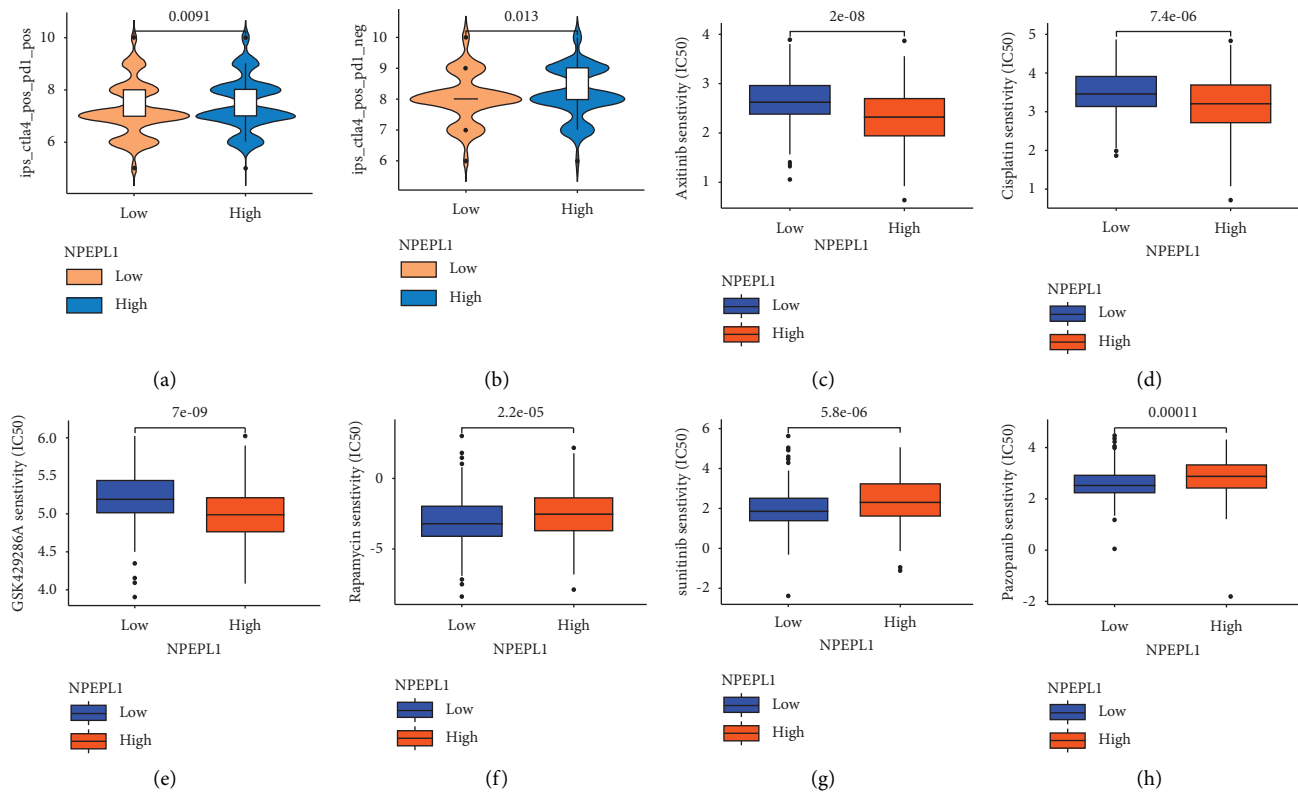
Figure 8: Analysis of drugs susceptibility. Sensitivity to immunotherapy (a, b), axitinib (c), cisplatin (d), GSK429286A (e), rapamycin (f), sunitinib (g), and pazopanib (h).

important roles in drug resistance resisting cell death, tumor stem cell differentiation, tumor microenvironment alteration, and tumors evading immune destruction [29–32]. The blocks of calcium channels and TRP channels were used to decrease occurrence risk of RCC, relieve drug resistance, and improve patient prognosis [33, 34]. Moreover, KEGG analysis was mainly concentrated on protein digestion and absorption, the cAMP signaling pathway, the calcium signaling pathway, and the Ras signaling pathway. The abnormal function of protein digestion and absorption following NPEPL1 expression dysregulation promoted invasion, migration, and drug resistance in ccRCC [35, 36]. With the in-depth understanding of the mechanism of ccRCC development, cAMP and the Ras signaling pathway played a crucial role in regulating biological behaviors [37, 38]. Regulation of some crucial signaling pathways could modulate the growth, invasion, migration, and drug resistance of tumor, become a new target of treatment, and improve the prognosis of tumor patients [39–41].

The eleven proteins coexpressed with NPEPL1 were identified, with six proteins upregulated and five proteins downregulated with the increase in NPEPL1 expression. Among them, PIDD1 has proved to play a positive role with an increase in stage in RCC patients [42]. The expression of SERINC1 exerted a protective effect in the progression of RCC, and ITGA6 expression may be a main factor in the treatment of drug-resistant RCC with valproic acid and interferon-alpha [43, 44]. Although CHTF18 and KMT5C have not been shown to correlate

with RCC, they played a role in the development of other tumors; abnormalities in CHTF18 promoted endometrial carcinoma, and KMT5C played a role in non-small cell lung cancer [45, 46].

Tumor immune cell infiltration has been approved to be associated with the prognosis of ccRCC and the response to immunotherapy [47, 48]. The importance of some infiltrating immune cells has been confirmed, including regulatory T cells, CD8 T cells, NK cells, and resting mast cells [49–52]. The immune cell infiltration analysis between high and low NPEPL1 expression also revealed differences in immune cells similar to previous studies. Interestingly, the infiltration level of CD8T cell was high in patients with high NPEPL1 expression, and CD8T cells were a kind of antitumor immune cell [53]. Regulatory T cells, which have a negative effect on antitumor activity, had a higher infiltration level in high NPEPL1 expression patients [54]. These results showed that the immune regulation in tumor tissues was multidirectional, and the antitumor effect was offset by a stronger immunosuppressive environment in patients with high expression of NPEPL1. Moreover, immune checkpoints (TNFRSF25 and TNFSF14) were positively correlated with NPEPL1, which was a prognostic factor of ccRCC and had been confirmed by previous studies [55, 56]. TNFRSF25 could increase the proliferation of regulatory T cells [57–59]. TNFSF15, as the ligand of TNFRSF25, presented a negative correlation with NPEPL1 and played a negative role in regulatory T cells' suppressive ability [57–60]. The inhibitory ability of regulatory T cells

was promoted by suppression of TNFSF15 and TNFRSF25 expression. Above all, NPEPL1 expression regulated the distribution of immune cells in tumor tissues through immune checkpoints, which affected the occurrence and development of ccRCC.

ICIs have been proven to play a significant effect in solid tumors, and the activation of tumor immune microenvironment can improve the outcome of ICIs treatment. We found that low and high NPEPL1 expression groups had a significant difference in response to ctla-4_pos_pd1_neg and ctla-4_pos_pd1_pos, which powerfully predicted that patients with different NPEPL1 expression had a significantly different immunotherapy response. Besides, the low NPEPL1 expression group was more sensitive to rapamycin, sunitinib, and pazopanib; the high NPEPL1 expression group was more sensitive to axitinib, cisplatin, and GSK429286A. Axitinib, sunitinib, and pazopanib were all ATP-competitive inhibitors of vascular endothelial growth factor receptors (VEGFRs), which were approved to treat RCC by the FDA [61]. The high NPEPL1 expression group was more sensitive to axitinib, since axitinib was more selective for VEGFRs but not PDGFRs, B-Raf, c-Kit, or Flt-3 [62, 63].

All in all, NPEPL1 expression was upregulated in ccRCC tissues compared to normal tissues and increased with the development and progression of ccRCC. The high NPEPL1 expression was related to poor prognosis and immune responses. Some potential limitations were not ignored in our study. First, more clinical samples were required to confirm that NPEPL1 was an important prognostic factor in ccRCC. Second, the mechanism of NPEPL1 in the development and progression of ccRCC was necessary to identify. Third, the interaction between NREPL1 expression and immune cell infiltration needs to be confirmed by more studies.

5. Conclusion

We confirmed the prognostic value of high NPEPL1 expression in ccRCC, which was upregulated with development and progression. NPEPL1 expression plays certain roles in metastasis, metabolism, and the immune microenvironment in ccRCC. We also predicted that patients with high NPEPL1 expression would be more sensitive to some common drugs, including axitinib, cisplatin, and GSK429286A. NPEPL1 could be regarded as a prognostic predictor and therapeutic target in ccRCC patients and guide clinical medication.

Data Availability

The datasets generated during and/or analyzed during the current study are available from the TGCA dataset and HPA dataset.

Disclosure

Xiaoyu Wei and Zhongbao Zhou are the co-first authors. Fengze Sun is the first corresponding author of this article, and Guikai Ma is the co-corresponding author of this article.

Conflicts of Interest

The authors declare that they have no conflicts of interest.

Authors' Contributions

SFZ and MGK designed the research, interpreted the data, and revised the paper. WXY, ZZB, MGK, and SFZ extracted the data and drew the picture. WXY and ZZB drafted the paper. All the authors approved the submitted and final versions. Xiaoyu Wei and Zhongbao Zhou contributed equally to this work.

References

[1] R. L. Siegel, K. D. Miller, and A. Jemal, "Cancer statistics," *CA: A Cancer Journal for Clinicians*, vol. 69, no. 1, pp. 7–34, 2019.

[2] J. J. Hsieh, M. P. Purdue, S. Signoretti et al., "Renal cell carcinoma," *Nature Reviews Disease Primers*, vol. 3, no. 1, Article ID 17009, 2017.

[3] L. D. Truong and S. S. Shen, "Immunohistochemical diagnosis of renal neoplasms," *Archives of Pathology & Laboratory Medicine*, vol. 135, no. 1, pp. 92–109, 2011.

[4] M. M. Wolf, W. Kimryn Rathmell, and K. E. Beckermann, "Modeling clear cell renal cell carcinoma and therapeutic implications," *Oncogene*, vol. 39, no. 17, pp. 3413–3426, 2020.

[5] L. Bella, S. Zona, G. Nestal de Moraes, and E. W. F. Lam, "FOXM1: a key oncofoetal transcription factor in health and disease," *Seminars in Cancer Biology*, vol. 29, pp. 32–39, 2014.

[6] C. M. Díaz-Montero, B. I. Rini, and J. H. Finke, "The immunology of renal cell carcinoma," *Nature Reviews Nephrology*, vol. 16, no. 12, pp. 721–735, 2020.

[7] R. Motzer, B. Alekseev, S. Y. Rha et al., "Lenvatinib plus pembrolizumab or everolimus for advanced renal cell carcinoma," *New England Journal of Medicine*, vol. 384, no. 14, pp. 1289–1300, 2021.

[8] T. K. Choueiri, T. Powles, M. Burotto et al., "Nivolumab plus cabozantinib versus sunitinib for advanced renal-cell carcinoma," *New England Journal of Medicine*, vol. 384, no. 9, pp. 829–841, 2021.

[9] S. A. Holstein, C. A. Heckman, F. E. Davies, G. J. Morgan, S. S. Gelius, and F. Lehmann, "Review: aminopeptidases in cancer, biology and prospects for pharmacological intervention," *Current Cancer Drug Targets*, vol. 23, no. 1, pp. 25–46, 2022.

[10] Q. Ren, S. Fu, D. Wang, W. Ju, and X. He, "Prognostic value of preoperative serum leucine aminopeptidases in hepatocellular carcinoma patients who underwent liver transplantation," *Cancer Management and Research*, vol. 13, pp. 1053–1066, 2021.

[11] T. Otsuki, T. Nakashima, H. Hamada et al., "Aminopeptidase N/CD13 as a potential therapeutic target in malignant pleural mesothelioma," *European Respiratory Journal*, vol. 51, no. 5, Article ID 1701610, 2018.

[12] J. Cao, C. Zhao, H. Dong, Q. Xu, and Y. Zhang, "Development of pyrazoline-based derivatives as aminopeptidase N inhibitors to overcome cancer invasion and metastasis," *RSC Advances*, vol. 11, no. 35, Article ID 21426, 2021.

[13] K. Flanagan, R. Kumari, J. J. Miettinen et al., "The peptide-drug conjugate melflufen modulates the unfolded protein response of multiple myeloma and amyloidogenic plasma cells and induces cell death," *HemaSphere*, vol. 6, no. 3, Article ID e687, 2022.

[14] A. J. Zhang, B. Zhang, Z. Zhang, H. Hu, and J. T. Dong, "Novel gene signatures predictive of patient recurrence-free survival and castration resistance in prostate cancer," *Cancers*, vol. 13, no. 4, p. 917, 2021.

[15] M. Ouchida, H. Kanzaki, S. Ito et al., "Novel direct targets of miR-19a identified in breast cancer cells by a quantitative proteomic approach," *PLoS One*, vol. 7, no. 8, Article ID e44095, 2012.

[16] P. Shen, L. Qu, J. Wang et al., "LncRNA LINC00342 contributes to the growth and metastasis of colorectal cancer via targeting miR-19a-3p/NPEPL1 axis," *Cancer Cell International*, vol. 21, no. 1, p. 105, 2021.

[17] K. Wallander, J. Thutkawkorapin, E. Sahlin, A. Lindblom, and K. Lagerstedt-Robinson, "Massive parallel sequencing in a family with rectal cancer," *Hereditary Cancer in Clinical Practice*, vol. 19, no. 1, p. 23, 2021.

[18] X. Meng, J. Li, Q. Zhang et al., "Multivariate genome wide association and network analysis of subcortical imaging phenotypes in Alzheimer's disease," *BMC Genomics*, vol. 21, no. S11, p. 896, 2020.

[19] G. Kang, H. Yun, C. H. Sun et al., "Integrated genomic analyses identify frequent gene fusion events and VHL inactivation in gastrointestinal stromal tumors," *Oncotarget*, vol. 7, no. 6, pp. 6538–6551, 2016.

[20] Y. Yang, X. Chu, M. Nie et al., "A novel long-range deletion spanning STX16 and NPEPL1 causing imprinting defects of the GNAS locus discovered in a patient with autosomal-dominant pseudohypoparathyroidism type 1B," *Endocrine*, vol. 69, no. 1, pp. 212–219, 2020.

[21] Z. Zhou, Y. Zhou, X. Zhou, Y. Huang, Y. Cui, and Y. Zhang, "Downregulation of PTCD1 in bladder urothelial carcinoma predicts poor prognosis and levels of immune infiltration," *Journal of oncology*, vol. 2022, Article ID 1146186, 16 pages, 2022.

[22] A. K. A. Lalani, B. A. McGregor, L. Albiges et al., "Systemic treatment of metastatic clear cell renal cell carcinoma in 2018: current paradigms, use of immunotherapy, and future directions," *European Urology*, vol. 75, no. 1, pp. 100–110, 2019.

[23] L. Albiges, N. M. Tannir, M. Burotto et al., "First-line nivolumab plus ipilimumab versus sunitinib in patients without nephrectomy and with an evaluable primary renal tumor in the CheckMate 214 trial," *European Urology*, vol. 81, no. 3, pp. 266–271, 2022.

[24] J. Bedke, L. Albiges, U. Capitanio et al., "The 2021 updated European association of Urology guidelines on renal cell carcinoma: immune checkpoint inhibitor-based combination therapies for treatment-naive metastatic clear-cell renal cell carcinoma are standard of care," *European Urology*, vol. 80, no. 4, pp. 393–397, 2021.

[25] M. Rabjerg, A. Oliván-Viguera, L. K. Hansen et al., "High expression of KCa3.1 in patients with clear cell renal carcinoma predicts high metastatic risk and poor survival," *PLoS One*, vol. 10, no. 4, Article ID e0122992, 2015.

[26] J. Song, Y. Wang, X. Li et al., "Critical role of TRPC6 channels in the development of human renal cell carcinoma," *Molecular Biology Reports*, vol. 40, no. 8, pp. 5115–5122, 2013.

[27] D. P. Hall, N. G. Cost, S. Hegde et al., "TRPM3 and miR-204 establish a regulatory circuit that controls oncogenic autophagy in clear cell renal cell carcinoma," *Cancer Cell*, vol. 26, no. 5, pp. 738–753, 2014.

[28] F. Moccia, S. Dragoni, V. Poletto et al., "Orai1 and transient receptor potential channels as novel molecular targets to impair tumor neovascularization in renal cell carcinoma and other malignancies," *Anti-Cancer Agents in Medicinal Chemistry*, vol. 14, no. 2, pp. 296–312, 2014.

[29] M. Flourakis, V. Lehen'kyi, B. Beck et al., "Orai1 contributes to the establishment of an apoptosis-resistant phenotype in prostate cancer cells," *Cell Death & Disease*, vol. 1, no. 9, e75 pages, 2010.

[30] J. Yu, S. Wang, W. Zhao et al., "Mechanistic exploration of cancer stem cell marker voltage-dependent calcium channel $\alpha 2\delta 1$ subunit-mediated chemotherapy resistance in small-cell lung cancer," *Clinical Cancer Research*, vol. 24, no. 9, pp. 2148–2158, 2018.

[31] L. J. Sang, H. Q. Ju, G. P. Liu et al., "LncRNA CamK-A regulates Ca(2+)-signaling-mediated tumor microenvironment remodeling," *Molecular Cell*, vol. 72, no. 3, p. 601, 2018.

[32] E. C. Schwarz, B. Qu, and M. Hoth, "Calcium, cancer and killing: the role of calcium in killing cancer cells by cytotoxic T lymphocytes and natural killer cells," *Biochimica et Biophysica Acta (BBA) - Molecular Cell Research*, vol. 1833, no. 7, pp. 1603–1611, 2013.

[33] G. H. Mickisch, J. Kössig, R. K. Tschada, G. Keilhauer, E. Schlick, and P. M. Alken, "Circumvention of multidrug resistance mediated by P-170 glycoprotein using calcium antagonists in primary human renal cell carcinoma," *Urologia Internationalis*, vol. 47, no. 3, pp. 118–125, 1991.

[34] K. B. Kristensen, L. A. Habel, J. J. Gagne et al., "Risk of renal cell carcinoma associated with calcium channel blockers: a nationwide observational study focusing on confounding by indication," *Epidemiology*, vol. 31, no. 6, pp. 860–871, 2020.

[35] R. Yin and S. Liu, "SHARPIN regulates the development of clear cell renal cell carcinoma by promoting von Hippel-Lindau protein ubiquitination and degradation," *Cancer Science*, vol. 112, no. 10, pp. 4100–4111, 2021.

[36] H. Huang, Y. Gao, A. Liu et al., "EIF3D promotes sunitinib resistance of renal cell carcinoma by interacting with GRP78 and inhibiting its degradation," *EBioMedicine*, vol. 49, pp. 189–201, 2019.

[37] K. Hui, Y. Yue, S. Wu et al., "The expression and function of RASAL2 in renal cell carcinoma angiogenesis," *Cell Death & Disease*, vol. 9, no. 9, 881 pages, 2018.

[38] B. Zhang, N. Sun, X. Mu et al., "G protein alpha S subunit promotes cell proliferation of renal cell carcinoma with involvement of protein kinase A signaling," *DNA and Cell Biology*, vol. 36, no. 3, pp. 237–242, 2017.

[39] S. Sinha, N. Dwivedi, S. Tao et al., "Targeting the vasopressin type-2 receptor for renal cell carcinoma therapy," *Oncogene*, vol. 39, no. 6, pp. 1231–1245, 2020.

[40] S. Wang, X. Hao, S. He, C. Liu, and Q. Wang, "Suppressive effects of RASAL2 on renal cell carcinoma via SOX2/ERK/p38 MAPK pathway," *Experimental and Therapeutic Medicine*, vol. 20, no. 6, p. 151, 2020.

[41] M. Cao, K. Nawalaniec, A. K. Ajay et al., "PDE4D targeting enhances anti-tumor effects of sorafenib in clear cell renal cell carcinoma and attenuates MAPK/ERK signaling in a CRAF-dependent manner," *Translational oncology*, vol. 19, Article ID 101377, 2022.

[42] S. Heikaus, I. Pejin, H. E. Gabbert et al., "PIDDosome expression and the role of caspase-2 activation for chemotherapy-induced apoptosis in RCCs," *Analytical Cellular Pathology*, vol. 32, no. 1-2, pp. 29–42, 2010.

[43] Y. Sun, Y. Xu, X. Che, and G. Wu, "Development of a novel sphingolipid signaling pathway-related risk assessment model to predict prognosis in kidney renal clear cell carcinoma," *Frontiers in Cell and Developmental Biology*, vol. 10, Article ID 881490, 2022.

[44] E. Juengel, M. Bhasin, T. Libermann et al., "Alterations of the gene expression profile in renal cell carcinoma after treatment with the histone deacetylase-inhibitor valproic acid and interferon-alpha," *World Journal of Urology*, vol. 29, no. 6, pp. 779–786, 2011.

[45] J. C. Price, L. M. Pollock, M. L. Rudd et al., "Sequencing of candidate chromosome instability genes in endometrial cancers reveals somatic mutations in ESCO1, CHTF18, and MRE11A," *PLoS One*, vol. 8, no. 6, Article ID e63313, 2013.

[46] A. S. Pal, A. Agredo, N. A. Lanman et al., "Loss of KMT5C promotes EGFR inhibitor resistance in NSCLC via linc01510-mediated upregulation of MET," *Cancer Research*, vol. 82, no. 8, pp. 1534–1547, 2022.

[47] D. A. Braun, Y. Hou, Z. Bakouny et al., "Interplay of somatic alterations and immune infiltration modulates response to PD-1 blockade in advanced clear cell renal cell carcinoma," *Nature Medicine*, vol. 26, no. 6, pp. 909–918, 2020.

[48] S. Zhang, E. Zhang, J. Long et al., "Immune infiltration in renal cell carcinoma," *Cancer Science*, vol. 110, no. 5, pp. 1564–1572, 2019.

[49] C. S. Kim, Y. Kim, T. Kwon et al., "Regulatory T cells and TGF-β1 in clinically localized renal cell carcinoma: comparison with age-matched healthy controls," *Urologic Oncology: Seminars and Original Investigations*, vol. 33, no. 3, Article ID 113.e19, 2015.

[50] A. Ziblat, X. L. R. Iraolagoitia, S. Y. Nuñez et al., "Circulating and tumor-infiltrating NK cells from clear cell renal cell carcinoma patients exhibit a predominantly inhibitory phenotype characterized by overexpression of CD85j, CD45, CD48 and PD-1," *Frontiers in Immunology*, vol. 12, Article ID 681615, 2021.

[51] X. Wu, D. Jiang, H. Liu, X. Lu, D. Lv, and L. Liang, "CD8(+) T cell-based molecular classification with heterogeneous immunogenomic landscapes and clinical significance of clear cell renal cell carcinoma," *Frontiers in Immunology*, vol. 12, Article ID 745945, 2021.

[52] G. Zhu, L. Pei, H. Yin et al., "Profiles of tumor-infiltrating immune cells in renal cell carcinoma and their clinical implications," *Oncology Letters*, vol. 18, no. 5, pp. 5235–5242, 2019.

[53] S. S. Tykodi, S. Satoh, J. D. Deming, J. Chou, R. Harrop, and E. H. Warren, "CD8+T-cell clones specific for the 5T4 antigen target renal cell carcinoma tumor-initiating cells in a murine xenograft model," *Journal of Immunotherapy*, vol. 35, no. 7, pp. 523–533, 2012.

[54] Y. Takeuchi and H. Nishikawa, "Roles of regulatory T cells in cancer immunity," *International Immunology*, vol. 28, no. 8, pp. 401–409, 2016.

[55] F. Xu, Y. Guan, P. Zhang et al., "The impact of TNFSF14 on prognosis and immune microenvironment in clear cell renal cell carcinoma," *Genes & genomics*, vol. 42, no. 9, pp. 1055–1066, 2020.

[56] R. S. Al-Lamki, J. Wang, J. S. Pober, and J. R. Bradley, "Co-expression and functional interactions of death receptor 3 and E-selectin in clear cell renal cell carcinoma," *American Journal Of Pathology*, vol. 192, no. 4, pp. 722–736, 2022.

[57] F. Meylan, Y. J. Song, I. Fuss et al., "The TNF-family cytokine TL1A drives IL-13-dependent small intestinal inflammation," *Mucosal Immunology*, vol. 4, no. 2, pp. 172–185, 2011.

[58] V. Y. Taraban, T. J. Slebioda, J. E. Willoughby et al., "Sustained TL1A expression modulates effector and regulatory T-cell responses and drives intestinal goblet cell hyperplasia," *Mucosal Immunology*, vol. 4, no. 2, pp. 186–196, 2011.

[59] T. H. Schreiber, D. Wolf, M. S. Tsai et al., "Therapeutic Treg expansion in mice by TNFRSF25 prevents allergic lung inflammation," *Journal of Clinical Investigation*, vol. 120, no. 10, pp. 3629–3640, 2010.

[60] T. H. Schreiber and E. R. Podack, "Immunobiology of TNFSF15 and TNFRSF25," *Immunologic Research*, vol. 57, no. 1-3, pp. 3–11, 2013.

[61] F. Hofmann, E. C. Hwang, T. B. Lam et al., "Targeted therapy for metastatic renal cell carcinoma," *Cochrane Database of Systematic Reviews*, vol. 10, no. 10, Article ID Cd012796, 2020.

[62] G. Scagliotti and R. Govindan, "Targeting angiogenesis with multitargeted tyrosine kinase inhibitors in the treatment of non-small cell lung cancer," *The Oncologist*, vol. 15, no. 5, pp. 436–446, 2010.

[63] P. Bhargava and M. O. Robinson, "Development of second-generation VEGFR tyrosine kinase inhibitors: current status," *Current Oncology Reports*, vol. 13, no. 2, pp. 103–111, 2011.

Research Article

Comprehensive Molecular Analyses of Notch Pathway-Related Genes to Predict Prognosis and Immunotherapy Response in Patients with Gastric Cancer

Yinsen Song,[1] Na Gao,[2] Zhenzhen Yang,[2] Sisen Zhang,[2] Tianli Fan ⑩,[3] and Baojun Zhang ⑩[4]

[1]*School of Basic Medical Sciences, Xi'an Jiaotong University, Translational Medicine Research Center,*
 Zhengzhou People's Hospital, Zhengzhou, China
[2]*Translational Medicine Research Center, Zhengzhou People's Hospital, Zhengzhou, China*
[3]*School of Basic Medical Sciences, Xi'an Jiaotong University, Zhengzhou People's Hospital, Zhengzhou University,*
 Zhengzhou, China
[4]*Department of Pathogenic Microbiology and Immunology, School of Basic Medical Sciences, Xi'an Jiaotong University,*
 Xi'an, China

Correspondence should be addressed to Baojun Zhang; bj.zhang@mail.xjtu.edu.cn

Gastric cancer (GC) is a highly molecular heterogeneous tumor with unfavorable outcomes. The Notch signaling pathway is an important regulator of immune cell differentiation and has been associated with autoimmune disorders, the development of tumors, and immunomodulation caused by tumors. In this study, by developing a gene signature based on genes relevant to the Notch pathway, we could improve our ability to predict the outcome of patients with GC. From the TCGA database, RNA sequencing data of GC tumors and associated normal tissues were obtained. Microarray data were collected from GEO datasets. The Molecular Signature Database (MSigDB) was accessed in order to retrieve sets of human Notch pathway-related genes (NPRGs). The LASSO analysis performed on the TCGA cohort was used to generate a multigene signature based on prognostic NPRGs. In order to validate the gene signature, the GEO cohort was utilized. Using the CIBERSORT method, we were able to determine the amounts of immune cell infiltration in the GC. In this study, a total of 21 differentially expressed NPRGs were obtained between GC specimens and nontumor specimens. The construction of a prognostic prediction model for patients with GC involved the identification and selection of three different NPRGs. According to the appropriate cutoff value, the patients with GC were divided into two groups: those with a low risk and those with a high risk. The time-dependent ROC curves demonstrated that the new model had satisfactory performance when it came to prognostic prediction. Multivariate assays confirmed that the risk score was an independent marker that may be used to predict the outcome of GC. In addition, the generated nomogram demonstrated a high level of predictive usefulness. Moreover, the scores of immunological infiltration of the majority of immune cells were distinctly different between the two groups, and the low-risk group responded to immunotherapy in a significantly greater degree. According to the results of a functional enrichment study of candidate genes, there are multiple pathways and processes associated with cancer. Taken together, a new gene model associated with the Notch pathway may be utilized for the purpose of predicting the prognosis of GC. One potential method of treatment for GC is to focus on NPRGs.

1. Introduction

Gastric cancer (GC) is one of the most prevalent malignant tumors in the world [1]. GC was ranked as the fifth biggest cancer burden in the world, according to data from the World Health Organization (WHO) [2]. This was based on the estimated occurrence of 1 million cases worldwide [3]. As a result of the late detection of the disease at a more advanced stage, the mortality rate of gastric cancer is significant; for example, in 2020, it was 768,793, which places it

as the fifth most prevalent cause of death due to cancer [4, 5]. Despite the fact that surgery is the primary treatment with the intention of curing the disease, 40%–60% of those patients who undergo resection surgery show disease relapse [6]. The prognosis is not good for these individuals, who have a survival rate of fewer than 10% over a period of 5 years [7, 8]. Patients with GC face an uphill battle when it comes to their prognosis because of intratumoral, interpatient, and intrapatient heterogeneity of the disease [9]. In addition, GC has a predisposition toward early metastasis, and the majority of these metastases are discovered in severe stages. This may be the single most important factor contributing to the high fatality rate of GC patients [10, 11]. As a result, it is essential to locate dependable predictors for the purpose of prognostic estimation, which might provide an incredible amount of guiding value to the administration of the GC. Patients suffering from GC would especially benefit from an improved prognostic prediction if a multiple-gene signature could be constructed.

The Notch signaling system is an intercellular signaling pathway that has been largely conserved throughout evolution. It is responsible for regulating cell proliferation and differentiation, determining cell fate decision, and participating in cellular activity in both embryonic and adult tissues [12, 13]. It is essential to have a good understanding of the structure of Notch proteins and the signaling pathways that are associated with them, since they are involved in the control of the promotion, proliferation, and development of cancer [14, 15]. Transmembrane glycoproteins make up Notch receptors, which range in the number from 1 to 4. Notch receptors have three distinct regions: an extracellular domain, a transmembrane domain, and an intramembrane or cytoplasmic region [16]. The extracellular domain is located outside of the cell. The activation of oncogenic signaling pathways makes aggressive GC harder to treat. One such pathway is the Notch signaling pathway. Notch signaling is an important mechanism in the process of the self-renewal of stem cells, the determination of cell fate and differentiation during embryonic and postnatal development, and the maintenance of adult cell homeostasis [17, 18]. Until now, it is not clear whether each Notch component acts as an oncogene or a tumor suppressor. This is a contentious issue. Researchers also focused on the connection between the Notch signaling pathway and stomach cancer [19, 20]. Although a rapidly expanding number of linked outcomes have been developed, conclusions are still debatable. For example, in contrast to conventional wisdom, researchers found that the expression of Notch 1 was lower in stomach cancers than that in normal tissue.

There is an increasing body of research studies suggesting that the tumor microenvironment (TME) plays an important part in the progression of tumors [21]. It is possible to divide solid tumors into two categories: immunologically hot tumors and cold tumors [22]. Cancer immunotherapy is successful in treating hot tumors, whereas the treatment is ineffective against cold tumors [23]. Cancers that are immunologically inert have a few mutations, a limited invasion of cytotoxic immune cells, and a substantial population of myeloid-derived suppressor cells [24, 25]. As a consequence, reactions seen in clinical trials involving immune checkpoint blockade (ICB) are poorer in immunologically cold tumors [26]. However, preliminary research has demonstrated that it is possible for cool tumors to become heated ones. Therefore, it is of the utmost importance to discover the comprehensive mechanism that lies at the root of immunologically cold tumors, as this would aid in the development of a method for bringing cold tumors up to temperature and turning them into hot tumors.

In this study, we built a predictive signature using genes related to Notch pathway-related genes (NPRGs), evaluated its utility for determining outcomes, diagnosis, treatment responses, and tumor immune infiltration of GC patients, and carried out internal verification. In addition, we accomplished functional enrichment analysis (GSEA) in order to investigate possible mechanisms.

2. Materials and Methods

2.1. Raw Data.
The data on RNA sequencing and clinical information related to STAD patients were received from the TCGA data portal. For the purpose of developing the risk model, the TCGA-STAD cohort served as the "training cohort," while the microarray data obtained from the GEO database was applied to the "validation cohort." We collected RNA-sequencing data on the TCGA-STAD cohort using the UCSC Xena browser (https://xenabrowser.net/datapages/) in raw count format. We then normalized the data for subsequent analysis by using Deseq2 software. GSE84437 included 433 GC samples with available clinical information. Downloads of gene sets relevant to the human Notch pathway were received from the Molecular Signature Database (MSigDB), and a total of 428 genes were retrieved from seven different Notch-related pathways (Table S1).

2.2. Identification of Differentially Expressed genes (DEGs) in GC.
Raw count data were first transformed into log2 form after being standardized with the transcript per million (TPM) method. The next step was the annotation of 19654 protein-coding genes. Limma, version 3.36.2 of the R package, was utilized in the determination of DEGs [27]. The detection of differentially expressed genes (DEGs) worthy of further investigation required both a log2 fold change (FC) of larger than one and an adjusted P value of less than 0.05.

2.3. Construction of the Prognostic Model by LASSO Cox Regression.
To determine which candidate DEGs in the two discovery sets were most strongly related to patients' overall survival times, we used univariate analysis with a significance level of $P < 0.05$. In order to perform univariate Cox regression analysis, the "survival" R program was utilized [28]. Least absolute shrinkage and selection operator (LASSO) Cox regression, together with ten times of cross-validation, was utilized in order to arrive at the value for the penalty regularization parameter. The coefficient of each gene was decreased to zero by artificial means, which got rid of the connection that existed between the genes that were chosen and stopped the model from being overfit. Genes

were chosen using a method called lamda.min, which stands for minimum deviance. In order to perform LASSO Cox regression analysis, the "glmnet" R program was utilized. Multivariate Cox regression analysis was used to create the coefficients for each gene, and then, the prognostic risk-score model was constructed using those coefficients. In order to carry out the multivariate Cox regression analysis, the "survminer" R program was utilized [29]. The risk score for each patient was determined using the risk-score model based on the expression of each gene that was found. After that, the model of risk scores was utilized to determine the prognosis of GC patients. The TCGA cohort served as the training set, whereas the samples from the GEO: GSE84437 project served as the test set.

2.4. Building Predictive Nomograms and Analyzing Gene Set Enrichment for Functional Relevance.
The "rms R package" was used in order to construct the nomogram and the calibration plot [30]. Gene set enrichment analysis (GSEA) was applied to GC patients in order to uncover associated pathways. It was determined that an enriched gene set was statistically significant if it had a false discovery rate of less than 0.25 percent and a nominal P value that was lower than 0.05 percent.

2.5. Principal Component Analysis (PCA).
In the field of computer vision, PCA is a method that is frequently used for dimensionality reduction and feature extraction [31]. In order to study the potential differences that may exist between high-risk and low-risk groups, the "scatterplot3d" R tool was used [32].

2.6. Immune Feature Analysis.
A brand new deconvolution algorithm known as CIBERSORT was used, which is based on linear support vector regression [33]. Taking into consideration the important roles that immune cells play in TME, the CIBERSORT program was applied to determine the scores of 22 immune cells in each tumor sample. Using the ggplot2 R tool, all of the results were displayed on stacked graphs, heatmaps, and box plots, respectively [34]. In addition, the Wilcoxon rank-sum test was utilized in order to conduct an analysis of disparate scores exhibited by these immune cells that were obtained from TCGA datasets.

2.7. Pathway Analysis.
The DEGs of low-risk and high-risk groups were compared using the "edgeR" tool of the R computer language. In this investigation, we compared the DEGs of the two groups. This was performed in order to perform functional annotation from the GO for DEGs. The KEGG database performs an analysis of metabolic pathways. After that, GSEA was then performed to reveal signaling pathways and BPs in which differentially expressed genes were enriched between high-risk and low-risk subgroups.

2.8. Statistical Analysis.
All analyses used in this study were performed by using R software (version 3.5.1, Boston,

Massachusetts, USA). The Kaplan–Meier curve, which was examined by the log-rank test, was utilized in the investigation of the connection between genes associated with the Notch pathway and overall survival. For the purpose of determining the sensitivity and specificity of the prognostic prediction model, time-dependent ROC curves were utilized. The performance of the nomogram was evaluated using the c-index and the calibration curve. The nomogram was produced using the regression coefficients that were derived from the Cox analysis. Statistical differences between the two groups were examined using the Wilcoxon test. When the P value was less than 0.05, statistical significance was considered.

3. Results

3.1. Identification of DEGs between Normal Specimens and GC Tissues.
Seven gene sets associated with the Notch pathway were obtained from the MSigDB database. Using data received from TCGA-STAD, we were able to obtain information on the linked gene expression of GC. The "limma" R program was applied in order to locate genes that displayed differential expression levels. TCGA-STAD was used to analyze the differential expression of 95 distinct NPRGs. As shown in Figures 1(a) and 1(b), a total of 21 DEGs were obtained: 16 genes (MIR302A, MIR200C, DLGAP5, E2F1, CDK6, FABP7, MFAP2, TSPEAR, MESP2, SIX1, H3C12, ONECUT1, DLL3, ADAM12, WNT2, and MAGEA1) were significantly upregulated and 5 genes (KCNA5, TMEM100, CFD, PLN, and FHL1) were significantly downregulated.

3.2. Establishment of the Prognostic Notch Pathway-Related Gene Signature.
For the purpose of predicting overall survival in patients from TCGA datasets, LASSO and Cox assays were employed to evaluate a gene signature connected with 3 Notch pathways, and the formula calculating the risk score was as follows: ADAM12 expression $*0.2035 +$ MFAP2 expression $*0.1361 +$ TMEM100 expression $*0.1554$ (Figures 2(a)–2(c)). To clearly differentiate GC samples, the risk-score model was applied (low or high-risk) (Figures 2(d) and 2(e)). According to the findings of patient survival, those patients who had a low-risk score had a greater survival rate than those patients who had a high-risk score (Figure 3(a)). In addition, these findings were reexamined and shown to be consistent for GSE84437 datasets (Figure 3(b)). According to the results of a time-dependent ROC analysis, the Notch pathway-related gene signature had a diagnostic accuracy of 0.586 after one year, 0.617 after three years, and 0.729 after five years (Figure 3(c)). The area under the ROC curves (AUC) demonstrated that the risk score (AUC = 0.729) had a better prognostic value than a single indicator, such as age (AUC = 0.606), gender (AUC = 0.559), grade (AUC = 0.548), and stage (AUC = 0.606) (Figure 3(d)). Cox survival studies were carried out so that we could find out whether or not the risk score was an independent factor for determining the outcome of GC. According to the results of a univariate study, the clinical stage and the risk score were associated

(a)

(b)
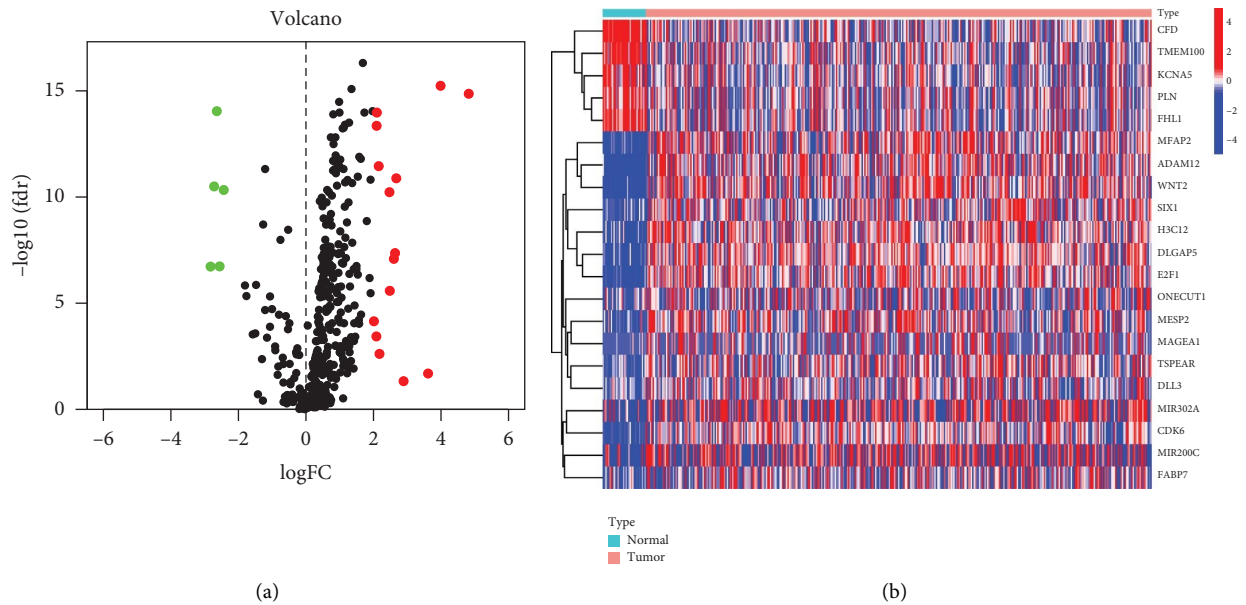
FIGURE 1: Differentially expressed NPRGs between GC specimens and nontumor specimens shown in the (a) volcano map and (b) heatmap.

with the patients' likelihood of survival with GC (Figure 4(a)). Furthermore, multivariate analysis revealed that a patient's risk score was an independent predictor of a poor prognosis for GC (HR = 2.336, 95% CI: 1.249–4.370). (Figure 4(b)).

3.3. Association between Clinicopathological Characteristics and Risk Scores.

The potential link between the risk score and clinicopathological features was then investigated. We discovered no correlation between the risk score and either age or gender (Figures 5(a) and 5(b)). In addition, we observed that a higher risk score was associated with the advanced grade (Figure 5(c)), clinical stage (Figure 5(d)), and T stage (Figure 5(e)). However, there was not a distinct difference in the risk score between the M and N stage (Figures 5(f) and 5(g)).

3.4. Construction of a Nomogram for Predicting Survival.

To better predict OS for GC data, a nomogram was constructed using age, gender, grade, pathological stage, T stage, M stage, and N stage information, in addition to a predictive risk-score model (Figure 6(a)). The nomogram's ability for the prediction of the overall survival of GC patients was demonstrated by calibration curves drawn at 1, 3, and 5 years (Figure 6(b)). Cox assays illustrated that the nomogram is an independent prognostic indicator for GC patients (Figures 6(c) and 6(d)). The nomogram was more predictive than a single indicator, as shown by AUC (Figure 6(e)).

3.5. Gene Set Variation Analysis (GSVA).

To investigate biological activities exhibited by the two groups, GSVA enrichment was carried out with the gene sets of "c2.cp.kegg.v7.2," which were obtained from the Molecular Signature Database (MSigDB). Interestingly, we found that many tumor-related were enriched in the high-risk score,

such as TGF_BETA_SIGNALING_PATHWAY, WNT_SIGNALING_PATHWAY, and KEGG_MAPK_-SIGNALING_PATHWAY (Figure 7). Our findings suggested that the above genes may be involved in tumor progression via regulating several different tumor-related pathways.

3.6. Relationships between the Gene Signature and Immune Cells.

We estimated the presence of 22 immune cell types in the TCGA cohort. Figure 8(a) displays the substantial difference in the presence of four types of immune cells between cases in the low-risk group and cases in the high-risk group (plasma cells, T cells CD4 memory activated, monocytes, and macrophages M2). Moreover, APC_-co_inhibition, APC_co_stimulation, CCR, Check-point, Cytolytic_activity, HLA, Parainflammation, T_cell_co-inhibition, T_cell_co-stimulation, Type_I_IFN_Response, and Type_II_IFN_Response were also activated in the high-risk group, indicating that it is possible that immunotherapy will be effective for people in the high-risk group who have immune suppression (Figure 8(b)).

3.7. Enrichment Analyses.

To isolate DEGs, we used the "limma" R package and filtered for FDR 0.05 and |log2FC| > 1. These steps were taken to delve deeper into how the risk model's categorization of individuals into subgroups affects gene function and pathway analysis. We found that there were a total of 686 DEGs that existed between the low-risk and high-risk groups in TCGA datasets. There were 627 upregulated genes and 58 downregulated genes in the high-risk group. As shown in Figures 9(a) and 9(b), we found that 627 genes were mainly associated with extracellular matrix organization, extracellular structure organization, skeletal system development, endoplasmic reticulum lumen, contractile fiber, myofibril, extracellular matrix structural

(a)

(b)

(c)

(d)
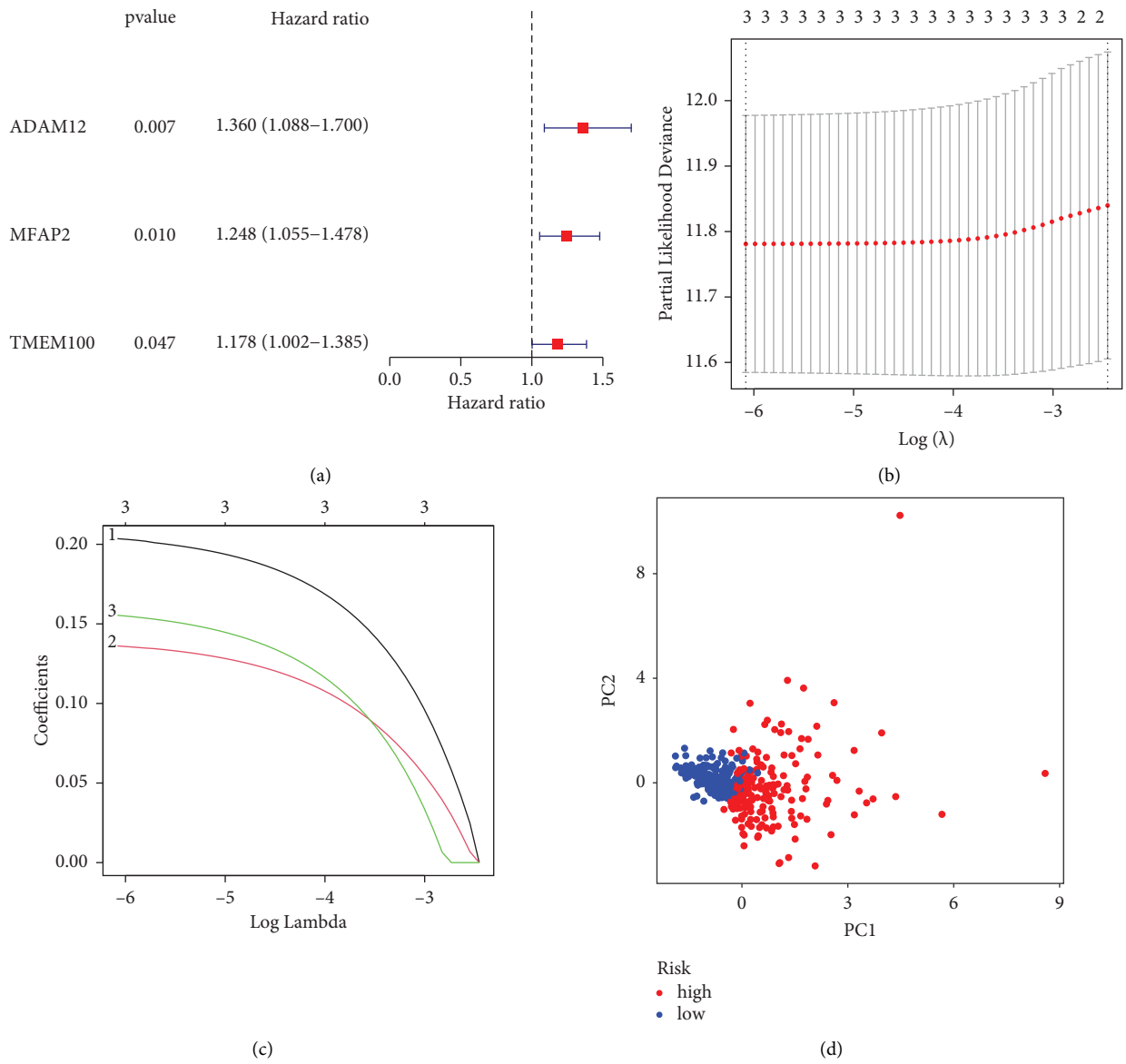
FIGURE 2: Continued.
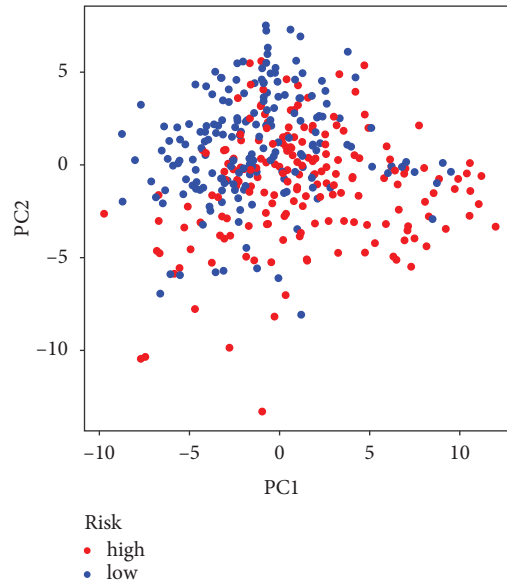
(e)

Figure 2: Construction of a prognostic signature in GC from TCGA. (a) Hazard ratios for three differentially expressed NPRGs that were implicated in overall survival plotted on a forest plot. (b) Three-fold cross-validation for tuning parameter selection in the LASSO model. (c) Profiles of differentially expressed NPRGs using the LASSO coefficient. The value determined using a three-fold cross-validation is indicated by the dashed line. (d) Principal component analysis based on NPRGs in GC. (e) In order to differentiate tumor samples from normal ones in the TCGA cohort, principal component analysis was performed based on a risk score. Patients who were considered to have a high risk were represented by the group that was colored green, while patients who were considered to have a low risk were represented by the group that was colored red.
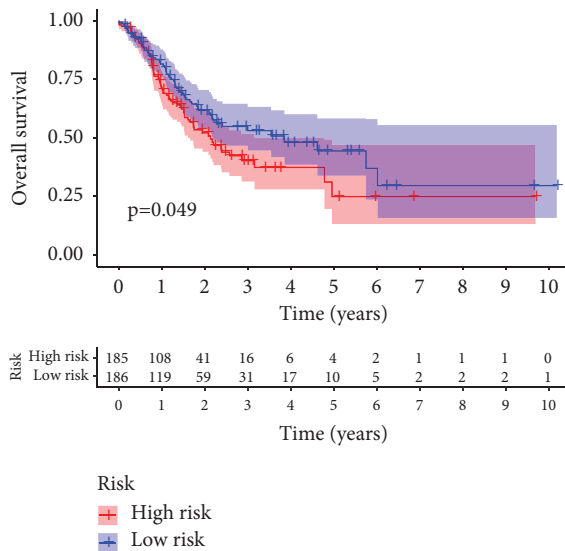
(a)

(b)

Figure 3: Continued.

(c)
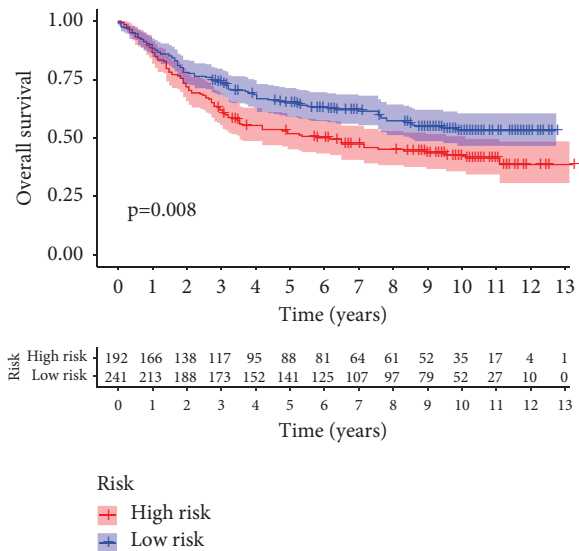
(d)
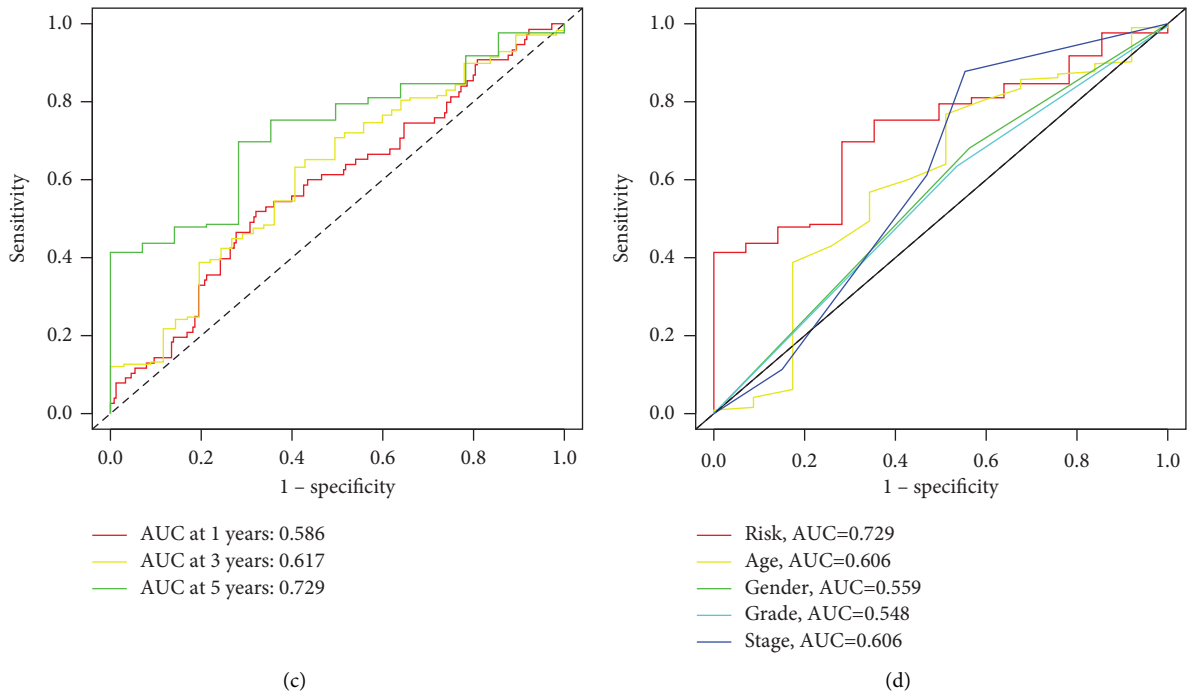
FIGURE 3: Validation of the risk-score model. (a, b) The survival value of the risk score was demonstrated in TCGA datasets and GSE84437. (c) Validation of the prognostic values of the index in TCGA datasets using a ROC curve. (d) ROC assays for both clinical factors and risk scores.

	pvalue	Hazard ratio
Age	0.004	1.026 (1.008−1.044)
Gender	0.234	1.249 (0.866−1.803)
Grade	0.075	1.361 (0.969−1.911)
Stage	<0.001	1.534 (1.241−1.896)
riskScore	0.004	2.433 (1.339−4.422)

(a)
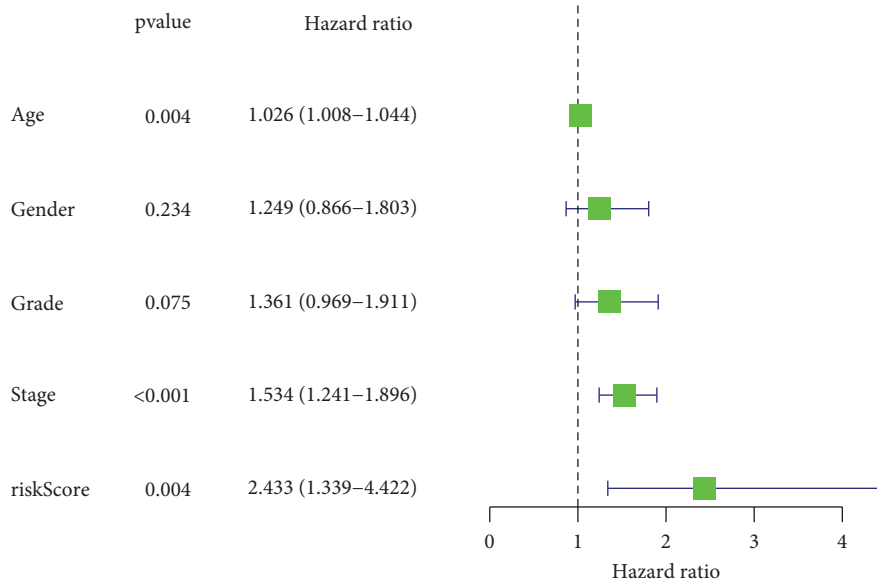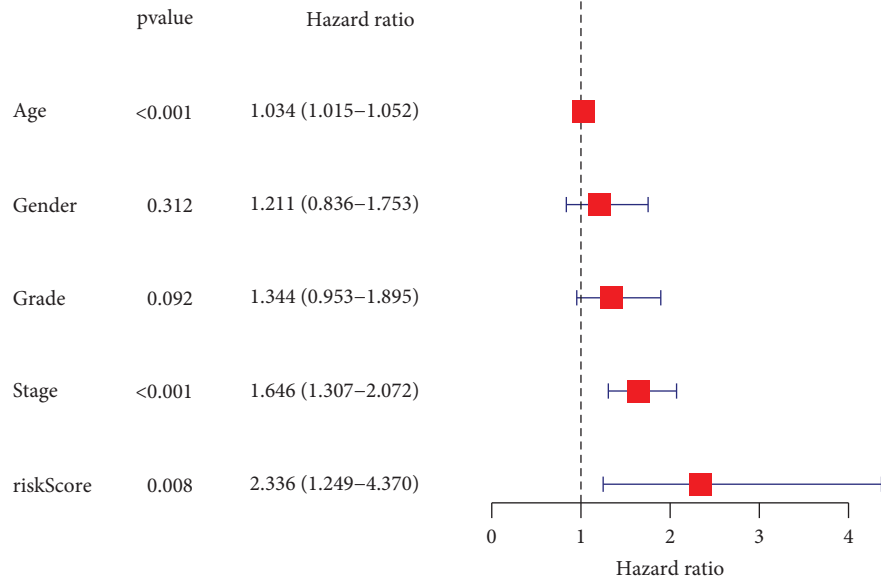
FIGURE 4: Continued.

(b)

FIGURE 4: (a) Univariate and (b) multivariate analysis of overall survival in GC patients from TCGA datasets.

(a)   (b)   (c)

(d)   (e)   (f)

FIGURE 5: Continued.

(g)
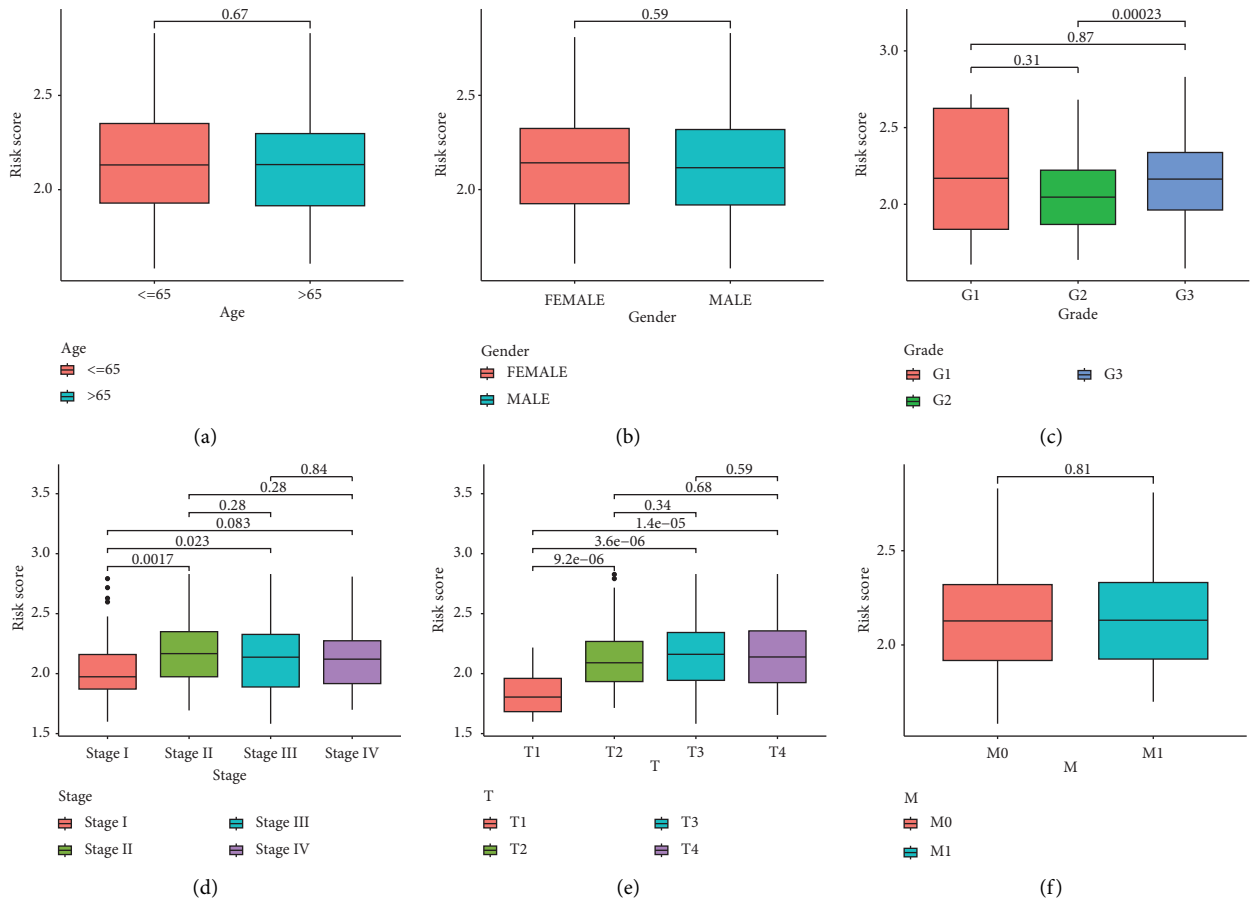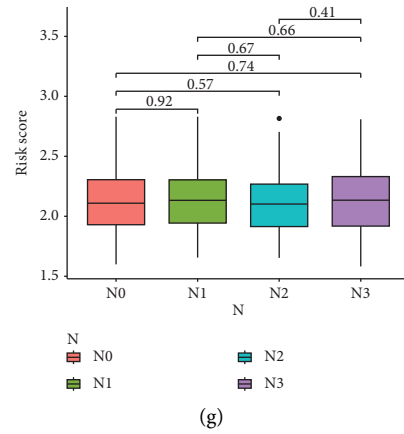
FIGURE 5: Indications of a link between the risk model and patient features. Correlation assays of the risk score with (a) age, (b) gender, (c) grade, (d) stage, (e) *T* stage, (f) *M* stage, and (g) *N* stage.

(a)

(b)

(c)

(d)

FIGURE 6: Continued.

(e)
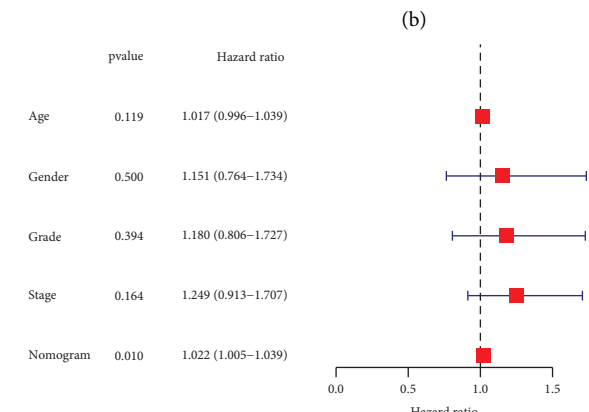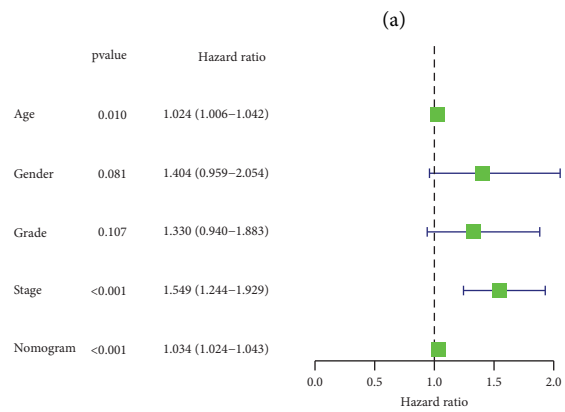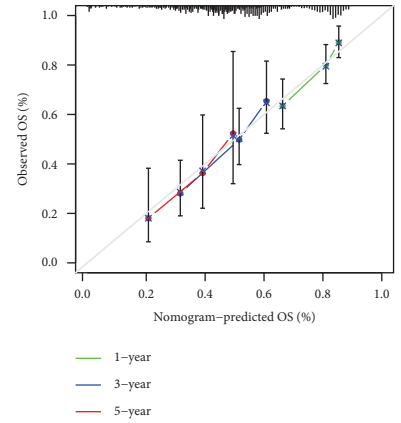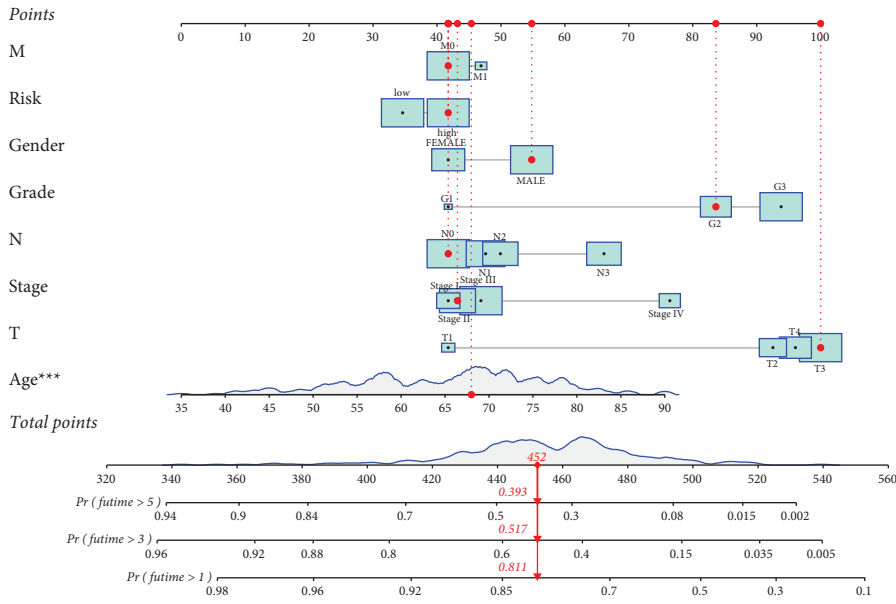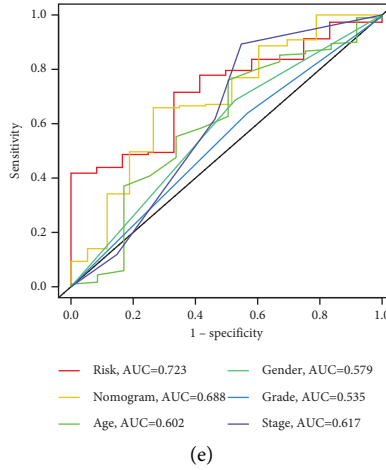
FIGURE 6: The development of the nomogram with the risk score. (a) A nomogram predicting survival. (b) A calibration plot for prediction. (c and d) Univariate and multivariate analyses of the nomogram with the risk score. (e) The nomogram with the risk score.
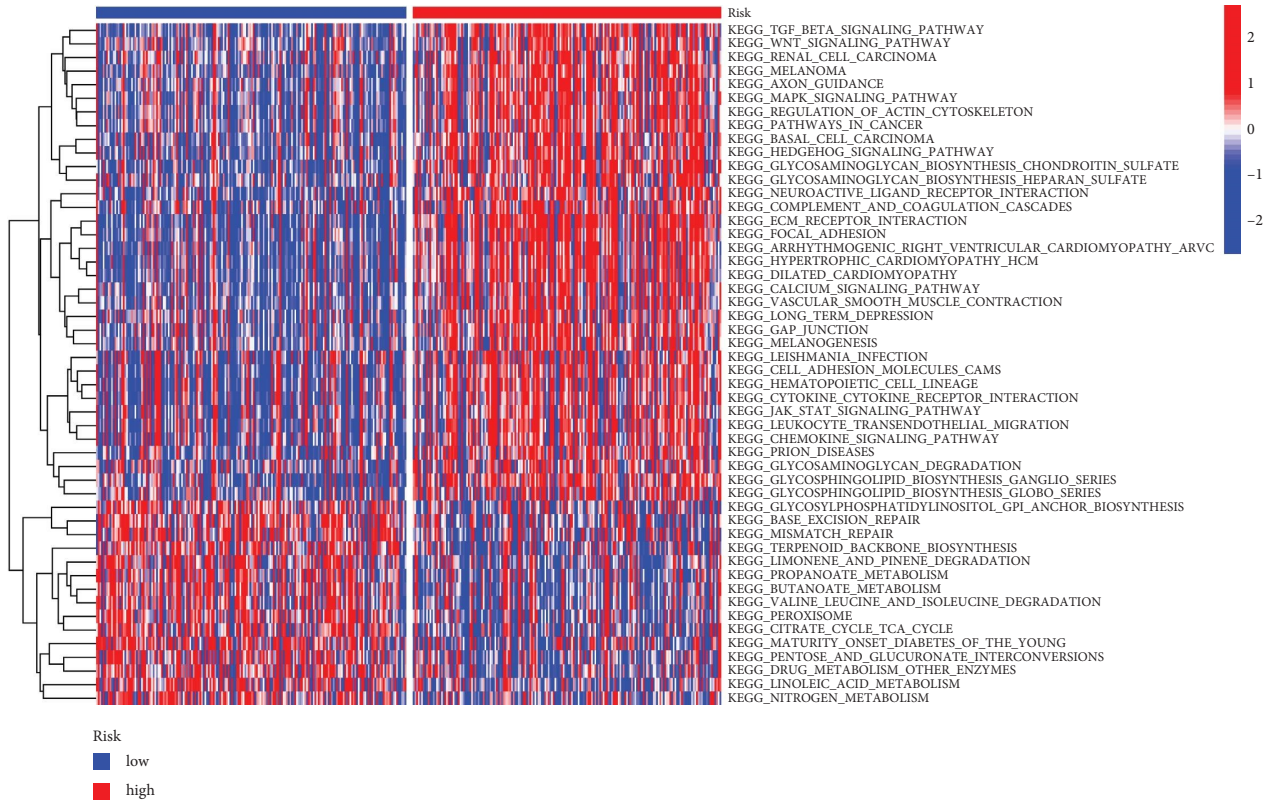
FIGURE 7: Comparison of GSVA enrichment for groups with low and high-risk scores as shown in a heatmap.

constituent, glycosaminoglycan binding, and sulfur compound binding. In addition, the results of KEGG assays revealed that 627 genes were mainly associated with focal adhesion, PI3K-Akt signaling pathway, human papillomavirus infection, proteoglycans in cancer, and ECM-receptor interaction (Figures 9(c) and 9(d)).

4. Discussion

GC is one of the most prevalent malignancies worldwide [35]. The most recent statistics available on the disease indicated that GC is currently ranked as the world's second most prevalent cause of death from cancer-related causes

(a)

(b)
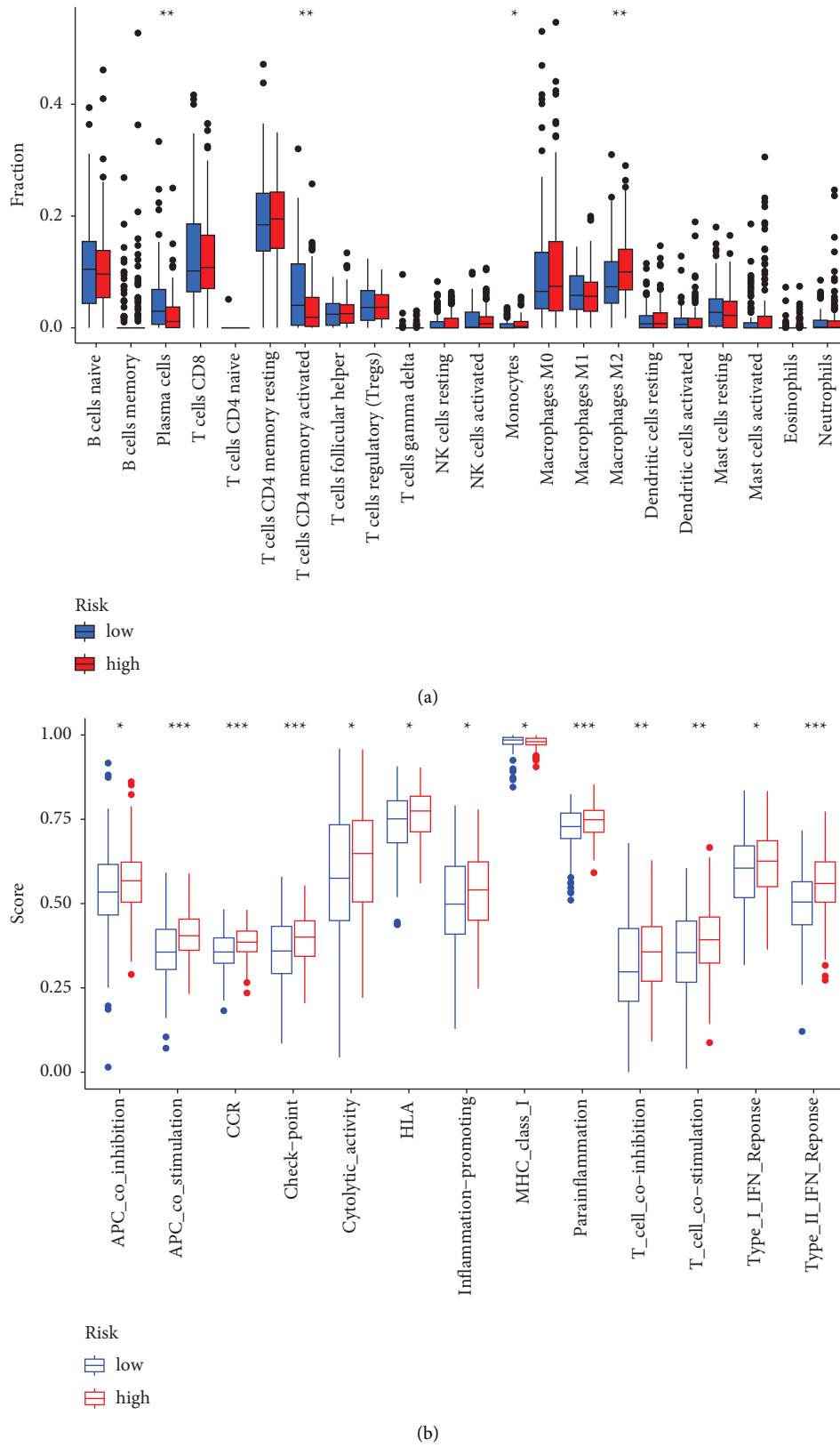
FIGURE 8: Modeling immunotherapy risk. (a) Changes in immune cell infiltration between people with low and high-risk scores. (b) Cases with a high-risk score and those with a low-risk score have different observable functions associated with immune system control.

(a)

(b)

(c)

(d)
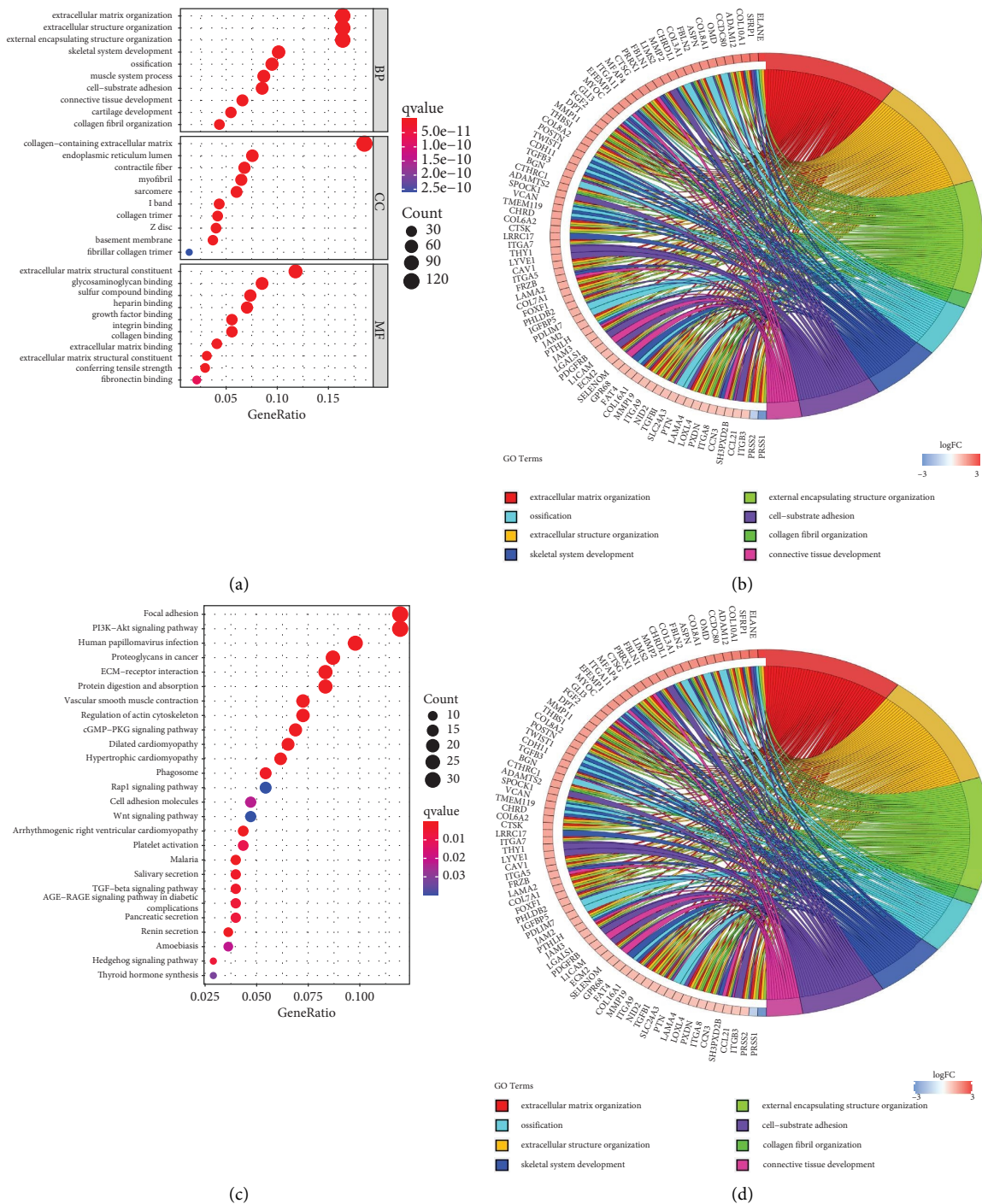
Figure 9: Comparing the TCGA cohort's two risk categories from the lens of functional analysis based on DEGs. (a, b) GO enrichment. (c, d) KEGG pathways.

[36, 37]. The majority of GC is caused by *Helicobacter pylori*'s complicated interplay with the host's components. According to the findings of a number of studies, a number of environmental factors, including trace elements, are thought to be contributors to the development of stomach cancer [38, 39]. Even with the breakthroughs that have been made in diagnosis and therapy over the course of the last few years, the primary therapeutic option for GC patients

remains surgery. The prognosis for individuals with GC is still not favorable due to the fact that a significant number of patients are still initially diagnosed at an advanced stage. As a result, it is of the utmost significance to look for promising prognostic indicators for early diagnosis and innovative therapy targets.

Notch was identified for the first time in 1917 and was given its name after the mutation that was found to cause

malformations in the wings of flies [40]. The Notch signaling pathway is an example of a chained signaling pathway. It is made up of ligands, receptors, and DNA binding proteins farther down the chain [41]. Notch1 and Notch2 are two different types of receptors, and jagged1 is considered to be a ligand [42]. In addition, the roles of the Notch signaling pathway in GC have been verified and proved. It has been observed that the Notch and mTOR signaling pathways are frequently activated in human stomach cancer, which contributes to the proliferation of cells [43, 44]. It is possible that a viable therapeutic strategy for treating GC would involve targeting these pathways in combination with one another. According to the findings of Yang et al., the Notch signaling pathway may play a key role in the course of GC as well as the prognosis of the disease by regulating the function of CD4+CD25+CD127-dim/- regulatory T cells and T helper 17 cells [45]. The findings brought attention to the significant functions that the Notch pathway plays in the evolution of GC. As a result, we were curious as to whether or not a unique prognostic model that was based on NPRGs could be utilized in the process of forecasting the prognosis of patients who had GC. In this study, using TGCA datasets, we were able to obtain a total of 21 NPRGs with differential expression in GC. The expression of ADAM12, MFAP2, and TMEM100 was then used to establish a diagnostic signature for the disease. Based on the TCGA database, this prognostic model displayed an outstanding performance for operating system prediction. According to comprehensive research, the Notch pathway-related prognostic model was shown to be an independent prognostic indicator when other clinical parameters were taken into account. Subsequently, a model comprising nine NPRGs was effectively verified as a predictive factor for an independent GEO dataset. This was accomplished after the model was initially developed. Integration with a subset of clinicopathological characteristics in a risk-assessment nomogram further enhanced the predictive value of this prognostic risk-score model. This resulted in the nomogram having a higher predictive capacity. All of these data pointed to the fact that the Notch pathway-related prognostic model has the potential to serve as an efficient marker for GC prognostic prediction.

The landscape of cancer treatment is now being altered as a result of the application of immunotherapy to the treatment of a variety of malignancies [46, 47]. For instance, inhibiting the interaction between PD-1 and PD-L1 can restore the function of effector T cells, allowing them to perform their intended role of eliminating tumor cells more effectively. The level of PD-L1 that was expressed in a patient's tumor is the most important element in identifying whether or not they are a candidate for PD-1/PD-L1 axis immunotherapy. However, in practice, many PD-L1-positive patients have a poor response to PD-1/PD-L1 axis treatment, whereas some PD-L1-negative patients have an unexpectedly excellent response. Our study showed that high-risk patients with up-regulated immunological checkpoints had a worse response to immunotherapy, which was the result that kept popping up. However, the existence of immune cell infiltration may be a predictor of how effectively immunotherapy works, as individuals in the low-risk

subgroup who had higher levels of immunological/inflammatory activity were more likely to benefit from the treatment.

However, this study also had certain limitations. First, the bioinformatic research for this work was only performed on publicly available datasets. Next, we need to make sure that the findings of this investigation are accurate by using clinical participants in a prospective study design. Second, the three genes that make up the prognostic signature are all known to be risk factors in patients diagnosed with GC. Their downstream molecular pathways require additional investigation through functional tests in order to discover potential novel treatment targets. Overall, our gene profile that is associated with the Notch pathway has a fair chance of accurately predicting the immunotherapy response; however, this hypothesis will need to be verified in the future using clinical studies that are carefully planned.

5. Conclusion

Overall, a strong Notch pathway-related prognostic model was created, and the characteristics of the tumor immune milieu were investigated; our findings could be beneficial to the diagnosis and treatment of patients with GC.

Data Availability

The data used to support the findings of this study are included in the article.

Conflicts of Interest

The authors declare no conflicts of interest.

Acknowledgments

Supplementary Materials

Table S1: all names of Notch-related genes. (*Supplementary Materials*)

References

[1] R. L. Siegel, K. D. Miller, and A. Jemal, "Cancer statistics," *CA: A Cancer Journal for Clinicians*, vol. 69, no. 1, pp. 7–34, 2019.

[2] R. E. Sexton, M. N. Al Hallak, M. Diab, and A. S. Azmi, "Gastric cancer: a comprehensive review of current and future treatment strategies," *Cancer and Metastasis Reviews*, vol. 39, no. 4, pp. 1179–1203, 2020.

[3] E. C. Smyth, M. Nilsson, H. I. Grabsch, N. C. van Grieken, and F. Lordick, "Gastric cancer," *The Lancet*, vol. 396, no. 10251, pp. 635–648, 2020.

[4] C. Resende, C. P. Gomes, and J. C. Machado, "Review: gastric cancer: basic aspects," *Helicobacter*, vol. 25, no. 1, Article ID e12739, 2020.

[5] T. Matsuoka and M. Yashiro, "Biomarkers of gastric cancer: current topics and future perspective," *World Journal of Gastroenterology*, vol. 24, no. 26, pp. 2818–2832, 2018.

[6] N. Bizzaro, A. Antico, and D. Villalta, "Autoimmunity and gastric cancer," *International Journal of Molecular Sciences*, vol. 19, no. 2, p. 377, 2018.

[7] F. Meric-Bernstam, A. M. Johnson, E. E. I. Dumbrava et al., "Advances in HER2-targeted therapy: novel agents and opportunities beyond breast and gastric cancer," *Clinical Cancer Research*, vol. 25, no. 7, pp. 2033–2041, 2019.

[8] V. E. Strong, "Progress in gastric cancer," *Updates in surgery*, vol. 70, no. 2, pp. 157–159, 2018.

[9] S. Shichijo and Y. Hirata, "Characteristics and predictors of gastric cancer after *Helicobacter pylori* eradication," *World Journal of Gastroenterology*, vol. 24, no. 20, pp. 2163–2172, 2018.

[10] M. Venerito, R. Vasapolli, T. Rokkas, and P. Malfertheiner, "Gastric cancer: epidemiology, prevention, and therapy," *Helicobacter*, vol. 23, no. 1, Article ID e12518, 2018.

[11] S. S. Joshi and B. D. Badgwell, "Current treatment and recent progress in gastric cancer," *CA: A Cancer Journal for Clinicians*, vol. 71, no. 3, pp. 264–279, 2021.

[12] M. Katoh and M. Katoh, "Precision medicine for human cancers with Notch signaling dysregulation (Review)," *International Journal of Molecular Medicine*, vol. 45, no. 2, pp. 279–297, 2020.

[13] C. Siebel and U. Lendahl, "Notch signaling in development, tissue homeostasis, and disease," *Physiological Reviews*, vol. 97, no. 4, pp. 1235–1294, 2017.

[14] D. Sprinzak and S. C. Blacklow, "Biophysics of Notch signaling," *Annual Review of Biophysics*, vol. 50, no. 1, pp. 157–189, 2021.

[15] R. Kopan and M. X. G. Ilagan, "The canonical Notch signaling pathway: unfolding the activation mechanism," *Cell*, vol. 137, no. 2, pp. 216–233, 2009.

[16] S. Majumder, J. S. Crabtree, T. E. Golde, L. M. Minter, B. A. Osborne, and L. Miele, "Targeting Notch in oncology: the path forward," *Nature Reviews Drug Discovery*, vol. 20, no. 2, pp. 125–144, 2021.

[17] F. Jundt, R. Schwarzer, and B. Dörken, "Notch signaling in leukemias and lymphomas," *Current Molecular Medicine*, vol. 8, no. 1, pp. 51–59, 2008.

[18] Z. Wang, Y. Li, and F. H Sarkar, "Notch signaling proteins: legitimate targets for cancer therapy," *Current Protein and Peptide Science*, vol. 11, no. 6, pp. 398–408, 2010.

[19] J. Tao, S. Chen, and B. Lee, "Alteration of Notch signaling in skeletal development and disease," *Annals of the New York Academy of Sciences*, vol. 1192, no. 1, pp. 257–268, 2010.

[20] R. Schwanbeck, S. Martini, K. Bernoth, and U. Just, "The Notch signaling pathway: molecular basis of cell context dependency," *European Journal of Cell Biology*, vol. 90, no. 6-7, pp. 572–581, 2011.

[21] B. Arneth, "Tumor microenvironment," *Medicina*, vol. 56, no. 1, p. 15, 2019.

[22] D. C. Hinshaw and L. A. Shevde, "The tumor microenvironment innately modulates cancer progression," *Cancer Research*, vol. 79, no. 18, pp. 4557–4566, 2019.

[23] L. Hui and Y. Chen, "Tumor microenvironment: sanctuary of the devil," *Cancer Letters*, vol. 368, no. 1, pp. 7–13, 2015.

[24] N. Wang, X. Li, R. Wang, and Z. Ding, "Spatial transcriptomics and proteomics technologies for deconvoluting the tumor microenvironment," *Biotechnology Journal*, vol. 16, no. 9, Article ID e2100041, 2021.

[25] T. Du, J. Gao, P. Li et al., "Pyroptosis, metabolism, and tumor immune microenvironment," *Clinical and Translational Medicine*, vol. 11, no. 8, p. e492, 2021.

[26] C. Ngambenjawong, H. H. Gustafson, and S. H. Pun, "Progress in tumor-associated macrophage (TAM)-targeted therapeutics," *Advanced Drug Delivery Reviews*, vol. 114, pp. 206–221, 2017.

[27] M. E. Ritchie, B. Phipson, D. Wu et al., "Limma powers differential expression analyses for RNA-sequencing and microarray studies," *Nucleic Acids Research*, vol. 43, no. 7, p. e47, 2015.

[28] M. Pohar and J. Stare, "Relative survival analysis in R," *Computer Methods and Programs in Biomedicine*, vol. 81, no. 3, pp. 272–278, 2006.

[29] A. Ozhan, M. Tombaz, O. Konu, and SmulTCan, "SmulTCan: a Shiny application for multivariable survival analysis of TCGA data with gene sets," *Computers in Biology and Medicine*, vol. 137, Article ID 104793, 2021.

[30] X. Zhang, S. Wang, E. R. Rudzinski et al., "Deep learning of rhabdomyosarcoma pathology images for classification and survival outcome prediction," *American Journal Of Pathology*, vol. 192, no. 6, pp. 917–925, 2022.

[31] M. Ringnér, "What is principal component analysis?" *Nature Biotechnology*, vol. 26, no. 3, pp. 303-304, 2008.

[32] C. Zhang, C. W. Tam, G. Tang, Y. Chen, N. Wang, and Y. Feng, "Spatial transcriptomic analysis using R-based computational machine learning reveals the genetic profile of Yang or yin deficiency syndrome in Chinese medicine theory," *Evidence-based Complementary and Alternative Medicine*, vol. 2022, pp. 5503181–13, 2022.

[33] K. E. Craven, Y. Gökmen-Polar, and S. S. Badve, "CIBERSORT analysis of TCGA and METABRIC identifies subgroups with better outcomes in triple negative breast cancer," *Scientific Reports*, vol. 11, no. 1, p. 4691, 2021.

[34] K. Ito and D. Murphy, "Application of ggplot2 to pharmacometric graphics," *CPT: Pharmacometrics & Systems Pharmacology*, vol. 2, no. 10, p. e79, 2013.

[35] K. G. O'Connor, "Gastric cancer," *Seminars in Oncology Nursing*, vol. 15, no. 1, pp. 26–35, 1999.

[36] I. Petrovchich and J. M. Ford, "Genetic predisposition to gastric cancer," *Seminars in Oncology*, vol. 43, no. 5, pp. 554–559, 2016.

[37] X. Y. Zhang and P. Y. Zhang, "Gastric cancer: somatic genetics as a guide to therapy," *Journal of Medical Genetics*, vol. 54, no. 5, pp. 305–312, 2017.

[38] R. Obermannová and F. Lordick, "Management of metastatic gastric cancer," *Hematology-Oncology Clinics of North America*, vol. 31, no. 3, pp. 469–483, 2017.

[39] A. M. Sterea, E. E. Egom, and Y. El Hiani, "TRP channels in gastric cancer: new hopes and clinical perspectives," *Cell Calcium*, vol. 82, Article ID 102053, 2019.

[40] F. Allen and I. Maillard, "Therapeutic targeting of Notch signaling: from cancer to inflammatory disorders," *Frontiers in Cell and Developmental Biology*, vol. 9, Article ID 649205, 2021.

[41] K. Zohorsky and K. Mequanint, "Designing biomaterials to modulate Notch signaling in tissue engineering and regenerative medicine," *Tissue Engineering Part B Reviews*, vol. 27, no. 5, pp. 383–410, 2021.

[42] X. Yuan, H. Wu, H. Xu et al., "Notch signaling: an emerging therapeutic target for cancer treatment," *Cancer Letters*, vol. 369, no. 1, pp. 20–27, 2015.

[43] E. S. Hibdon, N. Razumilava, T. M. Keeley et al., "Notch and mTOR signaling pathways promote human gastric cancer cell proliferation," *Neoplasia*, vol. 21, no. 7, pp. 702–712, 2019.

[44] Y. Cui, Q. Li, W. Li et al., "NOTCH3 is a prognostic factor and is correlated with immune tolerance in gastric cancer," *Frontiers in Oncology*, vol. 10, Article ID 574937, 2020.

[45] L. Yang, K. L. Zhao, L. Qin et al., "Notch signaling pathway regulates CD4(+)CD25(+)CD127(dim/-) regulatory T cells and T helper 17 cells function in gastric cancer patients," *Bioscience Reports*, vol. 39, no. 5, Article ID BSR20182044, 2019.

[46] L. B. Kennedy and A. K. S. Salama, "A review of cancer immunotherapy toxicity," *CA: A Cancer Journal for Clinicians*, vol. 70, no. 2, pp. 86–104, 2020.

[47] R. S. Riley, C. H. June, R. Langer, and M. J. Mitchell, "Delivery technologies for cancer immunotherapy," *Nature Reviews Drug Discovery*, vol. 18, no. 3, pp. 175–196, 2019.

Research Article

Comprehensive Analysis of NPSR1-AS1 as a Novel Diagnostic and Prognostic Biomarker Involved in Immune Infiltrates in Lung Adenocarcinoma

Hui Zhang,[1] Jin Yuan,[1] Yuehua Xiang [ID],[1] and Yong Liu [ID][2]

[1]*Department of Pulmonary and Critical Care Medicine, The Central Hospital of Enshi Tujia and Miao Autonomous Prefecture, Enshi, China*
[2]*Department of Pulmonary Disease Diabetes Mellitus, The National Hospital of Enshi Autonomous Prefecture, Enshi, China*

Correspondence should be addressed to Yuehua Xiang; xyh15200799@163.com and Yong Liu; liuyonglc@stu.cpu.edu.cn

The incidence of lung adenocarcinoma (LUAD), the most common subtype of lung cancer, continues to make lung cancer the largest cause of cancer-related deaths worldwide. Long noncoding RNAs (lncRNAs) have been shown to have a significant role in both the onset and progression of lung cancer. In this study, we aimed to investigate the clinical significance and underlying mechanism of lncRNA NPSR1-AS1 (NPSR1-AS1) in LUAD. First, we performed an analysis on TCGA and identified 229 differentially expressed lncRNAs (DELs) (including 216 upregulated lncRNAs and 13 downregulated lncRNAs). Then, we carried out a screening of the lncRNAs associated with survival, and a total of 382 survival-related lncRNAs were found. 15 survival-related DELs were identified. Among them, our attention focused on NPSR1-AS1. We found that the expression of NPSR1-AS1 was much higher in LUAD specimens compared to nontumor tissues. According to the results of the ROC assays, high NPSR1-AS1 expression had an AUC value of 0.904 for LUAD, with a 95% confidence interval ranging from 0.881 to 0.927. The expression of NPSR1-AS1 was shown to be significantly elevated in a wide variety of cancers, according to the findings of a pancancer investigation. Functional enrichment analysis confirmed that NPSR1-AS1 was involved in LUAD progression via regulating several tumor-related pathways. Patients with high levels of NPSR1-AS1 expression were shown to have a shorter disease-specific survival (DSS) or overall survival (OS) than those with low levels of NPSR1-AS1 expression, according to the findings of a clinical investigation. It was determined by multivariate analysis that NPSR1-AS1 expressions served as an independent prognostic factor for the overall survival of LUAD patients. The results of immune cell infiltration revealed that the expressions of NPSR1-AS1 were negatively associated with CD8 T cells, pDC, cytotoxic cells, mast cells, iDC, neutrophils, NK CD56dim cells, DC, Th17 cells, Tgd, and macrophages, while they were positively associated with NK CD56bright cells and B cells. Overall, our findings revealed that NPSR1-AS1 could serve as a potential biomarker to assess the clinical outcome and immune infiltration level in LUAD.

1. Introduction

It is estimated that 1.76 million people die every year from lung cancer, making it the top cause of death resulting from cancer worldwide (18.4% of all cancer-related deaths) [1]. Approximately forty percent of all instances of lung cancer are classified as lung adenocarcinoma (LUAD), making it the most frequent type [2, 3]. The frequency of this form of lung cancer is rising worldwide. The primary cause of lung cancer is still smoking, as it has been

for decades [4, 5]. Even though prolonged exposure to tobacco smoke is by far the most common cause of this form of cancer, nonsmokers account for anywhere from 15 to 20 percent of cases and are typically thought to have contracted the disease due to a confluence of hereditary and environmental factors [6, 7]. Despite the use of morphological analysis to classify patients into different risk groups, it is evident that the overall survival (OS) rates for LUAD patients with high invasiveness and early metastasis ranged from 13 to 58.3% at 5 years [8, 9]. This

was the case despite the use of morphological analysis to classify patients. It is difficult to diagnose non-small-cell lung cancer in its early stages, when the disease is also tough to treat [10]. Consequently, it is of the utmost importance and a pressing necessity to discover innovative prognostic biomarkers in order to provide helpful therapy methods for LUAD.

The discovery of the potential diagnostic usefulness of genetic biomarkers, such as long noncoding RNAs (lncRNAs), was made possible by the advent of high-throughput sequencing techniques and bioinformatics technologies [11, 12]. lncRNAs are becoming an increasingly important focus of attention in research on cancers [13]. lncRNAs are a category of nonprotein coding transcripts that are typically longer than 200 nucleotides without an open reading frame [14]. Their length is what defines them as "long noncoding RNAs." Numerous studies have shed light on the function of lncRNAs in several biological processes, such as the silencing of X-chromosome genes, the remodeling of chromatin, and transcriptional activity [15, 16]. In addition, a growing number of studies have indicated a link between lncRNAs and the onset and progression of many malignancies, including LAUD [17, 18]. For instance, Zhang et al. indicated that the expressions of SNHG17 were highly elevated in LUAD specimens and cells, and high SNHG17 expression was related to advanced stages of tumor node metastases and a bad prognosis for patients who had LUAD. The targeting of the microRNA-193a-5p/NETO2 axis by SNHG17 knockdown resulted in an inhibition of the EMT process as well as cell migration, invasion, and proliferation [19]. Cong et al. showed that it is possible that the lncRNA known as linc00665, which was found to be significantly overexpressed in lung adenocarcinoma (LUAD) tissues, can act as an independent predictor of a bad prognosis. According to the results of functional tests, linc00665 promoted LUAD cell proliferation and metastasis both in vitro and in vivo through modulating the AKR1B10-ERK signaling pathway and by sponging miR-98 [20]. These studies suggested that lncRNAs have the potential to be turned into potentially valuable biomarkers that can aid in the diagnosis and prognosis of LUAD.

Although immunotherapy has been used with promising results in the treatment of tumors, it is still only effective for a very small percentage of cancer patients [21]. This is despite the fact that it represents a unique approach to cancer treatment [22]. There is a strong correlation between the tumor microenvironment (TME) and the effectiveness of immunotherapy [23, 24]. The epigenetic differentiation of tumor cells and the metastasis and infiltration of the tumor are both linked to the suppression of the immune system caused by the tumor [25]. TME is a complex system that is made up of many distinct cell types, cytokines, and other extracellular components. Both the kind and the quantity of immune cells that invade a tumor are significant factors in establishing its development and evolution [26, 27]. Additionally, the make-up and proportion of TIICs and stroma can be used for the diagnosis, prognosis, and prediction of many cancers [28]. It is possible that new therapy targets for cancers could be found by mining related lncRNAs and

then examining how those lncRNAs affect immune cell infiltration in TME and the prognosis of the tumor.

In this study, NPSR1-AS1, a previously unknown long noncoding RNA associated to LUAD, was found to have abundant expression in LUAD. Previous researches from a number of different investigations have uncovered its roles in some cancers. For instance, Ni et al. revealed that NPSR1-AS1 was substantially expressed in thyroid cancer, and its overexpression boosted the proliferation and metastasis of thyroid cancer cells. It was accomplished by recruiting ELAVL1 to stabilize NPSR1 mRNA [29]. NPSR1-AS1 was found to be highly expressed in thyroid cancer. On the other hand, its expression and potential prognostic usefulness in LUAD have not been researched. The investigation of the immunological microenvironment in patients with LUAD has opened up new possibilities for the conventional therapy protocols that are now in use. Therefore, the improvement of patient survival is one of our primary objectives in the development of a universal immunodiagnostic marker.

2. Materials and Methods

2.1. Patient Datasets. Using the UCSC Xena browser, we were able to retrieve the gene expression data, phenotypic data, and extensive clinicopathological data for TCGA-LUAD. The Illumina HiSeq RNA-Seq platform was used to retrieve the sequence data that was needed. For the purposes of the subsequent studies, the HTSeq-FPKM gene expression data were converted into TPM. TPM produces results that are more comparable to those provided by an approach using microarrays, and it makes it easier to compare the results of different samples. In accordance with the associated annotation file, the probe ID was transformed into the gene symbol, and then, the average expression values for many probes that corresponded to the same gene were computed. The data were collected and analyzed in a way that was compliant with the publication standards provided by TCGA datasets. There was not a single study that directly involved human volunteers or animal testing that was included. The approval of the ethics committee and informed consent were not required.

2.2. Identification of Differentially Expressed lncRNAs (DELs). All samples were compared using a differential expression analysis between LUAD and nontumor samples, and the Wald significance test (as specified by the nbinom Wald test function) was utilized to determine statistical significance. RNA-seq data can be trusted when analyzed using the DESeq2 package in R, which employs this test. This package was based on raw read counts for each gene, making it a robust way for assessing RNA-seq data. A statistical limit for significance was set at a false discovery rate (FDR) of less than 0.05 and a fold change of more than 4.

2.3. Survival Analysis. A high-expression group was defined as having an expression level that was higher than the median expression level across all samples, and a low-expression cohort was defined as having an expression level

(a)

(b)

(c)

(d)

(e)
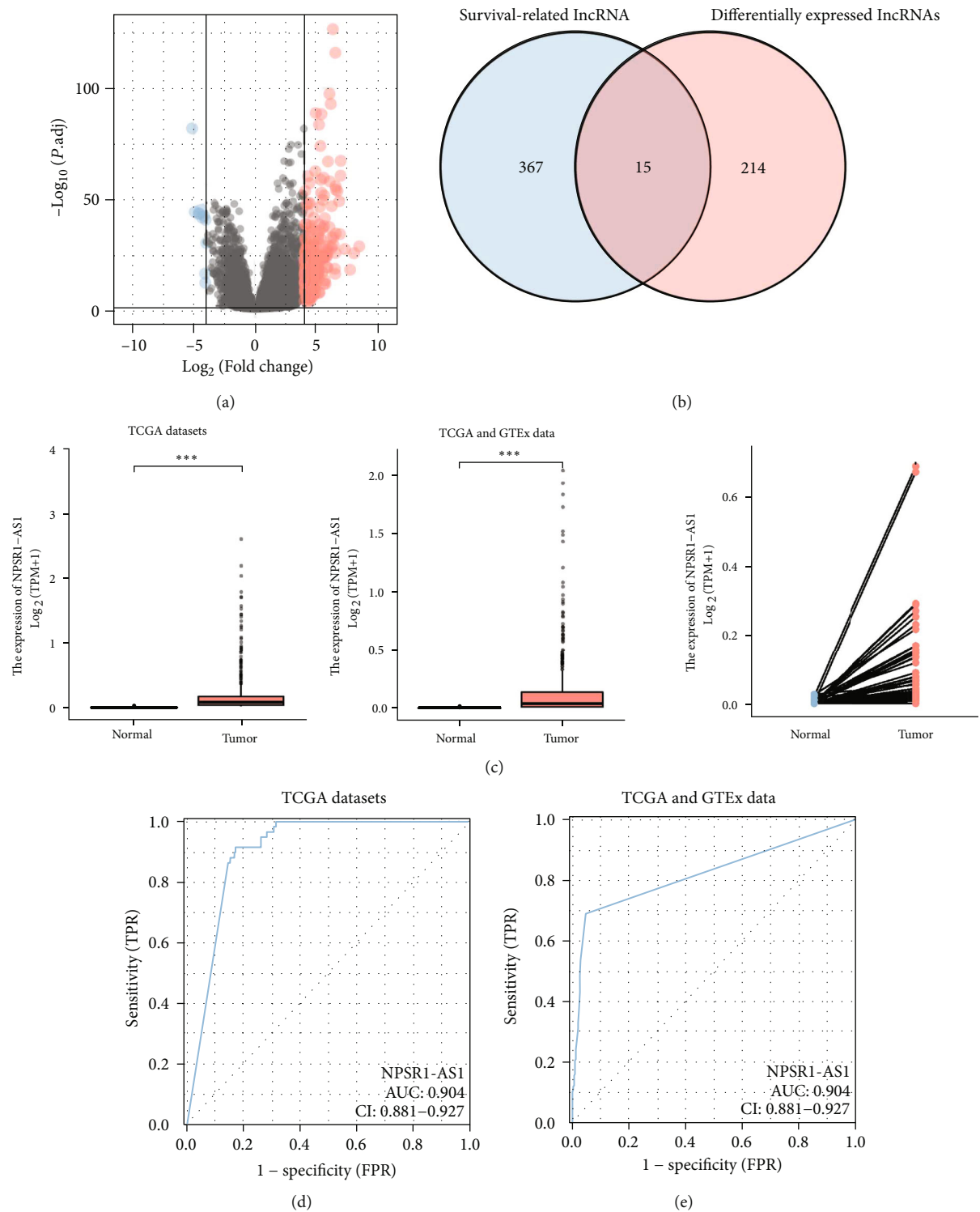
Figure 1: The expression of NPSR1-AS1 was distinctly increased in LUAD. (a) 229 DELs (including 216 upregulated lncRNAs and 13 downregulated lncRNAs) between LUAD specimens and nontumor specimens from TCGA datasets were shown in volcano map. (b) Venn diagram showed the overlapping lncRNA between 229 DELs and 382 survival-related lncRNAs. (c) The expression of NPSR1-AS1 in LUAD specimens and nontumor specimens. (d, e) ROC assays were used to investigate the diagnostic value of NPSR1-AS1 for LUAD patients in the datasets obtained from TCGA.
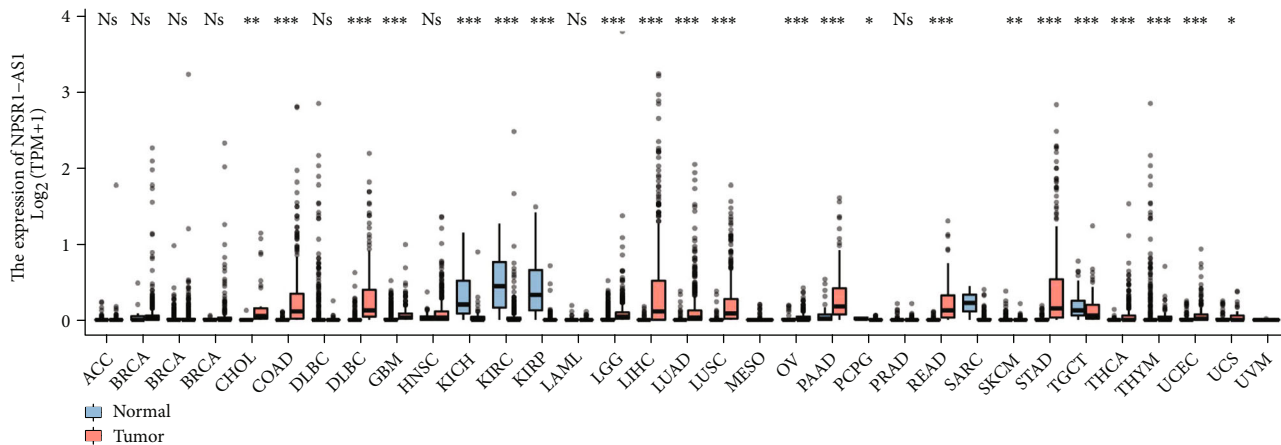
Figure 2: Pancancer analysis of NPSR1-AS1 expression.

(a)

Figure 3: Continued.

(b)
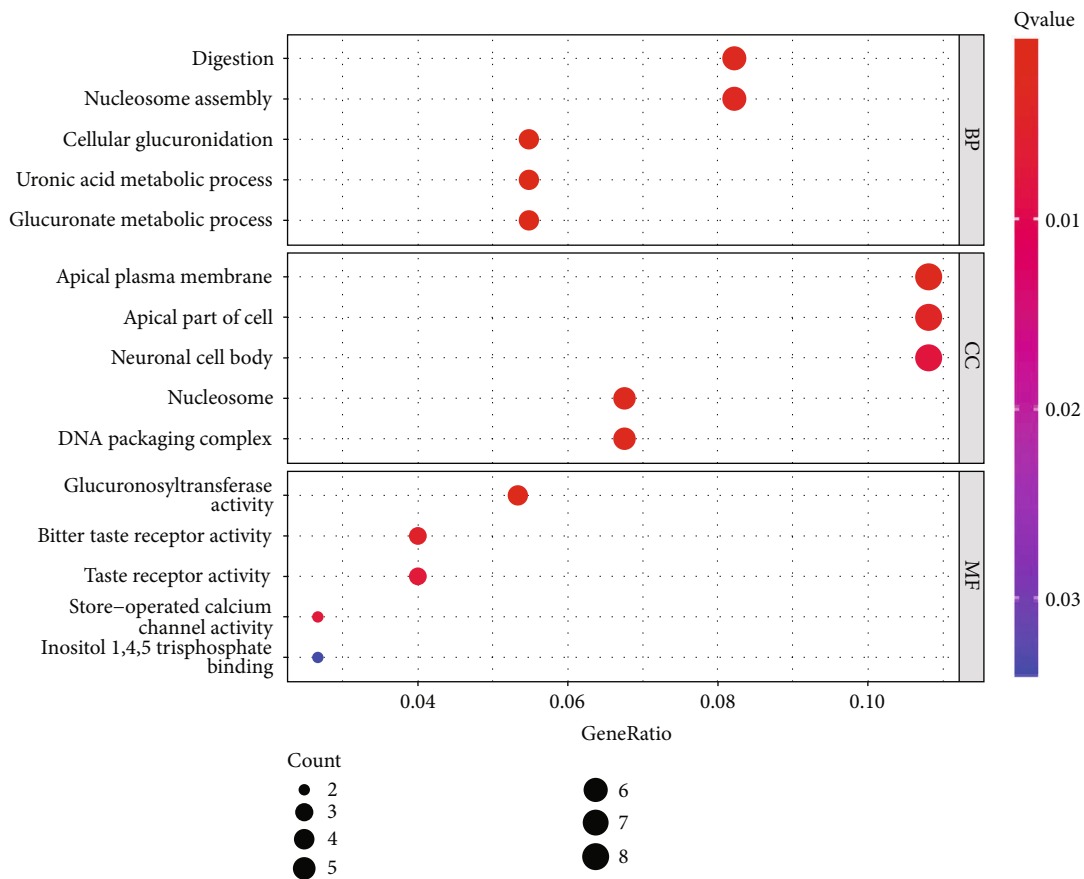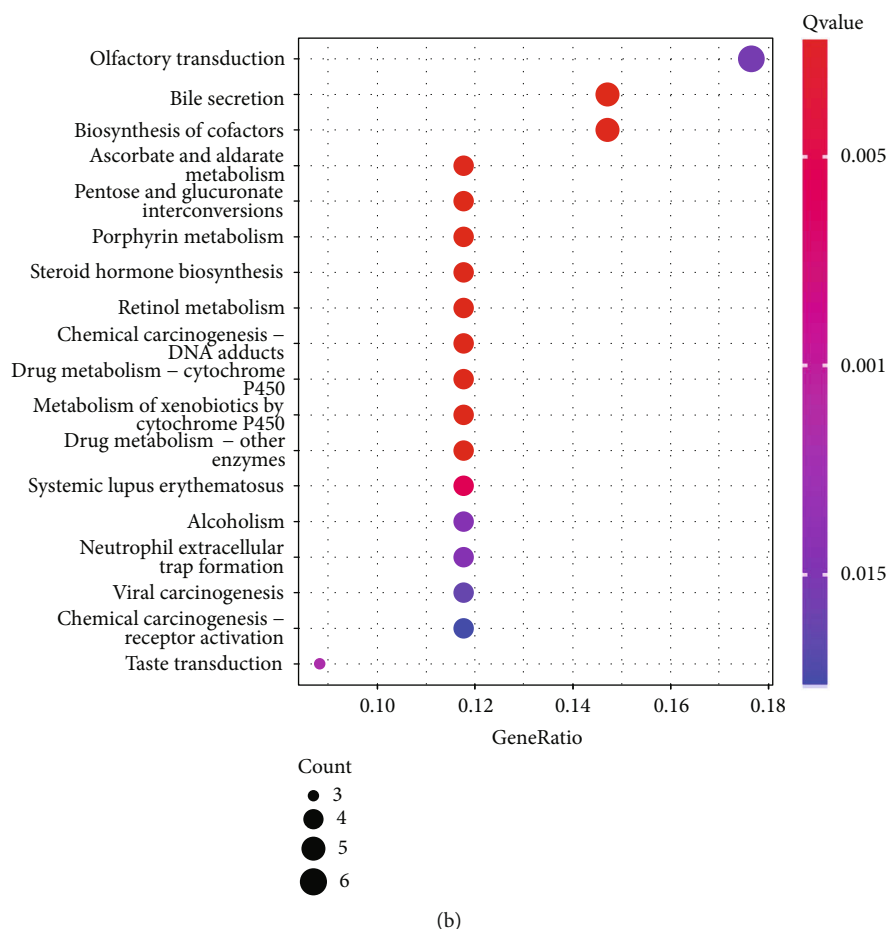
FIGURE 3: Functional enrichment analysis of DEGs between the high-NPSR1-AS1-expression group and low-NPSR1-AS1-expression group. (a) Significantly enriched GO terms of DEGs. (b) Significant KEGG pathway terms of DEGs.

that was lower than the median expression level across all samples. It was performed in order to facilitate the screening process for survival-related genes. A log-rank test was applied to compare the Kaplan-Meier curves of the high-expression cohort with those of the low-expression cohort. In order to determine the factors that are linked with survival, a multivariate analysis using the Cox proportional hazard model was carried out. Adjusted hazard ratios (HRs) and 95% confidence intervals (CIs) are reported. The level of significance for each test was two-sided and set at P less than 0.05. The "survival" package in R was utilized in order to successfully complete the procedure (https://cran.r-project.org/web/packages/survival/index.html).

2.4. Functional Enrichment Analysis. We separated the tumor groups into high- and low-expression subgroups based on the median expression values of NPSR1-AS1, and we used the "limma" R package to screen for differentially expressed genes (DEGs) between the two subgroups. In order to be considered statistically significant, the |logFoldChange (logFC)| value needed to be greater than 2, and the false discovery rate (FDR) needed to be lower than 0.05. The next step was to conduct a study of GO and KEGG enrichment of MMP14 coexpressed genes. The procedure was carried out with the assistance

of the R programming language and the clusterProfiler, Enrichment plot, and GGplot2 software programs.

2.5. Analysis of Infiltrating Immune Cell Types (TIICs) in the Microenvironment of LUAD. To examine the relative expression levels of 22 different TIICs in LUAD samples, the CIBERSORT package of the R software was utilized in its version 3.6.3 form [30]. We determined the percentages of each of these 22 TIIC subpopulations that were present in each sample.

2.6. Statistical Analysis. The statistical studies were carried out with the help of the R programming language. The Wilcoxon test was used to evaluate whether or not there were continuous variable differences between the two groups. The Kruskal-Wallis test was applied to make comparisons between more than two different groups. Either the chi-square test or Fisher's exact test was used to investigate the variations in frequency of occurrence between category variables. The log-rank test was utilized for the study of the variations in survival rates. In the analysis of disease-specific survival (DSS) or overall survival, the Cox assays was utilized for the purpose of calculating the hazard ratios (HRs) of variables together with their respective 95% confidence intervals (95% CIs). Moreover,
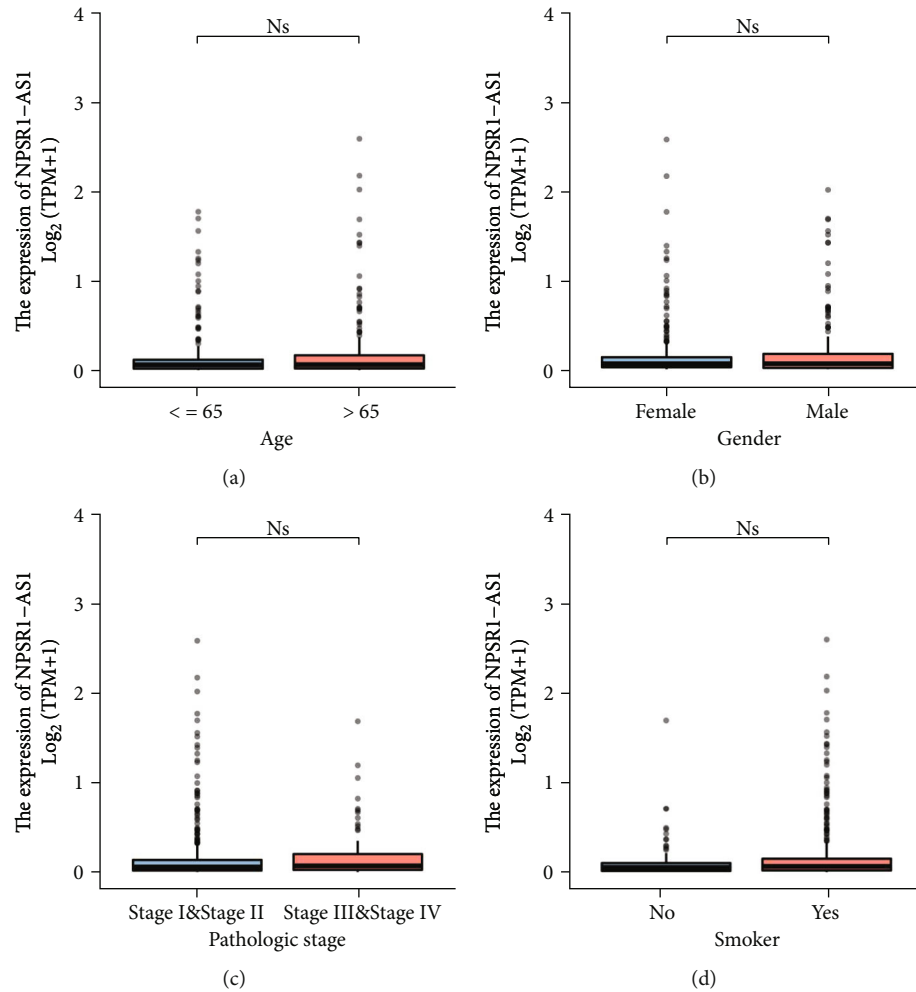
Figure 4: Relationships between NPSR1-AS1 expressions and clinicopathological parameters in LUAD patients. (a) Age. (b) Gender. (c) Pathologic stage. (d) Smoker.

Pearson's correlation and Spearman's correlation were used to assess the correlations between different genes. A $P < 0.05$ was considered statistically significant.

3. Results

3.1. Identification of the Survival-Related DELs in LUAD. The transcriptional profiles of 535 tumor samples and 59 normal samples were first retrieved from TCGA databases and then reanalyzed by our team. It was possible to determine the levels of expression for all lncRNAs. We were able to collect a total of 229 DELs, 216 of which were upregulated lncRNAs and 13 of which were downregulated lncRNAs (Figure 1(a)). Then, we screened the lncRNAs associated with survival, and we found 382 survival-related lncRNAs that had a P value of less than 0.01 (Table S1). Venn diagram showed the overlapping lncRNAs between 229 DELs and 382 survival-related lncRNAs, and 15 survival-related DELs were identified, including FAM83A-AS1, LINC01833, LASTR, AC022784.1, AC068228.1, AC010343.3, NPSR1-AS1, LINC01559, AC005256.1, AC125603.2, AL365181.3, AL365181.2, AC125603.1, LINC00973, and

LINC02535 (Figure 1(b)). NPSR1-AS1 was the primary focus of our study among the 15 survival-related DELs listed above. We observed that the expressions of NPSR1-AS1 were markedly elevated in LUAD tissues when compared to nontumor specimens (Figure 1(c)). Additionally, the diagnostic significance of NPSR1-AS1 for LUAD patients was investigated using data from TCGA datasets. According to the results of the ROC tests, high NPSR1-AS1 expression yielded an AUC value of 0.904 for LUAD with a 95% confidence interval ranging from 0.881 to 0.927 (Figure 1(d)). Moreover, based on the data from TCGA and GTEx data, the results of ROC assays indicated that high NPSR1-AS1 expression had an AUC value of 0.824 (95% CI: 0.801 to 0.847) for LUAD (Figure 1(e)).

3.2. Pancancer Analysis of NPSR1-AS1 Expression. In addition, we performed pancancer analysis of NPSR1-AS1 expression using TCGA and GTEx data. As shown in Figure 2, we found that the expression of NPSR1-AS1 was distinctly increased in many types of tumors, such as CHOL, COAD, and ESCA. Our findings suggested that NPSR1-AS1 upregulation may be a common event.

TABLE 1: The relationship between NPSR1-AS1 expression and clinicopathological characteristics in patients with LUAD.

Characteristic	Low expression of NPSR1-AS1	High expression of NPSR1-AS1	P
n	267	268	
Age, n (%)			1.000
≤65	128 (24.8%)	127 (24.6%)	
>65	130 (25.2%)	131 (25.4%)	
Gender, n (%)			0.968
Female	142 (26.5%)	144 (26.9%)	
Male	125 (23.4%)	124 (23.2%)	
Pathologic stage, n (%)			0.244
Stage I	158 (30%)	136 (25.8%)	
Stage II	57 (10.8%)	66 (12.5%)	
Stage III	36 (6.8%)	48 (9.1%)	
Stage IV	12 (2.3%)	14 (2.7%)	
Age, median (IQR)	66 (59, 72)	66 (59, 72)	0.616

3.3. Functional Enrichment Analysis.

To further explore the roles of NPSR1-AS1 in LUAD, we used the "limma" R package to separate the tumor groups into high- and low-expression subgroups based on median expression values of NPSR1-AS1. Following that, 79 DEGs were found. Then, we performed GO analysis using 79 DEGs. As shown in Figure 3(a), we found that the 79 DEGs were mainly enriched in digestion, nucleosome assembly, cellular glucuronidation, uronic acid metabolic process, glucuronate metabolic process, apical plasma membrane, apical part of cell, neuronal cell body, nucleosome, DNA packaging complex, glucuronosyltransferase activity, bitter taste receptor activity, taste receptor activity, store-operated calcium channel activity, and inositol 1,4,5-trisphosphate binding. Moreover, the results of KEGG assays indicated that the 79 DEGs were mainly enriched in olfactory transduction, bile secretion, biosynthesis of cofactors, ascorbate and aldarate metabolism, pentose and glucuronate interconversions, porphyrin metabolism, steroid hormone biosynthesis, retinol metabolism, viral carcinogenesis, and chemical carcinogenesis-receptor activation (Figure 3(b)).

3.4. Correlation of High NPSR1-AS1 Expression with Clinicopathological Features of LUAD.

In order to carry out statistical analysis, the level of NPSR1-AS1 expression was split between high- and low-expression groups. In individuals diagnosed with LUAD, an investigation was conducted to determine whether or not there was a correlation between the expression of NPSR1-AS1 and clinicopathological features. However, we find that the expressions of NPSR1-AS1 were not associated with age (Figure 4(a)), gender (Figure 4(b)), pathologic stage (Figure 4(c)), and smoker (Figure 4(d)). In addition, the results from the chi-square test also showed a similar finding (Table 1).

3.5. Relationship between NPSR1-AS1 Expression and Survival Outcomes in LUAD Patients.

Further, we investigated whether or not the expression of NPSR1-AS1 was connected with the fate of LUAD patients. Patients who had high levels of NPSR1-AS1 had a lower overall survival rate than those who had low levels of NPSR1-AS1 (Figure 5(a), $P = 0.003$), as shown by the findings of a Kaplan-Meier survival analysis. In addition, the group with high levels of NPSR1-AS1 showed a considerably lower DSS than the group with low levels of NPSR1-AS1 expression (Figure 5(b), $P = 0.043$).

3.6. Prognostic Factors Determined by Univariate and Multivariate Cox Regression Analysis.

The next step was to conduct univariate and multivariate analysis to determine whether the NPSR1-AS1 expression level was an independent predictive indicator of LUAD patient outcomes. According to the findings of our study, both the pathologic stage and the expression of NPSR1-AS1 functioned as independent prognostic indicators for overall survival (Table 2). In addition, it was demonstrated that the pathologic stage is an independent prognostic indication for patients diagnosed with LUAD (Table 3). However, no additional evidence of NPSR1-AS1 expression could be found in DSS (Table 3).

3.7. The Expression of NPSR1-AS1 Was Associated with Immune Cell Infiltration.

The ssGSEA methodology was utilized to analyze the transcriptomes of TCGA-LUAD cohort in order to determine the degree to which immune cell infiltration was present. Twenty-four immune-related phrases were included in the study in order to determine the number of immune cells that are present in the microenvironment of a tumor. Our group observed that the expressions of NPSR1-AS1 were negatively associated with CD8 T cells, pDC, cytotoxic cells, mast cells, iDC, neutrophils, NK CD56dim cells, DC, Th17 cells, Tgd, and macrophages, while they were positively associated with NK CD56bright cells and B cells (Figure 6).

4. Discussion

Tumor developments were dependent on the survivals and death of tumor cells [31]. The study of cell death can therefore assist us in understanding the underlying mechanisms that are responsible for the development of malignancies [32]. In addition to the well-known techniques of functional genes, researchers are uncovering other kinds of regulators that are involved in the progression of tumors. In recent years, for instance, lncRNAs have garnered a lot of attention from researchers [33, 34]. Research on lncRNAs has also become increasingly common. However, the majority of the attention has been directed toward conducting more in-depth basic studies. The question of whether lncRNAs can give doctors with some therapeutic insight has received very little attention in the published research. In the subject of LUAD research, there are likewise very few studies. Therefore, in the hopes of locating additional new approaches that may be utilized for clinical diagnosis and therapy, we decided to conduct research on the relationship that existed between lncRNAs and the clinical data associated with LUAD.

(a)

(b)
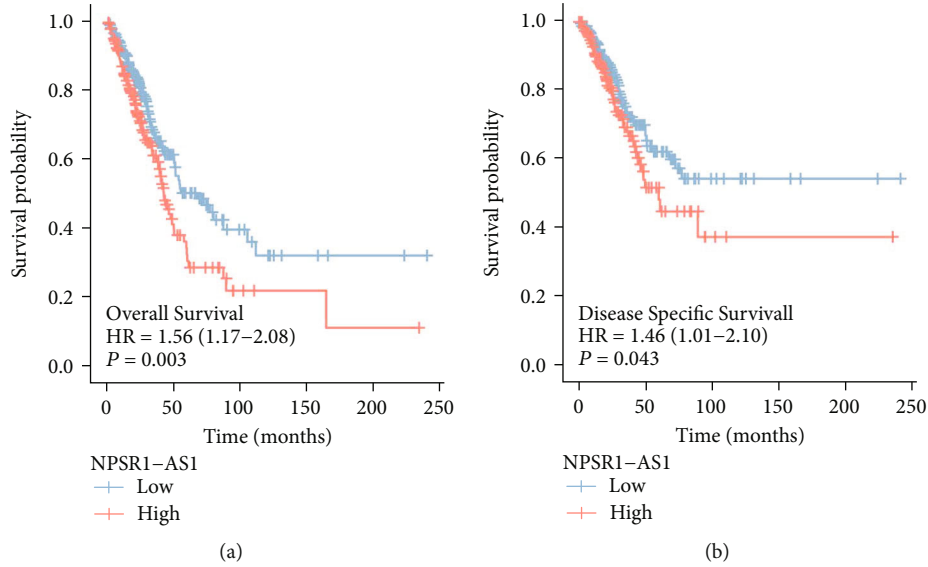
FIGURE 5: Kaplan-Meier survival analysis was applied to examine the prognostic value of NPSR1-AS1 expression in (a) OS and (b) DSS of LUAD patients.

TABLE 2: Univariate and multivariate analysis of different prognostic factors for overall survival in patients with LUAD.

Characteristics	Total (N)	Univariate analysis		Multivariate analysis	
		Hazard ratio (95% CI)	P value	Hazard ratio (95% CI)	P value
Gender	526				
Female	280	Reference			
Male	246	1.070 (0.803-1.426)	0.642		
Age	516				
≤65	255	Reference			
>65	261	1.223 (0.916-1.635)	0.172		
Pathologic stage	518				
Stage I & stage II	411	Reference			
Stage III & stage IV	107	2.664 (1.960-3.621)	<0.001	2.535 (1.860-3.455)	<0.001
NPSR1-AS1	526				
Low	263	Reference			
High	263	1.557 (1.165-2.081)	0.003	1.442 (1.074-1.936)	0.015

In our study, we performed an analysis on TCGA datasets, and as a result, we found a total of 229 DELs, which included 216 upregulated lncRNAs and 13 downregulated lncRNAs. NPSR1-AS1 was the primary focus of our attention. In the past, a number of studies have indicated that NPSR1-AS1 served a function in a variety of cancers. For instance, He et al. revealed that the expressions of NPSR1-AS1 were shown to be increased in hepatocellular carcinoma tissues and cell lines. In the following step, the ectopic expression of NPSR1-AS1 regulated the MAPK/ERK pathway, which in turn accelerated the proliferation and glycolysis of hepatocellular carcinoma cells [35]. Dastjerdi et al. showed that NPSR1-AS1 had the ability to make a considerable distinction between the tumor and the normal samples. These findings might have repercussions for the early diagnosis and focused treatment of colorectal cancer in the future [36]. He et al. discovered that NPSR1-AS1 activated

the MAPK pathway to promote the proliferation and metastasis of thyroid cancer cells by engaging ELAVL1 to stabilize NPSR1 mRNA. This was accomplished by facilitating the proliferation of thyroid cancer cells [35]. In the first part of our study, we observed that the level of NPSR1-AS1 was significantly higher in LUAD tissues compared to nontumor specimens. This finding was in line with findings from other studies. The findings of the ROC tests then revealed that NPSR1-AS1 may be utilized as an indicator to screen LUAD specimens vs. nontumor specimens. In addition, the expression of NPSR1-AS1 was shown to be significantly elevated in many other kinds of tumors, such as CHOL, COAD, and ESCA, according to the findings of a pancancer investigation. Our research led us to believe that an upregulation of NPSR1-AS1 is a rather typical occurrence. The GO and KEGG tests found evidence that NPSR1-AS1 may play a regulatory role in the course of LUAD by exerting an influence

TABLE 3: Univariate and multivariate analysis of different prognostic factors for disease specific survival in patients with LUAD.

Characteristics	Total (N)	Univariate analysis Hazard ratio (95% CI)	P value	Multivariate analysis Hazard ratio (95% CI)	P value
Gender	491				
Female	262	Reference			
Male	229	0.989 (0.687-1.424)	0.954		
Age	481				
≤65	243	Reference			
>65	238	1.013 (0.701-1.464)	0.944		
Pathologic stage	483				
Stage I & stage II	389	Reference			
Stage III & stage IV	94	2.436 (1.645-3.605)	<0.001	2.322 (1.562-3.450)	<0.001
NPSR1-AS1	491				
Low	251	Reference			
High	240	1.460 (1.013-2.105)	0.043	1.370 (0.943-1.988)	0.098
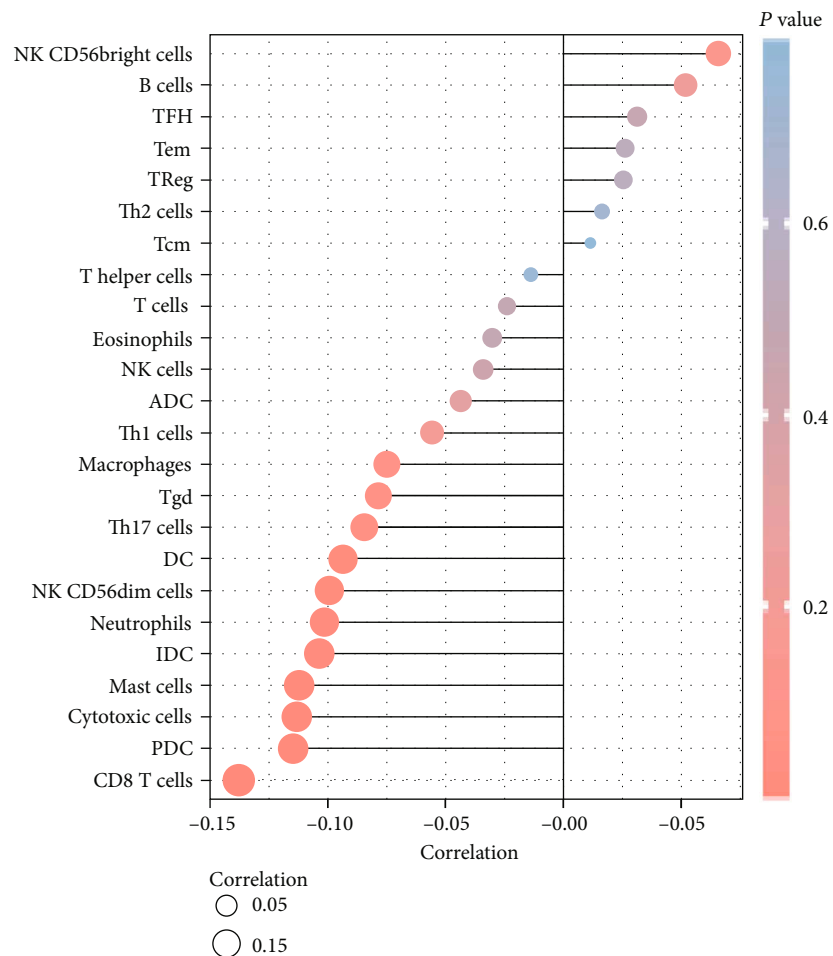
FIGURE 6: The expression of NPSR1-AS1 was associated with immune cell infiltration.

over a number of different tumor-related pathways. Patients who had a high level of NPSR1-AS1 expression in clinical studies were found to have a lower overall survival time and disease-free survival time than patients who had a low level of NPSR1-AS1 expression. Moreover, multivariate studies demonstrated that NPSR1-AS1 expression was an independent prognostic factor for overall survival of LUAD patients. Based on these findings, we hypothesized that NPSR1-AS1 could serve as a diagnostic and prognostic biomarker for patients with LUAD. The prognosis of LUAD

will be further investigated in subsequent studies in which we will also further evaluate the association between NPSR1-AS1-associated genes and the prognosis.

Tumor stromal cells are part of the tumor microenvironment and can influence how cancerous tumor cells behave [37]. One type of immune cell that plays a crucial role in tumor development and progression is called tumor-infiltrating lymphocytes (TILs). By building a complex intercellular contact network, TILs aid in the development and maintenance of an immunosuppressive environment, aid in immune escape, and eventually contribute to tumor progression [38]. Research on immune cell infiltration has revealed that there is a significant function for immune cells in the TME in the progression of cancer. New approaches to cancer immunotherapy may be easier to come up with if researchers had a better grasp of how immune cells infiltrate the immunological milieu. We found that the expression of NPSR1-AS1 was negatively associated with CD8 T cells, pDC, cytotoxic cells, mast cells, iDC, neutrophils, NK CD56dim cells, DC, Th17 cells, Tgd, and macrophages, while it was positively associated with NK CD56bright cells and B cells. It is possible that Th17 cells have an antitumor effect because the subgroup of patients with LUAD that has a greater infiltration of Th17 cells is less likely to develop lymph node metastases and more likely to have a better prognosis. Therefore, based on the findings of our study, immunosuppression, which is caused by the presence of less Th17 cells in the primary tumor microenvironment, may be the cause of a shorter survival rate at 10 years for patients with LUAD who have high levels of NPSR1-AS1.

Despite the fact that our research showed a relationship between NPSR1-AS1 and LUAD, there were still several limitations to our investigation that need to be addressed. Firstly, the number of patients who participated in this study was rather low, which meant that additional research including a substantial number of participants was necessary to validate our findings. Secondly, most of our findings were obtained from bioinformatics analysis and TCGA datasets, which lack experimental verification in in vitro and in vivo experiments.

5. Conclusion

It is possible that NPSR1-AS1 is a predictive biomarker for LUAD, which is the factor that determines how well cancer immunotherapy works. The findings of the current research have the potential to offer fresh perspectives on the formulation of efficient therapy methods directed against LUAD.

Data Availability

The datasets used and analyzed during the present study are available from the corresponding authors upon rational request.

Conflicts of Interest

The authors declare that they have no conflicts of interest regarding the publication of this paper.

Authors' Contributions

Hui Zhang and Jin Yuan contributed equally to this work.

Supplementary Materials

Table S1: the survival-related lncRNA in LUAD. (Supplementary Materials)

References

[1] R. L. Siegel, K. D. Miller, and A. Jemal, "Cancer statistics, 2019," *CA: a Cancer Journal for Clinicians*, vol. 69, no. 1, pp. 7–34, 2019.

[2] C. Mattiuzzi and G. Lippi, "Current cancer epidemiology," *J Epidemiol Glob Health*, vol. 9, no. 4, pp. 217–222, 2019.

[3] J. A. Barta, C. A. Powell, and J. P. Wisnivesky, "Global epidemiology of lung cancer," *Annals of Global Health*, vol. 85, no. 1, 2019.

[4] T. Deli, M. Orosz, and A. Jakab, "Hormone replacement therapy in cancer survivors-review of the literature," *Pathology Oncology Research*, vol. 26, no. 1, pp. 63–78, 2020.

[5] O. Tonyali, O. Gonullu, M. A. Ozturk, A. Kosif, and O. G. Civi, "Hepatoid adenocarcinoma of the lung and the review of the literature," *Journal of Oncology Pharmacy Practice*, vol. 26, no. 6, pp. 1505–1510, 2020.

[6] T. V. Denisenko, I. N. Budkevich, and B. Zhivotovsky, "Cell death-based treatment of lung adenocarcinoma," *Cell Death & Disease*, vol. 9, no. 2, p. 117, 2018.

[7] M. Saito, H. Suzuki, K. Kono, S. Takenoshita, and T. Kohno, "Treatment of lung adenocarcinoma by molecular-targeted therapy and immunotherapy," *Surgery Today*, vol. 48, no. 1, pp. 1–8, 2018.

[8] S. B. Goldberg, J. N. Contessa, S. B. Omay, and V. Chiang, "Lung cancer brain metastases," *Cancer Journal*, vol. 21, no. 5, pp. 398–403, 2015.

[9] G. Toyokawa, M. Takenoyama, and Y. Ichinose, "Multimodality treatment with surgery for locally advanced non-small-cell lung cancer with n2 disease: a review article," *Clinical Lung Cancer*, vol. 16, no. 1, pp. 6–14, 2015.

[10] P. Brennan, P. Hainaut, and P. Boffetta, "Genetics of lung-cancer susceptibility," *The Lancet Oncology*, vol. 12, no. 4, pp. 399–408, 2011.

[11] Y. Wang, W. Y. Pan, J. S. Ge et al., "A review of the relationship between long noncoding RNA and post-stroke injury repair," *The Journal of International Medical Research*, vol. 47, no. 10, pp. 4619–4624, 2019.

[12] Y. Li and X. Wang, "Role of long noncoding RNAs in malignant disease (review)," *Molecular Medicine Reports*, vol. 13, no. 2, pp. 1463–1469, 2016.

[13] W. Lin, Q. Zhou, C. Q. Wang et al., "LncRNAs regulate metabolism in cancer," *International Journal of Biological Sciences*, vol. 16, no. 7, pp. 1194–1206, 2020.

[14] P. K. Puvvula, "LncRNAs regulatory networks in cellular senescence," *International Journal of Molecular Sciences*, vol. 20, no. 11, p. 2615, 2019.

[15] M. Kazimierczyk, M. K. Kasprowicz, M. E. Kasprzyk, and J. Wrzesinski, "Human long noncoding RNA interactome: detection, characterization and function," *International Journal of Molecular Sciences*, vol. 21, no. 3, p. 1027, 2020.

[16] F. Bella and S. Campo, "Long non-coding RNAs and their involvement in bipolar disorders," *Gene*, vol. 796-797, article 145803, 2021.

[17] W. X. Peng, P. Koirala, and Y. Y. Mo, "LncRNA-mediated regulation of cell signaling in cancer," *Oncogene*, vol. 36, no. 41, pp. 5661–5667, 2017.

[18] J. Li, Z. Li, W. Zheng et al., "LncRNA-ATB: an indispensable cancer-related long noncoding RNA," *Cell Proliferation*, vol. 50, no. 6, 2017.

[19] Z. Zhang, Y. Yan, B. Zhang, Y. Ma, C. Chen, and C. Wang, "Long non-coding RNA SNHG17 promotes lung adenocarcinoma progression by targeting the microRNA-193a-5p/NETO2 axis," *Oncology Letters*, vol. 22, no. 6, p. 818, 2021.

[20] Z. Cong, Y. Diao, Y. Xu et al., "Long non-coding RNA linc00665 promotes lung adenocarcinoma progression and functions as ceRNA to regulate AKR1B10-ERK signaling by sponging miR-98," *Cell Death & Disease*, vol. 10, no. 2, p. 84, 2019.

[21] L. B. Kennedy and A. K. S. Salama, "A review of cancer immunotherapy toxicity," *CA: a Cancer Journal for Clinicians*, vol. 70, no. 2, pp. 86–104, 2020.

[22] A. Steven, S. A. Fisher, and B. W. Robinson, "Immunotherapy for lung cancer," *Respirology*, vol. 21, no. 5, pp. 821–833, 2016.

[23] Y. Igarashi and T. Sasada, "Cancer vaccines: toward the next breakthrough in cancer immunotherapy," *Journal of Immunology Research*, vol. 2020, Article ID 5825401, 13 pages, 2020.

[24] O. Zimmermannova, I. Caiado, A. G. Ferreira, and C. F. Pereira, "Cell fate reprogramming in the era of cancer immunotherapy," *Frontiers in Immunology*, vol. 12, article 714822, 2021.

[25] C. Hayes, "Cellular immunotherapies for cancer," *Irish Journal of Medical Science*, vol. 190, no. 1, pp. 41–57, 2021.

[26] L. Bejarano, M. J. C. Jordão, and J. A. Joyce, "Therapeutic targeting of the tumor microenvironment," *Cancer Discovery*, vol. 11, no. 4, pp. 933–959, 2021.

[27] I. Terrén, A. Orrantia, J. Vitallé, O. Zenarruzabeitia, and F. Borrego, "NK cell metabolism and tumor microenvironment," *Frontiers in Immunology*, vol. 10, p. 2278, 2019.

[28] X. Mao, J. Xu, W. Wang et al., "Crosstalk between cancer-associated fibroblasts and immune cells in the tumor microenvironment: new findings and future perspectives," *Molecular Cancer*, vol. 20, no. 1, p. 131, 2021.

[29] T. Ni, D. Guo, L. Tan, Z. Xiao, and Y. Shi, "NPSR1-AS1 activates the MAPK pathway to facilitate thyroid cancer cell malignant behaviors via recruiting ELAVL1 to stabilize NPSR1 mRNA," *Cell Cycle*, vol. 21, no. 5, pp. 439–449, 2022.

[30] A. M. Newman, C. L. Liu, M. R. Green et al., "Robust enumeration of cell subsets from tissue expression profiles," *Nature Methods*, vol. 12, no. 5, pp. 453–457, 2015.

[31] M. Yakubu, O. Meggetto, Y. Lai, L. Peirson, M. Walker, and A. Lofters, "Impact of postal correspondence letters on participation in cancer screening: a rapid review," *Preventive Medicine*, vol. 145, article 106404, 2021.

[32] B. Kretzler, H. H. König, L. Brandt, and A. Hajek, "Religion and cancer prevention: study protocol for a systematic review," *BMJ Open*, vol. 11, no. 12, article e046126, 2021.

[33] X. Pan, G. Zheng, and C. Gao, "LncRNA PVT1: a novel therapeutic target for cancers," *Clinical Laboratory*, vol. 64, no. 5, pp. 655–662, 2018.

[34] C. Hu, W. Xu, B. Wang et al., "Critical functions of lncRNA DGCR5 in cancers of the digestive system," *Current Pharmaceutical Design*, vol. 27, no. 40, pp. 4147–4151, 2021.

[35] H. He, T. Chen, H. Mo, S. Chen, Q. Liu, and C. Guo, "Hypoxia-inducible long noncoding RNA NPSR1-AS1 promotes the proliferation and glycolysis of hepatocellular carcinoma cells by regulating the MAPK/ERK pathway," *Biochemical and Biophysical Research Communications*, vol. 533, no. 4, pp. 886–892, 2020.

[36] S. Dastjerdi, M. Valizadeh, R. Nemati et al., "Highly expressed TLX1NB and NPSR1-AS1 lncRNAs could serve as diagnostic tools in colorectal cancer," *Human Cell*, vol. 34, no. 6, pp. 1765–1774, 2021.

[37] T. F. Gajewski, H. Schreiber, and Y. X. Fu, "Innate and adaptive immune cells in the tumor microenvironment," *Nature Immunology*, vol. 14, no. 10, pp. 1014–1022, 2013.

[38] S. T. Paijens, A. Vledder, M. de Bruyn, and H. W. Nijman, "Tumor-infiltrating lymphocytes in the immunotherapy era," *Cellular & Molecular Immunology*, vol. 18, no. 4, pp. 842–859, 2021.

Retraction

Retracted: SFRP2 is a Novel Diagnostic Biomarker and Suppresses the Proliferation of Pituitary Adenoma

Journal of Oncology

This article has been retracted by Hindawi following an investigation undertaken by the publisher [1]. This investigation has uncovered evidence of one or more of the following indicators of systematic manipulation of the publication process:

(1) Discrepancies in scope

(2) Discrepancies in the description of the research reported

(3) Discrepancies between the availability of data and the research described

(4) Inappropriate citations

(5) Incoherent, meaningless and/or irrelevant content included in the article

(6) Peer-review manipulation

The presence of these indicators undermines our confidence in the integrity of the article's content and we cannot, therefore, vouch for its reliability. Please note that this notice is intended solely to alert readers that the content of this article is unreliable. We have not investigated whether authors were aware of or involved in the systematic manipulation of the publication process.

Wiley and Hindawi regrets that the usual quality checks did not identify these issues before publication and have since put additional measures in place to safeguard research integrity.

We wish to credit our own Research Integrity and Research Publishing teams and anonymous and named external researchers and research integrity experts for contributing to this investigation.

The corresponding author, as the representative of all authors, has been given the opportunity to register their agreement or disagreement to this retraction. We have kept a record of any response received.

References

[1] R. Huang, D. Chen, H. Wang, B. Zhang, Y. Zhang, and W. Ren, "SFRP2 is a Novel Diagnostic Biomarker and Suppresses the Proliferation of Pituitary Adenoma," *Journal of Oncology*, vol. 2022, Article ID 4272525, 8 pages, 2022.

Hindawi

Research Article

SFRP2 is a Novel Diagnostic Biomarker and Suppresses the Proliferation of Pituitary Adenoma

Rongxi Huang,[1] Danyan Chen,[1] Hongman Wang,[1] Binghan Zhang,[1] Yu Zhang,[1] and Wei Ren [2]

[1]*Department of Endocrinology, Chongqing General Hospital, Chongqing, China*
[2]*Department of Instrument, Chongqing Emergency Medical Center, Chongqing, China*

Correspondence should be addressed to Wei Ren; 20140204368@cqu.edu.cn

Pituitary adenoma (PA) constitutes one of the most common intracranial tumors. The present study was designed to identify potential diagnostic markers for PA. We used gene expression profiles (GEO: GSE26966 and GEO: GSE63357 datasets) derived from human PA and nontumor samples that were made freely accessible by the gene expression omnibus (GEO) datasets. Differentially expressed genes (DEGs) were screened between 14 normal specimens and 34 PA specimens by the use of the limma package of the R. The diagnostic genes were determined using a LASSO regression model and SVM-RFE analysis. SFRP2 expression in PA cells was analyzed using RT-PCR, and the effect of SFRP2 dysregulation on PA cell proliferation was measured using CCK-8 analysis. In this study, 361 DEGs were identified: 309 genes were downregulated and 52 genes were upregulated. The results of KEGG assays revealed that the 361 DEGs were mainly enriched in the PI3K-Akt signaling pathway, MAPK signaling pathway, growth hormone synthesis, secretion and action, and AGE-RAGE signaling pathway in diabetic complications. Results from the LASSO regression model and the SVM-RFE analysis indicated that LOC101060391 and SFRP2 were diagnostic genes. In contrast to normal tissue, the expressions of LOC101060391 and SFRP2 were much lower in PA samples. According to the ROC assays, high LOC101060391 and SFRP2 expression had an AUC value >0.9 for PA. Upregulation of SFRP2 distinctly inhibited the proliferative capacity of PA cells, as shown by CCK-8 analysis. Furthermore, knockdown of SFRP2 had an influence on cell growth in both the AtT-20 and HP75 cell lines. Taken together, our findings indicate that LOC101060391 and SFRP2 have diagnostic potential for PA. Furthermore, SFRP2 may be an antioncogene and a therapeutic target for PA.

1. Introduction

Pituitary adenoma (PA), accounting for 10%–15% of all cranial tumors, is the third most common brain tumor [1]. Noninvasive pituitary adenocarcinomas (NIPAs), invasive pituitary adenocarcinomas (IPAs), and pituitary adenocarcinomas (PAs) are the three categories that can be used to classify PAs [2, 3]. IPAs have a tendency to infiltrate key surrounding structures, such as the cavernous sinus, the sphenoid bone, and the cranial nerves because of their highly proliferative and invasive nature [4, 5]. When a tumor presses on a nearby organ or tissue, it can create symptoms such as headaches or vision problems, which lead doctors to suspect PAs. This is because PAs do not typically present

with the typical symptoms that are associated with hormone hypersecretion [6, 7]. On the other hand, certain tumors have the potential to spread to the cavernous sinus or the region around the internal carotid artery, making it hard to do a total excision [8]. Surgical treatment is beneficial for NFPAs; however, complete removal of certain tumors is not achievable. The purposes of these three different treatment strategies are to lessen or remove the impact of tumor-occupying lesions, rectify excessive hormone release by the tumor, and maintain normal pituitary function [9, 10]. However, after surgery to remove a pituitary tumor, the recurrence rate is rather significant, ranging from 7 to 35 percent [11]. In addition, surgery to remove a pituitary tumor may result in problems such as diabetes insipidus,

sphenoid sinusitis, leakage of cerebrospinal fluid, worsening of visual impairment, cerebral palsy, and meningitis [12, 13]. Therefore, it is essential to research and develop effective treatments as well as innovative diagnostic biomarkers.

New disease-related genes have been discovered through the use of microarrays and integrated bioinformatics analysis in recent years. These genes have the potential to operate as biological markers that are diagnostic as well as predictive [14, 15]. For instance, Yang et al. showed that both PVT1 and EZH2 expression levels were elevated in human glioma tissues and cell lines, and this elevation was found to have a positive correlation with the malignancy of the glioma. In addition, inhibiting the expression of PVT1 led to a reduction in cell proliferation, an increase in apoptosis, and a reduction in both migration and invasion via targeting EZH2. In addition, there was a correlation between high expression of PVT1 and a bad prognosis in glioma patients [16]. Huang et al. reported that in patients who had pituitary tumors, the expression of SIRT1 was found to be downregulated in the tumor tissues. The present work indicated, through in vitro tests, that SIRT1 overexpression decreased pituitary tumor cell line growth by inhibiting PTTG1 expression, whereas SIRT1 downregulation demonstrated the reverse effects on pituitary tumor cell line growth [17]. Daniela et al. indicated that the expression of AP52 is significantly increased in gonadotroph and prolactin-secreting pituitary adenomas, where it corresponds with the expression of HMGA2. The above results are in contrast to the expression of AP52 in normal pituitary tissues. RPSAP52 overexpression, from a functional standpoint, stimulated cell multiplication by functioning as a miRNA sponge for HMGA proteins [18]. However, only a few studies have identified the functional genes involved in PA progression. With this study, we aimed to explore the critical diagnostic genes for PA by the use of machine learning.

2. Materials and Methods

2.1. Cell Culture and Transfection.
The HP75 and AtT-20 pituitary tumor cell lines were cultivated in accordance with the instructions provided by the manufacturer. At 37 degrees Celsius and 5% carbon dioxide, the media was supplemented with 1% penicillin-streptomycin and 10% fetal bovine serum (Gibco, USA). AtT-20 and HP75 cells were seeded in six-well plates at the optimal density a full twenty-four hours before the transfection, and the plates were left to incubate overnight. Both AtT-20 and HP75 cells were transfected with pcDNA-SFRP2, sh-SFRP2, and a control (blank plasmid) using Lipofectamine® 3000 reagent and Opti-MEM medium (Invitrogen Life Technologies, USA) in accordance with the methodology provided by the manufacturer. Tolo Biotech was responsible for the procurement of the pcDNA-SFRP2, sh-SFRP2, and blank plasmid (Shanghai, China).

2.2. RNA Extraction and Quantitative Real-Time Polymerase Chain Reaction (qRT-PCR).
In order to extract total RNA from cells in accordance with the instructions provided by the manufacturer for qRT-PCR, the FastPure Cell/Tissue Total RNA Isolation Kit V2 was utilized. After completing the reverse transcription of lncRNAs and mRNAs with the help of a reverse transcription system kit, the results were analyzed using quantitative polymerase chain reaction (qPCR) using a Universal SYBR qPCR Master Mix kit. According to the procedure manual, GAPDH was employed in the role of an internal control in order to ascertain the level of mRNAs. For relative quantification, the 2Δ-CT approach was applied. The experiments were repeated three times, and each experiment was triplicated.

2.3. Cell Proliferation Assay.
After receiving a variety of treatments, the level of cell proliferation was measured utilizing the Cell Counting Kit-8 (CCK-8; TargetMol, Shanghai, China) in accordance with the protocols provided by the manufacturer. To be more specific, 2×10^3 cells were seeded into each well of a 96-well plate, and the plates were then cultured overnight at 37 degrees Celsius and 5% carbon dioxide. Following this, $10\,\mu$L of CCK-8 was added to each well. Using a microplate reader set to 450 nm, the optical density of each well was measured. The experiments were repeated three times, and each experiment was triplicated.

2.4. Microarray Data.
The series of matrix files of the GSE26966 and GSE63357 datasets were obtained from https://www.ncbi.nlm.nih.gov/geo/. The GSE26966 dataset included 9 normal specimens and 14 tumor specimens, whereas the GSE63357 dataset included 5 normal specimens and 20 tumor specimens. The gene symbols corresponding to the probes in each dataset were converted into those symbols using the probe annotation files. When there was more than one probe that corresponded to the same gene symbol, the final expression value of the gene was computed based on the average of all of the probes. Because these two datasets use the same platform and are important for combining data from various datasets, they were combined into a metadata cohort so that additional integration analysis could be performed on the results of the combined datasets. In addition to this, the combat function contained inside the R software's SVA package was utilized in order to eliminate the batch effect.

2.5. Data Processing and DEG Screening.
After combining the two datasets into a single metadata cohort, the combat function of the SVA package was used to preprocess the data and eliminate any batch effects that may have been present. Differential expression analysis between 14 normal specimens and 34 tumor specimens was all performed with the help of the limma package of the R programming language (https://www.bioconductor.org/). The threshold points for differentially expressed genes (DEGs) were determined to be samples that had an adjusted false discovery rate P that was less than 0.05 and a |log fold change (FC)| that was more than 2.

2.6. Gene Functional Enrichment Analyses.
Using the "clusterProfiler" R package, functional enrichment was

(a)

(b)
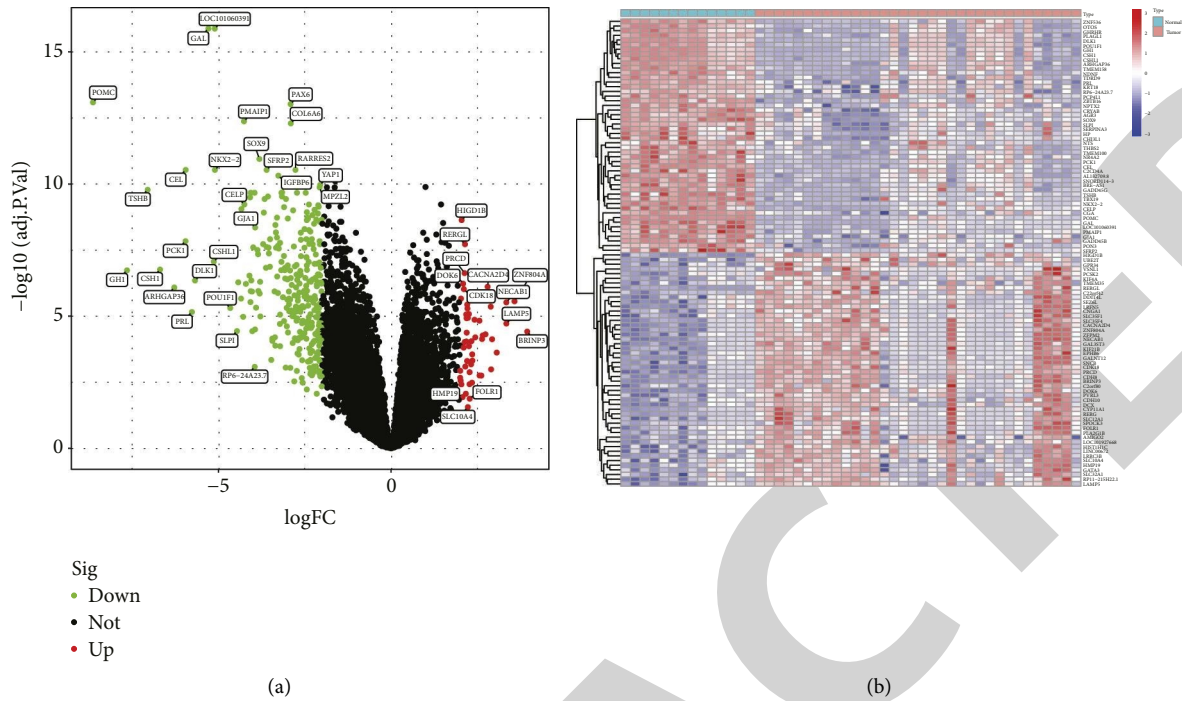
Figure 1: Differentially expressed genes between PA specimens and nontumor specimens. (a) Volcano plot of differentially expressed genes (DEGs). (b) Heat map of the top 100 differentially expressed genes in the analysis result (50 downregulated genes and 50 upregulated genes).

(a)

(b)
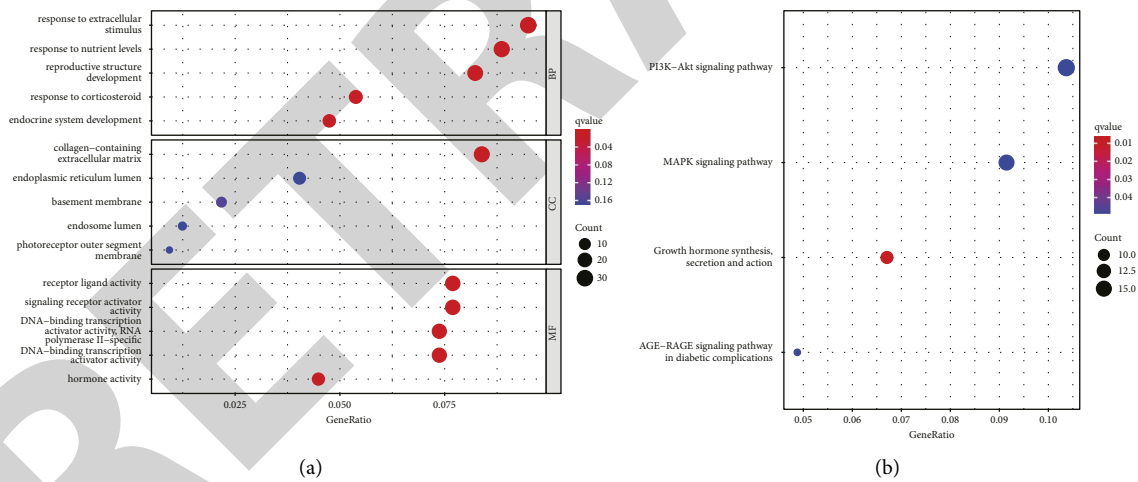
Figure 2: Representative results of GO and KEGG analyses. (a) The outcomes of the GO molecular function enrichment, GO cellular component enrichment, and GO biological process enrichment of DEGs. (b) The findings of an examination of DEGs using KEGG pathways.

determined in a thorough manner in order to examine the biological activities of DEGs [19]. This was accomplished by detecting gene ontology (GO) word enrichment and KEGG pathway enrichment. The results of the GO enrichment were divided into three categories: molecular functions, biological processes, and cellular components (MF). The GO enrichment and KEGG pathway were determined based on a threshold of p value 0.05, and the images that accompany this article represent the top 10 enrichment items.

2.7. Candidate Diagnostic Biomarker Screening. Two different machine-learning methods were employed to make predictions about the disease's progression in order to find meaningful prognostic variables. The least absolute shrinkage and selection operator (LASSO) algorithm is a form of regression analysis that makes use of regularization in order to increase the accuracy of prediction [20]. In order to determine the genes that are significantly linked with the differentiation of pituitary tumor samples from normal samples, the LASSO regression technique was implemented
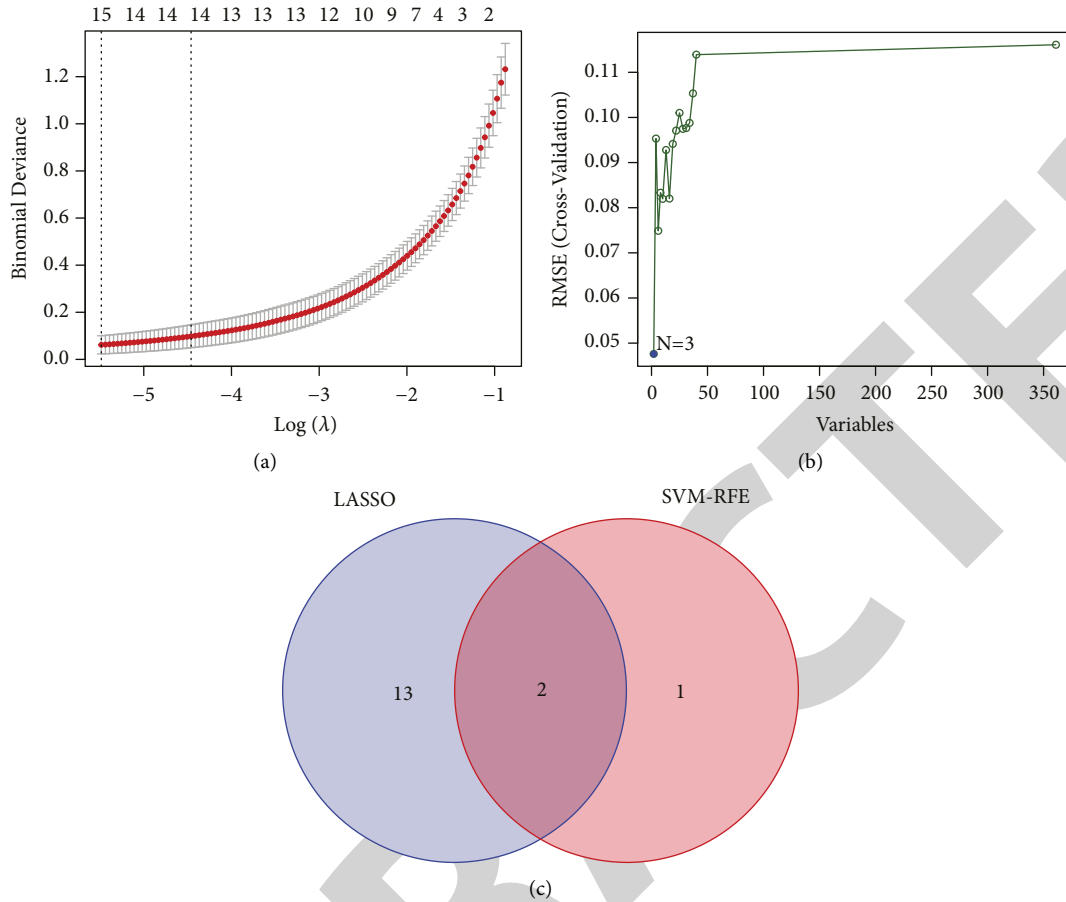
FIGURE 3: Screening process of diagnostic biomarkers for PA diagnosis. (a) Tuning feature selection in the LASSO. (b) A plot of biomarkers selection via SVM-RFE algorithm. (c) Venn diagram demonstrating two diagnostic markers.

in R and run with the "glmnet" package. The support vector machine (SVM) is a popular supervised method of machine learning that may be used for both classification and regression [21]. When selecting the best genes from the metadata cohort, an RFE algorithm was used so as not to fall into the trap of overfitting. Therefore, in order to determine the group of genes that have the greatest capacity for discrimination, support vector machine recursive feature elimination (SVM-RFE) was utilized in order to choose the pertinent characteristics.

2.8. Statistical Analysis. The statistical analyses were conducted in the R software (version 3.6.3) and GraphPad Prism 6.0 software. The Student's *t* test and the one-way analysis of variance (ANOVA) were used to compare the data obtained from the various groups. The final data were generated from three independent experiments. *p* values <0.05 were considered statistically significant.

3. Results

3.1. Identification of DEGs in Pituitary Tumor. In this work, a retrospective analysis was performed on the data obtained from a total of 14 normal specimens and 34 pituitary tumor

specimens taken from two different GEO datasets (GSE26966 and GSE63357). After taking into account the batch effects, the DEGs of the metadata were examined with the help of the limma software. 361 DEGs were obtained: 309 genes were downregulated and 52 genes were upregulated (Figures 1(a) and 1(b)).

3.2. GO Term and KEGG Pathway Enrichment Analyses of DEGs. To learn more about the biological roles and pathways played by DEGs, researchers can do gene enrichment analysis. As shown in Figure 2(a), the results of GO assays indicated that the 361 DEGs were mainly associated with response to extracellular stimulus, response to nutrient levels, reproductive structure development, response to corticosteroid, endocrine system development, collagen-containing extracellular matrix, endoplasmic reticulum lumen, basement membrane, endosome lumen, photoreceptor outer segment membrane, receptor ligand activity, signaling receptor activator activity, and hormone activity. In addition, the results of KEGG assays revealed that the 361 DEGs were mainly enriched in the PI3K-Akt signaling pathway, MAPK signaling pathway, growth hormone synthesis, secretion and action, and AGE-RAGE signaling pathway in diabetic complications (Figure 2(b)).
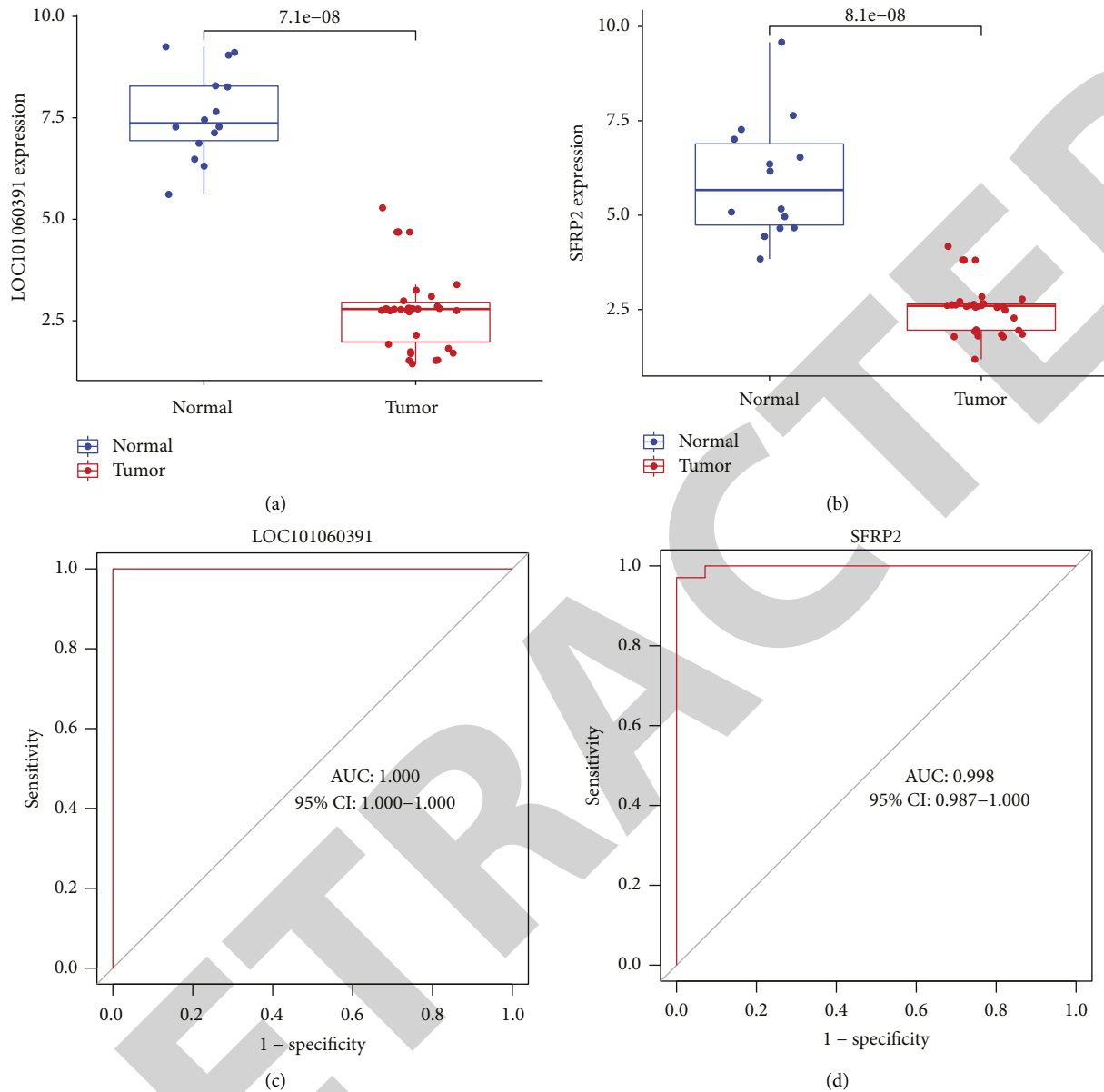
Figure 4: The expression of LOC101060391 and SFRP2 in PA and their diagnostic value. ((a) and (b)) The expression of LOC101060391 and SFRP2 was distinctly increased in PA specimens compared with nontumor specimens from GSE26966 and GSE63357 datasets. ((c) and (d)) ROC assays confirmed the diagnostic value of LOC101060391 and SFRP2 for PA based on GSE26966 and GSE63357 datasets.

3.3. Identification of Diagnostic Biomarkers in Pituitary Tumor. In order to search for relevant biomarkers, two different algorithms were utilized. Using the LASSO regression algorithm, the DEGs were narrowed down, and the result was the identification of 15 genes as diagnostic genes for PA (Figure 3(a)). Using the SVM-RFE technique, we were able to choose a subset of three genes from among the DEGs (Figure 3(b)). The two overlapping factors (LOC101060391 and SFRP2) between these two techniques were finally selected (Figure 3(c)). In addition, we analyzed the expressing pattern of LOC101060391 and SFRP2 and found that the expression of LOC101060391 and SFRP2 was noticeably decreased in PA specimens as compared to nontumor specimens (Figures 4(a) and 4(b)). Following

that, an investigation into the diagnostic utility of LOC101060391 and SFRP2 in patients suffering from pituitary tumors was carried out. According to the ROC tests, high expression levels of LOC101060391 and SFRP2 exhibited an AUC value that was more than 0.9 for PA (Figures 4(c) and 4(d)).

3.4. Effect of SFRP2 on the Growth of Pituitary Tumor Cells in Vitro. The purpose of this study is to investigate the influence that SFRP2 has on the proliferation of HP75 and AtT-20 cells. When compared with the NC group, the findings of the RT-PCR study revealed that the level of expression of SFRP2 was either increased or decreased in

(a)

(b)

(c)
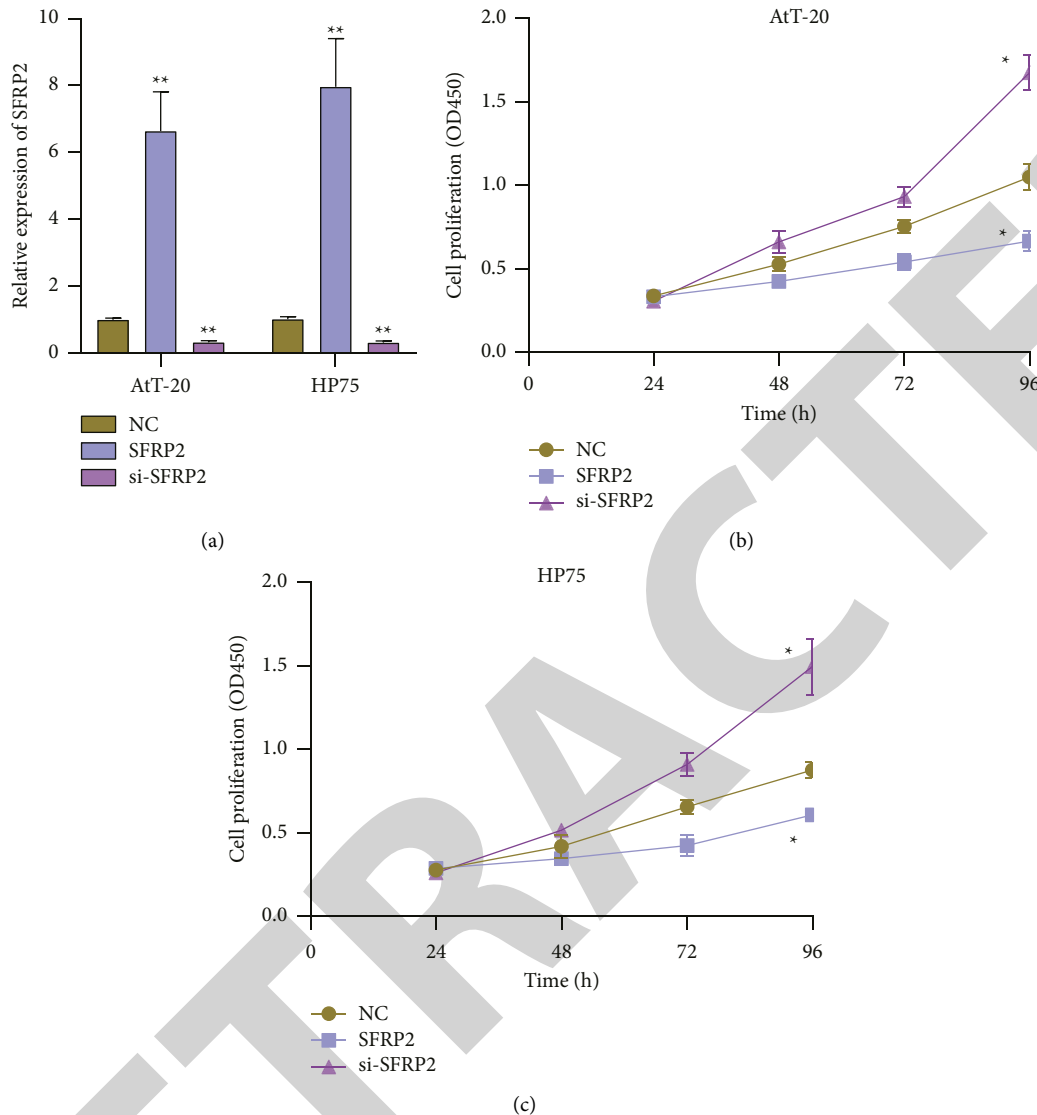
FIGURE 5: The effect of SFRP2 on the proliferation of AtT-20 and HP75 cells. (a) The RT-PCR method was utilized to analyze the level of SFRP2 expression. ((b) and (c)) The CCK-8 assay was utilized to evaluate the degree to which AtT-20 and HP75 cells were able to proliferate. $^{*}p < 0.05$ and $^{**}p < 0.01$.

HP75 and AtT-20 cells when transplanted with pcDNA-SFRP2 or si-SFRP2, respectively (Figure 5(a)). The findings of the CCK-8 assays revealed that forced SFRP2 expression had a significant inhibiting effect on the ability of AtT-20 and HP75 cells to proliferate in comparison to the NC group (both $p < 0.05$, Figures 5(b) and 5(c)). In addition to this, the effect of SFRP2 knockdown on the proliferation of AtT-20 cells as well as HP75 cells was observed (both $p < 0.05$, Figures 5(b) and 5(c)). As a result of these findings, we hypothesized that an increase in SFRP2 expression could inhibit the growth of pituitary tumors in vitro.

4. Discussion

Pituitary tumors come in a variety of subtypes, the most prevalent of which is the prolactin-secreting pituitary adenoma, which accounts for 30–40% of all pituitary tumors

[22, 23]. Accompanying this adenoma are headaches, vision problems, irregular periods, enlarged ovaries, infertility, and a lack of sexual desire. Most prolactinomas are benign and respond well to surgical removal, radiation therapy, or drug therapy [24, 25]. Highly effective medications for prolactinoma include cabergoline and dopamine agonists. Pathologically, aggressive prolactin pituitary tumors are intermediate between benign pituitary adenomas and malignant pituitary carcinomas [26, 27]. It is unknown how common malignant prolactin-secreting pituitary tumors are. It is common for them to develop resistance to standard treatments such as TMZ and to experience rapid recurrence after surgery [28, 29]. They have a relatively specific aggressive behavior that is characterized by a marked invasion of surrounding anatomical structures. An extensive study has been carried out in order to investigate the possible biomarkers that could be used for the early diagnosis and

treatment of aggressive pituitary tumors. The primary objective of this investigation was to locate previously undiscovered diagnostic biomarkers through the application of machine-learning techniques.

We first evaluated two GEO datasets (GSE26966 and GSE63357) to study the DEGs in PA. After removing the impacts of the batching, the DEGs of the metadata were evaluated by making use of the limma program. Then, we got these results: 309 genes had dramatically decreased expression, while 52 genes had significantly increased expression. To explore the possible function of the 361 DEGs, we performed KEGG assays and found that the 361 DEGs were mainly enriched in the PI3K-Akt signaling pathway, MAPK signaling pathway, growth hormone synthesis, secretion and action, and AGE-RAGE signaling pathway in diabetic complications. Our findings suggest the 361 DEGs may influence tumor progression via regulating the above tumor-related pathways. Importantly, we used two machine-learning methods (LASSO regression algorithm and SVM-RFE) and identified two critical diagnosis genes, including LOC101060391 and SFRP2. Their expression was distinctly decreased in PA specimens compared with nontumor specimens. In addition, ROC assays also confirmed their diagnostic value in screening PA specimens from nontumor specimens. Our findings suggest LOC101060391 and SFRP2 may be used as novel diagnostic biomarkers for PA patients.

SFRP1, SFRP2, SFRP3, SFRP4, and SFRP5 are the five members of the family of proteins known as secreted frizzled-related proteins (SFRP) [30]. It appears that the specific environment plays a role in determining whether the protein known as secreted frizzled-related protein 2 (SFRP2) acts as an antagonist or an agonist for the Wnt signaling pathway [31, 32]. There have been multiple reports of the expression of SFRP2 as well as its function in various cancers. For instance, Wu et al. reported that patients with glioma who were treated with radiotherapy had a decrease in their expression of SFRP2, and this decrease was connected to an advanced stage of the tumor and a bad prognosis. Through the activation of Wnt/-catenin signaling, the CRISP/Cas9-mediated reduction of SFRP2 facilitated the development of soft agar colonies, cancer stemness, and radioresistance in glioma cells [33]. Zhang et al. reported that when compared to the paired adjacent nontumor tissue, the amount of SFRP2 mRNA in NSCLC tissue was found to be significantly lower, while the amount of SFRP2 gene methylation was found to be significantly higher. In addition, the loss of SFRP2 that was mediated by methylation contributed to the increased invasiveness of nonsmall cell lung cancer cells. It was discovered that SFRP2 was weakly expressed in PA, and its knockdown increased the proliferation, migration, and invasion of PA cells by upregulating Wnt signaling [34]. According to these findings, SFRP2 may act as a tumor suppressor in the aforementioned malignancies. In this study, we also found that SFRP2 expression was distinctly decreased in PA specimens, which was consistent with previous findings. However, for the first time, we confirmed SFRP2 as a sensitive diagnostic biomarker for PA based on the results of machine-learning methods. Then, we further performed CCK-8 assays to explore the function of SFRP2 in PA progression and found that its overexpression distinctly suppressed the proliferation of PA cells. It has been known to us that disordered tumor growth is the most important characteristic. Our findings suggest SFRP2 may suppress tumor growth in PA, suggesting it as an antioncogene for PA.

However, our study has a few limitations. First, there were just 14 normal specimens and 34 pituitary tumor specimens combined in the GSE26966 and GSE63357 studies; hence, the sample sizes were quite modest. In a subsequent investigation, there is an urgent need for a larger dataset in order to further validate our results. Secondly, more in vitro and in vivo experiments were needed to further study the function of SFRP2 in the progression of PA.

5. Conclusion

We identified two novel diagnostic biomarkers (LOC101060391 and SFRP2) for PA patients. In addition, SFRP2 may be used as a novel therapeutic target for PA.

Data Availability

The original data are provided by the corresponding author upon request without any hesitation.

Conflicts of Interest

The authors declare that they have no conflicts of interest.

References

[1] S. Melmed, "Pituitary-tumor endocrinopathies," *New England Journal of Medicine*, vol. 382, no. 10, pp. 937–950, 2020.

[2] G. U. Mehta and R. R. Lonser, "Management of hormone-secreting pituitary adenomas," *Neuro-Oncology*, vol. 19, no. 6, pp. 762–773, 2017.

[3] F. Langlois and M. Fleseriu, "What to do with incidentally discovered pituitary abnormalities?" *Medical Clinics of North America*, vol. 105, no. 6, pp. 1081–1098, 2021.

[4] J. Fu, A. Wu, X. Wang, and H. Guan, "Concurrent graves' disease and tsh secreting pituitary adenoma presenting suppressed thyrotropin levels: a case report and review of the literature," *Frontiers in Endocrinology*, vol. 11, p. 523, 2020.

[5] C. L. Boguszewski, N. R. de Castro Musolino, and L. Kasuki, "Management of pituitary incidentaloma," *Best Practice & Research Clinical Endocrinology & Metabolism*, vol. 33, no. 2, Article ID 101268, 2019.

[6] A. F. Daly and A. Beckers, "The epidemiology of pituitary adenomas," *Endocrinology and Metabolism Clinics of North America*, vol. 49, no. 3, pp. 347–355, 2020.

[7] M. Elsarrag, P. D. Patel, A. Chatrath, D. Taylor, and J. A. Jane, "Genomic and molecular characterization of pituitary adenoma pathogenesis: review and translational opportunities," *Neurosurgical Focus*, vol. 48, no. 6, p. E11, 2020.

[8] J. H. Yoon, W. Choi, J. Y. Park et al., "A challenging TSH/GH co-secreting pituitary adenoma with concomitant thyroid cancer; a case report and literature review," *BMC Endocrine Disorders*, vol. 21, no. 1, p. 177, 2021.

Research Article

High Expression of COL10A1 Is an Independent Predictive Poor Prognostic Biomarker and Associated with Immune Infiltration in Advanced Gastric Cancer Microenvironment

Neng Shen ⓘ,[1] **Shisheng Zhu**,[2] **Zhongyan Zhang** ⓘ,[3] **and Xuejiao Yong** ⓘ[3]

[1]*Department of Gastroenterology, Chongqing University Cancer Hospital, Chongqing, China*
[2]*Faculty of Basic Medical Sciences, Chongqing Medical and Pharmaceutical College, Chongqing 401331, China*
[3]*Oncology Treatment Center of Traditional Chinese Medicine, Chongqing University Cancer Hospital, Chongqing 400030, China*

Correspondence should be addressed to Zhongyan Zhang; zhangzhongyan@cqu.edu.cn
and Xuejiao Yong; yongxuejiao@cqu.edu.cn

Medical technology has become more and more sophisticated recently, which, however, fails to contribute to a better prognosis for patients suffering advanced gastric cancer (GC). Hence, new biomarkers specific to GC diagnosis and prognosis shall be identified urgently. This study screened differentially expressed genes (DEGs) between 375 GC samples and 32 paracancer tissue samples from TCGA datasets. The expression of Collagen type X alpha 1 (COL10A1) in GC was analyzed. The chi-square test assisted in analyzing the relevance of COL10A1 to the clinicopathologic characteristics. The Kaplan-Meier method helped to assess the survival curves and log-rank tests assisted in the examination of the differences. The Cox proportional hazard regression model served for analyzing the risk factors for GC. Then, we developed a nomogram that contained the COL10A1 expression and clinical information. Finally, how COL10A1 expression was associated with the immune infiltration was also evaluated. In this study, 7179 upregulated and 3771 downregulated genes were identified. Among them, COL10A1 expression was distinctly increased in GC specimens compared with nontumor specimens. High COL10A1 expression exhibited an obvious relation to tumor T and pathologic stage. ROC assays confirmed the diagnostic value of COL10A1 expression in screening GC samples from normal samples. Survival data displayed that patients with high COL10A1 expression exhibited a shorter OS and DSS than those with low COL10A1 expression. We obtained a predictive nomogram, which could better predict the COL10A1 expression by virtue of discrimination and calibration. The prognostic value of COL10A1 expression was further confirmed in GSE84426 datasets. Immune assays revealed that COL10A1 expression was associated with tumor-filtrating immune cells, like CD8 T cells, cytotoxic cells, DC, eosinophils, iDC, macrophages, mast cells, NK CD56dim cells, NK cells, pDC, T helper cells, Tem, Th1 cells, Th17 cells, and Treg. Overall, we firstly proved that COL10A1 may be a novel and valuable prognostic and diagnostic factor for GC patients. In addition, COL10A1 has potential to be an immune indicator in GC.

1. Introduction

Gastric cancer (GC) is ranked fifth in incidence and fourth in mortality among numerous malignant tumors around the world [1]. Statistically, the year of 2015 saw 679,100 new GC cases and about 498,000 deaths caused by GC [2, 3]. Growing studies have proved the effect of personal lifestyle choices on GC, like inadequate fruits and vegetables, excessive drinking as well as high intake of salt [4, 5]. Besides, the risk of suffering GC can increase affected by a family history of GC and Helicobacter pylori infection [6, 7]. GC exhibits a low early diagnosis rate, and a majority of patients can only be diagnosed at an advanced stage; hence, its 5-year survival rate remains less than 10% [8, 9]. GC still exhibits poor prognosis despite the improvement made on the therapy methods, like chemotherapy, surgery, and targeted therapy [10]. On that account, it is

(a)   (b)   (c)
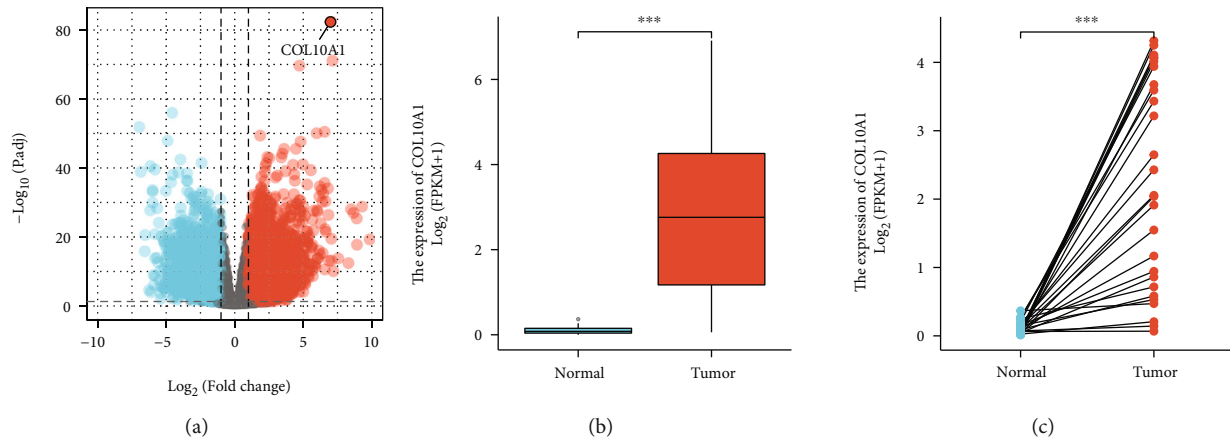
Figure 1: The COL10A1 expression in GC patients based on TCGA datasets. (a) Volcano plot served for visualizing the COL10A1 distribution of the DEGs. (b, c) Both paired and unpaired results found higher COL10A1 expression in tumor tissues relative to nontumor specimens. ***$p < 0.001$.

suggested to confirm useful biomarkers for better assessing tumor development, predicting the overall survival (OS), and enhancing the treatment effects.

Collagen type X alpha 1 (COL10A1) belongs to a family of collagen [11]. COL10A1 gene is the alpha chain encoding form X collagen, the small chain collagen in the form of hypertrophic chondrocytes in the endochondral ossification process [12, 13]. It is a major matrix component in the stroma, and studies have confirmed the vital effect of extracellular matrix on tumor cells in terms of growth, differentiation, progression, apoptosis, and metastasis [14, 15]. A panel of RNAs prepared from various cancers and cancer cell lines were screened, finding the frequent upregulation of COL10A1 in various cancers. However, COL10A1 expression was limited or even could not be detected in a majority of normal tissues. COL10A1 can exhibit specific expression in the vasculature and tumor microenvironment for breast cancer tissues via the immunofluorescence staining by using specific antibodies [16]. The above findings met the results of another study. Huang et al. reported that colorectal cancer tissues showed obviously higher COL10A1 expression. As revealed by biological functional experiments, COL10A1 overexpression strengthened colorectal cancer cells in terms of the proliferation, the migration, and the invasion, and COL10A1 knockdown hindered the tumorigenesis in vivo. According to western blot assays, COL10A1 was capable of facilitating the epithelial-mesenchymal transition (EMT) process. In addition, serum protein concentrations regarding COL10A1 exhibited an obvious increase in adenomas and colorectal cancer cases relative to the control samples. It was possible to treat the protein level regarding COL10A1 in serum as a biomarker for diagnosing tumor prognosis in early stage, thereby identifying colorectal cancer and adenoma [17]. However, whether COL10A1 could be a diagnostic and prognostic biomarker for GC remained largely unclear.

In this study, we screened differentially expressed genes (DEGs) to compare GC specimens and nontumor specimens based on TGCA datasets and confirmed that COL10A1 expression showed an obvious increase in GC specimens. Then, we analyzed its diagnostic and prognostic value in

two cohorts. Finally, the possible association of COL10A1 expression with immune microenvironment was explored.

2. Materials and Methods

2.1. Data Sources. The mRNA expression profiles regarding 375 GC samples and 32 paracancer tissue samples, together with related clinical data, came from The Cancer Genome Atlas (TCGA) database (https://www.cancer.gov/about-nci/organization/ccg/research/structural-genomics/tcga). 375 GC patients possessed matching mRNA expression profiles as well as survival data. Besides, the Gene Expression Omnibus (GEO) database (https://www.ncbi.nlm.nih.gov/geo/) provided the related dataset (GSE84426). The study strictly followed the publication guidelines of TCGA and GEO.

2.2. Differential Analysis of Genes. The "affy" and "limma" packages in R software (https://www.r-project.org/) served for differentiating specimens from the TCGA datasets, respectively, obtaining 375 GC samples and 32 paracancer tissue samples. The t-test assisted in screening DEGs following cut-off values: false discovery rate (FDR) < 0.05 and | log 2fold change| > 1.

2.3. Analysis on the Correlation of COL10A1 Expression Patterns with Clinicopathological Features. We selected the clinicopathological data [age, gender, pathological stage, infiltration depth (T), distant metastasis (M), lymph node metastasis (N), etc.] regarding the RC tissue specimens in the TCGA database for later analysis. The study included clinical data of 367 patients except data that were defective or incomplete. An independent sample t-test together with a paired t-test assisted in confirming the correlation of COL10A1 expression with the clinical-pathological parameters.

2.4. Statistical Analysis on Potential Prognostic Factors. The R version 4.0.2 software ("survival" and "survminer" packages) served for identifying the potential prognostic factors. Univariate Cox regression analysis assisted in confirming many prognostic factors, and multivariate Cox regression analysis assisted in confirming independent prognostic

Table 1: Association between COL10A1 expression and different clinicopathological features of human GC.

Characteristic	Low expression of COL10A1	High expression of COL10A1	p
n	187	188	
T stage, n (%)			<0.001
T1	18 (4.9%)	1 (0.3%)	
T2	44 (12%)	36 (9.8%)	
T3	78 (21.3%)	90 (24.5%)	
T4	45 (12.3%)	55 (15%)	
N stage, n (%)			0.901
N0	53 (14.8%)	58 (16.2%)	
N1	51 (14.3%)	46 (12.9%)	
N2	39 (10.9%)	36 (10.1%)	
N3	37 (10.4%)	37 (10.4%)	
M stage, n (%)			1.000
M0	166 (46.8%)	164 (46.2%)	
M1	13 (3.7%)	12 (3.4%)	
Pathologic stage, n (%)			0.012
Stage I	36 (10.2%)	17 (4.8%)	
Stage II	45 (12.8%)	66 (18.8%)	
Stage III	77 (21.9%)	73 (20.7%)	
Stage IV	19 (5.4%)	19 (5.4%)	
Gender, n (%)			0.884
Female	68 (18.1%)	66 (17.6%)	
Male	119 (31.7%)	122 (32.5%)	
Age, n (%)			0.899
≤65	82 (22.1%)	82 (22.1%)	
>65	101 (27.2%)	106 (28.6%)	
Histologic grade, n (%)			0.095
G1	5 (1.4%)	5 (1.4%)	
G2	77 (21%)	60 (16.4%)	
G3	98 (26.8%)	121 (33.1%)	
H pylori infection, n (%)			1.000
No	96 (58.9%)	49 (30.1%)	
Yes	12 (7.4%)	6 (3.7%)	
Barrett's esophagus, n (%)			0.612
No	122 (58.7%)	71 (34.1%)	
Yes	11 (5.3%)	4 (1.9%)	
Age, mean ± SD	65.52 ± 10.52	66.13 ± 10.79	0.580

factors. Nomograph was developed using R software. Finally, GSE84426 was used to validate the prognosis value of COL10A1 expression.

2.5. Protein Interaction Network Analysis. The STRING database (https://string-db.org/) served for exploring the predicted and actual correlations of protein interactions with COL10A1 expression patterns. Proteins interacting with the COL10A1 were screened.

2.6. Analysis on the Correlation of COL10A1 with Immune Cell Infiltration. The "cibersort" package (R version 4.0.2 software) assisted in analyzing the percentage occupied by 22 immune cell types (LM22 gene signature) in GC tissues. A further quantification was conducted on the correlation of COL10A1 expression with proportions occupied by different immune cells. The "ggplot2" and "limma" packages (R version 4.0.2 software) served for analyzing and plotting data at last. Also, we referenced the TIMER database for analyzing the tumor-infiltrating immune cells (CD8+ T cells, CD4+ T cells, B cells, macrophages, neutrophils, and DCs).

2.7. Gene Ontology (GO) and the Kyoto Encyclopedia of Genes and Genomes (KEGG) Pathway Analysis. GO enrichment that involves cellular components, molecular functions, and biological process is capable of defining special biological characteristics regarding certain genes in various respects. The KEGG enrichment served for investigating the biological pathways in some genes. GO and KEGG analysis were conducted under the assistance of the R 3.6 software together with "clusterProfiler" package. Moreover, "ggplot2" package was used for the outcome visualization.

2.8. GSEA. The median COL10A1 expression was taken into account for dividing patients into group with high expression and group with low expression by using the GSEA software; also, the gene enrichment pathways with the highest ranking in the two groups were detected (Molecular Signatures Database c2. Cp. Kegg. V7.2. Symbols). We used the Gene Matrix Transposed function dataset as a reference gene set specific to all analyses. FDR < 0.05 indicated significant enrichment.

2.9. Statistical Analysis. IBM SPSS Statistics for Windows, version 20.0 (IBM Corporation, Armonk, NY, USA) and R version 4.0.2 served for the statistical analyses. The gene expression data were in the form of mean ± standard deviation. A t-test assisted in comparing GC tissues and paracarcinoma tissues in terms of the COL10A1 expression in the TCGA and GEO databases. Wilcoxon's signed-rank test assisted in analyzing the correlation of the COL10A1 with clinical characteristic variables. The hazard ratio and 95% CI were calculated with the univariate and multivariate Cox analyses. Finally, R was used to draw nomogram and build a prediction model. We plotted ROC curve and calculated AUC by using "ROCR" package for assessing the ability to distinguish tumor and normal tissue. A p value < 0.05 reported statistical significance. FDR < 0.05 and $p < 0.01$ indicated significant enrichment.

3. Results

3.1. Microarray Data and Identification regarding DEGs in GC. For finding DEGs in GC, the current study included 375 GC samples and 32 paracancer tissue samples from the TCGA. At last, we identified 7179 upregulated and 3771 downregulated genes ($|\log FC| \geq 1$, $p < 0.05$). The

(a)

(b)

(c)

(d)

(e)
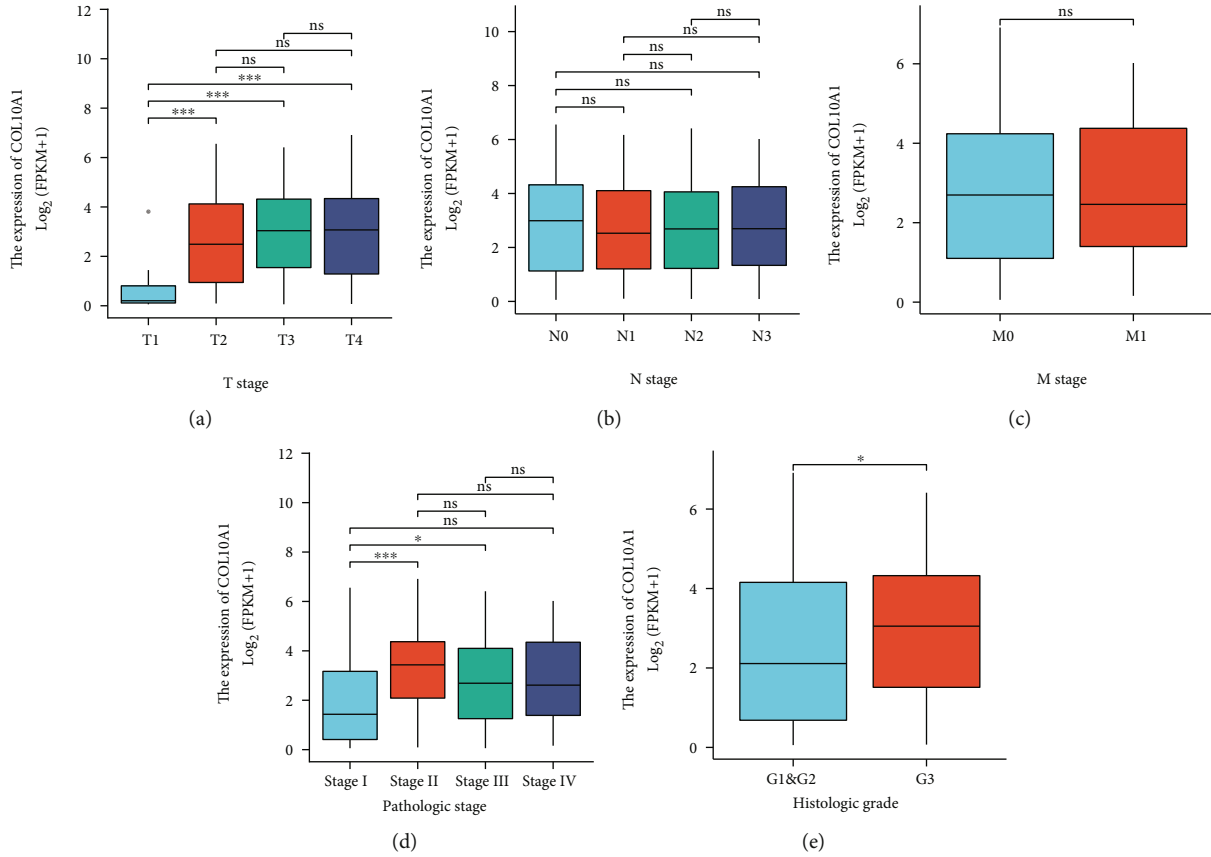
Figure 2: Relationship between clinicopathological characteristics and COL10A1 expression, namely (a) T stage, (b) N stage, (c) M stage, (d) pathologic stage, and (e) histologic grade. $^*p < 0.05$, $^{**}p < 0.01$, and $^{***}p < 0.001$. ns: no significance.
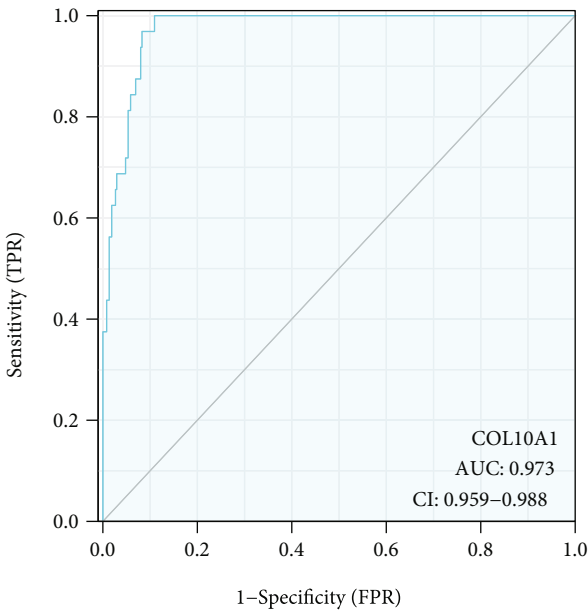
Figure 3: ROC curve of COL10A1 for the diagnosis of GC.

COL10A1 distribution of the DEGs was visualized in a volcano plot (Figure 1(a)). Both paired and unpaired results displayed the higher COL10A1 expression in tumor tissues relative to control adjacent tissues (Figures 1(b) and 1(c)).

3.2. Relationship of Clinicopathological Characteristics with COL10A1 Expression. The clinical significances of COL10A1 expression were examined using the TCGA datasets. High COL10A1 expression was significantly correlated with tumor T and pathologic stage (Table 1 and Figures 2(a)–2(e)). The level of COL10A1 can be used as a diagnosis tool for GC (AUC = 0.973) (Figure 3).

3.3. Prognosis Value of COL10A1 for GC. The R software "survival" package and Kaplan-Meier method together with log-rank test were applied to assess how COL10A1 affected GC patients' overall survival (OS) and disease-specific survival (DSS). We calculated the logarithmic rank p value and the 95% CI, followed by plotting a survival curve. The results showed that patients with high COL10A1 expression showed a shorter OS and DSS than those with low COL10A1 expression (Figures 4(a) and 4(b)). Univariate and multivariate Cox regression analyses were applied to investigate whether high COL10A1 expression could independently report poor prognosis of GC patients. Cox univariate
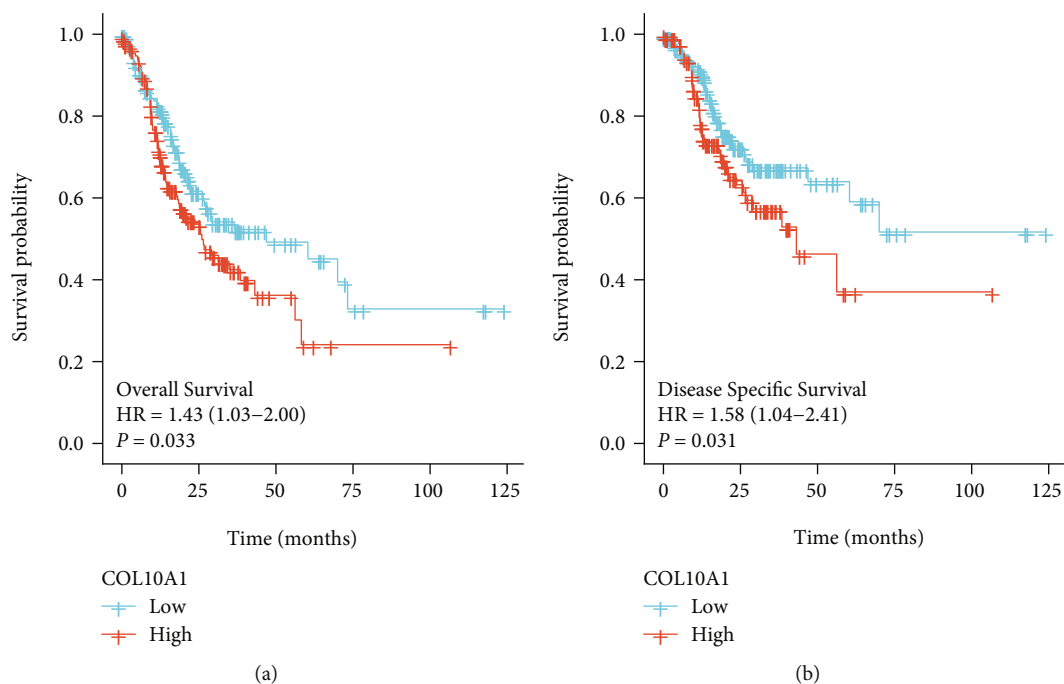
Figure 4: Kaplan-Meier analysis of (a) OS and (b) DSS in 375 GC patients in relation to COL10A1 expression level.

survival analysis revealed the important effect of T, N, M, stage, age, and COL10A1 on the OS duration, and multivariate Cox survival analysis showed that age ($p = 0.001$) and COL10A1 ($p = 0.014$) independently predicted a poor prognosis for GC patients (all, $p < 0.05$) (Table 2). Nomograph was built (Figures 5(a)–5(d)), and 1-, 3-, and 5-year AUCs of COL10A1 expression were 0.575, 0.622, and 0.764, respectively, for the survival prediction, that proved the large prognostic value possessed by COL10A1 (Figure 5(e)). GSE84426 was used to validate the prognosis value of COL10A1, and the results were consistent with TCGA (Figures 6(a) and 6(b)).

3.4. Interrelation with Tumor-Infiltrating Immune Cells in GC. Analysis by the ssGSEA software found the correlation of COL10A1 expression with the tumor-filtrating immune cells, namely, CD8 T cells, cytotoxic cells, DC, eosinophils, iDC, macrophages, mast cells, NK CD56dim cells, NK cells, pDC, T helper cells, Tem, Th1 cells, Th17 cells, and Treg (all $p < 0.05$, Figure 7(a)). Also, the TIMER database found the positive correlation of COL10A1 expression with infiltrating immune cell levels, namely, macrophage, NK, TH1, and iDC cells (Figure 7(b)).

3.5. GO, KEGG, and GSEA Analysis of COL10A1 Coexpression-Related Genes. Based on the GO analysis, these genes were mainly expressed in the extracellular matrix structural constituent, endopeptidase regulator activity, protein digestion and absorption, and pancreatic secretion (Figure 8(a)). Besides, as revealed by the GSEA analysis, these genes mainly affected the OLFACTORY_TRANSDUC-TION, OLFACTORY_SIGNALING_PATHWAY, KERATI-NIZATION, etc. (Figure 8(b)).

4. Discussion

Currently, the commonly used methods for treating GC in early stages are the endoscopic mucosal resection and the endoscopic submucosal dissection [18]. Nevertheless, GC can develop fast and can only be diagnosed at an advanced stage; hence, GC patients have a low 5-year survival rate [19, 20]. Hemotherapy regimens, i.e., SOX (oxaliplatin+S1)/CapeOX (oxaliplatin+capecitabine), FOLFOX (oxaliplatin+leucovorin+5-fluorouracil), and DCF (docetaxel+cisplatin+5-fluorouracil)/DOF (docetaxel+oxaliplatin+5-fluorouracil), mainly serve for GC patients in later stage, which, however, also exhibit limited efficacy. Based on studies, combining the chemotherapy with radiotherapy, surgery, or targeted therapy is treated as the most proper treatment method for improving patient survival, which, however, fails to greatly enhance GC patients' prognosis because chemotherapeutic drugs are toxic; it is hard to screen beneficiaries of targeted therapy drugs; and patients present drug resistance [21, 22].

Based on recent studies, abnormal COL10A1 expression in many cancer types has promoted the tumor growth. Some groups reported the ability of high COL10A1 expression to facilitate GC development in terms of cell proliferation, invasion, and migration. High COL10A1 plasma levels predicted poor OS, which could serve for detecting GC in early stage as a useful biomarker. Huang et al. found the higher COL10A1 expression in colorectal cancer tissues. High COL10A1 expression could cause tumor progression and independently predicted the OS of patients suffering colorectal cancer [23]. As for lung adenocarcinoma, COL10A1 upregulation exhibited positive relation to lymph node metastasis, and COL10A1 was treated as a novel target specific to lung cancer [24]. Breast cancer patients may present less improvement due to the neoadjuvant chemotherapy relative to patients

TABLE 2: Prognostic factor for OS of patients with GC determined by using univariate and multivariate COX analysis.

Characteristics	Total (N)	Univariate analysis		Multivariate analysis	
		Hazard ratio (95% CI)	p value	Hazard ratio (95% CI)	p value
T stage	362				
T1&T2	96	Reference			
T3&T4	266	1.719 (1.131-2.612)	0.011	1.189 (0.624-2.264)	0.599
N stage	352				
N0	107	Reference			
N1	97	1.629 (1.001-2.649)	0.049	1.329 (0.672-2.626)	0.413
N2	74	1.655 (0.979-2.797)	0.060	1.502 (0.650-3.469)	0.341
N3	74	2.709 (1.669-4.396)	<0.001	2.142 (0.933-4.917)	0.072
M stage	352				
M0	327	Reference			
M1	25	2.254 (1.295-3.924)	0.004	1.256 (0.534-2.954)	0.602
Pathologic stage	347				
Stage I	50	Reference			
Stage II	110	1.551 (0.782-3.078)	0.209	1.281 (0.474-3.458)	0.626
Stage III	149	2.381 (1.256-4.515)	0.008	1.256 (0.342-4.610)	0.731
Stage IV	38	3.991 (1.944-8.192)	<0.001	2.485 (0.655-9.436)	0.181
Gender	370				
Female	133	Reference			
Male	237	1.267 (0.891-1.804)	0.188		
Age	367				
≤65	163	Reference			
>65	204	1.620 (1.154-2.276)	0.005	1.849 (1.272-2.687)	0.001
COL10A1	370				
Low	185	Reference			
High	185	1.434 (1.030-1.996)	0.033	1.567 (1.096-2.242)	0.014
Histologic grade	361				
G1	10	Reference			
G2	134	1.648 (0.400-6.787)	0.489		
G3	217	2.174 (0.535-8.832)	0.278		

possessing high COL10A1 expression [14]. Our study found the obviously increased COL10A1 expression in GC patients. Importantly, we found that patients with COL10A1 expression showed an advanced clinical stage. It has been known to us that clinical stage can vitally help to determine proper candidates as well as design neoadjuvant treatment strategies specific to advanced tumors. In addition, patients with advanced clinical stage showed a poor prognosis. Thus, our findings suggested that COL10A1 may be associated with the clinical outcome of GC patients. Then, we analyzed survival data using Kaplan-Meier methods, finding that patients who had high COL10A1 expression predicted a shorter OS and DSS relative to patients possessing low COL10A1 expression. Importantly, multivariate Cox survival analysis showed that COL10A1 could independently predict GC patients' poor prognosis. Besides, we obtained a predictive nomogram, which could better predict the COL10A1 expression by virtue of discrimination and calibration. The ROC curve analysis found the better performance exhibited by nomogram relative to other single predictors. Our finding evidenced the advan-

tage of COL10A1 expression in predicting long-term survival as well as stratifying risks.

The immune system can greatly help to eliminate malignant cells inside healthy individuals [25]. However, tumor cells are capable of escaping via immune-mediated infiltration and hence can be hardly cleared by the immune infiltrating cells [26]. Considering the antitumor immunity ability associated with T cells, checkpoint inhibition is commonly applied for clinical cancer immunotherapy [27, 28]. Based on a lot of large clinical trials, immune checkpoint blockade (ICB) therapy could help patients with chemotherapy resistance in EGC and even be a specific agent for palliative treatment [29, 30]. Besides, tumor microenvironment component activity together with related treatment methods may assist in developing combined therapies for ICB [31, 32]. Hence, COL10A1 and immune cells were evaluated with regard to the clinical applicability. In this study, we found the relevance of COL10A1 expression to tumor-filtrating immune cells, namely, CD8 T cells, cytotoxic cells, DC, eosinophils, iDC, macrophages, mast cells, NK CD56dim

(a)

(b)

(c)

(d)

(e)
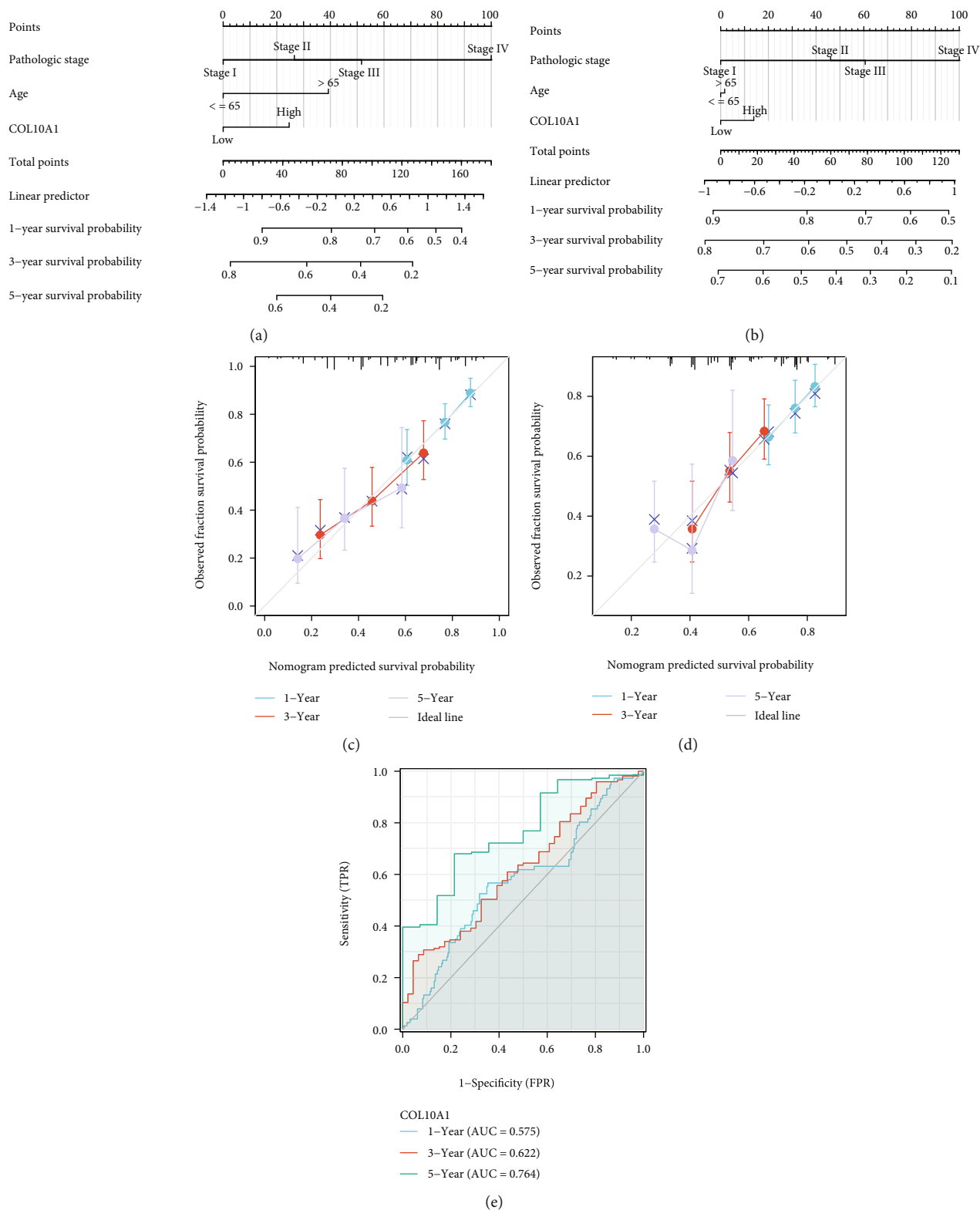
FIGURE 5: Nomograph of COL10A1 for GC and the time-dependent ROC curve showing the diagnosis value. (a) OS, (b) DSS. (c, d) The calibration curve of nomogram for GC patients in 1 year, 3 years, and 5 years, respectively. (e) The AUC regarding the prediction of 1-, 3-, and 5-year survival rate of GC.

(a)

(b)
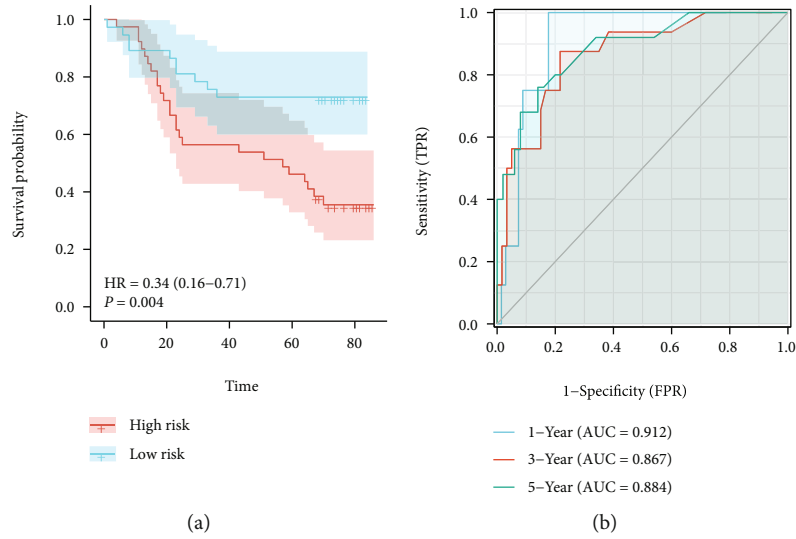
FIGURE 6: GSE84426 was used to validate the prognosis value of COL10A1. (a) High expression of COL10A1 reported shorter OS. (b) The AUC regarding the prediction of 1-, 3-, and 5-year survival rate of GC.

(a)

(b)
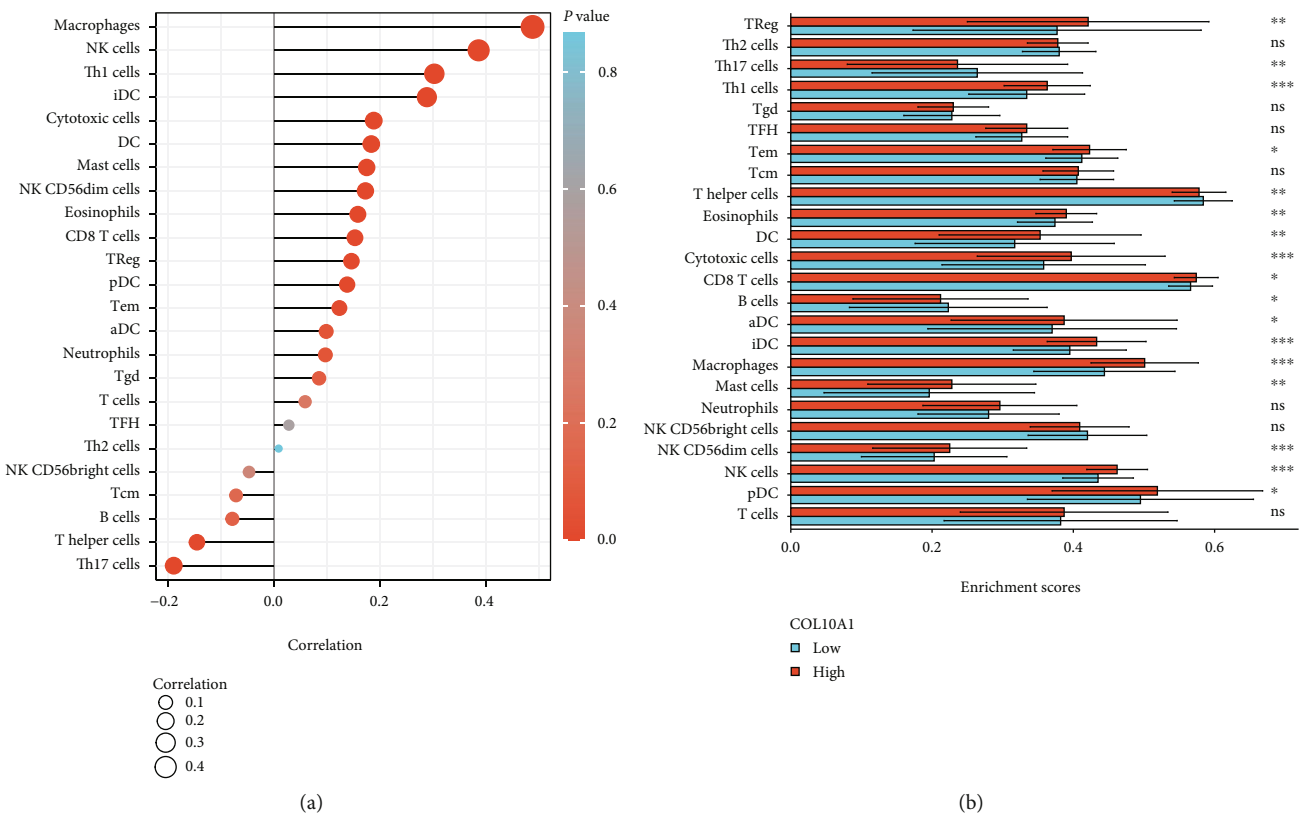
FIGURE 7: Interrelation with tumor-infiltrating immune cells in GC. (a) ssGSEA. (b) TIMER database. $^*p < 0.05$, $^{**}p < 0.01$, and$^{***}p < 0.001$. ns: no significance.

cells, NK cells, pDC, T helper cells, Tem, Th1 cells, Th17 cells, and Treg. Mast cells and DCs, the first groups of cells in the immune system, are capable of interacting with allergens, other antigens, as well as invading pathogens in the environment. Being in resting states, the two cells cannot play their roles, which may lead to tumor immune escape.

Our model was closely related to immunity, finding that COL10A1 expression well reported the immune status regarding the predicted samples.

Undoubtedly, some limitations must be addressed in the present study. Firstly, data in the study are based on public databases; hence, our results shall be validated in vitro and

(a)

(b)
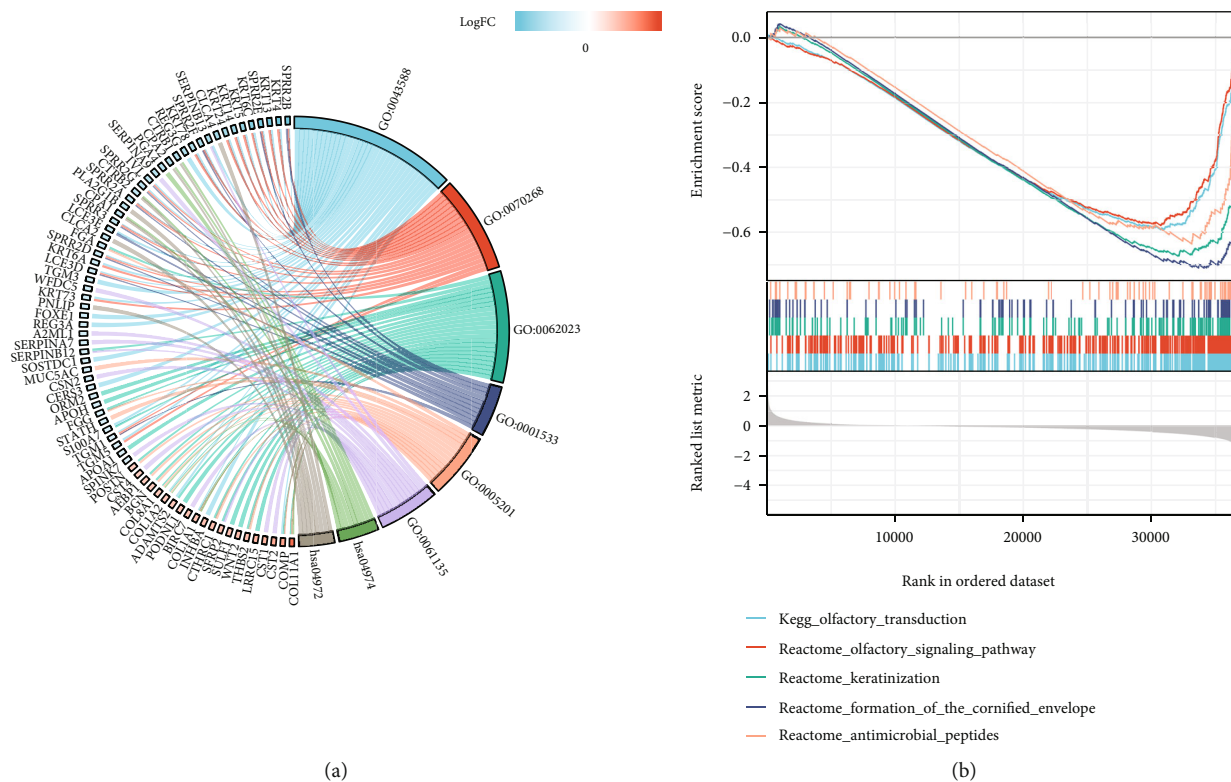
Figure 8: Enrichment analysis of COL10A1 coexpression-related genes. (a) GO assays. (b) GSEA analysis.

in vivo. Also, COL10A1 exhibited overexpression in tumor tissue from TCGA database relative to normal tissue; hence, COL10A1 expression shall be validated via other studies, such as RT-PCR and Western blot.

5. Conclusion

To our knowledge, this is the first study on clinical significance of COL10A1 expression in GC patients. Our study revealed that the expression levels of COL10A1 were upregulated in GC tissues. High expression of COL10A1 predicted poor prognosis for GC. COL10A1 may be useful for evaluating prognosis and added new possibilities for immunotherapy in patients with GC.

Data Availability

The data used to support the findings of this study are available from the corresponding authors upon request.

Conflicts of Interest

All authors declared that no conflicts of interest exist.

References

[1] R. L. Siegel, K. D. Miller, and A. Jemal, "Cancer statistics, 2020," CA: a Cancer Journal for Clinicians, vol. 70, no. 1, pp. 7–30, 2020.

[2] R. M. Feng, Y. N. Zong, S. M. Cao, and R. H. Xu, "Current cancer situation in China: good or bad news from the 2018 Global Cancer Statistics?," Cancer Communications, vol. 39, no. 1, p. 22, 2019.

[3] R. L. Siegel, K. D. Miller, H. E. Fuchs, and A. Jemal, "Cancer statistics, 2022," CA: a Cancer Journal for Clinicians, vol. 72, no. 1, pp. 7–33, 2022.

[4] Z. Tan, "Recent advances in the surgical treatment of advanced gastric cancer: a review," Medical Science Monitor, vol. 25, pp. 3537–3541, 2019.

[5] N. Y. Chia and P. Tan, "Molecular classification of gastric cancer," Annals of Oncology, vol. 27, no. 5, pp. 763–769, 2016.

[6] R. Santoro, G. M. Ettorre, and E. Santoro, "Subtotal gastrectomy for gastric cancer," World Journal of Gastroenterology, vol. 20, no. 38, pp. 13667–13680, 2014.

[7] J. P. Hamilton and S. J. Meltzer, "A review of the genomics of gastric cancer," Clinical Gastroenterology and Hepatology, vol. 4, no. 4, pp. 416–425, 2006.

[8] H. Hoshi, "Management of gastric adenocarcinoma for general surgeons," The Surgical Clinics of North America, vol. 100, no. 3, pp. 523–534, 2020.

[9] N. Khalighinejad, H. Hariri, O. Behnamfar, A. Yousefi, and A. Momeni, "Adenoviral gene therapy in gastric cancer: a review," World Journal of Gastroenterology, vol. 14, no. 2, pp. 180–184, 2008.

[10] T. Nakajima, "Review of adjuvant chemotherapy for gastric cancer," World Journal of Surgery, vol. 19, no. 4, pp. 570–574, 1995.

[11] H. Wu, S. Wang, G. Li et al., "Characterization of a novel COL10A1 variant associated with Schmid-type metaphyseal

chondrodysplasia and a literature review," *Molecular Genetics & Genomic Medicine*, vol. 9, no. 5, article e1668, 2021.

[12] K. Y. Tsang, D. Chan, and K. S. Cheah, "Fate of growth plate hypertrophic chondrocytes: death or lineage extension?," *Development, Growth & Differentiation*, vol. 57, no. 2, pp. 179–192, 2015.

[13] Y. Fang, J. F. Bateman, J. F. Mercer, and S. R. Lamandé, "Nonsense-mediated mRNA decay of collagen -emerging complexity in RNA surveillance mechanisms," *Journal of Cell Science*, vol. 126, Part 12, pp. 2551–2560, 2013.

[14] W. Yang, X. Wu, and F. Zhou, "Collagen type X alpha 1 (COL10A1) contributes to cell proliferation, migration, and invasion by targeting prolyl 4-hydroxylase beta polypeptide (P4HB) in breast cancer," *Medical Science Monitor*, vol. 27, article e928919, 2021.

[15] S. H. Aktas, T. Taskin-Tok, K. Al-Khafaji, and D. F. Akın-Balı, "A detailed understanding of the COL10A1 and SOX9 genes interaction based on potentially damaging mutations in gastric cancer using computational techniques," *Journal of Biomolecular Structure & Dynamics*, pp. 1–12, 2021.

[16] S. Chen, Y. Wei, H. Liu et al., "Analysis of collagen type X alpha 1 (COL10A1) expression and prognostic significance in gastric cancer based on bioinformatics," *Bioengineered*, vol. 12, no. 1, pp. 127–137, 2021.

[17] T. Li, H. Huang, G. Shi et al., "TGF-β1-SOX9 axis-inducible COL10A1 promotes invasion and metastasis in gastric cancer via epithelial-to-mesenchymal transition," *Cell Death & Disease*, vol. 9, no. 9, p. 849, 2018.

[18] A. Digklia and A. D. Wagner, "Advanced gastric cancer: current treatment landscape and future perspectives," *World Journal of Gastroenterology*, vol. 22, no. 8, pp. 2403–2414, 2016.

[19] M. Leja and A. Linē, "Early detection of gastric cancer beyond endoscopy - new methods," *Best Practice & Research Clinical Gastroenterology*, vol. 50, article 101731, 2021.

[20] F. Dhalla, S. P. da Silva, M. Lucas, S. Travis, and H. Chapel, "Review of gastric cancer risk factors in patients with common variable immunodeficiency disorders, resulting in a proposal for a surveillance programme," *Clinical and Experimental Immunology*, vol. 165, no. 1, pp. 1–7, 2011.

[21] B. Farran, S. Müller, and R. C. Montenegro, "Gastric cancer management: kinases as a target therapy," *Clinical and Experimental Pharmacology & Physiology*, vol. 44, no. 6, pp. 613–622, 2017.

[22] A. Thiel and A. Ristimäki, "Gastric cancer: basic aspects," *Helicobacter*, vol. 17, Supplement 1, pp. 26–29, 2012.

[23] H. Huang, T. Li, G. Ye et al., "High expression of COL10A1 is associated with poor prognosis in colorectal cancer," *Oncotargets and Therapy*, vol. 11, pp. 1571–1581, 2018.

[24] Y. Liang, W. Xia, T. Zhang et al., "Upregulated collagen COL10A1 remodels the extracellular matrix and promotes malignant progression in lung adenocarcinoma," *Frontiers in Oncology*, vol. 10, article 573534, 2020.

[25] B. Pulendran and M. M. Davis, "The Science and Medicine of Human Immunology," *Science*, vol. 369, no. 6511, 2020.

[26] H. Locy, S. de Mey, W. de Mey, M. De Ridder, K. Thielemans, and S. K. Maenhout, "Immunomodulation of the tumor microenvironment: turn foe into friend," *Frontiers in Immunology*, vol. 9, p. 2909, 2018.

[27] V. Roudko, B. Greenbaum, and N. Bhardwaj, "Computational prediction and validation of tumor-associated neoantigens," *Frontiers in Immunology*, vol. 11, p. 27, 2020.

[28] L. B. Kennedy and A. K. S. Salama, "A review of cancer immunotherapy toxicity," *CA: a Cancer Journal for Clinicians*, vol. 70, no. 2, pp. 86–104, 2020.

[29] R. S. Riley, C. H. June, R. Langer, and M. J. Mitchell, "Delivery technologies for cancer immunotherapy," *Nature Reviews Drug Discovery*, vol. 18, no. 3, pp. 175–196, 2019.

[30] Y. Yang, "Cancer immunotherapy: harnessing the immune system to battle cancer," *The Journal of Clinical Investigation*, vol. 125, no. 9, pp. 3335–3337, 2015.

[31] J. van den Bulk, E. M. Verdegaal, and N. F. de Miranda, "Cancer immunotherapy: broadening the scope of targetable tumours," *Open Biology*, vol. 8, no. 6, 2018.

[32] M. Abbott and Y. Ustoyev, "Cancer and the immune system: the history and background of immunotherapy," *Seminars in Oncology Nursing*, vol. 35, no. 5, article 150923, 2019.

Research Article

Lymph Node Metastasis-Related Gene ITGA4 Promotes the Proliferation, Migration, and Invasion of Gastric Cancer Cells by Regulating Tumor Immune Microenvironment

Tianyi Fang ⓘ **, Xin Yin, Yufei Wang, Hao Wang** ⓘ **, Xibo Wang, and Yingwei Xue** ⓘ

Department of Gastroenterological Surgery, Harbin Medical University Cancer Hospital, Harbin Medical University, Harbin 150081, China

Correspondence should be addressed to Yingwei Xue; xueyingwei@hrbmu.edu.cn

Tianyi Fang, Xin Yin, and Yufei Wang contributed equally to this work.

The Integrin Subunit Alpha 4 (ITGA4) plays important roles in cancers pathogenesis. However, the expression and association with clinicopathological and survival probability have not been previously assessed in gastric cancer (GC). Protein expression of ITGA4 was assessed in TMA using immunohistochemistry and correlated with clinicopathological factors and survival. The mRNA expression of ITGA4 was also assessed in the HMU-GC cohort. Bioinformatics function analysis was conducted through GSEA. The "CIBERSORT" package was used for immune infiltration analysis. "SvyNom" package is used to construct prognosis model. ITGA4 knock down using shRNA. The evaluation of cell function was performed by CCK-8 and Transwell invasion and migration experiments. ITGA4 was significantly associated with N classification ($P = 0.031$), tumor location ($P = 0.033$), WHO classification ($P = 0.007$), and poor prognosis in mRNA level. GSEA analysis of the validation cohort suggested that ITGA4 was associated with macrophage infiltration. Immunohistochemistry showed that ITGA4 was associated with poor prognosis. Multivariate Cox regression analysis found that ITGA4 ($P = 0.045$) and lymph node metastasis rate ($P = 0.026$) were independent prognostic factors and could construct a prognosis model. ITGA4 knockdown cell line significantly reduced the ability of proliferation, invasion, and metastasis. ITGA4 is associated with patient survival in GC and may be an important prognostic biomarker.

1. Introduction

Gastric cancer (GC) is one of the common malignant tumors in China. World Health Organization (WHO) reported that there were 479,000 new cases of GC and 374,000 deaths in China in 2020, accounting for 44.0% and 48.6% of the global new cases and deaths [1–3]. The incidence and mortality of GC have increased significantly, and the mortality rate of GC is the fourth among malignant tumors, which is one of the most threatening malignant tumors to the health and life of the population, resulting in a social burden that cannot be ignored [4, 5]. Lymph node metastasis plays a substantial role in the progression of GC

and is one of the most indispensable factors affecting the therapeutic. The 8th of the TNM staging system distinguishes patients into N3a and N3b in the final pathological stage [6]. This also shows that lymph node metastasis means irreversible tumor progression indicating that the biological characteristics of cancer cells have undergone a fundamental change and manifested as enhanced proliferation and invasion ability [7–9]. Whatever, lymph node metastasis is one of the important factors affecting the treatment and prognosis of GC. Therefore, finding biomarkers for early prediction of lymph node metastasis and developing therapeutic targets is crucial for the clinical treatment, especially for the molecular regulatory mechanisms related to lymph node
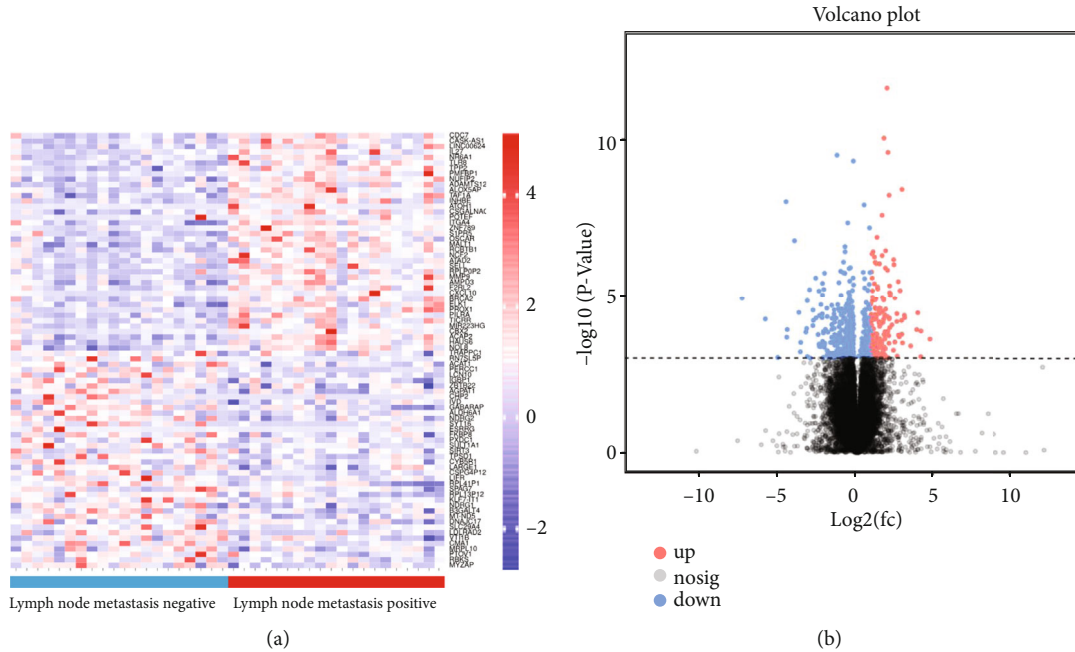
FIGURE 1: (a) Heatmap showing genes associated with lymph node metastasis of GC. (b) Volcano plot shows the differentially expressed genes between the two groups of samples.
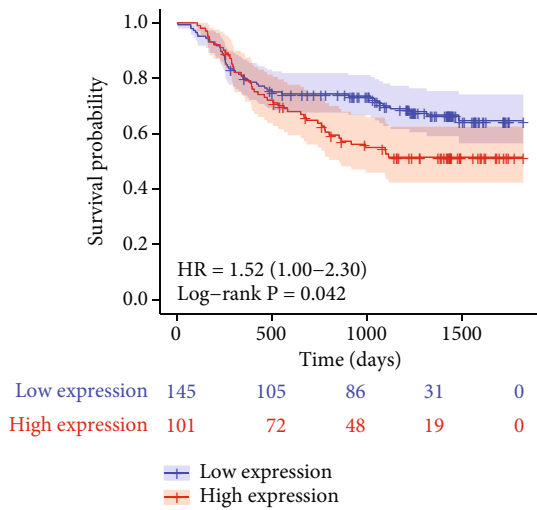
FIGURE 2: Kaplan–Meier survival analysis of the OS for patients with different ITGA4 expression in HMU-GC validation cohort.

metastasis, including chemotactic movement of GC cells and the formation of lymphatic vessels.

It is often found that patients with advanced GC may have significantly different prognosis even if their TNM stages are the same [10, 11]. Some GC primary sites are large in volume, but the degree of invasion is limited to the serosae, and lymph node metastasis and distant planting metastasis do not occur. If these patients are treated surgically and undergo postoperative chemotherapy according to the guidelines, the 5-year survival rate can often reach 84.0% [7]. Some patients' tumors only invade the muscle layer but have multiple lymph node metastases. Even if radical

surgery, postoperative chemotherapy or preoperative neoadjuvant treatment is performed, their 5-year and 10-year survival rates are significantly reduced [12, 13]. However, studies have shown that about 60% of GC has obvious tissue heterogeneity in transcriptomics sequencing, which makes it difficult to find molecules targeted at lymph node metastasis.

Therefore, this study is different from conventional transcriptomic sequencing analysis. We started with the clinicopathological characteristics of patients and took the pathological characteristics of lymph node metastasis as a separate variable to screen out the abnormal expression of ITGA4 in tumor with positive lymph node metastasis. The full name of ITGA4 is Integrin Subunit Alpha 4. Integrin is a heterodimeric integrated membrane protein, composed of α Chain and β Chain composition, which plays a role in cell surface adhesion and signaling [14]. The precursor protein encoded by ITGA4 is proteolytically processed to produce light and heavy chains containing Alpha4 subunits. This subunit is related to $\beta 1$ or $\beta 7$ subunits, which binds to form integrins that may play a role in cell motility and migration [15, 16]. This integrin is a therapeutic target for the treatment of multiple sclerosis, Crohn's disease, and inflammatory bowel disease. But up to now, little research of ITGA4 in GC has been reported [17]. In this study, we try to find the possibility of ITGA4 as a biomarker and its potential mechanism in the progression of GC.

2. Materials and Methods

2.1. Overview of GC RNA Dataset and Immunohistochemical Cohort. The training cohort included 20 patients with lymph node metastatic GC with N3+ stage and 20 patients with N0 stage. The HMU-CG validation set included 246 patients underwent gastrectomy as the primary treatment in the

TABLE 1: Relationship between ITGA4 mRNA expression and the clinical characteristics of GC in the HMU-GC validation cohort.

Characteristic	High expression ($n = 101$)	Low expression ($n = 145$)	P value
Sex, n (%)			0.711
Female	38 (15.4%)	50 (20.3%)	
Male	63 (25.6%)	95 (38.6%)	
T classification, n (%)			0.241
T1a	2 (0.8%)	4 (1.6%)	
T1b	1 (0.4%)	6 (2.4%)	
T2	7 (2.8%)	10 (4.1%)	
T3	64 (26%)	101 (41.1%)	
T4a	14 (5.7%)	16 (6.5%)	
T4b	13 (5.3%)	8 (3.3%)	
N classification, n (%)			0.031
N0	17 (6.9%)	32 (13%)	
N1	10 (4.1%)	19 (7.7%)	
N2	17 (6.9%)	25 (10.2%)	
N3a	28 (11.4%)	51 (20.7%)	
N3b	29 (11.8%)	18 (7.3%)	
M classification, n (%)			0.806
M0	95 (38.6%)	134 (54.5%)	
M1	6 (2.4%)	11 (4.5%)	
pTNM, n (%)			0.077
IA	3 (1.2%)	8 (3.3%)	
IB	4 (1.6%)	6 (2.4%)	
IIA	10 (4.1%)	13 (5.3%)	
IIB	7 (2.8%)	16 (6.5%)	
IIIA	18 (7.3%)	28 (11.4%)	
IIIB	24 (9.8%)	46 (18.7%)	
IIIC	29 (11.8%)	17 (6.9%)	
IV	6 (2.4%)	11 (4.5%)	
Borrmann type, n (%)			0.307
Borrmann I	4 (1.6%)	1 (0.4%)	
Borrmann II	22 (8.9%)	28 (11.4%)	
Borrmann III	60 (24.4%)	89 (36.2%)	
Borrmann IV	15 (6.1%)	27 (11%)	
Tumor location, n (%)			0.033
Lower third	41 (16.7%)	77 (31.3%)	
Middle third	20 (8.1%)	35 (14.2%)	
Upper third	22 (8.9%)	21 (8.5%)	
Entire stomach	18 (7.3%)	12 (4.9%)	
Lymphatic infiltration, n (%)			0.604
Negative	46 (18.7%)	60 (24.4%)	
Positive	55 (22.4%)	85 (34.6%)	
Nerve infiltration, n (%)			0.677
Negative	24 (9.8%)	30 (12.2%)	
Positive	77 (31.3%)	115 (46.7%)	
WHO classification, n (%)			0.007
Mucinous	8 (3.3%)	1 (0.4%)	
Poorly differentiated	26 (10.6%)	38 (15.4%)	
Signet ring cell	39 (15.9%)	47 (19.1%)	

Characteristic	High expression ($n = 101$)	Low expression ($n = 145$)	P value
Well to moderately differentiated	28 (11.4%)	59 (24%)	
Age, median (IQR)	61 (51, 67)	58 (47, 64)	0.144
CEA, median (IQR)	1.81 (1.16, 3.85)	2.25 (1.27, 3.9)	0.245
CA-199, median (IQR)	10.91 (6.17, 22.47)	11.57 (5.16, 22.81)	0.714
CA724, median (IQR)	2.49 (1.29, 11.86)	3.03 (1.29, 6.64)	0.706
CA125, median (IQR)	10.21 (8.08, 13.47)	10.21 (7.72, 15.67)	0.797

Histological type, T classification, N classification, and pTNM classification were according to the AJCC 8th edition of the Cancer Staging Manual of the American Joint Committee on Cancer. Vascular infiltration, nerve infiltration, and lymphatic infiltration were determined according to the postoperative pathology report. IQR: interquartile range.

Department of Gastroenterology, Harbin Medical University Cancer Hospital (GSE184336 and GSE179252). The quality control method is mainly completed through Agilent 2100 bioanalyzer. The kit used for library building is EBNext® Ultra™ Directional RNA Library Prep Kit for Illumina. Finally, use the Illumina platform for sequencing. All samples were collected from patients after obtaining written informed consent. The study was approved by the institutional review board of the Affiliated Tumor Hospital of Harbin Medical University. RNA isolation, library construction, and mRNA sequencing were performed by Novogene Biotech Co., Ltd. (Beijing, China). Data were stored in the Gene Expression Omnibus (GEO) repository.

Tissue microarray (TMA) samples included 180 patients underwent radical gastrectomy in the Department of Gastroenterology, Affiliated Tumor Hospital of Harbin Medical University between November 2018 and December 2019. Exclusion criteria included preoperative neoadjuvant therapy, serious heart disease, serious infectious diseases, recurrent GC, and distant metastasis.

For the preparation of tissue microarray, two experienced pathologists observed the pathological level of the whole tumor tissue through H&E staining under high-definition electron microscopy and selected a representative site to more accurately reflect the pathological characteristics of the tumor. Then, mark the position on the paraffin embedded tissue with special marker and select a sample with a diameter of 1.5 mm. The sites of sampling include tumor center and invasion front. The technical service is provided by Shanghai Aoduo Biotechnology Co., Ltd. (Shanghai, China).

2.2. Immunochemistry. GC tissues and paracancerous tissues were fixed in 4% paraformaldehyde. Then all tissue samples were paraffin embedded and prepared for at least 4 μm thick tissue sections. Pathologists performed hematoxylin and eosin (H&E) staining to select the representative location for preparing tissue chips, and the lattice diameter was 15 mm. In order to detect the protein expression in the tissue, the sections were first repaired with EDTA antigen repair solution in a 120°C pressure cooker environment for 3 minutes, then incubated with 3% H_2O_2 at room temperature for 30 minutes, goat serum at room temperature for 2 hours, and then incubated with primary antibodies specific for ITGA4 at 4°C overnight (1 : 1000, Affinity, #DF6135).

The secondary antibodies (Elabscience, No.E-IR-R217) were incubated at room temperature for 30 minutes, and the chromogenic reaction was performed via diaminobenzidine (DAB) staining. The assessment of immunohistochemistry used the H-score method. This score was derived from the dyeing intensity and was scored as negative (0), weak (1), medium (2), or strong (3) multiplied by percentage of dyed area under intensity. Immunohistochemical score data were divided into high expression or low expression according to survival rate by X-tile software.

2.3. Cell Culture. All cell lines (GES, AGS, BGC-823, HGC-27, MKN-28, and 293T) were obtained from the cell line service (Procell Biotechnology Co., Ltd., Wuhan, China) and authenticated by the provider. These cell lines were not included in the misidentified cell line database of the The International Cell Line Authentication Committee (ICLAC) (http://iclac.org/). In this study, BGC-823 cell line was used to investigate the effect of ITGA4 on the proliferation, migration, and invasion of GC. 293T cells were used for lentiviral infection. GES, BGC-823, HGC-27, and MKN-28 cell lines were cultured using modified McCoy's 5A medium RPMI-1640 (PM150110), 10% fetal bovine serum (164210-50), 1% Penicillin-Streptomycin Solution (PB180120), and 1% GlutaMax (PB180419). The AGS cell line used Ham's F-12 nutrient mixture (PM150810), 10% fetal bovine serum (164210-50), and 1% Penicillin-Streptomycin Solution (PB180120). The 293T cell line was cultured in Dulbecco's modified medium DMEM (PM150210), 10% fetal bovine serum (164210-50), and 1% Penicillin-Streptomycin Solution (PB180120). All cell lines were cultured in a humidified incubator containing 5% CO_2 at 37°C.

2.4. Cell Transfection. The shRNA against ITGA4 was designed and synthesized according to the known sequence, and then inserted into the lentiviral expression vector GV493 (Genechem, China). The sequences of shRNA targeting IGTA4 are shown in Supplementary Table S1. This lentivirus vector was transfected into 293T cells together with the packaging system plasmids psPAX2 and pMD2.G to obtain pseudolentivirus particles. 20 μg lentiviral vector, 15 μg psPAX2, and 10 μg pMD2.G were used to transfect a 5×10^6 293T cells. The supernatant of 293T was collected and concentrated by an ultracentrifuge at 25 000 rpm for 2 h at 4°C. BGC-823 cells were transduced with

(a)

(b)

(c)

(d)

(e)

(f)
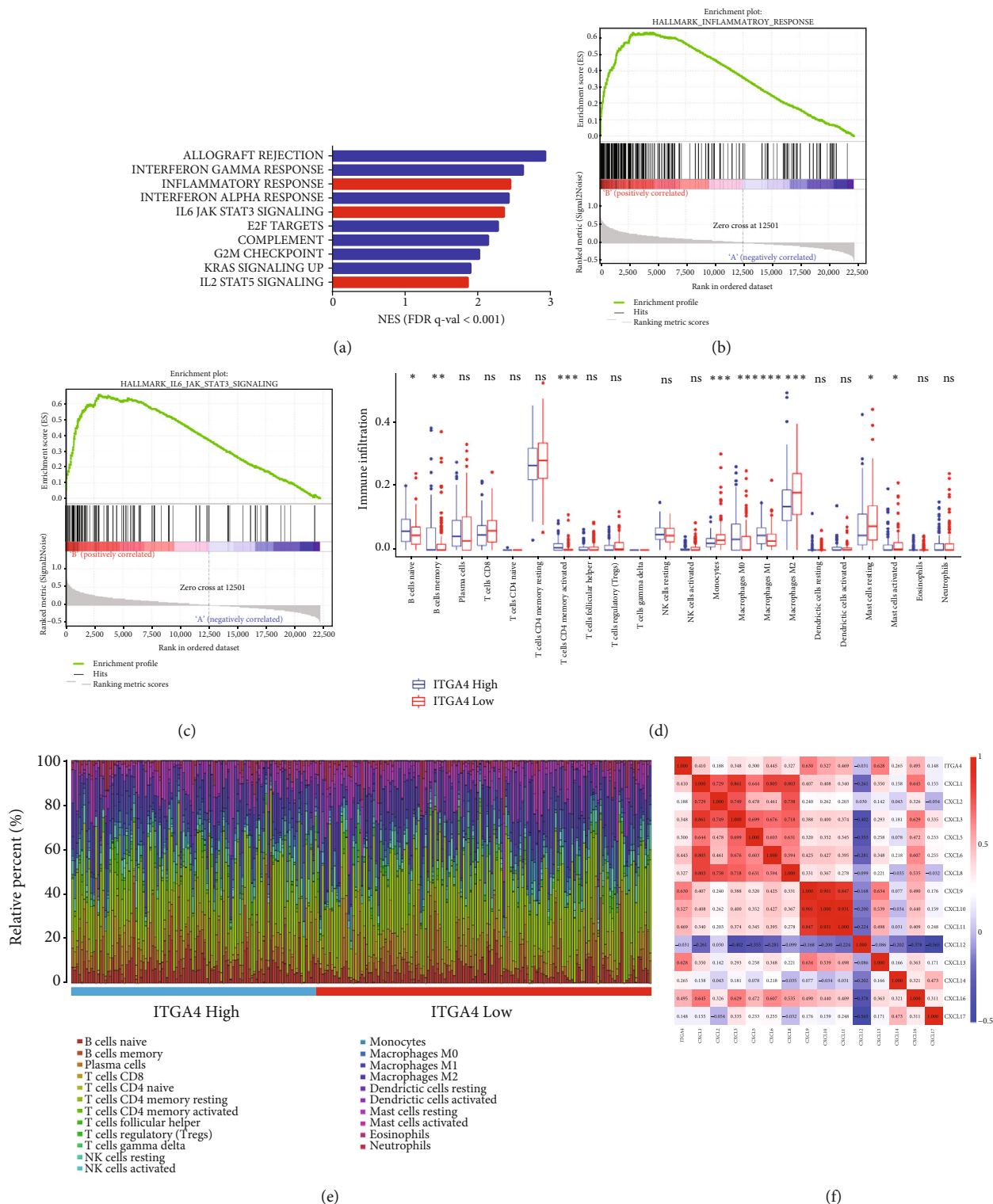
FIGURE 3: (a) ITGA4 expression correlated with inflammatory response, (b) IL6 JAK STAT3 signaling, (c) and IL2 STAT5 signaling from the HMU-GC validation cohort. (d, e) Analysis of immune cell components according to different ELN expression levels from the HMU-GC validation cohort. (f) Correlation analysis of ITGA4 and chemokines.

concentrated lentiviral particles. IGTA4 knock down was verified by Western blot. Scrambled sequences were inserted into these vectors for use as controls.

2.5. Western Blot. The proteins were extracted from gastric epithelial cells and cancer cells, and the extracted proteins were quantified using BCA Kit (Beyotime Institute of

(a)

(b)

(c)

(d)
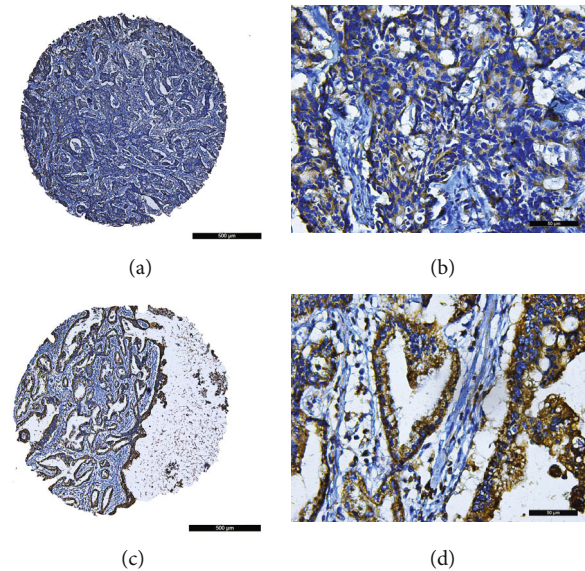
FIGURE 4: ITGA4 immunohistochemistry staining of TMA. (a) Low expression of ITGA4 at ×50. (b) Low expression of ITGA4 at ×400. (c) High expression of ITGA4 at ×50. (d) High expression of ITGA4 at ×400.

Biotechnology). The proteins were separated by sodium dodecyl sulphate-polyacrylamide gel electrophoresis (SDS-PAGE), transferred to PVDF membrane (Merck Millipore Ltd.), and sealed with BSA (5%) under RT for 2 hours. Subsequently, the membrane was incubated with ITGA4 specific primary antibody at 4°C overnight (1 : 1000, Affinity, DF6135). The membranes were incubated with horseradish peroxidase labeled secondary antibody at 37°C for 40 minutes, and then visualize by ECL (Thermo Scientific).

2.6. Cell Counting Kit-8 (CCK-8) Assay.
Cell viability in vitro was evaluated by cell counting kit-8 (CCK-8) assay. 4×10^3 cells were implanted into 96-well plates. After the cells adhered to the wall after 4 hours of culture, the medium in each well was replaced with 100 ml RPMI-1640 serum-free medium, and the adsorption rate after 2 hours was measured by a microplate reader at 450 nm in a medium containing 10 ml CCK-8 reagent (Meilunbio, MA0218-3). Then repeat the detection at 24 h, 48 h, and 72 h, respectively.

2.7. Cell Migration and Invasion Assay.
Migration and invasion analyses were performed using a 24-well Transwell chamber system (Costar, USA, #3422). Briefly, cells were resuspended in serum-free medium, washed twice, and seeded into the upper chamber (8×10^4 cells per 200 μl). The lower chamber contains 900 μl medium containing 20% FBS. After 24 hours of incubation, the cells were fixed with 95% ethanol for 15 minutes, and then stained with 0.1% crystal violet for 30 minutes. Use a cotton swab to remove the cells that failed to penetrate the filter from the upper chamber. Under the light microscope, migrating and invading cells were counted in three randomly selected regions. For the invasion test, the chamber was coated with 40 μl Corning Matrix Matrix (#356234, USA) before cell inoculation.

2.8. Statistical Analysis and Bioinformatics Analysis.
Data were analyzed using SPSS 22.0 (Chicago, USA, SPSS Inc.) software and shown as mean ± SD. Chi-square test was used to evaluate the relationship between ITGA4 expression and clinicopathological features if they meet the conditions that the theoretical frequency is more than 5 and the total sample size is more than 40. If they do not meet the conditions that the theoretical frequency is more than 5 or the total sample size is more than 40, so the Fisher exact test is recommended. The Wilcoxon rank sum test is selected if the normal distribution is not satisfied. Survival analysis of patients was analyzed using log-rank test and Cox regression. Survival curves and overall survival (OS) were determined by Kaplan-Meier and log Rank methods. Gene Ontology (GO) pathway enrichment analysis was used for genome functional annotation. The "clusterprofiler" package was used to study the functional enrichment of risk score-related genes in gene set enrichment analysis (GSEA). All bioinformatics analyses were performed using R Studio software (v4.0.2). A two tailed P value < 0.05 is considered significant.

3. Results

3.1. ITGA4 Was Highly Correlated with Lymph Node Metastasis in the Training Cohort.
In this study, we first searched for ITGA4 related to lymph node metastasis through transcriptome-level sequencing. There were 20 patients in each of the two groups in the training cohort. The pathological data were not statistically significant except for lymph node metastasis (Supplementary Table S2). The sequencing results showed that ITGA4 gene was significantly overexpressed in patients with positive lymph node metastasis ($P < 0.001$, Figure 1(a)). Figure 1(b) shows the differential genes of the two groups. In the group with positive lymph node metastasis, 309 genes were upregulated and 331 genes were downregulated.

TABLE 2: The relationship between ITGA4 expression in tumor tissue and the clinicopathological characteristics.

Characteristic	High expression (n = 74)	Low expression (n = 106)	P value
Age, mean ± SD	58.93 ± 9.75	61.2 ± 9.16	0.114
BMI, median (IQR)	22.51 (20.21, 24.48)	23.19 (21.12, 25.45)	0.092
Sex, n (%)			0.402
Female	16 (8.9%)	30 (16.7%)	
Male	58 (32.2%)	76 (42.2%)	
Tumor infiltration pattern, n (%)			0.189
INFa	12 (6.7%)	24 (13.3%)	
INFb	14 (7.8%)	30 (16.7%)	
INFc	34 (18.9%)	34 (18.9%)	
N/A	14 (7.8%)	18 (10%)	
Lymphatic infiltration, n (%)			0.163
Negative	47 (26.1%)	55 (30.6%)	
Positive	27 (15%)	51 (28.3%)	
Venous infiltration, n (%)			0.936
Negative	55 (30.6%)	77 (42.8%)	
Positive	19 (10.6%)	29 (16.1%)	
Nerve infiltration, n (%)			0.530
Negative	17 (9.4%)	30 (16.7%)	
Positive	57 (31.7%)	76 (42.2%)	
T classification, n (%)			0.028
T1	5 (2.8%)	5 (2.8%)	
T2	6 (3.3%)	21 (11.7%)	
T3	24 (13.3%)	44 (24.4%)	
T4	39 (21.7%)	36 (20%)	
N classification, n (%)			0.006
N0	18 (10%)	32 (17.8%)	
N1	8 (4.4%)	28 (15.6%)	
N2	17 (9.4%)	24 (13.3%)	
N3	31 (17.2%)	22 (12.2%)	
pTNM classification, n (%)			0.109
I	9 (5%)	14 (7.8%)	
II	17 (9.4%)	39 (21.7%)	
III	48 (26.7%)	53 (29.4%)	
Metastatic lymph node ratio, n (%)			0.018
< 0.3	50 (27.8%)	90 (50%)	
≥ 0.6	8 (4.4%)	4 (2.2%)	
0.3 ≥, < 0.6	16 (8.9%)	12 (6.7%)	
Borrmann type, n (%)			0.330
Borrmann I	6 (3.3%)	9 (5%)	
Borrmann II	20 (11.1%)	29 (16.1%)	
Borrmann III	38 (21.1%)	62 (34.4%)	
Borrmann IV	10 (5.6%)	6 (3.3%)	
Lauren classification, n (%)			0.514
Diffuse	30 (16.7%)	34 (18.9%)	
Intestinal	17 (9.4%)	32 (17.8%)	
Mixed	13 (7.2%)	23 (12.8%)	
Unknown	14 (7.8%)	17 (9.4%)	
Family cancer history, n (%)			0.441

Table 2: Continued.

Characteristic	High expression ($n = 74$)	Low expression ($n = 106$)	P value
No	69 (38.3%)	94 (52.2%)	
Yes	5 (2.8%)	12 (6.7%)	
Tumor location, n (%)			0.058
Entire stomach	5 (2.8%)	1 (0.6%)	
Lower third	35 (19.4%)	62 (34.4%)	
Middle and upper third	34 (18.9%)	43 (23.9%)	
HER2 expression, n (%)			0.330
Negative	61 (33.9%)	94 (52.2%)	
Positive	13 (7.2%)	12 (6.7%)	
CEA, n (%)			0.354
> 5 ng/ml	12 (6.7%)	11 (6.1%)	
≤ 5 ng/ml	62 (34.4%)	95 (52.8%)	
CA19-9, n (%)			0.003
> 37 U/ml	16 (8.9%)	6 (3.3%)	
≤ 37 U/ml	58 (32.2%)	100 (55.6%)	
CA72-4, n (%)			0.530
> 6 U/ml	17 (9.4%)	30 (16.7%)	
≤ 6 U/ml	57 (31.7%)	76 (42.2%)	

Histological type, T classification, N classification, and pTNM classification were according to the AJCC 8th edition of the Cancer Staging Manual of the American Joint Committee on Cancer. Vascular infiltration, nerve infiltration, and lymphatic infiltration were determined according to the postoperative pathology report. IQR: interquartile range; SD: standard deviation.

3.2. ITGA4 Expression Was Associated with Poor Clinicopathological Features in the Validation Cohort. We examined the relationship between ITGA4 mRNA expression and OS, clinicopathological features in the HMU-GC validation cohort. The cut-off of mRNA was calculated according to the ROC curve. There were 101 patients with high expression of ITGA4 and 145 patients with low expression. Kaplan-Meier analysis showed that ITGA4 was associated with poor prognosis, and the prognosis of patients with high expression of ITGA4 had a lower survival probability (Figure 2, $P = 0.045$). In addition, ITGA4 was highly correlated with poor pathological features such as N classification ($P = 0.031$), tumor location ($P = 0.033$), and WHO classification ($P = 0.007$) (Table 1).

3.3. Bioinformatics Analysis of the Validation Cohort Suggested that ITGA4 Was Associated with Macrophage Infiltration. We performed GSEA analysis related to ITGA4 in the HMU-GC validation cohort (Figure 3(a)), and the results showed that immune response pathways such as inflammatory response (Figure 3(b)) and IL6 JAK STAT3 signaling (Figure 3(c)) were activated in the tissues of patients with high expression of ITGA4 ($P < 0.001$). In order to explore which kind of immune cells plays the more important role in GC tissues with different levels of ITGA4, we analyzed the immune cell composition with different levels of expression of ITGA4. The results showed that macrophages were enriched higher in tissues with high expression of ITGA4 (Figure 3(d) and 3(e)). At the same time, we also found that ITGA4 maintained this immune response

mainly through a variety of chemokines, especially CXCL9 ($r = 0.630$) and CXCL1 ($r = 0.628$, Figure 3(f)).

3.4. Immunohistochemistry Showed that ITGA4 Was Associated with Poor Prognosis and Could Construct a Prognosis Model. We evaluated the expression of ITGA4 through immunohistochemistry, which is mainly expressed in the cytoplasm of tumor cells (Figure 4). Chi-square analysis showed that ITGA4 was mainly related to T classification ($P = 0.028$), N classification ($P = 0.006$), lymph node metastasis rate ($P = 0.018$), and serum CA19-9 ($P = 0.003$) (Table 2), which was basically consistent with the results of previous transcriptome level analysis. There are 180 samples of TMA, and 100 samples meet the 3-year follow-up, so the survival analysis includes 100 samples. Survival analysis showed that high expression of ITGA4 was significantly related to poor patient survival (Figure 5(a), $P = 0.011$). Univariate Cox regression analysis showed that ITGA4 ($P = 0.011$), lymph node metastasis rate ($P < 0.001$), and tumor location ($P = 0.003$) were correlated with prognosis. Multivariate Cox regression analysis found that ITGA4 ($P = 0.045$) and lymph node metastasis rate ($P = 0.026$) were independent prognostic factors (Table 3). Next, we construct a prognosis model (Figure 5(b)) based on independent prognostic factors of Cox regression analysis. The calibration curve analysis of the prognosis model has satisfactory accuracy, $C - index = 0.705$ (0.656-0.753) (Figure 5(c)). DCA analysis showed that the prognosis model had an acceptable predictive value in predicting the death risk in 2 years (Figure 5(d)) and 3 years (Figure 5(e)), ITGA4 $C - index =$
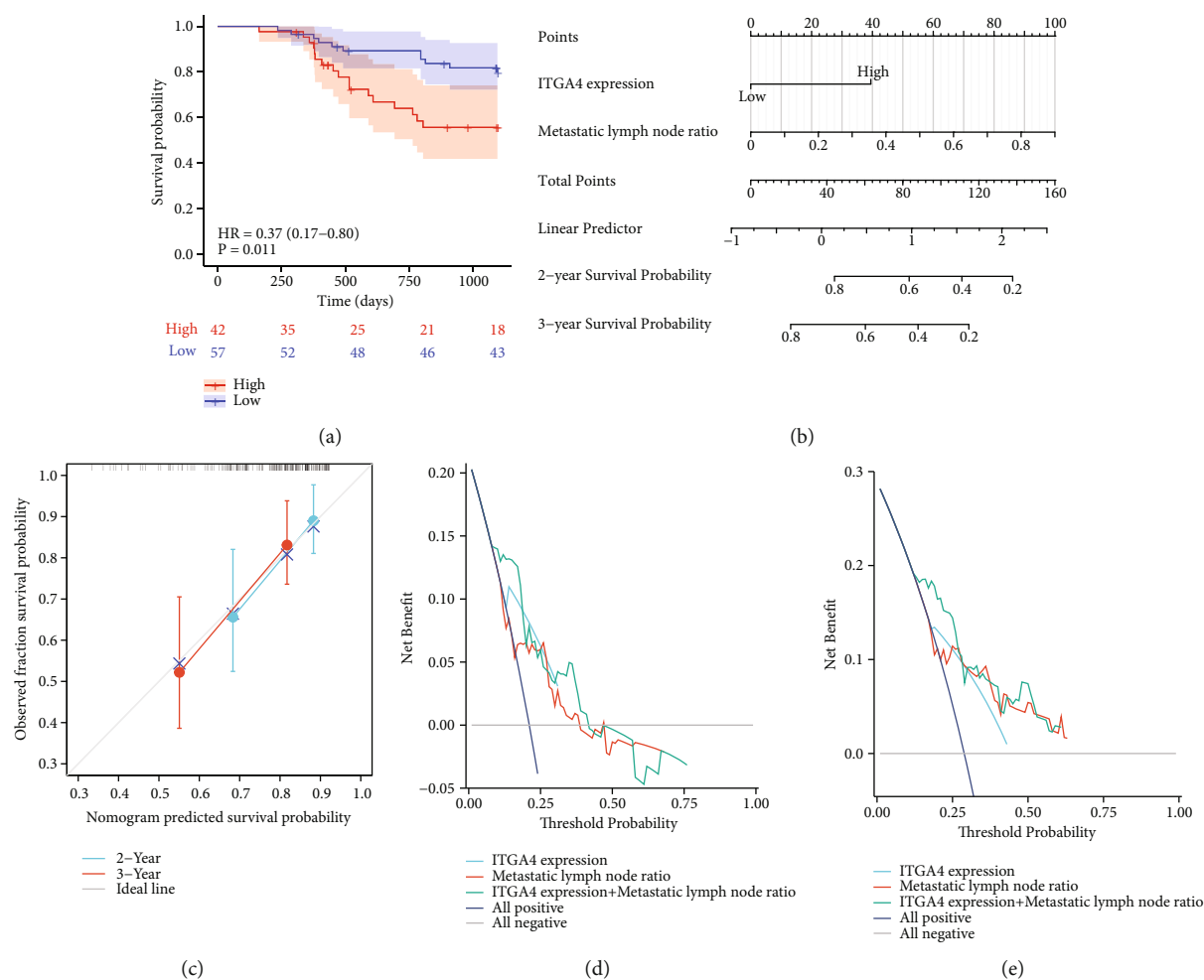
FIGURE 5: (a) Kaplan–Meier survival analysis of the OS for patients with different ITGA4 expression levels in TMAs. (b) Nomogram prognostic model. (c) Calibration analysis in 2 and 3 years. (d) Decision curve analysis in 2 years. (e) Decision curve analysis in 3 years.

0.623 (0.577-0.669), the lymph node metastasis rate C − index = 0.647 (0.593-0.702), and the combined C − index = 0.705 (0.656-0.753).

3.5. ITGA4 Knockdown Cell Line Significantly Reduced the Ability of Proliferation, Invasion, and Metastasis.

We first verified at the protein level that ITGA4 is generally highly expressed in GC cells compared with gastric epithelial cells (Figure 6(a)). Then we constructed the ITGA4 knockdown cell line of BGC-823 and verified it at the protein level (Figure 6(b)). Next, we evaluated the ability of ITGA4 to promote GC proliferation through CCK-8 experiment. The results showed that the proliferation ability of BGC-823 cell lines with ITGA4 knockdown was significantly inhibited than that of the control group (Figure 6(c)). The results of previous clinical immunohistochemical experiments suggested that the expression of ITGA4 was significantly correlated with the metastasis rate of lymph nodes. We tested the effect of ITGA4 gene on the migration and invasion ability of GC cells through Transwell experiments. The results showed that after knockdown of ITGA4 by BGC-823 cell line, the number of cells penetrating the membrane in

migration and invasion simulation experiment was significantly less than that in the control group (Figure 6(d)).

4. Discussion

The TNM staging system based on tumor invasion, regional lymph node, and distant metastasis in GC is recognized as an international standard to predict prognosis and guide postoperative treatment [18]. Adjuvant chemotherapy is recommended for patients with stage II or III pathological stage after radical surgery to reduce recurrence [5]. However, how to more accurately evaluate lymph node metastasis is a clinical problem that surgeons and pathologists have been working on for a long time. Therefore, we want to screen a reliable biomarker according to the difference of lymph node metastasis to evaluate the biological function and prognosis of GC. In this study, we first found that ITGA4 was highly correlated with lymph node metastasis in GC. Then, we analyzed the mRNA and immunohistochemical expression of ITGA4 and the relationship between expression level and clinicopathological factors. We found that the high expression of ITGA4 affects the immune infiltration status of

Table 3: Univariate and multivariate Cox analysis of ITGA4 expression and the clinicopathological variables.

Characteristics	Total (N)	Univariate analysis Hazard ratio (95% CI)	P value	Multivariate analysis Hazard ratio (95% CI)	P value
Group	100				
High expression	43	Reference			
Low expression	57	0.374 (0.174-0.801)	0.011	0.450 (0.206-0.984)	0.045
Sex	100				
Female	28	Reference			
Male	72	1.175 (0.499-2.765)	0.712		
Age	100	0.992 (0.957-1.028)	0.646		
BMI	100	0.944 (0.845-1.054)	0.303		
Tumor infiltration pattern	100				
INFc	48	Reference			
INFb	16	0.843 (0.280-2.541)	0.761		
INFa	20	0.568 (0.188-1.712)	0.315		
N/A	16	1.035 (0.376-2.848)	0.947		
Lymphatic infiltration	100				
Positive	45	Reference			
Negative	55	1.064 (0.503-2.249)	0.872		
Venous infiltration	100				
Positive	30	Reference			
Negative	70	1.689 (0.685-4.166)	0.255		
Nerve infiltration	100				
Positive	75	Reference			
Negative	25	0.446 (0.155-1.286)	0.135		
T classification	100				
T4	38	Reference			
T3	45	0.591 (0.268-1.302)	0.192		
T2	13	0.348 (0.079-1.533)	0.163		
T1	4	0.585 (0.077-4.452)	0.605		
Metastatic lymph node ratio	100	14.056 (3.348-59.004)	<0.001	7.032 (1.262-39.187)	0.026
Borrmann type	100	1.445 (0.769-2.715)	0.253		
Tumor location	100				
Lower third	54	Reference			
Middle and upper third	42	1.866 (0.847-4.113)	0.122	1.369 (0.590-3.177)	0.464
Entire stomach	4	7.426 (2.017-27.337)	0.003	1.838 (0.376-8.988)	0.452
HER2	100				
Positive	18	Reference			
Negative	82	0.602 (0.256-1.418)	0.246		
CEA	100				
≤ 5 ng/ml	86	Reference			
> 5 ng/ml	14	0.679 (0.205-2.250)	0.526		
CA-199	100				
≤ 37 U/ml	88	Reference			
> 37 U/ml	12	1.745 (0.663-4.593)	0.260		
CA724	100				
≤ 6 U/ml	74	Reference			
> 6 U/ml	26	1.096 (0.483-2.490)	0.826		

Histological type and T classification were according to the AJCC 8th edition of the Cancer Staging Manual of the American Joint Committee on Cancer. Vascular infiltration, nerve infiltration, and lymphatic infiltration were determined according to the postoperative pathology report.

(a)

(b)

(c)

(d)
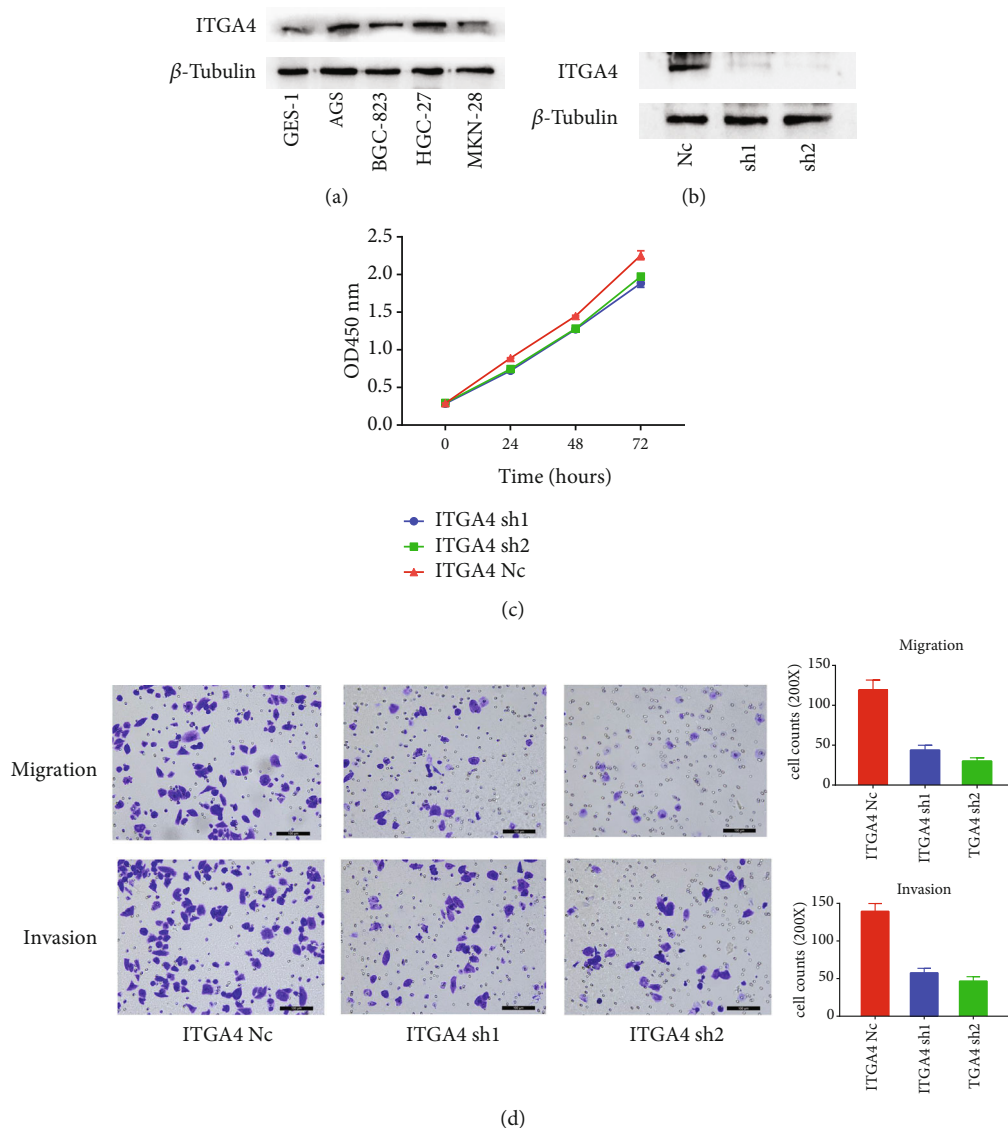
Figure 6: (a) Protein expression of ITGA4 in gastric epithelium and different GCs. (b) Verification of ITGA4 knockdown in protein level. (c) CCK-8 analysis of ITGA4 knockdown in BGC-823 cell line. (d) Transwell migration and invasion assay in BGC-823 cell line after ITGA4 knockdown.

cancer tissues, especially related to the enrichment of macrophages. We further confirmed that ITGA4 can promote GC cell migration and invasion in vitro. Finally, we constructed a prognostic model for GC based on ITGA4 expression and clinicopathological characteristics.

ITGA4 (Integrin Subunit Alpha 4) is a protein-coding gene. The gene encodes a member of the integrin alpha chain family of proteins. Integrin is a member of the superfamily of transmembrane glycoproteins α and β and a heterodimer membrane receptor protein composed of two subunits that function in cell surface adhesion and signaling. ITGA4 has been proved to be involved in cell proliferation, apoptosis, adhesion, and migration, which promoting tumor progression [19]. In addition, methylation of ITGA4 exists in many kinds of primary tumors, which may play a key role in the transformation of inflammatory cancer [20–22]. However, there are little studies that have confirmed the

prognostic value of ITGA4 in GC. In this study, we found that high expression of ITGA4 was significantly associated with vascular invasion and lymph node metastasis. At the same time, we further confirmed that ITGA4 promotes GC cell migration and invasion, which suggests that it may be a potential prognostic biomarker. Survival analysis showed that ITGA4 had satisfactory prognostic value in GC patients.

In order to further verify the reliability of ITGA4 as a biomarker, we found that ITGA4 is significantly related to the activation of IL6/JAK/STAT3, IL2/STAT5, and other immune response pathways through GSEA and GO enrichment analysis. In addition, the analysis of immune cell components in cancer tissues showed that there was more macrophages that were enriched in the tissues with high expression of ITGA4. Wei et al. [23] reasonably explains this result that tumor associated macrophages (TAMs-) derived IL-6 activated the JAK2/STAT3 signaling pathway. The

activated STAT3 transcriptional inhibition produces CCL2 to promote macrophage recruitment. It is worth noting that our results show that the overexpression of ITGA4 was related to the enrichment of M1 type TAMs. This is contrary to previous cognition. Previous studies have shown that TAMs can be polarized into tumor supporting M2 like macrophages and tumor inhibiting M1 like macrophages [24–26]. You et al. [27] found that M1 like TAMs significantly promoted the epithelial mesenchymal transformation (EMT) process and induced the formation of cancer stem cells by upregulating the expression of MME and MMP14 in oral squamous cell carcinoma. M1 like TAMs promote the invasion and migration of cell colonies by activating the JAK/STAT3 pathway. This is consistent with our results, indicating that M1 like TAMs do not play a diversified inhibitory role in tumor progression. In addition, our results show that undifferentiated M0 type TAMs is enriched in tissues with high expression of ITGA4. This means that the high expression of ITGA4 is closely related to macrophage polarization and may induce more TAMs [28]. In the future, researches should pay more attention to how ITGA4 in the GC microenvironment affects the dynamic polarization of macrophages. At the same time, our research results confirm that ITGA4 mainly maintains this specific immune infiltration state through a variety of chemokines, such as CXCL9. Relevant studies have found that M1 like TAMs may recruit CD8$^+$ tissue resident memory (TRM) T cells through CXCL9 overexpression and provide TRM with essential fatty acids to maintain immune infiltration [29].

Of course, our research has some limitations. First, the analysis of mRNA markers and immunoassays in tumors comes from transcriptome level sequencing, which has not been verified by rigorous molecular level experiments, and should be interpreted carefully. Second, functional characterization and verification of the role of ITGA4 in immune cells will be very important to determine whether the cancer promoting effect of ITGA4 in the GC microenvironment is a driver or a bystander. In the survival analysis of ITGA4, it is also necessary to conduct multicenter and multiethnic trials in a larger cohort to verify the role of ITGA4 in the treatment response to patient survival and other clinical features, such as immune efficacy and metastasis status.

Data Availability

The datasets used in this study are available from the corresponding author on reasonable request. More information can also be obtained from the Gastric Cancer Information Management System v1.2 of Harbin Medical University Cancer Hospital (Copyright No. 2013SR087424, http://www.sgihmu.com/). The datasets HMU-training cohort and HMU-validation cohorts presented in this study can be found in online repositories (GSE184336 and GSE179252).

Ethical Approval

All programs followed were according to the ethical standards of the Human Subjects Responsibility Committee (institutions and countries) as well as the 1964 Helsinki Declaration and subsequent editions. This research was approved by Harbin Medical University Cancer Hospital Ethics Committee (Approval Number: SHGC-1029).

Conflicts of Interest

The authors declare that they have no conflict of interest.

Authors' Contributions

Tianyi Fang, Xin Yin, and Yufei Wang designed and conceived this project, and they contributed equally to this work. Xin Yin, Tianyi Fang, Yufei Wang, and Xibo Wang interpreted and analyzed the data. Yingwei Xue revised the manuscript for important intellectual content. Xin Yin, Tianyi Fang, Hao Wang, and Yufei Wang participated in the patient information collection. Tianyi Fang, Xin Yin, and Yufei Wang contributed equally to this work.

Acknowledgments

Supplementary Materials

Table S1: the shRNA designed for ITGA4 knockdown. Table S2: baseline characteristics in the training cohort. (Supplementary Materials)

References

[1] R. L. Siegel, K. D. Miller, H. E. Fuchs, and A. Jemal, "Cancer statistics, 2022," CA: a Cancer Journal for Clinicians, vol. 72, no. 1, pp. 7–33, 2022.

[2] H. Sung, J. Ferlay, R. L. Siegel et al., "Global cancer statistics 2020: GLOBOCAN estimates of incidence and mortality worldwide for 36 cancers in 185 countries," CA: a Cancer Journal for Clinicians, vol. 71, no. 3, pp. 209–249, 2021.

[3] R. L. Siegel, K. D. Miller, and A. Jemal, "Cancer statistics, 2020," CA: a Cancer Journal for Clinicians, vol. 70, no. 1, pp. 7–30, 2020.

[4] T. Fang, X. Yin, Y. Wang et al., "Proposed models for prediction of mortality in stage-I and stage-II gastric cancer and 5 years after radical gastrectomy," Journal of Oncology, vol. 2022, Article ID 4510000, 14 pages, 2022.

[5] Japanese Gastric Cancer Association, "Japanese gastric cancer treatment guidelines 2018 (5th edition)," Gastric Cancer, vol. 24, no. 1, pp. 1–21, 2021.

[6] T. Sano, D. G. Coit, H. H. Kim et al., "Proposal of a new stage grouping of gastric cancer for TNM classification: international gastric cancer association staging project," Gastric Cancer, vol. 20, no. 2, pp. 217–225, 2017.

[7] Y. W. Moon, H. C. Jeung, S. Y. Rha et al., "Changing patterns of prognosticators during 15-year follow-up of advanced gastric cancer after radical gastrectomy and adjuvant

chemotherapy: a 15-year follow-up study at a single Korean institute," *Annals of Surgical Oncology*, vol. 14, no. 10, pp. 2730–2737, 2007.

[8] J. W. Kim, I. Hwang, M. J. Kim, and S. J. Jang, "Clinicopathological characteristics and predictive markers of early gastric cancer with recurrence," *Journal of Korean Medical Science*, vol. 24, no. 6, pp. 1158–1164, 2009.

[9] H. In, I. Solsky, B. Palis, M. Langdon-Embry, J. Ajani, and T. Sano, "Validation of the 8th edition of the AJCC TNM staging system for gastric cancer using the National Cancer Database," *Annals of Surgical Oncology*, vol. 24, no. 12, pp. 3683–3691, 2017.

[10] H. Katai, T. Ishikawa, K. Akazawa et al., "Five-year survival analysis of surgically resected gastric cancer cases in Japan: a retrospective analysis of more than 100,000 patients from the nationwide registry of the Japanese gastric cancer association (2001-2007)," *Gastric Cancer*, vol. 21, no. 1, pp. 144–154, 2018.

[11] T. Fang, Z. Wang, X. Yin et al., "Evaluation of immune infiltration based on image plus helps predict the prognosis of stage III gastric cancer patients with significantly different outcomes in northeastern China," *Disease Markers*, vol. 2022, Article ID 2893336, 16 pages, 2022.

[12] D. S. Lee, J. K. Park, S. J. Lee, and G. J. Cheon, "Clinical significance of regional lymph node enlargement in patients with EGC within the expanded criteria for ESD," *BMC Gastroenterology*, vol. 20, no. 1, p. 51, 2020.

[13] M. Arnold, J. Y. Park, M. C. Camargo, N. Lunet, D. Forman, and I. Soerjomataram, "Is gastric cancer becoming a rare disease? A global assessment of predicted incidence trends to 2035," *Gut*, vol. 69, no. 5, pp. 823–829, 2020.

[14] K. Kundu, M. Tardaguila, A. L. Mann et al., "Genetic associations at regulatory phenotypes improve fine-mapping of causal variants for 12 immune-mediated diseases," *Nature Genetics*, vol. 54, no. 3, pp. 251–262, 2022.

[15] Y. Nurzat, W. Su, P. Min, K. Li, H. Xu, and Y. Zhang, "Identification of therapeutic targets and prognostic biomarkers among integrin subunits in the skin cutaneous melanoma microenvironment," *Frontiers in Oncology*, vol. 11, article 751875, 2021.

[16] A. Andrzejewska, S. Dabrowska, B. Nowak, P. Walczak, B. Lukomska, and M. Janowski, "Mesenchymal stem cells injected into carotid artery to target focal brain injury home to perivascular space," *Theranostics*, vol. 10, no. 15, pp. 6615–6628, 2020.

[17] R. Dhondrup, X. Zhang, X. Feng et al., "Proteomic analysis reveals molecular differences in the development of gastric cancer," *Evidence-based Complementary and Alternative Medicine*, vol. 2022, Article ID 8266544, 18 pages, 2022.

[18] J. Y. Liu, C. W. Peng, X. J. Yang, C. Q. Huang, and Y. Li, "The prognosis role of AJCC/UICC 8th edition staging system in gastric cancer, a retrospective analysis," *American Journal of Translational Research*, vol. 10, no. 1, pp. 292–303, 2018.

[19] A. Zucchetto, T. Vaisitti, D. Benedetti et al., "The CD49d/CD29 complex is physically and functionally associated with CD38 in B-cell chronic lymphocytic leukemia cells," *Leukemia*, vol. 26, no. 6, pp. 1301–1312, 2012.

[20] H. R. Attia, M. H. Ibrahim, S. H. A. El-Aziz et al., "ITGA4gene methylation status in chronic lymphocytic leukemia," *Future Science OA*, vol. 6, no. 7, article FSO583, 2020.

[21] X. Zhang, S. Wan, Y. Yu et al., "Identifying potential DNA methylation markers in early-stage colorectal cancer," *Genomics*, vol. 112, no. 5, pp. 3365–3373, 2020.

[22] J. Yan, X. Yang, X. Jiao et al., "Integrative transcriptomic and proteomic analysis reveals CD9/ITGA4/PI3K-Akt axis mediates trabecular meshwork cell apoptosis in human glaucoma," *Journal of Cellular and Molecular Medicine*, vol. 24, no. 1, pp. 814–829, 2020.

[23] C. Wei, C. Yang, S. Wang et al., "Crosstalk between cancer cells and tumor associated macrophages is required for mesenchymal circulating tumor cell-mediated colorectal cancer metastasis," *Molecular Cancer*, vol. 18, no. 1, p. 64, 2019.

[24] H. Prenen and M. Mazzone, "Tumor-associated macrophages: a short compendium," *Cellular and Molecular Life Sciences*, vol. 76, no. 8, pp. 1447–1458, 2019.

[25] M. Mohme, S. Riethdorf, and K. Pantel, "Circulating and disseminated tumour cells – mechanisms of immune surveillance and escape," *Nature Reviews. Clinical Oncology*, vol. 14, no. 3, pp. 155–167, 2017.

[26] I. D. Nagtegaal, C. A. Marijnen, E. K. Kranenbarg et al., "Local and distant recurrences in rectal cancer patients are predicted by the nonspecific immune response; specific immune response has only a systemic effect - a histopathological and immunohistochemical study," *BMC Cancer*, vol. 1, no. 1, 2001.

[27] Y. You, Z. Tian, Z. Du et al., "M1-like tumor-associated macrophages cascade a mesenchymal/stem-like phenotype of oral squamous cell carcinoma via the IL6/Stat3/THBS1 feedback loop," *Journal of Experimental & Clinical Cancer Research*, vol. 41, no. 1, 2022.

[28] R. Thomas, V. Menon, R. Mani, and J. Pruszak, "Glycan Epitope and Integrin Expression Dynamics Characterize Neural Crest Epithelial-to-Mesenchymal Transition (EMT) in Human Pluripotent Stem Cell Differentiation," *Stem Cell Reviews and Reports*, 2022.

[29] E. M. Garrido-Martin, T. W. P. Mellows, J. Clarke et al., "M1(hot) tumor-associated macrophages boost tissue-resident memory T cells infiltration and survival in human lung cancer," *Journal for Immunotherapy of Cancer*, vol. 8, no. 2, 2020.

Hindawi

Research Article

Identification of Prognostic Markers and Potential Therapeutic Targets in Gastric Adenocarcinoma by Machine Learning Based on mRNAsi Index

Si Hong Guo,[1] Li Ma,[2] and Jie Chen [2]

[1]*Personal Health Management, Hong Kong Baptist University, Hong Kong 999077, China*
[2]*Department of Gynaecologic Oncology, Harbin Medical University Cancer Hospital, Harbin 150000, China*

Correspondence should be addressed to Jie Chen; cj2365255@hrbmu.edu.cn

Background. Cancer stem cells (CSCs), characterized by self-renewal and therapeutic resistance, play important roles in stomach adenocarcinoma (STAD). However, the molecular mechanism of STAD stem cells is still unclear. In this study, our purpose is to explore the expression of stem cell-related genes in STAD. *Methods.* The stemness index based on mRNA expression (mRNAsi) was used to analyze STAD cases in The Cancer Genome Atlas (TCGA). Firstly, mRNAsi was used and analyzed by differential expression, survival analysis, clinical stage, and gender in STAD. Then, weighted gene coexpression network analysis (WGCNA) was used to discover the fascinating modules and key genes. Enrichment analysis was carried out to annotate the functions and pathways of key genes. The gene expression comprehensive database (GEO) in STAD was used to verify the expression levels of key genes in all cancers. Protein-protein interaction networks is used to determine the relationships between key genes. *Results.* The mRNAsi was obviously upregulated in tumor cases. With the increase of tumor stage and T stage, the mRNAsi score decreased, and the overall survival rate of high score group patients was better. According to the degree of association with mRNAsi, different modules and key genes were screened out. A total of 6,740 differential genes were found, of which 1,147 genes were downregulated and 5,593 genes were upregulated. 19 key genes (BUB1, BUB1B, KIF14, NCAPH, RACGAP, KIF15, CENPF, TPX2, RAD54L, KIF18B, KIF4A, TTK, SGO2, PLK4, ARHGAP11A, XRCC2, C1orf112, NCAPG, and ORC6) were screened due to significant upregulation in STAD. And they had been proven that enriched from the cell cycle Kyoto Encyclopedia of Genes and Genomes (KEGG) pathway, relating to cell proliferation Gene Ontology (GO) terms, as well. Among them, 9 genes have been extensively associated to OS, and 3 genes had been associated to receive chemotherapy resistance. PPI protein network suggests that there is a sturdy correlation between these key genes. *Conclusion.* A total of 19 key genes were found to play an essential position in retaining the traits of STAD stem cells. These genes can be used to evaluate the prognosis of STAD patients or become specific therapeutic targets.

1. Introduction

The incidence rate and mortality of stomach cancer decreased significantly in five years, but it still ranked third among common malignant tumors and the second leading cause of cancer-related death [1]. Ninety percent of all tumors of the stomach are malignancies, and stomach adenocarcinoma (STAD) accounts for 95% of all cases of malignancies [2].

In current years, the characteristic of most cancers stem telephone has been mentioned such as self-renewal and unlimited proliferation [3–5]. CSC theory points out that tumor proliferation, therapeutic resistance, and recurrence are additionally pushed by way of a small range of tumor stem cells hidden in most cancers. It explains these clinical observations, such as tumor recurrence, tumor dormancy, and metastasis after successful surgical resection, chemotherapy, and radiotherapy [6]. CSCs have been found in several human malignancies, such as leukemia [7], breast cancer [8], colorectal cancer [9], and brain cancer [10]. In addition, strong preclinical data and clinical evidence have been added as supports of the existence of gastric CSCs [11]. Therefore,

(a)

(b)

(c)

(d)

(e)

(f)
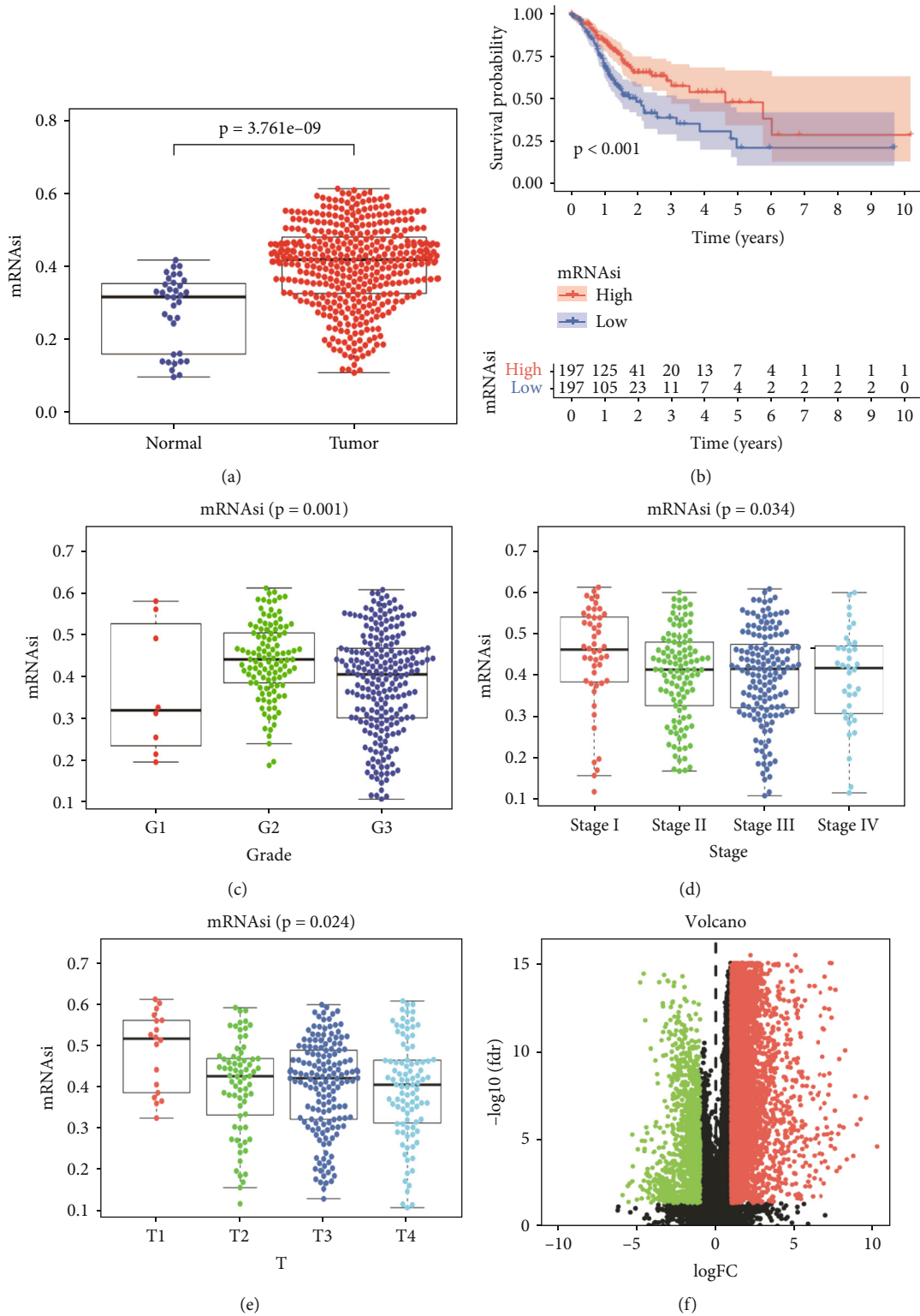
FIGURE 1: The correlation of mRNAsi profiles with STAD. (a) Scatter plot illustrating the difference of mRNAsi index expression between normal tissues and tumors. (b) Kaplan–Meier survival curve of correlation between mRNAsi score and OS of STAD patients. Detect the correlation between mRNAsi score and the Grade (c), Stage (d), and T degree (e) by the Kruskal-Wallis test. (f) Volcano map of DEGs between STAD tissues and normal tissues. Downregulated genes are indicated in green, and upregulated genes are indicated in red. STAD: stomach adenocarcinoma; DEGs: differentially expressed genes.

(a)

(b)

(c)

(d)

FIGURE 2: Continued.

(e)

(f)

(g)
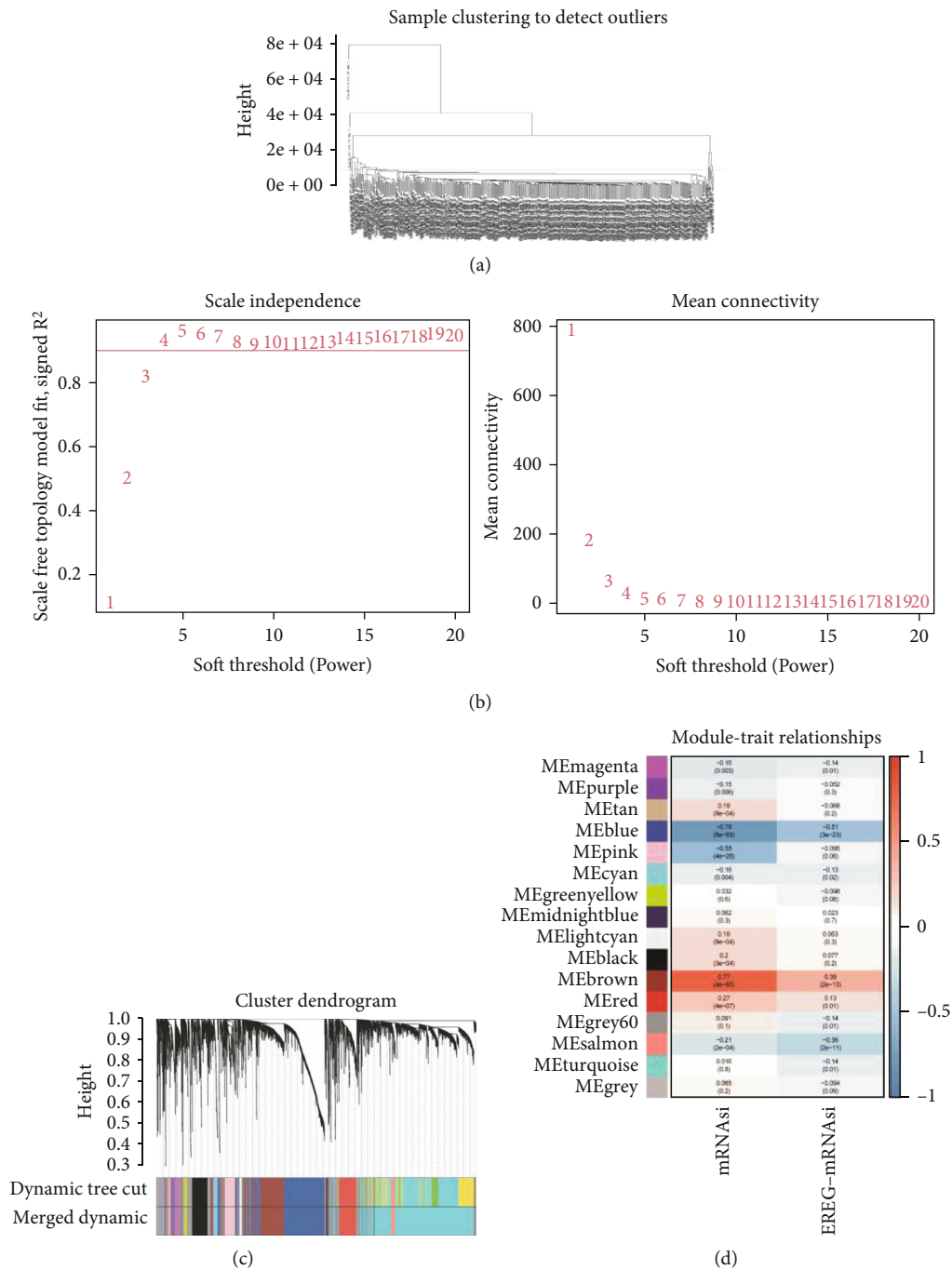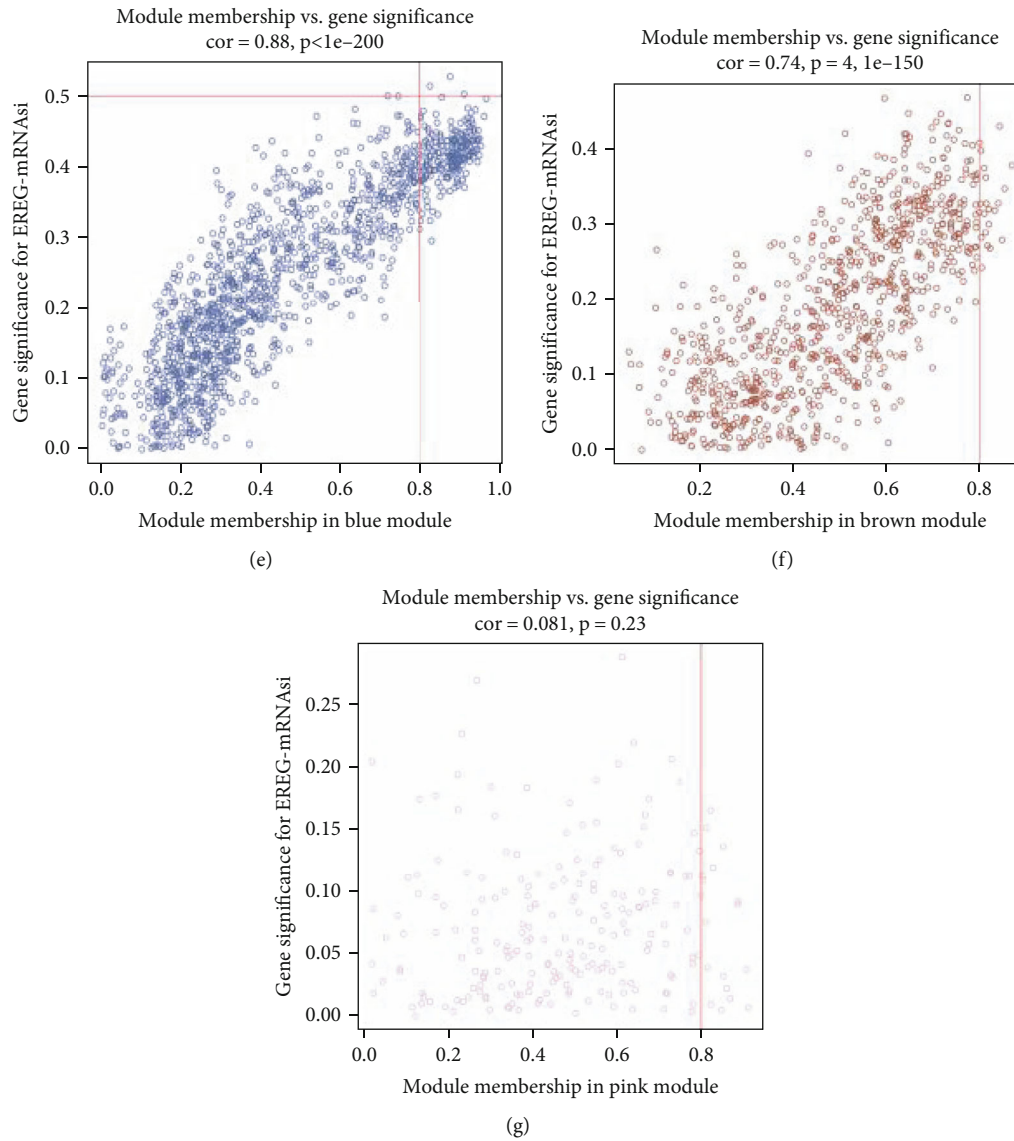
FIGURE 2: Construction of weighted gene coexpression network for STAD stemness related datasets. (a) Identify and remove outlier samples through average linkage hierarchical clustering. Samples exceeding the red line were considered deviations in gene expression. (b) Network topology analysis of different soft threshold powers. The left figure shows the influence of soft threshold power on the scale-free topological fitting index. The right figure shows the influence of soft threshold power on average connectivity. (c) Clustering dendrograms was done via mean linkage hierarchical. (d) Module-trait relationships. Each column represents a clinical phenotype, and each row denotes an ME. The correlation coefficient and P value are contained in each cell. (e–g) Scatterplots of GS for weight vs. MM to pick out the key genes from the blue, brown, and pink modules. STAD: stomach adenocarcinoma; ME: module eigengene; GS: gene significance; MM: module membership.

CSC research is able to provide a new paradigm for managing patients with STAD.

A growing number of studies have shown cancer stemness is associated with being transcriptomic, genomic, epigenomic, and proteomic [12]. Within the last decade, The Cancer Genome Atlas (TCGA) has elucidated the primary tumor landscapes by generating comprehensive multiomics characteristics, along with pathophysiological feature and clinical information annotations [13]. Machine learning has been increasing applied in various areas of society and has become a useful strategy in biotechnology [14].

Tathiane et al. used publicly available molecular profiles from TCGA to obtain two independent stemness indices by using original one-class logistic regression machine-learning algorithm (OCLR) to complete the integration of transcriptome, methylome, and transcription factor [15]. One was mDNAsi which reflects epigenetic features; the other was mRNAsi which reflects gene expression. Malta et al. identified the relationship between the two stem cell indices and new carcinogenesis pathways, somatic cell changes, microRNAs (miRNAs), and transcription regulatory networks. These characteristics are
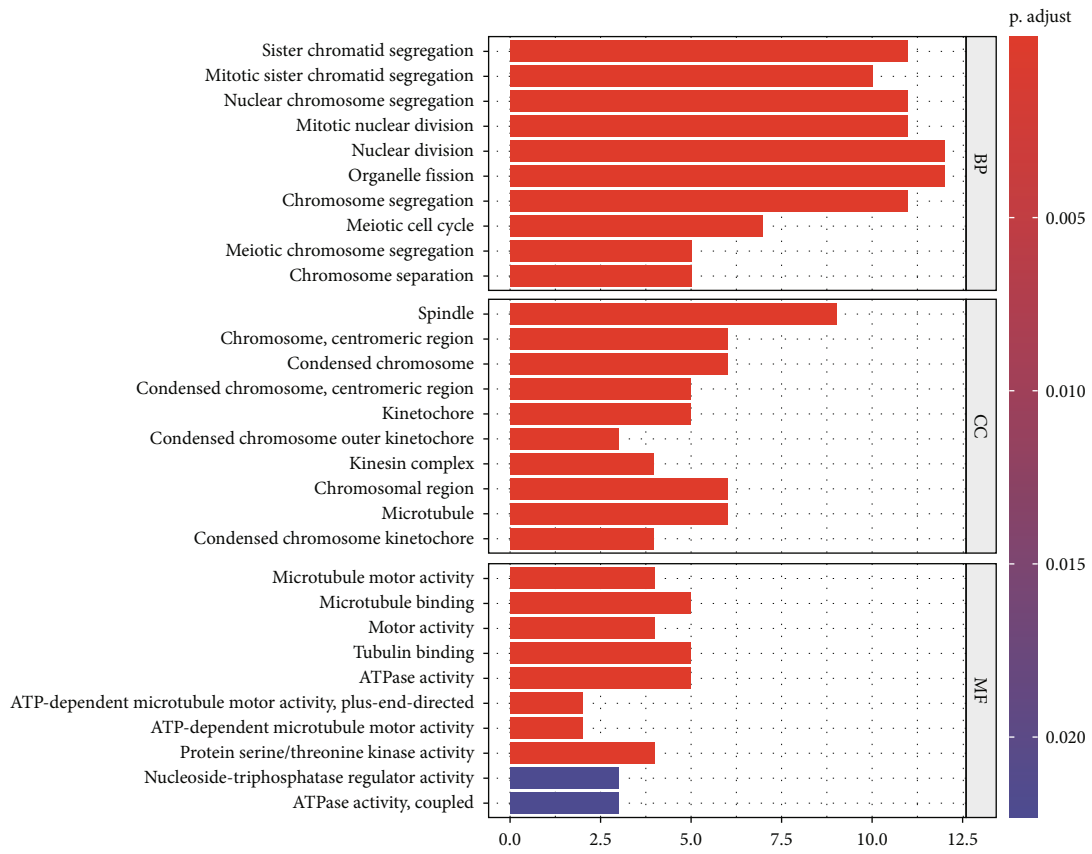
(a)

(b)
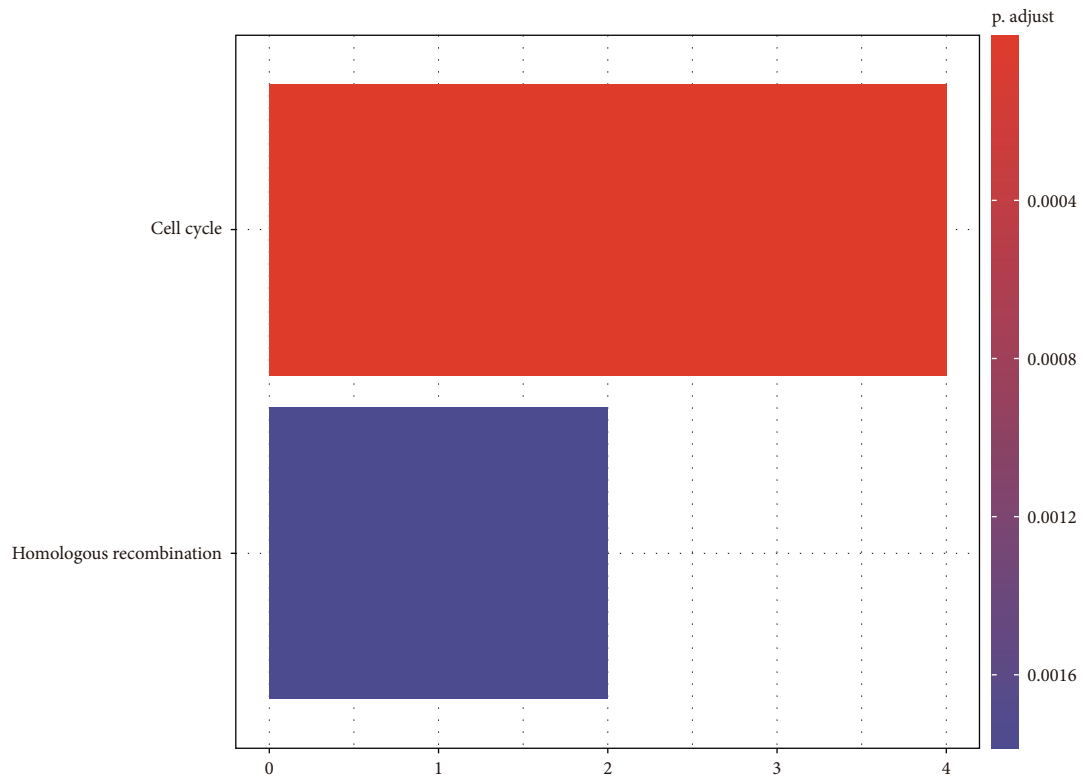
Figure 3: Functional analysis of brown module. (a) GO enrichment analysis. (b) KEGG enrichment analysis. GO: Gene Ontology; KEGG: Kyoto Encyclopedia of Genes and Genomes; BP: biological process; CC: cellular component; MF: molecular function.

related to cancer stem cells in specific molecular subtypes of TCGA tumors, which may be the factors controlling cancer stem cells. Importantly, higher stem cell index value is related to the active biological processes and greater tumor dedifferentiation in tumor stem cells, as reflected in histopathological grade. Metastatic tumor cells show more dedifferentiation in phenotype, which may contribute to their invasiveness. The stemness indices had positive correlation with tumor dedifferentiation and biological active in CSCs [16]. The mRNAsi and mDNAsi scores in TCGA samples had been calculated by applying the stemness indices.

Weighted gene coexpression network analysis (WGCNA), a method commonly used to explore biological networks, paired relationships between genes and phenotypes. WGCNA transforms gene expression data into coexpression module, providing insights into signaling networks, and mine the pathway-related modules [17]. It is widely applied in many physiological and pathological processes, including cancer, genetic therapy, and clinical data analysis, which can be useful for identifying biomarkers of disease or target points for therapy [18, 19].

In this study, our purpose is to identify key genes associated with STAD stemness in TCGA based on mRNAsi scores. The purpose of this study was to provide an interesting bioinformatics method for identifying stem cell-related genes and revealing the role of some CSC-related genes in STAD.

2. Materials and Methods

2.1. Software and R Packages. We used R Studio version 1.2.5042 (URL: https://rstudio.com/) with R version 3.6.2 (URL: https://www.r-project.org/) in this study. The programming software Perl version 64-bit (URL: https://www.perl.org/) was used for data processing. All R packages were downloaded from Bioconductor (URL: https://www.bioconductor.org/).

2.2. Database and mRNAsi Index. The RNA-sequencing (RNA-seq) of STAD and all pathological and clinical information were downloaded from TCGA database (URL: https://portal.gdc.cancer.gov/). These data were updated on 5 October 2019. The results of RNA-seq were including 375 cancer samples and 32 normal samples, structured for a matrix file. We used Ensemble data to exchange the gene names expressed by Ensembl IDs which are specifically converted into a gene symbol matrix. Moreover, to explore the mode of action of CSC-related genes in chemotherapy resistance, we download the microarray (GSE14210) results from the Gene Expression from the Gene Expression Omnibus (GEO) (URL: https://www.ncbi.nlm.nih.gov/geo/). We referred to the mRNAsi index data for all types of tissues in the supporting documents to Malta et al.'s article and specifically screened the mRNAsi index of patients with stomach adenocarcinoma for incorporation into TCGA data for stomach adenocarcinoma, with the unmatched cases deleted.

2.3. 2.3 Differential Expressed Gene (DEG) Analysis. We used the R package "limma" for differential expression analysis [20]. We used the cut-off values, which were fold change > 1 and adj.$P < 0.05$, to screen for DEGs between normal health and stomach adenocarcinoma samples. The volcano plot and the box-plots showing differences in key genes presented in this study were drawn by the R package "pheatmap" and "ggpubr," respectively.

2.4. WGCNA. WGCNA was performed using the WGCNA R package [17], which were "matrixStats," "Hmisc," "foreach," "doParallel," "fastcluster," dynamicTreeCut," "survival," and "WGCNA." Before the building of coexpression network, the rectangular Euclidean relative distance of every take a look at pattern was once calculated by means of practical adjacency method, and the integration connectivity of the total pattern community calculated via distance was once standardized via practical scaling method. Due to some exceptional genes with no tremendous trade in expression between samples which are surprisingly correlated in WGCNA as a whole, it appears that the genes with the most biased expression have been used in the subsequent WGCNA analysis. The gene with the highest DEG variance of 25% was selected. Clear ordinary value pattern information with connectivity is much less than -2.5. Function pickSoftThreshold was used to calculate scale-free topology becoming indices R^2 corresponding to one-of-a-kind smooth thresholding powers β. The β value was used as lengthy as R^2 reaching 0.8. After that, the gene expression matrix was converted into an adjacency matrix and a Topological Overlap Matrix (TOM), and then the corresponding dissimilarity of TOM (dissTOM) was calculated. For module detection, hierarchical clustering was used to produce a hierarchical clustering tree (dendrogram) of genes by using characteristic "hclust" based totally on dissTOM. The Dynamic Tree Cut approach was carried out for department reduction to generate modules. During this, a quite massive minimal module measurement of minClusterSize = 30 to department splitting had been chosen to avoid producing too many small or massive modules. To consider the magnitude of every module, gene significance (GS) was once calculated to measure the correlation coefficient between genes and pattern traits. The module eigengene (ME) is described as the first foremost thing of a given element and can be regarded as a consultant of the gene expression profile of the module integration. It was calculated by using purposeful module genes. If their MES correlation coefficient is higher than 0.75, the modules will be merged, with capacity that they have considerable comparable gene expression levels. Here, we can pick out mRNAsi and epigenetically regulated mRNAsi as scientific phenotypes.

After selecting the components of interest, let us calculate the GS and module membership of each key gene (MM, the significance between the module's own gene and gene expression profile), and set their threshold values. The thresholds for screening key genes in the module were defined as cor.gene MM > 0.8 and cor.gene GS > 0.5.

(a)

(b)

(c)

(d)

(e)

Figure 4: Continued.

(f)

(g)

(h)

(i)

(j)

(k)
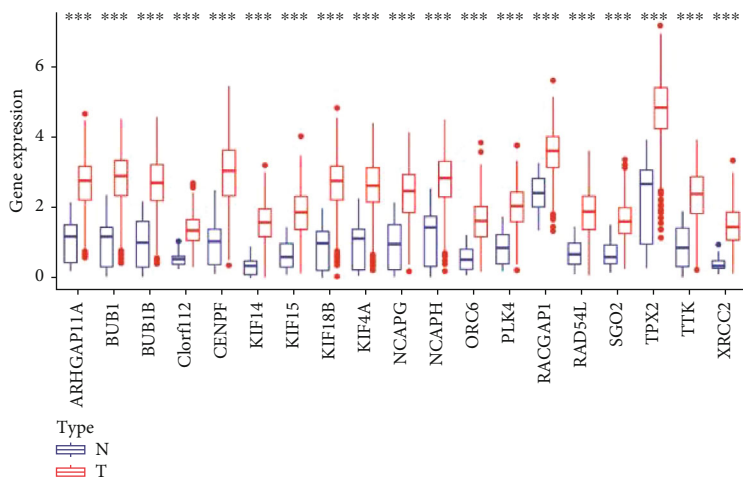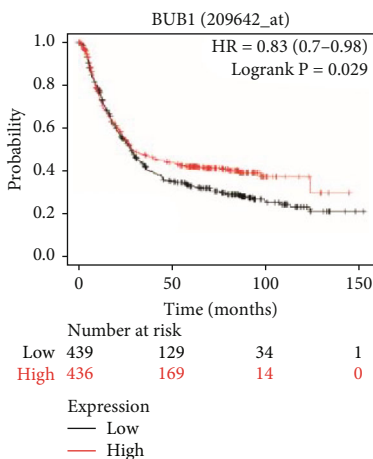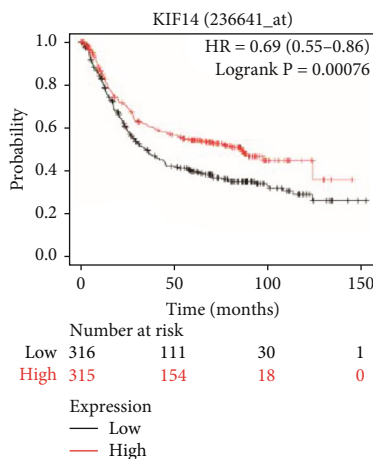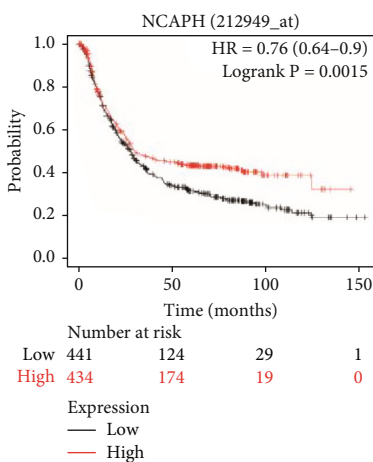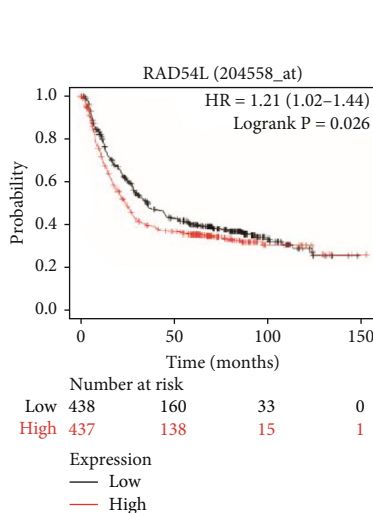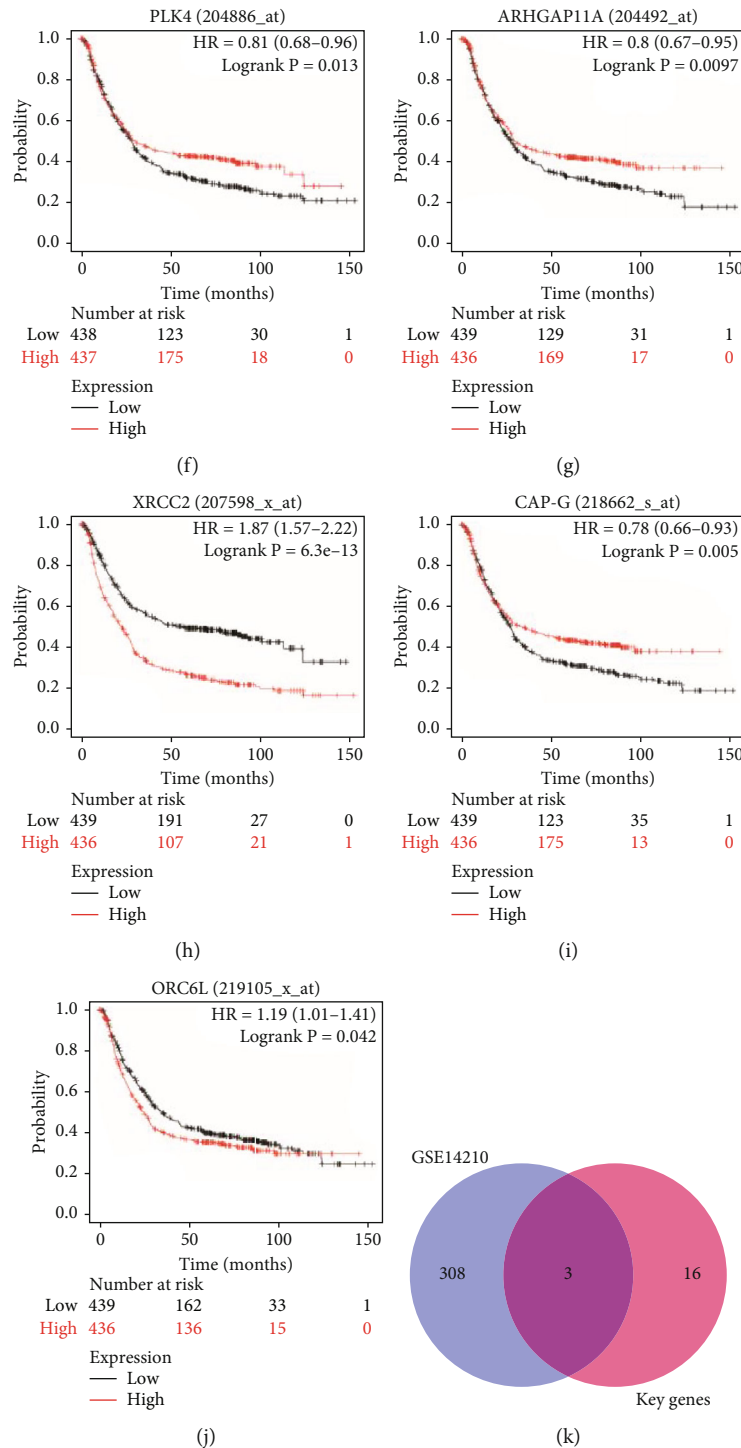
Figure 4: Verification of the influence of key genes on diseases. (a) The mRNA expression level of key genes between tumor and normal tissues in TCGA STAD dataset. The Kaplan–Meier plotter database was used to assess the correlation between the expression of BUB1 (b), KIF14 (c), NCAPH (d), RAD54L (e), PLK4 (f), ARHGAP11A (g), XRCC2 (h), NCAPG (i, also called CAP-G), ORC6 (j, also called ORC6L), and the OS of STAD patients. Kaplan–Meier survival plots (K–M plots) were generated using the on-line tool, Kaplan–Meier plotter. (k) Venn diagram of the relationship between 19 key genes and acquired chemoresistance by GSE14210.

2.5. Overall Survival Curve. Finally, to determine the prognostic significance and value of mRNAsi scores, we can draw the Kaplan–Meier diagram of mRNAsi index to explore the

overall survival deviation between patients with low and high mRNAsi index. In this part, R package "survival" and "surviminer" were used, and a log-rank test is used to test

the relationship between them. In key gene validation analysis, Kaplan–Meier survival curves of key genes were drawn with the online tool Kaplan–Meier plotter [21] (URL:http://www.kmplot.com/analysis/index.php?p= service).

2.6. Functional Annotation Gene Ontology (GO) and Kyoto Encyclopedia of Genes and Genomes (KEGG) Analyses. The GO functional annotations and KEGG pathway enrichment analysis shown in this study were obtained from the data analysis conducted by the R package "cluster Profiler" to investigate the biological functions of key genes. The threshold values were as follows: $P < 0.01$ and FDR < 0.05.

2.7. Gene Coexpression Analysis and Construction of Protein-Protein Interaction (PPI) Network. In order to further study the stability of these special relationships at the transcriptional level, we calculated the coexpression relationships among key genes within the module depending on the gene expression level. The R "corrlot" package is mainly used to calculate the Pearson correlation degree between genes. The STAD data set was selected from TCGA for analysis and research, and the routine data were analyzed by the Pearson correlation test. Results with a correlation coefficient > 0.3 and P value < 0.01 were considered statistically significant.

Accurately retrieve PPI network from STRING version 11.0 (URL: https://string-db.org/) [22]. And display the bar graph of the nodes in the network with top-level network connectivity. The minimum required interaction score was set to a medium confidence of 0.4, and now, the hidden branch nodes in the network are disconnected. The number of adjacent nodes of each gene in the PPI network was calculated, and then, the genes were sorted by the bar graph combined with the number of adjacent nodes.

3. Results

3.1. Clinical Characteristics of mRNAsi and DEGs in STAD. The mRNAsi is an index of CSCs that can quantitatively describe the similarity between tumor cells and stem cells. We observe large distinction in mRNAsi between tumor and ordinary tissues (Figure 1(a)). In the survival analysis, we divided gastric cancer patient into higher mRNAsi score group and lower mRNAsi group by using mRNAsi median value. Obviously, patients with higher mRNAsi scores have greater overall survival in contrast with sufferers with lower mRNAsi scores (Figure 1(b)), the five-year survival rate of higher scores group is 47.9% with CI (0.344, 0.668), and the lower scores group is 21.2% with CI (0.107, 0.421). Surprisingly, the mRNAsi scores tend to decline with the grade increasing with the exception of G1 (only 8 samples). Also, the mRNAsi score shows an overall decreasing trend in stage and T (Figures 1(c), 1(d), and 1(e)). The Kruskal Wallis test was once used to determine the value of variations between groups.

We download mRNA-seq data and did difference analysis to compare STAD and normal since the mRNAsi difference between tumor and normal. We find 6740 DEGs in which 1147 were downregulated and 5593 were upregulated (Figure 1(f)).

3.2. WGCNA: Identifying the Most Significant Modules and Genes. With WGCNA, we built a gene coexpression network to become aware of biologically significant gene modules. It can help us to understand the genes associated with STAD stemness. We put 6740 DEGs with the highest variance of 25% into the same module through cluster analysis. Before that, the outlier samples should be removed (Figure 2(a)). According to the lowest value of scale-free network, the β value is determined. What the pickSoftThreshold function does is to find the appropriate power. The selection of the power value is determined by β value. Calculate the correlation intensity (weighted correlation value) of expression levels among all genes to obtain the adjacency matrix. As a result, we choose $\beta = 4$ (scale-free $R^2 = 0.9$) as the soft threshold (Figure 2(b)). We find 16 modules for subsequent evaluation (Figure 2(c)).

Taking MS as the total gene expression level of the corresponding module, the correlation between MS and clinical phenotype was calculated. This is useful for us to discover the relationship between these modules and the dryness index of the sample. By calculating the Pearson correlation coefficient, a threshold value can be obtained. If the correlation coefficient is greater than 0.8 or so, it can be used as the basis of strong correlation between the two genes. The consequences confirmed that the blue and brown modules were extensively correlated with mRNAsi, and the correlation was once close to 0.8. However, the correlation coefficient of the brown module is 0.77, which is higher. In addition, the pink module was fantastically negatively correlated with mRNAsi (Figure 2(d)). Therefore, the brown module was chosen through us as the most fascinating module for subsequent analysis.

The threshold for screening key genes in the mRNAsi group was described as cor.MM > 0.8 and cor.GS > 0.5. We pick 19 key genes (BUB1, BUB1B, KIF14, NCAPH, RACGAP1, KIF15, CENPF, TPX2, RAD54L, KIF18B, KIF4A, TTK, SGO2, PLK4, ARHGAP11A, XRCC2, Clorf112, NCAPG, and ORC6), as shown in Figures 2(e)–2(g). And we exhibit the distinct expressions of key genes between most cancers and ordinary samples in TCGA; all these genes in brown module are upregulated in tumor cases (Figure 2(f)).

3.3. Enrichment Analysis of Brown Module. We use GO and KEGG analysis to elucidate the function similarities of module brown genes. The results show that nuclear division, spindle, and microtubule binding are the most great enrichments in cellular component (CC), biological process (BP), and molecular function (MF) groups (Figure 3(a)). KEGG pathway enrichment analysis suggested cell cycle and homologous recombination pathways are significant pathways (Figure 3(b)). All of them are related to cancer stem cells.

3.4. Data Validation. Firstly, the STAD dataset of TCGA showed significant differences in the expression of all key

(a)

(b)

Figure 5: Continued.

(c)
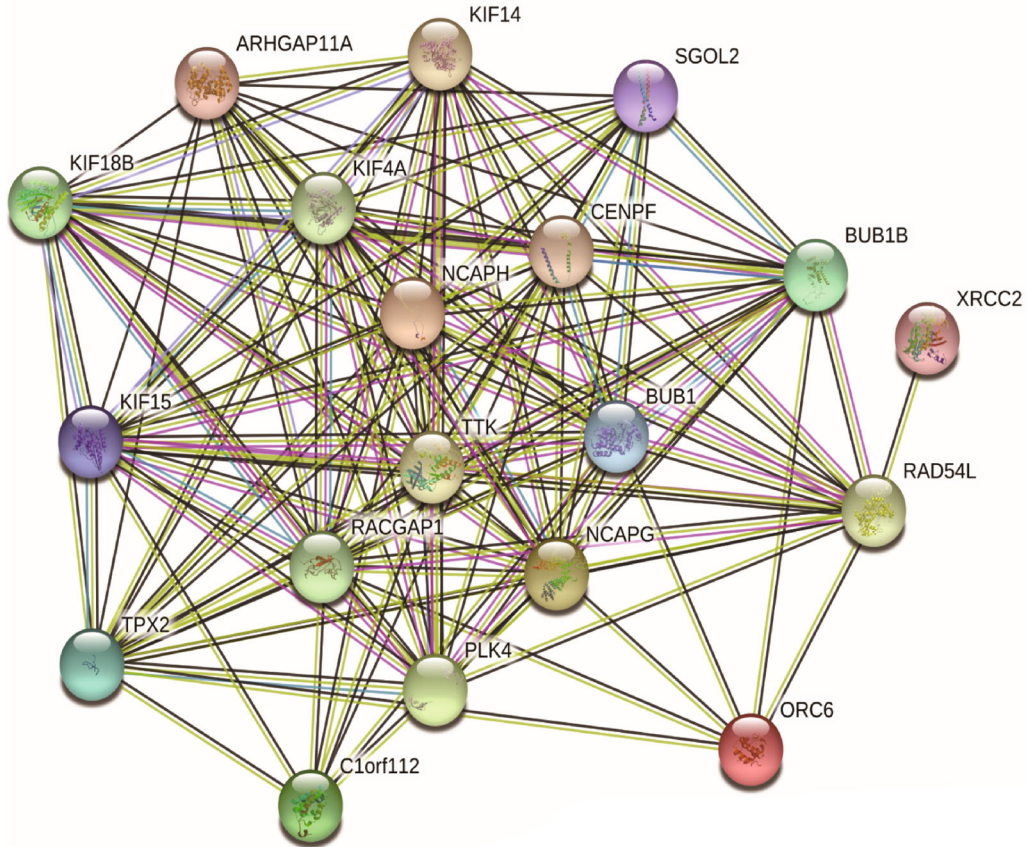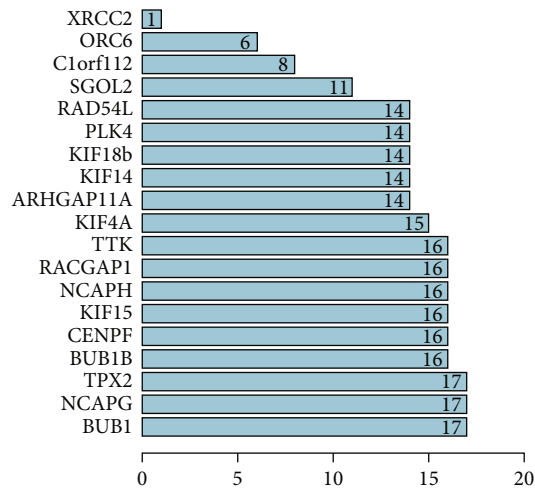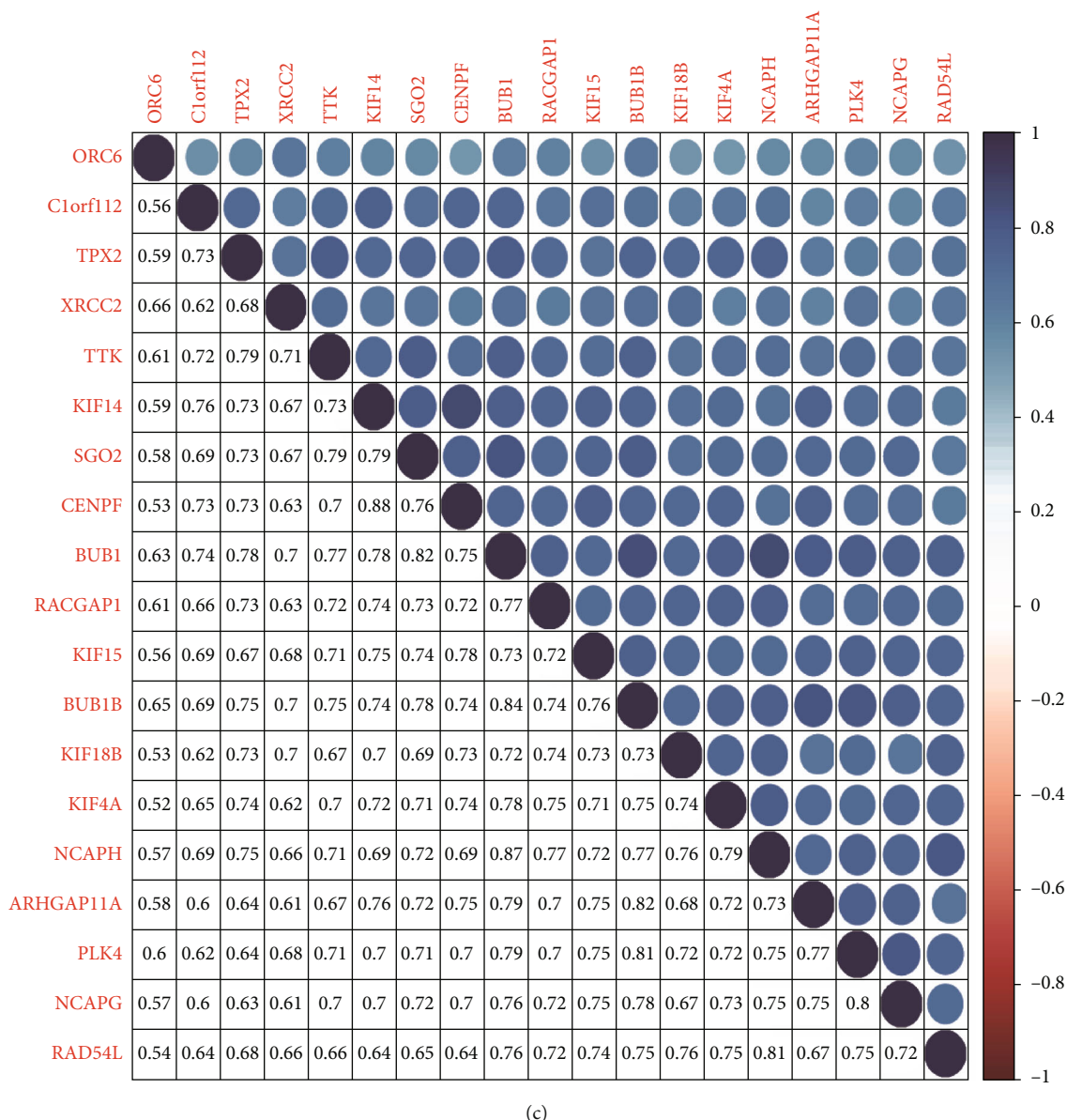
Figure 5: PPI interactive network. (a) String diagram composed of 19 key genes as nodes. (b) The bar-plot lists the connections of key genes in the brown module by the counts of connections. (c) Correlation analysis between key genes. The higher phase of the graph indicates the degree of correlation. The darker the color, the greater the correlation. The lower part shows the corresponding correlation value. PPI: protein-protein interaction.

genes between normal and tumor cases (Figure 4(a)). In all patients with STAD, the Kaplan–Meier curve and log rank test analysis showed that 7 genes in the brown module were significantly associated with OS ($P < 0.05$, FDR < 0.05) (Figures 4(b)–4(j)).

It is well known that CSCs have chemoresistance, and resistance is related to cancer-associated fibroblasts in the extracellular matrix [23]. The mapping of GSE14210 is based on Venn diagram. 19 key gene maps selected from the brown module were scored by GS and MM scores. Finally, SGO2, TTK, and CENPF were associated with the acquired chemoresistance to cisplatin and fluorouracil combination chemotherapy in gastric cancer (Figure 4(k)).

3.5. Protein-Protein Interactions (PPI) among Genes of Brown Module.

The application of the on-line device STRING (URL: http://string-db.org/) to protein-protein interaction networks for each module will assist us to explore the interplay between key genes extra deeply. There were 19 nodes and 129 edges in the shaped PPI network, and the PPI enrichment (P value < 0.01) (Figure 5(a)). In addition, the significant nodes shown in the bar-plot can identify the genes most closely related to other members of the module (Figure 5(b)).

The correlation between the key genes of this module was strong (Figure 5(c)), and the correlation was statistically significant ($P < 0.01$). The correlation between CENPF and

ORC6 (0.53), KIF18B, and ORC6 (0.53) was the lowest, whereas the correlation between CENPF and KIF14 (0.88) was the highest.

4. Discussion

The morbidity and mortality of gastric most cancers stay excessive all over the worldwide. In current years, CSCs have been mentioned to make vital contributions to tumor progression, recurrence, and therapeutic resistance [24, 25]. Therefore, therapy concentrating on STAD stem cells is essential. In addition, choosing out the emergence of these druggable genetic ameliorations in pancancer cases, and whether or not there are modifications in the expression of the equal mRNAsi-related genes, is additionally a query priceless of dialogue in the future work.

In this study, we tried to discover key genes associated to STAD stem cells in TCGA database. We used WGCNA based totally on mRNAsi scores, as calculated by Salomonis et al. [26]. The tumor case had a greater mRNAsi rating than the regular case. The mRNAsi scores reduced with the sickness grade, stage, and T stage, though the mRNAsi rating of G1 was once small which may also be associated to inadequate pattern size. The excessive mRNAsi team confirmed a decrease survival chance than the low team in the first 5 years, which used to be constant with the negative consequence related with stemness features.

We developed coexpression modules through WGCNA and pick out brown module as the best correlations with mRNAsi. Key genes have been screened from the blue module primarily based on the GS and MM scores. The expression degrees of key genes are appreciably upregulated in tumor samples. There have been robust coexpression relationships at the transcriptional degree in brown module. There was additionally a robust PPI community among proteins of this module. The key genes intently associated to pluripotent stem cells have been confirmed to be overexpressed in most tumors. Moreover, all organ tissues are developed from pluripotent stem cells, suggesting that key genes might also play a position in keeping stem cellphone residences in a range of cancers. The consequences led us to reassess the relationship between CSC traits and STAD progression.

Undifferentiated major tumors are more probably to reason most cancer cells to unfold to far-off organs, mainly to sickness development and negative prognosis. Moreover, CSCs are typically resistant to handy remedies [27]. The acquisition of progenitor cell-like and stem cell-like traits and loss of the differentiated phenotype are manifestations of most cancer development [28], regular with the expand in STAD stemness as the tumor progression. In our study, we observed that sufferers with greater corrected mRNAsi rankings had decreased ordinary survival rates, which used to be regular with the negative prognosis related with CSC characteristics. Disease stage 1 and T1 stage STAD had pretty greater CSC characteristics, indicating the stem telephone residences start to upward thrust from initiation of the cancer.

Functional annotations of the brown module had been chiefly associated to the stem cell self-renewal and proliferation characteristics. The pathway enrichment advised that the four key genes in the cycle pathway time period have been most possibly a useful gene set that impacts tumor stemness via regulating the cell cycle.

The gene units that keep the traits of stem cells in a range of cancers may additionally have similarities. Since the formation of a range of organ tissues takes place from pluripotent stem cells, their CSCs are dedifferentiated with stem mobile phone characteristics. This reverse improvement has made a range of CSCs possessing some traits of pluripotent stem cells. Moreover, their stage of overexpression was once associated to the stage of stemness, and their persisted expand might also promote modifications in tumor development and posttherapy progression. More than half of the key genes have been mentioned in STAD, and some have been proven to be related with the traits of CSCs. BUB1 is related with the most cancer stem cell attainable in breast cancer [29]. An issue highlights a study that links the presentation of kinetochores within mitosis to an essential requirement for BUB1 threonine kinase B (BUB 1B), broadening our understanding of the cell-cycle machinery in CSCs [30]. Kinesin family member 15 (KIF15) promotes the CSC phenotype and malignancy by means of PHGDH-mediated ROS imbalance in hepatocellular carcinoma [31]. TTK gene was overexpressed in the CSC-like cell populace remoted from human esophageal carcinoma phone strains as properly as in the human more than one myeloma stem cells sorted through aldehyde dehydrogenase 1 (ALDH1) [32, 33].

Survival curves have been generated to validate the prognostic fee of the key genes in brown module in STAD. In the K-M plots, 7 genes had been substantially related with prognoses ($P < 0.01, \text{FDR} < 0.05$). High expression of BUB1, TPX2, and X-ray repair cross complementing 2 (XRCC2) had been noticeably related with negative prognoses. The expression of NCAPH, NCAPG, RACGAP1, and SGO2 has been positively correlated with affected person prognosis. As known, CSCs can withstand clinical remedy and make contributions to tumor relapse. The key genes had been validated in GSE14210, and SGO2, TTK, and CENPF have been related with the obtained chemoresistance to cisplatin and fluorouracil mixture chemotherapy in gastric cancer. Several studies had proven that CSCs have one or greater abnormalities in signaling pathways that modify self-renewal. The Wnt/β-catenin, Notch, and Hedgehog pathways have been mentioned fully [34]. Wnt/β-catenin KIF14, TPX2, KIF18B, and PLK4 in the Wnt/β-catenin pathway [35–38], TTK and XRCC2 in the Hedgehog pathway [37, 38], and RACGAP1 and TTK in the Notch pathway [39, 40] may additionally be necessary for the tumorigenicity of CSCs. These genes are vital therapeutic aimed at inhibiting the self-renewal, proliferation, and tumor development of CSCs.

5. Conclusions

In summary, 19 key genes have been determined to play necessary roles in STAD stem phone maintenance. The validations confirmed that these genes ought to be beneficial for outlining the prognosis of STAD patients. These genes may

also be therapeutic pursuits for inhibiting STAD stemness characteristics. However, our conclusions are primarily based on the retrospective information, and similarly organic and scientific investigation of these genes should lead to novel insights into the manageable associations of CSCs with a STAD prognosis.

Data Availability

The datasets generated and/or analyzed during this research period can be obtained from the corresponding author.

Conflicts of Interest

The authors declare that the study was conducted in the absence of any commercial or financial relationships that may be interpreted as potential conflicts of interest.

Authors' Contributions

JC and SG designed the study and drafted the manuscript. SG and LM jointly collect, analyze data, and revise the manuscript. All authors have read and approved the final manuscript. SiHong Guo and Li Ma contributed equally to this work.

Acknowledgments

References

[1] R. Siegel, J. Ma, Z. Zou, and A. Jemal, "Cancer statistics, 2014," *CA: a Cancer Journal for Clinicians*, vol. 64, no. 1, pp. 9–29, 2014.

[2] E. Yakirevich and M. B. Resnick, "Pathology of gastric cancer and its precursor lesions," *Gastroenterology Clinics of North America*, vol. 42, no. 2, pp. 261–284, 2013.

[3] Y. Horikoshi, Y. Yan, M. Terashvili et al., "Fatty acid-treated induced pluripotent stem cell-derived human cardiomyocytes exhibit adult cardiomyocyte-like energy metabolism phenotypes," *Cell*, vol. 8, no. 9, article 1095, 2019.

[4] M. Paolillo, R. Colombo, M. Serra et al., "Stem-like cancer cells in a dynamic 3D culture system: a model to study metastatic cell adhesion and anti-cancer drugs," *Cell*, vol. 8, no. 11, article 1434, 2019.

[5] L. MacDonagh, S. G. Gray, E. Breen et al., "Lung cancer stem cells: the root of resistance," *Cancer Letters*, vol. 372, no. 2, pp. 147–156, 2016.

[6] E. Batlle and H. Clevers, "Cancer stem cells revisited," *Nature Medicine*, vol. 23, no. 10, pp. 1124–1134, 2017.

[7] F. M. Uckun, H. Sather, G. Reaman et al., "Leukemic cell growth in SCID mice as a predictor of relapse in high-risk B-lineage acute lymphoblastic leukemia," *Blood*, vol. 85, no. 4, pp. 873–878, 1995.

[8] M. Al-Hajj, M. S. Wicha, A. Benito-Hernandez, S. J. Morrison, and M. F. Clarke, "Prospective identification of tumorigenic breast cancer cells," *Proceedings of the National Academy of Sciences of the United States of America*, vol. 100, no. 7, pp. 3983–3988, 2003.

[9] C. A. O'Brien, A. Pollett, S. Gallinger, and J. E. Dick, "A human colon cancer cell capable of initiating tumour growth in immunodeficient mice," *Nature*, vol. 445, no. 7123, pp. 106–110, 2007.

[10] S. K. Singh, C. Hawkins, I. D. Clarke et al., "Identification of human brain tumour initiating cells," *Nature*, vol. 432, no. 7015, pp. 396–401, 2004.

[11] D. Brungs, M. Aghmesheh, K. L. Vine, T. M. Becker, M. G. Carolan, and M. Ranson, "Gastric cancer stem cells: evidence, potential markers, and clinical implications," *Journal of Gastroenterology*, vol. 51, no. 4, pp. 313–326, 2016.

[12] I. Ben-Porath, M. W. Thomson, V. J. Carey et al., "An embryonic stem cell-like gene expression signature in poorly differentiated aggressive human tumors," *Nature Genetics*, vol. 40, no. 5, pp. 499–507, 2008.

[13] K. Tomczak, P. Czerwińska, and M. Wiznerowicz, "The Cancer Genome Atlas (TCGA): an immeasurable source of knowledge," *Współczesna Onkologia*, vol. 19, no. 1A, pp. A68–A77, 2015.

[14] Y. Sun, M. Peng, Y. Zhou, Y. Huang, and S. Mao, "Application of machine learning in wireless networks: key techniques and open issues," *IEEE Communications Surveys Tutorials*, vol. 21, no. 4, pp. 3072–3108, 2019.

[15] A. Sokolov, E. O. Paull, and J. M. Stuart, "One-class detection of cell STATES in tumor subtypes," *Pacific Symposium on Biocomputing*, vol. 21, pp. 405–416, 2016.

[16] T. M. Malta, A. Sokolov, A. J. Gentles et al., "Machine learning identifies stemness features associated with oncogenic dedifferentiation," *Cell*, vol. 173, no. 2, pp. 338–354.e15, 2018.

[17] P. Langfelder and S. Horvath, "WGCNA: an R package for weighted correlation network analysis," *BMC Bioinformatics*, vol. 9, no. 1, p. 559, 2008.

[18] D. Perumal, V. V. Leshchenko, P. Y. Kuo et al., "Weighted gene co-expression network analysis (WGCNA) identifies highly proliferative myeloma subgroup responsive to CDK4/ARK5 inhibition," *Blood*, vol. 124, no. 21, pp. 3445–3445, 2014.

[19] S. Pan, Y. Zhan, X. Chen, B. Wu, and B. Liu, "Identification of biomarkers for controlling cancer stem cell characteristics in bladder cancer by network analysis of transcriptome data stemness indices," *Frontiers in Oncology*, vol. 9, p. 613, 2019.

[20] M. E. Ritchie, B. Phipson, D. Wu et al., "limma powers differential expression analyses for RNA-sequencing and microarray studies," *Nucleic Acids Research*, vol. 43, no. 7, article e47, 2015.

[21] A. M. Szász, A. Lánczky, Á. Nagy et al., "Cross-validation of survival associated biomarkers in gastric cancer using transcriptomic data of 1,065 patients," *Oncotarget*, vol. 7, no. 31, pp. 49322–49333, 2016.

[22] D. Szklarczyk, A. L. Gable, D. Lyon et al., "STRING v11: protein-protein association networks with increased coverage, supporting functional discovery in genome-wide experimental datasets," *Nucleic Acids Research*, vol. 47, no. D1, pp. D607–D613, 2019.

[23] J. Huelsken and D. Hanahan, "A subset of cancer-associated fibroblasts determines therapy resistance," *Cell*, vol. 172, no. 4, pp. 643-644, 2018.

[24] Y. C. Chae and J. H. Kim, "Cancer stem cell metabolism: target for cancer therapy," *BMB Reports*, vol. 51, no. 7, pp. 319–326, 2018.

[25] F. Ricci, L. Brunelli, R. Affatato et al., "Overcoming platinum-acquired resistance in ovarian cancer patient-derived *xeno-grafts*," *Medical Oncology*, vol. 11, article 1758835919839543, 2019Published 2019 Jun 24.

[26] N. Salomonis, P. J. Dexheimer, L. Omberg et al., "Integrated genomic analysis of diverse induced pluripotent stem cells from the progenitor cell biology consortium," *Stem Cell Reports*, vol. 7, no. 1, pp. 110–125, 2016.

[27] T. Shibue and R. A. Weinberg, "EMT, CSCs, and drug resistance: the mechanistic link and clinical implications," *Nature Reviews. Clinical Oncology*, vol. 14, no. 10, pp. 611–629, 2017.

[28] D. Friedmann-Morvinski and I. M. Verma, "Dedifferentiation and reprogramming: origins of cancer stem cells," *EMBO Reports*, vol. 15, no. 3, pp. 244–253, 2014.

[29] J. Y. Han, Y. K. Han, G. Y. Park, S. D. Kim, and C. G. Lee, "Bub1 is required for maintaining cancer stem cells in breast cancer cell lines," *Scientific Reports*, vol. 5, article 15993, 2015Published 2015 Nov 2.

[30] M. Venere, T. E. Miller, and J. N. Rich, "Mitotic control of cancer stem cells," *Cancer Discovery*, vol. 3, no. 2, pp. 141–144, 2013.

[31] Q. Li, J. Qiu, H. Yang et al., "Kinesin family member 15 promotes cancer stem cell phenotype and malignancy via reactive oxygen species imbalance in hepatocellular carcinoma," *Cancer Letters*, vol. 482, pp. 112–125, 2020.

[32] D. Huang, Q. Gao, L. Guo et al., "Isolation and identification of cancer stem-like cells in esophageal carcinoma cell lines," *Stem Cells and Development*, vol. 18, no. 3, pp. 465–474, 2009.

[33] W. Zhou, Y. Yang, Z. Gu et al., "ALDH1 activity identifies tumor-initiating cells and links to chromosomal instability signatures in multiple myeloma," *Leukemia*, vol. 28, no. 5, pp. 1155–1158, 2014.

[34] N. Takebe, L. Miele, P. J. Harris et al., "Targeting Notch, Hedgehog, and Wnt pathways in cancer stem cells: clinical update," *Nature Reviews. Clinical Oncology*, vol. 12, no. 8, pp. 445–464, 2015.

[35] T. Yang, X. N. Li, L. Li et al., "Sox17 inhibits hepatocellular carcinoma progression by downregulation of KIF14 expression," *Tumour Biology*, vol. 35, no. 11, pp. 11199–11207, 2014.

[36] L. Ding, S. Zhang, S. Chen, L. Zheng, and L. Xiao, "Effect and mechanism of lentivirus-mediated silencing of TPX2 gene on proliferation and apoptosis of human hepatoma cells," *Journal of Cellular Biochemistry*, vol. 120, 2018.

[37] Y. Wu, A. Wang, B. Zhu et al., "KIF18B promotes tumor progression through activating the Wnt/β-catenin pathway in cervical cancer," *Oncotargets and Therapy*, vol. 11, pp. 1707–1720, 2018, Published 2018 Mar 28.

[38] Z. Liao, H. Zhang, P. Fan et al., "High PLK4 expression promotes tumor progression and induces epithelial-mesenchymal transition by regulating the Wnt/β-catenin signaling pathway in colorectal cancer," *International Journal of Oncology*, vol. 54, no. 2, pp. 479–490, 2019.

[39] B. D. Wilson, L. J. Ricks-Santi, T. E. Mason et al., "Admixture mapping links RACGAP1 regulation to prostate cancer in African Americans," *Cancer Genomics & Proteomics*, vol. 15, no. 3, pp. 185–191, 2018.

[40] J. Sun, L. Smith, A. Armento, and W. M. Deng, "Regulation of the endocycle/gene amplification switch by Notch and ecdysone signaling," *The Journal of Cell Biology*, vol. 182, no. 5, pp. 885–896, 2008.

Research Article

A Retrospective Study of Chemotherapy and 3D-Image-Guided Afterloading Intracavitary Radiotherapy in Locally Advanced Cervical Cancer

Xiaojun Li [ID],[1] Cunlian An [ID],[2] Chunlan Feng,[2] Jieren Sun,[1] Huixiang Lu,[1] Xiaodong Yang,[1] Kaiping Wang,[1] and Ruimei Wang[2]

[1]*Heavy Ion Radiotherapy Department, Wuwei Cancer Hospital and Institute, Wuwei Academy of Medical Sciences, Gansu, China 733000*
[2]*Department of Gynecology and Oncology, Wuwei Cancer Hospital, Gansu, China 733000*

Correspondence should be addressed to Cunlian An; clianan@hbut.edu.cn

Aim. To investigate the value of neoadjuvant chemotherapy combined with 3D-image-guided afterloading intracavitary radiotherapy in locally advanced cervical cancer (LACC). *Methods*. Patients with cervical cancer admitted to our hospital from January 1, 2020 to January 1, 2021 were retrieved and analyzed. Cases treated with neoadjuvant chemotherapy and 3D-image-guided afterloading intracavitary radiotherapy were assigned into the observation group (OG), while cases with neoadjuvant chemotherapy alone were assigned into the control group (CG). The short-term effects were determined by RECIST 1.1. Total effective rate (TR) = complete remission (CR) + partial remission (PR). The serum levels of squamous epithelial cell carcinoma antigen (SCC-Ag), glycoantigen 125 (CA125), carcinoembryonic antigen (CEA), and vascular endothelial growth factor (VEGF) were assessed. In view of the difference between tumor markers and diameters before and after treatment, the correlation between them was analyzed by Pearson test. The adverse events were compared, and the amount of operative bleeding and operation time were evaluated. Cox regression analysis was conducted to assess the influencing factors of 1-year disease-free survival time. *Results*. Sixty-seven patients were retrieved, including 30 cases in the OG and 37 cases in the CG. There were no significant differences in age, pathological type, tumor size, FIGO stage, past medical history, or smoking history between the two groups ($P > 0.05$). The TR of patients in the OG was higher than that in the CG ($P < 0.05$). The SCC-Ag, CA125, CEA, and VEGF levels in the OG decreased markedly after treatment ($P < 0.001$). The difference in SCC-Ag, CA125, CEA, and VEGF was positively correlated with the difference in tumor diameter before and after treatment ($P < 0.05$). The incidence of adverse events revealed no obvious difference between the OG and CG ($P > 0.05$). Cox regression analysis showed that FIGO stage and treatment regimens were independent prognostic factors for 1-year disease-free survival ($P < 0.05$). *Conclusion*. Neoadjuvant chemotherapy combined with 3D-image-guided afterloading intracavitary radiotherapy can improve the TR rate and 1-year disease-free survival of LACC patients without increasing the incidence of adverse events.

1. Introduction

Globally, cervical cancer (CC) ranks among malignancies with the highest number of new cases and deaths, posing a serious threat to the health of women [1]. In China, CC screening still needs to be popularized due to uneven regional healthcare development, and many patients are already in the stage of locally advanced cervical cancer (LACC) at initial diagnosis [2, 3], who are unable to be treated solely by surgeries [4, 5]. The 5-year survival rates of CC patients in stage IB1 and IIA1 are 80%-90% and 79.7%, respectively, while those of stage IB2 and IIA2 decreased to 50%-60% [6, 7].

Radical concurrent radiotherapy is the standard of care for advanced CC with NCCN guideline class 1 evidence, but the optimal treatment regimen for LACC is currently

highly controversial, and there is no consensus worldwide [8]. The standard treatment recommended in the United States and Canada is concurrent radiotherapy, while countries in Europe, Asia, and Latin America use neoadjuvant chemotherapy followed by surgery as first-line treatment [9]. LACC patients are difficult to cure and have a poor prognosis due to the large localized extent of the tumor and the high risk factors [10]. For LACC with tumor diameter ≥ 4 cm, it is not easily controlled by surgical treatment alone and is prone to distant metastases and lymph node metastases after surgery [11]. Currently, the preoperative adjuvant treatment options mainly include neoadjuvant chemotherapy and radiotherapy. Radiotherapy is a local treatment, while chemotherapy can treat distant metastases and lymph node metastases while reducing the tumor [12]. Despite the international controversy regarding preoperative adjuvant therapy for LACC, preoperative adjuvant radiotherapy, neoadjuvant chemotherapy, or their combination are still popular in developing countries by reducing tumor volume, improving the tissue environment around the uterus, and facilitating surgical operation. Also, they can reduce the difficulty of surgery, improve the surgical resection rate of patients, and control tumors effectively [13]. Research has proven that combining radiotherapy with chemotherapy is an even more effective way to improve the local control rate of advanced CC [14]. However, radiotherapy alone can increase drug resistance and lead to many side effects.

To reduce the side effects of radiotherapy toxicity and to ensure efficient and sustainable treatment, it has been a hot topic of research in the gynecologic oncology field. In this study, neoadjuvant chemotherapy combined with 3D-image-guided afterloading intracavitary radiotherapy was offered to LACC patients prior to radical hysterectomy to observe the short-term clinical impact and outcome as well as adverse events, so as to evaluate the clinical significance of this regimen in future treatment.

2. Methods and Materials

CC patients treated at our hospital from January 1, 2020 to January 1, 2021 were analyzed retrospectively. Cases treated with neoadjuvant chemotherapy and 3D-image-guided afterloading intracavitary radiotherapy were assigned into the observation group (OG), while cases with neoadjuvant chemotherapy alone were enrolled into the control group (CG). All patients received radical CC surgery after treatment. The research was conducted with the approval of the medical ethics committee of Wuwei Cancer Hospital and Institute.

The inclusion criteria were cases confirmed through histopathology. The gynecologic examinations were performed by two gynecologic oncologists of associate chief physician or above and diagnosed according to the FIGO stage IB2 and IIA2 (FIGO staging 2009) [15]. Patients should not receive targeted treatment before this research. Patients' clinical data were complete. All of them were informed and signed an informed consent form. The exclusion criteria were as follows: cases with serious complications or underly-

TABLE 1: Clinical characteristics of enrolled patients.

Factor	Control group (n = 37)	Observation group (n = 30)	P value
Age			
≥55 years old	23	18	0.856
<55 years old	14	12	
Pathological type			
Squamous cell carcinoma	33	28	0.554
Adenocarcinoma	4	2	
Tumor size			
≥ 5 cm	33	24	0.293
< 5 cm	4	6	
FIGO stage			
IB2	17	13	0.830
IIA2	20	17	
Past medical history			
Hypertension	12	15	0.144
Diabetes	10	8	0.973
Smoking history			
Yes	8	3	0.202
No	29	27	

ing diseases that could not tolerate the treatment plan; cases complicated with other malignancies; surgical history of cervical disease; history of radiotherapy, chemotherapy, or antitumor therapy; infectious or metabolic diseases; abnormal blood clotting function; cognitive impairment or mental illness; patients with allergic symptoms of chemotherapeutic drugs; and patients during lactation or pregnancy.

2.1. Treatment Regimens. Patients received neoadjuvant chemotherapy with paclitaxel plus platinum, which was sensitive to CC. Specifically, paclitaxel 135-175 mg/m^2 was given intravenously on day 1, and cisplatin 50-75 mg/m^2 was given on days 1 to 3. The chemotherapy was administered at 3-week intervals for 2 cycles, during which symptomatic treatments such as hydration and antiemetic were routinely used. The 3D-afterloading intracavitary radiation therapy with 5.5-6 Gy each time was performed twice and completed within 1 week [16]. Radical hysterectomy and pelvic lymph node dissection was performed 2 weeks after adjuvant therapy.

2.2. Outcome Determinations. The main outcomes include: the near-term outcomes were compared by the Response evaluation criteria in solid tumors version 1.1 (RECIST 1.1) [17]. Total response rate (TR) = complete response (CR) + partial response (PR). The squamous cell carcinoma antigen (SCC-Ag), carbohydrate antigen (CA125), and carcinoembryonic antigen (CEA) of squamous cell carcinoma before and after treatment were tested by chemiluminescence method [18], and the level of serum vascular endothelial growth factor (VEGF) was determined by enzyme linked
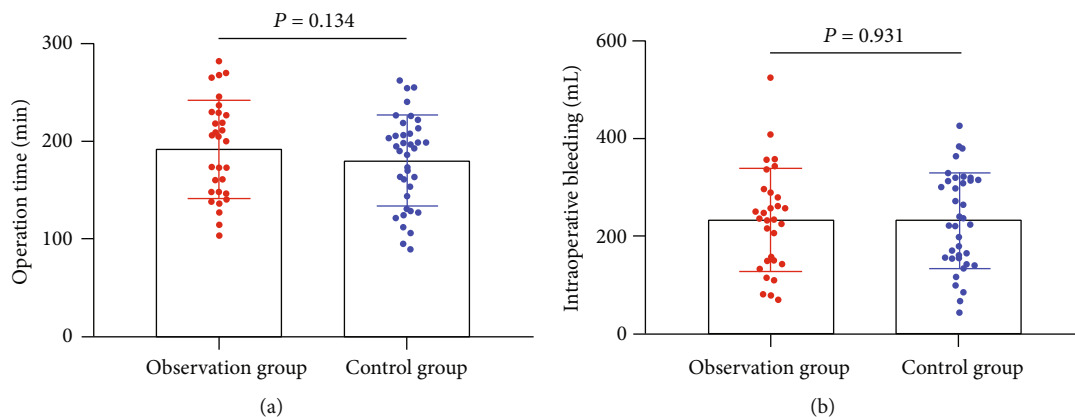
FIGURE 1: Blood loss and operation time during operation. (a) Difference of operation time between groups. (b) Difference of intraoperative blood loss between groups.

TABLE 2: Comparison of near-term efficacy [n (%)].

Groups	Complete remission	Partial remission	Stable	Ineffective	RR
Control group ($n = 37$)	4 (10.80)	10 (27.00)	21 (56.80)	2 (5.4)	14 (37.80)
Observation group ($n = 30$)	6 (20.00)	13 (43.30)	9 (30.00)	2 (6.70)	19 (63.30)
χ^2/Z value			-1.808		4.309
P value			0.071		0.037
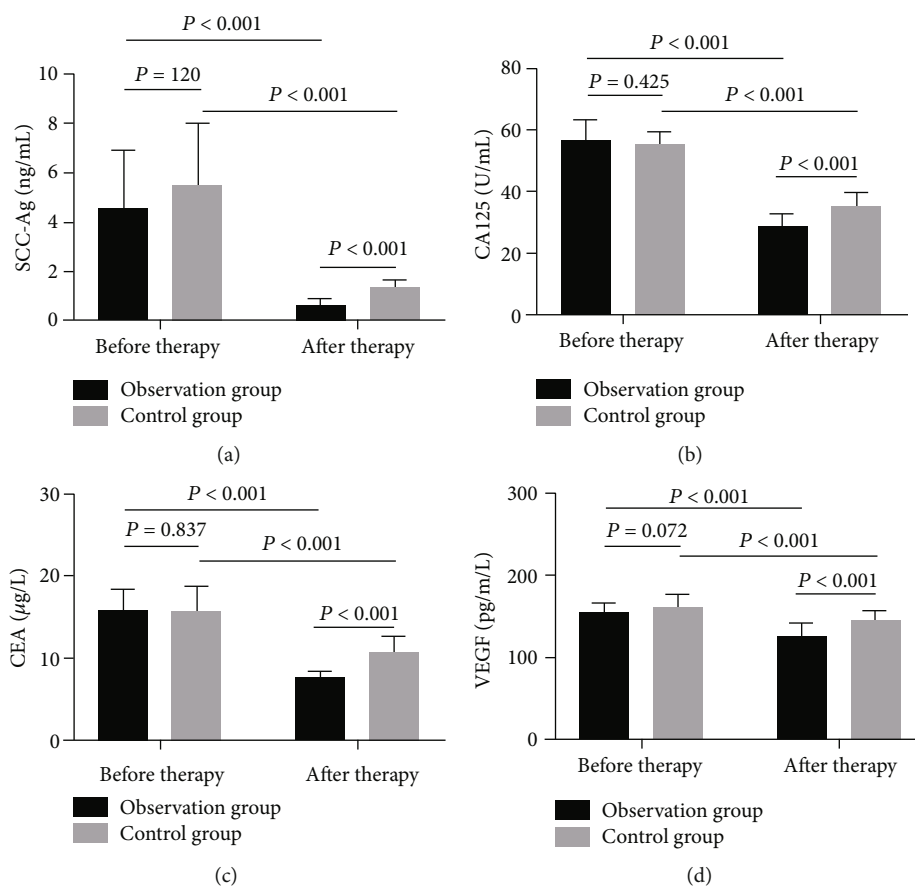
FIGURE 2: Comparison of serum tumor markers and VEGF levels in patients before and after treatment. (a) Comparison of serum SCC-Ag levels between groups before and after treatment. (b) Comparison of serum CA125 levels between groups before and after treatment. (c) Comparison of serum CEA levels between groups before and after treatment. (d) Changes of serum VEGF levels before and after treatment.

TABLE 3: Difference of various indexes before and after treatment.

Indexes	Observation group ($n = 37$)			Control group ($n = 30$)		
	Before treatment	After treatment	Difference	Before treatment	After treatment	Difference
SCC-ag	4.54 ± 2.38	0.65 ± 0.25	3.95 ± 2.30	5.50 ± 2.55	1.36 ± 0.31	4.17 ± 2.53
CA125	56.59 ± 6.64	28.64 ± 4.21	27.95 ± 8.97	55.53 ± 4.06	35.47 ± 4.29	20.06 ± 6.39
CEA	15.85 ± 2.41	7.63 ± 0.89	8.23 ± 2.48	15.71 ± 3.08	10.76 ± 1.97	5.28 ± 2.79
VEGF	154.06 ± 11.65	125.15 ± 15.66	29.75 ± 18.66	160.36 ± 15.71	145.29 ± 11.76	20.95 ± 15.18
Tumor diameter	6.26 ± 1.20	4.51 ± 2.10	2.23 ± 1.66	6.22 ± 0.95	5.10 ± 1.67	1.51 ± 1.23

immunosorbent assay (ELISA). The correlation between tumor markers and diameter changes was assessed by Pearson's test according to the difference between patients before and after treatment.

The secondary outcomes include: the clinical characteristics and adverse events of both groups were compared. The amount of intraoperative bleeding and operation time were assessed. Cox regression analysis was conducted to assess the influencing factors of 1-year disease-free survival time.

2.3. Statistical Analysis. Data were analyzed through SPSS 20.0 (IBM Corp., Armonk, N.Y., USA). The enumeration data were expressed as n (%) and analyzed using the chi-squared test, and the measurement data were shown as mean ± standard deviation (SD) and evaluated by independent t-test. The association between tumor markers and diameter was assessed via Pearson test. Patients' disease-free survivals were plotted using the Kaplan-Meier survival curves, and then analyzed through log-rank test. The prognostic factor affecting patients' disease-free survival time was assessed through Cox regression. A two-tailed p value <0.05 indicated statistical difference.

3. Results

3.1. Comparison of Clinical Characteristics. Sixty-seven CC patients were retrieved, including 30 cases in the OG and 37 cases in the CG. There were no statistical differences in age, pathological type, tumor size, FIGO stage, past medical history, or smoking history between the two groups ($P > 0.05$, Table 1). There was no marked difference in operation time and intraoperative blood loss between groups ($P > 0.05$, Figure 1).

3.2. Comparison of Near-Term Efficacy after Radiotherapy and Chemotherapy. There was significantly higher TR of patients in the OG than that in the CG ($P < 0.05$, Table 2).

3.3. Changes of Tumor Markers and VEGF Expression before and after Treatment. The changes of serum tumor markers and VEGF expression were compared after radiotherapy and chemotherapy before operation. The SCC-Ag, CA125, CEA, and VEGF levels in serum after treatment were lower than those before treatment ($P < 0.001$). After treatment, the levels of SCC-Ag, CA125, CEA, and VEGF in the OG were significantly lower than those in the CG ($P < 0.001$, Figure 2).
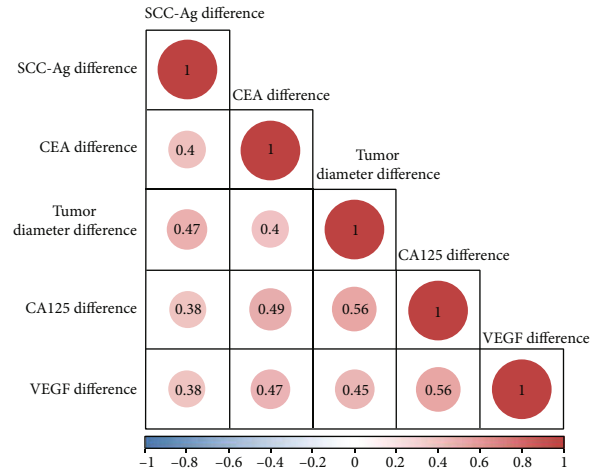
FIGURE 3: Correlation between tumor diameter, markers, and VEGF. Note: red indicates positive correlation, and blue indicates negative correlation.

3.4. Correlation between Tumor Markers, VAGF, and Diameter. We performed a correlation analysis based on the differences of indicators before and after treatment (Table 3). The differences of SCC-Ag, CA125, CEA, and VEGF before and after treatment were positively correlated with those of tumor diameter ($P < 0.05$, Figure 3).

3.5. Comparison of Adverse Events in Patients. There was no obvious difference in the incidence of adverse events between groups ($P > 0.05$, Table 4).

3.6. Analysis of Prognostic Factors of Disease-Free Survival Time. The 1-year disease-free survival rate of 67 patients was 74.62%. Subsequently, we analyzed the clinical data of patients using univariate analysis and found that age, FIGO stage, and treatment regimens were prognostic factors affecting disease-free survival (Figure 4). Further analysis revealed that FIGO staging and treatment regimens were independently tied to patients' disease-free survival ($P < 0.05$, Table 5).

4. Discussion

CC is a malignancy with high incidence in female patients. LACC accounts for a relatively large proportion among CC, and the 5-year survival rate is about 60% [19]. The tumor diameter of LACC patients is relatively large, which

TABLE 4: Adverse events of patients.

Groups	Leukopenia	Malignant vomiting	Abnormal liver function	Fever	Total incidence rate
Control group ($n = 37$)	3 (8.10)	2 (5.40)	2 (5.40)	1 (2.70)	8 (21.62)
Observation group ($n = 30$)	2 (6.67)	2 (6.67)	2 (6.67)	0 (0.00)	6 (20.00)
χ^2 value					0.026
P value					0.871

(a)

(b)

(c)
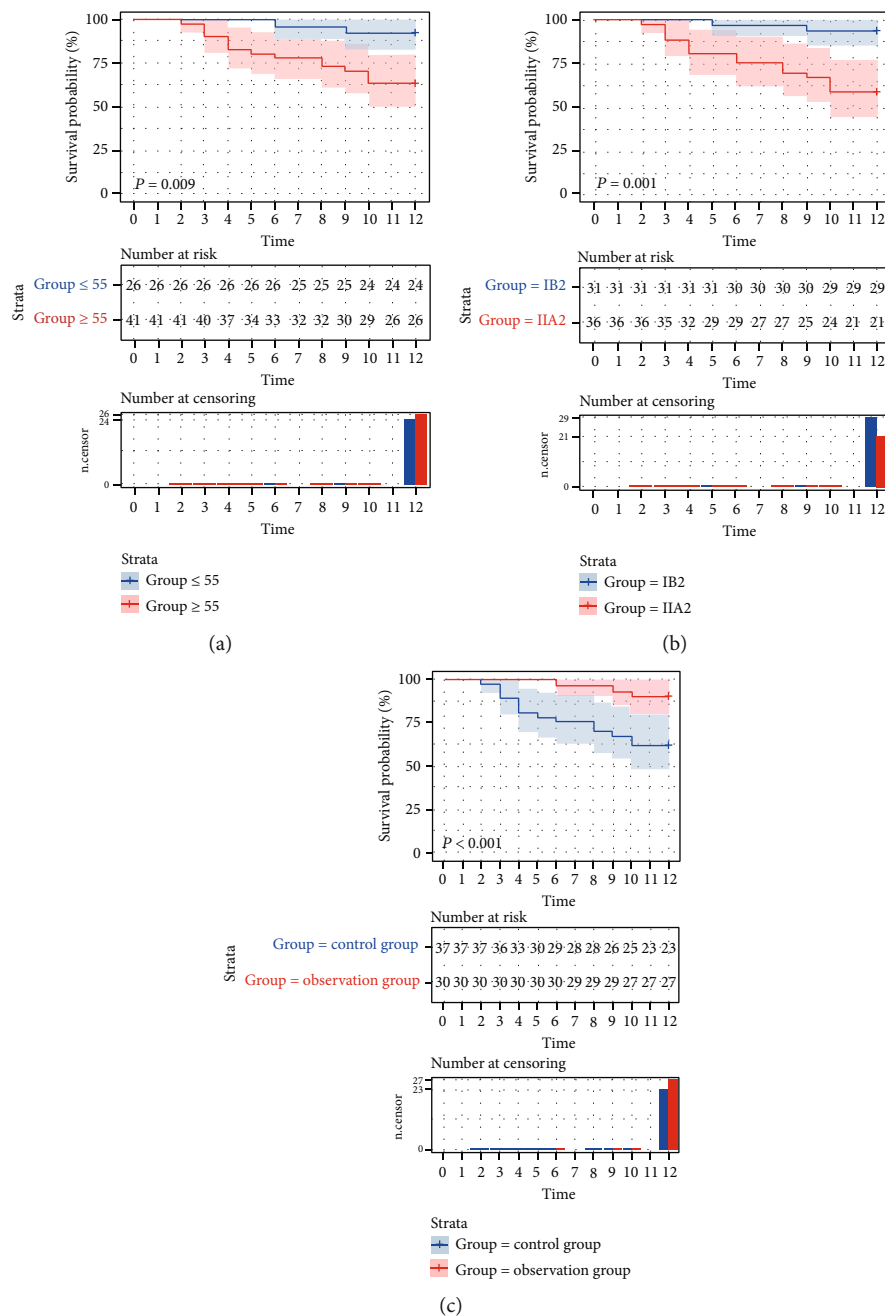
FIGURE 4: Analysis of age, FIGO stage, treatment plan, and disease-free survival of patients. (a) Analysis of age and disease-free survival of patients. (b) Analysis of FIGO staging and disease-free survival of patients. (c) Analysis of treatment plans and disease-free survival time of patients.

Table 5: Analysis of risk factors for disease-free survival time.

Factor	Univariate analysis			Multivariate analysis		
	HR value	P value	95% CI	HR value	P value	95% CI
Age (≥55 VS <55)	5.617	0.022	1.284~24.578	4.346	0.053	0.983~19.208
Pathological type (adenocarcinoma VS squamous cell carcinoma)	0.951	0.947	0.217~4.160			
Tumor size (≥5 cm VS <5 cm)	0.815	0.747	0.234~2.836			
FIGO stage (IB2 VS IIA2)	0.127	0.006	0.029~0.558	0.144	0.011	0.033~0.637
Hypertension (yes VS no)	0.301	0.059	0.086~1.048			
Diabetes (yes VS no)	1.503	0.422	0.556~4.065			
Smoking history (yes VS no)	0.036	0.218	0.000~7.086			
Treatment plans (combination VS single)	0.218	0.017	0.062~0.759	0.188	0.009	0.054~0.657

increases the difficulty of operation to a certain extent. The incidence of postoperative complications, metastasis, and recurrence rate are high, and the prognosis is not ideal [20]. Not only that, clinical treatment is difficult and more controversial. Although concurrent chemoradiation is considered an international standard treatment option, there are still many problems and limitations [21]. The number of patients treated tends to be younger, and radical surgery after preoperative adjuvant treatment is more in line with clinical needs. Neoadjuvant chemotherapy and 3D-image-guided afterloading intracavitary radiotherapy combines the advantages of precision radiotherapy and chemotherapy, so that CC with large tumor size can be well controlled, creating favorable conditions for surgical resection, and reducing surgical risks and complications. It improves the effect of treatment and quality of life of patients effectively [22]. Nevertheless, there are few studies on whether there is a difference in the efficacy between combination therapy and neoadjuvant chemotherapy alone in LACC treatment [23].

In the present study, we analyzed the efficacy of the two regimens in LACC patients. In our study, we found no marked effect of the two regimens on overall outcomes and adverse events. But our further analysis revealed that the TR rate of patients in the OG was higher than that of those in the CG. Previously, research found that 3D-image-guided afterloading intracavitary radiotherapy combined with chemotherapy improved the treatment outcome of advanced CC [24]. This is due to the fact that 3D conformal HDR brachytherapy can calculate the radiation dose received by the target area and surrounding normal organ tissues more accurately, which is conducive to the development of reasonable individualized treatment plans [25]. Neoadjuvant chemotherapy and radiotherapy have synergistic effects, acting on different cell cycles, respectively. Chemotherapy synchronizes cancer cells with radiotherapy-sensitive cycles, increases radiotherapy sensitivity while shrinking tumor cells, accelerates the apoptotic process of cancer cells, and reduces the chance of CC metastasis, thus, improving the histopathology [26]. Radiotherapy shrinks the local mass and leads to narrowing and occlusion of some capillaries and lymphatic vessels in the pelvis, which facilitates surgical operations and reduces the difficulty of surgery, thus, improving the efficiency of surgery [27]. We also found no difference in intraoperative bleeding and operative time dur-

ing surgery. It is theoretically believed that combined treatment can reduce the local tumor volume and improve the parametrial tissue gap, which in turn reduces the difficulty of surgery. It showed that the combined treatment did not reduce the difficulty of the procedure, and we believe that the physiology of patients was diminished after the combined treatment. In addition, after the combined treatment, the reactive adhesion of lymphoid tissue and the para-uterine tissue fibrosis increased, thus, increasing the difficulty of the operation.

Currently, tumor markers such as SCC-Ag, CA125, CEA, and VEGF are of clinical value in CC diagnosis and treatment [28]. SCC-Ag is a relevant antigen reflecting the proliferation of squamous epithelial cells [29]. CA125 is one of the specific tumor markers, mostly found in adult pleura, endometrium, fallopian tube endothelium, and endocervical lining, and its expression is relevant to the tumor load in patients [30]. CEA may reflect the risk of tumor cell infiltration [18]. VEGF is an essential vascular endothelial growth factor for distant metastasis and tumor recurrence [31]. We found the SCC-Ag, CA125, CEA, and VEGF expression in LACC patients decreased after treatment. Besides, we confirmed a positive correlation between the difference of SCC-Ag, CA125, CEA, VEGF, and tumor diameter, which indicates that SCC-Ag, CA125, CEA, and VEGF are relevant to tumor growth. It is suggested that joint observation of changes in the levels of these markers may have vital monitoring value for assessing the disease progression and treatment efficacy.

At the end of the research, we measured patients' disease-free survival time. Cox regression analysis revealed that FIGO staging and treatment regimens were relevant to their disease-free survival. Earlier studies have shown that patients with higher FIGO stage have shorter disease-free survival time, which is consistent with our findings [32]. We first found that neoadjuvant chemotherapy combined with 3D-image-guided afterloading intracavitary radiotherapy was effective in improving the short-term disease-free survival of LACC patients. We believe this is due to the fact that preoperative radiotherapy shrinks the local mass. Moreover, preoperative radiotherapy can reduce local cervical tumors in varying degrees, which can not only eliminate tumor cells or reduce their activity, block tumor vessels, improve para-uterine infiltration, increase surgical resection

rate but also reduce intraoperative dissemination and improve survival rate.

We found that neoadjuvant chemotherapy combined with 3D-image-guided afterloading intracavitary radiotherapy can increase the TR rate of LACC patients and improve their short-term disease-free survival. Nevertheless, there are still some limitations. First of all, the study period is relatively short. We were only able to count the disease-free survival time of patients for one year, and the effect of combined therapy on long-term overall survival and disease-free survival needs further study. Second, we only collected a relatively small number of patients for this study. Finally, this was a retrospective study, the results of which might be biased. We hope to continue to follow patients in subsequent studies and retrieve more patients to confirm our findings. It might be more intriguing to consider the combined therapy in other complicated cases, such as infection, hypoxia, fulminant hepatitis, or wound healing problems [33–39].

To sum up, neoadjuvant chemotherapy combined with 3D-image-guided afterloading intracavitary radiotherapy in LACC patients improves the TR rates and 1-year disease-free survival and does not increase the incidence of adverse events.

Data Availability

The data used to support the findings of this study are available from the corresponding author upon request.

Conflicts of Interest

The authors declare that they have no conflicts of interest.

Acknowledgments

References

[1] F. Bray, J. Ferlay, I. Soerjomataram, R. L. Siegel, L. A. Torre, and A. Jemal, "Global cancer statistics 2018: GLOBOCAN estimates of incidence and mortality worldwide for 36 cancers in 185 countries," *CA: a Cancer Journal for Clinicians*, vol. 68, no. 6, pp. 394–424, 2018.

[2] A. Gadducci and S. Cosio, "Neoadjuvant chemotherapy in locally advanced cervical cancer: review of the literature and perspectives of clinical research," *Anticancer Research*, vol. 40, no. 9, pp. 4819–4828, 2020.

[3] H. B. Musunuru, P. M. Pifer, P. Mohindra, K. Albuquerque, and S. Beriwal, "Advances in management of locally advanced cervical cancer," *The Indian Journal of Medical Research*, vol. 154, no. 2, pp. 248–261, 2021.

[4] S. Chopra, M. Gupta, A. Mathew et al., "Locally advanced cervical cancer: a study of 5-year outcomes," *Indian Journal of Cancer*, vol. 55, no. 1, pp. 45–49, 2018.

[5] R. Benson, S. Pathy, L. Kumar, S. Mathur, V. Dadhwal, and B. K. Mohanti, "Locally advanced cervical cancer - neoadjuvant chemotherapy followed by concurrent chemoradiation and targeted therapy as maintenance: a phase II study," *Journal of Cancer Research and Therapeutics*, vol. 15, no. 6, pp. 1359–1364, 2019.

[6] T. Shu, B. Li, D. Zhao, Y. T. Wang, and S. H. Liu, "Open nerve-plane sparing radical hysterectomy in locally advanced cervical cancer: evaluation on efficacy and long-term survival outcomes," *Zhonghua Fu Chan Ke Za Zhi*, vol. 56, no. 1, pp. 43–51, 2021.

[7] K. G. G. van Kol, R. M. F. Ebisch, J. M. J. Piek, P. L. M. Zusterzeel, T. F. M. Vergeldt, and R. L. M. Bekkers, "Salvage surgery for patients with residual disease after chemoradiation therapy for locally advanced cervical cancer: a systematic review on indication, complications, and survival," *Acta Obstetricia et Gynecologica Scandinavica*, vol. 100, no. 7, pp. 1176–1185, 2021.

[8] V. A. Fabri, A. C. M. Queiroz, H. Mantoan et al., "The impact of addition of consolidation chemotherapy to standard cisplatin-based chemoradiotherapy in uterine cervical cancer: matter of distant relapse," *Journal of Oncology*, vol. 2019, Article ID 1217838, 9 pages, 2019.

[9] W. Zou, Y. Han, Y. Zhang et al., "Neoadjuvant chemotherapy plus surgery versus concurrent chemoradiotherapy in stage IB2-IIB cervical cancer: a systematic review and meta-analysis," *PLoS One*, vol. 14, no. 11, article e0225264, 2019.

[10] M. Toure, A. T. Bambara, K. K. Y. Kouassi et al., "Level of concordance of pre-, intra-, and postoperative staging in cervical cancers (TREYA study)," *Journal of Oncology*, vol. 2017, Article ID 8201462, 5 pages, 2017.

[11] N. Sakuragi, M. Kaneuchi, T. Kato et al., "Tailored radical hysterectomy for locally advanced cervical cancer," *International Journal of Gynecological Cancer*, vol. 30, no. 8, pp. 1136–1142, 2020.

[12] X. Tian, F. Yang, F. Li et al., "A comparison of different schemes of neoadjuvant chemotherapy followed by concurrent chemotherapy and radiotherapy for locally advanced cervical cancer: a retrospective study," *Cancer Management and Research*, vol. 13, pp. 8307–8316, 2021.

[13] L. C. Wei, X. Li, Y. Zhang et al., "Individualized pelvic lymphadenectomy should follow neoadjuvant concurrent chemoradiotherapy for locally advanced cervical cancer," *Medicine*, vol. 97, no. 14, article e0331, 2018.

[14] T. Asakij, J. Khunnarong, S. Tangjitgamol et al., "Salvage treatment and outcomes of locally advanced cervical cancer after failed concurrent chemoradiation with or without adjuvant chemotherapy: post hoc data analysis from the ACTLACC trial," *Asian Pacific Journal of Cancer Prevention*, vol. 23, no. 7, pp. 2263–2269, 2022.

[15] A. Mohamud, C. Hogdall, and T. Schnack, "Prognostic value of the 2018 FIGO staging system for cervical cancer," *Gynecologic Oncology*, vol. 165, no. 3, pp. 506–513, 2022.

[16] J. Itami, N. Murakami, M. Watanabe et al., "Combined interstitial and intracavitary high-dose rate brachytherapy of cervical cancer," *Frontiers in Oncology*, vol. 11, p. 809825, 2022.

[17] R. L. Wahl, H. Jacene, Y. Kasamon, and M. A. Lodge, "From RECIST to PERCIST: evolving considerations for PET response criteria in solid tumors," *Journal of Nuclear Medicine*, vol. 50, Suppl 1, pp. 122S–150S, 2009.

[18] L. Gao, J. Lv, L. Hou, Y. Yuan, and Q. Wan, "Clinical effects of Chinese herbal decoction combined with basic chemoradiotherapy and nursing intervention in the treatment of cervical cancer and the effect on serum CEA, CA125, and TNF-α

levels," *Evidence-based Complementary and Alternative Medicine*, vol. 2021, Article ID 1446864, 7 pages, 2021.

[19] J. Ge, J. Sun, J. Li, Q. Zhang, X. Lv, and B. Chen, "Operation for locally advanced cervical cancer after concurrent chemoradiotherapy," *International Journal of Clinical Oncology*, vol. 25, no. 5, pp. 948–954, 2020.

[20] F. Landoni, A. Colombo, R. Milani, F. Placa, V. Zanagnolo, and C. Mangioni, "Randomized study between radical surgery and radiotherapy for the treatment of stage IB-IIA cervical cancer: 20-year update," *Journal of Gynecologic Oncology*, vol. 28, no. 3, article e34, 2017.

[21] S. Tangjitgamol, K. Katanyoo, M. Laopaiboon, P. Lumbiganon, S. Manusirivithaya, and B. Supawattanabodee, "Adjuvant chemotherapy after concurrent chemoradiation for locally advanced cervical cancer," *Cochrane Database of Systematic Reviews*, vol. 12, article CD010401, 2014.

[22] A. Mousavi, M. Modarres Gilani, S. Akhavan, S. Sheikh Hasani, A. Alipour, and H. Gholami, "The outcome of locally advanced cervical cancer in patients treated with neoadjuvant chemotherapy followed by radical hysterectomy and primary surgery," *The Iranian Journal of Medical Sciences*, vol. 46, no. 5, pp. 355–363, 2021.

[23] T. Kokabu, K. Masui, Y. Tarumi et al., "3D-image-guided multi-catheter interstitial brachytherapy for bulky and high-risk stage IIB-IVB cervical cancer," *Cancers*, vol. 14, no. 5, p. 1257, 2022.

[24] P. Naga Ch, L. Gurram, S. Chopra, and U. Mahantshetty, "The management of locally advanced cervical cancer," *Current Opinion in Oncology*, vol. 30, no. 5, pp. 323–329, 2018.

[25] N. B. Chen, B. Qiu, J. Zhang et al., "Intensity-modulated radiotherapy versus three-dimensional conformal radiotherapy in definitive chemoradiotherapy for cervical esophageal squamous cell carcinoma: comparison of survival outcomes and toxicities," *Cancer Research and Treatment*, vol. 52, no. 1, pp. 31–40, 2020.

[26] K. Nam, J. R. Eisenbrey, M. Stanczak et al., "Monitoring neoadjuvant chemotherapy for breast cancer by using three-dimensional subharmonic aided pressure estimation and imaging with US contrast agents: preliminary experience," *Radiology*, vol. 285, no. 1, pp. 53–62, 2017.

[27] M. Jirkovska, T. Novak, B. Malinova, and R. Lohynska, "Three-dimensional conformal radiotherapy versus intensity modulated radiotherapy with simultaneous integrated boost in the treatment of locally advanced head and neck carcinoma," *Neoplasma*, vol. 66, no. 5, pp. 830–838, 2019.

[28] J. P. Hoogendam, A. Zaal, E. G. Rutten et al., "Detection of cervical cancer recurrence during follow-up: a multivariable comparison of 9 frequently investigated serum biomarkers," *Gynecologic Oncology*, vol. 131, no. 3, pp. 655–660, 2013.

[29] J. Fu, W. Wang, Y. Wang, C. Liu, and P. Wang, "The role of squamous cell carcinoma antigen (SCC ag) in outcome prediction after concurrent chemoradiotherapy and treatment decisions for patients with cervical cancer," *Radiation Oncology*, vol. 14, no. 1, p. 146, 2019.

[30] N. Kim, W. Park, W. K. Cho et al., "Significance of serum CA125 level in surgically resected cervical adenocarcinoma with adverse features," *Journal of Gynecologic Oncology*, vol. 32, no. 5, article e72, 2021.

[31] L. Zhang, Q. Chen, J. Hu, Y. Chen, C. Liu, and C. Xu, "Expression of HIF-2alpha and VEGF in cervical squamous cell carci-

noma and its clinical significance," *BioMed Research International*, vol. 2016, Article ID 5631935, 7 pages, 2016.

[32] L. Li, X. Song, R. Liu et al., "Chemotherapy versus radiotherapy for FIGO stages IB1 and IIA1 cervical carcinoma patients with postoperative isolated deep stromal invasion: a retrospective study," *BMC Cancer*, vol. 16, no. 1, p. 403, 2016.

[33] Z. Shi, J. Vasquez-Vivar, K. Luo et al., "Ascending lipopolysaccharide-induced intrauterine inflammation in near-term rabbits leading to newborn neurobehavioral deficits," *Developmental Neuroscience*, vol. 40, no. 5-6, pp. 534–546, 2019.

[34] L. Deng, X. Li, Z. Shi, P. Jiang, D. Chen, and L. Ma, "Maternal and perinatal outcome in cases of fulminant viral hepatitis in late pregnancy," *International Journal of Gynecology & Obstetrics*, vol. 119, no. 2, pp. 145–148, 2012.

[35] Z. Shi, K. Luo, S. Jani et al., "Mimicking partial to total placental insufficiency in a rabbit model of cerebral palsy," *Journal of Neuroscience Research*, 2021.

[36] Y. Yang, L. Deng, X. Li et al., "Evaluation of the prognosis of fulminant viral hepatitis in late pregnancy by the MELD scoring system," *European Journal of Clinical Microbiology & Infectious Diseases*, vol. 31, no. 10, pp. 2673–2678, 2012.

[37] Y. Yang, L. Deng, X. Li et al., "Analysis of prognosis-associated factors in fulminant viral hepatitis during pregnancy in China," *International Journal of Gynaecology and Obstetrics*, vol. 114, no. 3, pp. 242–245, 2011.

[38] X. M. Li, L. Ma, Y. B. Yang, Z. J. Shi, and S. S. Zhou, "Prognostic factors of fulminant hepatitis in pregnancy," *Chinese Medical Journal*, vol. 118, no. 20, pp. 1754–1757, 2005.

[39] Z. Shi, L. Ma, H. Wang et al., "Insulin and hypertonic glucose in the management of aseptic fat liquefaction of post-surgical incision: a meta-analysis and systematic review," *International Wound Journal*, vol. 10, no. 1, pp. 91–97, 2013.

Research Article

Risk Predictive Model Based on Three DDR-Related Genes for Predicting Prognosis, Therapeutic Sensitivity, and Tumor Microenvironment in Hepatocellular Carcinoma

Renzhi Hu, Xiping Liang, Qiying Li, and Yao Liu [ID]

Department of Hematology-Oncology, Chongqing University Cancer Hospital, Chongqing Key Laboratory of Translational Research for Cancer Metastasis and Individualized Treatment, Chongqing, China

Correspondence should be addressed to Yao Liu; liuyao77@cqu.edu.cn

Hepatocellular carcinoma (HCC) is the seventh most common malignancy and the second most common cause of cancer-related deaths. Tumor mutational load, genomic instability, and tumor-infiltrating lymphocytes were associated with DNA damage response and repair gene changes. The goal of this study is to estimate the chances of patients with HCC surviving their disease by constructing a DNA damage repair- (DDR-) related gene profile. The International Cancer Genome Consortium (ICGC) and The Cancer Genome Atlas (TCGA) provided us with the mRNA expression matrix as well as clinical information relevant to HCC patients. Using Cox regression and LASSO analysis, DEGs strongly related to general survival were discovered in the differentially expressed gene (DEG) study. In order to assess the model's accuracy, Kaplan-Meier (KM) and receiver operating characteristic (ROC) were used. In order to compute the immune cell infiltration score and immune associated pathway activity, a single-sample gene set enrichment analysis was performed. A three-gene signature (CDC20, TTK, and CENPA) was created using stability selection and LASSO COX regression. In comparison to the low-risk group, the prognosis for the high-risk group was surprisingly poor. In the ICGC datasets, the predictive characteristic was confirmed. A receiver operating characteristic (ROC) curve was calculated for each cohort. The risk mark for HCC patients is a reliable predictor according to multivariate Cox regression analysis. According to ssGSEA, this signature was highly correlated with the immunological state of HCC patients. There was a significant correlation between the expression levels of prognostic genes and cancer cells' susceptibility to antitumor therapies. Overall, a distinct gene profile associated with DDR was identified, and this pattern may be able to predict HCC patients' long-term survival, immune milieu, and chemotherapeutic response.

1. Introduction

Hepatocellular carcinoma (HCC) remains one of the most aggressive solid malignancies throughout the world, and fatty liver, alcoholic liver, and hepatitis B and C infections are the three most significant risk factors for HCC [1, 2]. The incidence of HCC is highest in underdeveloped nations, but chronic hepatitis C virus infection, which causes liver cirrhosis, is also increasing in wealthy nations [3, 4]. Researchers have been investigating the molecular pathways underlying the pathogenesis of hepatocellular carcinoma for several decades [5]. Gene mutations, epigenetic changes, and dysregulation of coding or noncoding genes were found to influence HCC growth [6, 7]. Although we have made great progresses in integrating treatment plans for HCC and our understanding of its epidemiology, etiology, biology, diagnostics, and therapy, the long-term prognosis of HCC patients remains unfavorable [8, 9]. Metastatic illness, in which tumor cells invade nearby tissues and organs and spread cancer throughout the body, is responsible for the vast majority of cancer-related deaths. Therefore, identifying molecular markers for early diagnosis, survival prediction, and recurrence monitoring of HCC is very important. In this way, patient categorization can be improved, and medical intervention can be more effective.
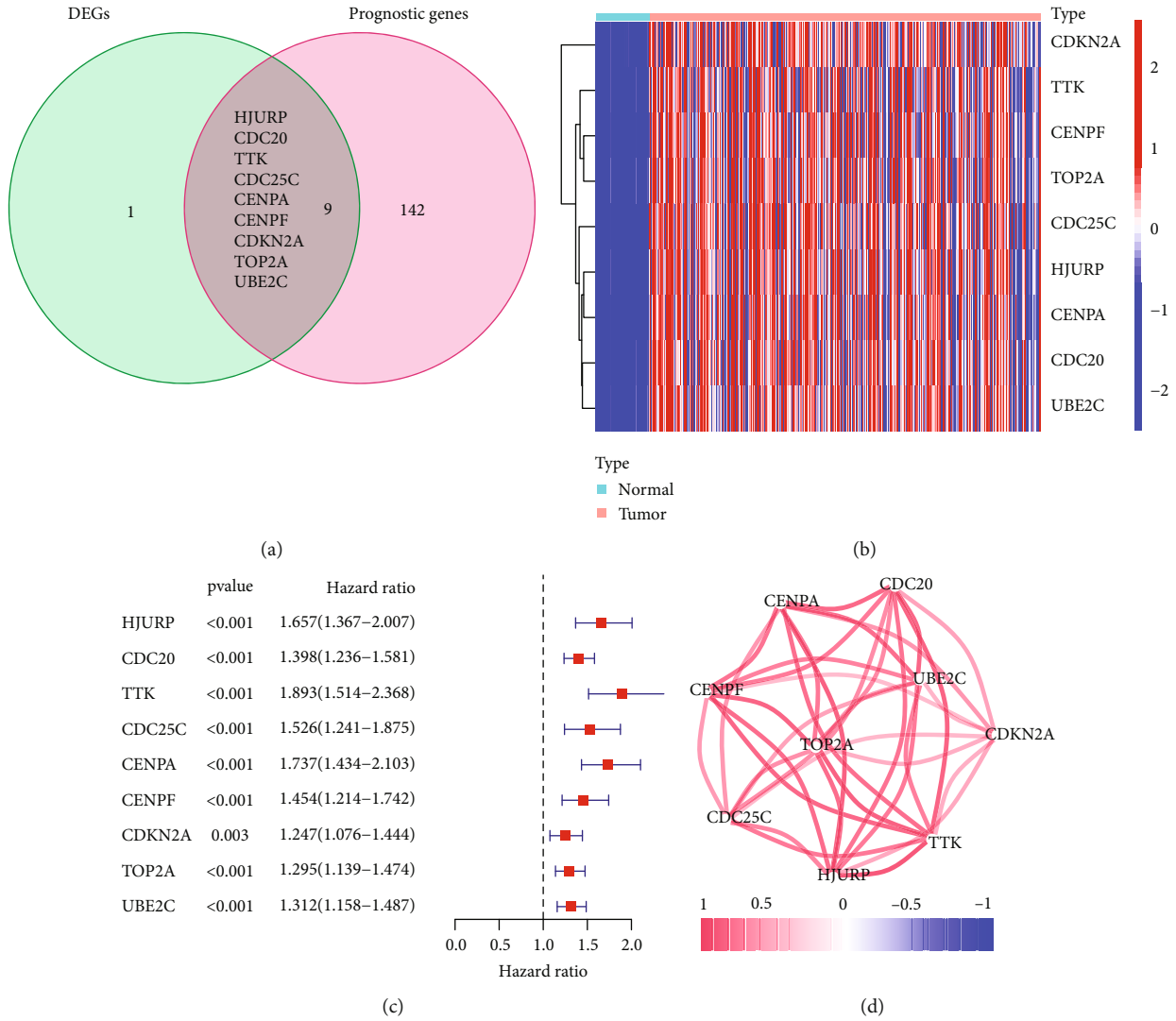
FIGURE 1: A list of possible DDR-related genes identified in the TCGA cohort. DEGs between nearby normal specimens and HCC specimens are calculated using a Venn diagram (a). (b) Expression of nine genes that overlap between neighboring normal tissues and HCC tissues. (c) Forest plots showing the associations between OS and the expression of 9 overlapping genes. (d) Correlation network of candidate genes.

All biological activities result in DNA damage because DNA damage repair keeps the genome stable and intact [10]. Several chronic illnesses, including cancer, are characterized by genomic instability. The integrity of DNA is of utmost importance in this respect, as it may prevent genomic instability [11]. In spite of the relatively low frequency of DNA damage, it should be repaired as soon as possible to demonstrate the accurate transmission of genetic information [12, 13]. Inability of the DDR to repair the following endogenous and external insults would lead to (1) a future malignant transformation, (2) the emergence of cancer, and (3) further deterioration of the DNA repair system [14]. The DDR mechanism can be modified during tumor formation or during therapy-induced tumor evolution to provide tumor clones with new growth abilities when they have lost genomic integrity and are outgrowing their original hosts [15, 16]. Cancer cells may also be more resistant to chemotherapy if DDR genes are expressed differently. Ovar-

ian and prostate cancers may benefit from therapeutic targeting of DDR-related genes [17, 18]. Numerous studies have shown that the numerous DDR gene polymorphisms together affect the chance of developing HCC [19, 20]. In the wake of immunotherapy, researchers are placing a renewed emphasis on DDR pathways, the modifications of which are associated with hereditary traits, such as elevated TMB, caused by the accumulation of certain uncorrected DNA damage [21, 22]. DDR-related genes are linked to a poor prognosis for HCC, but the evidence is limited.

Clinical data and the expressing pattern of mRNAs of HCC patients were obtained from a publicly accessible dataset. A predictive signature of differentially expressed genes associated with DDR was then created in TCGA cohorts, and its stability and dependability were tested in the ICGC cohorts. Moreover, we examined the relationship between immune infiltrates and the expressions of prognostic genes. Furthermore, we examined the relationships between
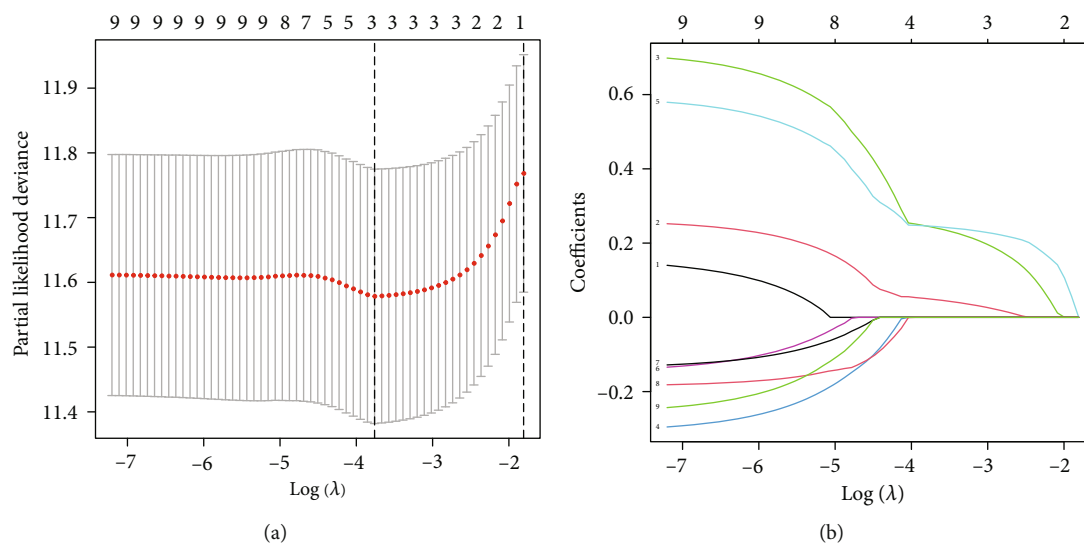
Figure 2: Gene signatures associated with DDR were identified in TCGA datasets using LASSO regression analysis. (a) Choosing the optimal LASSO model parameter (lambda). (b) LASSO coefficient profiles of the nine prognostic DDR genes.

prognostic genes' expressions and characteristics of cancer that make it resistant to chemotherapy. New treatment plans for HCC patients can be created based on our discoveries.

2. Materials and Methods

2.1. The Acquisition and Processing of Data. 374 HCC samples and 50 nontumor samples were presented on the UCSC Xena website (https://xenabrowser.net/). The raw gene microarray expression data of International Cancer Genome Consortium (ICGC-LIRI-JP) and associated clinical information were downloaded from ICGC. Furthermore, we eliminated datasets without clinical data. An average value was assigned to genes with two or more probe matches, while probes with two or more matches were disqualified.

2.2. Identification of Variation in the Expression of DDR Genes in HCC. Our statistical analysis and data visualization were performed using the R programming language. A differentially expressed gene from the DDR gene sets was also analyzed using the limma program at a significance threshold of p less than 0.05 and a fourfold change. "Pheatmap" was used to display the heatmap graphic.

2.3. Identification of Survival-Related DDR Genes in HCC. A single-variate Cox analysis was used to identify survival-related DDR genes, and the Benjamini and Hochberg correction was applied to alter the p value. A $p < 0.05$ was considered statistically significant.

2.4. Creation and Validation of the DD-Related Prognostic Signature for HCC. In order to reduce the dimensionality of intersecting genes, we used a LASSO regression analysis. DDR score-related predictive risk signatures were then optimized by including both forward and backward components. According to various fitting results, we also obtained the minimal AIC value. In the end, three gene construction models were achieved: CDC20, TTK, and CENPA. There

are three components to the risk score: $(0.0496 \times CDC20) + (0.244 \times TTK) + (0.245 \times CENPA)$. Each patient's risk score was calculated by the use of above algorithm. The performance of the prognostic risk model was evaluated between the training cohort and validation cohort by dividing patients into low- and high-risk groups based on median and ideal cut-off points. A survival study was conducted using the Kaplan-Meier method. It was determined whether the risk mark was accurate by using a ROC curve. The survival-ROC R package was utilized to assess the t-ROC prediction capability. We also assessed the relevance of each parameter to overall survival (OS) using Cox proportional hazard regression.

2.5. Microenvironmental and Immune Analysis of Tumors. We examined the amount of stromal and immune cell infiltration in various tumor tissues according to the stromal score and immune score. Spearman correlations were used to investigate the relationship between the risk score and those scores.

2.6. Chemotherapy Sensitivity Analysis. NCI-60, which contains 60 distinct cancer cell lines from 9 different cancer types, can be accessed through the CellMiner interface (https://discover.nci.nih.gov/cellminer). A Pearson correlation analysis was performed to determine whether the critical genes were related to medication sensitivity. A correlation analysis was done on 263 FDA-approved and clinically trialed medications to determine their therapeutic impact.

2.7. Statistical Analysis. Analysis and installation of the R packages mentioned above were performed using the R software version 3.6.3 (The R Foundation for Statistical Computing, 2020). There are two sides to every statistical test. Statistical significance was defined as a p value less than 0.05. The chi-square test or Fisher exact test was used for

(a)

(b)

(c)

(d)
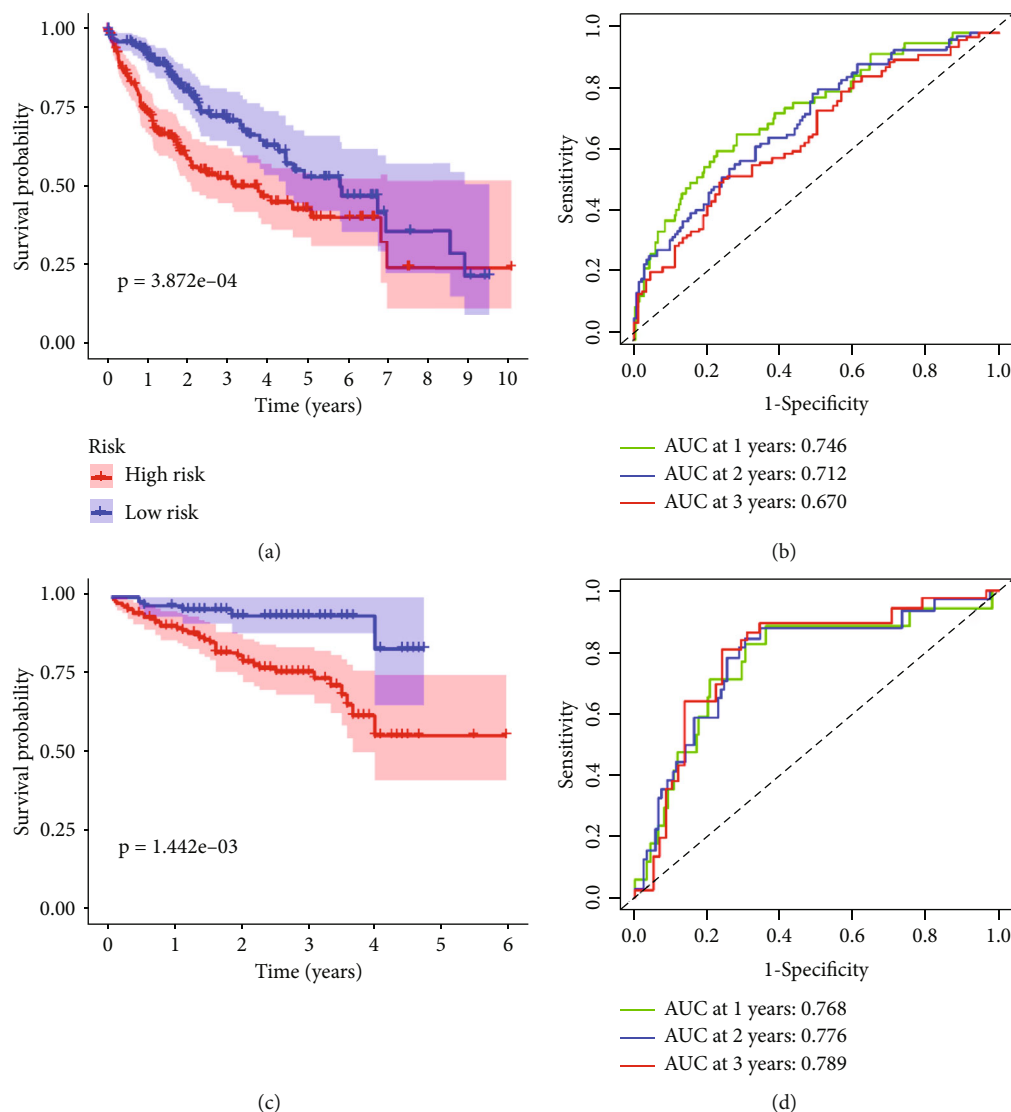
FIGURE 3: The performance of DDR-related gene signature in TCGA and ICGC datasets. Based on Kaplan-Meier analysis of the (a) TCGA and (c) ICGC datasets, patients with lower risk ratings had greater overall survival than those with higher risk scores. ROC curves were used to assess the prognostic signature's accuracy in the (b) TCGA and (d) ICGC datasets.

categorical variables, and the *t*-test or Wilcoxon rank-sum test was used for continuous variables. Kaplan-Meier analysis was also performed to determine OS. Log-rank tests were used to compare survival rates between subgroups. With R's "survival" package, we conducted univariate and multivariate Cox proportional hazard analyses. Hazard ratios (HR), 95% confidence intervals, and *p* values were calculated.

3. Results

3.1. Identification of Prognostic DDR-Related DEGs in HCC. TCGA datasets were used to screen dysregulated DDR-related DEGs between HCC cases and nontumor specimens. A total of ten DDR-related genes were differentially expressed between nontumorous tissues and tumorous tissues. Using a univariate Cox analysis (Figure 1(a)), a link was found between OS and 9 of them. A heatmap was used to show the expression pattern of the nine prognostic DDR-

related DEGs (Figure 1(b)). As a prognostic marker, 9 DDR-related genes were kept (Figure 1(c)), and the overall risk ratio for each gene was calculated. As shown in Figure 1(d), these genes are related. In addition, we performed GO assays and found that the 151 survival-related DDR-related genes were mainly associated with regulation of cell cycle phase transition, nuclear division, chromosomal region, nuclear chromosome, ATPase activity, and damaged DNA binding (Figure S1A). Moreover, the results of KEGG assays confirmed that the 151 survival-related DDR-related genes were mainly associated with cell cycle, PI3K-AKT pathway, DNA replication, p53 signaling pathway, and platinum drug resistance (Figure S1B).

3.2. Development of a Prognostic Gene Signature Based on DDR-Related Genes. Three DDR-related gene signatures were screened using LASSO and Cox regression analyses in order to predict OS in HCC patients from TCGA datasets:

	pvalue	Hazard ratio
Age	0.174	1.010 (0.996–1.025)
Gender	0.188	0.776 (0.531–1.132)
Grade	0.330	1.133 (0.881–1.457)
Stage	<0.001	1.680 (1.369–2.062)
riskScore	<0.001	3.326 (2.220–4.984)

(a)

	pvalue	Hazard ratio
Stage	<0.001	1.506 (1.211–1.872)
riskScore	<0.001	2.665 (1.765–4.025)

(b)

	pvalue	Hazard ratio
Gender	0.031	0.502 (0.268–0.940)
Age	0.800	1.004 (0.973–1.036)
Stage	<0.001	2.203 (1.519–3.195)
riskScore	<0.001	5.897 (3.074–11.312)

(c)

	pvalue	Hazard ratio
Gender	0.003	0.371 (0.194–0.710)
Stage	<0.001	2.060 (1.453–2.920)
riskScore	<0.001	5.175 (2.650–10.104)

(d)

FIGURE 4: The OS by Cox regression model's univariate and multivariate evaluations. Datasets (a, b) from the TCGA. Datasets (c, d) from the ICGC.

expression of CDC20 (∗0.0496), TTK (∗0.244), and CENPA (∗0.245) (Figures 2(a) and 2(b)). Patients were divided equally into low-risk and high-risk groups. Patients with low-risk marks had a greater survival rate than those with high-risk marks ($p < 0.01$, Figure 3(a)). According to time-dependent ROC analysis, the predictive precision of the DDR-related gene signature was 0.746 at 1 year, 0.712 at 2 years, and 0.670 at 3 years (Figure 3(b)). To examine the stability of the model built from the TCGA cohort, we divided the patients in the ICGC cohort into high-risk or low-risk groups based on the median value from the TCGA cohort. According to Figure 3(c), patients with a high-risk score had a shorter OS, similar to the results reported in the TCGA cohort. AUCs for the 8-gene signature were 0.768, 0.776, and 0.789 at 1, 2, and 3 years (Figure 3(d)). In univariate Cox analysis of TCGA cohorts, OS and risk markers showed a strong correlation (Figure 4(a)). After controlling for additional confounding variables, the risk score remained an independent predictor of OS (Figure 4(b)). A similar effect was also observed in the ICGC group (Figures 4(c) and 4(d)).

3.3. Risk Score for the Prognostic Model and Clinical Characteristics. The relationship between risk mark and clinical features of HCC patients in the TCGA cohort revealed no relationship between age and sex (Figures 5(a) and 5(b)). In contrast, HCC specimens with advanced grade and clinical stage had a greater risk mark (Figures 5(c) and

5(d)). A similar outcome was found in the ICGC cohort as well (Figures 5(e)–5(g)).

3.4. Immunity and Tumor Microenvironment Analysis. To better understand the relationship between risk marks and immunological state, we measured enrichment scores of various immune cell subpopulations, functions, and pathways. High-risk groups had significantly more components of the antigen presentation pathway in the TCGA cohort, such as aDCs, macrophages, Tfh, Th1 cells, and MHC class I. (Figures 6(a) and 6(b)). Figures 6(c) and 6(d) show that the high-risk group had significantly more DCs, iDCs, macrophages, and Th2 cells in ICGC datasets. The immune infiltration types C1 (wound healing), C2 (IFN-g dominant), C3 (inflammatory), C4 (lymphocyte deficient), C5 (immunologically silent), and C6 (tumor-inhibiting) have been identified in malignancies (TGF-β dominant). The HCC C6 immune subtype can be classified only in one patient sample, and the C5 immune subtype cannot be classified in any patient sample. Therefore, the immunological subtypes C5 and C6 were omitted. A correlation was discovered between the two risk scores for HCC and immune infiltration, according to the TCGA-HCC data. A strong correlation was found between high-risk marks and C1 and a strong correlation between low-risk marks and C3 (Figure 6(e)).

3.5. The Expression of Prognostic Genes and Chemotherapy Response in Cancer Cells. Gene expression levels and

(a)

(b)

(c)

(d)

(e)

(f)

(g)
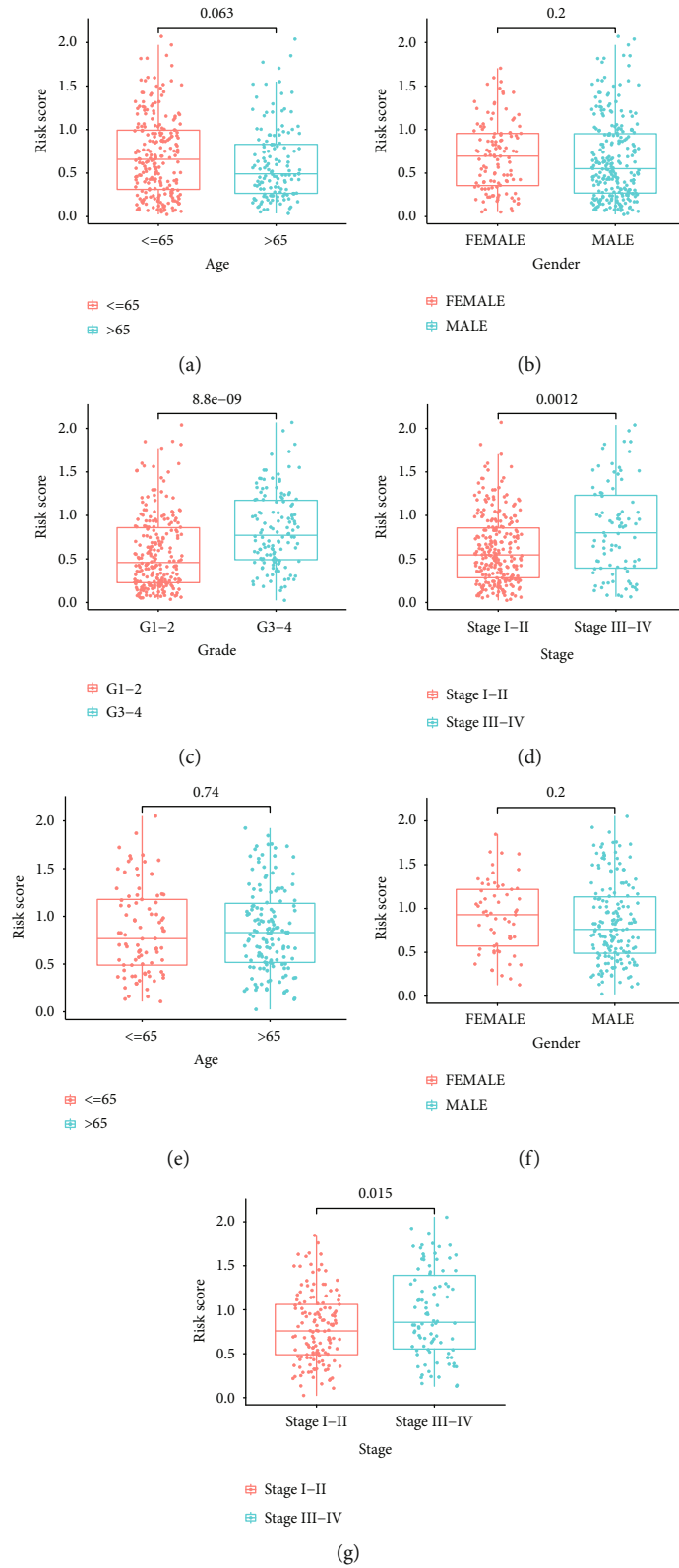
Figure 5: The risk score in different groups divided by clinical factors. TCGA cohort (a–d) and ICGC cohort (e, f): (a) age; (b) gender; (c) grade; (d) clinical stage; (e–g) age, gender, and clinical stage.

medication sensitivity were examined in NCI-60 cell lines to identify prognostic genes. Several genes were found to correlate with chemotherapy treatment sensitivity (Figure 7). For example, the enhanced expression of CENPA was related to increased treatment resistance to nelarabine, asparaginase, dexamethasone decadron, cladribine, and hydroxyurea. In

(a)

(b)

(c)

(d)

Figure 6: Continued.

(e)
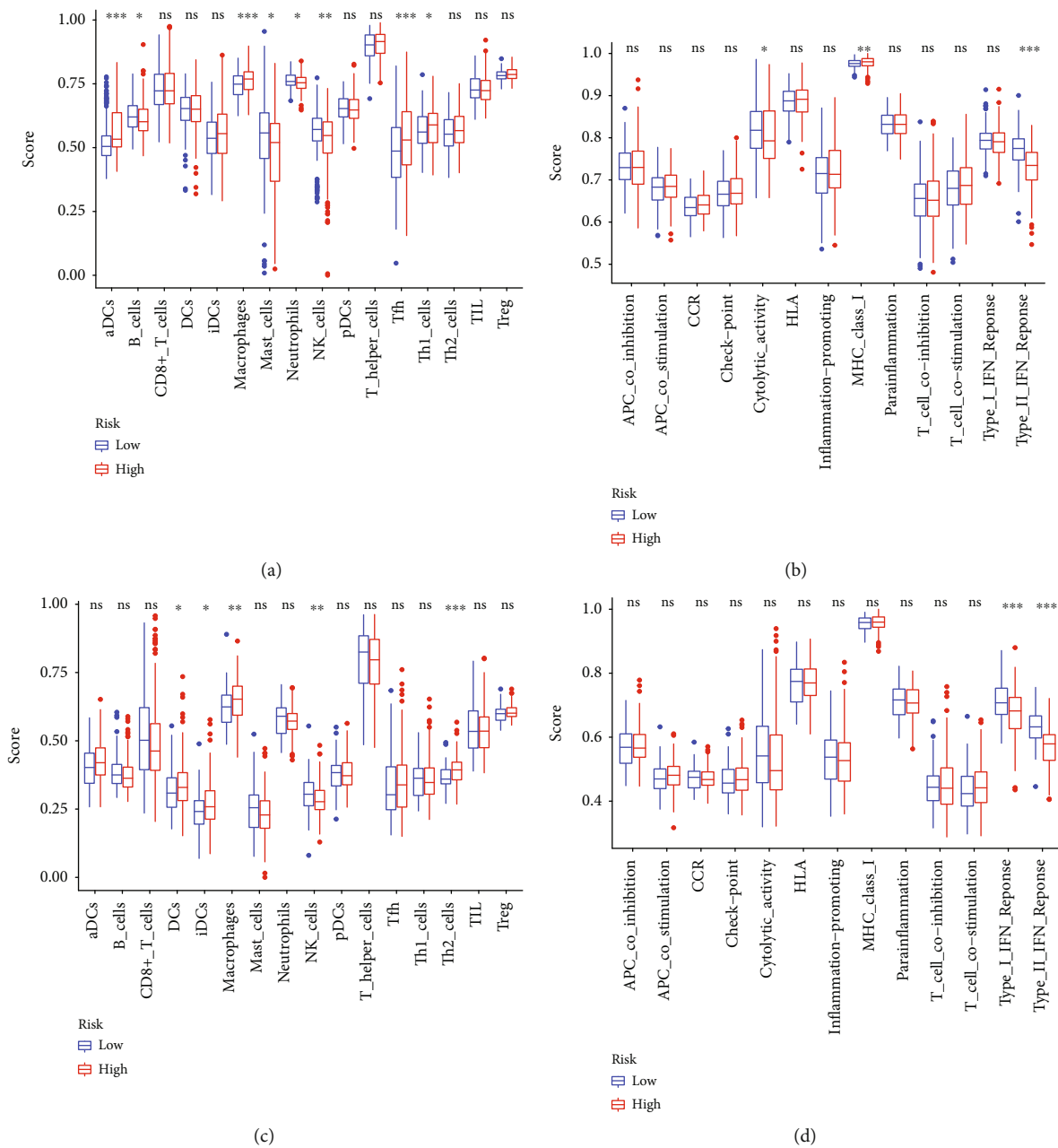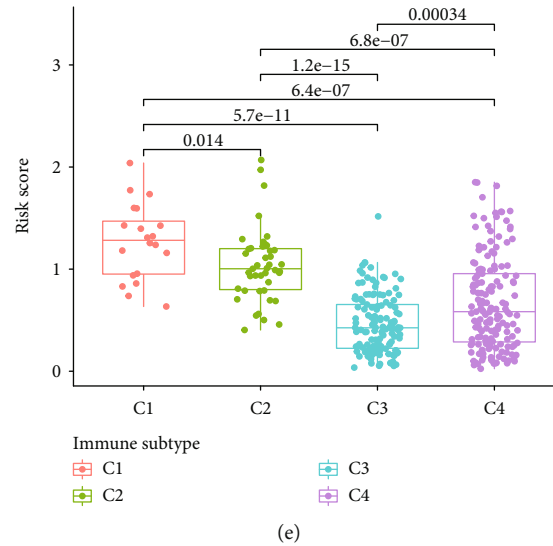
FIGURE 6: A correlation between the tumor microenvironment and risk markers. The characteristics of 16 immune cells (a, c) and 13 immune-related activities (b, d) were illustrated in boxplots. (e) Comparison of risk scores across several subtypes of immune infiltration.

cancer cells, increased TTK expression was linked to increased resistance to nelarabine, mithramycin, and actinomycin D, 6-thioguanine. CDC20 expression was also associated with higher treatment resistance to denileukin diftitox Ontak, 6-thioguanine, paclitaxel, vinorelbine, irofulven, and celecoxib.

4. Discussions

Cirrhosis is the leading cause of death in the liver, and HCC is on the rise [23]. A multidisciplinary approach is required to treat HCC, including hepatologists, surgeons, radiologists, pathologists, and oncologists [24, 25]. Researchers have studied the pathophysiology and epidemiology of HCC for several years. The prognosis for HCC remains dismal, despite substantial advances in surgical and medicinal treatments. This illness develops because early-stage detection methods are lacking [26, 27]. As well as being a very diverse illness, median survival times vary greatly between individuals of comparable TNM stages. In order to tailor prevention and treatment for HCC, it will be crucial to find a powerful prognostic marker that can dynamically reflect the biological progression of the disease [28, 29]. The DDR process affects treatment response and tumor development in patients with HCC. To predict the prognosis of HCC, Li et al. developed a seven-gene signature linked to DNA repair [30]. In order to create a prediction model, genes involved in DDR should be analyzed for their expression patterns.

By analyzing the expression profiles of DDR-related genes in the TCGA database, this study examined the association between DDR-related genes and the prognosis of HCC patients. DDR-related genes were not observed to be differentially expressed between HCC specimens and nontumor specimens at first. Based on the univariate Cox regression analysis, nine DDR-related genes were associated with OS. We also developed the OS-related prediction model, a

standalone prognostic indicator for HCC patients, using multivariate Cox regression to identify the three DDR-related genes (CDC20, TTK, and CENPA). As high-throughput sequencing technology and bioinformatics have advanced rapidly, many signals have been developed for predicting prognosis in HCC patients. In contrast to our investigations, these investigations lacked independent validation using external datasets. Additionally, they ignored conventional clinical measures in favor of genetic biomarkers. The study shows promise for therapeutic applications by integrating clinical indicators with the autophagy-related signature to predict survival in HCC patients.

There is evidence that CDC20, TTK, and CENPA were expressed and active in several types of cancer. Zhao et al. demonstrated that knocking down CDC20 improved radiation treatment of growth retardation in HepG2 after radiation activated P53. HCC cells may undergo DNA damage, DNA repair loss, G2/M arrest, and apoptosis when CDC20 is downregulated and radiation is applied [31]. According to Yang et al., CDC20 expression in HCC and HCC cell lines is associated with poor prognosis. Cell proliferation, migration, and invasion of HCC were inhibited by silencing CDC20. Furthermore, silencing CDC20 increased E-cadherin expression while decreasing N-cadherin, vimentin, and Ki-67 expression [32]. A total of 77.63 percent (118/152) of HCC tissues overexpressed TTK, according to Liu et al. [33]. TTK expression and portal vein tumor thrombus presence showed a positive correlation. In HCC, TTK's promoter was demethylated, increasing its expression. Tests in vitro found that TTK improved anchorage-independent proliferation, cell migration, and anchorage independence. Based on the results of the following study, TTK activated the Akt/mTOR pathway in a p53-dependent manner. In several studies, TTK has also been shown to be predictive of HCC. A prior study found that tumor tissues exhibited a marked increase in CENPA mRNA compared to
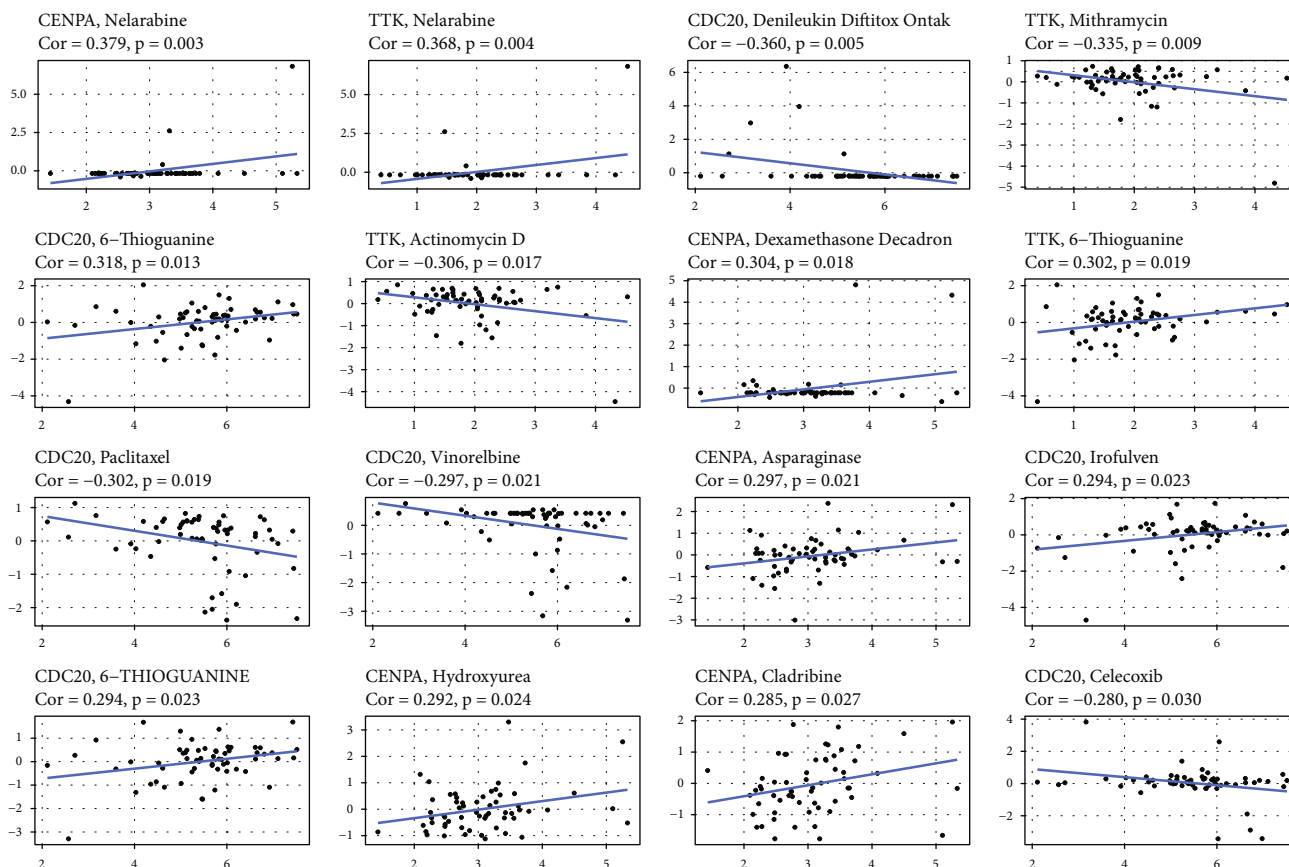
FIGURE 7: The scatter plot showed the relationship between prognostic gene expression and medication sensitivity.

neighboring tissues. In HCC patients, increased CENPA mRNA was associated with elevated alpha-fetoprotein, advanced TNM stage, larger tumor size, advanced AJCC stage, and advanced pathology grade. CENPA, however, was not examined in earlier research. There have been few studies on the roles of CDC20, TTK, and CENPA. This study validated earlier findings that CDC20, TTK, and CENPA are upregulated in HCC. CDC20, TTK, and CENPA prognostic models showed remarkable capability in predicting clinical prognoses for patients with HCC.

According to new research, immune cells in the TME play an important role in cancer development [34]. Among the innate immune cells that can promote or support tumor growth are macrophages, neutrophils, dendritic cells, innate lymphoid cells, myeloid-derived suppressor cells, and natural killer cells [35, 36]. In the TME, cancer cells showed iron ion aggregation during active proliferation. Controlling ferroptosis, therefore, may effectively eliminate tumor cells in terms of iron homeostasis. Besides monitoring tumors and tumor immunity, ferroptosis also has an important immunological function. By combining an examination of distinct immune infiltration densities in the tumor core and the invasive margin, it has been shown that the prognosis of BC patients with poor clinicopathological criteria may be accurately predicted [37, 38]. According to a previous study, the prognosis for patients with HCC is related to the pattern

of infiltrating immune cells in TME, and macrophage-associated cytokines may be used to predict PD-L1 levels in these patients [39]. Immune score models based on immune cell infiltration can also predict the prognosis and efficacy of chemotherapy treatment for HCC patients [40, 41]. A study of the prognostic value of the immune infiltration alteration is therefore worthwhile and practical. This study demonstrated that high levels of aDCs, macrophages, Tfh, Th1 cells, and MHC class I were detected in the high-risk group, indicating disruption of immune regulation. Due to this, it may be logical to believe that the antitumor immunity of the high-risk group is weakening, which may explain its poor prognosis.

The drug sensitivity of various anticancer medicines was determined in the treatment of patients with HCC [42, 43]. Data from NCI-60 cell lines showed that higher expression of several prognostic genes was associated with enhanced drug resistance to numerous FDA-approved chemotherapeutic medicines, including denileukin diftitox Ontak, paclitaxel, vinorelbine, and irofulven [44]. Few medicines were also more sensitive to drugs due to a range of prognostic genes. CENPA expression was associated with higher drug resistance to nelarabine, asparaginase, dexamethasone Decadron, cladribine, and hydroxyurea in cancer cells. In order to overcome drug resistance, chemotherapeutic drugs must be tested according to the molecular subtypes of patients.

A range of studies were applied to construct prognostic signatures and numerous verifications using bioinformatics tools and statistical approaches, but there were still some limitations. The samples were provided by a single database, so they may be unrepresentative. Besides, no in vitro or in vivo experiments were conducted. Our future study will focus on the shortcomings listed above.

5. Conclusions

A DDR-related signature has been identified as an independent predictor of HCC. A comprehensive analysis of the signature's role in the immune landscape and therapies was conducted. Informing the treatment of HCC with this hallmark could be powerful and promising.

Data Availability

The data supporting the conclusions of this article will be made available by the authors, without undue reservation.

Conflicts of Interest

The authors declare that there are no conflicts of interest.

Acknowledgments

Supplementary Materials

Figure S1: function analysis of 151 survival-related DDR-related genes. (A) GO enrichment analysis. (B) KEGG analysis. (Supplementary Materials)

References

[1] A. Villanueva, "Hepatocellular carcinoma," *The New England Journal of Medicine*, vol. 380, no. 15, pp. 1450–1462, 2019.

[2] G. M. Mranda, Z. P. Xiang, J. J. Liu, T. Wei, and Y. Ding, "Advances in prognostic and therapeutic targets for hepatocellular carcinoma and intrahepatic cholangiocarcinoma: the Hippo signaling pathway," *Frontiers in Oncology*, vol. 12, article 937957, 2022.

[3] M. Komuta and M. M. Yeh, "A review on the update of combined hepatocellular cholangiocarcinoma," *Seminars in Liver Disease*, vol. 40, no. 2, pp. 124–130, 2020.

[4] K. M. Kee and S. N. Lu, "Diagnostic efficacy of ultrasound in hepatocellular carcinoma diagnosis," *Expert Review of Gastroenterology & Hepatology*, vol. 11, no. 4, pp. 277–279, 2017.

[5] R. G. Gish, "Hepatocellular carcinoma: overcoming challenges in disease management," *Clinical Gastroenterology and Hepatology: the official clinical practice journal of the American Gastroenterological Association*, vol. 4, no. 3, pp. 252–261, 2006.

[6] A. S. Befeler and A. M. Di Bisceglie, "Hepatocellular carcinoma: diagnosis and treatment," *Gastroenterology*, vol. 122, no. 6, pp. 1609–1619, 2002.

[7] Q. Gao, Y. Shi, X. Wang, J. Zhou, S. Qiu, and J. Fan, "Translational medicine in hepatocellular carcinoma," *Frontiers of Medicine*, vol. 6, no. 2, pp. 122–133, 2012.

[8] V. Vilgrain, M. Abdel-Rehim, A. Sibert, and M. Ronot, "Clinical studies in hepatocellular carcinoma," *Future Oncology*, vol. 10, no. 15s, 15 Suppl, pp. 13–16, 2014.

[9] L. Bolondi, "State of the art: hepatocellular carcinoma," *Future Oncology*, vol. 10, no. 15s, pp. 1–6, 2014.

[10] N. Chatterjee and G. C. Walker, "Mechanisms of DNA damage, repair, and mutagenesis," *Environmental and Molecular Mutagenesis*, vol. 58, no. 5, pp. 235–263, 2017.

[11] R. P. Sinha and D. P. Häder, "UV-induced DNA damage and repair: a review," *Photochemical & Photobiological Sciences: Official journal of the European Photochemistry Association and the European Society for Photobiology*, vol. 1, no. 4, pp. 225–236, 2002.

[12] W. L. Santivasi and F. Xia, "Ionizing radiation-induced DNA damage, response, and repair," *Antioxidants & Redox Signaling*, vol. 21, no. 2, pp. 251–259, 2014.

[13] W. P. Roos, A. D. Thomas, and B. Kaina, "DNA damage and the balance between survival and death in cancer biology," *Nature Reviews Cancer*, vol. 16, no. 1, pp. 20–33, 2016.

[14] M. Goldstein and M. B. Kastan, "The DNA damage response: implications for tumor responses to radiation and chemotherapy," *Annual Review of Medicine*, vol. 66, no. 1, pp. 129–143, 2015.

[15] M. Dizdaroglu and P. Jaruga, "Mechanisms of free radical-induced damage to DNA," *Free Radical Research*, vol. 46, no. 4, pp. 382–419, 2012.

[16] A. Agarwal, M. K. Panner Selvam, S. Baskaran, and C. L. Cho, "Sperm DNA damage and its impact on male reproductive health: a critical review for clinicians, reproductive professionals and researchers," *Expert Review of Molecular Diagnostics*, vol. 19, no. 6, pp. 443–457, 2019.

[17] U. S. Srinivas, B. W. Q. Tan, B. A. Vellayappan, and A. D. Jeyasekharan, "ROS and the DNA damage response in cancer," *Redox Biology*, vol. 25, p. 101084, 2019.

[18] T. Reisländer, F. J. Groelly, and M. Tarsounas, "DNA damage and cancer immunotherapy: a STING in the tale," *Molecular Cell*, vol. 80, no. 1, pp. 21–28, 2020.

[19] C. Wang, H. Wang, C. Lieftink et al., "CDK12 inhibition mediates DNA damage and is synergistic with sorafenib treatment in hepatocellular carcinoma," *Gut*, vol. 69, no. 4, pp. 727–736, 2020.

[20] M. Lulli, L. Del Coco, T. Mello et al., "DNA damage response protein CHK2 regulates metabolism in liver cancer," *Cancer Research*, vol. 81, no. 11, pp. 2861–2873, 2021.

[21] Z. Zhao, K. He, Y. Zhang et al., "XRCC2 repairs mitochondrial DNA damage and fuels malignant behavior in hepatocellular carcinoma," *Cancer Letters*, vol. 512, pp. 1–14, 2021.

[22] A. L. Gomes, A. Teijeiro, S. Burén et al., "Metabolic inflammation-associated IL-17A causes non-alcoholic steatohepatitis and hepatocellular carcinoma," *Cancer Cell*, vol. 30, no. 1, pp. 161–175, 2016.

[23] A. M. Moon, A. G. Singal, and E. B. Tapper, "Contemporary epidemiology of chronic liver disease and cirrhosis," *Clinical Gastroenterology and Hepatology*, vol. 18, no. 12, pp. 2650–2666, 2020.

[24] A. Garrido and N. Djouder, "Cirrhosis: a questioned risk factor for hepatocellular carcinoma," *Trends in Cancer*, vol. 7, no. 1, pp. 29–36, 2021.

[25] G. Fattovich, T. Stroffolini, I. Zagni, and F. Donato, "Hepatocellular carcinoma in cirrhosis: incidence and risk factors," *Gastroenterology*, vol. 127, no. 5, pp. S35–S50, 2004.

[26] B. Sangro, P. Sarobe, S. Hervás-Stubbs, and I. Melero, "Advances in immunotherapy for hepatocellular carcinoma," *Nature Reviews Gastroenterology & Hepatology*, vol. 18, no. 8, pp. 525–543, 2021.

[27] T. El Jabbour, S. M. Lagana, and H. Lee, "Update on hepatocellular carcinoma: pathologists' review," *World Journal of Gastroenterology*, vol. 25, no. 14, pp. 1653–1665, 2019.

[28] J. C. Nault and A. Villanueva, "Biomarkers for hepatobiliary cancers," *Hepatology (Baltimore, Md)*, vol. 73, no. S1, pp. 115–127, 2021.

[29] F. De Stefano, E. Chacon, L. Turcios, F. Marti, and R. Gedaly, "Novel biomarkers in hepatocellular carcinoma," *Digestive and Liver Disease: official journal of the Italian Society of Gastroenterology and the Italian Association for the Study of the Liver*, vol. 50, no. 11, pp. 1115–1123, 2018.

[30] N. Li, L. Zhao, C. Guo, C. Liu, and Y. Liu, "Identification of a novel DNA repair-related prognostic signature predicting survival of patients with hepatocellular carcinoma," *Cancer Management and Research*, vol. Volume 11, pp. 7473–7484, 2019.

[31] S. Zhao, Y. Zhang, X. Lu et al., "CDC20 regulates the cell proliferation and radiosensitivity of P 53 mutant HCC cells through the Bcl-2/Bax pathway," *International Journal of Biological Sciences*, vol. 17, no. 13, pp. 3608–3621, 2021.

[32] G. Yang, G. Wang, Y. Xiong et al., "CDC20 promotes the progression of hepatocellular carcinoma by regulating epithelial-mesenchymal transition," *Molecular Medicine Reports*, vol. 24, no. 1, 2021.

[33] M. Liu, Y. Zhang, Y. Liao et al., "Evaluation of the antitumor efficacy of RNAi-mediated inhibition of CDC20 and heparanase in an orthotopic liver tumor model," *Cancer Biotherapy & Radiopharmaceuticals*, vol. 30, no. 6, pp. 233–239, 2015.

[34] L. Bejarano, M. J. C. Jordão, and J. A. Joyce, "Therapeutic targeting of the tumor microenvironment," *Cancer Discovery*, vol. 11, no. 4, pp. 933–959, 2021.

[35] D. Chen, X. Zhang, Z. Li, and B. Zhu, "Metabolic regulatory crosstalk between tumor microenvironment and tumor-associated macrophages," *Theranostics*, vol. 11, no. 3, pp. 1016–1030, 2021.

[36] L. Laplane, D. Duluc, A. Bikfalvi, N. Larmonier, and T. Pradeu, "Beyond the tumour microenvironment," *International Journal of Cancer*, vol. 145, no. 10, pp. 2611–2618, 2019.

[37] T. Wu and Y. Dai, "Tumor microenvironment and therapeutic response," *Cancer Letters*, vol. 387, pp. 61–68, 2017.

[38] D. C. Hinshaw and L. A. Shevde, "The tumor microenvironment innately modulates cancer progression," *Cancer Research*, vol. 79, no. 18, pp. 4557–4566, 2019.

[39] C. Donisi, M. Puzzoni, P. Ziranu et al., "Immune checkpoint inhibitors in the treatment of HCC," *Frontiers in Oncology*, vol. 10, article 601240, 2021.

[40] H. Li, C. W. Li, X. Li et al., "MET inhibitors promote liver tumor evasion of the immune response by stabilizing PDL1," *Gastroenterology*, vol. 156, no. 6, pp. 1849–1861.e13, 2019.

[41] B. Zhang, B. Tang, J. Gao, J. Li, L. Kong, and L. Qin, "A hypoxia-related signature for clinically predicting diagnosis, prognosis and immune microenvironment of hepatocellular carcinoma patients," *Journal of Translational Medicine*, vol. 18, no. 1, p. 342, 2020.

[42] T. Inoue and Y. Tanaka, "Novel biomarkers for the management of chronic hepatitis B," *Clinical and Molecular Hepatology*, vol. 26, no. 3, pp. 261–279, 2020.

[43] G. Yildiz, "Integrated multi-omics data analysis identifying novel drug sensitivity-associated molecular targets of hepatocellular carcinoma cells," *Oncology Letters*, vol. 16, no. 1, pp. 113–122, 2018.

[44] L. Shen, Y. Kondo, S. Ahmed et al., "Drug sensitivity prediction by CpG island methylation profile in the NCI-60 cancer cell line panel," *Cancer Research*, vol. 67, no. 23, pp. 11335–11343, 2007.

Research Article

Prognostic Value of UBE2T and Its Correlation with Immune Infiltrates in Lung Adenocarcinoma

Feng Xu,[1] Na Xiong,[2] Yuhong Yuan,[3] and Jun Liu [4]

[1]*Department of Respiratory Diseases, Qingdao Chengyang District People's Hospital, Qingdao, China*
[2]*Critical Care Medicine, Qingdao Eighth People's Hospital, Qingdao, China*
[3]*Department of Pharmacy Qingdao Chengyang District People's Hospital, Qingdao, China*
[4]*Department of General Surgery, Gaomi Hospital of Traditional Chinese Medicine, Gaomi, China*

Correspondence should be addressed to Jun Liu; ljzhuren@sina.com

Non-small cell lung cancer has a subtype with a high morbidity and mortality rate called lung adenocarcinoma (LUAD). It is critical to locate reliable prognostic biomarkers for LUAD at this time. Ubiquitin-conjugating enzyme E2T (UBE2T) has been found in numerous malignancies; however, its expression level and potential functions in LUAD are not completely understood at this time. A differentially expressed gene (DEG) screening method was used to identify genes that were expressed differently in 516 samples from LUAD and 59 samples from TCGA datasets. Clinicopathological markers were correlated with UBE2T expression. Using the Kaplan–Meier plotter database, UBE2T was evaluated for its prognostic value in the context of LUAD. In order to examine the importance of independent prognostic factors, both univariable and multivariable Cox regression models were applied. TIMER and CIBERSORT were utilized in order to investigate the connection that exists between UBE2T expression and tumor-infiltrating immune cells. This study collected 578 DEGs in total, as follows: 171 genes were significantly increased, while 408 genes were significantly decreased. We identified 9 survival-related DEGs in LUAD, including ASF1B, CA9, CCNB2, CCNE1, RRM2, SAPCD2, TCN1, TPX2, and UBE2T. Our attention focused on UBE2T, which was highly expressed in LUAD. A correlation was also found between high UBE2T expression and gender, age, advanced clinical stage, and decreased overall survival. In addition, multivariate analysis demonstrated UBE2T expression to be a significant independent diagnostic factor for patients suffering from LUAD. UBE2T was positively correlated with resting T cell CD4+ memory, myeloid dendritic cell resting, mast cell activated, macrophage M2, and B cell plasma, whereas it was negatively correlated with resting T cell CD4+ memory, MDC resting, MDC activated, macrophage M2, and B cell plasma. Overall, high expression levels of UBE2T correlated with poor overall survival in patients with LUAD, and UBE2T was an independent predictor involved in immune infiltration of LUAD. These findings offer fresh perspectives that contribute to our comprehension of the evolution of LUAD.

1. Introduction

Lung cancer is considered to be one of the most common malignant tumors all over the world [1, 2]. It has virtually reached the position of being the first major contributor to death among those living in China's urban areas [3, 4]. The majority of lung malignancies, approximately 70–80 percent, are diagnosed as non-small cell lung cancer (NSCLC) [5, 6]. Lung adenocarcinoma is a main subtype of NSCLC and is often diagnosed at an advanced disease stage [7]. Early surgical resection is currently the recommended course of treatment for patients diagnosed with LUAD. Following the completion of any necessary surgical procedures, the patient will undergo further chemotherapy to further increase their chances of survival [8, 9]. However, half of all people who have LUAD will suffer a relapse at some point and will ultimately pass away as a result of the disease's return. A reliable method of predicting patient survival status is needed in order to facilitate the diagnosis of early-stage LUAD and to provide patients with reasonable treatment regimens without wasting medical resources or delaying their recovery.

There has been a shift in the therapy paradigm for LUAD over the past few years due to the use of immunotherapies for the therapy of patients suffering from LUAD [10, 11]. Since January 2015, there have been substantial advancements made in cancer immunotherapy [12]. Inhibiting programmed cell death protein 1 is successful in treating Hodgkin's lymphoma, generating optimism about its potential to change the way the disease is typically treated [13, 14]. Immunotherapy using inhibitors of programmed death-1, programmable death ligand-1, and cytotoxic T lymphocyte associated antigen-4 has been demonstrated to possess potential anticancer benefits in malignant melanoma [15, 16]. Growing data suggest that tumor-infiltrating immune cells in the tumor microenvironment contribute to tumor development, aggressiveness, and responsiveness to therapy [17, 18]. Growing evidence supporting the idea that cancer lymphocytes, such as cancer macrophages and cancer neutrophils, affect the prognosis and the efficiency of chemotherapy and immunotherapy is also rising [19]. Additionally, it has become more and more common to block immunological checkpoints like PD-1/PD-L1 and CTLA-4 in malignant tumors [20, 21]. The majority of malignancies do not react well to immunotherapy with a single drug because the tumor microenvironment contains immune elements. Clarifying immunogen types of tumor-immune interactions as well as finding new immune-related biomarkers and targeted therapies in LUAD are urgently needed.

The TCGA project, which was completed just recently, includes matched clinical and molecular data of numerous tumors, which makes it possible to conduct a systematic investigation of the impact that single gene expression has on patients' chances of survival. In this study, we aimed to explore novel biomarkers via analyzing TCGA datasets. Using LUAD cohorts-based TCGA datasets, we screened differentially expressed genes (DEGs). We identified a novel LUAD-related gene ubiquitin-conjugating enzyme E2T (UBE2T) which was significantly expressed in LUAD and predicted a poor prognosis. UBE2T plays a significant function in a variety of pathological processes in a manner that is E2-enzyme-dependent. The reason for this is that it belongs to the E2 family of proteins, which are responsible for conjugating ubiquitin to substrates [22]. The expression of UBE2T has been reported to be dysregulated in several tumors, including cancers of the stomach, liver, and esophagus [23–25]. Despite this, there has been no investigation of the prognostic value of UBE2T in LUAD. Based on our findings, a new prognostic biomarker that is involved in the microenvironment of tumors may be developed for LUAD.

2. Materials and Methods

2.1. Acquiring and Processing Raw Data.
Over 10,000 cancer patients whose tumors were classified into one of 33 categories have been assessed and evaluated by the TCGA research network. To obtain transcriptome data of 33 different tumor types, we searched the TCGA database (https://portal.gdc.cancer.gov/). A total of 33 cancer types were studied.

They were OV, PAAD, PRAD, READ, SKCM, STAD, TGCT, THCA, THYM, UCEC, and UCS. ACC, BLCA, BRCA, COAD, DLBC, ESCA, GBM, HNSC, KICH, KIRC, KIRP, LAML, LGG, LIHC, and UCS. The full names of all tumors are shown in Table S1.

2.2. Genes Differentially Expressed in LUAD Identified.
Data from our research were mapped against version 38 (hg38) of the human genome using the STAR2 software. This allowed us to generate data on gene expression. The Sam Tools were utilized in order to identify the mapped reads that had a quality of 10 or higher. The feature count served as the reference transcriptome to define the read counts for each gene. With the aid of the edger package in R, differential expression analysis was conducted, and tumor samples were compared with normal samples that were matched to them in order to identify DEGs [26]. Among the genes that were selected for differential expression between tumor and normal samples, their false discovery rates (FDR) are less than 0.05 and their absolute log2 fold changes (log FC) are greater than 4.

2.3. An Analysis of the Expression of UBE2T in Pan-Cancers.
The TCGA and Genotype Tissue Expression (GTEx) projects provided data on the differential expression of UBE2T between tumor and normal tissue that was matched to a tumor. A tissue bank and data resource called GTEx has been established by the National Institutes of Health Common Fund (https://gtexportal.org). A total of 53 human normal tissues from about 1,000 people were examined for genetic variants, RNA sequencing, and additional molecular traits. We chose log2 (TPM+1) converted expression data for plotting, which was how we chose the parameters.

2.4. Infiltration Cells and Their Marker Genes Are Correlated with the UBE2T Expression.
Whether UBE2T expression and immune cell presence were correlated was investigated using the Tumor Immune Estimation Resource database (TIMER) [27]. The TIMER database greatly assisted in the evaluation and integration of immune cells for RNA sequencing samples from the TCGA. These immune cells are thought to contain human B cells, human CD4+ T cells, human CD8+ T cells, human macrophages, human neutrophils, and human dendritic cells. The proportional fractions of 22 different immune cell types invading each tumor sample were calculated using the R tool CIBERSORT.

2.5. An Analysis of the Relationship between UBE2T Gene Expression and Immune Markers.
In this research, we examined the relationship between more than 40 immune checkpoint genes and UBE2T expression. The R software program "GGplot2" was used to retrieve these immune checkpoint genes, estimate the correlation between gene expression and immune checkpoint gene expression, and generate a diagonal heat map [28]. Using a diagonal heat map, we were able to illustrate the association. As shown in the upper triangle, the P value and significance of the

correlation are expressed in color, while the correlation coefficient is illustrated in the lower triangle. The * in the graph indicates a significant correlation P less than 0.05, the ** represents a significant correlation P less than 0.01, and the *** indicates a significant personality P less than 0.001.

2.6. Statistical Analysis.

The data were examined using the R program (Version 3.6.3, The R Foundation for Statistical Computing). The unpaired t test was applied to test the differential expression of UBE2T in cancer tissues compared to adjacent nonmalignant tissues. The log-rank test was used to evaluate the Kaplan–Meier survival curves. The Cox regression model for multivariate analysis was used to ascertain the existence of independent prognostic variables. A P value of less than 0.05 was used to determine a statistical significance.

3. Results

3.1. LUAD DEG Identification.

This study retrospectively analyzed data from 516 LUAD samples and 59 control samples from TCGA datasets. The DEGs were analyzed using the limma package. In total, 578 DEGs were identified: 171 were significantly upregulated and 408 were significantly downregulated (Figures 1(a) and 1(b)).

3.2. DEGs Associated with Survival in LUAD.

Then, we performed a Kaplan–Meier analysis on LUAD to screen for DEGs associated with survival in the context of survival caused by DEGs, with P less than 0.01. As shown in Figure 2, we identified 9 survival-related DEGs in LUAD, including ASF1B, CA9, CCNB2, CCNE1, RRM2, SAPCD2, TCN1, TPX2, and UBE2T. A PubMed search revealed that several of them have been reported in various types of tumors, including LUAD. However, no research has been conducted on the expression and function of UBE2T in LUAD. Thus, we focused on UBE2T.

3.3. Pan-Cancer Assays of UBE2T.

We examined the expression of UBE2T in several tumors and the normal tissues that bordered them to evaluate whether or not it is associated with malignancy. According to TCGA data, UBE2T mRNA expression was significantly higher in tumor tissues from the BLCA, BRCA, CESC, CHOL, COAD, ESCA, GBM, HNSC, KIRC, KIRP, LIHC, LUAD, LUSC, PAAD, PCPG, PRAD, READ, STAD, THCA, and UCEC than in normal tissues, suggesting that this molecule may play an oncogenic role in tumor progression (Figure 3). The analysis of UBE2T expression in cancer utilizing the TCGA and GTEx databases revealed a similar result as well (Figure S1). Besides, we further assessed the prognostic value of UBE2T for pancancer. The correlation between increased UBE2T expression and reduced overall survival in ACC, BRCA, KIRC, KIRP, LGG, LIHC, LUAD, MESO, OV, PAAD, STAD, and THYM is shown in Figure S2.

3.4. UBE2T in LUAD: Clinical Significance and Prognostic Value.

First, in contrast to nontumor specimens, we discovered a clear increase in UBE2T expression in LUAD tissues (Figures 4(a) and 4(b)). The link between UBE2T expression and a number of clinical variables was then investigated. Additionally, we discovered that high UBE2T expression was associated with gender (Figure 4(c)), age (Figure 4(d)), and advanced clinical stage (Figure 4(e)). Additionally, pTNM-stage and UBE2T expression were significantly correlated, according to univariate analysis (Figure 5(a)). The UBE2T expression and pTNM-stage were shown to be independent predictive variables after multivariate data analysis (Figure 5(b)).

The degree of immune infiltration in malignancies and the expression of UBE2T are correlated.

As a result of tumorigenesis, the growth process is a difficult one that is accompanied by several different phenomena, such as increased proliferation, resistance to apoptosis, increased angiogenesis, and escape from immunity, among other phenomena. TME is one of them that plays an important part. TILs not only inhibited the growth of tumors but also shielded cancer cells from being destroyed, making them an important player in the fight against cancer. To look into the potential connection between UBE2T expression and immune cell infiltration, data on immune cell infiltration from two independent sources were used in a correlation study. The findings of the TIMER2 and CIBERSOR tests revealed that UBE2T was favorably linked with the amount of immune cell infiltration in the TCGA pan-cancer model (Figure S3 and Figure 6). This study's key finding was that UBE2T correlated favorably with T cell gamma delta, T cell follicular helper, T cell CD4+ memory activated, NK cell activated, macrophage M0, and B cell naive and adversely with T cell CD4+ memory resting, myeloid dendritic cell resting, mast cell activated, macrophage M2, and B cell plasma (Figure 6). Data on immune cell infiltration from three sources were consistently examined.

3.5. Inhibition of Immune Checkpoints by the UBE2T Expression.

The relationship between the UBE2T expression and immunological checkpoint genes was examined using eight popular immune checkpoint genes. Figure S4 presents the findings. In a variety of cancers, UBE2T expression was associated favorably with the levels of numerous immune checkpoint genes, including UVM, THCA, LIHC, LGG, KIRC, and BLCA (Figure S4). On the other hand, it was discovered that the LAG3 expression and UBE2T expression were positively associated. The expression of UBE2T and immunological checkpoint genes was examined to see whether there was a relationship between them. The research used eight popular immune checkpoint genes.

4. Discussions

Everyone knows that lung cancer is the sort of cancer that causes the most fatalities worldwide [29]. Over 80% of all

(a)

(b)
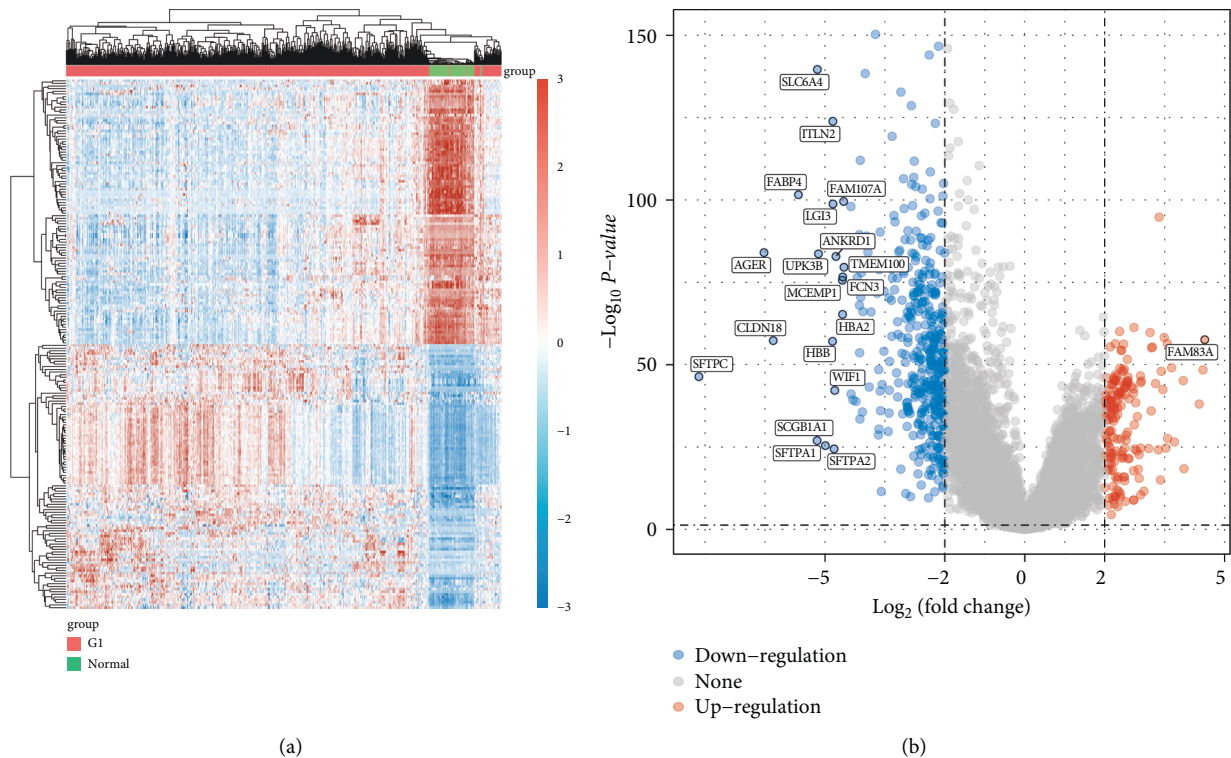
Figure 1: The identification of differentially expressed genes between LUAD specimens and nontumor specimens based on TCGA datasets. Both the heat map (a) and the volcano map (b) show differentially expressed genes in LUAD samples compared to normal samples. False discovery rates (FDR) are less than 0.05 and absolute log2 fold changes (log FC) are greater than 4.

instances of lung cancer are diagnosed in individuals with NSCLC, and about 50% of these patients have LUAD [30]. Despite improvements in medication regimens, the survival rate of individuals with LUAD remains very poor. In addition to the high-level variability of LUAD, there are a plethora of complicated etiologic factors that may make it challenging to predict the prognosis [31, 32]. Therefore, the creation of creative prognostic models is urgently required.

The TCGA database was used to get clinical and mRNA expression data from LUAD level 3 RNA seq for the present research. Then, we carried out a comparison of the differential expression between LUAD-positive samples and normal lung tissue. There were found to be 408 substantially downregulated genes and 171 significantly upregulated genes out of a total of 578 DEGs. Then, we discovered 9 DEGs in LUAD that were associated with survival. UBE2T was one among those that caught our interest. Previous studies have hypothesized that UBE2T may contribute to a variety of tumor forms. For instance, Yu et al. found that RACK1 was ubiquitinated and degraded at the lysine K172, K225, and K257 residues without the aid of an E3 ligase by UBE2T, which overactivated the Wnt/-catenin signaling pathway. This opens up a new window of possibility for particular GC patients who have abnormal Wnt/-catenin signaling [23]. Liu and his colleagues found that both the mRNA and protein levels of UBE2T were considerably greater in HCC tissues compared to nontumor tissues close to the tumor. It was also shown that UBE2T overexpression prevented hepatoma cell proliferation, colony formation,

tumorigenesis, migration, and invasion, but UBE2T inhibition had the reverse effect [24]. Additionally, it was shown that the UBE2T expression was markedly increased in GBM tissues and was associated with a bad prognosis. Blocking UBE2T dramatically decreased cell invasion and migration, according to in vitro study. This was done by stabilizing GRP78 and controlling EMT [33]. UBE2T may have previously been shown to promote both autophagy and proliferation, which raises the possibility that by inhibiting this gene, lung cancer cells may not go through autophagy. It was discovered that the p53/AMPK/mTOR signaling pathway was engaged during UBE2T-mediated autophagy, proving that UBE2T induced autophagy via this mechanism. However, the prognostic value of UBE2T has not been investigated. In this study, we examined the associations between the expression of UBE2T and several clinical factors. We also found that advanced clinical stages, gender, and age were associated with higher UBE2T expression. Multivariate analysis was used to identify the p-TNM stage and UBE2T expression as independent prognostic factors. Our study showed that UBE2T has the potential to be used as a sophisticated prognostic biomarker for LUAD patients. Our findings were consistent with previous results that UBE2T may serve as a tumor promotor.

According to current thinking, TME significantly affects the clinical treatment response and prognosis of patients with malignancies [34]. This idea is supported by the advancement of precise and high-throughput technology. Immune cells that have invaded tumor patients' TMEs have
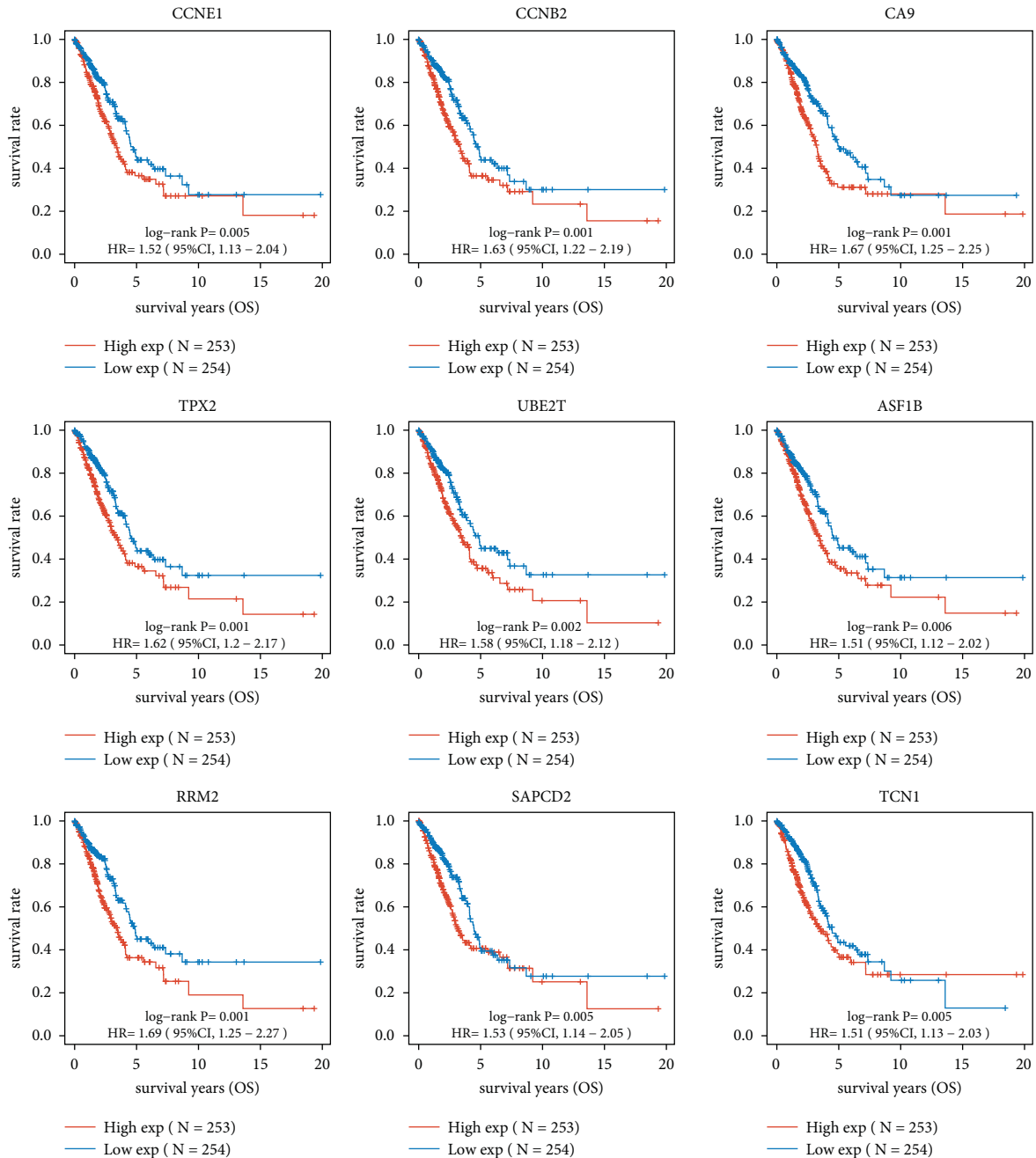
FIGURE 2: Identification of survival-related DEGs in LUAD by the use of Kaplan–Meier curves.

been proven in an increasing number of studies to have either a pro- or an antitumorigenic function [35, 36]. A positive prognosis for LUAD patients is related to immune cell infiltration in tumors, according to Rachel and others. The TCGA database has made it feasible to gather several global gene expression profiles as well as clinical information. In accordance with our findings, UBE2T was negatively correlated with T cell CD4+ memory resting, myeloid dendritic cell resting, mast cell activated, macrophage M2, and B cell plasma, and positively correlated with T cell gamma delta, T cell follicular helper, T cell CD4+

memory activated, NK cell activated, and B cell naive. Pancancer tests have also shown that UBE2T is critical for TME.

The field of cancer treatment, LUAD in particular, has lately experienced a drastic upheaval as a result of considerable advancements in immunotherapy [37]. First-line pembrolizumab, an immune checkpoint inhibitor that targets PD-1, in combination with pemetrexed-carboplatin continues to demonstrate increased response and survival in advanced NSCLC in comparison to chemotherapy alone [38, 39]. Durvalumab, a human IgG1 monoclonal antibody that targets PD-L1, may prolong overall survival in Stage III
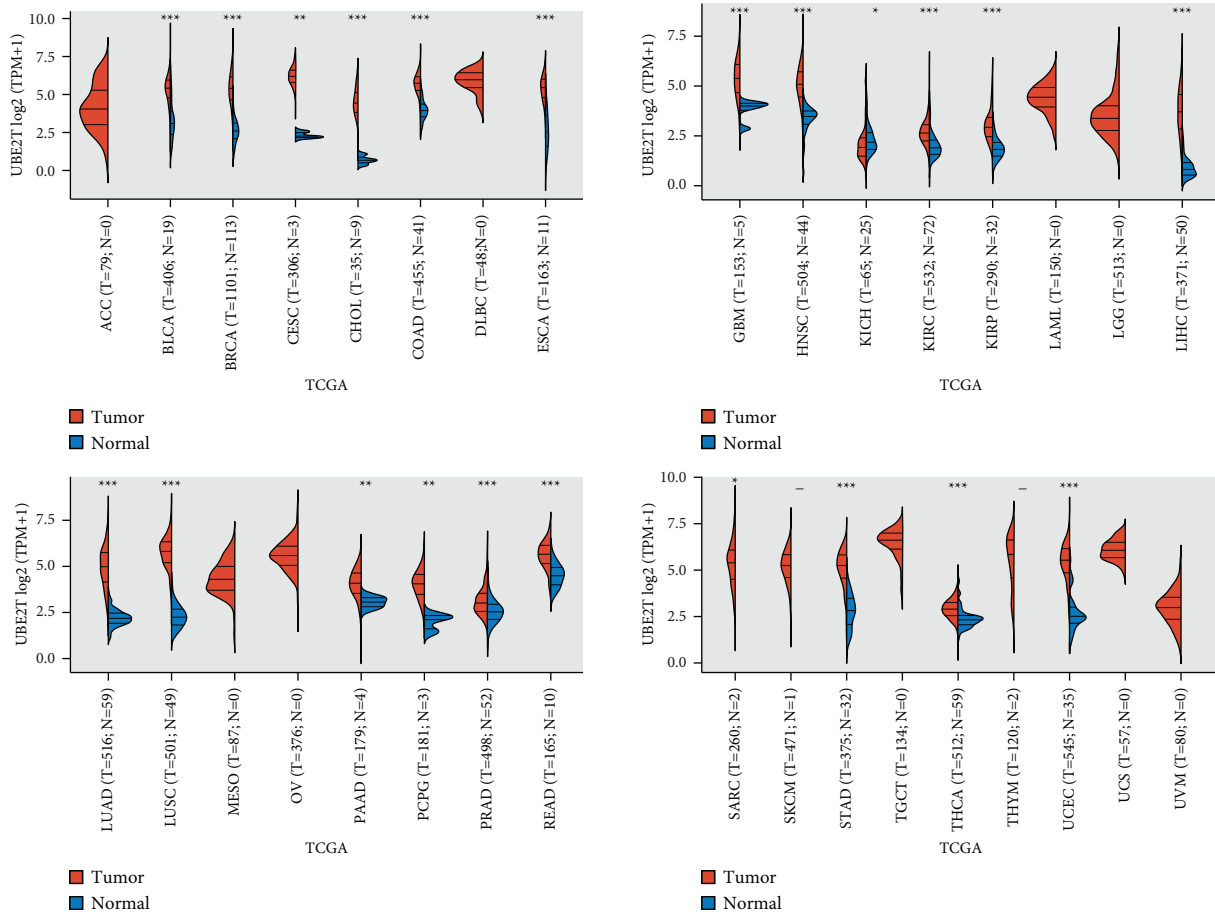
FIGURE 3: Pan-cancer expression of UBE2T between tumor tissues and normal tissues from TCGA datasets.

(a)

(b)

(c)

FIGURE 4: Continued.

(d)

(e)
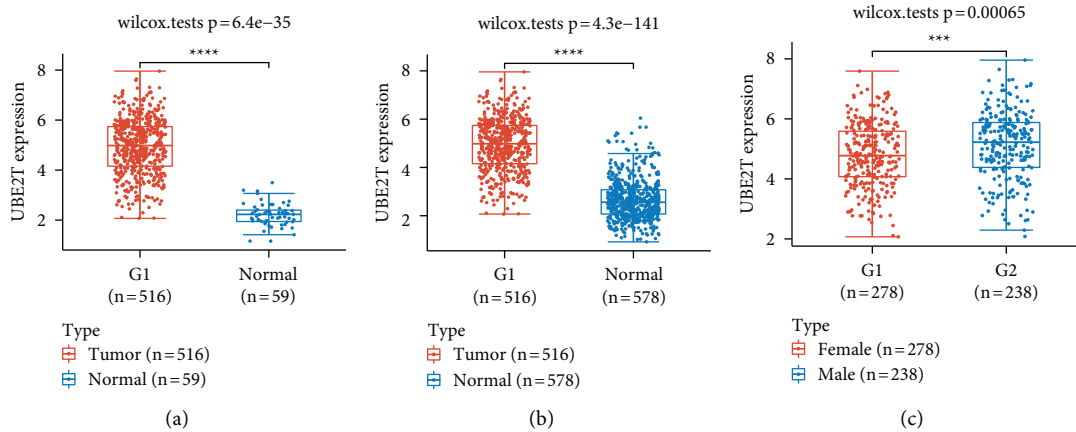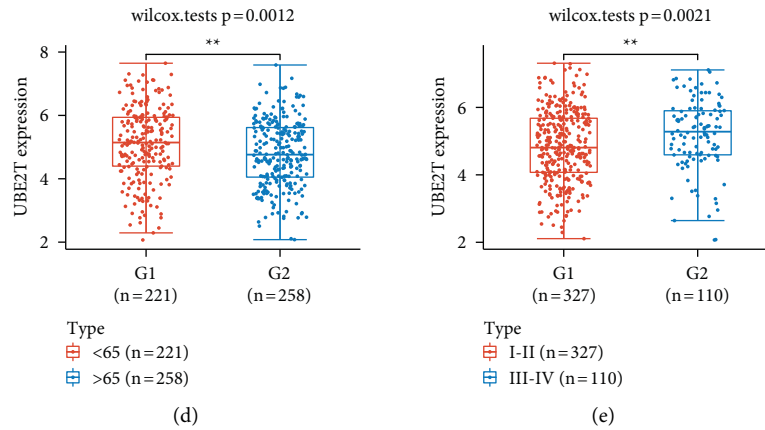
Figure 4: The clinical importance of the UBE2T expression in LUAD. (a and b) In LUAD samples, UBE2T expression was noticeably higher than in nontumor samples from the TCGA datasets or the TCGA and GTEx databases. (c–e) Clinical parameters that affect UBE2T expression, including (c) gender, (c) age, and (e) clinical stage.
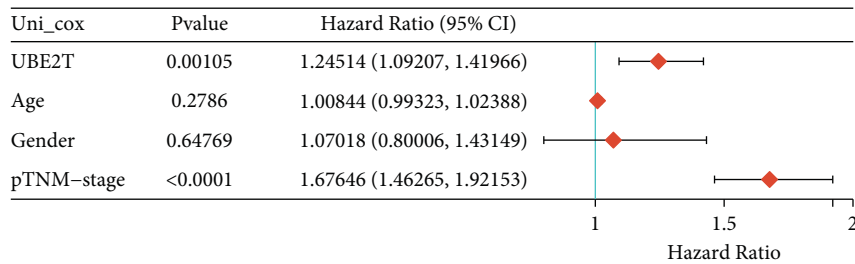
(a)
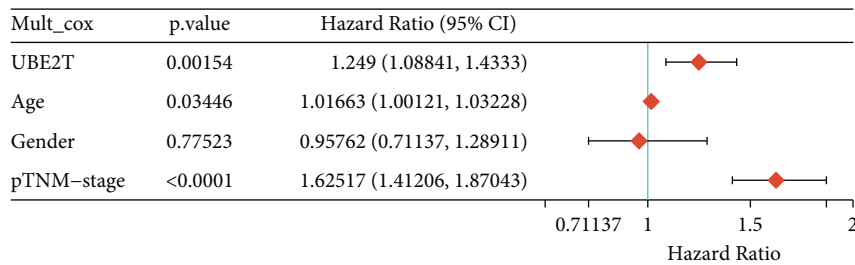
(b)

Figure 5: (a) Univariate and (b) multivariate analyses for overall survival of LUAD patients by Cox regression model.

non-small-cell lung cancer patients following chemo-radiation [40]. Immunotherapy, however, could only benefit a tiny portion of patients if they are not picked correctly. Therefore, identifying reliable biomarkers to screen the majority of immunotherapy patients is critical. The expression of PD-L1 and TMB may serve as predictive indicators for the efficacy of ICBs, according to prior research. There are, however, restrictions to be aware of. For instance, because of the high geographical and temporal variation in the expression of PD-L1, the use of TMB is constrained since there are no uniform criteria that can be utilized to establish the cut-off value. In this study, we found that UBE2T expression was positively correlated with the expression of many immunological checkpoint genes, including UVM, THCA, LIHC, LGG, KIRC, and BLCA. However, we recently found a favorable correlation between the LAG3 expression and UBE2T expression. We infer from the aforementioned results that the immune infiltration's function in regulating UBE2T expression may have an impact on the onset and development of LUAD.

This study inevitably contains several limitations that need to be taken into account. Firstly, because the prognosis for UBE2T in this study was based on information from the TCGA databases, new clinical data are required to confirm it. Additionally, UBE2T's involvement in the mechanism that it used in LUAD samples is not currently explained by wet experimental evidence. Therefore, more works is needed to shed light on the potential connection between UBE2T and the prognosis of LUAD. We intend to investigate the impact of UBE2T on LUAD cells by in vitro invasion and
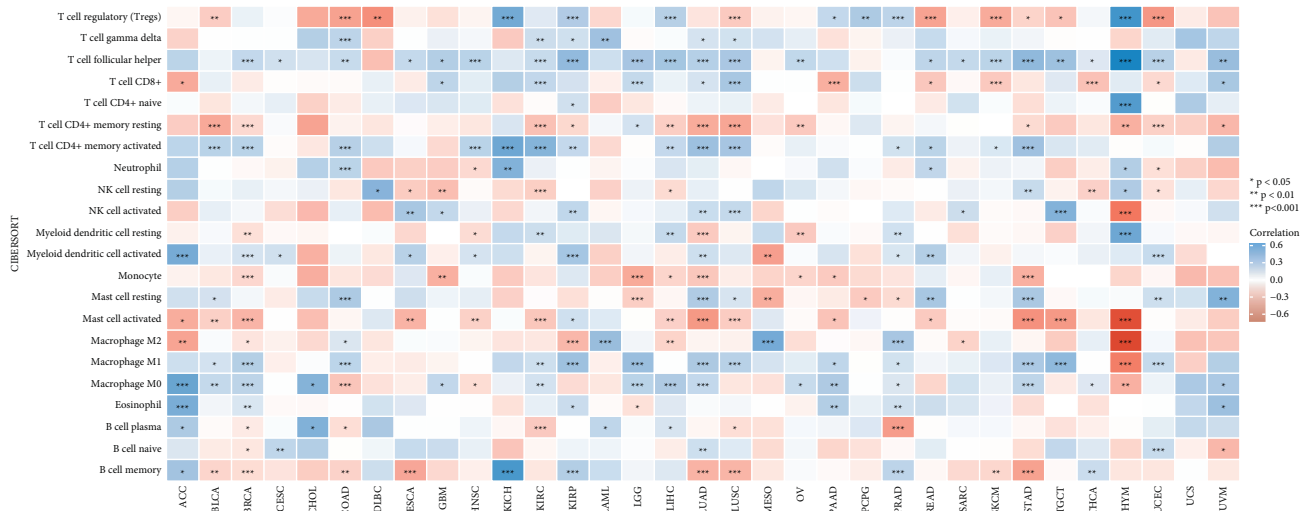
Figure 6: Correlation of the UBE2T expression with immune infiltration level in cancer.

migration experiments, confirm the regulatory relationship between UBE2T and EMT development, and, finally, suggest investigating the impact of UBE2T on LUAD using animal models.

5. Conclusions

LUAD had an increased expression of UBE2T and its expression was significantly correlated with variables such as gender, age, and advanced clinical stage. Patients with high levels of UBE2T expression exhibited significantly shorter overall survival rates, and UBE2T could be used as a biomarker for LUAD prognosis. These findings not only offered crucial cues for the identification of novel treatment targets in LUAD but they also established a framework for the investigation of potential UBE2T pathways in LUAD.

Data Availability

The data used to support the findings of this study are included within the article.

Conflicts of Interest

The authors declare that they have no conflicts of interest.

Supplementary Materials

Figure S1 displays the pan-cancer expression of UBE2T in tumor tissues out from the TCGA database as well as in normal tissues from the TCGA and GTEx datasets. Figure S2 The predictive relevance of UBE2T in the above tumor types was assessed using univariate analysis from the TCGA database. The median UBE2T value was chosen as the cut-off value for each tumor. Figure S3 UBE2T expression and immune infiltration levels in malignancies were correlated using TIMER2. Figure S4 Immune checkpoints and UBE2T expression are related. Table S1 The extension of tumor abbreviations. (*Supplementary Materials*)

References

[1] R. L. Siegel, K. D. Miller, and A. Jemal, "Cancer statistics, 2019," *CA: A Cancer Journal for Clinicians*, vol. 69, no. 1, pp. 7–34, 2019.

[2] R. L. Siegel, K. D. Miller, H. E. Fuchs, and A. Jemal, "Cancer statistics, 2022," *CA: A Cancer Journal for Clinicians*, vol. 72, no. 1, pp. 7–33, 2022.

[3] F. Wu, L. Wang, and C. Zhou, "Lung cancer in China: current and prospect," *Current Opinion in Oncology*, vol. 33, no. 1, pp. 40–46, 2021.

[4] S. Gao, N. Li, S. Wang et al., "Lung cancer in people's Republic of China," *Journal of Thoracic Oncology*, vol. 15, no. 10, pp. 1567–1576, 2020.

[5] G. A. Rivera and H. Wakelee, "Lung cancer in never smokers," *Advances in Experimental Medicine & Biology*, vol. 893, pp. 43–57, 2016.

[6] B. C. Bade and C. S. Dela Cruz, "Lung cancer 2020: epidemiology, etiology, and prevention," *Clinics in Chest Medicine*, vol. 41, no. 1, pp. 1–24, 2020.

[7] H. Hoy, T. Lynch, and M. Beck, "Surgical treatment of lung cancer," *Critical Care Nursing Clinics of North America*, vol. 31, no. 3, pp. 303–313, 2019.

[8] A. G. Pallis and K. N. Syrigos, "Lung cancer in never smokers: disease characteristics and risk factors," *Critical Reviews In Oncology-Hematology*, vol. 88, no. 3, pp. 494–503, 2013.

[9] F. Oberndorfer and L. Müllauer, "Molecular pathology of lung cancer: current status and perspectives," *Current Opinion in Oncology*, vol. 30, no. 2, pp. 69–76, 2018.

[10] M. B. Schabath and M. L. Cote, "Cancer progress and priorities: lung cancer. Cancer epidemiology, biomarkers & prevention: a publication of the American Association for cancer research," *Cancer Epidemiology, Biomarkers & Prevention*, vol. 28, no. 10, pp. 1563–1579, 2019.

[11] A. Steven, S. A. Fisher, and B. W. Robinson, "Immunotherapy for lung cancer," *Respirology*, vol. 21, no. 5, pp. 821–833, 2016.

[12] S. Yang, Z. Zhang, and Q. Wang, "Emerging therapies for small cell lung cancer," *Journal of Hematology & Oncology*, vol. 12, no. 1, p. 47, 2019.

[13] S. R. Gordon, R. L. Maute, B. W. Dulken et al., "PD-1 expression by tumour-associated macrophages inhibits

phagocytosis and tumour immunity," *Nature*, vol. 545, no. 7655, pp. 495–499, 2017.

[14] L. Ai, A. Xu, and J. Xu, "Roles of PD-1/PD-L1 pathway: signaling, cancer, and beyond," *Advances in Experimental Medicine & Biology*, vol. 1248, pp. 33–59, 2020.

[15] J. Naidoo, X. Wang, K. M. Woo et al., "Pneumonitis in patients treated with anti-programmed death-1/programmed death ligand 1 therapy," *Journal of Clinical Oncology*, vol. 35, no. 7, pp. 709–717, 2017.

[16] M. Ayers, J. Lunceford, M. Nebozhyn et al., "IFN-γ-related mRNA profile predicts clinical response to PD-1 blockade," *Journal of Clinical Investigation*, vol. 127, no. 8, pp. 2930–2940, 2017.

[17] T. Wu and Y. Dai, "Tumor microenvironment and therapeutic response," *Cancer Letters*, vol. 387, pp. 61–68, 2017.

[18] D. C. Hinshaw and L. A. Shevde, "The tumor microenvironment innately modulates cancer progression," *Cancer Research*, vol. 79, no. 18, pp. 4557–4566, 2019.

[19] I. Vitale, G. Manic, L. M. Coussens, G. Kroemer, and L. Galluzzi, "Macrophages and metabolism in the tumor microenvironment," *Cell Metabolism*, vol. 30, no. 1, pp. 36–50, 2019.

[20] B. Rowshanravan, N. Halliday, and D. M. Sansom, "CTLA-4: a moving target in immunotherapy," *Blood*, vol. 131, no. 1, pp. 58–67, 2018.

[21] W. Jiang, S. Pan, X. Chen, Z. W. Wang, and X. Zhu, "The role of lncRNAs and circRNAs in the PD-1/PD-L1 pathway in cancer immunotherapy," *Molecular Cancer*, vol. 20, no. 1, p. 116, 2021.

[22] J. Sun, Z. Zhu, W. Li et al., "UBE2T-regulated H2AX monoubiquitination induces hepatocellular carcinoma radioresistance by facilitating CHK1 activation," *Journal of Experimental & Clinical Cancer Research*, vol. 39, no. 1, p. 222, 2020.

[23] Z. Yu, X. Jiang, L. Qin et al., "A novel UBE2T inhibitor suppresses Wnt/β-catenin signaling hyperactivation and gastric cancer progression by blocking RACK1 ubiquitination," *Oncogene*, vol. 40, no. 5, pp. 1027–1042, 2021.

[24] L. L. Liu, J. M. Zhu, X. N. Yu et al., "UBE2T promotes proliferation via G2/M checkpoint in hepatocellular carcinoma," *Cancer Management and Research*, vol. 11, pp. 8359–8370, 2019.

[25] X. Wang, Y. Liu, X. Leng et al., "UBE2T contributes to the prognosis of esophageal squamous cell carcinoma," *Pathology and Oncology Research*, vol. 27, Article ID 632531, 2021.

[26] M. E. Ritchie, B. Phipson, D. Wu et al., "Limma powers differential expression analyses for RNA-sequencing and microarray studies," *Nucleic Acids Research*, vol. 43, no. 7, p. e47, 2015.

[27] T. Li, J. Fan, B. Wang et al., "TIMER: TIMER: a web server for comprehensive analysis of tumor-infiltrating immune cells," *Cancer Research*, vol. 77, no. 21, pp. e108–e110, 2017.

[28] E. K. Gustavsson, D. Zhang, R. H. Reynolds, S. Garcia-Ruiz, and M. Ryten, "ggtranscript: an R package for the visualization and interpretation of transcript isoforms using ggplot2," *Bioinformatics*, vol. 38, no. 15, pp. 3844–3846, 2022.

[29] H. Kato, "Photodynamic therapy for lung cancer--a review of 19 years' experience," *Journal of Photochemistry and Photobiology B: Biology*, vol. 42, no. 2, pp. 96–99, 1998.

[30] H. Duan, S. Y. Zheng, C. Luo et al., "Cryoablation for advanced non-small cell lung cancer: a protocol for a systematic review," *BMJ Open*, vol. 10, no. 9, Article ID e033460, 2020.

[31] G. Veronesi, "Lung cancer screening: the European perspective," *Thoracic Surgery Clinics*, vol. 25, no. 2, pp. 161–174, 2015.

[32] A. Amann, M. Corradi, P. Mazzone, and A. Mutti, "Lung cancer biomarkers in exhaled breath," *Expert Review of Molecular Diagnostics*, vol. 11, no. 2, pp. 207–217, 2011.

[33] P. Huang, Y. Guo, Z. Zhao et al., "UBE2T promotes glioblastoma invasion and migration via stabilizing GRP78 and regulating EMT," *Aging (Albany NY)*, vol. 12, no. 11, pp. 10275–10289, 2020.

[34] L. Bejarano, M. J. C. Jordāo, and J. A. Joyce, "Therapeutic targeting of the tumor microenvironment," *Cancer Discovery*, vol. 11, no. 4, pp. 933–959, 2021.

[35] N. Wang, X. Li, R. Wang, and Z. Ding, "Spatial transcriptomics and proteomics technologies for deconvoluting the tumor microenvironment," *Biotechnology Journal*, vol. 16, no. 9, Article ID e2100041, 2021.

[36] I. Terrén, A. Orrantia, J. Vitallé, O. Zenarruzabeitia, and F. Borrego, "NK cell metabolism and tumor microenvironment," *Frontiers in Immunology*, vol. 10, p. 2278, 2019.

[37] J. Y. Noh, H. Seo, J. Lee, and H. Jung, "Immunotherapy in hematologic malignancies: emerging therapies and novel approaches," *International Journal of Molecular Sciences*, vol. 21, no. 21, p. 8000, 2020.

[38] E. B. Ehlerding, C. G. England, D. G. McNeel, and W. Cai, "Molecular imaging of immunotherapy targets in cancer," *Journal of Nuclear Medicine*, vol. 57, no. 10, pp. 1487–1492, 2016.

[39] I. Mikelez-Alonso, A. Aires, and A. L. Cortajarena, "Cancer nano-immunotherapy from the injection to the target: the role of protein corona," *International Journal of Molecular Sciences*, vol. 21, no. 2, p. 519, 2020.

[40] S. J. Antonia, A. Villegas, D. Daniel et al., "Durvalumab after chemoradiotherapy in stage III non-small-cell lung cancer," *New England Journal of Medicine*, vol. 377, no. 20, pp. 1919–1929, 2017.

Research Article

MIR548P and TRAV39 Are Potential Indicators of Tumor Microenvironment and Novel Prognostic Biomarkers of Esophageal Squamous Cell Carcinoma

Jian Xu, Long Tang, Zhiqiang Wang, Qi Zhang, and Yuequan Jiang [ID]

Chongqing Key Laboratory of Translational Research for Cancer Metastasis and Individualized Treatment, Chongqing University Cancer Hospital, Chongqing 400030, China

Correspondence should be addressed to Yuequan Jiang; jyq63849075@cqu.edu.cn

Esophageal squamous cell carcinoma (ESCC) remains a common aggressive malignancy in the world. Multiple studies have shown evidence to support the hypothesis that certain functional genes that are engaged in the microenvironment of tumors played a role in the progression of ESCC. Thus, to better analyze the prognostic values of important genes in ESCC, there is an immediate need for an in-depth research study. From the TCGA database, the RNA-seq data and clinical features of 163 ESCC patients were obtained. Using the ESTIMATE technique, we were able to calculate the ImmuneScore, the StromalScore, and the ESTIMATEScore for each ESCC sample. The samples from the ESCC were split up into high score and low score groups based on the median of the various scores. In this study, ImmuneScore, StromalScore, and ESTIMATEScore were not found to be linked with overall survival of ESCC patients, according to our findings. Higher StromalScores were linked to more advanced T stages and clinical stages. The intersection analysis that was exhibited by the use of a Venn diagram indicated that there was a total of 944 upregulated genes that shared the same high score in both the ImmuneScore and the StromalScore and that there was 0 downregulated gene that shared the same low score. Survival experiments confirmed MIR548P and TRAV39 as critical prognostic biomarkers for ESCC patients. Importantly, we found that TRAV39 expression was positively associated with T cell CD4 memory activated while negatively associated with B cell memory, dendritic cells activated, and mast cells activated. In addition, we found that MIR548P expression was negatively associated with mast cells activated while positively associated with T cell CD4 memory activated. Overall, we identified MIR548P and TRAV39 as new modulators for ESCC, affecting the immune microenvironment of ESCC patients and may be a target of immunotherapy.

1. Introduction

Esophageal cancer has become a common malignant tumor in this world [1]. In addition, it is a significant contributor to deaths caused by cancer [2]. The number of cases of esophageal cancer, which are sadly rising at an alarming rate, will not stop rising [3]. Esophageal squamous cell carcinoma (ESCC) is the predominant histological type of esophageal cancer worldwide [4]. Due to the absence of typical symptoms in the early stage, patients who have ESCC are always detected at a late stage in the disease's progression [5, 6]. On the other hand, metastasis is one of the primary causes that leads to recurrence following surgical therapy, which

ultimately results in the failure of the therapeutic attempt [7]. If the progression of the disease can be forecasted based on the identification of pertinent signs in patients, then the clinical prognosis of those patients will significantly improve [8, 9]. Although relevant immunotherapies involving ESCC are still in the basic stages of development, certain related immunosuppressants have been applied in specific patients and demonstrated long-lasting anticancer effectiveness as well as controlled adverse responses [10, 11]. The ability to make an accurate prognostic assessment of ESCC is essential to the efficacy of clinical screen and treatments, as well as customized medicine. Therefore, it is highly vital to identify unique and reliable prognostic biomarkers from different

(a)

(b)
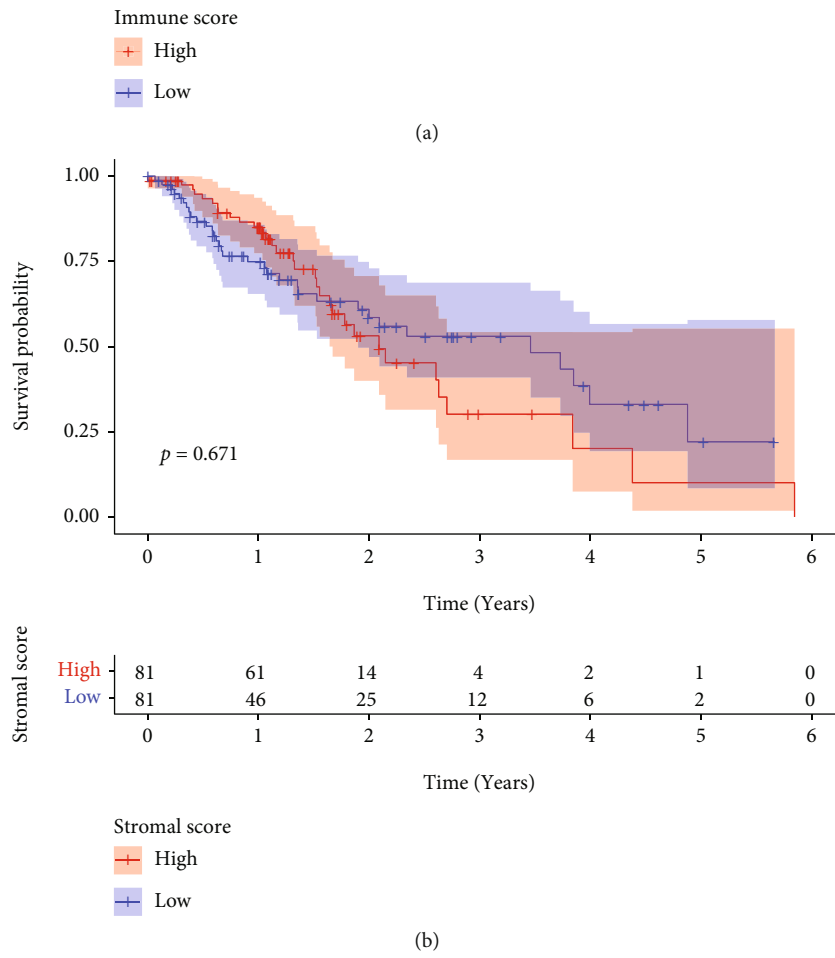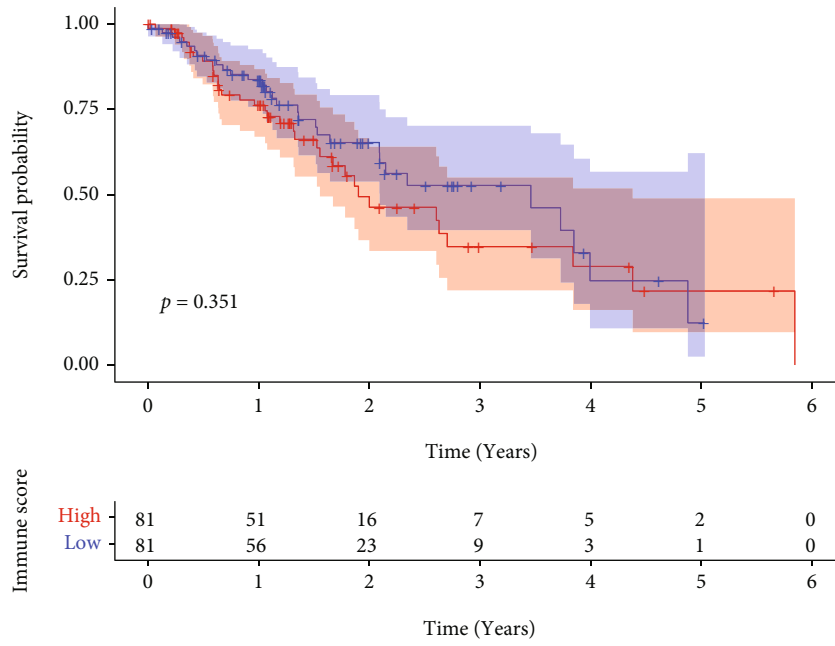
Figure 1: Continued.
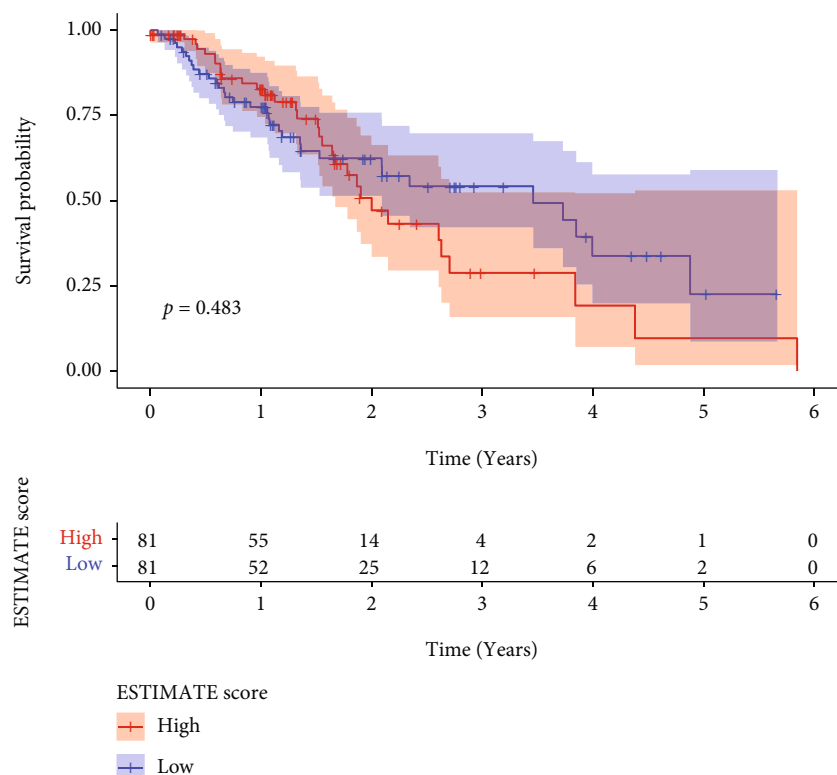
(c)

FIGURE 1: Associations between Immune/Stromal/ESTIMATE scores and survival rates in ESCC patients from TCGA datasets. Kaplan-Meier survival analysis for (a) ImmuneScore, (b) StromalScore, and (c) ESTIMATEScore.

dimensions in order to determine the best appropriate therapy plans and improve the dismal outcome of patients with ESCC.

The beginning, the course, and the development of ESCC are all determined by the genes that are inherent to the tumor cells, particularly the master transcription factors [12, 13]. On the other hand, it has been observed that the microenvironment of the tumor has a significant impact on the gene expressions of the tumor specimens and, as a result, the long-term survivals [14, 15]. The microenvironment of tumor refers to the cellular milieu in which the tumor itself is situated. Inflammatory mediators and extracellular matrix (ECM) molecules are also a part of it, along with immune cells, endothelial cells, and mesenchymal cells [16, 17]. In the microenvironment of tumor, immune and stromal cells are two major types of nontumor components that could be useful for the diagnosis of tumors [18, 19]. Immune cells can help diagnose cancer, while stromal cells help predict how aggressive a tumor will become. It has been suggested that tumor-infiltrating immune cells (TIICs) and stromal cells, which are two important categories of nontumor cell components, are useful in the prediction of clinical outcome of malignancies [20, 21]. Previous researches have shown evidence that tumor-infiltrating lymphocytes (TILs) play a key role in determining the clinical progression of a variety of malignancies [22, 23]. Recently, several types of cancers, including renal, prostate, colorectal, ovarian, bladder, and lung cancers, have been linked to TILs, specifically cytotoxic T cells, memory T cells, and T helper 1 cells, which

are positively related to good clinical outcomes [24, 25]. In addition to this, it was observed that the tumor microenvironment (TME) had an effect on the gene expression in the cancer specimens as well as the prognostic results. These findings shed light on the connection between the tumor microenvironment and the evolution of cancer, suggesting new approaches that could make the management of cancerous tumors more effective.

Through the use of the ESTIMATE algorithm, we were able to acquire the ImmuneScore and StromalScore of ESCC patients that were stored in the TCGA database. The purpose of this work was to determine which genes with key functional roles were implicated in TME. After that, we further explored their clinical significance.

2. Methods

2.1. Datasets and Data Processing. The TCGA-ESCA RNA-seq FPKM data, together with clinical data and survival data, were retrieved from the UCSC Xena database. There were 163 cases with ESCA and 11 normal cases, all of which had their clinical data extracted from the above datasets.

2.2. Generation of ImmuneScore, StromalScore, and ESTIMATEScore. Each sample's ratio of immune-stromal component in TME was estimated using the ESTIMATE algorithm implemented in R language version 3.5.1 with the estimate package and displayed as one of three scores: ImmuneScore, StromalScore, or ESTIMATEScore.
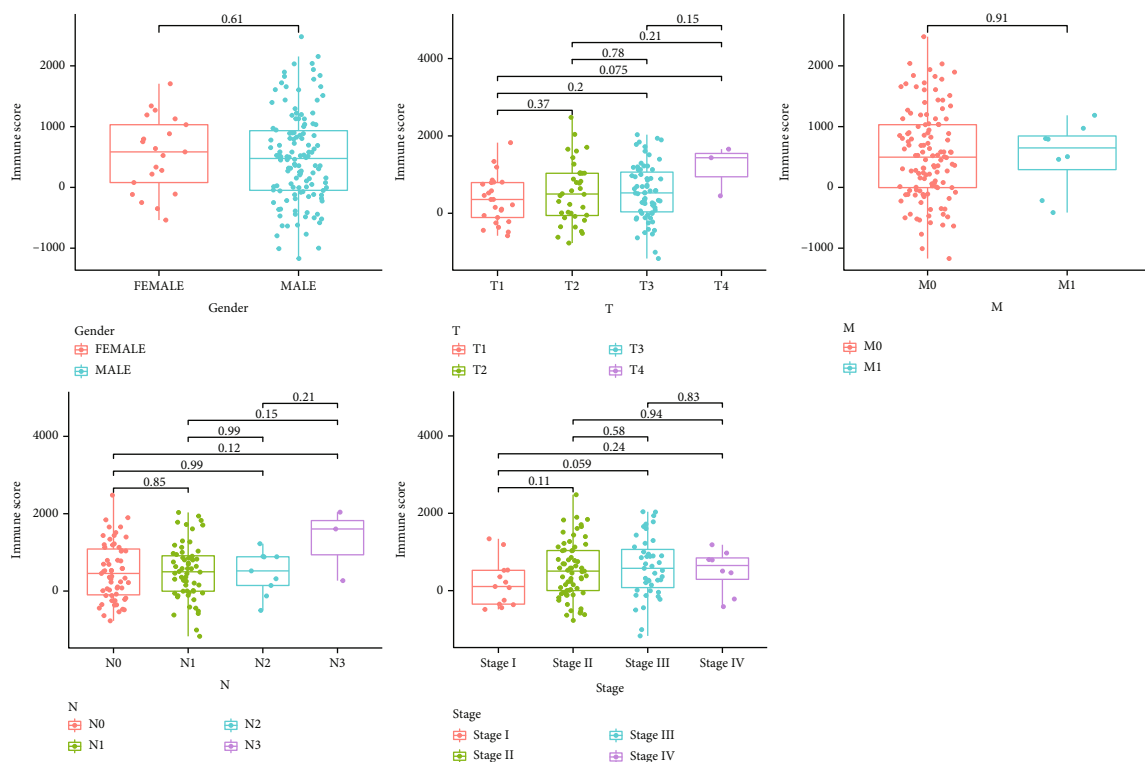
(a)

(b)

Figure 2: Continued.

(c)
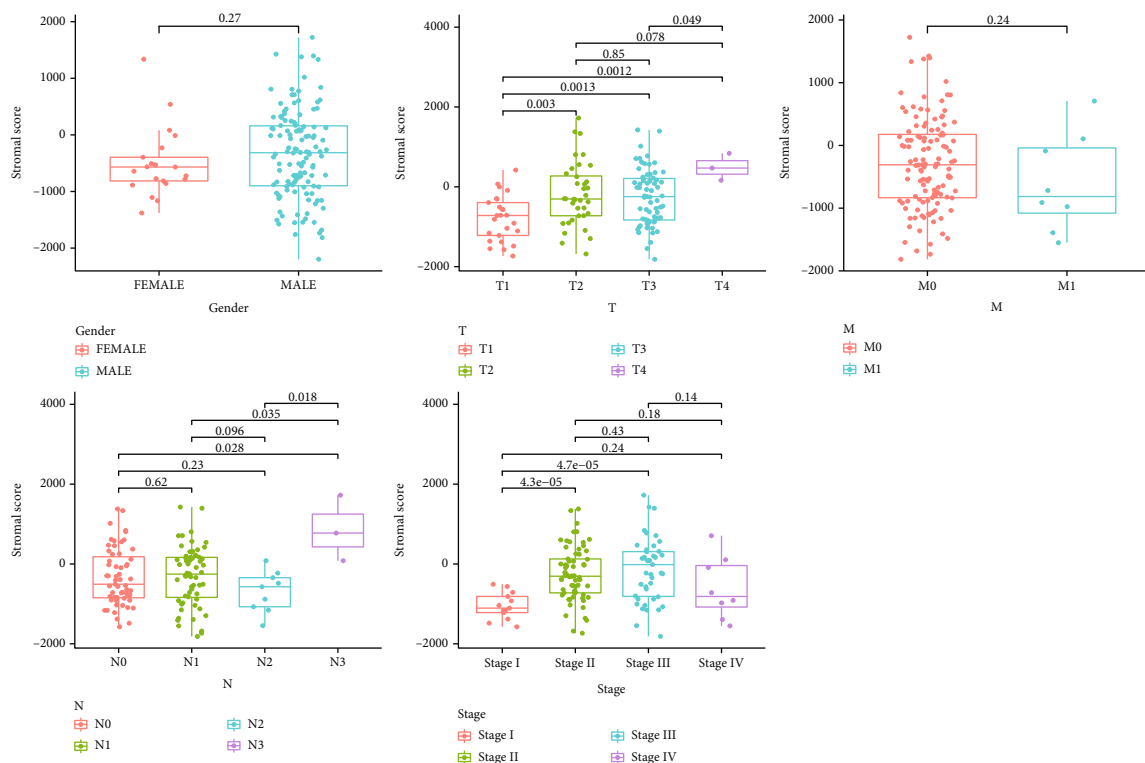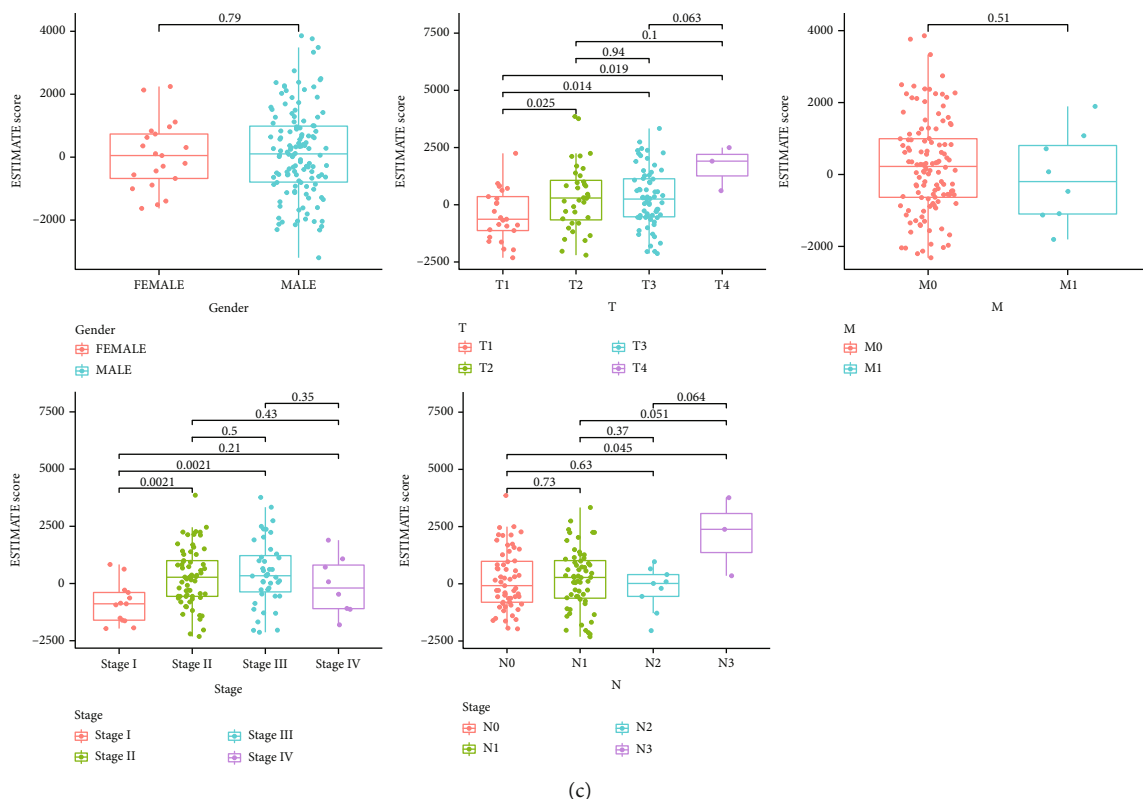
Figure 2: Associations of Immune/Stromal/ESTIMATE scores with clinical factors. (a) ImmuneScore, (b) StromalScore, and (c) ESTIMATEScore.

ImmuneScore, StromalScore, and ESTIMATEScore all showed positive correlations with the ratio of immune, stromal, and the sum of the two components in TME, so higher scores indicated larger ratios of the respective component.

2.3. Distinguishing of Differentially Expressed Genes (DEGs).
The "limma" algorithm was used to perform preprocessing on the raw data that TCGA collected. The cut-offs for identifying DEGs were determined to be adjusted p values (adj. p) less than 0.05 and |Log2 (FC)| greater than 1.

2.4. Heatmaps and Clustering Analysis.
The web application "ClustVis" was utilized in order to produce heatmaps [26].

2.5. Enrichment Assays of DEGs.
R 4.0.2 and the related R packages were utilized to carry out Gene Ontology (GO) and the Kyoto Encyclopedia of Genes and Genomes (KEGG) enrichment assays, and the DEGs were utilized as the data source. Only terms whose p and q values were lower than 0.05 were judged to have significantly increased abundance.

2.6. TME Component-Related Survival Analysis.
After performing survival analysis on all of the ESCC samples, we separated them into two groups, one with high scores and one with low scores. The Kaplan-Meier methods were applied to generate the survival curve, and the log-rank test was performed to establish whether or not there was any statistical significance. When the p value was less than 0.05, it was considered statistically significant.

2.7. Cox Regression Analysis.
We used the "survival" package in R to carry out a univariate Cox analysis on the DEGs [27].

2.8. Difference Analysis of Scores with Clinical Stages.
The data on the clinicopathological characteristics of the ESCC samples that corresponded to them were retrieved from TCGA. The analysis was carried out using the R programming language, and the significance test used was either the Wilcoxon rank sum or the Kruskal-Wallis rank sum test, depending on the number of clinical stages that were being compared.

2.9. Immune Infiltration Analysis in ESCC Dataset.
We made use of CIBERSORT so that we could investigate the enrichment of immune cells in the tumor microenvironment of ESCC patients. Analyses were performed on the relative abundance of 22 different types of invading immune cells, including T, B, and NK cells, as well as macrophages, for each sample. Spearman's correlation was utilized in order to explore the correlations between essential gene expression and immune cells that were inferred by CIBERSORT. In order to compare the locations of immune cells in groups with high and low levels of gene expression, a Wilcoxon test was carried out.

2.10. Statistical Analysis.
Utilizing the R programming language, statistical analyses were carried out. A $p < 0.05$ was considered statistically significant.

(a)

Figure 3: Continued.

(b)

(c)
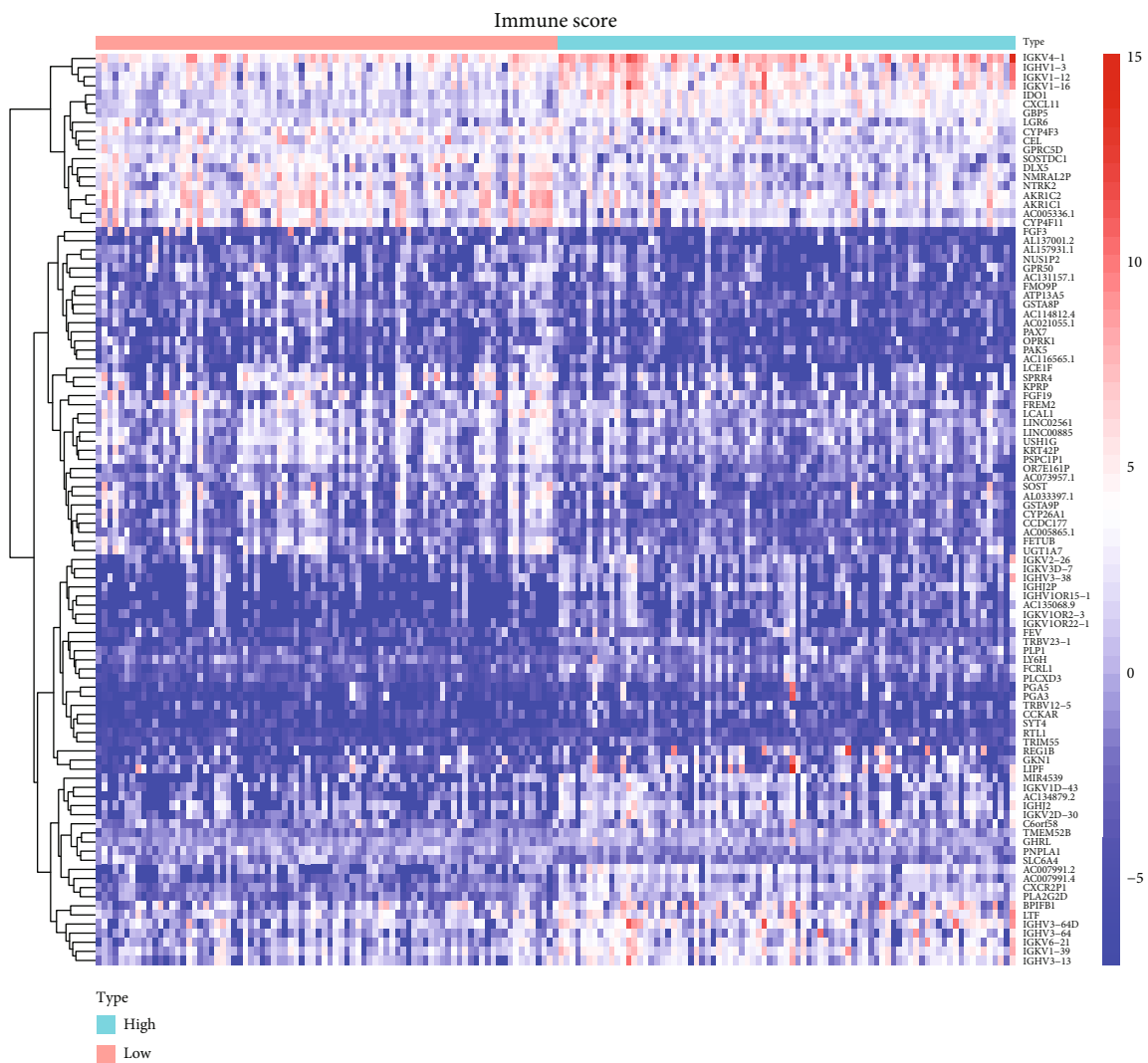
(d)
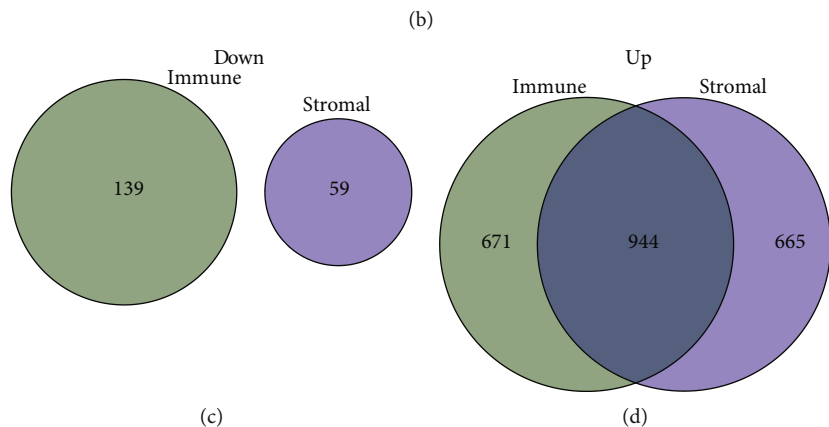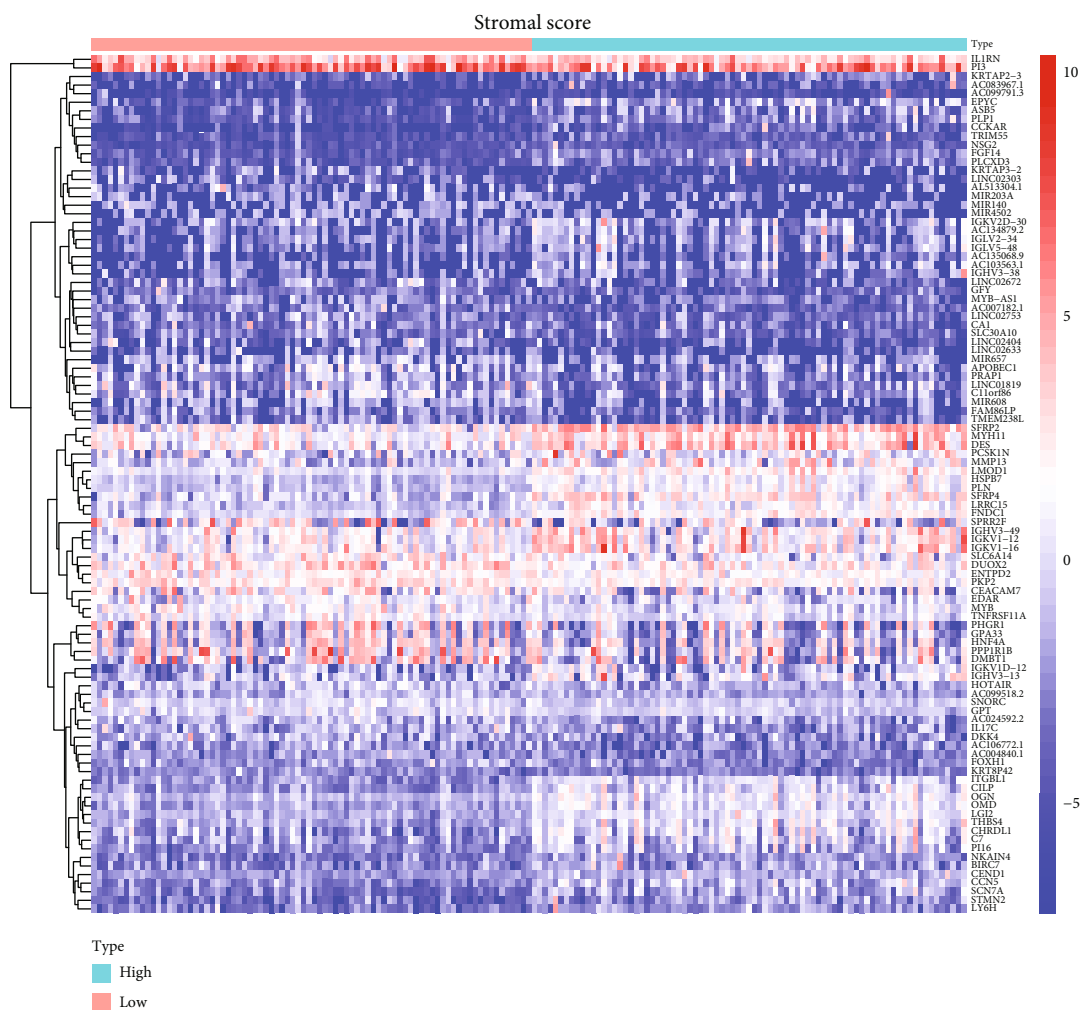
FIGURE 3: The discovery of DEGs that are common to both the ImmuneScore and the StromalScore. (a) A heatmap for DEGs that was developed by comparing the group with the high score to the group with the low score using ImmuneScore. (b) Heatmap for DEGs in StromalScore. (c, d) Diagrams in the form of Venn plots illustrating upregulated and downregulated DEGs that are common to both ImmuneScore and StromalScore.

3. Results

3.1. Survival Analysis of ESCC Patients in Three Different Scores. In order to profile the relationship that existed between the various scores and the outcomes of the patients,

we employed a combination of ESTIMATE algorithms and Kaplan-Meier survival analyses. ImmuneScore (Figure 1(a)), StromalScore (Figure 1(b)), and ESTIMATE-Score (Figure 1(c)) were found to have no correlation with overall survival in ESCC patients.

(a)

FIGURE 4: Continued.

(b)
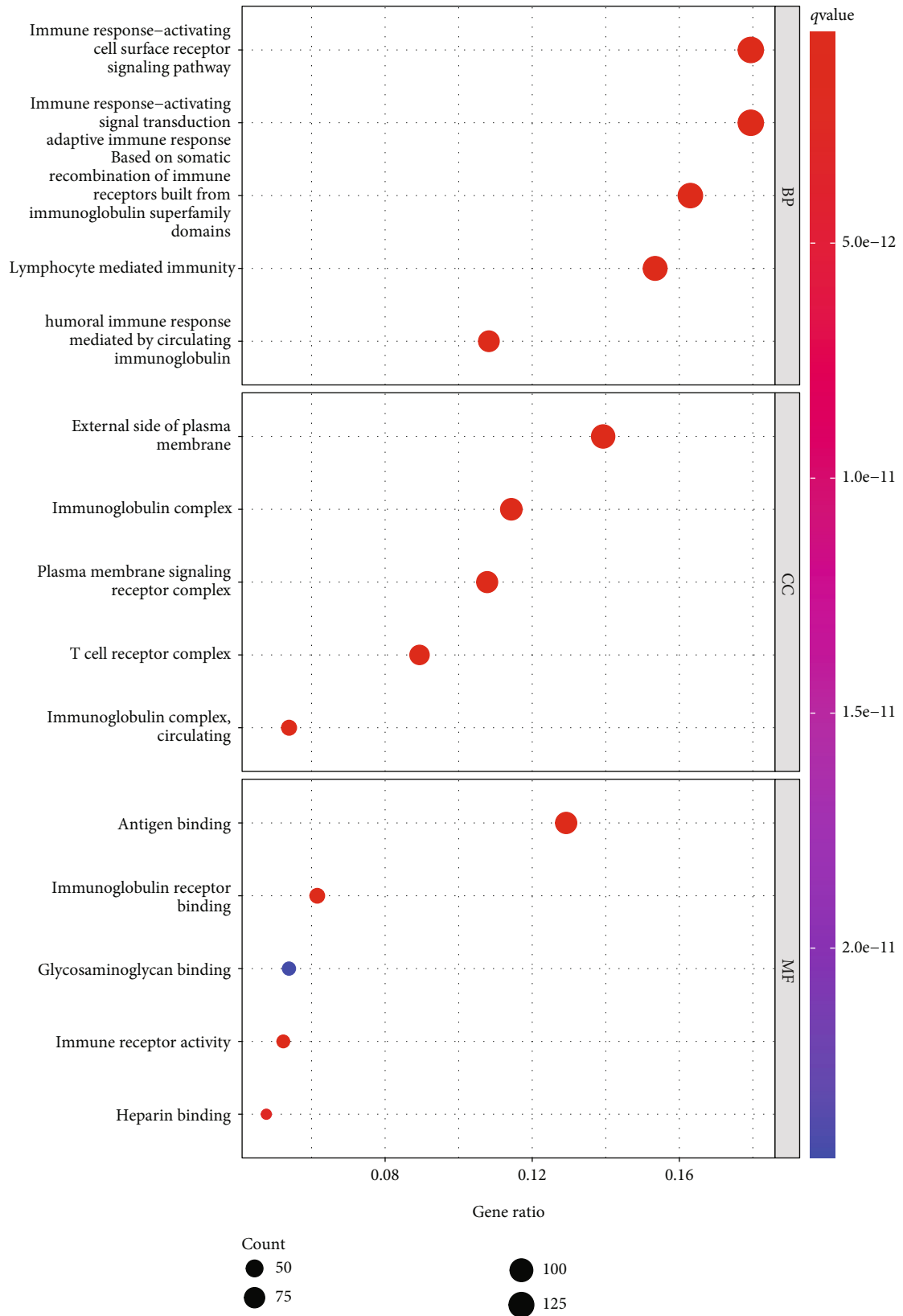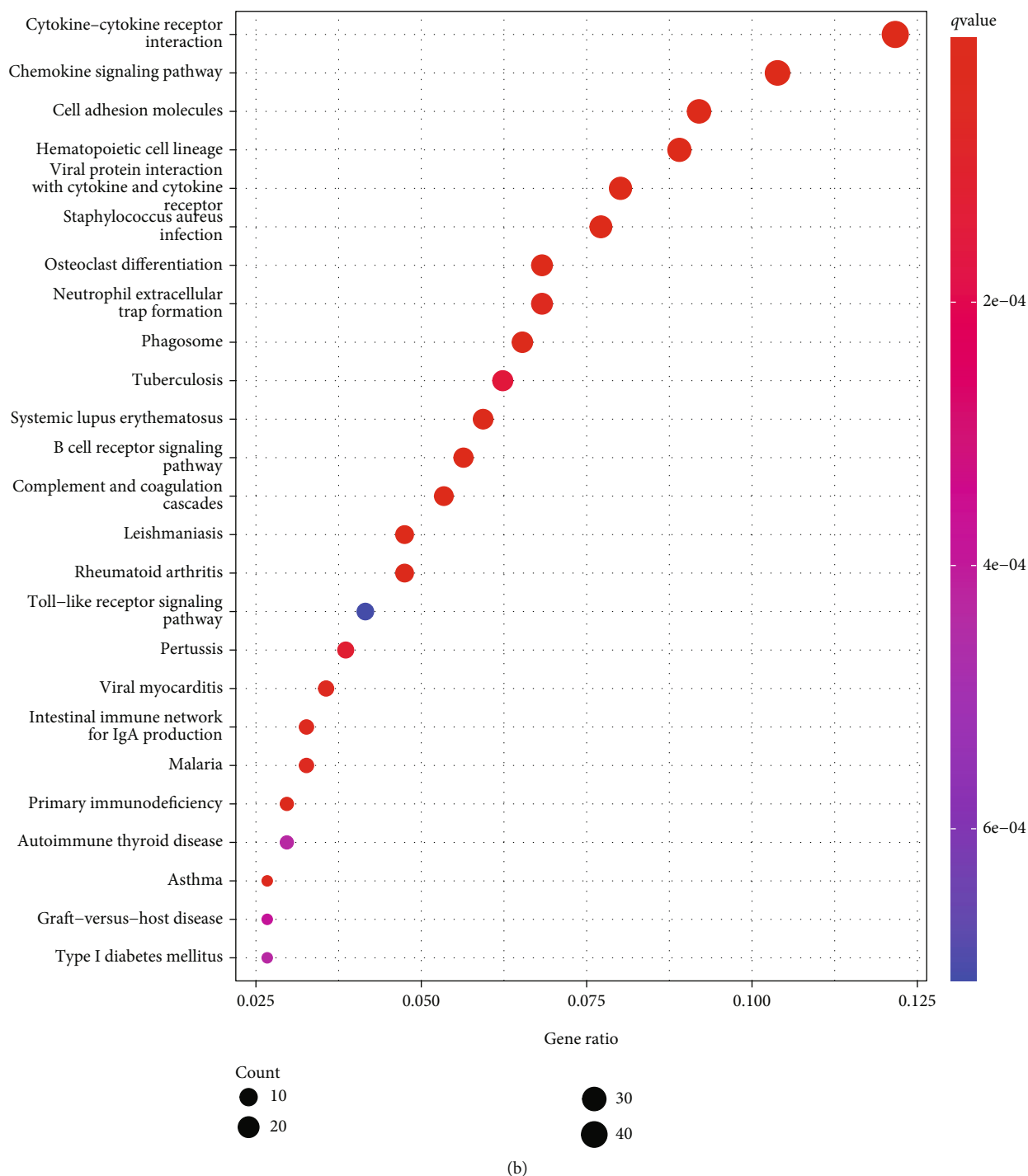
FIGURE 4: Enrichment analysis of DEGs. (a) GO enrichment analysis. (b) EGG pathway analysis.

3.2. Analysis of the Correlations between Scores and Clinical Features of Patients with ESCC. After that, we performed an analysis to see whether or not there was a correlation between clinical factors of ESCC patients and the scores. We observed that ImmuneScore did not have a significant link with a number of clinical features of ESCC patients, including gender and TMN stage (Figure 2(a)). However, we observed that a higher StromalScore was related to advanced T stages and clinical stages (Figure 2(b)). Mover,

we found that higher ESTIMATEScore predicted an advanced T stages and clinical stages (Figure 2(c)).

3.3. DEGs Shared by ImmuneScore and StromalScore. The comparative analysis between samples with high scores and those with low scores was carried out in order to determine the precise variations of gene profile in TME relating immunological and stromal components. ImmuneScore provided a total of 1754 DEGs, which are significantly different from

	*p*value	Hazard ratio
MIR548P	0.050	0.286 (0.082−0.999)
TRAV39	0.029	0.142 (0.024−0.822)

Hazard ratio

(a)

(b)
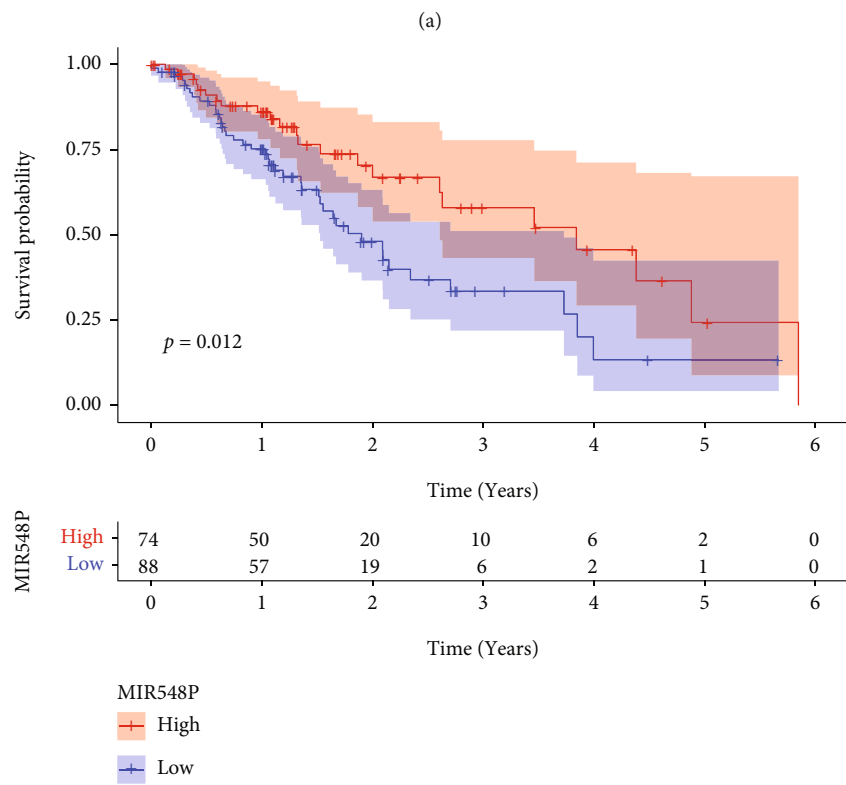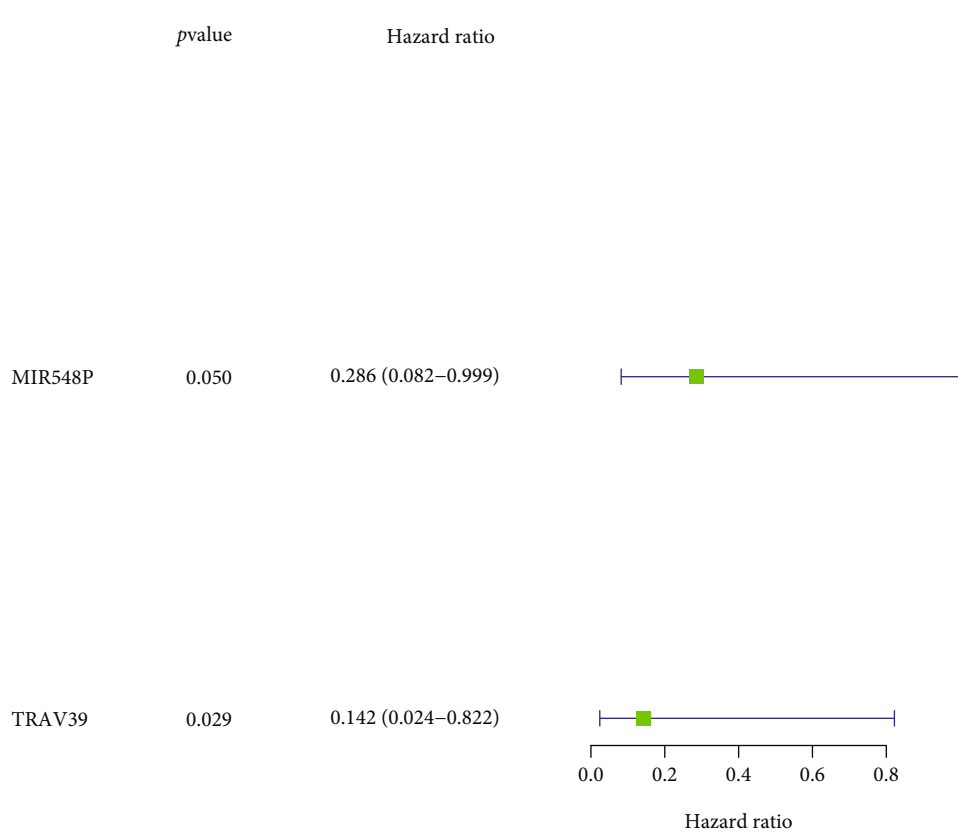
Figure 5: Continued.

(c)
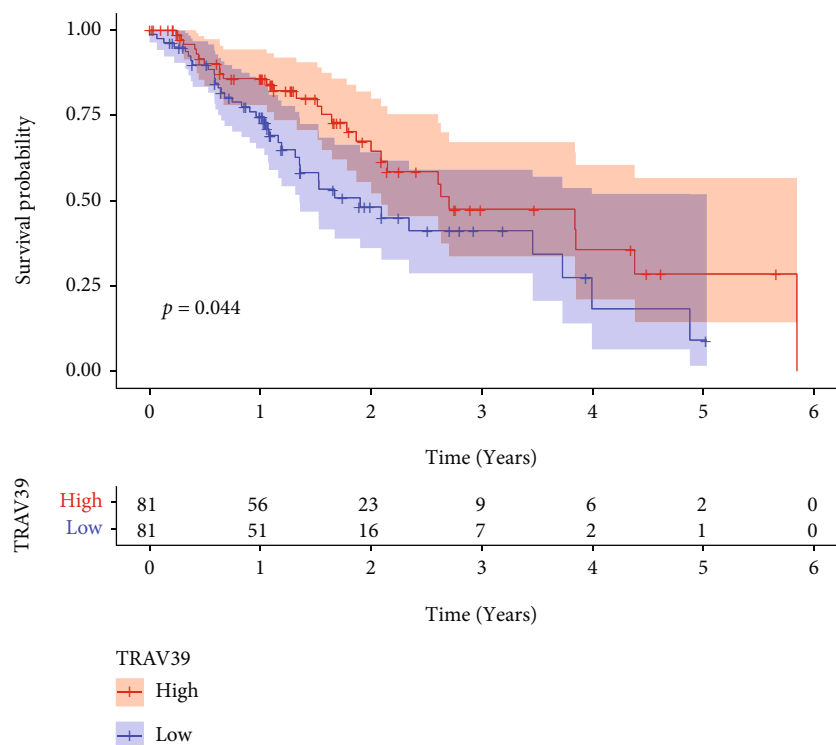
FIGURE 5: The identification of survival-related DEGs. (a) Univariate analysis was applied to screen the survival-related DEGs in ESCC patients based on TCGA datasets. (b) Kaplan-Meier curves for overall survival after surgery according to expression of MIR548P and TRAV39 expression in ESCC patients.

the median (samples with high score vs. low score). There were 1615 genes that showed an increase in expression, whereas 139 genes showed a decrease (Figure 3(a)). In a similar fashion, 1668 DEGs were derived using StromalScore. These differentially expressed genes included 1609 genes with an increase in expression and 59 genes with a decrease in expression (Figure 3(b)). The intersection analysis that was presented in the form of a Venn diagram revealed that there was a total of 944 upregulated genes that had the same high score in both the ImmuneScore and the StromalScore and that there was a total of 0 downregulated gene that had the same low score. Both of these scores were determined by the ImmuneScore and the StromalScore (Figures 3(c) and 3(d)). These DEGs could have been the deciding factor in determining the status of the TME.

3.4. Functional Correlation Assays. Enrichment analyses of GO were carried out in order to learn more about the role of DEGs. The results indicated that the DEGs were mainly related to immune response-activating cell surface receptor signaling pathway, immune response-activating signal transduction, lymphocyte-mediated immunity, external side of plasma membrane, immunoglobulin complex, plasma membrane signaling receptor complex, T cell receptor complex, immune receptor activity, glycosaminoglycan binding, immunoglobulin receptor binding, and antigen binding (Figure 4(a)). The results of KEGG assays revealed that the DEGs were mainly enriched in chemokine signaling pathway, cytokine-cytokine receptor interaction, cell adhesion

molecules, osteoclast differentiation, neutrophil extracellular trap formation, phagosome, tuberculosis, and B cell receptor signaling pathway (Figure 4(b)).

3.5. The Identification of Survival-Related DEGs in ESCC Patients. We carried out a univariate Cox regression on 944 DEGs in order to investigate the crucial genes that play functional roles in ESCC. Only MIR548P and TRAV39, as can be shown in Figure 5(a), were found to be related to an increased likelihood of overall survival among ESCC patients. According to the findings of the Kaplan-Meier method, the 5-year overall survival rate of patients whose MIR548P expression was low was noticeably lower than that of patients whose MIR548P expression was high. This difference was statistically significant (Figure 5(b)). A finding that was quite similar to this one was noticed when patients exhibited a low expression of TRAV39 (Figure 5(c)).

3.6. Relationships between MIR548P and TRAV39 Expressions and Clinicopathological Features in ESCC. In order to investigate the connection between the expressions of MIR548P and TRAV39 and the clinicopathological factors of human ESCC, clinical follow-up information was gathered from all of ESCC patients. Our research revealed that an elevated level of TRAV39 expression was associated with an advanced clinical stage in ESCC patients (Figure 6(a)). On the other hand, we did not discover any data that supported the hypothesis that there was a positive

(a)

(b)
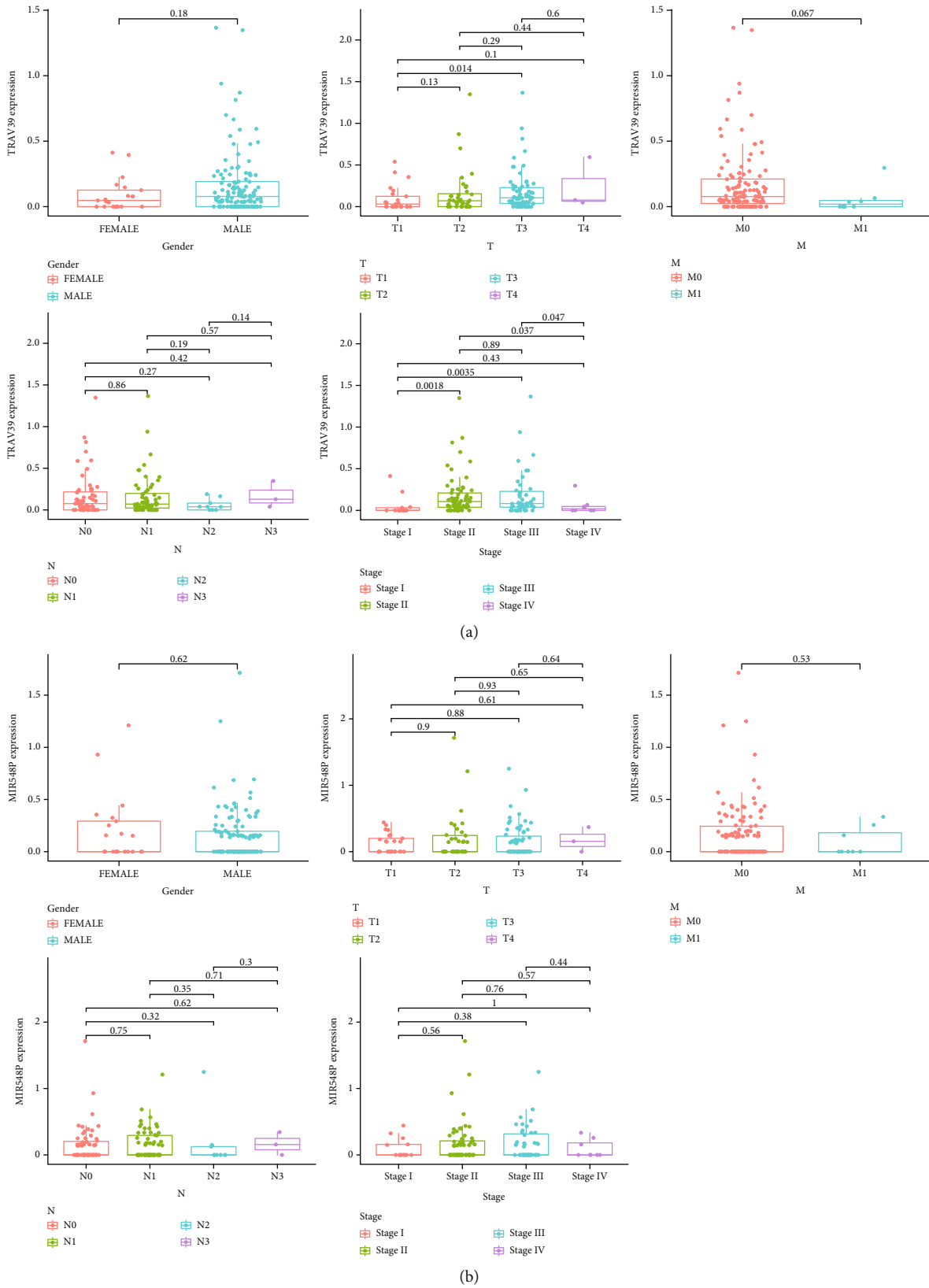
FIGURE 6: Relationships between (a) MIR548P and (b) TRAV39 expressions and clinicopathological features in ESCC.
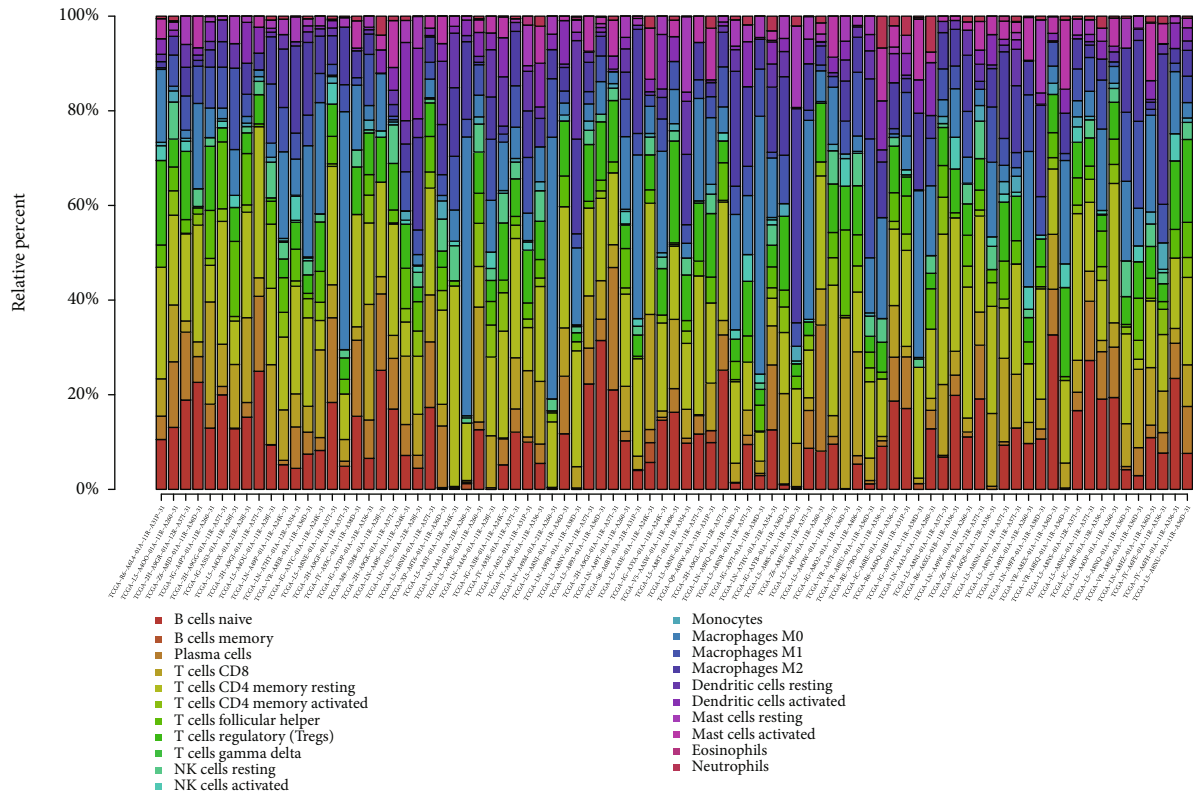
(a)

Figure 7: Continued.
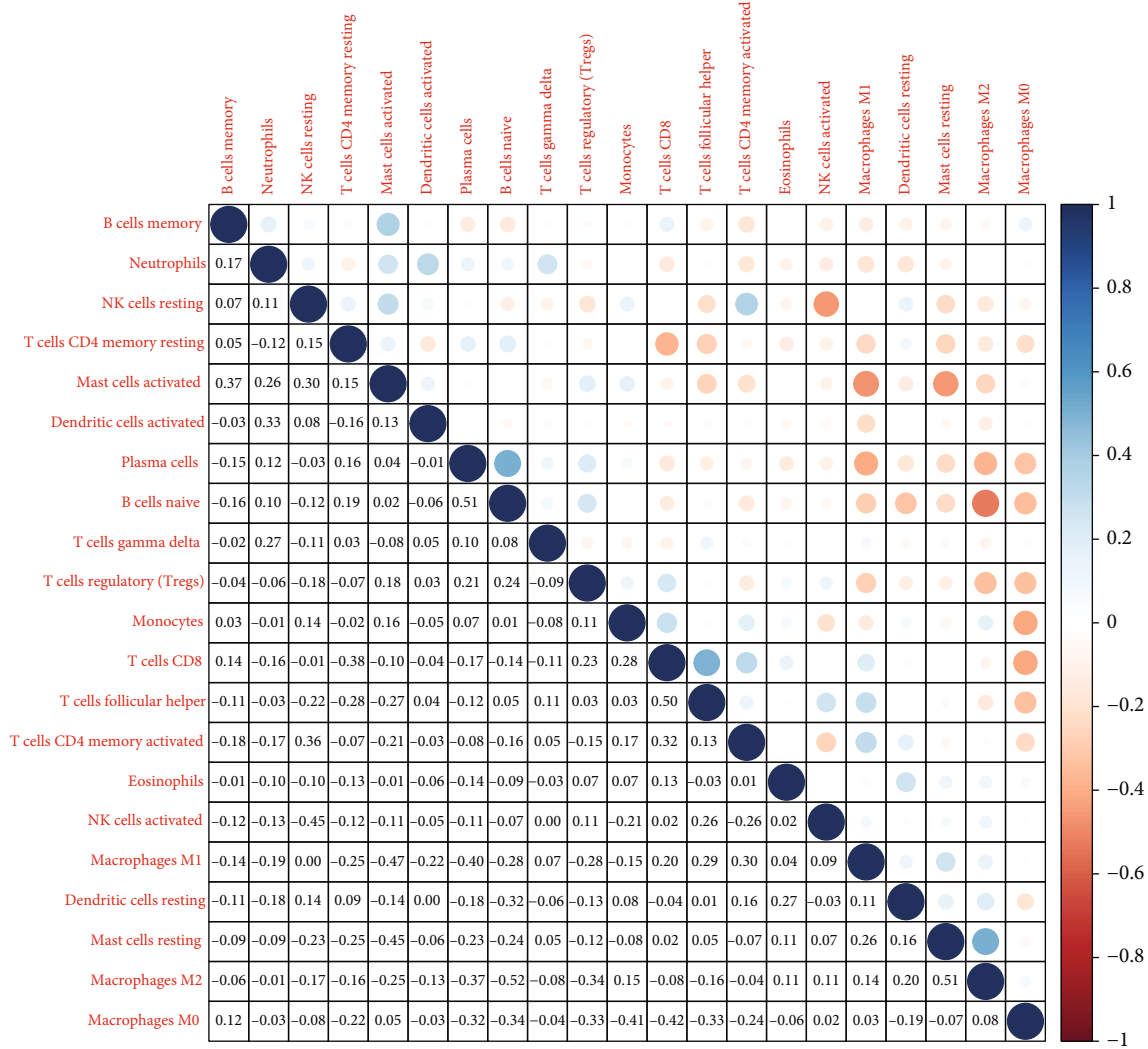
(b)

FIGURE 7: Continued.
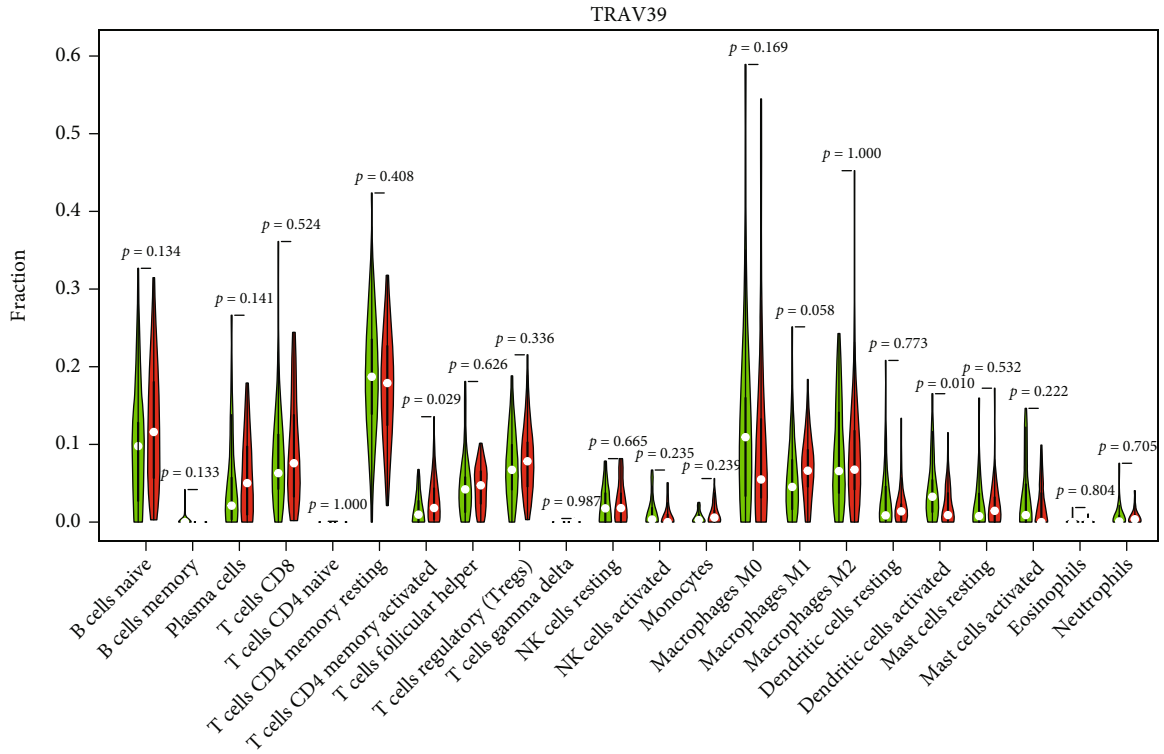
(c)
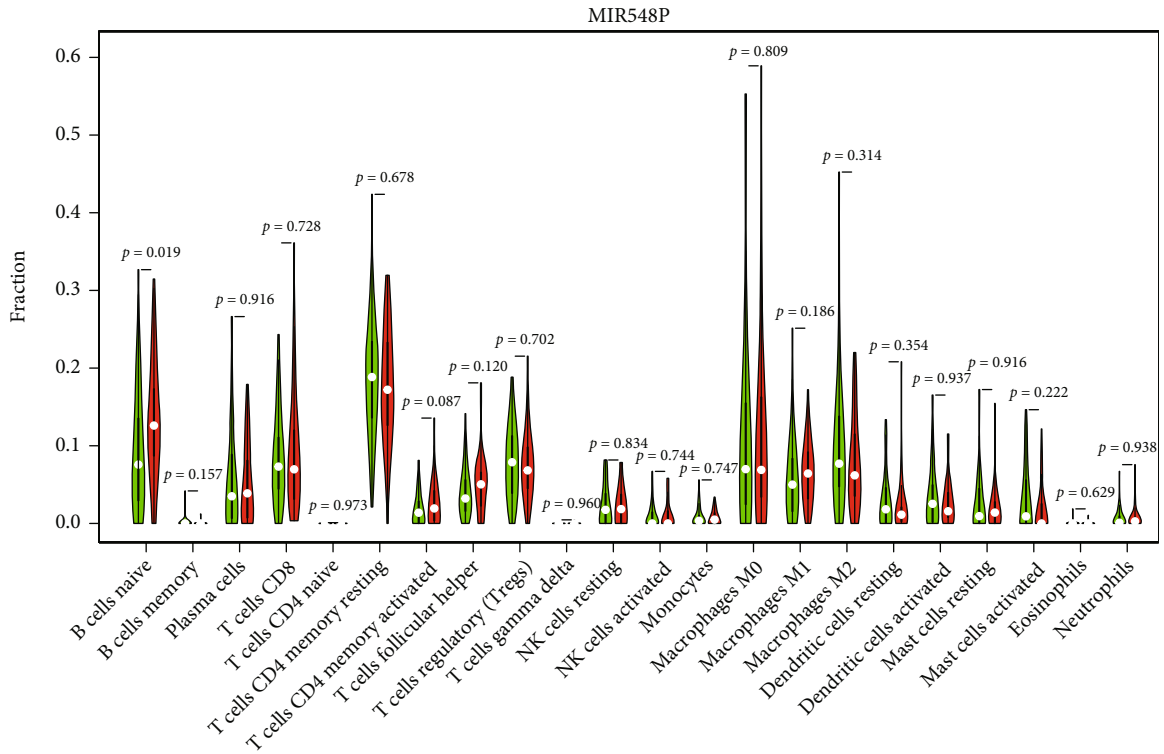
(d)

Figure 7: TIC profile in the tissue samples from the tumors and correlation analysis. (a) The distribution of the 21 different types of TICs found in ESCC tumor samples is shown as a barplot. (b) A heatmap displaying the correlation between 21 different types of TICs, with a number in each little box reflecting the p value of correlation between two different types of cells. (c, d) All ESCC cases were divided into the high and low (c) MIR548P and (d) TRAV39 expression groups, based on the median of MIR548P and TRAV39 expressions, and the Wilcoxon rank-sum test was carried out.
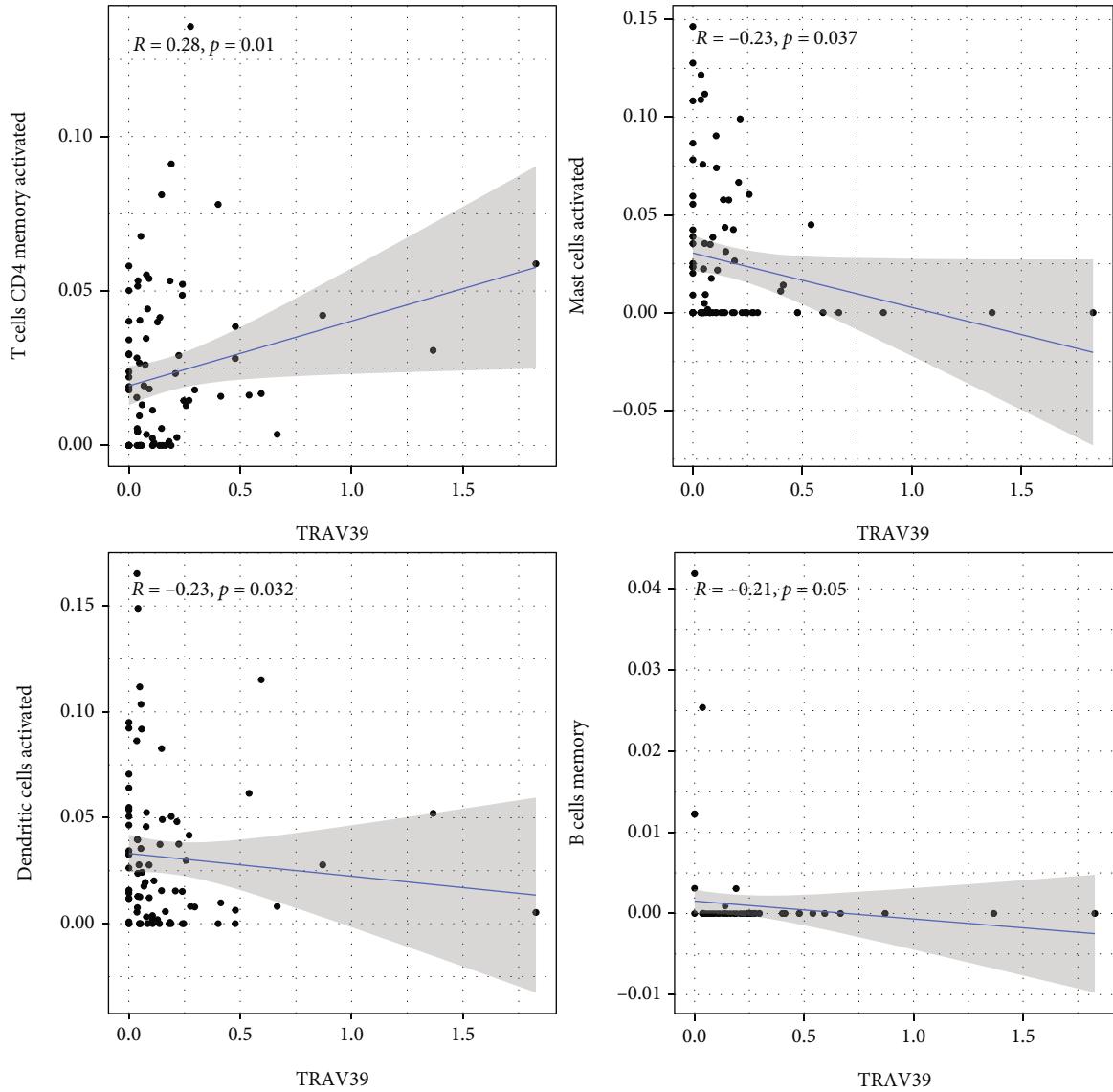
(a)

Figure 8: Continued.

(b)
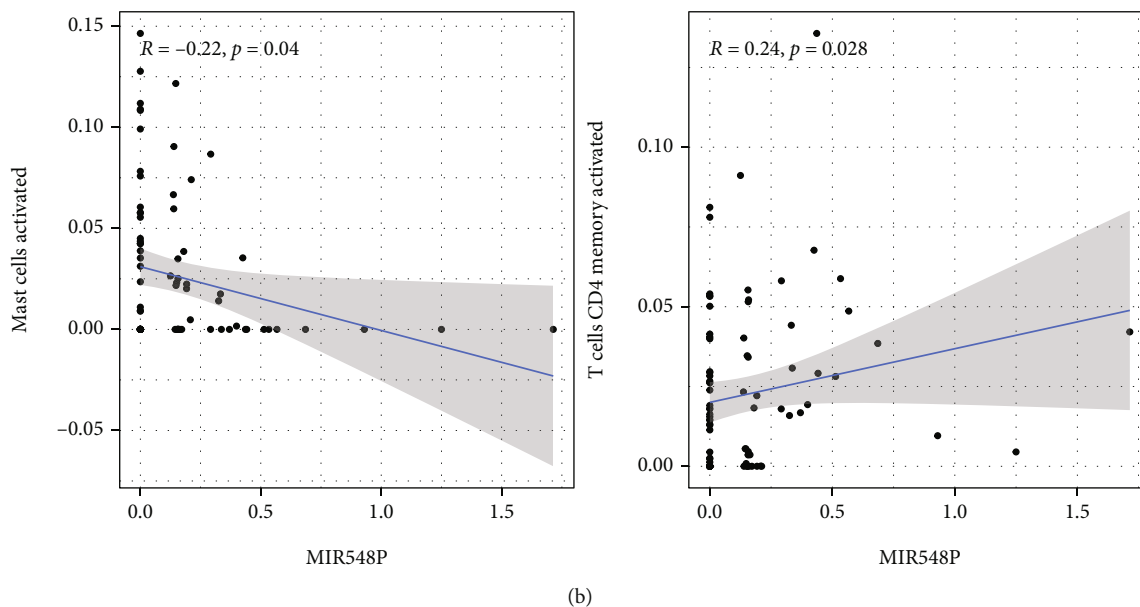
Figure 8: Correlation of TIC proportion with the expression of (a) TRAV39 and (b) MIR548P.

link between the expression of MIR548P and the clinicopathological characteristics of ESCC patients (Figure 6(b)).

3.7. Correlation of MIR548P and TRAV39 with the Proportion of TICs. In order to provide additional evidence that MIR548P and TRAV39 expressions were correlated with the immune microenvironment, it was determined with the use of the CIBERSORT algorithm what proportion of immune subsets had invaded the tumor, and 21 different immune cell profiles were constructed using ESCC samples (Figures 7(a) and 7(b)). The dysregulated levels of immune cells are shown in Figures 7(c) and 7(d). Importantly, we found that TRAV39 expression was positively associated with T cell CD4 memory activated while negatively associated with B cell memory, dendritic cells activated, and mast cells activated (Figure 8(a)). In addition, we found that MIR548P expression was negatively associated with mast cells activated while positively associated with T cell CD4 memory activated (Figure 8(b)). Thus, our findings suggested MIR548P and TRAV39 were involved in the function of immune microenvironment.

4. Discussion

ESCC is one of the most common forms of aggressive cancer worldwide, and it is especially prevalent in China, where it ranks as the fourth most common reason for people to pass away from cancer-related causes [28, 29]. The 5-year survival rate for ESCC patients is roughly 17%. Due to the absence of a single, reliable clinical approach for early identification, ESCC is associated with a typically dismal prognosis globally [30, 31]. ESCC accounts for approximately 90% of all occurrences of esophageal cancer. The ongoing dismal clinical outcome suggested that there was an immediate need to increase our understanding of the molecular mechanism behind the carcinogenesis of ESCC [32, 33]. The

above knowledge could help in the creation of innovative ways for predicting the patient's prognosis. There was an increasing body of evidence suggesting that aberrant regulation of certain proteins was essential for the advancement of ESCC [34, 35]. Therefore, the mortality rate of ESCC patients can be lowered and clinical outcomes can be improved by the discovery of novel biomarkers that can be used in early diagnosis and prognostic assessment to better personalize therapy.

The TME was home to a wide variety of cell types, all of which are integral parts of tumor tissues and play a crucial part in both the beginning and progression of cancers [36]. The cells and substances that make up the TME were constantly undergoing change, which served to both identify characteristics of the tumor and encourage immune evasion, growth, and metastasis [37]. Multiple studies have shed light on the therapeutic relevance of the TME in the prediction of therapy efficacy and patient prognosis [38]. In recent years, various medications that target the TME, such as immune checkpoint inhibitors and angiogenesis inhibitors, have shown significant success in regulating the progression and spread of malignancies [39, 40]. These drugs included angiogenesis inhibitors. In this study, we determined the percentages of TME components and carried out survival analysis pertaining to those findings. However, according to the findings, neither the ESTIMATEScore nor the StromalScore nor the ImmuneScore was substantially connected to the overall survival rate of patients with ESCC. The immunological state was shown to be connected with the clinical outcome of ESCC patients, which was not consistent with our data but has been corroborated by an increasing number of research. I hypothesized that the small number of participants could be responsible for this outcome. Then, DEGs were discovered by TME score-related gene expression difference analysis, and GO and KEGG enrichment analyses were carried out. The results illustrated that the DEGs were enriched in

cytokine-cytokine receptor interaction, chemokine signaling pathway, cell adhesion molecules, osteoclast differentiation, neutrophil extracellular trap formation, phagosome, tuberculosis, and B cell receptor signaling pathway. The univariate Cox regression analysis was also performed using the DEGs. Only MIR548P and TRAV39 were related with an increased likelihood of overall survival in ESCC patients, according to our findings. In addition, survival experiments demonstrated that a high expression of MIR548P and TRAV39 predicted a decreased overall survival rate. Moreover, we found that TRAV39 was positively associated with an advanced clinical stage. It has been known to us that clinical stage is a very important index to predict the prognosis of patients. In clinical practice, doctors also make different treatment plans according to the clinical stages. Our findings highlighted the important roles of TRAV39 expression in ESCC progression. To date, the expression and function of MIR548P and TRAV39 were rarely reported.

Immune cells have the ability to mediate chemotherapeutic resistance and sensitivity, which can increase patients' chances of survival when they have ESCC [14]. It has been established beyond a reasonable doubt that the primary immune cell subtypes that are positively associated to the important genes include immune effector cells (M1 macrophages and CD8 T cells), plasma cells that have the capacity to secrete antibodies, Treg cells, and activated memory CD4 T cells [41, 42]. Immune cells such as naive CD4 T cells and M0 macrophages, activated DC cells, and memory B cells are examples of immune cells that have a negative relationship with important genes. One of the hallmark host immunological responses to tumor cells is the infiltration of immune cells, which has been linked in numerous studies to both the initiation and progression of cancers. This reaction is one of the hallmarks of the immune system of the host. It has been observed that a high expression of Tregs and a low ratio of M0 macrophages are two factors that lead to a positive prognosis of overall survival and disease-free survival in patients with ESCC [43, 44]. It is commonly accepted that CD8+ T lymphocytes destroy tumor cells by attaching to MHCI antigens. Additionally, the total number of CD8+ cells has been shown to have a favorable correlation with tumor grade and a better patient prognosis in cases of ESCC [14, 43]. Memory CD4+ T cells, meantime, suppress the expansion of tumor cells by encouraging the multiplication of CD8+ cells. The anticancer activity of memory CD4+ T cells is further supported by previous findings demonstrating that an increase in disease-free survival of ESCC patients is directly associated to an increase in activated memory CD4+ T cells [44, 45]. In this study, we found that TRAV39 expression was positively associated with T cell CD4 memory activated while negatively associated with B cell memory, dendritic cells activated, and mast cells activated. In addition, we found that MIR548P expression was negatively associated with mast cells activated while positively associated with T cell CD4 memory activated. Our findings suggested that high expression of TRAV39 and MIR548P predicted a poor prognosis due to the promotion of antitumor immunity in ESCC.

5. Conclusion

Our findings identified two novel regulators involved in ESCC progression. The expressions of TRAV39 and MIR548P might aid in the prediction of the clinical outcome of ESCC patients, especially the status of TME. TRAV39 and MIR548P can be utilized as a promising modulator in the development of immunotherapy for ESCC.

Data Availability

The authors confirm that the data supporting the findings of this study are available within the article.

Conflicts of Interest

The authors declared no conflicts of interest.

Authors' Contributions

Jian Xu and Long Tang contributed equally to this work.

Acknowledgments

References

[1] M. A. Patel, J. D. Kratz, S. J. Lubner, N. K. Loconte, and N. V. Uboha, "Esophagogastric cancers: integrating immunotherapy therapy into current practice," *Journal of Clinical Oncology: Official Journal of the American Society of Clinical Oncology*, vol. 40, no. 24, pp. 2751–2762, 2022.

[2] E. Uche-Anya, A. Anyane-Yeboa, T. M. Berzin, M. Ghassemi, and F. P. May, "Artificial intelligence in gastroenterology and hepatology: how to advance clinical practice while ensuring health equity," *Gut*, vol. 71, no. 9, pp. 1909–1915, 2022.

[3] Z. Wang, C. Shao, Y. Wang et al., "Efficacy and safety of neoadjuvant immunotherapy in surgically resectable esophageal cancer: a systematic review and meta-analysis," *International Journal of Surgery (London, England)*, vol. 104, article 106767, 2022.

[4] J. E. Rogers, M. Sewastjanow-Silva, R. E. Waters, and J. A. Ajani, "Esophageal cancer: emerging therapeutics," *Expert Opinion on Therapeutic Targets*, vol. 26, no. 2, pp. 107–117, 2022.

[5] J. K. Waters and S. I. Reznik, "Update on management of squamous cell esophageal cancer," *Current Oncology Reports*, vol. 24, no. 3, pp. 375–385, 2022.

[6] T. Liu, X. Wang, W. Guo et al., "RNA sequencing of tumor-educated platelets reveals a three-gene diagnostic signature in esophageal squamous cell carcinoma," *Frontiers in Oncology*, vol. 12, article 824354, 2022.

[7] L. van Tilburg, S. E. M. van de Ven, M. C. W. Spaander et al., "Prevalence of lung tumors in patients with esophageal squamous cell carcinoma and vice versa: a systematic review and meta-analysis," *Journal of Cancer Research and Clinical Oncology*, 2022.

[8] Y. Zhang, J. Shi, J. Luo, C. Liu, and L. Zhu, "Regulatory mechanisms and potential medical applications of HNF1A-AS1 in cancers," *American Journal of Translational Research*, vol. 14, no. 6, pp. 4154–4168, 2022.

[9] A. Sánchez-Danés and C. Blanpain, "Deciphering the cells of origin of squamous cell carcinomas," *Nature Reviews Cancer*, vol. 18, no. 9, pp. 549–561, 2018.

[10] D. K. Li, S. Haffar, M. Horibe et al., "Verrucous esophageal carcinoma is a unique indolent subtype of squamous cell carcinoma: a systematic review and individual patient regression analysis," *Journal of Gastroenterology*, vol. 56, no. 1, pp. 12–24, 2021.

[11] Y. Ishibashi, H. Tsujimoto, H. Sugasawa et al., "Prognostic value of platelet-related measures for overall survival in esophageal squamous cell carcinoma: a systematic review and meta-analysis," *Critical Reviews in Oncology/Hematology*, vol. 164, article 103427, 2021.

[12] M. Tarazi, S. Chidambaram, and S. R. Markar, "Risk factors of esophageal squamous cell carcinoma beyond alcohol and smoking," *Cancers*, vol. 13, no. 5, p. 1009, 2021.

[13] Y. Baba, D. Nomoto, K. Okadome et al., "Tumor immune microenvironment and immune checkpoint inhibitors in esophageal squamous cell carcinoma," *Cancer Science*, vol. 111, no. 9, pp. 3132–3141, 2020.

[14] Y. Zheng, Z. Chen, Y. Han et al., "Immune suppressive landscape in the human esophageal squamous cell carcinoma microenvironment," *Nature Communications*, vol. 11, no. 1, p. 6268, 2020.

[15] Y. Zhao, J. Sun, Y. Li et al., "Tryptophan 2, 3-dioxygenase 2 controls M2 macrophages polarization to promote esophageal squamous cell carcinoma progression via AKT/GSK3β/IL-8 signaling pathway," *Acta Pharmaceutica Sinica B*, vol. 11, no. 9, pp. 2835–2849, 2021.

[16] R. J. Kelly, "Emerging multimodality approaches to treat localized esophageal cancer," *Journal of the National Comprehensive Cancer Network: JNCCN*, vol. 17, no. 8, pp. 1009–1014, 2019.

[17] J. J. Shi, H. Xing, Y. X. Wang et al., "PI3Kα inhibitors sensitize esophageal squamous cell carcinoma to radiation by abrogating survival signals in tumor cells and tumor microenvironment," *Cancer Letters*, vol. 459, pp. 145–155, 2019.

[18] M. F. Chen, C. C. Hsieh, P. T. Chen, and M. S. Lu, "Role of nutritional status in the treatment outcome for esophageal squamous cell carcinoma," *Nutrients*, vol. 13, no. 9, p. 2997, 2021.

[19] T. Yamauchi, F. Fujishima, M. Hashimoto et al., "Necroptosis in esophageal squamous cell carcinoma: an independent prognostic factor and its correlation with tumor-infiltrating lymphocytes," *Cancers*, vol. 13, no. 17, p. 4473, 2021.

[20] Y. Chen, R. Feng, B. He et al., "PD-1H expression associated with CD68 macrophage marker confers an immune-activated microenvironment and favorable overall survival in human esophageal squamous cell carcinoma," *Frontiers in Molecular Biosciences*, vol. 8, article 777370, 2021.

[21] L. R. C. Barros, P. T. Souza-Santos, M. A. M. Pretti et al., "High infiltration of B cells in tertiary lymphoid structures, TCR oligoclonality, and neoantigens are part of esophageal squamous cell carcinoma microenvironment," *Journal of Leukocyte Biology*, vol. 108, no. 4, pp. 1307–1318, 2020.

[22] T. Yagi, Y. Baba, T. Ishimoto et al., "PD-L1 expression, tumor-infiltrating lymphocytes, and clinical outcome in patients with surgically resected esophageal cancer," *Annals of Surgery*, vol. 269, no. 3, pp. 471–478, 2019.

[23] T. Yao, P. Shooshtari, and S. M. M. Haeryfar, "Leveraging public single-cell and bulk transcriptomic datasets to delineate MAIT cell roles and phenotypic characteristics in human malignancies," *Frontiers in Immunology*, vol. 11, p. 1691, 2020.

[24] L. Zhang, S. B. Ye, G. Ma et al., "The expressions of MIF and CXCR4 protein in tumor microenvironment are adverse prognostic factors in patients with esophageal squamous cell carcinoma," *Journal of Translational Medicine*, vol. 11, no. 1, p. 60, 2013.

[25] N. Sadanaga, H. Kuwano, M. Watanabe, S. Maekawa, M. Mori, and K. Sugimachi, "Local immune response to tumor invasion in esophageal squamous cell carcinoma. The expression of human leukocyte antigen-DR and lymphocyte infiltration," *Cancer*, vol. 74, no. 2, pp. 586–591, 1994.

[26] T. Metsalu and J. Vilo, "ClustVis: a web tool for visualizing clustering of multivariate data using principal component analysis and heatmap," *Nucleic Acids Research*, vol. 43, no. W1, pp. W566–W570, 2015.

[27] A. A. Rizvi, E. Karaesmen, M. Morgan et al., "Gwasurvivr: an R package for genome-wide survival analysis," *Bioinformatics (Oxford, England)*, vol. 35, no. 11, pp. 1968–1970, 2019.

[28] P. Anandavadivelan and P. Lagergren, "Cachexia in patients with oesophageal cancer," *Nature Reviews Clinical Oncology*, vol. 13, no. 3, pp. 185–198, 2016.

[29] C. M. Shahbaz Sarwar, J. D. Luketich, R. J. Landreneau, and G. Abbas, "Esophageal cancer: an update," *International Journal of Surgery (London, England)*, vol. 8, no. 6, pp. 417–422, 2010.

[30] A. S. Borggreve, B. F. Kingma, S. A. Domrachev et al., "Surgical treatment of esophageal cancer in the era of multimodality management," *Annals of the New York Academy of Sciences*, vol. 1434, no. 1, pp. 192–209, 2018.

[31] L. Goense, P. S. van Rossum, D. Kandioler et al., "Stage-directed individualized therapy in esophageal cancer," *Annals of the New York Academy of Sciences*, vol. 1381, no. 1, pp. 50–65, 2016.

[32] O. S. Jackie, S. Han, W. Lee, and A. C. Lockhart, "Emerging immunotherapy for the treatment of esophageal cancer," *Expert Opinion on Investigational Drugs*, vol. 25, no. 6, pp. 667–677, 2016.

[33] Y. Song, X. Zhong, P. Gao et al., "Aspirin and its potential preventive role in cancer: an umbrella review," *Frontiers in Endocrinology*, vol. 11, p. 3, 2020.

[34] V. Patel and R. A. Burbridge, "Endoscopic approaches for early-stage esophageal cancer: current options," *Current Oncology Reports*, vol. 17, no. 1, p. 421, 2015.

[35] W. P. Tew, D. P. Kelsen, and D. H. Ilson, "Targeted therapies for esophageal cancer," *The Oncologist*, vol. 10, no. 8, pp. 590–601, 2005.

[36] T. Guo, W. Li, and X. Cai, "Applications of single-cell omics to dissect tumor microenvironment," *Frontiers in Genetics*, vol. 11, article 548719, 2020.

[37] T. Wu and Y. Dai, "Tumor microenvironment and therapeutic response," *Cancer Letters*, vol. 387, pp. 61–68, 2017.

[38] Y. Li, L. Zhao, and X. F. Li, "Hypoxia and the tumor microenvironment," *Technology in Cancer Research & Treatment*, vol. 20, 2021.

[39] A. Aponte-López and S. Muñoz-Cruz, "Mast cells in the tumor microenvironment," *Advances in Experimental Medicine and Biology*, vol. 1273, pp. 159–173, 2020.

[40] K. C. Corn, M. A. Windham, and M. Rafat, "Lipids in the tumor microenvironment: from cancer progression to treatment," *Progress in Lipid Research*, vol. 80, article 101055, 2020.

[41] X. Zhang, L. Peng, Y. Luo et al., "Dissecting esophageal squamous-cell carcinoma ecosystem by single-cell transcriptomic analysis," *Nature Communications*, vol. 12, no. 1, p. 5291, 2021.

[42] W. Guo, F. Tan, Q. Huai et al., "Comprehensive analysis of PD-L1 expression, immune infiltrates, and m6A RNA methylation regulators in esophageal squamous cell carcinoma," *Frontiers in Immunology*, vol. 12, article 669750, 2021.

[43] H. Yang, Q. Zhang, M. Xu et al., "CCL2-CCR2 axis recruits tumor associated macrophages to induce immune evasion through PD-1 signaling in esophageal carcinogenesis," *Molecular Cancer*, vol. 19, no. 1, p. 41, 2020.

[44] T. Lu, R. Xu, Q. Li et al., "Systematic profiling of ferroptosis gene signatures predicts prognostic factors in esophageal squamous cell carcinoma," *Molecular Therapy Oncolytics*, vol. 21, pp. 134–143, 2021.

[45] L. Han, Q. L. Gao, X. M. Zhou et al., "Characterization of CD103(+) CD8(+) tissue-resident T cells in esophageal squamous cell carcinoma: may be tumor reactive and resurrected by anti-PD-1 blockade," *Cancer Immunology, Immunotherapy: CII*, vol. 69, no. 8, pp. 1493–1504, 2020.

Research Article

miR-187/PDLIM1 Gets Involved in Gastric Cancer Progression and Cisplatin Sensitivity of Cisplatin by Mediating the Hippo-YAP Signaling Pathway

Yeru Tan [1] **Yuehua Li,**[1] **Hongbo Zhu** [1] **Xiaoping Wu,**[1] **Kai Mei,**[2] **Pian Li,**[2] **and Qiao Yang** [2]

[1]*The First Affiliated Hospital, Department of Medical Oncology, Hengyang Medical School, University of South China, Hengyang, Hunan 421001, China*
[2]*The First Affiliated Hospital, Department of Oncology Radiotherapy, Hengyang Medical School, University of South China, Hengyang, Hunan 421001, China*

Correspondence should be addressed to Qiao Yang; 2018012084@usc.edu.cn

Gastric cancer (GC) is one of the most prevalent malignancies in the digestive system across the world. The function and mechanism of PDLIM1, a cancer-suppressing gene, in gastric cancer progression remain unclear. This study is aimed at investigating the expression features and function of PDLIM1 in GC. RT-qPCR and western blot were used to compare the profiles of PDLIM1 and miR-187 between GC and normal tissues. The cell models of PDLIM1 overexpression and low expression were established in gastric cancer cell lines MKN45 and AGS. CCK8 and BrdU assays measured cell proliferation. Flow cytometry monitored cell apoptosis. Transwell analyzed cell invasion and migration. The influence of miR-187 overexpression on gastric cancer development was assessed. We predicted the targeted correlation between miR-187 and PDLIM1 through bioinformatics, which was corroborated via dual luciferase activity assay and RIP. Meanwhile, the cell model of PDLIM1 overexpression was built in AGS cells transfected with miR-187 mimics. A rescue experiment was conducted to assess the impact of PDLIM1 overexpression on the procancer function of miR-187. As a result, in contrast with normal paracancer tissues, PDLIM1 was substantially downregulated in GC tissues. Moreover, PDLIM1 overexpression considerably dampened proliferation, invasion, and migration in GC cells, boosted the cell apoptosis, and bolstered their sensitivity to cisplatin. PDLIM1 knockdown or miR-187 overexpression dramatically fostered GC cell proliferation, invasion, and migration and repressed cell apoptosis. Mechanism studies demonstrated that PDLIM1 vigorously restrained the profiles of the Hippo-YAP signaling pathway and the downstream target genes. miR-187 targeted PDLIM1, while miR-187 overexpression cramped PDLIM1 expression. The rescue experiment suggested that PDLIM1 overexpression weakened the procancer function of miR-187 in GC cells. In conclusion, our study demonstrated that PDLIM1 presented a low expression in GC tissues, while miR-187/PDLIM1 participated in GC development and cisplatin sensitivity by mediating the Hippo-YAP signaling pathway.

1. Introduction

The incidence rate of gastrointestinal tumors is increasing in recent years [1]. Gastric cancer (GC), one of the most prevailing malignancies in the digestive system across the world, is also the fifth biggest contributor to cancer and the third biggest cause of cancer-related death worldwide

[2, 3]. It mainly arises from helicobacter pylori infection, age, high salt intake, and diets deficient in fruits and vegetables [4]. Existing treatment strategies for GC includes genome classification, surgical resection and treatment, systemic radiotherapy, and chemotherapy as well as targeted therapy and immunotherapy. The onset of GC is not easy to be found, and the recurrence and metastasis rate after sur-

gery is high. Therefore, there are still many difficulties in its treatment [5, 6]. Cisplatin (DDP), an efficacious chemotherapy drug, is of great value in treating various cancers like GC [7]. However, GC patients often experience relapse and metastasis due to resistance to DDP therapy, with limited therapeutic effect [8]. Thus, the exact mechanism that influences GC progression and DDP resistance needs to be clarified. This is pivotal to exploring efficacious targets for GC treatment.

MicroRNAs (miRNAs), small noncoding RNAs about 18-25 nucleotides in length, can combine with the 3'-untranslated region (3'UTR) of target mRNAs to suppress the profiles of target genes [9, 10]. miRNAs can be used as prognostic biomarkers. They can exert a crucial function in modulating many biological processes of multiple human diseases, such as cancer [11]. miR-187, a member of the miRNA family, partakes in the development of umpteen cancers, including nonsmall cell lung cancer [12] and cervical cancer [13]. More of note, miR-187 can serve as a new serum biomarker for the early detection of GC [14]. Furthermore, miR-187 acts as a tumor suppressor in the context of GC, which hints that it may be a biomarker and therapeutic target for GC patients [15]. Nevertheless, the exact mechanism of miR-187 influencing GC development needs to be improved.

PDLIM1 (PDZ and LIM domain protein 1), also called CLP36, Elfin, or CLIM1, reportedly interacts with many proteins, including a-actinin, paladin, FHL1, and EGFR, thus playing a significant part in cytoskeletal tissues, neuronal signals, and organ development [16]. Increasing evidence has indicated that PDLIM1 expression is dysregulated in many tumors like glioma [17] and breast cancer [18]. Additionally, the anti-PDLIM1 auto-antibody can serve as a novel serum marker for ovarian cancer [19], but its function in GC development has been rarely reported.

The Hippo (Hpo) pathway was first identified in Drosophila. It has been reported to be an evolutionarily conserved signaling pathway that modulates cell proliferation, tissue homeostasis, and tissue regeneration [20, 21]. Reportedly, dysregulation of the pathway pertains to abnormal tissue growth and tumorigenesis. In the mammalian system, the relevant phosphorylated protein (YAP) is replaced in the cytoplasm to promote degradation when the Hippo signaling pathway is initiated. Inactivation of the Hippo pathway moves unphosphorylated YAP into the nucleus, hence eliciting the transcriptional activities of genes associated with cell growth [22, 23]. The Hippo pathway has a huge function in different cancers, but its correlation with PDLIM1 has not been elucidated. Thus, confirming the correlation between PDLIM1 and the regulation of the Hippo pathway seems to be of great significance in human cancers, particularly GC.

In this study, we investigated the function and exact mechanism of PDLIM1 during GC progression. The miR-187/PDLIM1 is involved in GC development and cisplatin sensitivity by regulating the Hippo-YAP signaling pathway. This provides a new idea for the clinical treatment of GC and its resistance to DDP.

2. Materials and Methods

2.1. Clinical Specimen Collection and Processing. The cancer tissues and normal paracancer tissues of 45 GC patients who received gastrectomy from October 2015 to March 2016 in our hospital were harvested. Prior to the surgery, they were not subjected to chemotherapy, radiotherapy, or other adjuvant therapies. The specimens in the control group were taken from the paracancer tissues of the same patients (at least 3 cm away from the surgical margin). No cancer tissues were detected during pathological examination following the surgery. In accordance with the standards of the World Health Organization (WHO), we substantiated the diagnosis of GC from the perspective of pathology. All specimens were kept in -196°C liquid nitrogen in preparation for RNA extraction.

2.2. Cell Culture and Transfection. Human GC cell lines (MKN-45, AGS) and human DDP-resistant GC cell lines (AGS/DDP) were obtained from American Type Culture Collection (ATCC; Manassas, Virginia, USA). The cells were grown in the PRMI-1640 medium supplemented with 10% FBS (Invitrogen, Carlsbad, CA, US) at 37°C with 5% CO_2. The cells were passaged every two or three days.

The cells were inoculated into 6-well plates with a density of 5×10^6/well. We transfected PDLIM1 overexpression plasmid (pcDNA3.1-PDLIM1), PDLIM1 low expression plasmid (sh-PDLIM1) and its corresponding negative control (sh-NC), and miR-187 mimics and their corresponding negative control fragment (miR-NC) into MKN-45 and AGS cells according to the instructions of FuGENE®HD Transfection Reagent (Roche, Shanghai, China), respectively. Cells in each group were incubated in an incubator with 5% CO_2 at 37°C. 24 hours posttransfection, the steadily growing cells in each group were harvested.

2.3. Cell Counting Kit-8 (CCK8) Assay. MKN45 and AGS cells were seeded into 96-well plates with a density of 1×10^3 cells/well and incubated for 24 hours. Subsequently, $10 \mu l$ of CCK8 reagent (Dojindo Molecular Technologies, Kumamoto, Japan) was added into each well. After the cells were incubated for an hour at 37°C, the OD450 value of each well was determined by a spectrophotometer (Bio-Rad, CA, USA).

2.4. DDP Sensitivity Detection. We measured the viability of DDP-resistant GC cells under the impact of different DDP concentrations using 3-(4,5-dimethyl-2-thiazolyl)-2,5-diphenyl-2H-tetrazolium bromide (MTT; Sigma-Aldrich) with a view to confirming and visualizing the semi-inhibitory concentration (IC50) value of DDP. The IC50 value was defined as the concentration of DDP corresponding to 50% of cell viability inhibition rates in the curve [24].

2.5. Bromodeoxyuridine (BrdU) Staining. Following transfection, GC cells in each group were moved onto coverslips (Beyotime, Shanghai, China) for 12 hours of culture. Later, the cells were incubated with BrdU solution (Beyotime, Shanghai, China) for 6 hours. The culture medium was dis-

carded. GC cells were immobilized with 4% paraformaldehyde for 30 minutes, incubated with anti-BrdU antibody (Beyotime, Shanghai, China) for an hour at room temperature (RT), and flushed with phosphate buffer saline (PBS). The number of positive BrdU cells was calculated [25].

2.6. Transwell Assay. Transwell examined cell invasion and migration. The cells posttransfection were harvested. With the cell density set to 4×10^4, the cells were suspended in a serum-free medium supplemented with 1 μg/mL mitomycin C. Then, the cells were inoculated into an upper compartment precoated with Matrigel, while 10% fetal bovine serum (FBS) was given to the lower compartment. Subsequent to 24 hours of incubation at 37°C, substrates and cells that failed to pass the membrane surface in the upper compartment were wiped off. The cells were rinsed, immobilized with paraformaldehyde for 10 minutes, and dyed with 0.5% crystal violet. A microscope was adopted to observe cell invasion. As for the cell migration test, Matrigel was not administered to the upper Transwell chamber, but the other steps were similar to those in the invasion test.

2.7. Flow Cytometry. Annexin V-FITC double staining was implemented to measure cell apoptosis. Following 24 hours of transfection, the cells were digested with trypsin, harvested, and inoculated into 6-well plates for 24 hours of further culture, with the cell density adjusted to 2×10^6 cells/well. The supernatant was removed. The cells were flushed with precooled PBS twice and resuspended with $1 \times$ binding buffer. Later, 5 μL Annexin V-FITC and 5 μL PI were administered to the cell suspension, and they were conflated thoroughly. The cells were incubated at RT for 15 minutes, and the cell apoptosis rate was confirmed by a flow cytometry instrument within an hour. Apoptosis rate = number of apoptotic cells/(number of apoptotic cells + number of normal cells) × 100%. All procedures were done as instructed by the apoptosis kit (Yeasen Biotech Co., Ltd., Shanghai, China).

2.8. RT-qPCR. TRIzol reagent was utilized to extract total RNA from the cells. As per the supplier's instructions, the PrimeScript™ RT Reagent kit (Invitrogen, Shanghai, China) was taken to reverse-transcribe the RNA into cDNA. The Bio-Rad CFX96 quantitative PCR system and SYBR were utilized for qPCR in line with the supplier's stipulation. The conditions for PCR were as follows: 5 minutes of predenaturation at 95°C, 15 seconds of denaturation at 95°C, and 30 seconds of annealing at 60°C. β-Actin was adopted as the internal parameter for confirming PDLIM1 and miR-187 expressions. The $2^{-\Delta\Delta Ct}$ approach was adopted for statistical analysis. Each experiment was duplicated three times. Guangzhou Ruibo Company took on the design and synthesis of the primers. The primer sequences are detailed in Table 1.

2.9. Western Blot. The cellular protein was isolated with protein lysis buffer (Roche, USA). Subsequently, 50 μg of the total protein was subjected to SDS-PAGE and transferred onto polyvinylidene fluoride (PVDF) membranes. After blocked with 5% skimmed milk in PBST for an hour, the

TABLE 1: The primers used in this study.

Gene name	Primer sequence (5'-3')
PDLIM1	Forward: CCCAGCAGATAGACCTCCAG
	Reverse: GTTGTCTGTGCAGCCTTTGA
miR-187	Forward: TCGTGTCTTGTGTTGCAGC
	Reverse: GTGCAGGGTCCGAGGT
β-Actin	Forward: GGCATCCTCACCCTGAAGTA
	Reverse: GAAGGTGTGGTGCCAGATTT

membranes were washed with TBST three times, and incubated with primary antibodies including Anti-Bax antibody (ab32503, 1 : 1000, Abcam, USA), Anti-Bcl-2 antibody (ab32124, 1 : 1000, Abcam, USA), Anti-Bad antibody (ab32445, 1 : 1000, Abcam, USA), Anti-PDLIM1 antibody (ab129015, 1 : 1000, Abcam, USA), Anti-Amphiregulin antibody (ab89119, 1 : 1000, Abcam, USA), Anti-Myc antibody (ab185656, 1 : 1000, Abcam, USA), Anti-CCND2 antibody (ab267318, 1 : 1000, Abcam, USA), Anti-YAP antibody (ab52771, 1 : 1000, Abcam, USA), Anti-p-YAP antibody (ab254343, 1 : 1000, Abcam, USA), Anti-β-actin antibody (ab115777, 1 : 1000, Abcam, USA), and Anti-Lamin A antibody (ab108595, 1 : 1000, Abcam, USA) at 4°C overnight. The membranes were washed with TBST and then incubated with the horseradish peroxidase (HRP)-labeled anti-rabbit secondary antibody (1 : 3000, Abcam, USA) for an hour at RT. The bands were developed with Pierce™ ECL Western Blotting Substrate (Invitrogen, USA). The gray value of each protein was analyzed using Image J analysis software (National Institutes of Health, USA).

2.10. Dual Luciferase Reporter Assay. We predicted the target genes of miR-187 through TargetScan. Pmir-GLO-NC, pmir-GLO-PDLIM1-wt, pmir-GLO-PDLIM1-mut, miR-NC, and miR-187, ordered from Sangon Biotech (Shanghai, China), were transfected into the cells with Lipofectamine™2000 (Invitrogen, Carlsbad, CA, USA). Subsequent to incubation, the cells were harvested and flushed with PBS twice. The Dual-Lucy Assay Kit (Progema, Madison, WI, USA) was used for the assay [26].

2.11. RIP Assay. To further confirm the correlation between miR-187 and PDLIM1, we utilized the Magna RIP™ RNA Binding Protein Immunoprecipitation Kit (Millipore, Bedford, MA, USA) for RIP analysis. Then, AGS cells (2×10^7) transfected with miR-187 or its negative control were harvested and subjected to 200 μL of RIP lysis buffer. They were lysed on ice for 5 minutes and centrifuged at 1500 rpm for 15 minutes to produce the supernatant. The extracts were incubated with Anti-Ago2 or Anti-IgG (Sigma) overnight. Subsequently, magnet beads were flushed with a washing buffer five times, and the supernatant was removed. The beads were lysed with the protease K lysate at 55°C for 30 minutes. The supernatant was put in a new centrifuge tube. The total RNA was extracted through phenol–chloroform-isoamyl alcohol extraction and purified via isopropanol

(a)

(b)

(c)

(d)

(e)
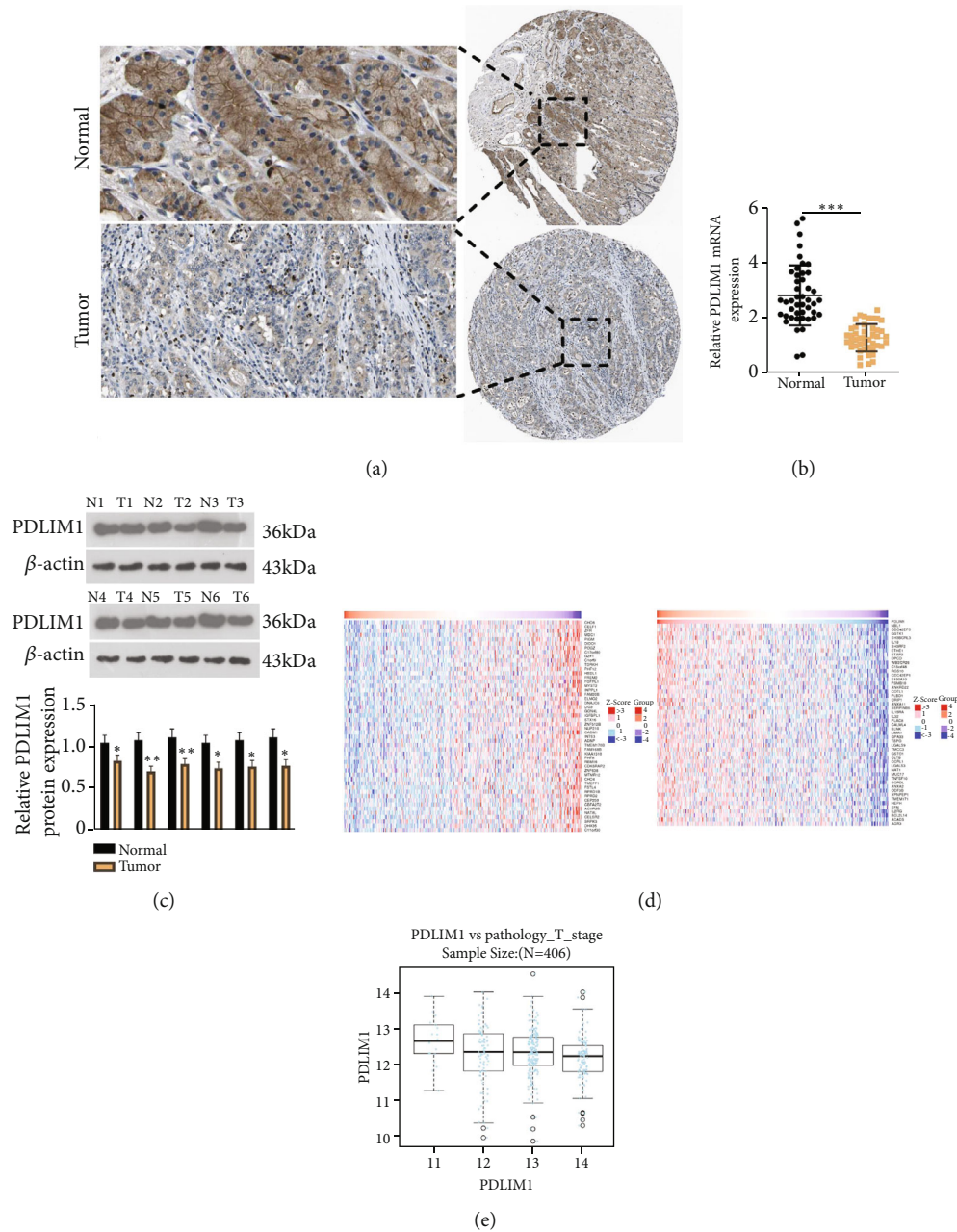
Figure 1: PDLIM1 expression is lowered in GC tissues and cell lines. (a) The database (https://www.proteinatlas.org/) was introduced to examine the positive profile of PDLIM1 in GC tissues. (b, c) RT-PCR and western blot evaluated the profile of PDLIM1 in GC tissues and normal paracancer tissues. (d) The coexpressed genes of PDLIM1 in GC (LindOmics). The heat maps exhibited the positively and negatively coexpressed Top-50 genes of PDLIM1 in GC. (e) The staging of tumors. $***P < 0.001$ (vs. the Normal group). $N = 45$.

centrifugation. The coprecipitated RNA was isolated and analyzed through RT-qPCR.

2.12. Statistical Analysis. GraphPad Prism 8 was used for statistical analysis. Experimental data were presented as mean ± standard deviation (SD). One-way ANOVA and Student's t-test were taken for comparison. Two-sided $P < 0.05$ was regarded as statistically significant. The experiment was duplicated three times.

3. Results

3.1. PDLIM1 Expression Is Lowered in GC Tissues and Cell Lines. To determine whether PDLIM1 could exert a significant function in GC development, we uncovered that PDLIM1 expression was remarkably attenuated in GC tissues (vis-a-vis normal paracancer tissues) through the database (https://www.proteinatlas.org/) (Figure 1(a)). RT-PCR ($P < 0.05$, Figure 1(b)) and western blot (Figure 1(c)) confirmed that the profile of PDLIM1 was lowered in GC tissues

Table 2: The correlation between PDLIM1 expression and clinical characteristics in the tissue specimens of GC patients.

| Characteristics | Patients | Expression of PDLIM1 | | P value |
		High-PDLIM1	Low-PDLIM1	
Total	45	23	22	
Age (years)				0.661
<63	21	10	11	
≥63	24	13	11	
Gender				0.668
Male	26	14	12	
Female	19	9	10	
Tumor location				0.837
Bottom	20	10	10	
Body	12	7	5	
Gastric antrum	13	6	7	
Diameter				0.023*
< 3 cm	25	9	16	
≥ 3 cm	20	14	6	
Clinical stage				0.005*
Early	24	17	7	
Middle and late	21	6	15	
Distant metastasis				0.025*
Without	22	15	7	
With	23	8	15	
Vascular invasion				0.023*
Yes	25	9	16	
No	20	14	6	

in contrast with normal paracancer tissues. Additionally, the coexpressed genes of PDLIM1 in the context of GC were analyzed through the LinkedOmics database (Figure 1(d)). They were negatively correlated with the staging of tumors (Figure 1(e)). The correlation between PDLIM1 expression and clinical characteristics in the tissue specimens of GC patients was shown in Table 2. These discoveries revealed that PDLIM1 pertained to the malignant phenotype of GC cells and possibly played a procancer role.

3.2. PDLIM1 Hampers GC Cell Proliferation, Migration, and Invasion and Boosts Apoptosis.

To confirm the impact of PDLIM1 on GC development, we established a cell model of PDLIM1 overexpression in MKN-45 and AGS ($P < 0.05$, Figure 2(a)). CCK8 and BrdU denoted that PDLIM1 overexpression brought about a substantial reduction in cell proliferation ($P < 0.05$, Figures 2(b) and 2(c)). Transwell indicated that PDLIM1 overexpression vigorously lessened cell invasion and migration ($P < 0.05$, Figure 2(d)). Flow cytometry revealed that cell apoptosis was remarkably augmented in the PDLIM1 group vis-a-vis the control group ($P < 0.05$,

Figure 2(e)). Western blot suggested that PDLIM1 overexpression notably attenuated the profile of the anti-apoptotic protein Bcl-2 and augmented the profiles of proapoptotic proteins Bax and Bad ($P < 0.05$, Figure 2(f)). These outcomes demonstrated that PDLIM1 overexpression weakened the malignant biological behaviors of GC cells.

3.3. PDLIM1 Knockdown Bolsters GC Cell Proliferation, Migration, and Invasion and Hinders Apoptosis.

To confirm the influence of PDLIM1 on GC development, we built a PDLIM1 knockdown model in MKN-45 and AGS cells ($P < 0.05$, Figure 3(a)). CCK8 and BrdU denoted that PDLIM1 knockdown considerably augmented cell viability ($P < 0.05$, Figures 3(b) and 3(c)). Transwell indicated that PDLIM1 knockdown greatly strengthened cell invasion and migration ($P < 0.05$, Figure 3(d)). Flow cytometry unraveled that by contrast to the control group, the PDLIM1 group had a distinct decline in cell apoptosis ($P < 0.05$, Figure 3(e)). Western blot suggested that PDLIM1 knockdown dramatically heightened Bcl2 expression and lowered Bax and Bad expressions ($P < 0.05$, Figure 3(f)). These findings demonstrated that PDLIM1 inhibition boosted the malignant biological behaviors of GC cells.

3.4. PDLIM1 Overexpression Strengthens the Sensitivity of GC Cells to Cisplatin.

To better understand the function of PDLIM1 overexpression in modulating DDP-resistance in AGS/DDP cells, we synthesized PDLIM1 or NC. First, they were transfected into AGS/DDP cells. PDLIM1 expression was confirmed via RT-qPCR. It turned out that the profile of PDLIM1 was notably higher than that of NC ($P < 0.05$, Figure 4(a)). To verify whether PDLIM1 presented different expressions in the two cell lines, we performed RT-qPCR for analysis. As a result, the mRNA level of PDLIM1 was evidently lower in AGS/DDP than in AGS ($P < 0.05$, Figure 4(b)). Moreover, CCK8 was performed to confirm the IC50 value, thus testing the resistance of AGS/DDP to DDP. The outcomes suggested that the IC50 value to DDP in AGS/DDP was 81.3 μg/mL ($P < 0.05$, Figure 4(c)). Later, AGS/DDP cells, treated with DDP, were transfected with PDLIM1 or NC. CCK8 examined cell viability. PDLIM1 overexpression culminated in a notably lower survival rate in contrast with the DDP group ($P < 0.05$, Figure 4(d)). These findings confirmed that an increase in PDLIM1 markedly bolstered AGS/DDP cell apoptosis, whereas PDLIM1 overexpression vigorously attenuated the resistance of AGS/DDP cells to DDP.

3.5. miR-187 Overexpression Facilitates GC Progression.

To determine the influence of miR-187 on GC development, we established a cell model of miR-187 overexpression in MKN-45 and AGS cells ($P < 0.05$, Figure 5(a)). RT-PCR exhibited that the profile of miR-187 was greatly heightened in GC tissues as compared with normal paracancer tissues ($P < 0.05$, Figure 5(b)). CCK8 and BrdU indicated that overexpression of miR-187 contributed to a conspicuous increase in cell proliferation ($P < 0.05$, Figures 5(c) and 5(d)). Transwell denoted that overexpression of miR-187 dramatically strengthened cell invasion and migration ($P < 0.05$, Figure 5(e)). Flow cytometry revealed that as opposed to
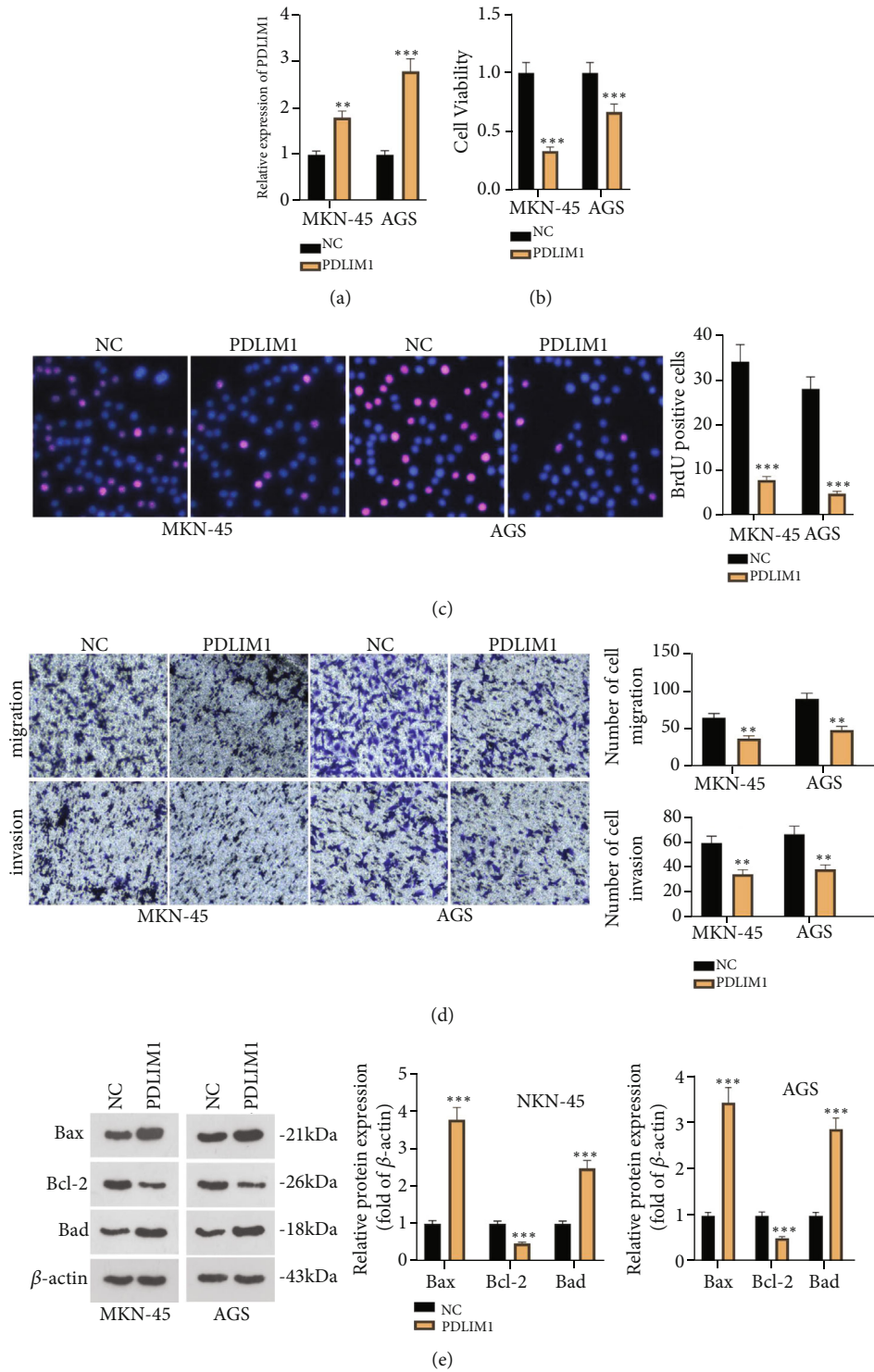
FIGURE 2: PDLIM1 hampers GC cell proliferation, migration, and invasion and boosts apoptosis. A cell model of PDLIM1 overexpression was built in MKN-45 and AGS cells. (a) RT-qPCR confirmed the profile of PDLIM1. (b, c) CCK8 and BrdU verified the viability of MKN-45 and AGS cells. (d) Transwell detected GC cell invasion and migration. (e) Flow cytometry examined cell apoptosis. $^{**}P < 0.01$, $^{***}P < 0.001$ (vs. the NC group). $N = 3$.
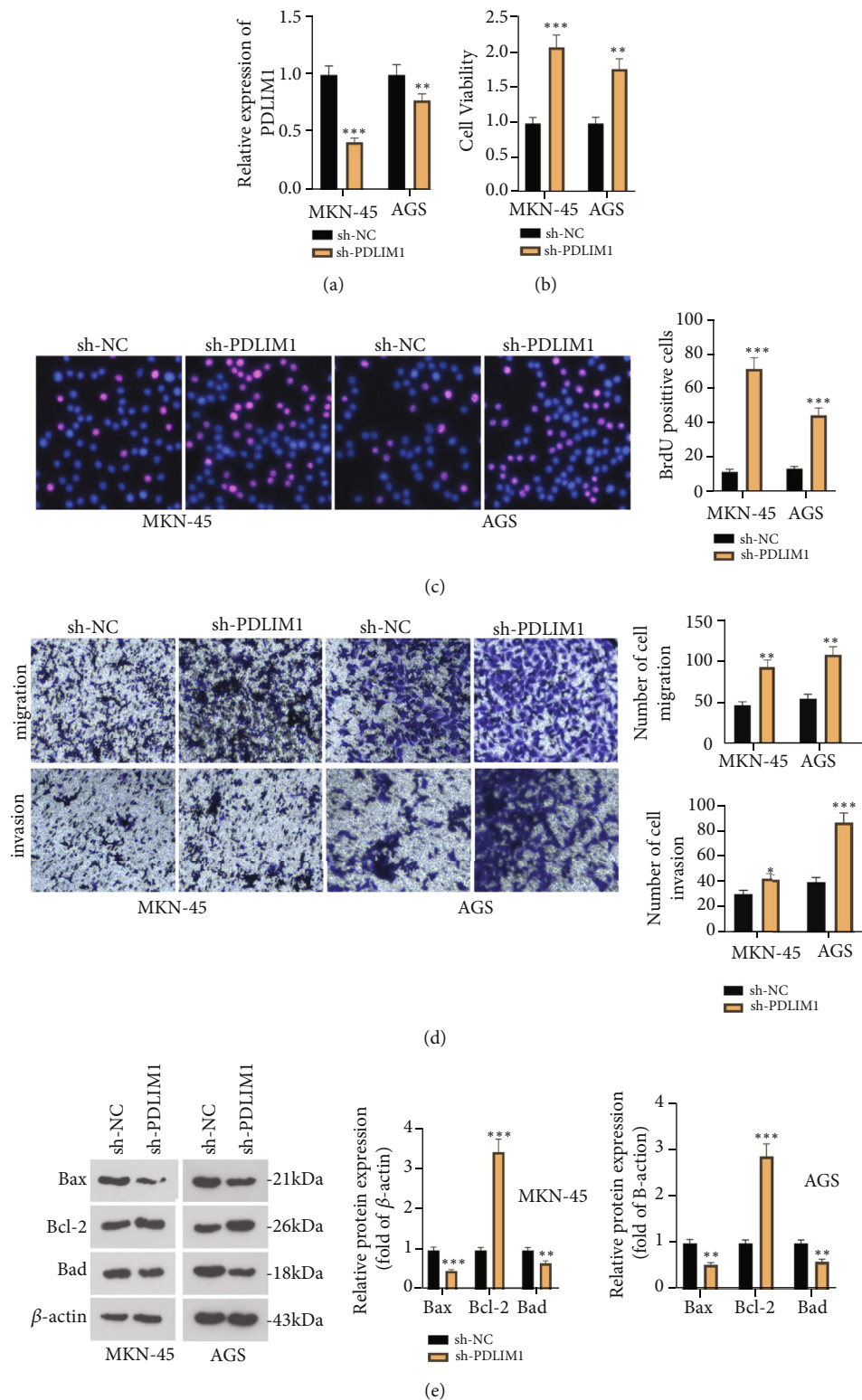
Figure 3: PDLIM1 knockdown bolsters GC cell proliferation, migration, and invasion and suppresses apoptosis. A cell model of PDLIM1 knockdown was established in MKN-45 and AGS cells. (a) RT-PCR determined PDLIM1 expression. (b, c) CCK8 and BrdU examined the viability of MKN-45 and AGS cells. (d) Transwell monitored cell invasion and migration. (e) Flow cytometry measured cell apoptosis. $^{**}P < 0.01$, $^{***}P < 0.001$ (vs. the sh-NC group). $N = 3$.

(a)

(b)

(c)

(d)
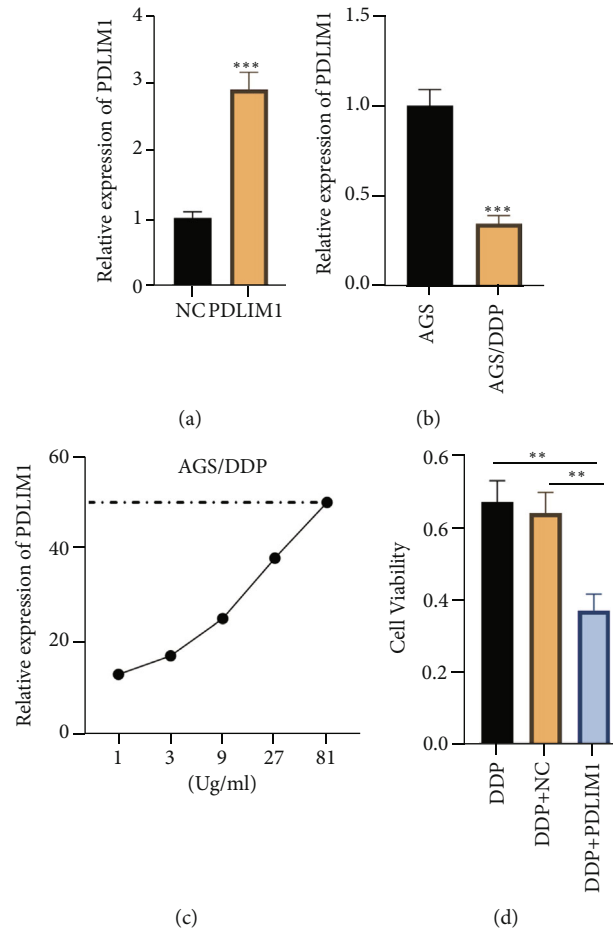
Figure 4: PDLIM1 overexpression strengthens the sensitivity of GC cells to cisplatin. (a) PDLIM1 or NC was transfected into AGS/DDP cells resistant to DDP. The profile of PDLIM1 was determined via RT-qPCR. (b) RT-qPCR confirmed the mRNA profile of PDLIM1 in the two cell lines. (c) The IC50 value to DDP in the cell lines was determined by CCK8. (d) The DDP-resistant cells were transfected with PDLIM1 and then treated with $1 \mu g/mL$ DDP. CCK8 monitored cell proliferation. The apoptosis rate of each group was calculated. $^{**}P < 0.01$, $^{***}P < 0.001$ vs. the DDP group). $N = 3$.

the control group, the miR-187 group had a considerable reduction in cell apoptosis ($P < 0.05$, Figure 5(f)). These discoveries demonstrated that the transfection of miR-187 mimics stepped up the malignant development of GC cells.

3.6. miR-187 Targets PDLIM1. By using the Starbase database (http://starbase.sysu.edu.cn/), we predicted that PDLIM1 was the target of miR-187 (Figure 6(a)). To better understand the targeted correlation between miR-187 and PDLIM1, we implemented dual luciferase activity assay. It transpired that miR-187 vigorously suppressed PDLIM1-WT activity ($P < 0.05$, Figure 6(b)) but exerted little impact on PDLIM1-MUT ($P < 0.05$, Figure 6(b)). RIP revealed that following miR-187 transfection, PDLIM1 precipitated in the Ago2 antibody group was more than that in the IgG group. This hinted that PDLIM1 combined with Ago2 protein via miR-187 ($P < 0.05$, Figure 6(c)). To probe the potential mechanism of miR-187, we evaluated the coexpressed genes of miR-187 in the context of GC via the LinkedOmics database. As a result, PDLIM1 was negatively associated with miR-187 in GC (Figures 6(d) and 6(e)). Later, the profile of PDLIM1 subsequent to miR-187 overexpression in MKN-45 cells was measured. By contrast

to the control group, miR-187 overexpression vigorously repressed PDLIM1 expression ($P < 0.05$, Figure 6(f)). These phenomena demonstrated that miR-187 targeted and negatively modulated PDLIM1 expression in GC cells.

3.7. PDLIM1 Influences the Hippo-YAP Pathway. The Hippo pathway exerted a significant function in cancer progression [27]. We delved into the regulatory impact of PDLIM1 on the Hippo-YAP pathway. In Figures 7(a) and 7(b), RT-qPCR denoted that the mRNA levels of YAP and its target genes AREG, Myc, and CCND2 were negatively modulated by PDLIM1 in MKN-45 and AGS cells ($P < 0.05$, Figures 7(a) and 7(b)). This outcome was also substantiated by western blot subsequently ($P < 0.05$, Figure 7(c)). As YAP was translocated into the nucleus and influenced the transcription of its target genes, we checked the abundance of nuclear and phosphorylated YAP in the nucleus. Figure 7(d) displayed that the levels of YAP and phosphorylated YAP were lowered in the nuclei of cells with PDLIM1 overexpression ($P < 0.05$, Figure 7(d)). These discoveries unraveled that PDLIM1 impeded the Hippo/YAP signaling pathway.

(a)

(b)

(c)

(d)

(e)

(f)
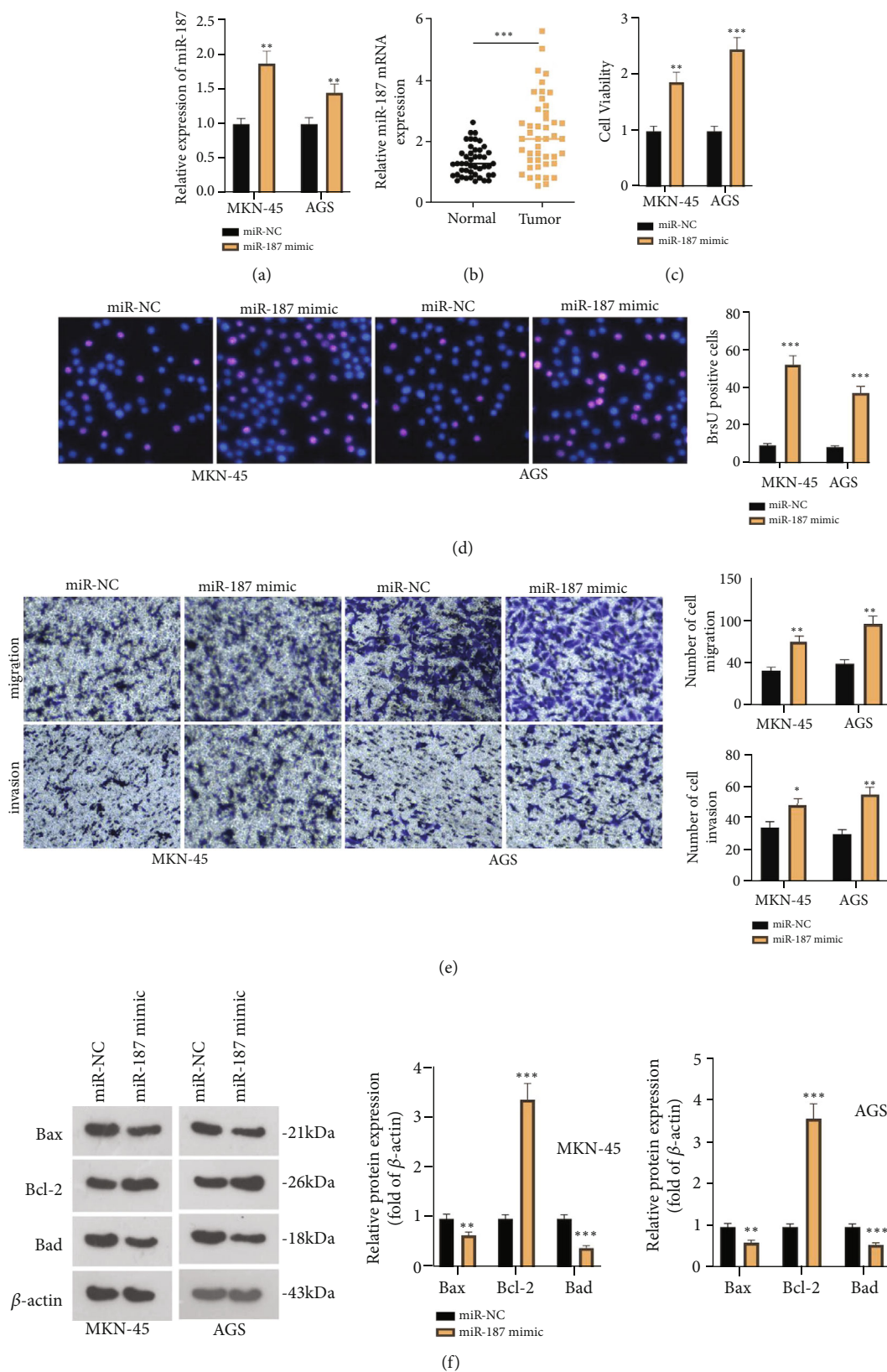
FIGURE 5: miR-187 overexpression facilitates GC development. A cell model of miR-187 overexpression was established in MKN-45 and AGS cells. (a) RT-qPCR examined miR-187 expression. (b) RT-qPCR confirmed miR-187 expression in GC tissues and normal paracancer tissues. (c, d) CCK8 and BrdU measured MKN-45 and AGS cell viability. (e) Transwell monitored invasion and migration in MKN-45 and AGS cells. (f) Flow cytometry evaluated cell apoptosis. (g) Western blot verified the profiles of Bcl2, Bax, and Bad. $^{**}P < 0.01$, $^{***}P < 0.001$ (vs. the miR-NC group). $N = 3$.
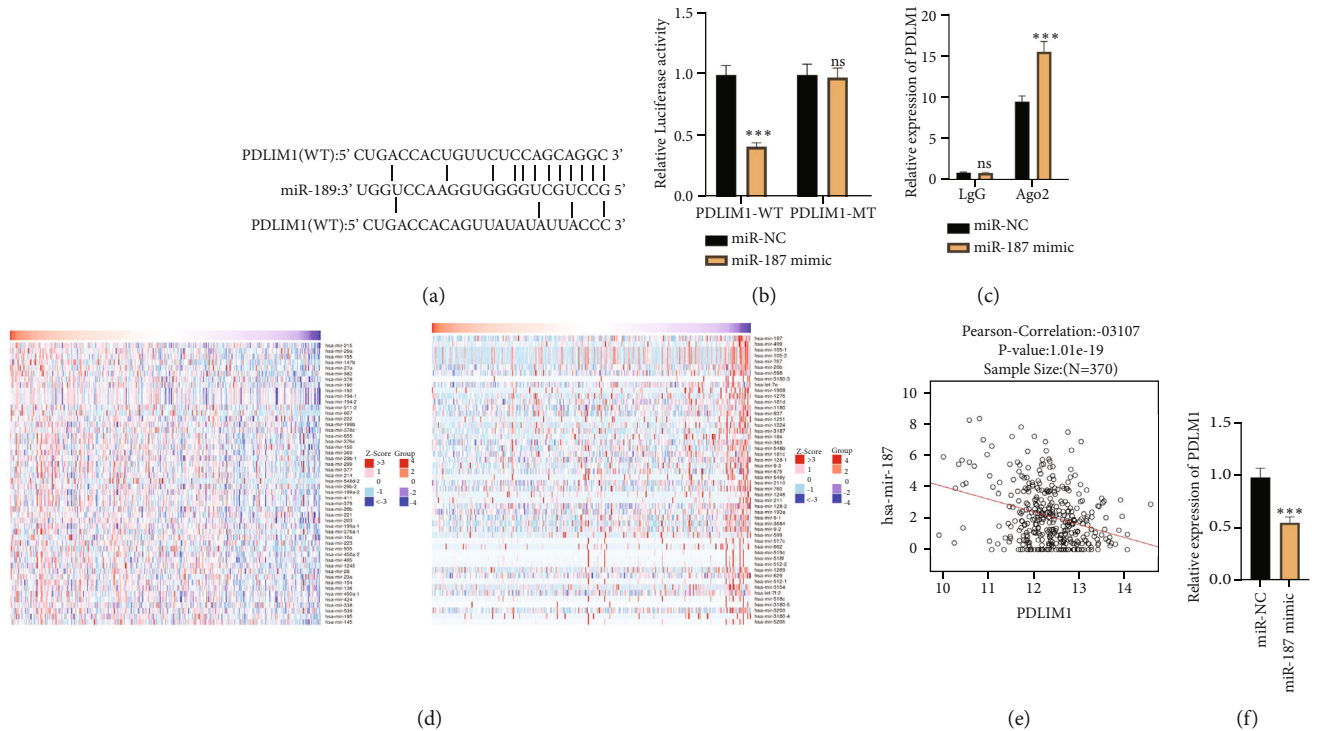
FIGURE 6: miR-187 targets PDLIM1. (a) The Starbase database (http://starbase.sysu.edu.cn/) forecast the binding target of PDLIM1 and miR-187. (b, c) Dual luciferase activity assay and RIP corroborated the binding relationship between PDLIM1 and miR-187. (d) The coexpressed genes of miR-187 in GC (LindOmics). The heat maps exhibited the positively and negatively coexpressed Top-50 genes of miR-187 in GC. (e) PDLIM1 was negatively correlated with miR-187 in GC. (f) RT-qPCR confirmed PDLIM1 expression in MKN-45 cells. ns $P > 0.05$, ***$P < 0.001$. $N = 3$.

3.8. PDLIM1 Overexpression Weakens the Procancer Function of miR-187 in GC Cells. To dig deeper into the influence of PDLIM1 overexpression on the procancer function of miR-187 in GC cells, we transfected PDLIM1 overexpression plasmid into AGS cells already transfected with miR-187 mimics and confirmed the transfection efficiency via RT-qPCR. As a consequence, in contrast with the control group, miR-187 expression was notably heightened in the miR-187 group, whereas PDLIM1 lowered the profile of miR-187 ($P < 0.05$, Figure 8(a)). CCK8 and BrdU staining measured cell proliferation. As opposed to the control group, the miR-187 group went through a notable increase in cell proliferation. But in contrast with the miR-187 group, PDLIM1 overexpression vigorously dampened AGS cell proliferation ($P < 0.05$, Figures 8(b) and 8(c)). Transwell revealed that in contrast with the control group, the miR-187 group experienced a distinct increase in cell migration and invasion. But as compared with the miR-187 group, the miR − 187 + PDLIM1 group had a substantial decline in AGS cell migration and invasion ($P < 0.05$, Figure 8(d)). Flow cytometry confirmed that by contrast to the NC group, there was a reduction in AGS cell apoptosis in the miR-187 group. As compared with the miR-187 group, AGS cell apoptosis was augmented in the miR − 187 + PDLIM1 group ($P < 0.05$, Figure 8(e)). Western blot determined the profiles of Bax, Bad, and Bcl2. It turned out that the protein profiles of Bax and Bad were abated, and Bcl2 expression was elevated in the miR-187 group vis-a-vis the miR-NC group.

By contrast to the miR-187 group, Bax and Bad expressions were evidently heightened, while Bcl2 expression was lowered in the miR − 187 + PDLIM1 group ($P < 0.05$, Figure 8(f)). The mRNA levels of YAP, AREG, Myc, and CCND2 were dramatically downregulated in the miR − 187 + PDLIM1 group vis-a-vis the miR-187 group ($P < 0.05$, Figure 8(g)). This finding was also corroborated by western blot later ($P < 0.05$, Figure 8(h)). These phenomena demonstrated that PDLIM1 overexpression weakened the procancer function of miR-187, thus slowing GC progression.

4. Discussion

Recently, because of changes in dietary habits, the incidence rate of GC has been relatively lowered. Nevertheless, GC shows strong invasive and metastatic features, and its early detection is poor. Many GC patients have already entered into the advanced stage upon the first diagnosis, demonstrating fast progression and poor prognosis [28–30]. mRNAs have high specificity and are aberrantly expressed under different pathological and physiological circumstances. Therefore, they have drawn enormous attention as underlying diagnostic and predictive biomarkers these years [31, 32]. Here, we confirmed that PDLIM1 was a novel GC inhibitor. PDLIM1 overexpression vigorously hampered proliferation, invasion, and migration in GC cells and strengthened their sensitivity to cisplatin. These discoveries exhibited that PDLIM1 could be utilized as a novel target for GC treatment.
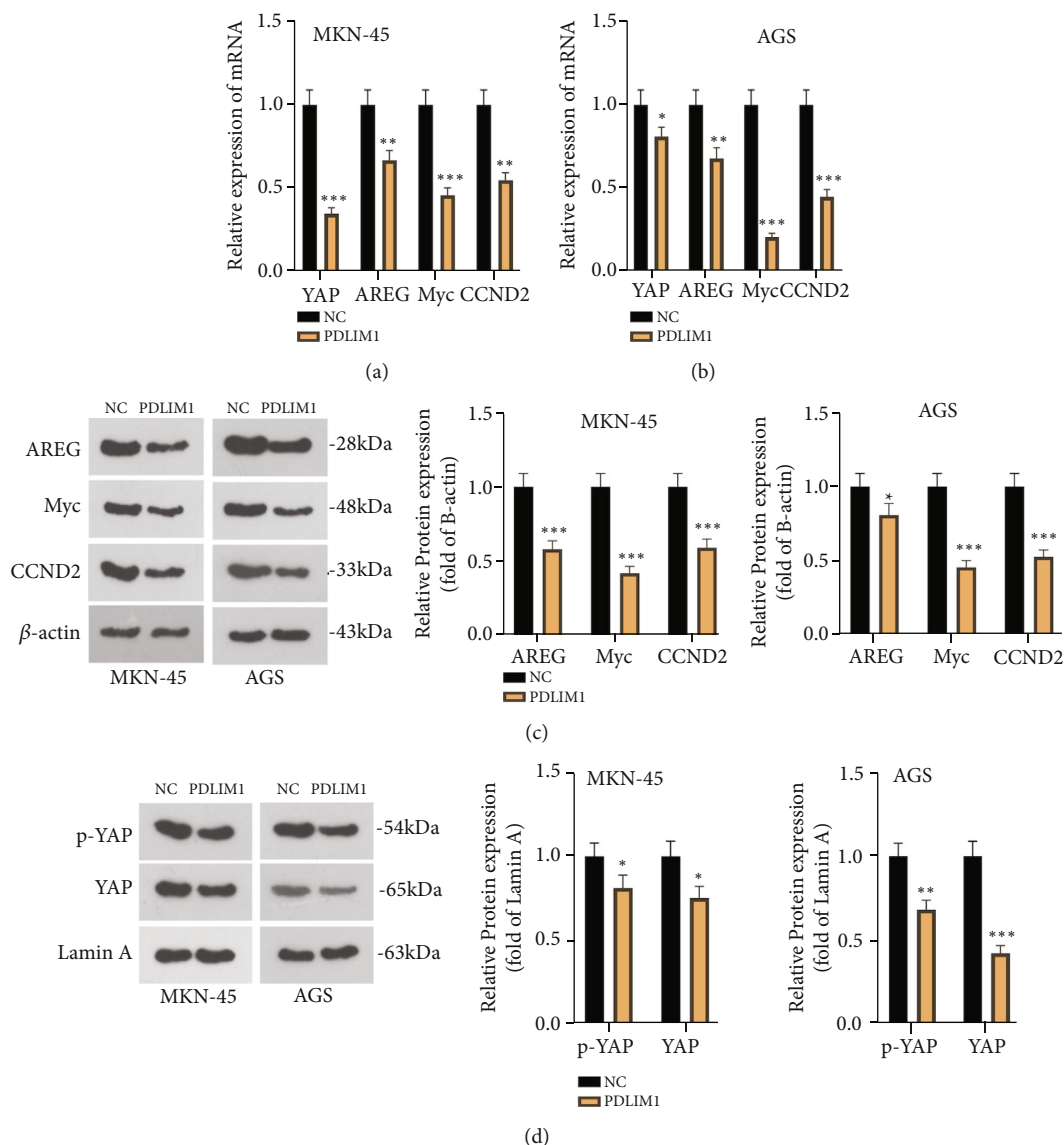
FIGURE 7: PDLIM1 influences the Hippo-YAP pathway. (a, b) RT-qPCR confirmed the profiles of YAP and its target genes in the cells. (c) Western blot verified the profiles of YAP and its target genes in the cells. (d) Western blot measured the abundance of YAP and phosphorylated YAP in the cell nucleus. $^{*}P < 0.05$, $^{**}P < 0.01$, $^{***}P < 0.001$ (vs. the NC group). $N = 3$.

PDLIM1 exerts a significant function in umpteen cancers. For instance, PDLIM1 stabilizes β-catenin at the cell-to-cell junction to suppress epithelial mesenchymal transformation and metastatic potential in colorectal cancer [33]. Moreover, PDLIM1 promotes proliferation and impedes apoptosis to play a carcinogenic part in chronic myeloid leukemia (CML) [34]. PDLIM1, also called CLP36, has been identified as a tumor antigen that elicits antibody response [35]. These findings represent the diverse functions of PDLIM1 in multiple cancers. Notwithstanding, the function and mechanism of PDLIM1 in the context of GC remain obscure. Here, we discovered that PDLIM1 expression was lowered in GC tissues and cell lines; the function of PDLIM1 was inextricably associated with a lot of physiological parameters of GC, including proliferation, invasion, migration, and apoptosis. These statistics demonstrated that PDLIM1 overexpression repressed GC

cell proliferation, invasion, and migration and bolstered apoptosis, whereas PDLIM1 inhibition facilitated the malignant development of GC cells.

Chemotherapy has been utilized to treat patients with unresectable gastric tumors with a view to reducing recurrence and metastasis [36]. Furthermore, perioperative chemotherapy can dramatically ameliorate the prognosis of patients with resectable tumors [37]. Nevertheless, 70%~90% of GC patients may relapse on account of chemotherapy resistance [38, 39]. It is still a big challenge in GC treatment. Further research on the mechanism of chemical resistance is in urgent need. Here, we discovered that PDLIM1 expression was attenuated in AGS/DDP cells; PDLIM1 overexpression boosted AGS/DDP cell apoptosis and elevated the sensitivity of AGS/DDP cells to DDP.

(a)

(b)

(c)

(d)

(e)

(f)

Figure 8: Continued.

(g)

(h)
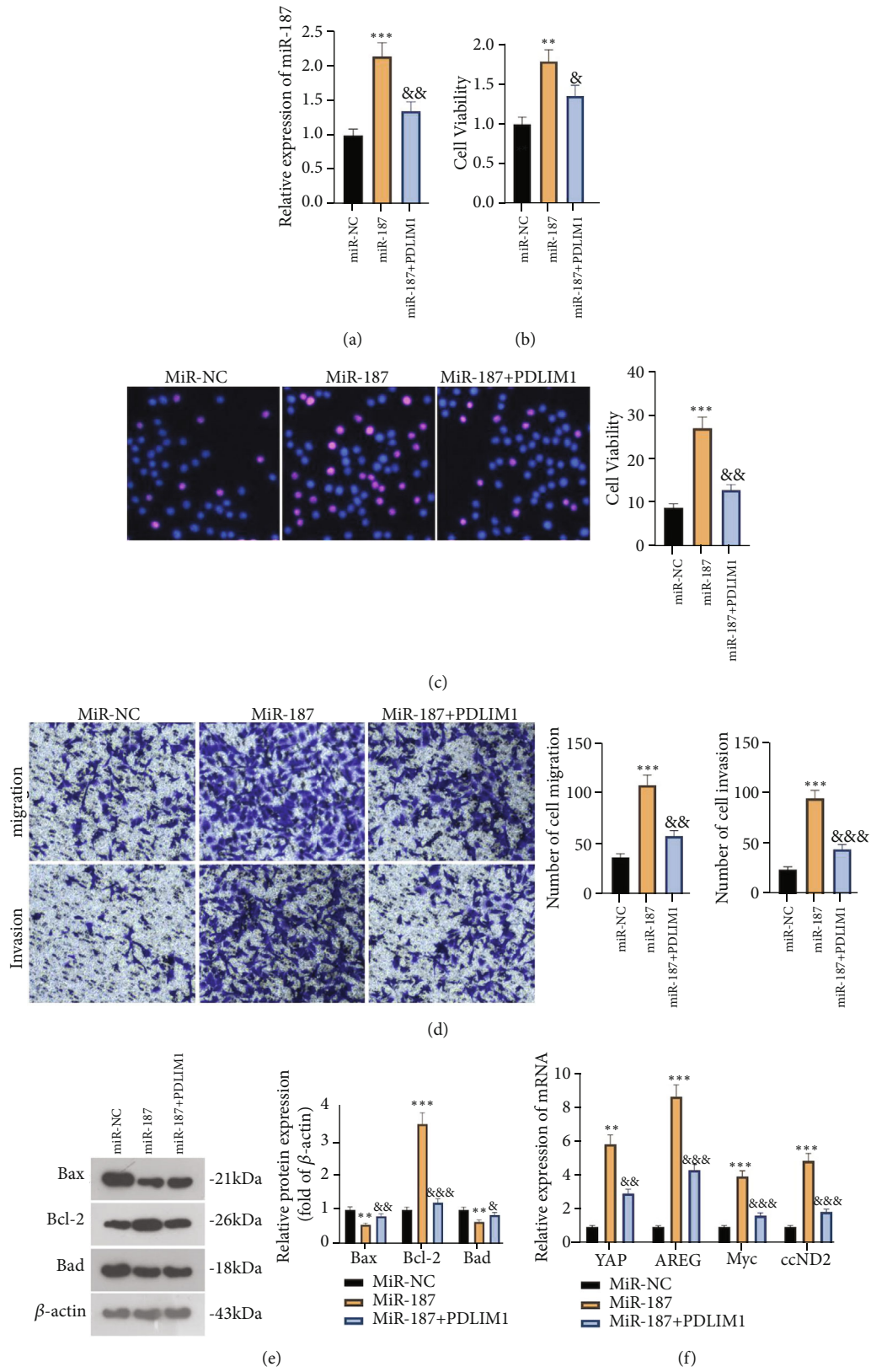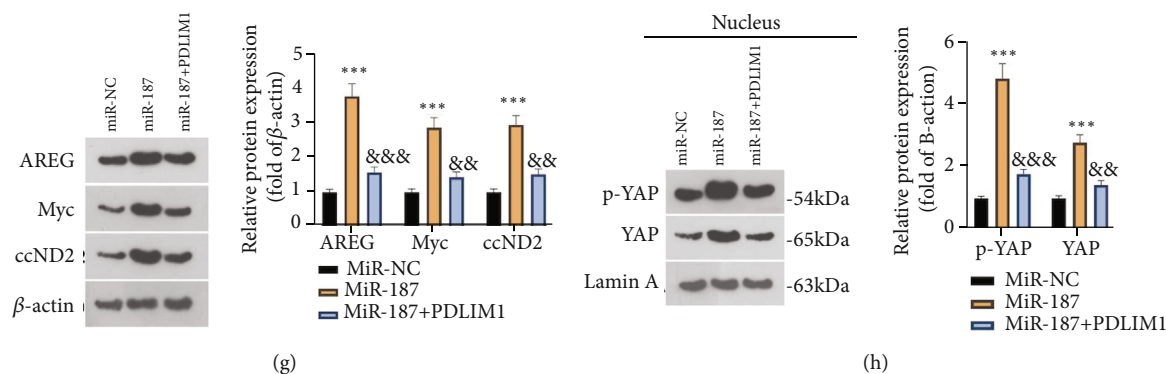
FIGURE 8: PDLIM1 overexpression weakens the procancer function of miR-187 in GC cells. AGS cells, already transfected with miR-187 mimics, were transfected with PDLIM1 overexpression plasmid. (a) RT-qPCR confirmed miR-187 expression. (b-c) CCK8 and BrdU staining measured cell proliferation. (d) Transwell monitored AGS cell migration and invasion. (e) Flow cytometry evaluated cell apoptosis. (f) Western blot determined the protein profiles of Bax, Bad, and Bcl2. (g) RT-qPCR verified the mRNA levels of YAP, AREG, Myc, and CCDN2. (h) Western blot tested the levels of AREG, Myc, and CCND2 as well as those of YAP and phosphorylated YAP in the nucleus. $^{**}P < 0.01$, $^{***}P < 0.001$ (vs. the miR-NC group). $^{\&}P < 0.05$, $^{\&\&}P < 0.05$, $^{\&\&\&}P < 0.001$ (vs. the miR-187 group). $N = 3$.

Reportedly, miR-187, a member of the miRNA family, participates in GC development. For instance, miR-187 modulates CRMP1 expression to facilitate GC cell migration and invasion, thus fostering GC development [40]. miR-187 represses FOXA2 to bolster GC growth and metastasis [41]. More of note, miR-187 overexpression dampens the TGF-β/Smad signaling pathway to mitigate the resistance of GC cells to DDP [42]. Here, we uncovered that miR-187 expression was heightened in GC; miR-187 overexpression dramatically boosted GC malignant phenotype. Dual luciferase assay revealed that miR-187 targeted PDLIM1, and they were negatively correlated; miR-187 overexpression vigorously impeded PDLIM1 progression. The rescue experiment indicated that PDLIM1 overexpression weakened the procancer function of miR-187 in GC cells.

The Hippo signaling pathway exerts a pivotal function in modulating organ size, migration, and invasion as well as sustaining the balance between cell proliferation and apoptosis [43, 44]. Reportedly, YAP is the primary effector of the Hippo pathway. Dephosphorylated YAP moves into the nucleus, thus promoting gene transcription that modulates proliferation and migration [45]. An increasing amount of evidence has shown that the aberrant activation of YAP incurs the growth-promoting transcription procedure that facilitates cell proliferation, migration, epithelial-mesenchymal transformation, and the stem-cell features of cancer [46]. YAP presents a high expression in GC and other tumors, which bolsters tumor proliferation and metastasis. This is extremely detrimental to the prognosis of cancer patients [47, 48]. For instance, when the nuclear translocation and dephosphorylation of YAP are boosted, GC development also gets promoted [49–51]. Meanwhile, targeting and suppressing YAP and β-catenin signaling cramps the malignant behaviors of GC [52]. Here, we discovered that the YAP pathway also partakes in GC progression; PDLIM1 overexpression vigorously represses the mRNA and protein levels of YAP and its target genes AREG, Myc, and CCND2; the levels of nuclear and phosphorylated YAP were lowered in the nucleus. These findings confirmed that PDLIM1 served as a tumor-suppressing factor and hindered the Hippo/YAP signaling pathway in GC.

To conclude, our research has unveiled a novel molecular mechanism for GC treatment: PDLIM1 mediates the Hippo-YAP signaling pathway to exert a cancer-suppressing function and strengthen the sensitivity of GC to cisplatin. Our observation affords significant insights into GC treatment and prognosis. Nevertheless, we have not completely corroborated the reliability of the mechanism *in vivo*, which will be improved in the future.

Data Availability

The datasets analyzed during the current study are available from the corresponding author on reasonable request.

Ethical Approval

Our research had been approved by the ethics committee of our hospital. The participants had signed the informed consent.

Conflicts of Interest

The authors declared no conflict of interest.

Acknowledgments

References

[1] P. Petryszyn, N. Chapelle, and T. Matysiak-Budnik, "Gastric cancer: where are we heading?," *Digestive Diseases*, vol. 38, no. 4, pp. 280–285, 2020, Epub 2020 Feb 17.

[2] D. E. Guggenheim and M. A. Shah, "Gastric cancer epidemiology and risk factors," *Journal of Surgical Oncology*, vol. 107, no. 3, pp. 230–236, 2013.

[3] P. Correa, "Gastric cancer: overview," *Gastroenterology Clinics of North America*, vol. 42, no. 2, pp. 211–217, 2013.

[4] E. C. Smyth, M. Nilsson, H. I. Grabsch, N. C. van Grieken, and F. Lordick, "Gastric cancer," *The Lancet*, vol. 396, no. 10251, pp. 635–648, 2020.

[5] F. M. Johnston and M. Beckman, "Updates on management of gastric cancer," *Current Oncology Reports*, vol. 21, no. 8, p. 67, 2019.

[6] P. Petryszyn, N. Chapelle, and T. Matysiak-Budnik, "Gastric cCancer: wWhere aAre wWe hHeading?," *Digestive Diseases.*, vol. 38, no. 4, pp. 280–285, 2020.

[7] N. Lipinska, A. Romaniuk, A. Paszel-Jaworska, E. Toton, P. Kopczynski, and B. Rubis, "Telomerase and drug resistance in cancer," *Cellular and Molecular Life Sciences*, vol. 74, no. 22, pp. 4121–4132, 2017.

[8] M. M. Gottesman, O. Lavi, M. D. Hall, and J. P. Gillet, "Toward a better understanding of the complexity of cancer drug resistance," *Annual Review of Pharmacology and Toxicology*, vol. 56, no. 1, pp. 85–102, 2016, Epub 2015 Oct 28.

[9] A. Wilczynska and M. Bushell, "The complexity of mi RNA-mediated repression," *Cell Death & Differentiation*, vol. 22, no. 1, pp. 22–33, 2015.

[10] Z. Ali Syeda, S. S. S. Langden, C. Munkhzul, M. Lee, and S. J. Song, "Regulatory mechanism of microRNA expression in cancer," *International Journal of Molecular Sciences*, vol. 21, no. 5, p. 1723, 2020.

[11] M. S. Adil, D. Khulood, and P. R. Somanath, "Targeting Akt-associated microRNAs for cancer therapeutics," *Biochemical Pharmacology*, vol. 189, article 114384, 2021.

[12] Z. Liang, J. Xu, Z. Ma, G. Li, and W. Zhu, "miR-187 suppresses non-small-cell lung cancer cell proliferation by targeting FGF9," *Bioengineered*, vol. 11, no. 1, pp. 70–80, 2020.

[13] P. S. Hung, F. J. Chuang, C. Y. Chen, C. H. Chou, H. F. Tu, and S. S. Lo, "miR-187 enhances SiHa cervical cancer cell oncogenicity via suppression of WWOX," *Anticancer Research*, vol. 40, no. 3, pp. 1427–1436, 2020.

[14] H. Liu, L. Zhu, B. Liu et al., "Genome-wide microRNA profiles identify miR-378 as a serum biomarker for early detection of gastric cancer," *Cancer Letters*, vol. 316, no. 2, pp. 196–203, 2012.

[15] W. Chen, Y. Cui, J. Wang et al., "Effects of downregulated expression of microRNA-187 in gastric cancer," *Experimental and Therapeutic Medicine*, vol. 16, no. 2, pp. 1061–1070, 2018.

[16] J. K. Zhou, X. Fan, J. Cheng, W. Liu, and Y. Peng, "PDLIM1: structure, function and implication in cancer," *Cell Stress*, vol. 5, no. 8, pp. 119–127, 2021.

[17] B. Y. Ahn, R. F. Saldanha-Gama, J. J. Rahn et al., "Glioma invasion mediated by the p75 neurotrophin receptor (p75 (NTR)/CD271) requires regulated interaction with PDLIM1," *Oncogene*, vol. 35, no. 11, pp. 1411–1422, 2016.

[18] Z. Liu, Y. Zhan, Y. Tu, K. Chen, Z. Liu, and C. Wu, "PDZ and LIM domain protein 1(PDLIM1)/CLP36 promotes breast cancer cell migration, invasion and metastasis through interaction with α-actinin," *Oncogene*, vol. 34, no. 10, pp. 1300–1311, 2015.

[19] C. Qiu, Y. Duan, B. Wang et al., "Serum anti-PDLIM1 autoantibody as diagnostic marker in ovarian cancer," *Frontiers in Immunology*, vol. 12, article 698312, 2021.

[20] K. F. Harvey, X. Zhang, and D. M. Thomas, "The Hippo pathway and human cancer," *Nature Reviews. Cancer*, vol. 13, no. 4, pp. 246–257, 2013.

[21] P. C. Calses, J. J. Crawford, J. R. Lill, and A. Dey, "Hippo pathway in cancer: aberrant regulation and therapeutic opportunities," *Trends Cancer*, vol. 5, no. 5, pp. 297–307, 2019, Epub 2019 May 16.

[22] S. Ma, Z. Meng, R. Chen, and K. L. Guan, "The Hippo pathway: biology and pathophysiology," *Annual Review of Biochemistry*, vol. 88, no. 1, pp. 577–604, 2019, Epub 2019 Dec 19.

[23] G. Halder and R. L. Johnson, "Hippo signaling: growth control and beyond," *Development*, vol. 138, no. 1, pp. 9–22, 2011.

[24] Y. Chen and Y. Wu, "Downregulation of LINC01857 increases sensitivity of gastric carcinoma cells to cisplatin," *Computational and Mathematical Methods in Medicine*, vol. 2022, Article ID 3325686, 8 pages, 2022.

[25] F. Tao, L. Qi, and G. Liu, "Long intergenic non-protein coding RNA 662 accelerates the progression of gastric cancer through up-regulating centrosomal protein 55 by sponging microRNA-195-5p," *Bioengineered*, vol. 13, no. 2, pp. 3007–3018, 2022.

[26] L. Zhang, W. Kang, X. Lu, S. Ma, L. Dong, and B. Zou, "lncRNA CASC11 promoted gastric cancer cell proliferation, migration and invasion in vitro by regulating cell cycle pathway," *Cell Cycle*, vol. 17, no. 15, pp. 1886–1900, 2018.

[27] M. Yin and L. Zhang, "Hippo signaling: a hub of growth control, tumor suppression and pluripotency maintenance," *Journal of Genetics and Genomics*, vol. 38, no. 10, pp. 471–481, 2011.

[28] Z. Song, Y. Wu, J. Yang, D. Yang, and X. Fang, "Progress in the treatment of advanced gastric cancer," *Tumour Biology*, vol. 39, no. 7, article 101042831771462, 2017.

[29] A. Digklia and A. D. Wagner, "Advanced gastric cancer: current treatment landscape and future perspectives," *World Journal of Gastroenterology*, vol. 22, no. 8, pp. 2403–2414, 2016.

[30] G. B. Baretton and D. E. Aust, "Current Biomarkers for Gastric Cancer," *Der Pathologe*, vol. 38, no. 2, pp. 93–97, 2017.

[31] M. Wang, Z. Li, Y. Peng et al., "Identification of immune cells and mRNA associated with prognosis of gastric cancer," *BMC Cancer*, vol. 20, no. 1, 2020.

[32] C. Wang, J. Luo, J. Rong, S. He, L. Zhang, and F. Zheng, "Distinct prognostic roles of S100 mRNA expression in gastric cancer," *Pathology, Research and Practice*, vol. 215, no. 1, pp. 127–136, 2019, Epub 2018 Nov 2.

[33] H. N. Chen, K. Yuan, N. Xie et al., "PDLIM1 stabilizes the E-cadherin/β-catenin complex to prevent epithelial-mesenchymal transition and metastatic potential of colorectal cancer cells," *Cancer Research*, vol. 76, no. 5, pp. 1122–1134, 2016, Epub 2015 Dec 23.

[34] L. M. Li, F. J. Luo, and X. Song, "MicroRNA-370-3p inhibits cell proliferation and induces chronic myelogenous leukaemia cell apoptosis by suppressing PDLIM1/Wnt/β-catenin signalling," *Neoplasma*, vol. 67, no. 3, pp. 509–518, 2020.

[35] S. H. Hong, "Identification of CLP36 as a tumor antigen that induces an antibody response in pancreatic cancer," *Cancer Research and Treatment*, vol. 37, no. 1, pp. 71–77, 2005.

[36] D. Liu, M. Lu, J. Li et al., "The patterns and timing of recurrence after curative resection for gastric cancer in China," *World Journal of Surgical Oncology*, vol. 14, no. 1, p. 305, 2016.

[37] Y. Yang, X. Yin, L. Sheng, S. Xu, L. Dong, and L. Liu, "Perioperative chemotherapy more of a benefit for overall survival than adjuvant chemotherapy for operable gastric cancer: an

updated meta-analysis," *Scientific Reports*, vol. 5, no. 1, article 12850, 2015.

[38] S. Russi, H. K. Verma, S. Laurino et al., "Adapting and surviving: intra and extra-cellular remodeling in drug-resistant gastric cancer cells," *International Journal of Molecular Sciences*, vol. 20, no. 15, p. 3736, 2019.

[39] Y. Jiang, J. Xie, W. Huang et al., "Tumor immune microenvironment and chemosensitivity signature for predicting response to chemotherapy in gastric cancer," *Cancer Immunology Research*, vol. 7, no. 12, pp. 2065–2073, 2019, Epub 2019 Oct 15.

[40] L. Ren, F. Li, M. Di et al., "MicroRNA-187 regulates gastric cancer progression by targeting the tumor suppressor CRMP1," *Biochemical and Biophysical Research Communications*, vol. 482, no. 4, pp. 597–603, 2017.

[41] C. Li, S. Lu, and Y. Shi, "MicroRNA-187 promotes growth and metastasis of gastric cancer by inhibiting FOXA2," *Oncology Reports*, vol. 37, no. 3, pp. 1747–1755, 2017, Epub 2017 Jan 16.

[42] Q. L. Zhu, Z. Li, C. M. Lv, and W. Wang, "miR-187 influences cisplatin-resistance of gastric cancer cells through regulating the TGF-β/Smad signaling pathway," *European Review for Medical and Pharmacological Sciences*, vol. 23, no. 22, pp. 9907–9914, 2019.

[43] F. X. Yu, B. Zhao, and K. L. Guan, "Hippo pathway in organ size control, tissue homeostasis, and cancer," *Cell*, vol. 163, no. 4, pp. 811–828, 2015.

[44] Y. Wang, X. Xu, D. Maglic et al., "Comprehensive molecular characterization of the Hippo signaling pathway in cancer," *Cell Reports*, vol. 25, no. 5, pp. 1304–1317.e5, 2018.

[45] M. Maugeri-Saccà and R. De Maria, "The Hippo pathway in normal development and cancer," *Pharmacology & Therapeutics*, vol. 186, pp. 60–72, 2018.

[46] T. Wang, B. Mao, C. Cheng et al., "YAP promotes breast cancer metastasis by repressing growth differentiation factor-15," *Biochimica et Biophysica Acta - Molecular Basis of Disease*, vol. 1864, no. 5 Part A, pp. 1744–1753, 2018.

[47] Q. Zhao, X. Jia, Y. Zhang et al., "Tetrandrine induces apoptosis in human neuroblastoma through regulating the Hippo/YAP signaling pathway," *Biochemical and Biophysical Research Communications*, vol. 513, no. 4, pp. 846–851, 2019, Epub 2019 Apr 16.

[48] K. Yin, S. Dang, L. Cui et al., "Netrin-1 promotes metastasis of gastric cancer by regulating YAP activity," *Biochemical and Biophysical Research Communications*, vol. 496, no. 1, pp. 76–82, 2018.

[49] C. Qi, P. Min, Q. Wang et al., "MICAL2 contributes to gastric cancer cell proliferation by promoting YAP dephosphorylation and nuclear translocation," *Oxidative Medicine and Cellular Longevity*, vol. 2021, Article ID 9955717, 17 pages, 2021.

[50] J. Wei, K. Peng, J. Zhu et al., "Geranylgeranylation promotes proliferation, migration and invasion of gastric cancer cells through the YAP signaling pathway," *American Journal of Translational Research*, vol. 12, no. 9, pp. 5296–5307, 2020.

[51] H. Wang, S. Dong, Y. Liu et al., "DAB2 suppresses gastric cancer migration by regulating the Wnt/β-catenin and Hippo-YAP signaling pathways," *Translational Cancer Research*, vol. 9, no. 2, pp. 1174–1184, 2020.

[52] Q. Liu, H. Xia, S. Zhou et al., "Simvastatin inhibits the malignant behaviors of gastric cancer cells by simultaneously suppressing YAP and β-catenin signaling," *OncoTargets and Therapy*, vol. 13, pp. 2057–2066, 2020.

Research Article

Epithelioid Hemangioendothelioma: Incidence, Mortality, Prognostic Factors, and Survival Analysis Using the Surveillance, Epidemiology, and End Results Database

Zhen Liu [ID][1] **and Shuting He**[2]

[1]*Department of Burns and Plastic Surgery, Beijing Children's Hospital, Capital Medical University, National Center for Children's Health, Beijing 100034, China*
[2]*Department of Anesthesiology, Peking University First Hospital, Beijing 100034, China*

Correspondence should be addressed to Zhen Liu; bdyywklz@163.com

Background. Although epithelioid hemangioendothelioma (EHE) is a rare and aggressive vascular tumor, its demographic characteristics remain unclear. We used the surveillance, epidemiology, and end results (SEER) database to determine the clinical features, incidence, and prognostic factors associated with overall survival in patients with EHE. *Methods.* The demographic and clinical data of patients with EHE were extracted from the SEER database (1975-2019) to calculate the incidence of EHE and survival rate in these patients. The Cox proportional hazards model and Kaplan-Meier method were used to analyze the prognostic factors of overall survival in these patients. A nomogram and time-dependent receiver operating characteristic (ROC) curve were employed to predict the 3- and 5-year survival rate. *Results.* The overall incidence rate (IR) of EHE was 0.230 (95%confidence interval $[CI] = 0.201 – 0.263$) per 1,000,000 person-years. According to the age-stratified IR, the highest age-adjusted IR was observed in patients aged 60–79 years (0.524 per 1,000,000 person-years, 95%CI = 0.406 – 0.665). The majority (30.8%) of the tumors were located in the soft tissue and skin, followed by lesions in the abdomen (28%), respiratory system (19%), bone and joint (8.6%), and others. The 5-year overall survival rate was 55.6% (95%CI = 32.8 – 73.5%). Multiple Cox regression analysis revealed that age >80 years (hazard ratio $[HR] = 8.57$, 95%CI = 2.32 – 31.63, $P < 0.001$), African-American race (HR = 2.52, 95%CI = 1.31 – 4.85, $P < 0.01$), "American Indian/Alaska Native" or "Asian or Pacific Islander" (HR = 2.99, 95%CI = 1.5 – 5.96, $P < 0.01$) race, and respiratory tumors (HR = 2.55, 95%CI = 1.37 – 4.75, $P < 0.01$) were distinctly related to worse overall survival. The calibration plots demonstrated good consistency between nomogram-predicted and actual survival. The area under the time-dependent ROC curve was 0.721 (95%CI = 0.63 – 0.81) and 0.719 (95%CI = 0.63 – 0.81) for the 3- and 5-year survival, respectively. For the convenience of researchers and clinicians, we designed an online dynamics nomogram to predict the survival rate. *Conclusion.* EHE is a relatively rare vascular tumor, which principally occurs in the soft tissue and skin. It most commonly occurs in patients aged 60–79 years and its incidence has increased in recent years. Age at diagnosis, race, and tumor location may affect the overall survival outcomes.

1. Introduction

Epithelioid hemangioendothelioma (EHE) is considered an intermediate or borderline malignant vascular tumor. It was first described in 1982 and involves various organs, including the liver, soft tissues, and bone [1, 2]. Its typical histological features include irregular vasculature, malignant endothelial cell lining, pinocytotic vesicles, and occasional

Weibel-Palade bodies [3, 4]. The tumor has an aggressive clinical course, with a tendency for both local recurrence and regional lymph node metastasis. Certain types of the tumor could develop a life-threatening hemoptysis upon invasion into the trachea and pleura [5]. Moreover, EHE is considered as the most common malignant vascular tumor of bone and can easily result in recurrence and metastasis [6, 7]. The overlapping morphologic features make diagnosis
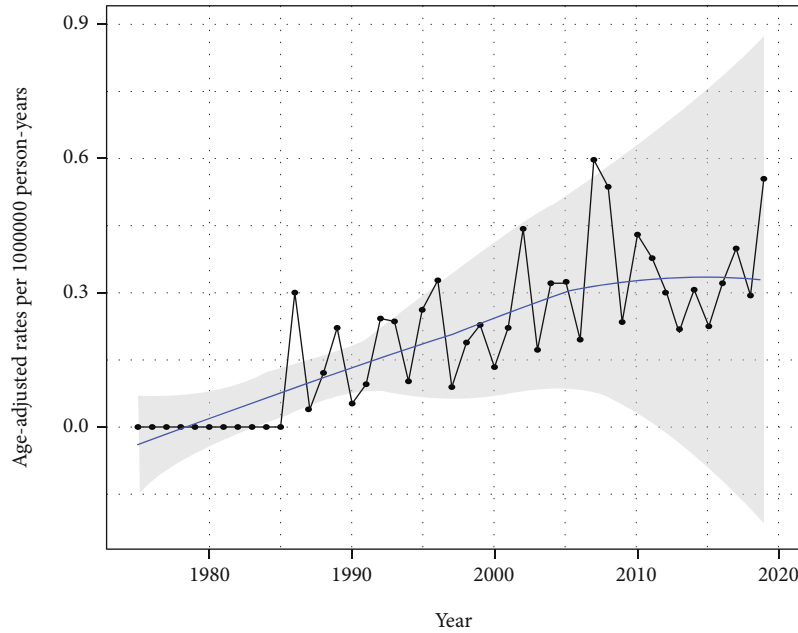
FIGURE 1: The age-adjusted incidence rate of epithelioid hemangioendothelioma from 1975 to 2019.

and management challenging [8, 9]. The incidence of EHE is approximately one in one million people, making it an extremely uncommon kind of cancer. Due to the fact that it is so uncommon, the majority of the research that has been published so far consists of case reports, with a few retrospective descriptive case series thrown in for good measure. The purpose of these case series is to better characterize the clinical, pathologic, and molecular characteristics, as well as to derive insight into treatment approaches [10, 11]. Currently, no comprehensive study exists on the demographic characteristics and prognostic factors of the overall survival of EHE.

Considering the challenging diagnosis and treatment of EHE, we designed this study using demographic and clinical data from the surveillance, epidemiology, and end results (SEER) database to understand the features of onset and risk factors of prognosis in patients with EHE. The SEER datasets, which contains cancer statistics from roughly twenty-eight percent of the population of the United States, could be considered a relatively large population-based cohort of patients with EHE [12].

2. Materials and Methods

2.1. Data Collection. The SEER database was searched for the pertinent information on cases diagnosed with EHE from 1975 all the way up till 2019. The variable titles based on the International Classification of Diseases for Oncology (ICD-O-3) histology codes, 9133/1 EHE and 9133/3 EHE, malignant, were considered the diagnosis of EHE. The basic information of these patients including age, race, sex, tumor location, lymph node metastasis, survival time, treatment, SEER cause-specific death classification, and tumor size, was recorded.

Based on the SEER database policy, the overall incidence rate (IR) and survival rate were analyzed using SEER∗Stat software [12]. The rates are per 1,000,000 and age-adjusted to the 2000 US standard population standard, with 95% confidence intervals (CI, Tiwari mod) for the rates and ratios. Moreover, the rates were calculated based on the age at diagnosis, sex, and race. Age was divided into five groups: 0–19, 20–39, 40–59, 60–79, and ≥80 years. The study population was categorized into male and female groups. Race was classified into three groups: white (Caucasians), black (African American), and other ("American Indian/Alaska Native" or "Asian or Pacific Islander"). The IR was considered significantly different when the P value is <0.05. The tumor location was divided into the following groups: soft tissue and skin, bone and joints, respiratory system, abdomen, head and neck, and others. Treatment regimens were classified into surgery and no surgery groups.

2.2. Statistical Analysis. Descriptive statistics were utilized in order to conduct the analysis on the demographic and clinical data. The data were analyzed using R version 3.6.0 (R Foundation for Statistical Computing, Vienna, Austria). The significance of the variables associated with the overall survival was evaluated using the univariate cox proportional hazards model. Multivariate cox regression analysis was subsequently used to analyze the significant variables as independent predictors for the overall survival. The Kaplan–Meier method and log-rank test were used to analyze the survival curves. These results of the multivariate analysis were represented as a nomogram [13]. The performance of the nomogram was evaluated using the concordance index (also known as the C-index), in addition to the calibration curve [14]. Time-dependent ROC curve assays were also used to evaluate the predictive value. Significance was assumed for two-sided P values <0.05.

TABLE 1: Age-adjusted incidence rates of epithelioid hemangioendothelioma.

Groups	Total number of cases	IR (per 1,000,000)	95% CI	P value
All years	221	0.230	0.201-0.263	—
0-19 years	10	0.036	0.017-0.066	<0.001
20-39 years	48	0.168	0.123-0.222	<0.05
40-59 years	85	0.349	0.278-0.431	<0.01
60-79 years	68	0.524	0.406-0.665	<0.001
80+ years	10	0.332	0.159-0.612	0.338
Gender	221	0.230	0.201-0.263	—
Male	98	0.212	0.172-0.259	0.545
Female	123	0.246	0.204-0.293	0.604
All races	221	0.230	0.201-0.263	—
White	179	0.233	0.200-0.270	0.949
Black	21	0.272	0.165-0.421	0.547
Others	18	0.164	0.010-0.260	0.192

3. Results

3.1. Patient Characteristics. Following relevant data retrieval, a total of 221 patients were enrolled. The overall IR of EHE was 0.230 per 1,000,000 person-years. The IR of EHE is gradually increasing in recent years in the United States population (Figure 1). According to the age-stratified IR, the highest age-adjusted IR was in patients aged 60–79 years (0.524 per 1,000,000 person-years, 95%CI = 0.406 – 0.665) followed by patients aged 40–59 years (0.349 per 1,000,000 person-years, 95%CI = 0.278 – 0.431) (Table 1). Tumors were rarely observed in 0–19-year-old patients, with an age-adjusted IR of 0.036 per 1,000,000 person-years (95%CI = 0.017 – 0.066). A total of 198 patients, including 98 male and 123 female participants, were enrolled in the study; the sex-stratified IR was 0.212 (95%CI = 0.172 – 0.259) and 0.246 (95%CI = 0.204 – 0.293) per 1,000,000 person-years in males and females, respectively. According to the SEER database data, the race-stratified IR was 0.230 (95%CI = 0.200 – 0.270), 0.272 (95%CI = 0.165 – 0.421), and 0.164 (95%CI = 0.010 – 0.260) in Caucasians, African Americans, and other races (American Indian/AK Native, Asian/Pacific Islander), respectively. The IR showed no statistical difference in terms of sex and race. Our results also revealed that EHE was observed in various organs. The majority (30.8%) of tumors were located in the soft tissue and skin, followed by the abdomen (28%), respiratory system (19%), bone and joints (8.6%), head and neck (5%), and other (8.6%) organs, such as the vulva, and other miscellaneous lesions (Figure 2). The liver (24%) and lung and bronchus (13%) are the most commonly affected organs in the abdominal and thoracic cavities, respectively. Among these patients, only 11 had regional lymph node metastasis and 3 patients had distant lymph node metastases. The average diameter of the tumor was 49.90 ± 44.28 mm (median = 39 mm, range 6 – 250 mm). Approximately 47.1% of the patients underwent surgery for EHE. In the operation group, 42.6% lesions were located in the soft tissue and skin, wherein most of the patients (60.3%) had a better overall survival than those in the no surgery group (P < 0.01,

FIGURE 2: Lesion site and proportion of epithelioid hemangioendothelioma.

Figure 3(a)). However, in the other organ groups, patients who underwent operation showed no distinct differences in the overall survivals with the patients in the no surgery group (Figures 3(b)–3(e)). Our result also demonstrated that no significant difference was observed between the surgery and no surgery groups in the overall survival in final multi-factor models. The overall 1-, 3-, and 5-year survival rates were 70.8% (95%CI = 48.4 – 84.9%), 61.2% (95%CI = 38.5 – 77.7%), and 55.6% (95%CI = 32.8 – 73.5%), respectively.

3.2. Survival Analysis. Owing to the lack of related data on the unknown death classification (3 patients) and race data (3 patients), only 215 patients were finally enrolled. In the

(a)

(b)

(c)

(d)

(e)
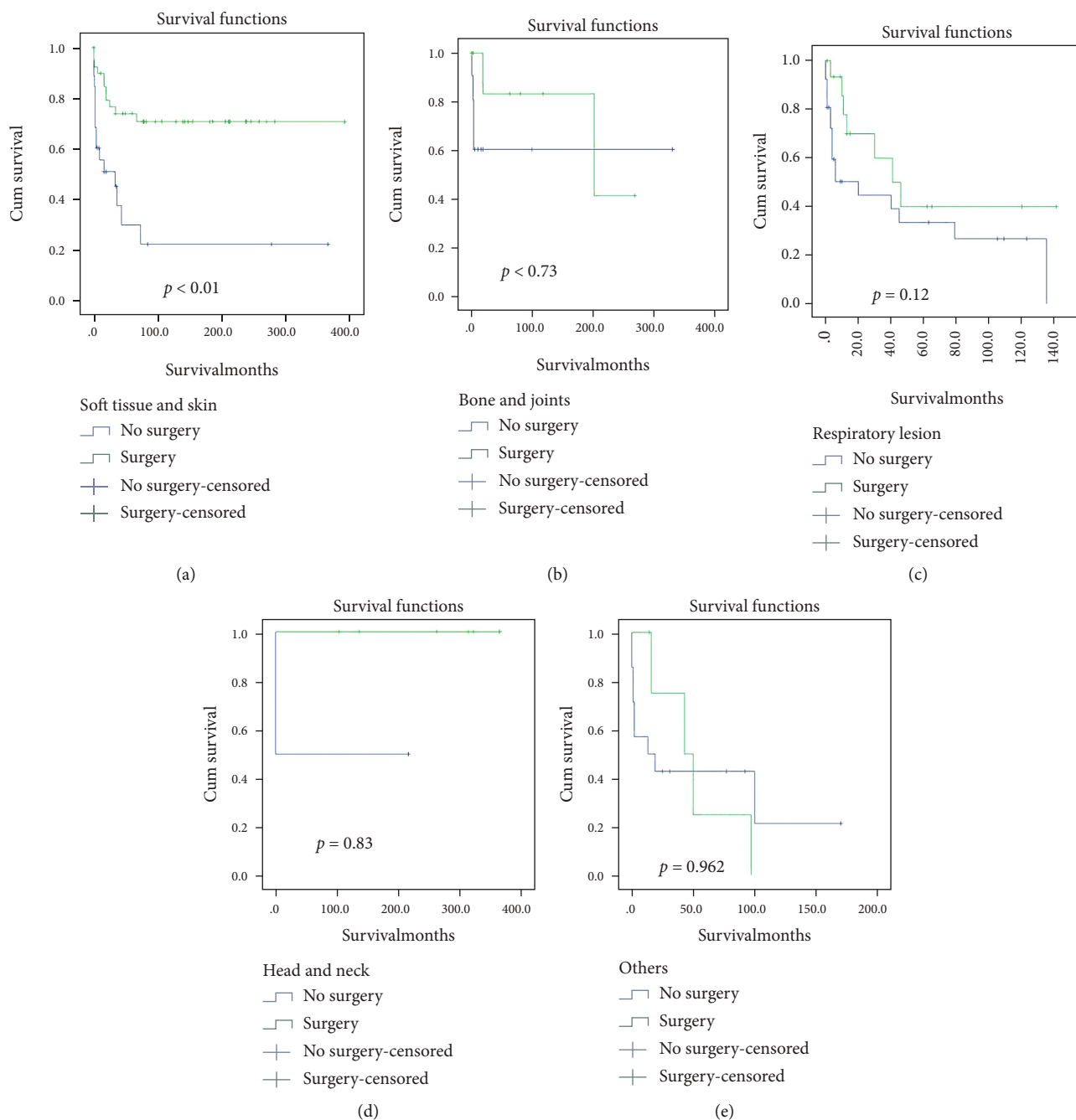
FIGURE 3: Kaplan-Meier (KM) survival curves in different locations according to the surgery and no surgery groups. (a) KM survival curves in soft tissues and skin. (b) KM survival curves in bone and joints. (c) KM survival curves in respiratory lesions. (d) KM survival curves in head and neck. (e) KM survival curves in other organs.

univariate analysis, compared to patients aged 0–19 years, a significant difference was observed in the patients aged >80 years (HR = 8.199, 95%CI = 2.400 – 28.009, $P < 0.001$, Figure 4(a)). Respiratory lesions could increase the risk of death to a certain extent (HR = 2.311, 95%CI = 1.272 – 4.198, $P < 0.001$) compared to soft tissue and skin tumors (Table 2 and Figure 4(b)). Patients of other races (American Indian/AK Native, Asian/Pacific Islander) showed significant difference compared to those of Caucasian origin (HR = 2.322, 95%CI = 1.198 – 4.501, $P = 0.013$

< 0.05, Figure 4(c)). The multivariate analysis revealed that age >80 years (HR = 8.566, 95%CI = 2.320 – 31.626, $P < 0.001$), African American race (HR = 2.520, 95%CI = 1.309 – 4.853, $P < 0.01$), "American Indian/Alaska Native" or "Asian or Pacific Islander" (HR = 2.989, 95%CI = 1.498 – 5.964, $P < 0.01$), and respiratory tumors (HR = 2.551, 95% CI = 1.370 – 4.749, $P < 0.01$) were significantly associated with worse overall survival. However, no statistical difference was observed in terms of sex and treatment regimen (Table 2 and Figures 4(d) and 4(e)). According to the results obtained,

(a)

(b)

(c)

(d)
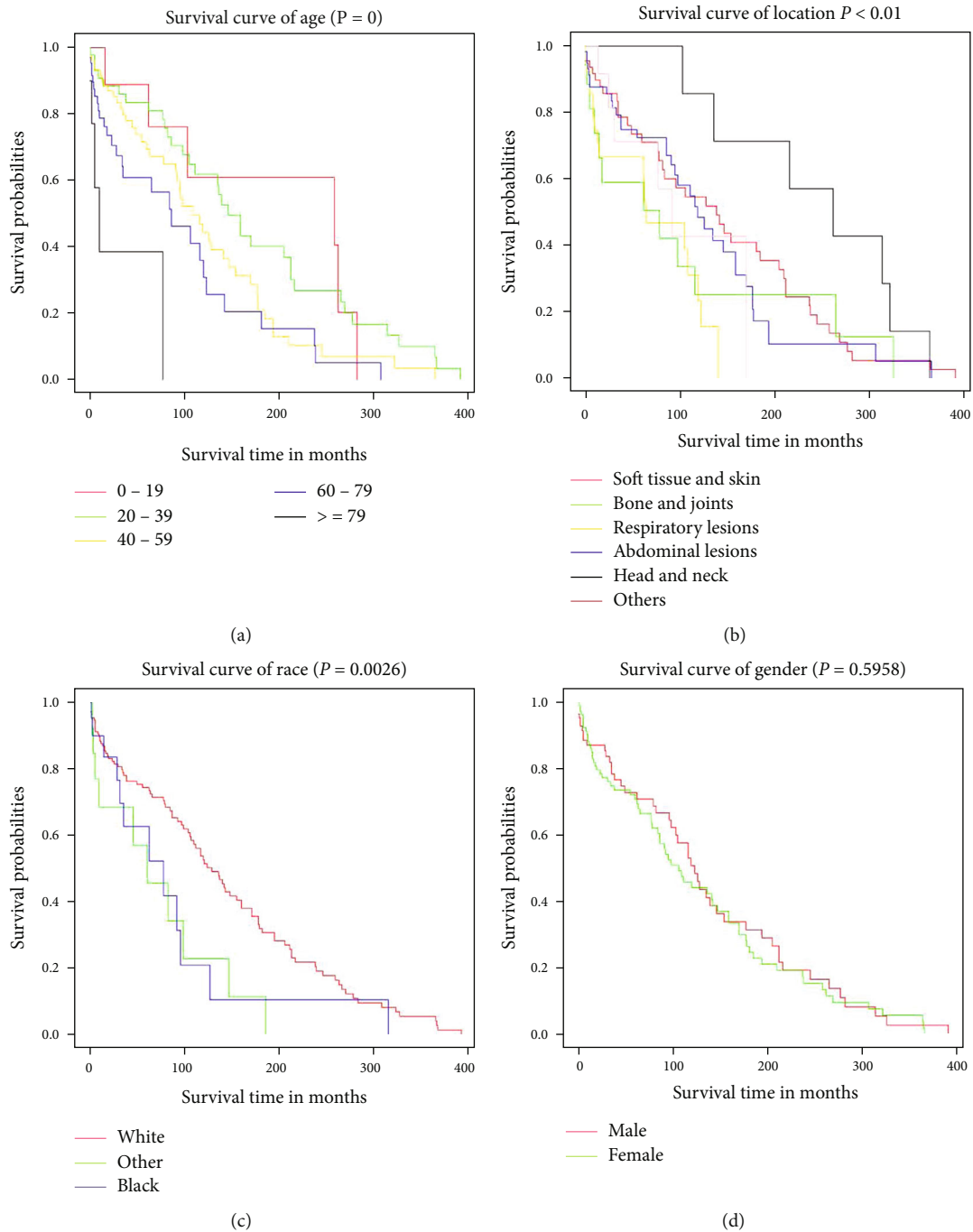
Figure 4: Continued.

(e)
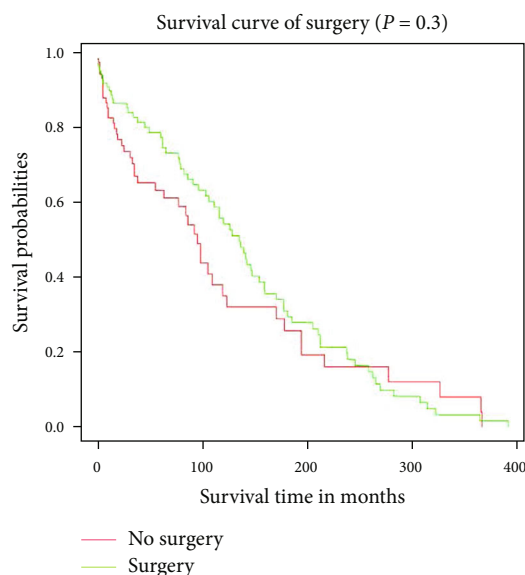
FIGURE 4: Kaplan-Meier survival curves for different variables by the use of by the log-rank test. (a) KM survival curves in age at diagnosis. (b) KM survival curves different locations. (c) KM survival curves in gender. (d) KM survival curves in surgery and no surgery groups.

TABLE 2: Univariate and multivariate cox analysis of overall survival.

Variable	Groups	Patients	Univariate analysis HR (95% CI) P	Multivariate analysis HR (95% CI) P
Age	Age 0-19	10	1 (reference) -	1 (reference) -
	Age 20-39	47	1.038 (0.431-2.500) 0.933	0.784 (0.316-1.945) 0.599
	Age 40-59	80	1.696 (0.716-4.017) 0.230	1.320 (0.538-3.240) 0.545
	Age 60-79	68	2.431 (0.999-5.914) 0.050	2.000 (0.804-4.978) 0.136
	Age 80+	10	8.199 (2.400-28.009) <0.001	8.566 (2.320-31.626) <0.01
Sex	Male	95	1 (reference) -	1 (reference) -
	Female	120	1.10404 (0.763-1.597) 0.6	0.903 (0.600-1.359) 0.625
Race	White	177	1 (reference) -	1 (reference) -
	Black	21	1.768 (0.962-3.250) 0.067	2.520 (1.309-4.853) <0.01
	Other	17	2.322 (1.198-4.501) 0.013	2.989 (1.498-5.964) <0.01
Location	Soft tissue and skin	67	1 (reference) -	1 (reference) -
	Respiratory lesions	42	2.311 (1.272-4.198) <0.001	2.551 (1.370-4.749) <0.01
	Bone and joints	18	1.418 (0.739-2.721) 0.29	1.877 (0.921-3.823) 0.083
	Abdominal lesions	61	1.205 (0.758-1.916) 0.431	1.252 (0.771-2.035) 0.364
	Head and necks	8	0.542 (0.240-1.225) 0.141	0.609 (0.254-1.459) 0.266
	Others	19	1.463 (0.605-3.533) 0.398	1.360 (0.523-3.530) 0.530
Surgery	No surgery	115	1 (reference) -	1 (reference) -
	Surgery	100	0.820 (0.563-1.193) 0.299	0.970 (0.640-1.474) 0.887

a prognostic nomogram was constructed for survival at 3 and 5 years (Figure 5). The C-index for survival prediction was 0.69 (95%CI = 0.635 – 0.744). The calibration plots demonstrated good consistency between nomogram-predicted and actual survival (Figures 6(a) and 6(b)). Moreover, the area under the time-dependent ROC curve was 0.721 (95%CI = 0.63 – 0.81) and 0.719 (95%CI = 0.63 – 0.81) for the 3- and 5-year survival (Figures 6(c) and 6(d)). For the convenience

of researchers and clinicians, we designed an online dynamic nomogram to predict the survival rate, which is available at https://plasticlz.shinyapps.io/DynNomapp/.

4. Discussion

EHE is a rare locally aggressive vascular neoplasm, which is considered an intermediate neoplasm between entirely benign
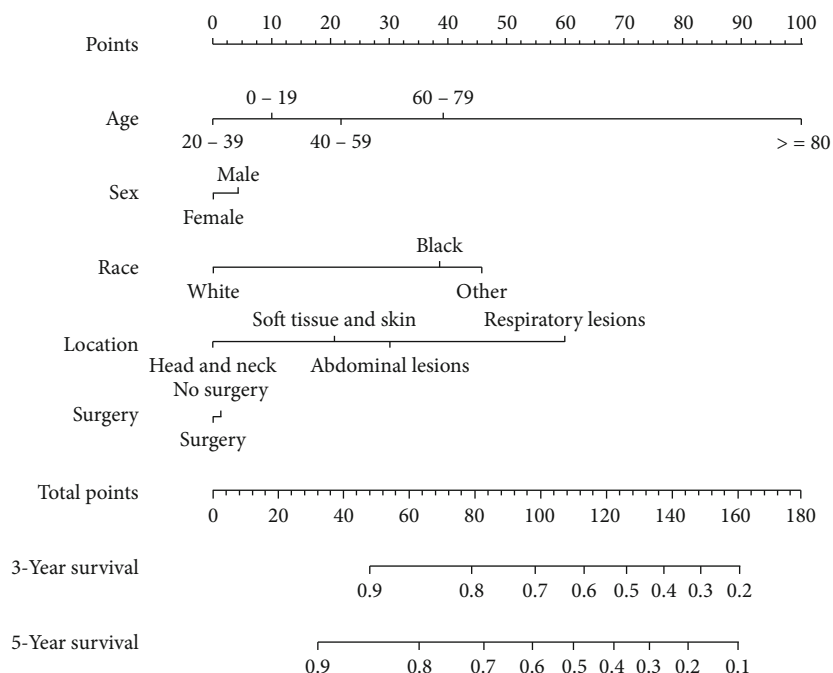
FIGURE 5: Nomograms predicting 3- and 5-year survivals of patients with epithelioid hemangioendothelioma. The C-index for survival prediction was 0.69 (95%CI = 0.635 – 0.744).

hemangiomas and highly malignant angiosarcomas [2, 15, 16]. To date, only few case series or case reports concerning EHE have been reported. [6, 16–19] Moreover, owing to lack of high-quality clinical research, diagnosis and management of this tumor is challenging [20]. To the best of our knowledge, the data from the SEER database, which was primarily used to analyze the clinical characteristics of patients with EHE, comprise the largest published cohort of patients until now.

Some reports have suggested the IR of EHE to be less than one person per 1,000,000 person-years [21, 22]. Upon evaluating the data in the SEER database, we found similar results wherein the IR of EHE was 0.23 per 1,000,000 person-years. The IR of EHE is gradually increasing in recent years in the United States population. Some studies have found EHE to be more common in the fourth to fifth decade with rare occurrence in pediatric patients [5, 23, 24]. However, our results showed that this kind of tumor was more common in patients aged 60–79 years followed by patients aged 40–59 years. We also found that EHE was rarely seen in pediatric patients. In addition, the sex-stratified IR of this tumor was different in correlational research. Some studies suggested that EHE was more common in males [6, 19, 25]; however, Lau et al. and Stacchiotti et al. observed increased occurrence in females [5, 17, 20]. Our results demonstrated that the sex-stratified IR showed no significant difference (Table 1). Moreover, IR in our results also showed no significant difference in terms of race (Table 1). EHE occurs in various organs, such as the skin, liver, mediastinum, lung and bronchus, and oral cavity [5, 16, 20, 24]. Our study also revealed that the tumor could occur in more than 20 kinds of organs or tissues. The most common site of EHE was the soft tissue and skin

(30.8%), followed by the abdomen (28%), and respiratory system (19%).

Owing to the relatively low IR of EHE, research on the overall survival rate of EHE has been limited. Based on the SEER database, our results demonstrated that the overall 1- and 5-year survival rates to be 70.8% and 55.6%, respectively. Moreover, age >80 years, African-American, and "American Indian/Alaska Native" or "Asian or Pacific Islander" race, and respiratory tumors were significantly associated with a worse overall survival. Although Lau et al. reported that male sex and a diagnosis during middle age could be related with a worse overall survival [5]. Data from the SEER database suggested that overall survival showed no statistical difference in terms of sex ($P = 0.64$). Our multivariate cox analysis did not indicate any significant difference in the overall survival between male and female patients. In our model, age >80 years was suggested to be an independent predictor for overall survival. This could be attributed to the comorbid conditions in older patients resulting in increased mortality. Moreover, tumor-related systemic symptoms, including fever, fatigue, or weight loss added to the severity of the condition in older patients [26]. Race-related overall survival rate difference may be attributed to various reasons. First, owing to the complexity of the patients' racial and ethnic backgrounds, limited relevant EHE data exist on African American and American Indian/Alaska Native patients compared to Caucasian patients [27]. Second, access to high-quality medical services for African American and American Indian/Alaska Native patients is challenging owing to economic factors. [28, 29] Lastly, differences in living habits and ethnicity between different races could contribute to the difference in the overall survival. Respiratory tumors were also associated with a

$n = 215$ d $= 118$ $p = 13$, 60 subjects per group
Gray: ideal
Nomogram-predicted probability of 3-year survival
X-resamping optimism added, B = 1000
based on observed-predicted

(a)

$n = 215$ d $= 118$ $p = 13$, 60 subjects per group
Gray: ideal
Nomogram-predicted probability of 5-year survival
X-resamping optimism added, B = 1000
based on observed-predicted

(b)

3–year survival AUC = 0.721

5–year survival AUC = 0.7187

(c)

(d)

FIGURE 6: (a, b) Calibration plots of the nomogram for overall survival prediction at 3- and 5-years. (c, d) Time-dependent receiver operating characteristic curves of the nomogram for overall survival prediction at 3- and 5-years.

worse overall survival in our model. Previous studies have reported EHE to rarely occur in the lung [5]; however, in our study, the number of EHEs in the lung and bronchus (13%) EHE was comparable among the included patients. It has been reported that once the tumor invades the bilateral lung or pleura, the life expectancy decreases significantly, even to less than 1 year [5, 17, 30]. Thus, the lesion characteristics of respiratory EHE could have contributed to the worse overall survival in our model.

Surgery is considered the primary treatment for confirmed unifocal EHE, especially in the soft tissue [20, 31]. However, in our study, fewer than half (47%) the patients underwent surgery for EHE. In the surgery group, the majority (42.6%) of the lesions were located in the soft tissue and skin. However, among the patients who underwent operations, only the patients with EHE in the soft tissue

and skin group had a good overall survival. ($P < 0.01$). Moreover, in the other organ groups, patients who underwent surgery showed no significance difference in the overall survival compared to patients who did not undergo surgery. Moreover, patients in the surgery group showed no significant difference in the overall survival from those in the no surgery group in the final multifactor models ($P = 0.3$, Figure 4(e)). This could be attributed to the rare nature and highly variable clinical course of EHE. No widely accepted treatment strategy exists for EHE. Moreover, according to Kaltenmeier's report, most patients with hepatic EHE (HEHE) in the United States (93.8%) did not undergo surgery owing to the comorbidities or patient preference [21]. In our study, the most common lesion location was the liver (28.2%) and followed by the lung and bronchus (19.7%) in the patients who did not undergo surgery. The

liver is reportedly the most common organ for EHE lesions [21]. While the treatment strategies for HEHE remain uncertain, some studies suggest surgery as the first treatment for HEHE [17]. However, other studies suggest liver transplantation as the best treatment option [18, 32]. The treatment for respiratory EHE also remains controversial. In unilateral focal lesions, surgery could be effective; however, in bilateral multiple nodules or pleural invasion, no effective treatment, including lung transplantation, exists [5, 30]. Owing to the low IR of EHE, the course and clinical characteristics concerning EHE remain unclear, and various treatment strategies exist. Hence, more high-quality studies defining the criteria for optimizing the selection of treatment modalities for EHE are warranted in the future.

Owing to the rare IR of EHE, certain limitations of this study should be considered. Although, the SEER database provided considerable EHE patient record, specific data, including the type of surgical resection, adequacy of the resection performed, and surgical timing, were not included. Accurate records on systemic therapy, such as chemotherapy and radiotherapy, was missing. As a retrospective database, the SEER database included certain unknown and incomplete data. Similarly, the symptoms of EHE in the SEER database were missing. Thus, the survival analysis should be interpreted with caution.

In conclusion, EHE is a relatively rare vascular tumor; however, its incidence has been increasing in recent years. It occurs principally in the soft tissue and skin, most common in patients aged 60–79 years. For patients with EHE, the age at diagnosis, race, and tumor location could affect the overall survival outcomes. The nomogram proposed in this study could estimate individualized survival for patients with EHE.

Abbreviations

EHE: Epithelioid hemangioendothelioma
SEER database: The surveillance, epidemiology, and end results database
ROC curve: Receiver operating characteristic curve
IR: Incidence rate
HR: Hazard ratio
C-index: concordance index.

Data Availability

The datasets generated for this study are available on request to the corresponding author.

Conflicts of Interest

The authors declare that the research was conducted in the absence of any commercial or financial relationships that could be construed as a potential conflict of interest.

Authors' Contributions

Zhen Liu and Shuting He contributed equally to this work.

References

[1] M. A. Costa, A. Sousa, and E. Vieira, "Hemangioendothelioma: a rare vascular tumor in childhood and adolescence," *Pediatric Hematology and Oncology*, vol. 13, no. 4, pp. 333–337, 1996.

[2] S. W. Weiss and F. M. Enzinger, "Epithelioid hemangioendothelioma: a vascular tumor often mistaken for a carcinoma," *Cancer*, vol. 50, no. 5, pp. 970–981, 1982.

[3] N. Nakagawa, M. Takahashi, K. Maeda, N. Fujimura, and M. Yufu, "Case report: adrenal haemangioma coexisting with malignant haemangioendothelioma," *Clinical Radiology*, vol. 37, no. 1, pp. 97–99, 1986.

[4] M. Vasquez, N. G. Ordóñez, G. W. English, and B. Mackay, "Epithelioid hemangioendothelioma of soft tissue: report of a case with ultrastructural observations," *Ultrastructural Pathology*, vol. 22, no. 1, pp. 73–78, 1998.

[5] K. Lau, M. Massad, C. Pollak et al., "Clinical patterns and outcome in epithelioid hemangioendothelioma with or without pulmonary involvement: insights from an internet registry in the study of a rare cancer," *Chest*, vol. 140, no. 5, pp. 1312–1318, 2011.

[6] C. Sardon, C. Foster, J. De Luca-Johnson, and A. Fehringer, "Epithelioid hemangioendothelioma of the foot," *Journal of Radiology Case Reports*, vol. 15, no. 12, pp. 20–28, 2021.

[7] Y. I. Liu, S. S. Brown, A. Elihu et al., "Hepatic epithelioid hemangioendothelioma," *Digestive Diseases and Sciences*, vol. 56, no. 2, pp. 303–306, 2011.

[8] J. Naqvi, N. G. Ordonez, M. A. Luna, M. D. Williams, R. S. Weber, and A. K. El-Naggar, "Epithelioid hemangioendothelioma of the head and neck: role of podoplanin in the differential diagnosis," *Head and Neck Pathology*, vol. 2, no. 1, pp. 25–30, 2008.

[9] D. Marchiano, F. Fisher, and S. Hofstetter, "Epithelioid hemangioendothelioma of the heart with distant metastases. A case report and literature review," *The Journal of Cardiovascular Surgery*, vol. 34, no. 6, pp. 529–533, 1993.

[10] A. Rosenberg and M. Agulnik, "Epithelioid hemangioendothelioma: update on diagnosis and treatment," *Current Treatment Options in Oncology*, vol. 19, no. 4, p. 19, 2018.

[11] W. Song, Z. Zhen, L. Li et al., "Epithelioid hemangioendothelioma of the sternum," *Thoracic Cancer*, vol. 11, no. 6, pp. 1741–1745, 2020.

[12] K. M. Doll, A. Rademaker, and J. A. Sosa, "Practical guide to surgical data sets: surveillance, epidemiology, and end results (SEER) database," *JAMA Surgery*, vol. 153, no. 6, pp. 588-589, 2018.

[13] F. E. Harrell Jr., K. L. Lee, and D. B. Mark, "Multivariable prognostic models: issues in developing models, evaluating assumptions and adequacy, and measuring and reducing errors," *Statistics in Medicine*, vol. 15, no. 4, pp. 361–387, 1996.

[14] M. J. Pencina and R. B. D'Agostino, "Overall C as a measure of discrimination in survival analysis: model specific population value and confidence interval estimation," *Statistics in Medicine*, vol. 23, no. 13, pp. 2109–2123, 2004.

[15] L. Requena and H. Kutzner, "Hemangioendothelioma," *Seminars in Diagnostic Pathology*, vol. 30, no. 1, pp. 29–44, 2013.

[16] L. L. Studer and D. M. Selby, "Hepatic epithelioid hemangioendothelioma," *Archives of Pathology & Laboratory Medicine*, vol. 142, no. 2, pp. 263–267, 2018.

[17] S. Stacchiotti, N. Simeone, S. L. Vullo et al., "Activity of sirolimus in patients with progressive epithelioid hemangioendothelioma: a case-series analysis within the Italian rare cancer network," *Cancer*, vol. 127, no. 4, pp. 569–576, 2021.

[18] M. Brahmbhatt, S. Prenner, and T. Bittermann, "Liver transplantation for hepatic epithelioid hemangioendothelioma is facilitated by exception points with acceptable long-term outcomes," *Transplantation*, vol. 104, no. 6, pp. 1187–1192, 2020.

[19] A. Weissferdt and C. A. Moran, "Epithelioid hemangioendothelioma of the bone," *Advances in Anatomic Pathology*, vol. 21, no. 4, pp. 254–259, 2014.

[20] S. Stacchiotti, A. B. Miah, A. M. Frezza et al., "Epithelioid hemangioendothelioma, an ultra-rare cancer: a consensus paper from the community of experts," *ESMO Open*, vol. 6, no. 3, article 100170, 2021.

[21] C. Kaltenmeier, S. Stacchiotti, A. Gronchi et al., "Treatment modalities and long-term outcomes of hepatic hemangioendothelioma in the United States," in *Hepato Pancreato Biliary*, Elsevier, 2022.

[22] C. E. Woodall, C. R. Scoggins, A. M. Lewis, K. M. McMasters, and R. C. Martin, "Hepatic malignant epithelioid hemangioendothelioma: a case report and review of the literature," *The American Surgeon*, vol. 74, no. 1, pp. 64–68, 2008.

[23] B. G. Zelger, B. Wambacher, H. Steiner, and B. Zelger, "Cutaneous epithelioid hemangioendothelioma, epithelioid cell histiocytoma and Spitz nevus," *Journal of Cutaneous Pathology*, vol. 24, no. 10, pp. 641–647, 1997.

[24] E. Cournoyer, A. Al-Ibraheemi, E. Engel, G. Chaudry, S. Stapleton, and D. M. Adams, "Clinical characterization and long-term outcomes in pediatric epithelioid hemangioendothelioma," *Pediatric Blood & Cancer*, vol. 67, no. 2, article e28045, 2020.

[25] N. Maruyama, Y. Kumagai, Y. Ishida et al., "Epithelioid haemangioendothelioma of the bone tissue," *Virchows Archiv. A, Pathological Anatomy and Histopathology*, vol. 407, no. 2, pp. 159–165, 1985.

[26] S. Shiba, H. Imaoka, K. Shioji et al., "Clinical characteristics of Japanese patients with epithelioid hemangioendothelioma: a multicenter retrospective study," *BMC Cancer*, vol. 18, no. 1, p. 993, 2018.

[27] X. Yin, H. Duan, Z. Yi, C. Li, R. Lu, and L. Li, "Incidence, Prognostic factors and survival for hemangioblastoma of the central nervous system: analysis based on the surveillance, epidemiology, and end results database," *Frontiers in Oncology*, vol. 10, 2020.

[28] P. J. Salsberry and P. B. Reagan, "Comparing the influence of childhood and adult economic status on midlife obesity in Mexican American, white, and African American women," *Public health Nursing*, vol. 26, no. 1, pp. 14–22, 2009.

[29] E. Chen, G. E. Miller, T. Yu, and G. H. Brody, "The great recession and health risks in African American youth," *Brain, Behavior, and Immunity*, vol. 53, pp. 234–241, 2016.

[30] P. Bagan, M. Hassan, F. L. P. Barthes et al., "Prognostic factors and surgical indications of pulmonary epithelioid hemangioendothelioma: a review of the literature," *The Annals of Thoracic Surgery*, vol. 82, no. 6, pp. 2010–2013, 2006.

[31] D. Tong, A. Constantinidou, B. Engelmann et al., "The role of local therapy in multi-focal epithelioid haemangioendothelioma," *Anticancer Research*, vol. 39, no. 9, pp. 4891–4896, 2019.

[32] J. A. Rodriguez, N. S. Becker, C. A. O'Mahony, J. A. Goss, and T. A. Aloia, "Long-term outcomes following liver transplantation for hepatic hemangioendothelioma: the UNOS experience from 1987 to 2005," *Journal of Gastrointestinal Surgery*, vol. 12, no. 1, pp. 110–116, 2008.

Retraction

Retracted: PRR15 Is a Novel Diagnostic and Prognostic Biomarker in Papillary Thyroid Cancer and Modulates the Tumor Microenvironment

Journal of Oncology

This article has been retracted by Hindawi following an investigation undertaken by the publisher [1]. This investigation has uncovered evidence of one or more of the following indicators of systematic manipulation of the publication process:

(1) Discrepancies in scope

(2) Discrepancies in the description of the research reported

(3) Discrepancies between the availability of data and the research described

(4) Inappropriate citations

(5) Incoherent, meaningless and/or irrelevant content included in the article

(6) Peer-review manipulation

The presence of these indicators undermines our confidence in the integrity of the article's content and we cannot, therefore, vouch for its reliability. Please note that this notice is intended solely to alert readers that the content of this article is unreliable. We have not investigated whether authors were aware of or involved in the systematic manipulation of the publication process.

Wiley and Hindawi regrets that the usual quality checks did not identify these issues before publication and have since put additional measures in place to safeguard research integrity.

We wish to credit our own Research Integrity and Research Publishing teams and anonymous and named external researchers and research integrity experts for contributing to this investigation.

The corresponding author, as the representative of all authors, has been given the opportunity to register their agreement or disagreement to this retraction. We have kept a record of any response received.

References

[1] L. Wang, X. Deng, Y. Chen, Y. Zhao, and Z. Li, "PRR15 Is a Novel Diagnostic and Prognostic Biomarker in Papillary Thyroid Cancer and Modulates the Tumor Microenvironment," *Journal of Oncology*, vol. 2022, Article ID 3290479, 11 pages, 2022.

Research Article

PRR15 Is a Novel Diagnostic and Prognostic Biomarker in Papillary Thyroid Cancer and Modulates the Tumor Microenvironment

Lingli Wang,[1] Xiaoqing Deng,[2] Yi Chen,[1] Yixia Zhao ⓘ,[3] and Zhirong Li ⓘ[4]

[1]Department of Breast and Thyroid Surgery, Daping Hospital, Army Medical University, Chongqing, China
[2]Department of Nephrology, The First Affiliated Hospital of Chongqing Medical University, Chongqing, China
[3]Department of Pharmacy, Chongqing University Cancer Hospital, Chongqing, China
[4]Digestive Center, University-Town Hospital of Chongqing Medical University, Chongqing, China

Correspondence should be addressed to Yixia Zhao; zhaoyixia@cqu.edu.cn and Zhirong Li; lzr2012vip@126.com

Papillary thyroid cancer (PTC), accounting for more than 80 percent of all cases of thyroid cancer, is a form of a cancerous tumor that has a very favorable prognosis. However, patients diagnosed with PTC who are already in an advanced state have a dismal outlook. This study aimed to establish the diagnostic relevance of PRR15 expression in PTC patients as well as its levels in PTC samples and its connection with immune infiltrates. The TCGA and GEO datasets were combed through to obtain information on PTC patients. The "Limma" program was used to screen for differentially expressed mRNAs (DEMs), and the results were displayed using volcano plots and heat maps. The Wilcoxon test was used to examine the level of PRR15 expression in PTC patients in comparison with that of normal tissues. To study the connection between the immune infiltration level and PRR15 expression in PTC, the single-sample sequence set enrichment analysis (ssGSEA) from the R package was utilized. The expression of PRR15 was analyzed with RT-PCR in PTC cells and normal cells. In order to evaluate the diagnostic significance of PRR15 expression, ROC assays were carried out. Experiments using CCK-8 were carried out to investigate the impact that PRR15 knockdown could have on the proliferation of PTC cells. In this study, 17 overlapped DEMs between PTC specimens and normal specimens were identified, including MPPED2, IPCEF1, SLC4A4, PKHD1L1, DIO1, CRABP1, TPO, TFF3, SPX, TCEAL2, ZCCHC12, SYTL5, PRR15, CHI3L1, SERPINA1, GABRB2, and CITED1. Our attention focused on PRR15 which was highly expressed in PTC specimens as compared with nontumor specimens. PRR15 had an AUC value of 0.926 (95% CI 0.902–0.950) for PTC based on TCGA datasets. Pan-cancer assays suggested PRR15 as an oncogenic gene in many types of tumors. Moreover, we found that PRR15 expression was positively correlated with eosinophils, NK cells, NK CD56bright cells, IDC, macrophages, DC, mast cells, and Th1 cells. Further investigations with CCK-8 demonstrated that inhibiting PRR15 resulted in a decrease in the proliferation of PTC cells. Overall, PRR15 was confirmed to be a biomarker for PTC patients and a predictor of response to immunotherapy.

1. Introduction

Thyroid cancer, which is the most prevalent kind of endocrine malignant tumor, is increasing at a rate of one percent per year around the world and has shown a rapid increase in morbidity [1]. Papillary thyroid carcinoma (PTC) is the most common kind of thyroid cancer [2]. It accounts for around 60–70 percent of all thyroid cancers, and it most

frequently affects women in their fourth and fifth decades of life [3]. Many PTCs are well differentiated and have a low risk of recurrence, but a small proportion of tumors reveal heterogeneity with more aggressive variations [4, 5]. Because so little is known about the potential mechanisms of aggressive variations, the therapy for PTC cases is frequently insufficient or less than ideal. Therefore, diagnostic and prognostic biomarkers are desperately needed as soon as

possible because these would assist doctors in implementing early and suitable steps for maximum treatment benefit.

PTCs encompass several subtypes, including a classical variant of tall cell variant of PTC (tPTC), follicular variant of PTC (fVPTC), and papillary thyroid carcinoma (cPTC) [6]. According to the established criteria recognized by the World Health Organization, other histologic variations include diffuse sclerosing, columnar, and others [7]. It is possible that the prognosis for various histologic subtypes of PTC will be varied. Based on the developing idea of "precision medicine," recent years have seen significant advancements in molecular pathology detection tools and tailored therapy, both of which have contributed to a dramatically increased overall survival rate for patients diagnosed with PTC [8, 9]. In the field of precision medicine, the genes that are most responsible for the development of cancer could be applied as therapeutic targets [10]. Several molecules are involved in adenocarcinoma including the anaplastic lymphoma kinase gene, echinoderm microtubule-associatedprotein-like gene, and epidermal growth factor receptor mutations [11, 12]. Even while molecularly targeted medicines have shown promising outcomes in clinical testing, there is still a long way to go before patients diagnosed with PTC may be cured, particularly due to the evolution of drug resistance. Therefore, patients diagnosed with PTC require the identification of more accurate indicators for diagnosis and prognosis of PTC patients.

Immunotherapy has recently garnered a great deal of attention as a potentially effective treatment for a variety of malignancies [13]. Immune checkpoint inhibitors (ICIs) are another name for T cell-based immunotherapy [14]. Immunotherapy and associated treatments targeting T cell exhaustion indicators can improve the long-term survival of tumor patients by increasing antitumor immunity, which has exhibited considerable therapeutic benefit in immunogenic cancers such as liver cancer, glioma, rectal cancer, renal cell carcinoma, and melanoma [15, 16]. However, the therapy provided by ICIs is not effective for all patients. The varying response is also connected with the genetic characteristics of the patients, such as the tumor microenvironment (TME) [17]. Research conducted throughout time has accumulated evidence that tumor cells can alter the TME to function as contributors that assure fast cell proliferation [18]. The dynamic alteration of molecular and cellular processes in TME relays on the interactions between tumor cells and immune cells, which highlights the role of TILs in the context of protumorigenic inflammation and anticancer immunosurveillance.

In this study, we analyzed GEO datasets and identified several differentially expressed mRNAs (DEMs) in PTC. Among them, our attention focused on proline-rich 15 (PRR15). PRR15 is a nuclear protein with a low-molecular weight that is expressed by the trophoblast in the early stages of pregnancy. The death of the embryo on day 15 of gestation was caused by lentivirus-mediated reduction of PRR15 mRNA in ovine trophectoderm [19]. This provides solid evidence that PRR15 expression is crucial during this precarious window of development. In recent years, PRR15 has been reported to be dysregulated in several tumors, such as

breast cancer, esophageal cancer, and human gastrointestinal tumors [20, 21, 22]. However, its specific function and clinical significance were rarely reported. In this study, we aimed to explore the prognostic value of PRR15 expression and its association with the tumor microenvironment.

2. Methods

2.1. Cell Culture and Cell Transfection. The human normal thyroid epithelial cell line (Nthy-ori 3-1) and the PTC cell lines (FTC-133, 8505C, TPC1, and BCPAP) were purchased. All of the cell lines were kept alive in DMEM (Invitrogen, China), which was supplemented with 10 percent FBS (PAN, China). The cells were cultured at a temperature of 37°C in an atmosphere that contained 5 percent carbon dioxide.

RiboBio (Guangzhou, China) was the supplier for both PRR15 small interfering RNA (siRNA) and negative control siRNA (si-NC). The Lipofectamine 2000 reagent (manufactured by Invitrogen) was used to achieve cell transfection in accordance with the manufacturer's instructions.

2.2. qRT-PCR Analysis. In order to get total RNA from TPC tissues or cells, the TRIzol (Invitrogen, USA) kit was used, and the process followed the procedure provided by the manufacturer. To perform reverse transcription on the shared gene and miRNA, the HiScript® III 1st Strand cDNA Synthesis Kit (+gDNA wiper) (Vazyme, China) was used. To carry out reverse transcription of miRNA, a First Strand cDNA Synthesis Kit (by stem-loop) (Vazyme, China) was utilized. Amplification of the target genes was done by qPCR, and the ChamQ-Universal-SYBR qPCR Master Mix was applied for the quantification (Vazyme). The following describes the cycle conditions for RT-qPCR: first, denaturation was performed at 95°C for ten minutes, followed by forty cycles of denaturation at 95°C for fifteen seconds and annealing/elongation at 60°C for sixty seconds each. Internal controls were determined using either GAPDH or U6. The 2-CT technique was utilized in order to carry out the task of determining the extent to which the target gene was amplified. The involved primers were as follows: PRR15 forward: 5′-GCTCACCAACAGCAGAAAGAA-3′, PRR15 reverse: CGGATTTGTCCCCGTATAACTTG; GAPDH forward: 5′- ACAACTTTGGTATCGTGGAAGG-3′, GAPDH reverse: 5′-GCCATCACGCCACAGTTTC-3′.

2.3. Cell Counting Kit-8 (CCK-8) Experiment. We used a commercial product called CCK-8 to determine the vitality of the cells. PTC cells with a density of 5×10^3 cells per well were seeded onto 96-pore dishes, and a further 10 μl of CCK-8 solution was added for an additional two hours of growth. It was determined that each well had an absorbance of 450 nm.

2.4. Data Processing. The datasets for papillary thyroid carcinoma, also known as THCA, were gathered from two different platforms. There was a search conducted in The Cancer Genome Atlas (TCGA) database (https://portal.gdc.

cancer.gov/repository) using the THCA database level 3 count. The values in the datasets that are part of TCGA have been converted into transcripts per million (TPM). The THCA clinical data were gathered by utilizing the UCSC Xena browser, which may be found online at https://xenabrowser.net/. In this retrospective study, we only considered patients who had primary tumors and who had not previously been treated with neoadjuvant chemotherapy or radiation. Their survival data, together with their clinicopathological, genetic, and epigenetic information, were downloaded for a secondary study. The datasets containing 510 tumor samples and 58 normal samples were utilized in this research project. The clinical information of all PTC is shown in Table 1. Two different Gene Expression Omnibus (GEO) datasets were examined for this study. Downloads were made up of the series matrix files of GSE33630 (which had 60 cases of thyroid cancer and 45 cases of normal tissue) and GSE3678 (which contained 7 cases of papillary thyroid carcinoma and 7 cases of normal tissue). Afterwards, the gene expression in PTC and normal thyroid tissue was compared using the normalized values of the genes.

2.5. Identification of Differentially Expressed mRNA (DEMs) in PTC. The raw count data were first transformed into log2 form after being standardized with the transcripts per million (TPM) method. The next step was the annotation of 19654 protein-coding genes. "Limma," in its version 3.36.2 for the R programming language, was used in the DEM calculations [23]. DEMs that had an absolute log2 fold change (FC) of >1 and an adjusted P value of <0.05 were taken into consideration for further study.

2.6. Estimation of TME Immune Infiltration. Bindea et al. provided us with the gene set that could be used to represent many sorts of immune cells that infiltrated the tissue. After that, ssGSEA was applied to compute the number of immune cells present based on the expression of the reference gene contained within the gene set that was obtained from the transcriptomic data. 24 types of immune cells were enrolled in our study.

2.7. Statistical Analyses. R software version 3.5.3 was used to carry out the statistical analyses. Student's t-test and the chi-square test were used to do a comparison between the two groups. The ROC was an invaluable tool in establishing the diagnostic value of PRR15 for PTC patients. Kaplan–Meier analysis and the log-rank test were performed to identify survival differences in TPC patients. A heat map and volcano map were used to show the DEMs between PTC specimens and nontumor specimens. A $p < 0.05$ was considered to indicate a statistically significant difference.

3. Results

3.1. Identification of DEMs between PTC Samples and Normal Samples. In the first step of our research, we examined the GSE3678 datasets, which contained both PTC and normal

samples. The limma program was utilized in order to perform an analysis on the DEMs of the metadata. 574 DEMs were collected: 244 genes were upregulated and 330 genes were downregulated (Figure 1(a)). Similarly, we analyzed GSE33630 datasets which included 60 tumor samples and 45 normal samples, and 1229 mRNAs were collected in which 615 mRNAs were upregulated and 614 mRNAs were downregulated (Figure 1(b)). To further screen the critical functional genes involved in PTC progression, we used a heat map to show the top 20 dysregulated mRNAs between PTC samples and normal samples in GSE3678 (Figure 1(c)) and GSE33630 (Figure 1(d)). Finally, 17 overlapped DEMs were identified, including MPPED2, IPCEF1, SLC4A4, PKHD1L1, DIO1, CRABP1, TPO, TFF3, SPX, TCEAL2, ZCCHC12, SYTL5, PRR15, CHI3L1, SERPINA1, GABRB2, and CITED1 (Figure 1(e)).

3.2. The Distinct Upregulation of PRR15 in PTC and Its Diagnostic Value. Among the 17 genes, our attention was focused on PRR15 which was highly expressed in PTC specimens compared with nontumor specimens in both GSE3678 (Figure 2(a)) and GSE33630 datasets (Figure 2(b)). Then, we analyzed TCGA datasets and also confirmed PRR15 as an overexpressed gene in PTC (Figures 2(c) and 2(d)). In addition, the results based on TCGA datasets and GTEx data were in line (Figure 2(e)). Then, we further explored the possible diagnostic potential of higher PRR15 expression in screening PTC patients. As presented in Figure 2(f), PRR15 had an AUC value of 0.926 (95% CI 0.902–0.950) for PTC based on TCGA datasets. Moreover, a similar finding was observed based on TCGA datasets and GTEx data (Figure 2(g)).

3.3. The mRNA Expression of PRR15 in Cancers. Data from the TCGA datasets showed that PRR15 expressions were distinctly higher in BRCA, CHOL, LIHC, LUSC, PAAD, STAD, THCA, and UCEC, while its expression was distinctly lower in COAD, KICH, KIRC, KIRP, and PRAD (Figure 3(a)). Based on TCGA and GTEx databases, we found that more tumor specimens exhibited a higher level of PRR15 (Figure 3(b)). Thus, our findings suggested that PRR15 may exhibit a different role based on the types of tumors. According to our results, its main function may be a tumor promotor.

3.4. Association between PRR15 Levels and Clinicopathological Parameters of PTC. We studied the relationship between PRR15 levels and the clinicopathological features of PTC so that we might gain a better understanding of the clinical relevance of PRR15 expression in patients with PTC. We did not find distinct differences between the PRR15 expression and several clinicopathological parameters of PTC, including age (Figure 4(a)), gender (Figure 4(b)), T stage (Figure 4(c)), and M stage (Figure 4(d)). However, we found that PTC specimens with advanced N stage exhibited a higher level of PRR15 than those with low N stage (Figure 4(e)).

TABLE 1: Association of PRR15 with clinicopathological characteristics of PTC patients.

Characteristics	The low expression of PRR15	The high expression of PRR15	P
N	255	255	
Gender, n (%)			0.691
Female	183 (35.9%)	188 (36.9%)	
Male	72 (14.1%)	67 (13.1%)	
Age, n (%)			0.723
≤45	118 (23.1%)	123 (24.1%)	
>45	137 (26.9%)	132 (25.9%)	
M stage, n (%)			0.505
M0	138 (46.8%)	148 (50.2%)	
M1	3 (1%)	6 (2%)	
N stage, n (%)			0.025
N0	123 (26.7%)	106 (23%)	
N1	99 (21.5%)	132 (28.7%)	
T stage, n (%)			0.500
T1	65 (12.8%)	78 (15.4%)	
T2	85 (16.7%)	82 (16.1%)	
T3	89 (17.5%)	86 (16.9%)	
T4	14 (2.8%)	9 (1.8%)	
Age, median (IQR)	48 (35.5, 60)	46 (34, 56)	0.096

(a)

(b)

FIGURE 1: Continued.

(c)

(d)

(e)
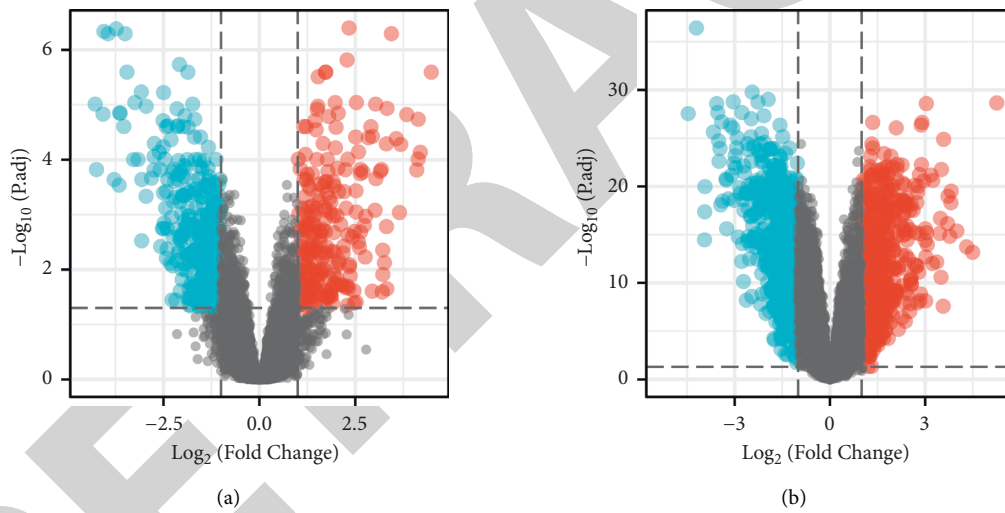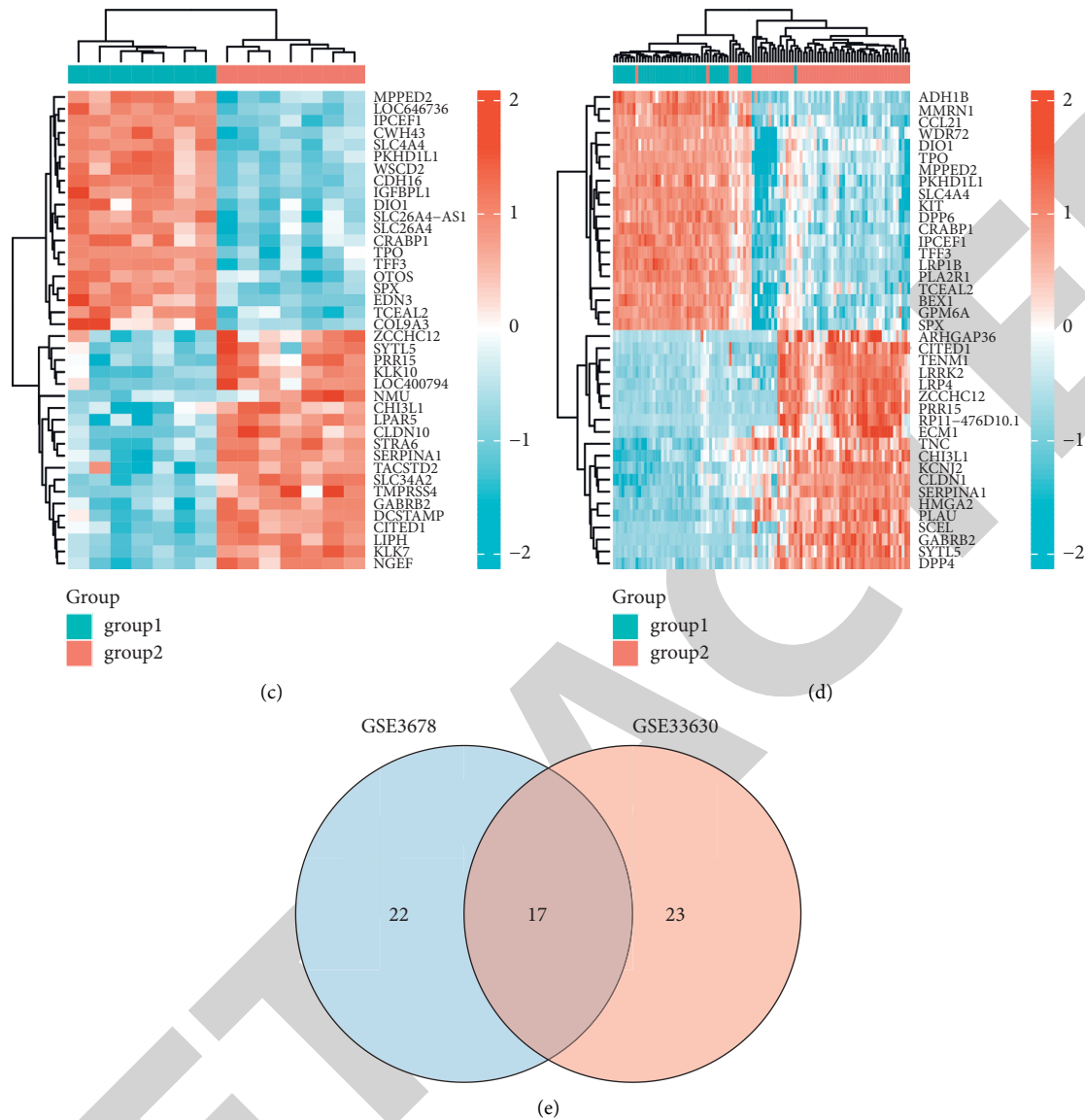
Figure 1: Identification of the DEMs between PTC specimens and nontumor specimens. (a)-(b) The number of DEMs found in the GSE3678 and GSE33630 datasets is displayed using volcano charts. (c)-(d) The top 20 DEMs found in the GSE3678 and GSE33630 datasets are displayed on a heat map. (e) The genes that are shared by both GSE3678 and GSE33630 datasets are depicted in a Venn diagram.

3.5. PRR15 Expression Is Correlated with Immune Infiltration Level in PTC. As shown in Figure 5(a), we found that PRR15 expression was positively correlated with eosinophils, NK cells, NK CD56bright cells, IDC, macrophages, DC, mast cells, and Th1 cells. The representative diagram of the correlation analysis between PRR15 expression and immune-infiltrating cells is shown in Figure 5(b).

3.6. Knockdown of PRR15 Suppressed the Proliferation of PTC Cells. We used RT-PCR to see if PRR15 expression was abnormal in PTC cells, Nthy-ori 3-1 cells had decreased PRR15 expression compared to PTC cell lines FTC-133, 8505C, TPC1, and BCPAP cells (Figure 6(a)). Loss-of-function experiments in vitro were carried out to examine the biological significance of PRR15 in PTC cells. An

oligonucleotide (si-PRR15) transfection reduced the expression level of PRR15 considerably in 8505C and TPC1 cells (Figure 6(b)). CCK-8 assays showed that PRR15 knockdown significantly reduced 8505C and TPC1 cell growth when compared to negative control transfection (Figures 6(c) and 6(d)).

4. Discussion

PTC has been shown to correlate with external radiation exposure, dietary iodine content, and the subsequent disturbance of thyroid stimulating hormone (TSH) levels throughout the course of the past few decades [24, 25]. Today, a rising number of investigations are beginning to focus on acquired genetic alterations that can discriminate paratumor normal tissue from PTC specimens. The early
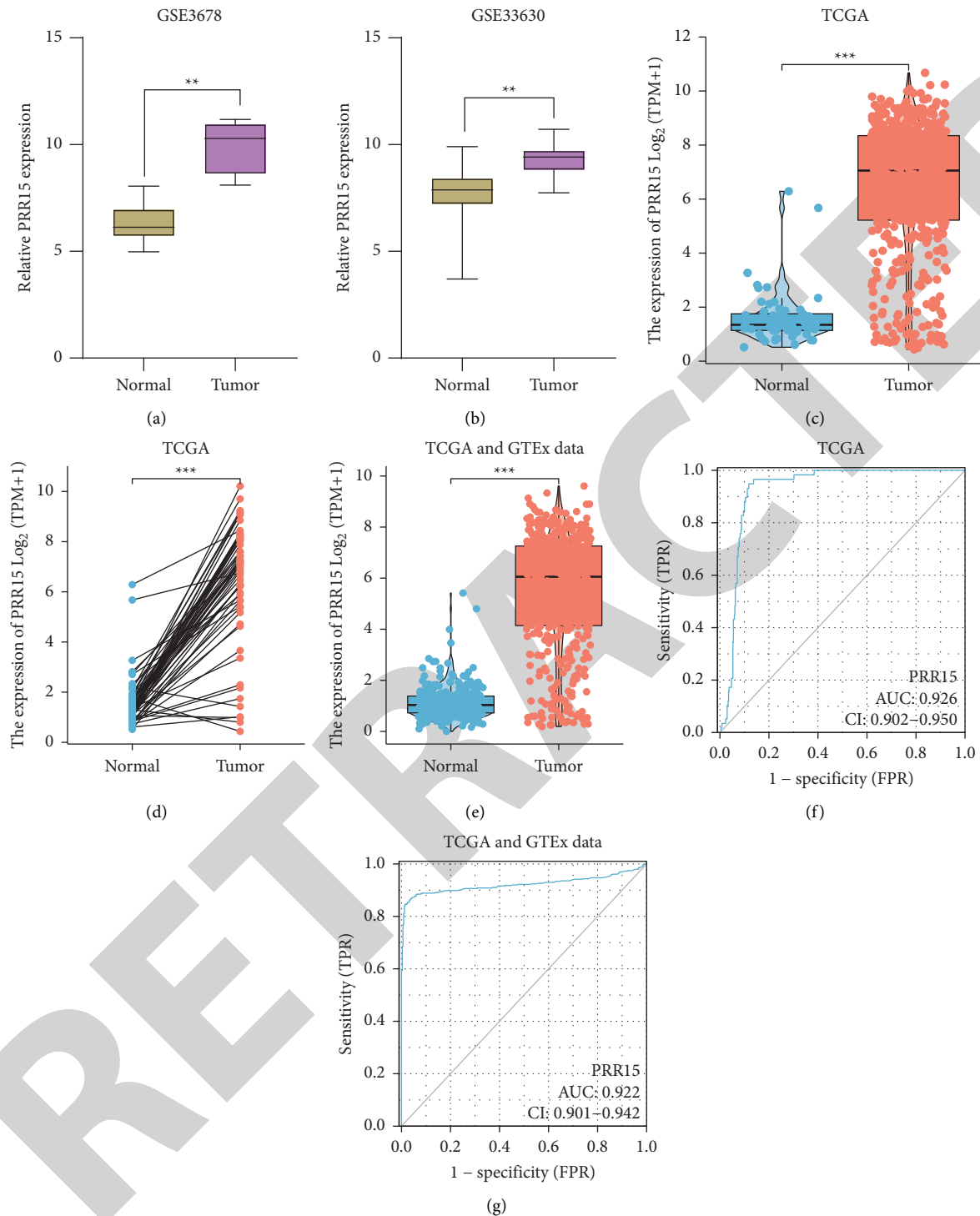
Figure 2: The expression of PRR15 in PTC patients and its diagnostic value. ((a)-(d)) PRR15 expression distinctly increased in PTC specimens compared with nontumor specimens in (a) GSE3678, (b) GSE33630, and (c)-(d) TCGA datasets. (e) The upregulation of PRR15 in PTC patients further confirmed in TCGA and GTEx data. (f)-(g) ROC assays applied to determine the diagnostic value of PRR15 expression in screening PTC specimens from nontumor specimens in TCGA or TCGA and GTEx data.

diagnosis of PTC patients is very important, which can help doctors develop the best treatment plan. As a result, our understanding of the molecular etiology of PTC has

significantly expanded. In clinical settings, a number of other biomarkers, such as RET/PTC rearrangement, PAX8-PPAR rearrangement, BRAF mutations, and RAS mutations, have
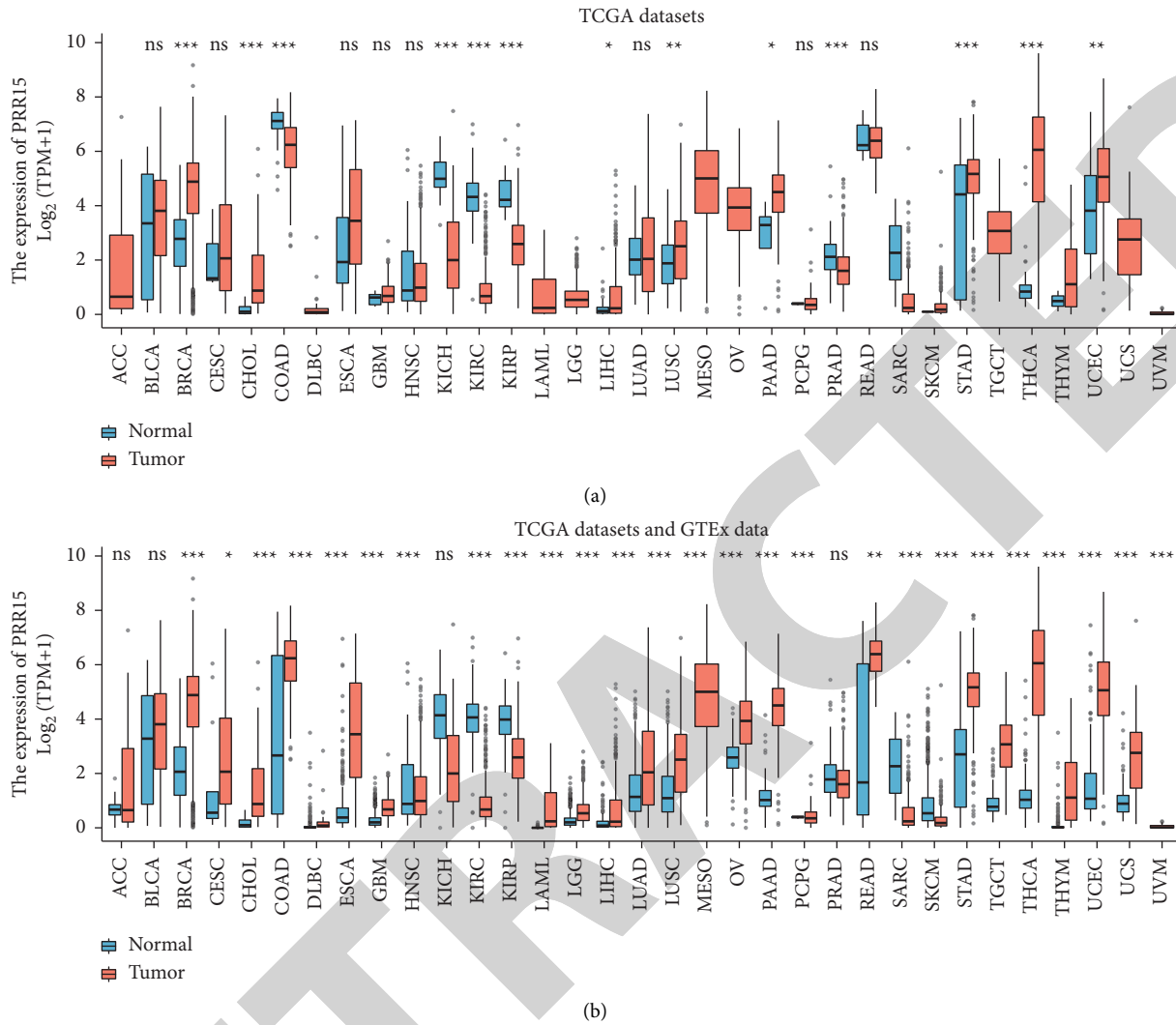
Figure 3: Expression level of PRR15 in different cancer types from (a) TCGA or (b) TCGA and GTEx data.

been employed [26, 27]. Therefore, screening sensitive biomarkers would be of tremendous value for the customized prevention and treatment of patients suffering from PTC.

First, we analyzed the GSE3678 and GSE33630 datasets. DEMs were analyzed by the use of the limma package. We overlapped 17 DEMs, including MPPED2, IPCEF1, SLC4A4, PKHD1L1, DIO1, CRABP1, TPO, TFF3, SPX, TCEAL2, ZCCHC12, SYTL5, PRR15, CHI3L1, SERPINA1, GABRB2, and CITED1. Among the above DEMs, several of them have been reported to be involved in the progression of several tumors. For instance, Zhang et al. reported that in PTC, miR-222-3p had a high level of expression, while SLC4A4 had a low level of expression. PTC cells were shown to benefit from the presence of miR-222-3p in terms of their ability to proliferate, invade, and migrate. These stimulatory effects of miR-222-3p were able to be inhibited by SLC4A4, as expected [28]. Lin et al. showed that TFF3 expression was shown to be increased in PTC tissue, and this increase in expression was associated with lymph node

metastasis, pathological grade, and snail expression. TPC1 cells were significantly hindered in their capacity for proliferation, adhesion, colony formation, migration, and invasion after having their TFF3 levels significantly reduced. The findings showed that TFF3 might potentially activate the MAPK/ERK signaling pathways mechanically [29]. Wang and his group reported that the ZCCHC12 gene was shown to be significantly amplified in primary PTC cancers. Overexpression of ZCCHC12 was found to correlate with lymph node metastases in both cohorts. In trials conducted in vitro, a decrease in ZCCHC12 expression led to a considerable inhibition of PTC cell colony formation, motility, and invasion [30]. These findings suggested DEMs as important regulators in progression of PTC. However, the expression and function of PRR15 have not been investigated in PTC. In this study, we first reported that PRR15 expression was distinctly increased in PTC cell lines. PRR15 had an AUC value of 0.926 (95% CI 0.902–0.950) for PTC based on TCGA datasets. Moreover, a similar finding was observed based on TCGA datasets and

(a)

(b)

(c)

(d)

(e)
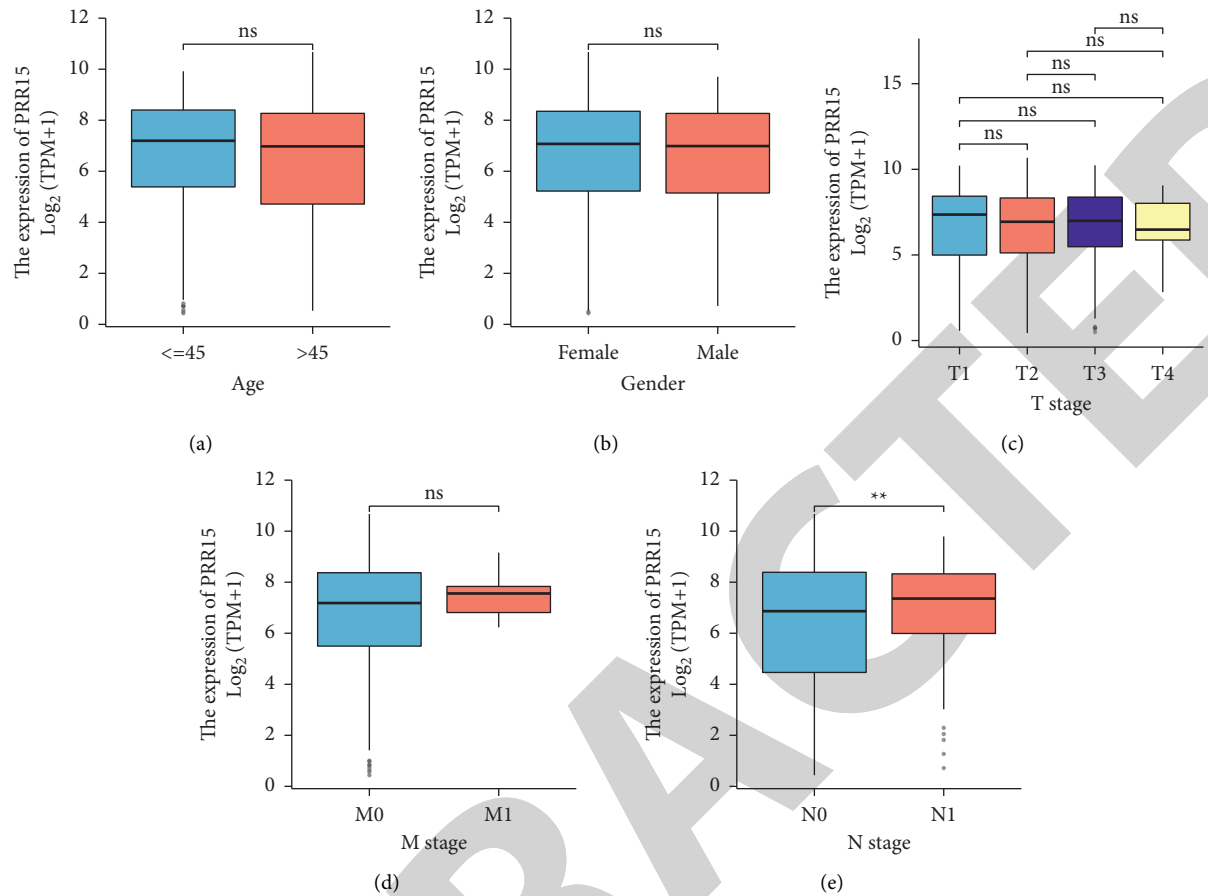
FIGURE 4: The association between PRR15 expression and clinicopathological parameters of PTC, including (a) age, (b) gender, (c) T stage, (d) M stage, and (e) N stage.

GTEx data, which confirmed the diagnostic value of PRR15 in screening PTC specimens from normal specimens. In addition to this, we were able to demonstrate that inhibiting PRR15 in PTC cells led to a reduction in their rate of proliferation. In general, our research indicated that PRR15 may serve as both a new diagnostic biomarker and an oncogene in individuals with PTC.

Equally as crucial, our research revealed the connection between PRR15 expressions and immune infiltration in PTC by utilizing ssGSEA and Spearman correlation. We found that PRR15 expression was positively correlated with eosinophils, NK cells, NK CD56bright cells, IDC, macrophages, DC, mast cells, and Th1 cells. Many tumors, including bladder cancer, lung cancer, and melanoma, have Th1/Th2 balanced drift in the body, and Th2 cells are often dominant, which may be related to the immune escape of tumors [31, 32]. There is a growing trend in research to try and develop medications and technologies that can either stabilize the Th1/Th2 balance or bring about a reversal of it [33]. For example, the use of cytokines or cytokine antagonists in the therapy of cancers and other disorders to reestablish a healthy balance between Th1 and Th2 cells: cytokines produced by Th1 cells have the ability to shift the Th1/Th2 equilibrium toward a Th1 state while simultaneously decreasing the dominant expression of Th2 cells.

The opposite impact was produced by Th2 cytokines. Patients who have a higher than average number of infiltrating DC in many different kinds of cancers have a better prognosis than patients who do not have a higher than average number of these cells [34]. There is a close association between DC and the occurrence and progression of cancers [35, 36]. The generation of a cellular immune response that is dominated by CD8+ T cells is essential to the production of an effective antitumor immune response. These cells are also the foundation of DC as an immunotherapy.

There are still some limitations in the current study. First, this investigation looked back at previous events. Therefore, in the future, there ought to be a prospective study carried out in order to eliminate the analysis bias that is linked with studies that are retrospective. Second, since the number of healthy subjects who participated in the study to serve as controls was significantly lower than the number of patients who participated in the study to have cancer, additional research was required to ensure that there was an equal distribution of patients and healthy subjects among the samples. Last, the purpose of this work, which was carried out in vitro, was to investigate the possible role that PRR15 expression plays in PTC progression. To validate our findings, we needed to conduct additional tests on living animals.
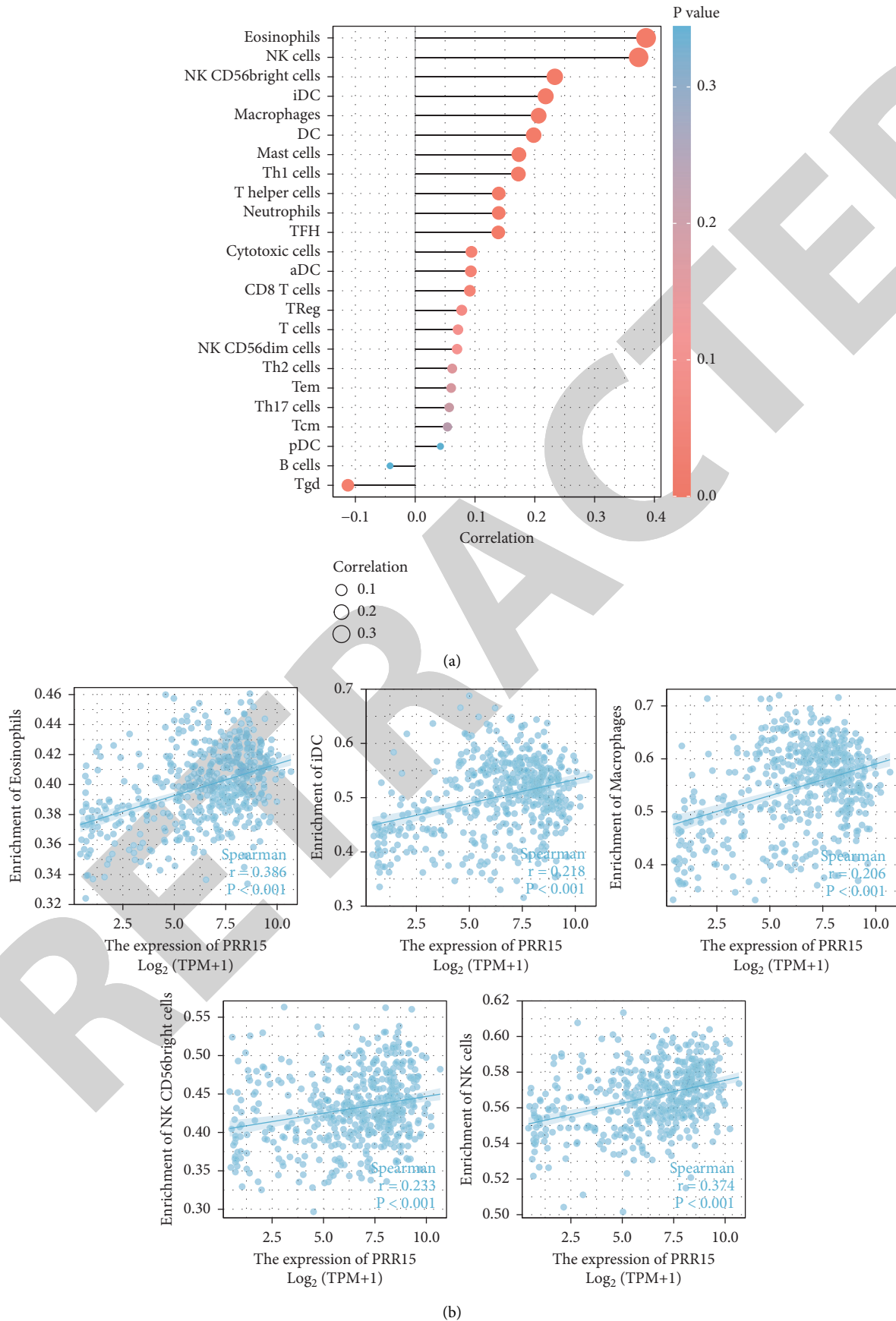
Figure 5: The expression level of PRR15 is related to the immune infiltration in the tumor microenvironment. (a) The amount of PRR15 expression shown to have a correlation with the relative abundances of 24 immune cells. The magnitude of the dots is representative of the absolute value of Spearman (R). (b) A diagrammatic representation of the correlation analysis performed between PRR15 expression and immune-infiltrating cells.

(a)

(b)

(c)

(d)
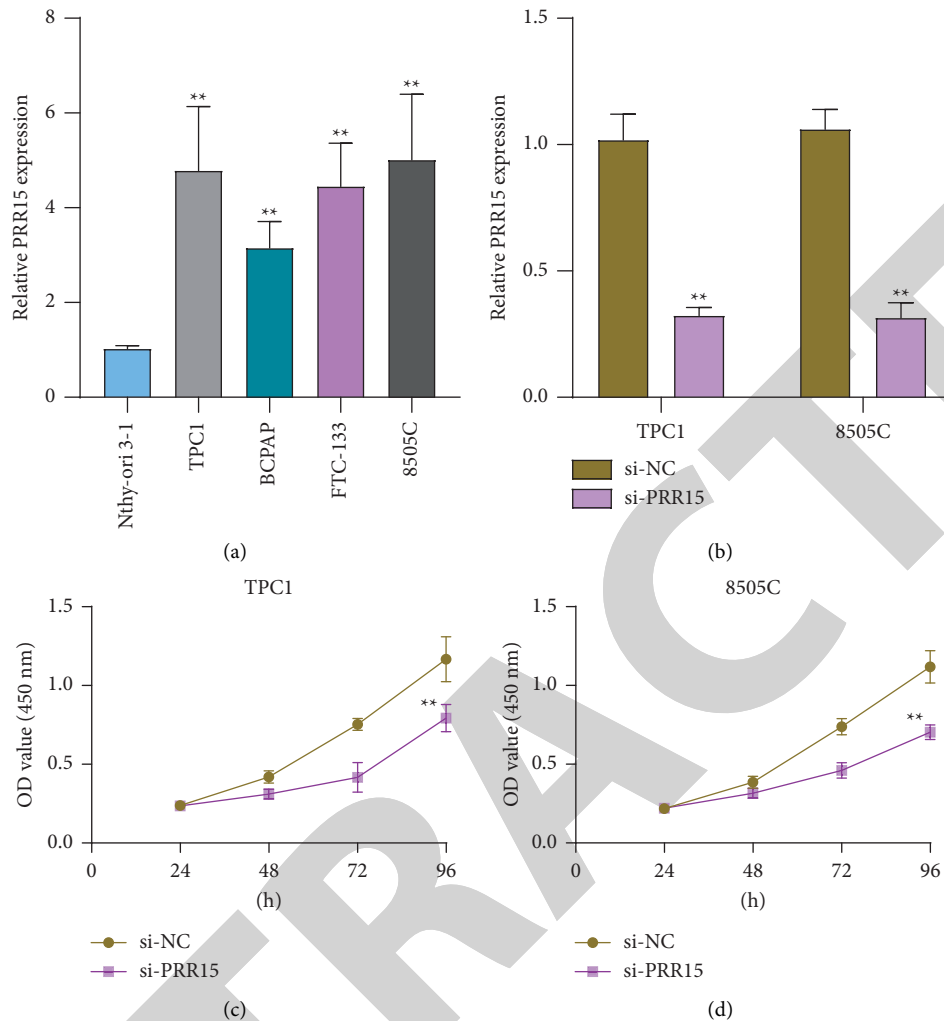
Figure 6: PRR15 overexpressed in PTC and its knockdown suppressed the proliferation of PTC cells. (a) In order to establish the level of PRR15 expression in FTC-133, 8505C, TPC1, and BCPAP cells, RT-PCR analysis is utilized. (b) The expression of PRR15 distinctly decreased in TPC1 and 8505C cells after the transfection of si-PRR15. (c)-(d) CCK-8 experiments applied to examine the function of PRR15 knockdown on TPC1 and 8505C cells. The experiments are repeated three times and each experiment is triplicated.

5. Conclusion

In our study, PRR15 was shown to be an important molecular biomarker with diagnostic significance and may have a major impact on the modulation of immune infiltration in PTC. This research work provides promising visions for future research to elucidate the molecular pathogenesis of PTC as well as its clinicopathological importance. It is necessary to conduct randomized clinical trials in addition to more research studies to investigate the underlying mechanism and clinical applications for PTC patients.

Data Availability

The databases generated during the current study are available from the corresponding author upon request.

Conflicts of Interest

The authors declare that they have no conflicts of interest.

Acknowledgments

References

[1] M. E. Cabanillas, D. G. McFadden, and C. Durante, "Durante C: thyroid cancer," *The Lancet*, vol. 388, no. 10061, pp. 2783–2795, 2016.

Hindawi

Research Article

Identification of the Diagnostic Biomarker VIPR1 in Hepatocellular Carcinoma Based on Machine Learning Algorithm

Song Ge,[1,2] Chen-rui Xu,[1,2] Yan-ming Li,[1,2] Yu-lin Zhang,[1] Na Li,[3] Fei-tong Wang,[1] Liang Ding,[1] and Jian Niu [1]

[1]*Department of General Surgery, The Affiliated Hospital of Xuzhou Medical University, Xuzhou, China*
[2]*Institute of Digestive Diseases, Xuzhou Medical University, Xuzhou, China*
[3]*Department of Oncology, Xuzhou Central Hospital, Xuzhou, China*

Correspondence should be addressed to Jian Niu; njnj_001@163.com

The purpose of this study was to identify the potential diagnostic biomarkers in hepatocellular carcinoma (HCC) by machine learning (ML) and to explore the significance of immune cell infiltration in HCC. From GEO datasets, the microarray datasets of HCC patients were obtained and downloaded. Differentially expressed genes (DEGs) were screened from five datasets of GSE57957, GSE84402, GSE112790, GSE113996, and GSE121248, totalling 125 normal liver tissues and 326 HCC tissues. In order to find the diagnostic indicators of HCC, the LASSO regression and the SVM-RFE algorithms were utilized. The prognostic value of VIPR1 was analyzed. Finally, the difference of immune cell infiltration between HCC tissues and normal liver tissues was evaluated by CIBERSORT algorithm. In this study, a total of 232 DEGs were identified in 125 normal liver tissues and 326 HCC tissues. 11 diagnostic markers were identified by LASSO regression and SVM-RFE algorithms. FCN2, ECM1, VIRP1, IGFALS, and ASPG genes with AUC>0.85 were regarded as candidate biomarkers with high diagnostic value, and the above results were verified in GSE36376. Survival analyses showed that VIPR1 and IGFALS were significantly correlated with the OS, while ASPG, ECM1, and FCN2 had no statistical significance with the OS. Multivariate assays indicated that VIPR1 gene could be used as an independent prognostic factor for HCC, while FCN2, ECM1, IGFALS, and ASPG could not be used as independent prognostic factors for HCC. Immune cell infiltration analyses showed that the expression of VIPR1 in HCC was positively correlated with the levels of several immune cells. Overall, VIPR1 gene can be used as a diagnostic feature marker of HCC and may be a potential target for the diagnosis and treatment of liver cancer in the future.

1. Introduction

Liver cancer is the sixth most common cancer in the world and the fourth leading cause of cancer death [1]. The main risk factors for primary liver cancer are viral infection (mainly HBV and HCV), alcoholic and nonalcoholic steatohepatitis, aflatoxin and parasitic infections, etc. Hepatocellular carcinoma (HCC) is the most common primary liver malignancy, accounting for about 75% of all liver cancers [2, 3]. Although some progresses have been made in the diagnosis and treatments of HCC [4], more than 70%-80% of patients are still diagnosed with liver cancer at a later stage, and more than 15% of patients have extrahepatic spread at

the time of diagnosis, which leads to a poor outcome [5–7]. Up to now, early surgical resection of liver cancer is still the most important and effective treatment. If the tumor is detected at an early stage and surgically removed, the 5-year survival rate of patients can exceed 70% and the prognosis is better [8]. In recent decades, alpha-fetoprotein (AFP) has been applied for HCC diagnosis [9]. The abnormal level of AFP in plasma is closely related to the malignancy of liver cancer, but due to insufficient sensitivity and specificity, the effect of early diagnosis of liver cancer is still not ideal [8]. In addition, AFP also increases in other benign and malignant diseases, such as other forms of chronic liver disease, other malignant tumors, pregnancy, and so on [7, 9]. So far,

specific biomarkers are still needed to improve the accurate detection of early or very early liver cancer [9]. Therefore, it is particularly important for the early diagnosis of HCC and the search for specific diagnostic markers.

In recent years, bioinformatics has developed rapidly in the field of medicine. Comprehensive bioinformatics analysis and microarray technology can be used to identify various disease-related genes and their biological functions, which is helpful to clarify the potential mechanisms of disease occurrence and development [10–13]. However, with the increase of the amount and complexity of cancer omics research data, cutting-edge technologies such as ML algorithms have been developed to deal with the increasingly large and complex cancer and other multiomics data [14, 15]. ML is a rapidly growing core subfield of artificial intelligence (AI), which enables computer technology to learn from data processing and selfimproves to predict results without explicit programming [16, 17]. There are two goals for the use of ML in medical biology: the first is to make accurate predictions in the absence of experimental data and to guide the follow-up research work through these predictions; the second is to use machine learning to deepen our understanding of medical biology [18]. Today, ML is widely recognized as a significant innovation and a pioneering method in the field of cancer multiomics data analysis. This method, which seeks to predict, diagnose, categorize, and identify biomarkers, plays a vital role in cancer research. The combination of ML and traditional bioinformatics is used to classify and identify diagnostic biomarkers of cancer, which can greatly improve the accuracy of identifying biomarkers of cancer and provide new guidance for the early diagnosis and treatment of cancer [14, 15, 19].

We downloaded several HCC microarray datasets from the GEO database for the identification of DEGs between HCC tissues and nontumor tissues and combined with ML algorithms to identify diagnosis biomarkers in DEGs for further research. Our findings suggested VIPR1 as a novel diagnostic and prognostic biomarker for HCC patients.

2. Materials and Methods

2.1. Data Download and Processing. The microarray datasets of HCC samples were downloaded from the GEO database (http://www.ncbi.nlm.nih.gov). After screening, GSE57957, GSE84402, GSE112790, GSE113996, GSE121248, and GSE36376 datasets were included in our research (Table 1). Among them, GSE57957 included 39 normal specimens and 39 liver cancer specimens, and the platform was from GPL10558; GSE84402 included 14 normal specimens and 14 liver cancer tissues, and the platform was from GPL570; GSE112790 included 15 normal specimens and 183 liver cancer tissues, and the platform was from GPL570; GSE113996 included 20 adjacent nontumor tissues and 20 liver cancer tissues, and the platform was from GPL16043; GSE121248 included 37 adjacent tissues and 70 liver cancer tissues, and the platform was from GPL570; and GSE36376

Table 1: Characteristics of mRNA expression profiles of HCC.

GEO series	Expression type	Platform	Sample number	
			Normal	Tumor
GSE57957	mRNA	GPL10558	39	39
GSE84402	mRNA	GPL570	14	14
GSE112790	mRNA	GPL570	15	183
GSE113996	mRNA	GPL16043	20	20
GSE121248	mRNA	GPL570	37	70
GSE3637	mRNA	GPL10558	193	240

included 193 adjacent nontumor tissues and 240 liver cancer tissues, and the platform was from GPL10558. Following the instructions in the platform file, the probes were renamed to their corresponding gene terms, and the samples were separated into tumor and normal subgroups. Using the limma and SVA packages of R software, the data of GSE57957, GSE84402, GSE112790, GSE113996, and GSE121248 chips were collected into a metadata queue and corrected in batches. The experimental group consisted of 125 cases of nontumor liver tissues and 326 cases of HCC liver tissues. The verification group consisted of the GSE36376 dataset. The clinical data of HCC patients were downloaded from TCGA datasets.

2.2. Screening of Differentially Expressed Genes (DEGs). Using the limma package of R software, the experimental group microarray datasets (GSE57957, GSE84402, GSE112790, GSE113996, and GSE121248) were filtered with $|\log FC| \geq 1.0$ and adj. $P.\text{val} < 0.05$ as the thresholds to obtain DEGs. DEGs were visually drawn with heat map and volcano map through the pheatmap and ggplot2 packages of R software.

2.3. Functional Enrichment Analyses of DEGs. Gene Ontology (GO) is the most comprehensive gene function database at present. To explore the biological pathways and functions of related genes, KEGG can be used for biological interpretation of genomic sequences and other high-throughput data [20] and can provide additional information about how genes interact in pathways [21]. Disease Ontology (DO) integrates data about human diseases. It can be used to annotate the human genome and better show the characteristics of current human diseases to see which diseases are enriched for differential genes [22–24]. In this study, we used the clusterProfiler package to carry out GO, KEGG, and DO enrichment analyses of DEGs under the conditions of P-value < 0.05 and q-value < 0.05 to understand the biological functions and involved diseases of DEGs.

2.4. Gene Set Enrichment Analysis (GSEA). Enrichment analysis using GSEA was performed in order to identify the functional items that differed most significantly between the HCC group and the control group. The GSEA enrichment analysis of the gene set was performed by the use of the clusterProfiler package of the R software. The

c2.cp.kegg.v7.4.symbols.gmt gene set was chosen as the enrichment analysis gene set.

2.5. Identification of Diagnostic Biomarkers by LASSO Regression and SVM-RFE Algorithms.

LASSO is a regression-based algorithm performed through successive shrinking operations that minimize regression coefficients to reduce the possibility of overfitting [25], thereby reducing redundancy and eliminating irrelevant genes from these analyses [26]. SVM is one of the best choices for feature selection, and it is also the most commonly used classifier for the microarray data [27]. SVM-RFE is a feature selection algorithm based on SVM [28]. In order to define the minimum classification error and avoid overfitting, the SVM-RFE algorithm is used to select the optimal genes [27, 29]. Therefore, two ML algorithms have been widely used to identify biomarkers and predict accurate and interpretable models. In our research, we used glmnet package to run LASSO regression algorithm and e1071 package to build SVM model. The value with the least cross-validation error was found as the feature markers of HCC by two ML algorithms of LASSO regression and SVM-RFE.

2.6. Diagnostic Value of Feature Biomarkers in HCC.

The AUC value was analyzed to determine how valuable each feature gene was as a diagnostic tool. The ROC curve of each feature gene was generated from the mRNA expression data of 125 normal liver tissues and 326 HCC tissues in the experimental group by using the pROC package of R software. The accuracy of disease diagnosis was judged by AUC value, and genes with AUC > 0.85 were identified as high diagnostic value genes for further research.

2.7. Validation of the Differential Expression and Diagnostic Value.

We used the GSE36376 dataset to verify expressions and diagnostic values of the candidate genes in order to further investigate whether the candidate genes exhibited a diagnostic significance for HCC patients.

2.8. The Correlations of Diagnostic Genes with OS and Clinicopathological Characteristics of Patients.

Analyses of the associations of diagnostic genes with overall survival and clinicopathological characteristics of patients were performed using data from the TCGA-LIHC transcriptome as well as clinical information. Kaplan–Meier methods were applied to investigate the connections between diagnostic genes and OS, and the survminer package of the R software was applied to develop the survival curves. Both of these analyses were performed using the survival package. The univariate and multivariate assays were applied to investigate the predictive power of each diagnostic gene in HCC.

2.9. Evaluation of Immune Cell Infiltration.

In recent years, we have come to the realization that immune cell infiltration was involved in tumor progression. The percentage of infiltrating immune cells that can be found in malignant tumors has a direct bearing on the growth and spread of tumors, as well as the development of cancer and the patients' overall prognoses [30, 31]. CIBERSORT is a bioinformatics analysis tool that can evaluate the proportions of immune cells [32]. The content of immune cell infiltration can be obtained from each sample, and then the correlations between immune cells can be analyzed. When comparing the amounts of immune cell infiltration seen in liver cancer tissues and normal liver tissues, we employed the CIBERSORT algorithm to do our comparisons. Following the exclusion of the data containing the value 0, the corrplot package of the R software was utilized to generate the pertinent heat map in order to identify correlations between the immune cells contained within the samples.

2.9.1. Correlations between Diagnostic Genes and Immune Cells.

Spearman rank correlation analysis was applied for the study of the relationships between the identified diagnostic markers and immune cells.

2.10. Statistical Analysis.

All the above analyses were performed using R (4.1.3) and Perl software. Comparisons between two independent groups were analyzed by Student's t-test. The survival curves were calculated by the Kaplan–Meier method and the difference by the log-rank test. Moreover, the prognostic significance of the related genes was valued by Cox regression analysis. A $P < 0.05$ was considered statistically significant.

3. Results

3.1. Identification of the DEGs in HCC Datasets.

In this study, the data of 125 normal liver tissues and 326 HCC tissues in the experimental group (GSE57957, GSE84402, GSE112790, GSE113996, and GSE121248) were analyzed by the use of the limma package. A total of 232 DEGs were screened, of which 58 genes were significantly upregulated and 174 genes were significantly downregulated (Figures 1(a) and 1(b)).

3.2. Functional Enrichment Analyses of DEGs.

The biological functions of DEGs were analyzed by GO, KEGG, and DO enrichment analyses. GO enrichment analysis showed that BP of DEGs was enriched in terpenoid metabolic process, olefinic compound metabolic process, amino acid metabolic process, and small molecule catabolic process. The CC is mainly enriched in collagen-containing extracellular matrix; MF was remarkably enriched in oxidoreductase activity (Figure 2(a)). KEGG assays revealed that DEGs were mainly concentrated in retinol metabolism, cytochrome P450, chemical carcinogenesis-DNA adducts, various amino acids, and other biological metabolic activities, etc (Figure 2(b)). DO assays indicated that DEGs were involved in cancer-related diseases such as hepatitis, nonsmall cell lung carcinoma, liver cirrhosis, biliary tract cancer, cholangiocarcinoma, esophageal cancer, and so on (Figure 2(c)).

(a)   (b)
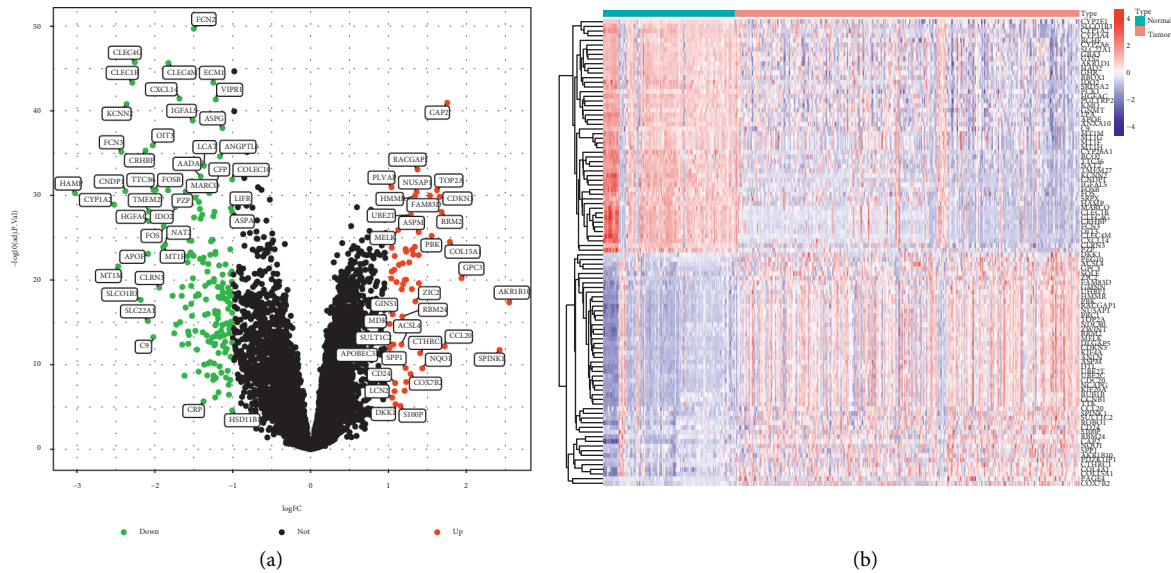
FIGURE 1: DGSs between normal liver tissues and HCC tissues in GSE57957, GSE84402, GSE112790, GSE113996, and GSE121248 datasets. (a) The volcano plots of DEGs. (b) The heat map of DEGs.

3.3. GSEA Enrichment Analysis. The GSEA enrichment analysis showed that complement and coagulation cascades, cytochrome P450, glycine serine and threonine metabolism, retinol metabolism, and tryptophan metabolism were highly active in normal liver tissues, while spliceosome, ribosome, proteasome, DNA replication, and cell cycle were highly active in HCC samples (Figures 3(a) and 3(b)).

3.4. Identification of Feature Biomarkers. We used two different ML algorithms of LASSO regression and SVM-RFE to identify potential biomarkers of HCC. 26 genes were obtained as diagnostic markers of HCC by using LASSO regression algorithm to narrow the range of DEGs (Figure 4(a)). 31 feature genes in DEGs were identified by the SVM-RFE algorithm (Figure 4(b)). Then, 11 diagnostic feature genes were obtained by intersecting the two sets of algorithms (Figure 4(c)).

3.5. Diagnostic Value of Feature Biomarkers in HCC. With AUC > 0.85 as the threshold, five diagnostic feature genes of FCN2, ECM1, VIPR1, IGFALS, and ASPG were identified for further research. As shown in the Figures 5(a)–5(e), the AUC values of FCN2, ECM1, VIPR1, IGFALS, and ASPG were 0.877 (95% CI 0.832-0.915), 0.870 (95% CI 0.827-0.908), 0.871 (95% CI 0.827-0.912), 0.856 (95% CI 0.811-0.899), and 0.857 (95% CI 0.813-0.898), which indicated that these five feature genes had a high diagnostic ability.

3.6. Validation of the Differential Expressions and Diagnostic Values. In order to obtain more reliable results, we used the GSE36376 dataset to validate our results. The results showed that the expressions of FCN2, ECM1, VIPR1, IGFALS, and ASPG were significantly downregulated in HCC ($P < 0.05$,

Figures 6(a)–6(e)), and all of them had high diagnostic values (AUC > 0.85) (Figures 6(f)–6(j)).

3.7. The Correlations of Diagnostic Genes with OS and Clinicopathological Characteristics of Patients. First of all, we analyzed the relationships between diagnostic genes and OS of patients. The results showed that the patients with lower expression of VIPR1 and IGFALS predicted shorter OS ($P < 0.05$), while the expressions of FCN2, ECM1, and ASPG had no statistical significance with OS (Figure 7(a)). To further screen the diagnostic genes with clinical prognostic value, we analyzed the relationships between the diagnostic genes and clinicopathological characteristics of HCC patients and performed Cox regression analyses. The results showed that the lower expression of VIPR1 was associated with the poor differentiation of tumor grade classification and malignant progression of clinical stage ($P < 0.05$) (Figures 7(b) and 7(c)). Multivariate assays demonstrated that VIPR1 could be used as an independent prognostic factor for HCC ($P < 0.05$), while other diagnostic genes could not be used as independent prognostic factors for HCC (Figures 8(a)–8(e)). Finally, we identified VIPR1 as a prognostic feature biomarker gene for diagnosing HCC.

3.8. Evaluation of Immune Cell Infiltration. We used the CIBERSORT algorithm to calculate the proportions of immune cells in the data set of normal liver tissues and HCC tissues (Figure 9(a)). Then, the correlations between different immune cells were evaluated. The heat map showed that T cells CD8 was positively correlated with T cells CD4 memory activated ($R = 0.35$), T cells follicular helper ($R = 0.33$), and macrophages M1 ($R = 0.30$); mast cells activated was positively correlated with neutrophils ($R = 0.33$); and monocytes were positively related to dendritic cells activated and NK cells resting ($R = 0.33$). The heat map also showed that T cells CD4 memory resting was negatively

(a)

(b)

(c)
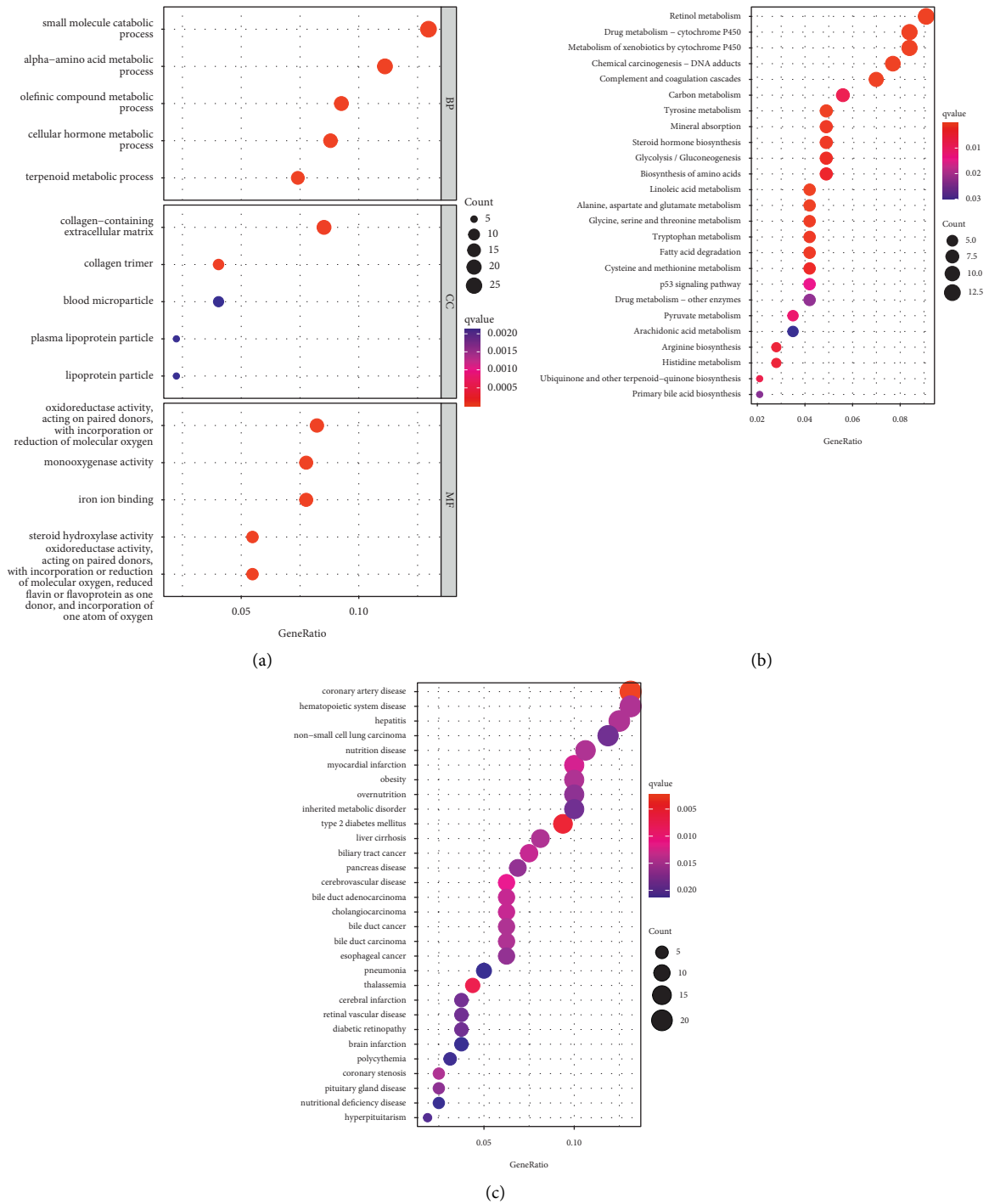
Figure 2: Functional enrichment analyses of DEGs. (a) GO enrichment analysis of DEGs, including BP, CC, and MF. (b) KEGG enrichment analysis of DEGs. (c) DO enrichment analysis of DEGs.

correlated with T cells CD8 ($R = -0.52$) and T cells follicular helper($R = -0.41$); mast cells activated was negatively related to mast cells resting ($R = -0.42$); and macrophages M0 was negatively correlated with macrophages M1($R = -0.41$) (Figure 9(b)). In addition, the results of the CIBERSORT algorithm showed that the proportions of T cell regulatory(Tregs) and macrophages M0 in HCC tissues were significantly higher than that in normal tissues ($P < 0.05$), while the proportions of T cell gamma delta and macrophages M1 in HCC tissues were significantly lower than that in normal tissues ($P < 0.05$) (Figure 9(c)).

3.9. Correlation between VIPR1 and Immune-Infiltrating Cells. As shown, VIPR1 was positively correlated with T cell gamma delta ($R = 0.33$), T cell CD4 memory

(a)

(b)
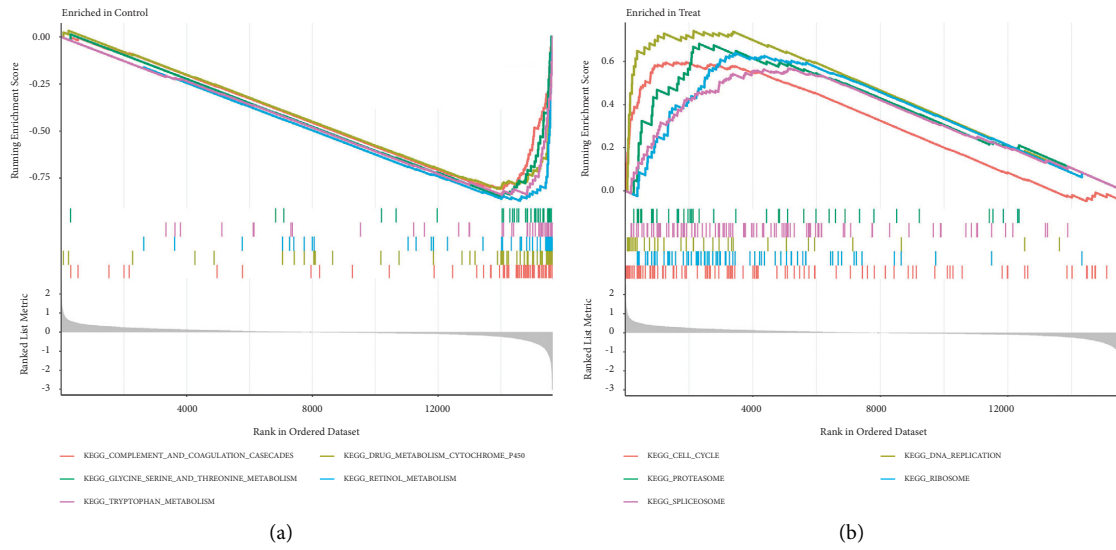
Figure 3: (a) GSEA enrichment analysis showed the signal pathways in normal liver tissues. (b) GSEA enrichment analysis showed the signal pathways in liver cancer tissues.

(a)

(b)

(c)
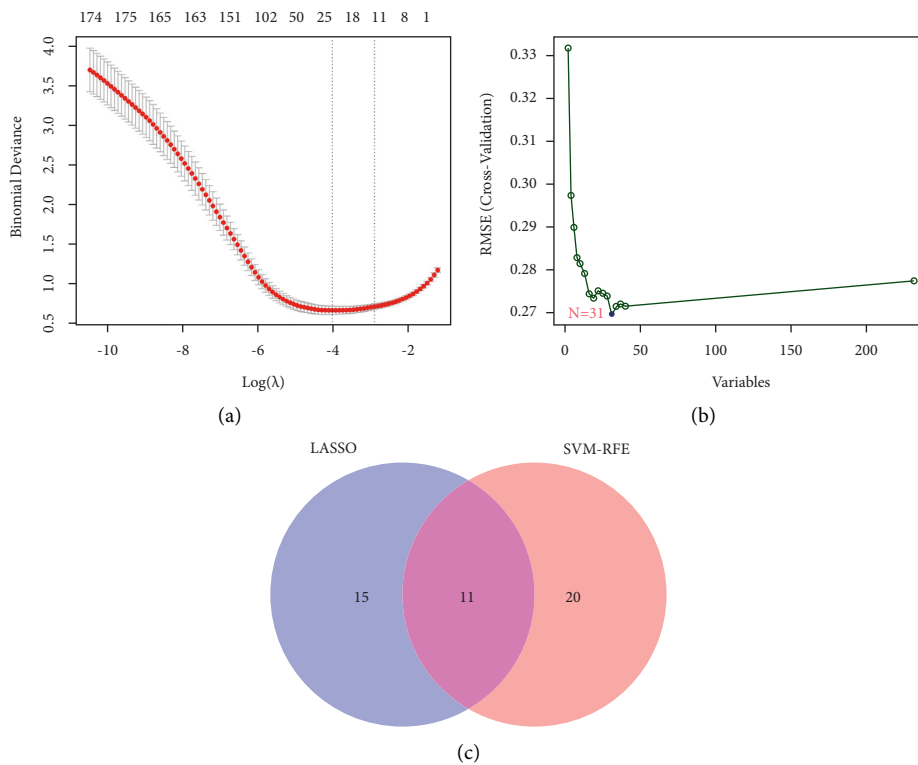
Figure 4: Screening process of diagnostic biomarker candidates for HCC diagnosis and several biomarkers were identified. (a) LASSO regression algorithm. (b) SVM-RFE algorithm. (c) Two ML algorithms take intersection to identify diagnostic feature genes.

resting ($R = 0.25$), macrophages M2 ($R = 0.2$), and monocytes ($R = 0.2$) ($P < 0.05$). VIPR1 was negatively correlated with macrophages M0 ($R = -0.41$), NK cells activated ($R = -0.29$), T cell regulatory (Tregs) ($R = -0.25$), and T cells follicular helper ($R = -0.23$) ($P < 0.05$) (Figures 10 and 11).

4. Discussion

Despite the significant leaps forward that have been achieved in both the diagnosis and treatment of HCC, there are still a significant number of patients who are diagnosed with the disease at a more advanced stage, which results in a low rate
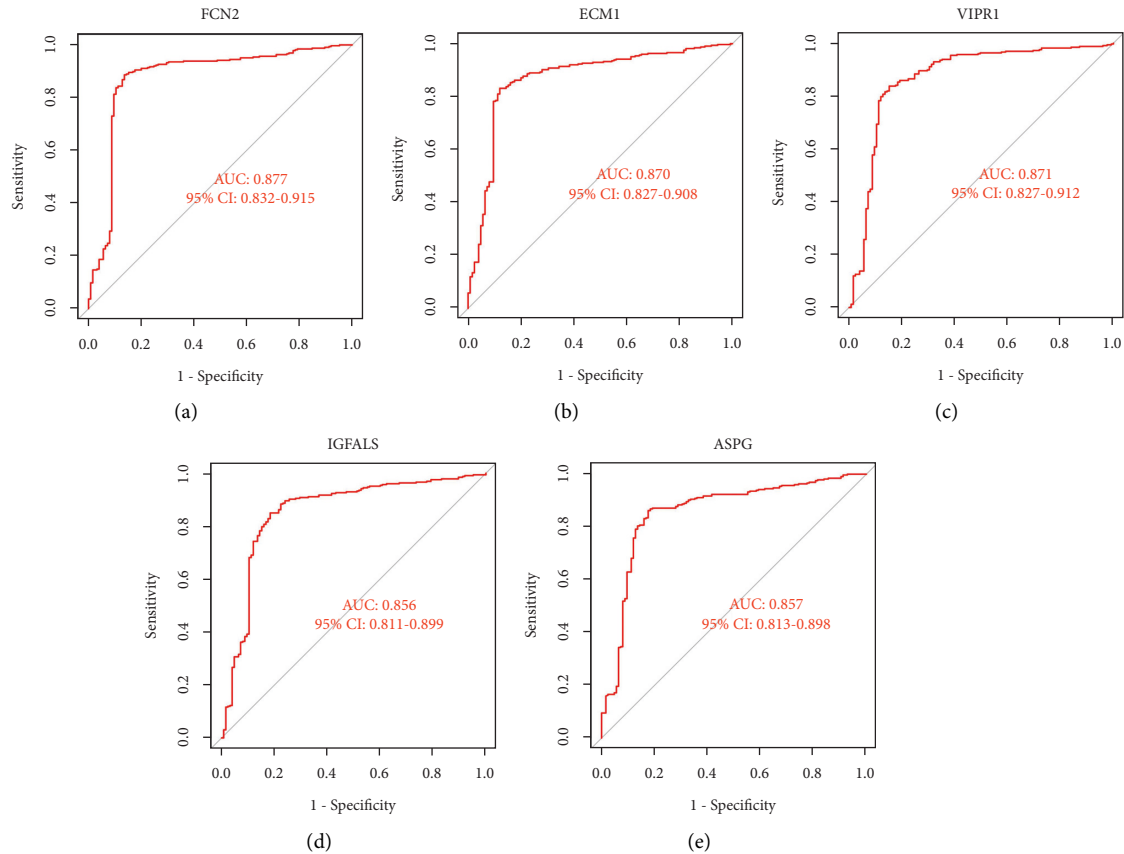
FIGURE 5: ROC curves of feature genes in experimental data set. (a) FCN2. (b) ECM1. (c) VIPR1. (d) IGFALS. (e) ASPG.

of patient survival. AFP is the most commonly used biomarker for monitoring liver cancer, but it is still not ideal for early diagnosis of liver cancer due to its lack of sensitivity and specificity. Therefore, it is of great significance to find and study specific biomarkers for early diagnosis of HCC. In this study, we identified VIPR1 as a diagnostic feature biomarker for HCC based on a combination of the ML algorithms and traditional bioinformatics. In addition, we compared the immune cell infiltration seen in HCC tissues to that shown in normal liver tissues, and we also investigated the relationship between VIPR1 and immune cell infiltration.

We downloaded multiple HCC microarray datasets from the GEO database. 232 DEGs were identified in 125 normal liver tissues and 326 HCC tissues. The DEGs were mainly enriched in small molecule catabolic process, amino acid metabolic process, and other biological processes. Small molecules are natural compounds with relatively small molecular weight, usually referring to biological molecules with relative molecular weight less than 1000 Dalton (especially less than 400 Dalton), which can participate in many biological processes including metabolic reactions. Studying the small molecules in metabolic pathway will help people design drugs for human diseases more effectively [33]. In addition, small molecular metabolites are sensitive to endogenous and exogenous changes in the body and have great potential and value in identifying the state and phenotype of liver cancer cells [34, 35].

In cancer, malignant cells usually exhibit greater proliferative capacity and metabolism than nonmalignant cells. Due to the increased demand for growth and metabolism, an adequate supply of amino acids is necessary for cancer cells to maintain their ability to proliferate. In addition, this rapid growth and metabolism may also exhibit a vulnerability specific to cancer, which is an increase in the demand for amino acids [36, 37]. KEGG assays revealed that DEGs were mainly enriched in retinol metabolism, cytochrome P450, chemical carcinogenesis-DNA adducts, various amino acids, and other biological metabolic activities and other tumor-related pathways. DO assays suggested that DEGs were involved in various cancers and related diseases such as hepatitis, nonsmall cell lung carcinoma, liver cirrhosis, biliary tract cancer, cholangiocarcinoma, and esophageal cancer. These results suggest that DESs are activated in many cancer-related pathways.

The retinoid metabolites are involved in a wide range of biological processes, such as cell differentiation, apoptosis, and inflammatory reaction [38]. In the human body, more than 70% of retinol metabolites are stored in the liver, so changes in their content may be involved in the occurrence and development of liver cancer [39]. Cytochrome P450 (CYP450) refers to an enzyme that is abundant in the smooth endoplasmic reticulum of hepatocytes and small intestinal epithelial cells. It is involved in the synthesis of various hormones and affects hormone-related cancer,
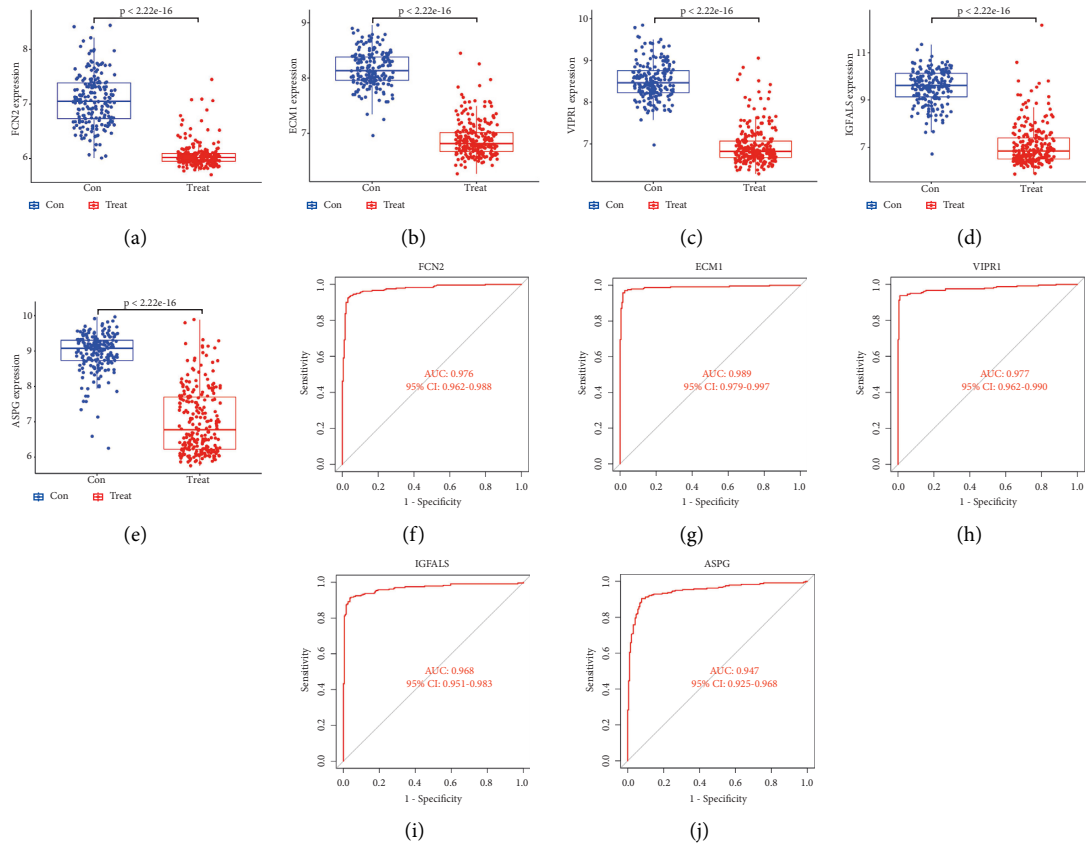
FIGURE 6: Validation of diagnostic genes differential analysis and diagnostic value. (a)-(e) Differential analysis of diagnostic genes in the GSE36376 dataset. (f)-(j) ROC curves of diagnostic genes in the GSE36376 dataset.
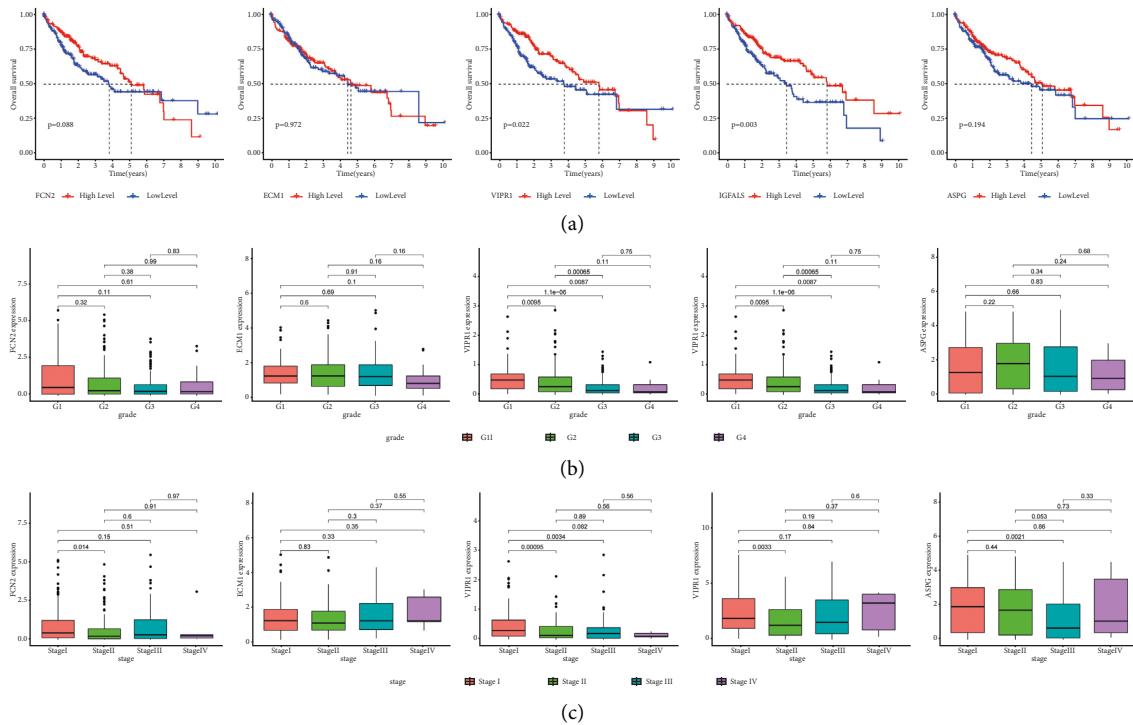
FIGURE 7: Correlations of diagnostic genes with OS and clinicopathological characteristics. (a) The correlations of diagnostic genes with OS, (b) the correlations of diagnostic genes with tumor grade classification, and (c) the correlations of diagnostic genes with clinical stage.
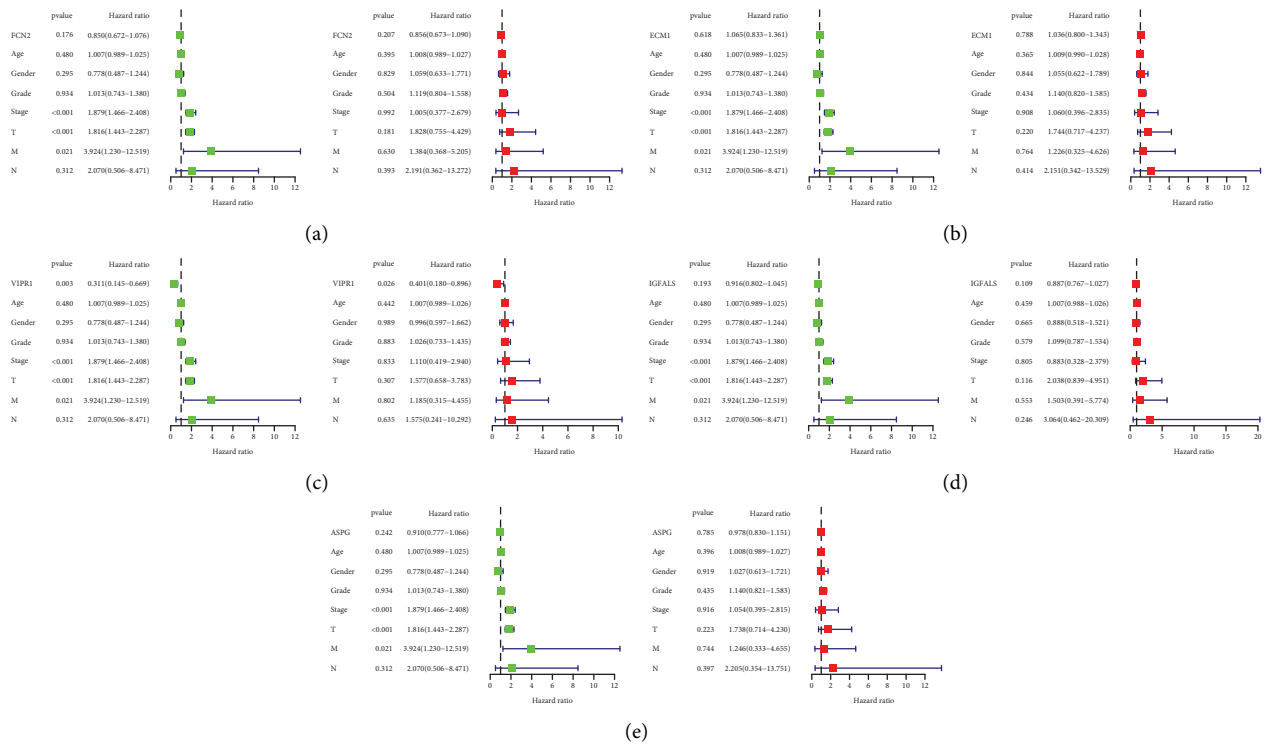
Figure 8: Univariate and multivariate Cox regression analyses between diagnostic genes and other clinical characteristics. (a) FCN2, (b) ECM1, (c) VIPR1, (d) IGFALS, and (e) ASPG.

which plays an important role in the metabolism of many anticancer drugs [40]. Long-term exposure to chemical carcinogens has been linked in certain studies to the formation of DNA adducts, and experts believe that a higher concentration of these adducts may raise the risk of tumorigenesis [41].

GSEA enrichment results showed that cell cycle, DNA replication, proteasome, ribosome, and spliceosome were highly active in hepatocellular carcinoma, which may be closely related to the occurrence and development of hepatocellular carcinoma. In order to improve the diagnostic and clinical availability of HCC diagnostic markers, we used the LASSO regression algorithm to minimize regression coefficients to reduce overfitting and the SVM-RFE algorithm to generate the minimal classification error, and the two ML algorithms took the intersection to select the optimal feature genes. Then, the feature genes were analyzed for the correlations with survival prognosis and clinicopathological characteristics for further screening. Finally, VIPR1 was identified as a diagnostic feature marker of HCC.

VIPR1 is a G protein-coupled receptor that is primarily found in normal tissues and plays a vital role in a variety of physiological tasks, including the metabolism of glycogen and the regulation of the immune system [42]. According to the findings of earlier research, VIPR1 has been found to have a variety of expressions and functions, depending on the specific type of malignant tumor. For example, VIPR1 was highly expressed in breast, gastric, and colon cancers, while it was significantly low expressed in lung, liver, and other cancers [42–45]. In breast cancer, VIP or VPAC1 receptor antagonists can enhance the killing ability of chemotherapy on breast cancer cells [46]. Functionally, elevated VIPR1 expression in gastric cancer promotes the malignant progression of gastric cancer by increasing the potential of gastric cancer cells to metastasis to distant regions. Ca2+ signaling is required for the carcinogenesis and progression of gastric cancer, and activation of VIPR1 by VIP can stimulate TRPV4-mediated Ca2+ entry [43]. It has been shown that the overexpression of VIPR1 in colon cancer may be related to the activation of EGFR, which can lead to poor differentiation of colon cancer, thereby promoting cancer progression. In addition, the overexpression of VIPR1 in tumor vessels and macrophages may play an important role in cancer invasion [44]. However, the expression of VIPR1 is lower in lung cancer tissues than in adjacent tissues, and overexpression of VIPR1 in lung cancer cells can inhibit cell proliferation, invasion, and migration [45, 47]. In HCC, VIPR1 mRNA expression is negatively correlated with DNA methylation, and the transcriptional silencing of VIPR1 caused by DNA methylation may contribute to the development of HCC [42]. The above studies have shown that VIPR1 plays different roles in different cancers, which is involved in the proliferation, invasion, migration, and differentiation of cancer cells.

(a)

(b)

(c)
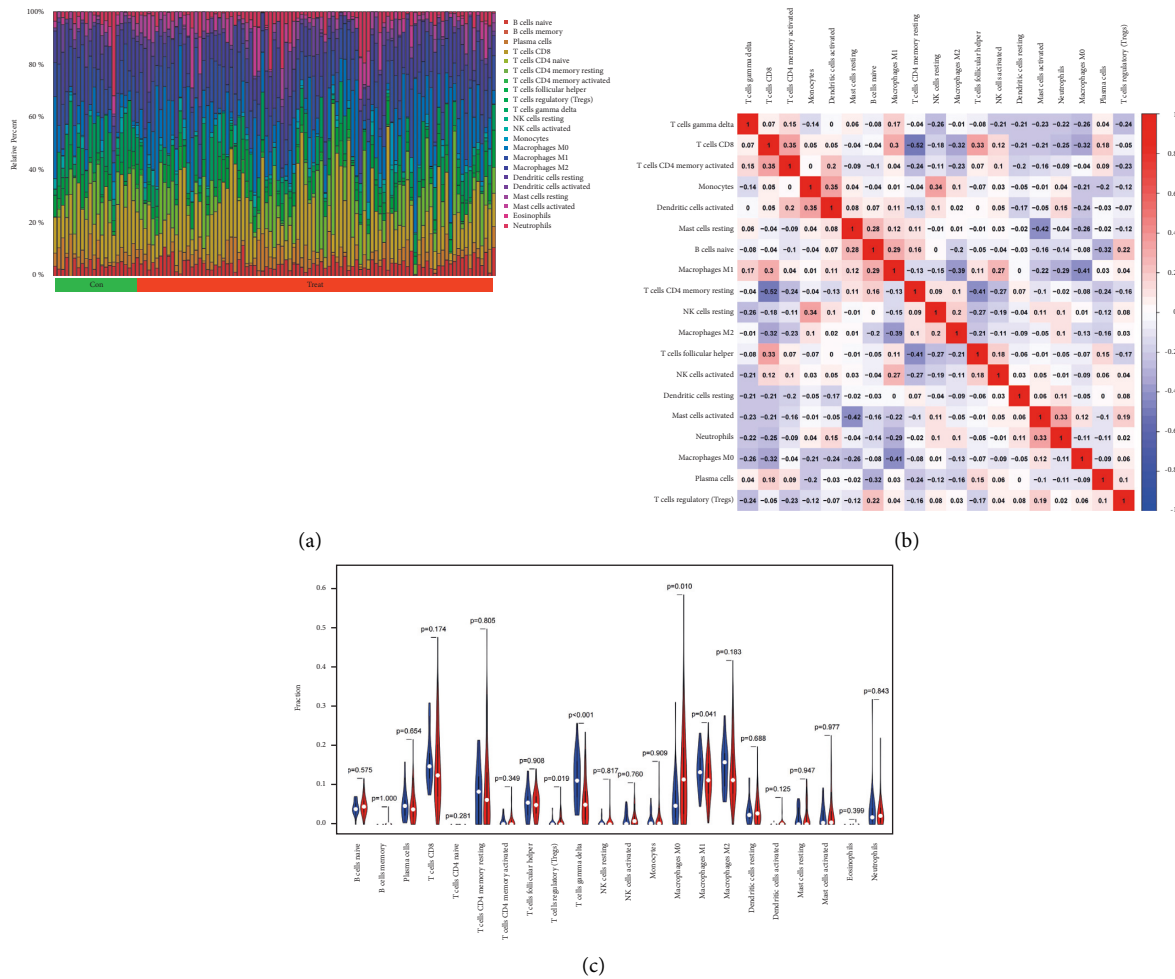
FIGURE 9: Evaluation of immune cell infiltration. (a) Pattern of infiltration of immune cells in normal and tumor tissues. (b) Correlations between different immune cells. (c) The difference of immune cell infiltration between normal liver tissues and HCC tissues.

In recent years, it has been abundantly obvious that the infiltration of immune cells plays a key role in both the beginning and the progression of malignancies. This information was uncovered as a direct consequence of recent research. Therefore, investigating the components of immune infiltration cells in HCC and locating diagnostic biomarkers for the diagnosis of HCC could potentially impact the clinical results of HCC patients. We used a bioinformatics technique known as CIBERSOTR to determine the relative amounts of immune cell infiltration in normal liver tissues and HCC tissues so that we could further investigate the function that immune cell infiltration plays in the development of HCC. We found that the proportions of T cell regulatory (Tregs) and macrophages M0 in HCC tissues were significantly higher than that in normal tissues.

In addition, the expression of VIPR1 in HCC was positively correlated with the levels of T cell gamma delta (0.33), T cell CD4 memory resting (0.25), macrophages M2 (0.2), and monocytes (0.2), while the expression of VIPR1 was negatively correlated with macrophages M0

(0.41), NK cells activated (0.29), T cell regulatory (Tregs), and T cell follicular helper (0.23). According to the previous studies, macrophages are central players in liver fibrosis and play a bidirectional role in the regulation of matrix deposition and catabolism [48]. Monocytes can influence the tumor microenvironment through mechanisms such as induction of immune tolerance, angiogenesis, and increased tumor cell dissemination [49]. In addition, peritumoral monocytes can induce autophagy of tumor cells and promote the occurrence and development of liver cancer [50]. In hepatocellular carcinoma (HCC), T cell gamma delta shows potent antitumor efficacy and has played an important role in tumor monitoring and antitumor immunity [51]. Tregs have the ability to produce an immunosuppressive tumor environment by releasing a variety of inhibitory cytokines. Additionally, Tregs have the potential to lead to immunological dysfunction in HCC through a number of different mechanisms [52]. The above research evidence and our findings suggested that various types of immune cell infiltrations played an important role in the pathogenesis of HCC.
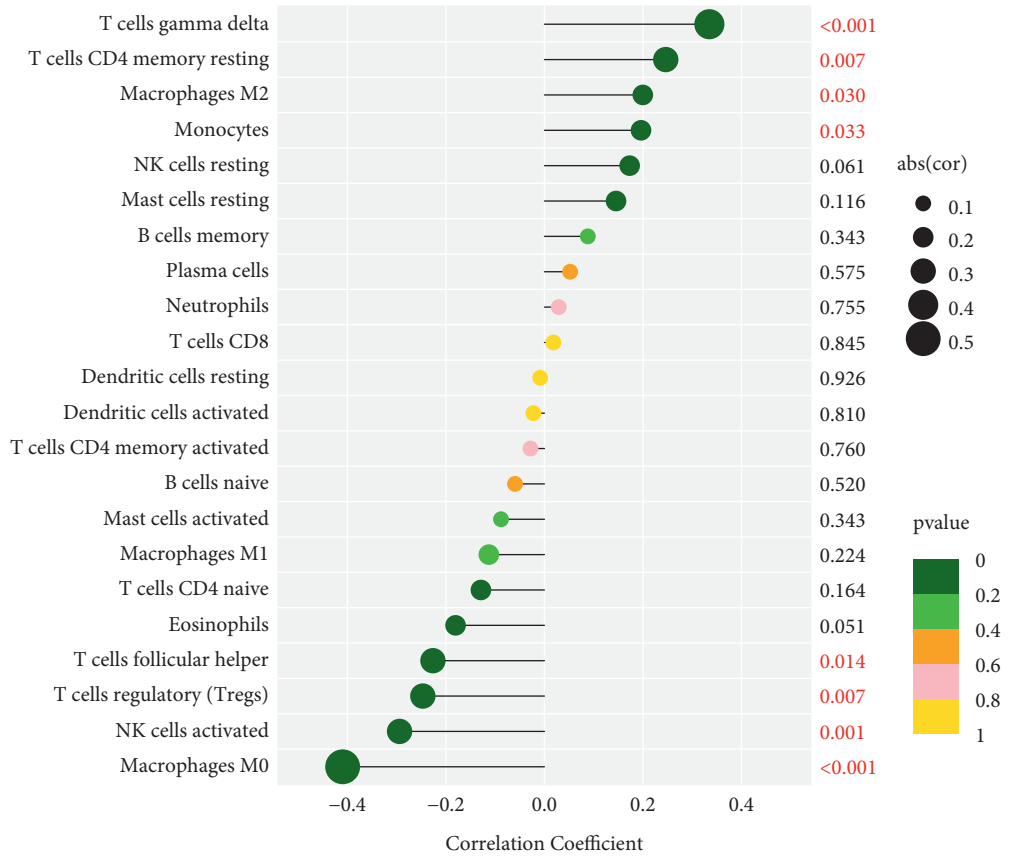
Figure 10: Lollipop plot of the correlations between VIPR1 and infiltrating immune cells.
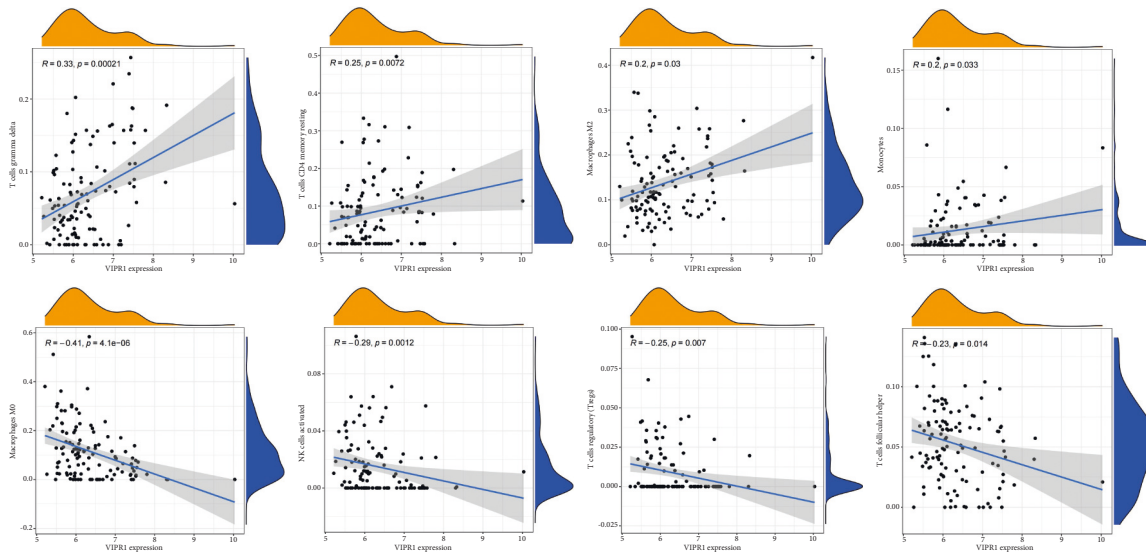
Figure 11: Scatter plot of the correlations between VIPR1 and infiltrating immune cells.

5. Conclusions

In summary, VIPR1 can be used as a diagnostic feature marker of HCC, which is distinctly related to the occurrences, developments, and immune cell infiltration of HCC. It can also be used as an independent prognostic factor of HCC and may become a potential target for the early diagnosis and treatment of HCC in the future.

Data Availability

The data sets used in this study can be obtained from TCGA and GEO public databases.

Conflicts of Interest

The authors declare that there are no conflicts of interest regarding the publication of this paper.

Authors' Contributions

Song Ge designed and analyzed the research study and prepared the original draft. Chenrui Xu, Yanming Li, and Yulin Zhang contributed to conception and design. Na Li, Feitong Wang, and Liang Ding were responsible for study supervision. Jian Niu provided financial support and revised the paper.

Acknowledgments

References

[1] F. Bray, J. Ferlay, I. Soerjomataram, R. L. Siegel, L. A. Torre, and A. Jemal, "Global cancer statistics 2018: GLOBOCAN estimates of incidence and mortality worldwide for 36 cancers in 185 countries," *CA: A Cancer Journal for Clinicians*, vol. 68, no. 6, pp. 394–424, 2018.

[2] S. Muppala, "Significance of the tumor microenvironment in liver cancer progression," *Critical Reviews in Oncogenesis*, vol. 25, no. 1, pp. 1–9, 2020.

[3] M. C. Kew, "Hepatocellular carcinoma: epidemiology and risk factors," *Journal of Hepatocellular Carcinoma*, vol. 1, pp. 115–125, 2014.

[4] J. D. Yang and J. K. Heimbach, "New advances in the diagnosis and management of hepatocellular carcinoma," *Bmj*, vol. 371, p. m3544, 2020.

[5] T. Demir, S. S. Lee, and A. O. Kaseb, "Systemic therapy of liver cancer," in *Mechanisms and Therapy of Liver Cancer 2021*, pp. 257–294, Pubmed, United state, 2021.

[6] D. Anwanwan, S. K. Singh, S. Singh, V. Saikam, and R. Singh, "Challenges in Liver Cancer and Possible Treatment Approaches," *Biochimica Et Biophysica Acta-Reviews on Cancer*, no. 1, p. 1873, 2020.

[7] J. Hartke, M. Johnson, and M. Ghabril, "The diagnosis and treatment of hepatocellular carcinoma," *Seminars in Diagnostic Pathology*, vol. 34, no. 2, pp. 153–159, 2017.

[8] W. Wang and C. Wei, "Advances in the early diagnosis of hepatocellular carcinoma," *Genes & Diseases*, vol. 7, no. 3, pp. 308–319, 2020.

[9] F. Pinero, M. Dirchwolf, and M. G. Pessoa, "Biomarkers in Hepatocellular Carcinoma: Diagnosis, Prognosis and Treatment Response Assessment," *Cells*, vol. 9, no. 1, p. 1370, 2020.

[10] M. Bednár, "DNA microarray technology and application," *Medical Science Monitor: International Medical Journal of Experimental and Clinical Research*, vol. 6, no. 4, pp. 796–800, 2000.

[11] M. G. Marzancola, A. Sedighi, and P. C. H. Li, "DNA microarray-based diagnostics," *Methods in Molecular Biology*, vol. 1368, pp. 161–178, 2016.

[12] T. Li, J. Fan, B. Wang et al., "TIMER: a web server for comprehensive analysis of tumor-infiltrating immune cells," *Cancer Research*, vol. 77, no. 21, pp. e108–e110, 2017.

[13] M. Chen, R. Hofestädt, and J. Taubert, "Integrative bioinformatics: history and future," *Journal of Integrative Bioinformatics*, vol. 16, no. 3, 2019.

[14] N. Auslander, A. B. Gussow, and E. V. Koonin, "Incorporating machine learning into established bioinformatics frameworks," *International Journal of Molecular Sciences*, vol. 22, no. 6, p. 2903, 2021.

[15] B. Arjmand, S. K. Hamidpour, A. Tayanloo-Beik et al., "Machine learning: a new prospect in multi-omics data analysis of cancer," *Frontiers in Genetics*, vol. 13, p. 824451, 2022.

[16] S. J. Goodswen, J. L. N. Barratt, P. J. Kennedy, A. Kaufer, L. Calarco, and J. T. Ellis, "Machine learning and applications in microbiology," *Fems Microbiology Reviews*, vol. 45, no. 5, p. fuab015, 2021.

[17] Y. Bastanlar and M. Ozuysal, "Introduction to machine learning," *Methods in Molecular Biology (Clifton, N.J.)*, vol. 1107, pp. 105–128, 2014.

[18] J. G. Greener, S. M. Kandathil, L. Moffat, and D. T. Jones, "A guide to machine learning for biologists," *Nature Reviews Molecular Cell Biology*, vol. 23, no. 1, pp. 40–55, 2022.

[19] S. Zhao, Y. Zhang, X. Lu et al., "CDC20 regulates the cell proliferation and radiosensitivity of P53 mutant HCC cells through the Bcl-2/Bax pathway," *International Journal of Biological Sciences*, vol. 17, no. 13, pp. 3608–3621, 2021.

[20] M. Kanehisa, Y. Sato, M. Kawashima, M. Furumichi, and M. Tanabe, "KEGG as a reference resource for gene and protein annotation," *Nucleic Acids Research*, vol. 44, no. D1, pp. D457–D462, 2016.

[21] M. Kanehisa and Y. Sato, "KEGG Mapper for inferring cellular functions from protein sequences," *Protein Science*, vol. 29, no. 1, pp. 28–35, 2020.

[22] S. M. Bello, M. Shimoyama, E. Mitraka et al., "Augmenting the disease ontology improves and unifies disease annotations across species," *Disease Models & Mechanisms*, vol. 11, no. 3, p. dmm032839, 2018.

[23] L. M. Schriml, C. Arze, S. Nadendla et al., "Disease Ontology: a backbone for disease semantic integration," *Nucleic Acids Research*, vol. 40, no. D1, pp. D940–D946, 2012.

[24] L. M. Schriml, E. Mitraka, J. Munro et al., "Human Disease Ontology 2018 update: classification, content and workflow expansion," *Nucleic Acids Research*, vol. 47, no. D1, pp. D955–D962, 2019.

[25] A. J. McEligot, V. Poynor, R. Sharma, and A. Panangadan, "Logistic LASSO Regression for Dietary Intakes and Breast Cancer," *Nutrients*, vol. 12, 2020.

[26] J. Friedman, T. Hastie, and R. Tibshirani, "Regularization paths for generalized linear models via coordinate descent," *Journal of Statistical Software*, vol. 33, no. 1, pp. 1–22, 2010.

[27] Z. Li, W. Xie, and T. Liu, "Efficient feature selection and classification for microarray data," *Plos One*, vol. 13, no. 8, p. e0202167, 2018.

[28] X. Lin, C. Li, Y. Zhang, B. Su, M. Fan, and H. Wei, "Selecting feature subsets based on SVM-RFE and the overlapping ratio with applications in bioinformatics," *Molecules*, vol. 23, no. 1, p. 52, 2017.

[29] M.-L. Huang, Y.-H. Hung, W. M. Lee, R. K. Li, and B.-R. Jiang, "SVM-RFE Based Feature Selection and Taguchi Parameters Optimization for Multiclass SVM Classifier," *Scientific World Journal*, vol. 2014, Article ID 795624, 2014.

[30] A. M. Newman, C. L. Liu, M. R. Green et al., "Robust enumeration of cell subsets from tissue expression profiles," *Nature Methods*, vol. 12, no. 5, pp. 453–457, 2015.

[31] B. Chen, M. S. Khodadoust, C. L. Liu, A. M. Newman, and A. A. Alizadeh, "Profiling tumor infiltrating immune cells with CIBERSORT," *Methods in Molecular Biology*, vol. 1711, pp. 243–259, 2018.

[32] X. Li, Y. Huang, N. Ye, and J. He, "Analysis of immune-related genes in idiopathic pulmonary fibrosis based on bioinformatics and experimental verification," *Annals of Palliative Medicine*, vol. 10, no. 11, pp. 11598–11614, 2021.

[33] J. Lu, B. Niu, L. Liu, W.-C. Lu, and Y.-D. Cai, "Prediction of small molecules metabolic pathways based on functional group composition," *Protein & Peptide Letters*, vol. 16, no. 8, pp. 969–976, 2009.

[34] J. K. Nicholson, E. Holmes, J. M. Kinross, A. W. Darzi, Z. Takats, and J. C. Lindon, "Metabolic phenotyping in clinical and surgical environments," *Nature*, vol. 491, no. 7424, pp. 384–392, 2012.

[35] X. Wang, A. Zhang, and H. Sun, "Power of metabolomics in diagnosis and biomarker discovery of hepatocellular carcinoma," *Hepatology*, vol. 57, no. 5, pp. 2072–2077, 2013.

[36] M. Endicott, M. Jones, and J. Hull, "Amino acid metabolism as a therapeutic target in cancer: a review," *Amino Acids*, vol. 53, no. 8, pp. 1169–1179, 2021.

[37] L. Vettore, R. L. Westbrook, and D. A. Tennant, "New aspects of amino acid metabolism in cancer," *British Journal of Cancer*, vol. 122, no. 2, pp. 150–156, 2020.

[38] Y. Shirakami, H. Sakai, and M. Shimizu, "Retinoid roles in blocking hepatocellular carcinoma," *Hepatobiliary Surgery and Nutrition*, vol. 4, pp. 222–228, 2015.

[39] S. M. O'Byrne and W. S. Blaner, "Retinol and retinyl esters: biochemistry and physiology," *Journal of Lipid Research*, vol. 54, no. 7, pp. 1731–1743, 2013.

[40] B. Mittal, S. Tulsyan, S. Kumar, R. D. Mittal, and G. Agarwal, "Cytochrome P450 in cancer susceptibility and treatment," *Advances in Clinical Chemistry*, vol. 71, pp. 77–139, 2015.

[41] M. C. Poirier, "Linking DNA adduct formation and human cancer risk in chemical carcinogenesis," *Environmental and Molecular Mutagenesis*, vol. 57, no. 7, pp. 499–507, 2016.

[42] S. Lu, H. Lu, R. Jin, and Z. Mo, "Promoter methylation and H3K27 deacetylation regulate the transcription of VIPR1 in hepatocellular carcinoma," *Biochemical and Biophysical Research Communications*, vol. 509, no. 1, pp. 301–305, 2019.

[43] B. Tang, J. Wu, M. X. Zhu et al., "VPAC1 couples with TRPV4 channel to promote calcium-dependent gastric cancer progression via a novel autocrine mechanism," *Oncogene*, vol. 38, no. 20, pp. 3946–3961, 2019.

[44] S. Liu, Y. Zeng, Y. Li, W. Guo, J. Liu, and N. Ouyang, "VPAC1 overexpression is associated with poor differentiation in colon cancer," *Tumor Biology*, vol. 35, no. 7, pp. 6397–6404, 2014.

[45] L. Zhao, Z. Yu, and B. Zhao, "Mechanism of VIPR1 gene regulating human lung adenocarcinoma H1299 cells," *Medical Oncology*, vol. 36, no. 11, p. 91, 2019.

[46] T. W. Moody, J. Leyton, D. Chan et al., "VIP receptor antagonists and chemotherapeutic drugs inhibit the growth of breast cancer cells," *Breast Cancer Research and Treatment*, vol. 68, no. 1, pp. 55–64, 2001.

[47] V. Mlakar, M. Stražišar, M. Sok, and D. Glavač, "Oligonucleotide DNA microarray profiling of lung adenocarcinoma revealed significant downregulation and deletions of vasoactive intestinal peptide receptor 1," *Cancer Investigation*, vol. 28, no. 5, pp. 487–494, 2010.

[48] P.-F. Ma, C.-C. Gao, J. Yi et al., "Cytotherapy with M1-polarized macrophages ameliorates liver fibrosis by modulating immune microenvironment in mice," *Journal of Hepatology*, vol. 67, no. 4, pp. 770–779, 2017.

[49] S. Ugel, S. Cane, F. De Sanctis, and V. Bronte, "Monocytes in the tumor microenvironment," *Annual Review of Pathology: Mechanisms of Disease*, vol. 16, pp. 93–122, 2021.

[50] D.-P. Chen, W.-R. Ning, X.-F. Li et al., "Peritumoral monocytes induce cancer cell autophagy to facilitate the progression of human hepatocellular carcinoma," *Autophagy*, vol. 14, no. 8, pp. 1335–1346, 2018.

[51] A. Makkouk, X. C. Yang, T. Barca et al., "Off-the-shelf Vδ1 gamma delta T cells engineered with glypican-3 (GPC-3)-specific chimeric antigen receptor (CAR) and soluble IL-15 display robust antitumor efficacy against hepatocellular carcinoma," *Journal for Immunotherapy of Cancer*, vol. 9, no. 12, Article ID e003441, 2021.

[52] B. Langhans, H. D. Nischalke, B. Kraemer et al., "THU-492-Role of regulatory T cells and checkpoint inhibition in hepatocellular carcinoma," *Journal of Hepatology*, vol. 70, no. 1, p. E377, 2019.

Research Article

Comprehensive Exploration of M2 Macrophages and Its Related Genes for Predicting Clinical Outcomes and Drug Sensitivity in Lung Squamous Cell Carcinoma

Yansong Han ⓘ **and Yuexia Li**

Department of Pharmacy, The Second Affiliated Hospital Haybin Medical University, Haybin, China

Correspondence should be addressed to Yansong Han; h02433@hrbmu.edu.cn

Background. M2 macrophages play an important role in cancers. However, the role of M2 macrophages has not been clarified in lung squamous cell carcinoma. *Methods*. All the open-accessed data were downloaded from The Cancer Genome Atlas database. All the analysis was performed in the R software. The CIBERSORT algorithm was utilized to quantify the immune cell infiltration in the tumor microenvironment. LASSO regression and multivariate Cox regression analysis were carried out for the creation of the prognostic model. Pathway enrichment analysis was performed using the single sample Gene Set Enrichment Analysis (ssGSEA) and clueGO algorithm. *Results*. In our study, we comprehensively explored the role of M2 macrophages and its related genes in LUSC patients. We found that the patients with high M2 macrophage infiltration tend to have a worse prognosis. Also, some oncogenetic pathways were activated in the patients with high M2 macrophage infiltration. Further, a prognosis model based on six M2 macrophage-related genes was established, including TRIM58, VIPR2, CTNNA3, KIAA0408, CLEC4G, and MATN4, which showed a good prognosis prediction efficiency in both training and validation cohort. Pathway enrichment analysis showed that the pathway of allograft rejection, bile acid metabolism, coagulation, inflammatory response, IL6/JAK/STAT3 signaling, hedgehog signaling, peroxisome, and myogenesis were significantly activated in the high-risk patients. Based on the results of an investigation of immune infiltration, risk score was found to have a positive correlation with M2 macrophages and resting CD4+ memory T cells, but a negative correlation with follicular helper T cells, M1 macrophages, and Tregs. In addition, we discovered that patients in high-risk groups may respond better to immunotherapy than individuals in lower-risk groups. However, low-risk patients might be more sensitive to cisplatin. *Conclusions*. Our model is a powerful tool to predict LUSC patient prognosis and could indicate the sensitivity of immunotherapy and chemotherapy.

1. Introduction

Lung cancer is a common malignant tumor globally and is approximately responsible for 2 million new cases and 1.5 million cancer-related deaths each year [1]. The incidence of lung cancer is related to several pathogenesis factors, including environmental exposure, smoking, lifestyle, and genetic predisposition [2]. Non-small-cell lung cancer (NSCLC) is the most frequently pathological subtype of lung cancer, mainly consisting of lung adenocarcinoma (LUAD) and lung squamous cell carcinoma (LUSC) [3, 4]. For the moment, surgery resection is still the best option for early-stage lung cancer. However, the overall survival rate for advanced lung cancer remains unsatisfactory, despite immunotherapy and targeted therapy providing some therapeutic benefits [5, 6]. Consequently, in order to diagnose and treat LUAD, it is essential to discover new molecular markers that are both effective and innovative.

Tumor cells are affected by various factors in the tumor microenvironment, rather than being isolated individuals [7]. Macrophages are a member of the tumor microenvironment and have been reported to affect tumor progression through intercellular interactions, secretion of cytokines, and other effects [8]. Generally speaking, macrophages are classified into three groups: M0, M1, and M2 types, of which M1 and M2 are different from M0 macrophages [8]. M2 macrophages have been widely reported to be involved in tumor development [9]. For example, Lan and colleagues found that the M2 macrophage-derived exosomes miR-21-5p and miR-155-5p could significantly promote cancer cell invasion and are potential therapeutic targets for colon cancer [10]. Weng and colleagues found that the polarization process of M2 macrophages could be induced by the MCT-1/miR-34a/IL-6/IL-6R axis, therefore facilitating breast cancer progression [11]. Wang and colleagues revealed that tumor-derived exosome miR-301a was induced by hypoxia and can mediate M2 Macrophage polarization through PTEN/PI3Kγ pathway to enhance pancreatic cancer metastasis [12]. Therefore, it is meaningful to explore the underlying role of M2 macrophages and its related molecules in lung cancer.

In our study, we aimed to develop a novel prognostic model for LUSC patients. We comprehensively explored the role of M2 macrophages and its related genes in LUSC patients. Meanwhile, a prognosis model based on six M2 macrophage-related genes was established, including TRIM58, VIPR2, CTNNA3, KIAA0408, CLEC4G, and MATN4, which showed a good prognosis prediction efficiency. In order to investigate the underlying clinical and biological differences that exist between patients with a high risk and patients with a low risk, clinical correlation, route enrichment, and immune infiltration studies were carried out. In addition, we discovered that patients in high-risk groups may respond better to immunotherapy than individuals in lower-risk groups. However, low-risk patients might be more sensitive to cisplatin.

2. Materials and Methods

2.1. Data Acquisition. The open-accessed data of LUSC patients were obtained from TCGA datasets. Detailed, the transcriptional profile data were in "STAR-Counts" form and were integrated with R code. Clinical information of each patient were downloaded in "bcr-xml" form. All data were preprocessed before data analysis.

2.2. Immune Cell Infiltration and Identification of M2 Macrophage-Related Genes. The CIBERSORT algorithm was utilized to quantify the immune cell infiltration in the tumor microenvironment [13]. The CIBERSORT port is a general calculation method, which is used to quantify the immune cell fraction from the tissue gene expression profile, and can accurately estimate the immune component of tumor biopsy. Limma package was used to perform differentially expressed genes (DEGs) analysis between patients high and low M2 macrophage infiltration with the threshold of |

logFC| > 1 and $P < 0.05$. The DEGs above were defined as M2 macrophage-related genes.

2.3. Pathway Enrichment and Genomic Analysis. Pathway enrichment analysis was performed using the single sample Gene Set Enrichment Analysis (ssGSEA) and clueGO algorithm to explore the underlying biological differences between two specific groups [14]. The reference pathway set was Hallmark. The TMB, MSI, and tumor stemness scores were obtained from TCGA.

2.4. Prognosis Model Construction. In the first step of the process, patients were randomly assigned to either the training or validation cohort. A univariate Cox regression analysis was carried out in order to locate the genes associated with the prognosis. After that, LASSO regression and multivariate Cox regression analysis were carried out for the creation of the prognostic model with the formula of "

risk score = gene A ∗ Coef A + gene B ∗ Coef B + ⋯+gene N ∗ Coef N" [15, 16]. For the purpose of model evaluation, Kaplan-Meier survival curves and Receiver Operating Characteristic (ROC) curves were utilized.

2.5. Immunotherapy and Drug Sensitivity Assays. The Tumor Immune Dysfunction and Exclusion (TIDE) algorithm was used to measure the efficacy of immunotherapy for patients with LUSC [17]. The Genomics of Drug Sensitivity in Cancer database served as the basis for the drug sensitivity analysis that was carried out [18].

2.6. Statistical Analysis. All the statistical analyses were performed using the R software v4.0.0. For the data that had a normal distribution, a Student T-test was carried out. When analyzing data with a nonnormal distribution, the Mann–Whitney U test was utilized. $P < 0.05$ was considered statistically significant.

3. Results

3.1. Quantification of M2 Macrophages in LUSC. In the patients with LUSC, the infiltration level of M2 macrophages was measured using the CIBERSORT method (Figure 1(a)). KM survival curves showed that the patients with high M2 macrophage infiltration tend to have a worse prognosis (Figure 1(b)). Limma package was used to perform differentially expressed gene (DEG) analysis between patients high and low M2 macrophage infiltration with the threshold of | logFC| > 1 and $P < 0.05$. A total of 81 downregulated genes and 38 upregulated genes were defined as M2 macrophage-related genes (Figure S1). Pathway enrichment analysis showed that in the patients with high M2 macrophage infiltration, the pathway of KRAS signaling, HEME metabolism, adipogenesis, coagulation, xenobiotic metabolism, and epithelial-mesenchymal transition (EMT) were significantly enriched (Figure 1(c)). ClueGO analysis showed that the DEGs between high and low macrophages were mainly involved in dopaminergic neuron differentiation, mast cell activation, cell adhesion mediator activity, positive regulation of insulin-like growth factor

Figure 1: M2 macrophages in LUSC. (a) The infiltration level of M2 macrophages was quantified using the CIBERSORT algorithm; (b) the patients with higher M2 macrophage infiltration tend to have a worse prognosis; (c) pathway enrichment analysis M2 macrophages; (d) ClueGO analysis.

receptor signaling pathway, regulation of action potential, potassium channel activity, and acylglycerol homeostasis (Figure 1(d)).

3.2. Prognosis Model Construction. A univariate Cox regression analysis was performed as the first step of the method in order to discover the genes that were connected with the prognosis. After that, LASSO regression was carried out in order to reduce the dimensionality of the data (Figures 2(a) and 2(b)). Multivariate Cox regression analysis finally identified six genes for model construction, including TRIM58, VIPR2, CTNNA3, KIAA0408, CLEC4G, and MATN4

(Figure 2(c)). Within the training group, a larger percentage of fatalities was seen in patients who were considered to be at high risk (Figure 2(d)). KM survival curve showed that the patients in the high-risk group had a worse overall survival (OS) (Figure 2(e)). ROC curves indicated a good prediction of patients 1-, 3-, and 5-year OS (Figures 2(f)–2(h), 1-year AUC = 0.728, 3-year AUC = 0.75, and 5-year AUC = 0.81). The same trend was also found in the validation cohort (Figures 2(i)–2(m), 1-year AUC = 0.661, 3-year AUC = 0.705, and 5-year AUC = 0.746). Next, we explored the prognosis value of six model genes. The result showed the genes TRIM58, VIPR2, CTNNA3, KIAA0406, and CLEC4G might

(a)

(b)

(c)

(d)

(e)

(f)

Figure 2: Continued.

(g)

(h)

(i)

(j)

(k)

(l)

(m)
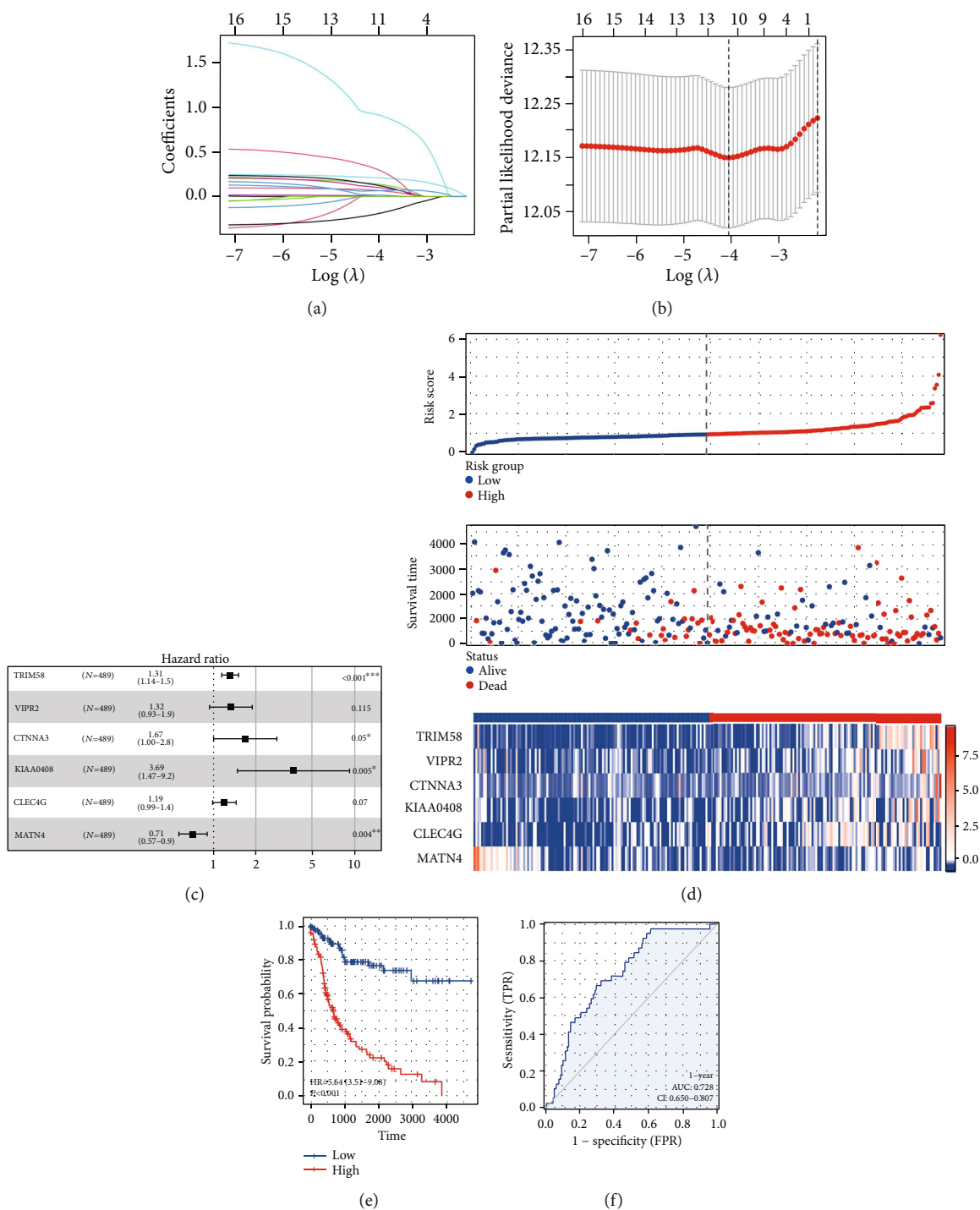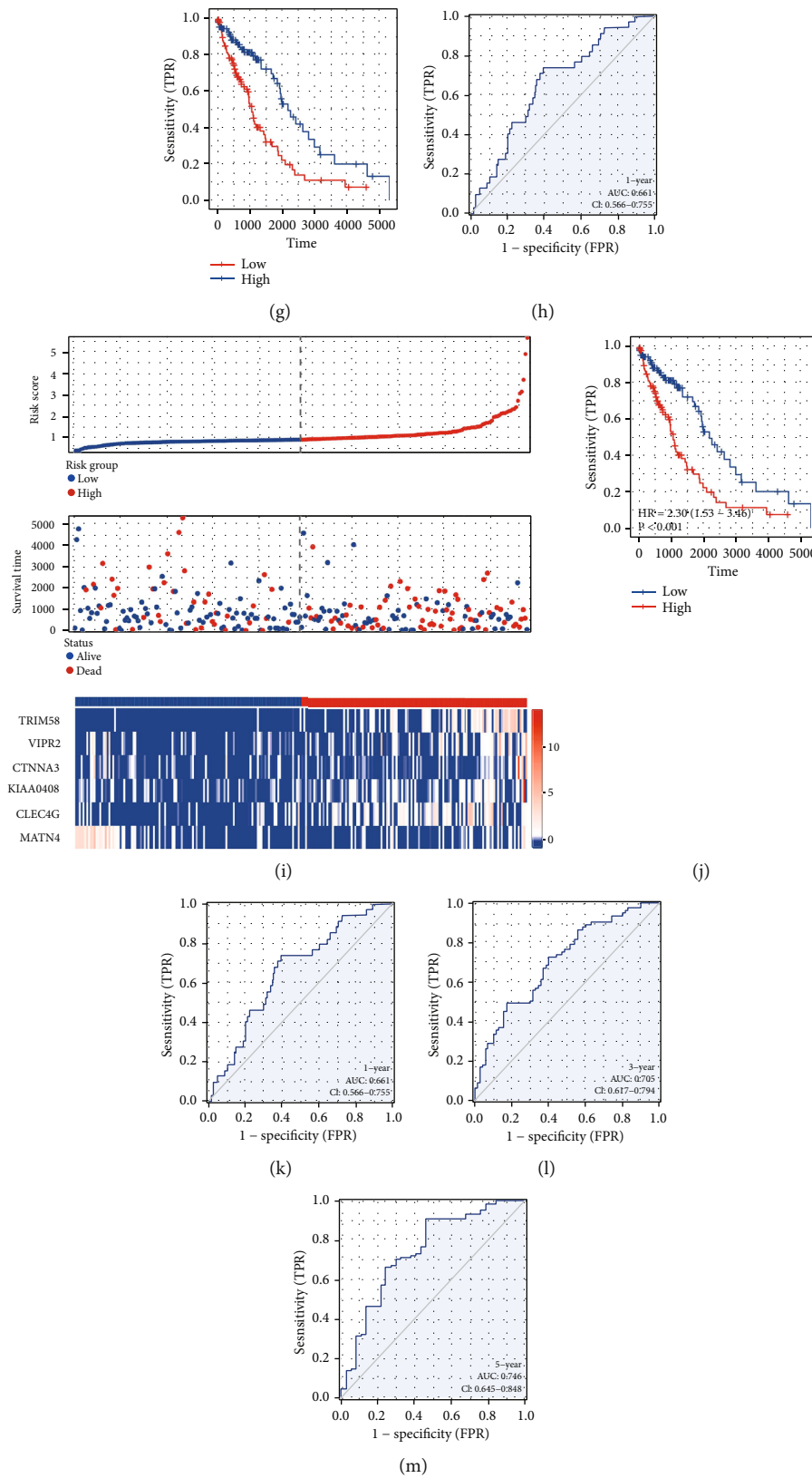
FIGURE 2: Prognosis model construction. (a, b) LASSO regression algorithm; (c) multivariate Cox regression analysis; (d) overview of the prognosis model in the training cohort; (e) KM survival curve of the model in the training cohort; (f–h) ROC curve was used for model evaluation in the training cohort; (i) overview of the prognosis model in the validation cohort; (j) KM survival curve of the model in the validation cohort; (k–m) OC curve was used for model evaluation in the validation cohort.

(a)

(b)

(c)
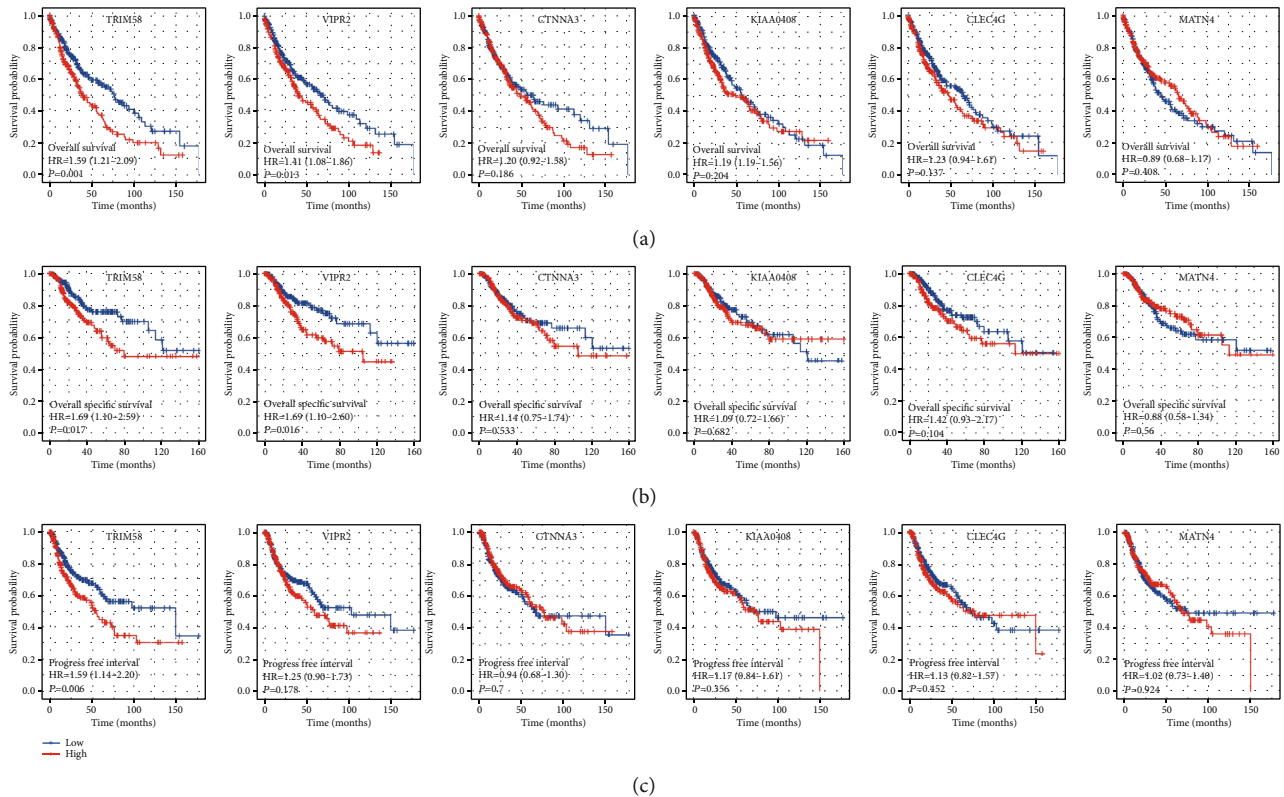
Figure 3: Prognosis effect of model genes. (a) The OS difference in patients with high and low model gene expression; (b) the DSS difference in patients with high and low model gene expression; (c) the PFS difference in patients with high and low model gene expression.

be associated with poor OS and disease-free survival (DSS), while MATN4 was associated with better prognosis (Figures 3(a) and 3(b)). Meanwhile, the patient with higher TRIM58 expression might have a shorter progression-free survival (Figure 3(c)).

3.3. Clinical Correlation Analysis. Both univariate and multivariate analyses demonstrated that our model is a risk factor that is not reliant on any other clinical characteristics, including age, gender, T classification, N classification, and clinical stage (Figure 4(a), univariate analysis, HR = 1.79, P < 0.001; Figure 4(b), multivariate analysis, HR = 1.864, P < 0.001). Clinical correlation analysis indicated no significant difference of model genes and risk score in patients of different ages (Figure 4(c)). Interestingly, we found that the female patients might have a higher risk score than male patients (Figure 4(d)). Also, we observed a lower CLEC4G level in patients with a worse clinical stage (Figure 4(e)). No significant difference of model genes and risk score was observed in patients of different TNM classifications (Figures 4(f)–4(h)).

3.4. Pathway Enrichment, Immune Infiltration, and Genomic Instability Analysis. Moreover, we made an effort to determine the potential variations in biological pathways that exist between patients who have a high risk and those who have a low risk. The result showed that the pathway of allograft rejection, bile acid metabolism, coagulation, inflammatory response, IL6/JAK/STAT3 signaling, hedgehog

signaling, peroxisome, and myogenesis were significantly activated in the high-risk patients (Figure 5). The CIBERSORT algorithm was used to quantify the immune microenvironment of LUSC patients (Figure 6(a)). Based on the results of an investigation of immune infiltration, risk score was found to have a positive correlation with M2 macrophages and resting CD4+ memory T cells, but a negative correlation with follicular helper T cells, M1 macrophages, and Tregs (Figure 6(b)). Genomic instability analysis showed that risk score had no remarkable correlation with TMB and MSI (Figures 7(a) and 7(b)). However, we found a negative correlation between risk score and mRNAsi (Figure 7(c)).

3.5. Immunotherapy and Drug Sensitivity Analysis. Both immunotherapy and chemotherapy were considered to be the most essential treatment options for lung cancer. Next, we investigated the underlying variations in immunotherapy and chemotherapy sensitivity between patients with a high chance of developing the disease and those with a low risk. The TIDE algorithm was used to quantify the immunotherapy response rate of LUSC patients (Figure 7(d)). The result showed that the immunotherapy responders might have a higher risk score (Figure 7(e)). Also, the patients in the high-risk group might have a higher proportion of immunotherapy responders (Figure 7(f)). The results of the drug sensitivity test suggested that people in the low-risk group would be more susceptible to the effects of cisplatin (Figure 7(g)). However, no significant difference was found
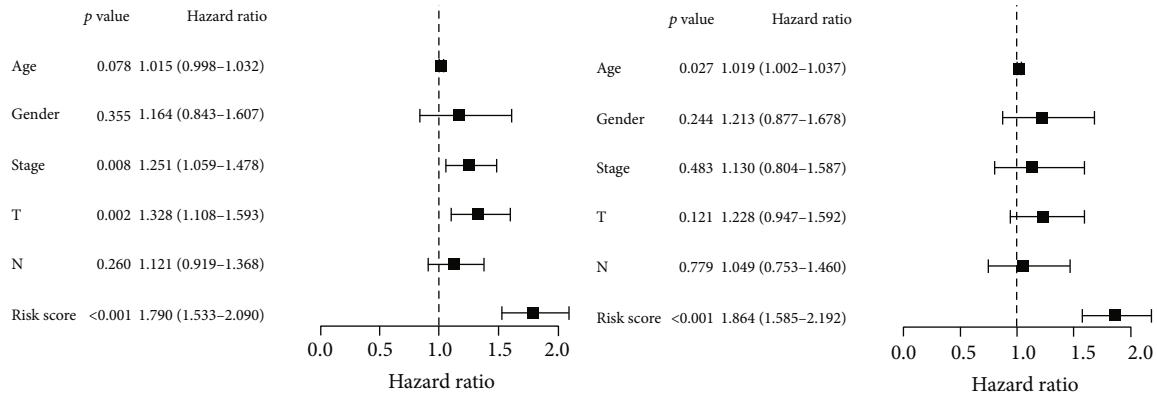
(a)

(b)

(c)

(d)

(e)

(f)

FIGURE 4: Continued.

(g)

(h)
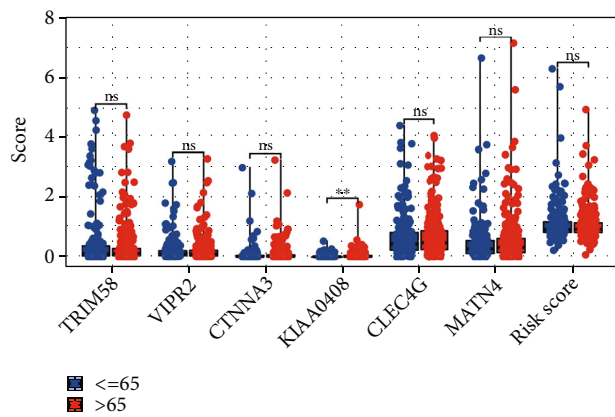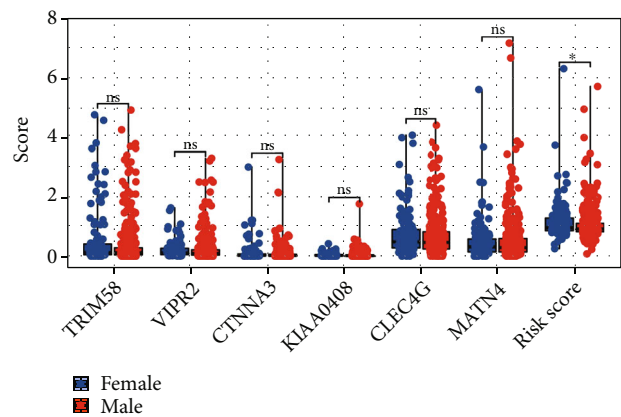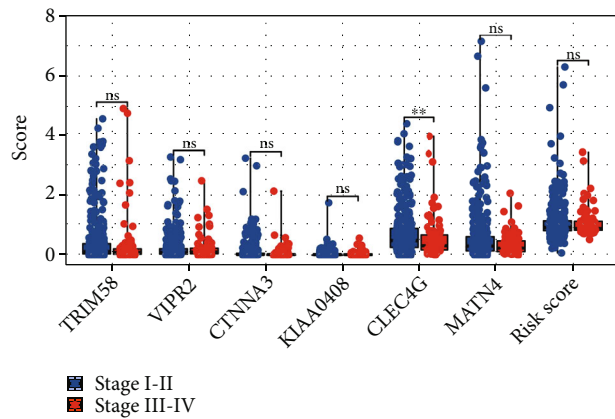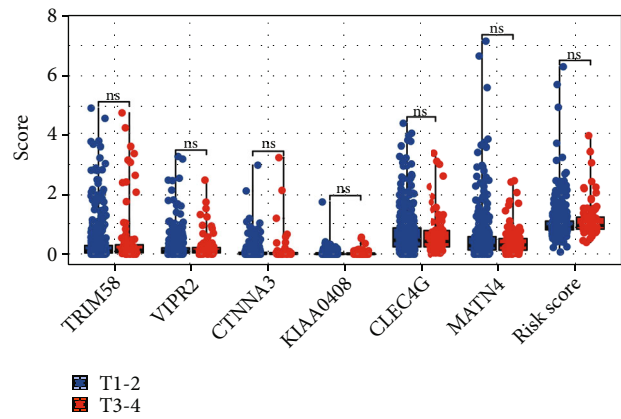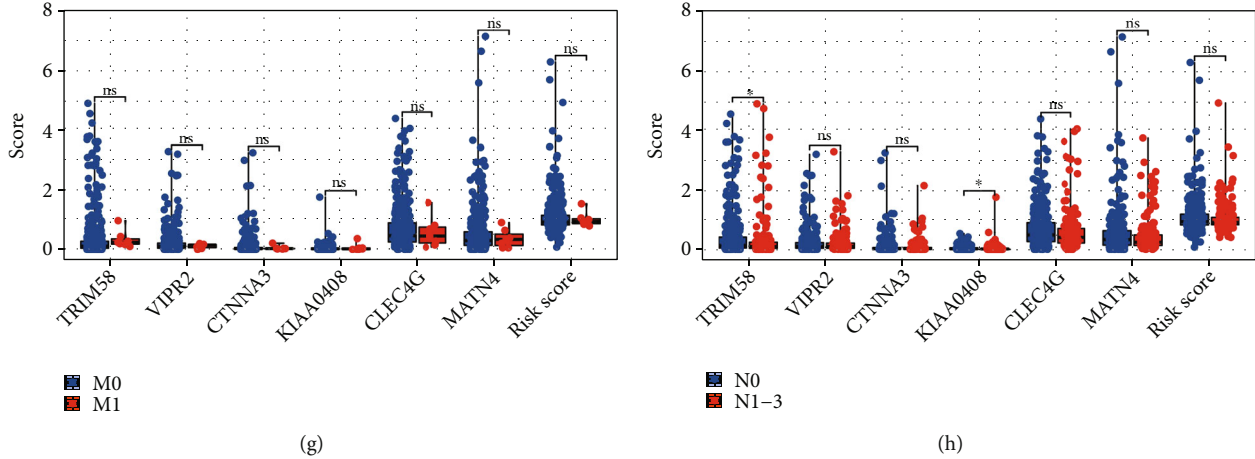
Figure 4: Clinical correlation analysis. (a, b) Both univariate and multivariate analyses were performed on the risk score and clinical characteristics; (c–h) clinical correlation of model genes and risk score.

Pathway	Gene ranks	NES	p val	p adj
Hallmark_allograft_rejection		1.23	2.0e−02	5.0e−01
Hallmark_bile_acid_metabolism		1.12	2.2e−01	1.0e+00
Hallmark_coagulation		1.07	3.2e−01	1.0e+00
Hallmark_angiogenesis		1.10	3.4e−01	1.0e+00
Hallmark_pancreas_beta_cells		1.04	4.5e−01	1.0e+00
Hallmark_inflammatory_response		0.99	5.3e−01	1.0e+00
Hallmark_IL6_JAC_STAT3_signaling		0.93	6.6e−01	1.0e+00
Hallmark_hedgehog_signaling		0.88	6.9e−01	1.0e+00
Hallmark_peroxisome		0.90	7.4e−01	1.0e+00
Hallmark_myogenesis		0.92	7.4e−01	1.0e+00
Hallmark_epithelial_mesenchymal_transition		−0.88	1.0e+00	1.0e+00
Hallmark_androgen_response		−0.81	9.5e−01	1.0e+00
Hallmark_oxidative_phosphorylation		−1.21	3.3e−01	1.0e+00
Hallmark_MYC_targets_v1		−2.22	3.3e−01	1.0e+00
Hallmark_G2M_checkpoint		−1.53	2.5e−01	1.0e+00
Hallmark_E2F_targets		−1.74	2.5e−01	1.0e+00
Hallmark_TGF_BETA_signaling		−1.13	2.2e−01	1.0e+00
Hallmark_DNA_repair		−1.44	1.4e−01	1.0e+00
Hallmark_WMT_beta_catenin_signaling		−1.32	7.0e−02	1.0e+00
Hallmark_MYC_targets_v2		−2.00	5.1e−03	2.5e+01

Figure 5: Pathway enrichment analysis.

in axitinib, bexarotene, bleomycin, bortezomib, docetaxel, gemcitabine, and sunitinib (Figure 7(g)).

4. Discussion

Lung cancer, the leading cause of cancer death throughout the world, claims the lives of more than 350 people every day [19]. During the last decade, although there was a steep decline in lung cancer incidence for advanced cases based on the changes in cancer screening and treatment, only 15% of patients with NSCLC can live beyond five years [20]. LUSC, the most common pathological subtype of NSCLC, known for its high tumor heterogeneity, showed a significant therapeutic difference in immunotherapy response rate [21]. A key objective of our research is to identify prognostic and therapeutic targets for LUSC.
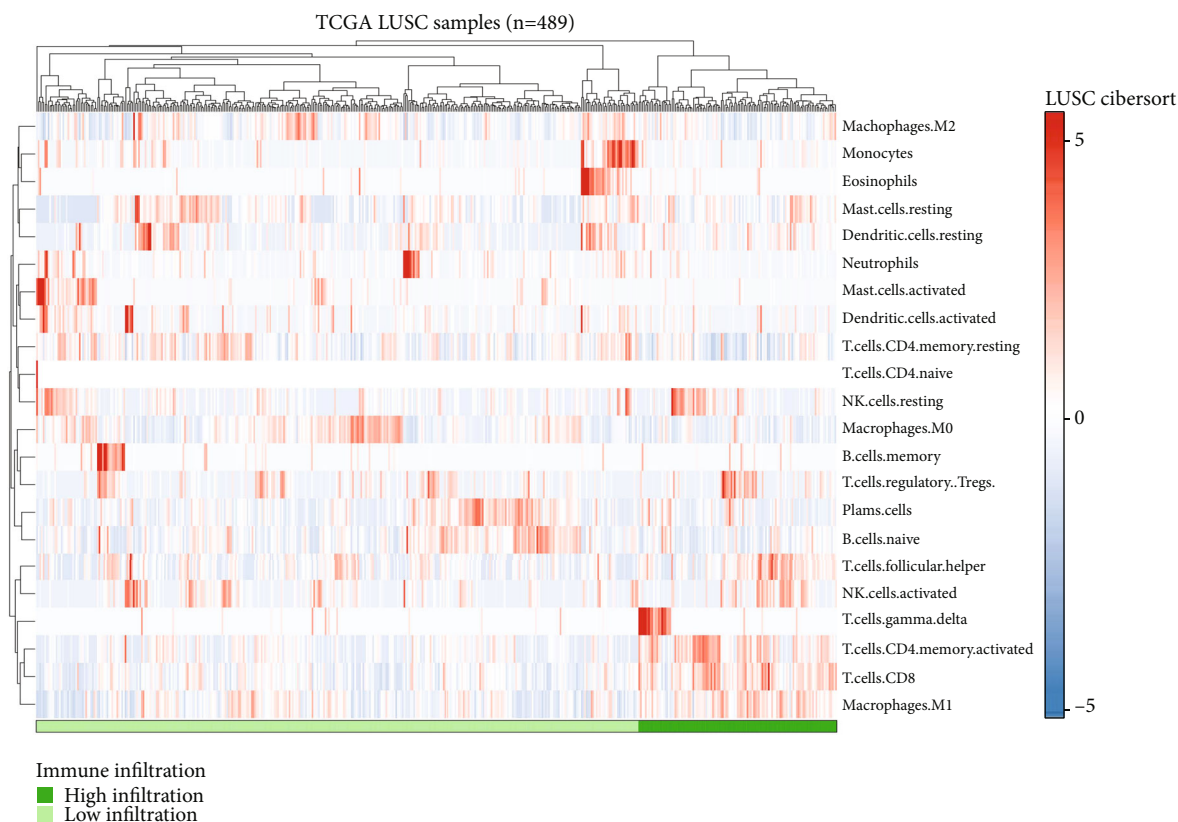
(a)
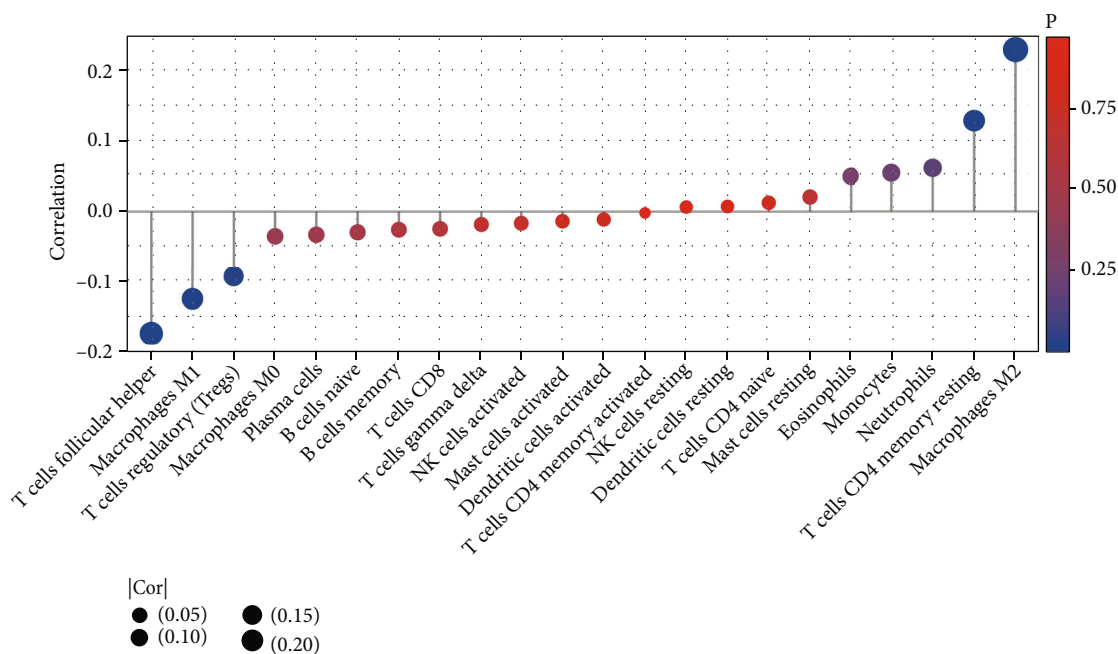
(b)

FIGURE 6: Immune infiltration analysis. (a) In order to quantify the immunological microenvironment, the CIBERSORT algorithm was utilized; (b) the correlation of risk score and quantified immune cells.

In this study, we comprehensively explored the role of M2 macrophages and its related genes in LUSC patients. Meanwhile, a prognosis model based on six M2 macrophage-related genes was established, including TRIM58, VIPR2, CTNNA3, KIAA0408, CLEC4G, and MATN4, which showed a good prognosis prediction efficiency in both training and validation cohort. In order to investigate the underlying clinical and biological differences

(a)

(b)

(c)

(d)

(e)

(f)

Figure 7: Continued.

(g)
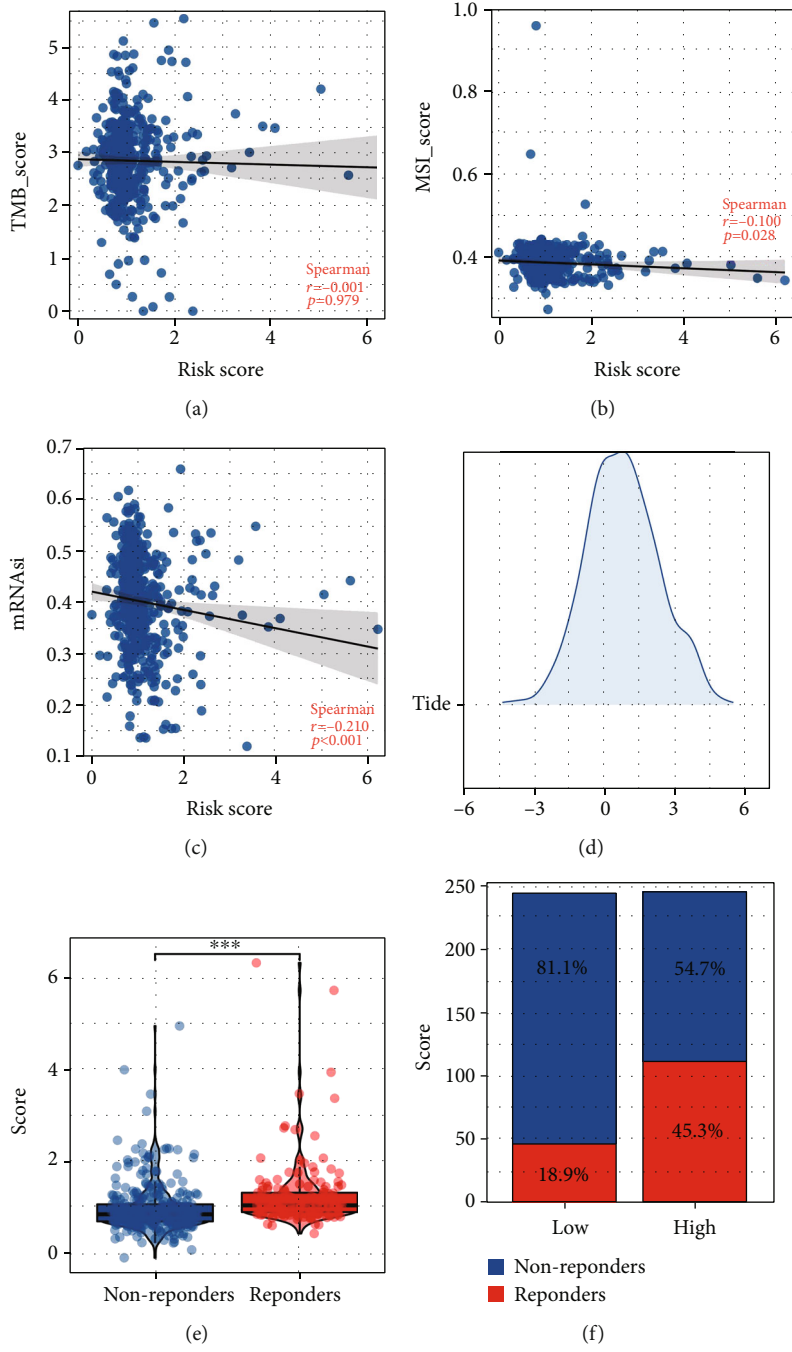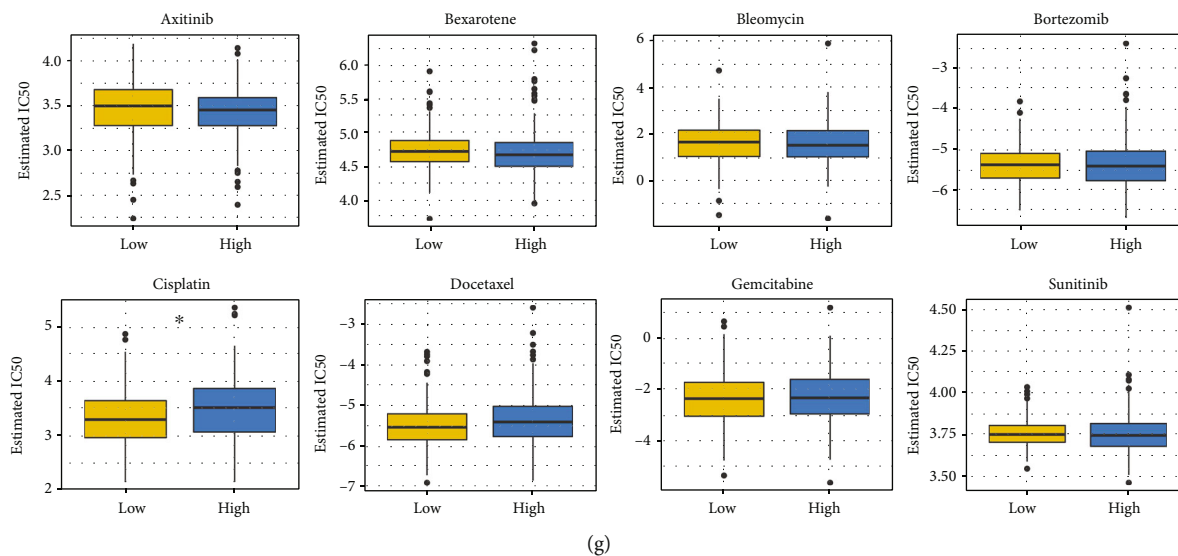
FIGURE 7: Immunotherapy and drug sensitivity analysis. (a) The correlation between risk score and TMB; (b) the correlation between risk score and MSI; (c) the correlation between risk score and mRNAsi; (d) TIDE algorithm was used to quantify the immunotherapy response; (e) the TIDE score in low- and high-risk patients; (f) the proportion of immunotherapy responders and non-responders in low- and high-risk patients; (g) drug sensitivity differences between low- and high-risk patients.

that exist between patients with a high risk and patients with a low risk, clinical correlation, route enrichment, and immune infiltration studies were carried out. In addition, we discovered that patients in high-risk groups may respond better to immunotherapy than individuals in lower-risk groups. However, low-risk patients might be more sensitive to cisplatin.

M2 macrophage is an essential part of the tumor microenvironment. In our study, we identified six model genes TRIM58, VIPR2, CTNNA3, KIAA0408, CLEC4G, and MATN4 that were associated with patients' prognosis and M2 macrophage infiltration. In lung cancer, Chen et al. found that TRIM58 was a prognostic biomarker that could remodel the tumor microenvironment of lung cancer [22]. Based on the whole-exome sequencing, Liu et al. indicated that CTNNA3 has the potential to be a promising druggable target in LUSC therapy [23]. However, there have been few studies examining the role of other genes playing in lung cancer, as well as their underlying association with M2 macrophage infiltration. The result of our study could provide a novel insight into the research direction of model genes.

The result in the present study showed that the pathway of allograft rejection, bile acid metabolism, coagulation, inflammatory response, IL6/JAK/STAT3 signaling, hedgehog signaling, peroxisome, and myogenesis were significantly activated in the high-risk patients. Through the large-scale metabonomic analysis of cancer tissue and plasma, Nie et al. found that bile acid metabolism was correlated with poor clinical features, which might be an underlying therapeutic target in lung cancer [24]. Meanwhile, Tantawy et al. found that the imbalance of IL6/JAK/STAT3 pathway and its related downstream pathways is the main reason for the progression of NSCLC [25]. The abnormal activation of the hedgehog pathway is responsible for causing and progressing several types of cancer [26]. In lung cancer, the hedgehog pathway was considered associated with

lung cancer development [27]. Meanwhile, risk score was found positively correlated with M2 macrophage infiltration. In lung cancer, high level of M2 macrophages was associated with more progressive biological behavior. From our result, it is possible that the aberrant activation of the pathways mentioned above, along with the link with M2 macrophages, is to blame for the dismal prognosis of patients who fall into the high-risk group.

Nowadays, immunotherapy and chemotherapy were important therapy options for lung cancer. According to the findings of our study, patients who were in the high-risk group would respond better to immunotherapy, whereas those who were in the low-risk group might respond better to cisplatin. Therefore, aside from predicting the prognosis of lung cancer patients, our model also provides some therapeutic guidance. In the clinical setting, the application of our model could indicate the therapy option of LUSC patients.

It is important to be aware of some restrictions. Firstly, the majority of people who participated in our research were from Western countries. The underlying race bias might hamper the credibility of the application of our model to other races. Secondly, the M classification information of a considerable part of the population is unknown. If all clinical information is complete, our data will be richer and more reliable. Moreover, further experimental research is required to elucidate the protein expression levels of the prognostic genes as well as their molecular mechanisms in the pathogenesis and progression of LUSC.

5. Conclusion

Our study identified a novel signature that reliably predict overall survival in pancreatic cancer. The findings may be beneficial to therapeutic customization and medical decision-making.

Data Availability

The data used in this research are available from the corresponding author upon reasonable request.

Conflicts of Interest

The authors have declared that no competing interest exists.

Supplementary Materials

Figure S1: identification of M2 macrophages-related genes. *(Supplementary Materials)*

References

[1] F. Nasim, B. F. Sabath, and G. A. Eapen, "Lung cancer," *The Medical Clinics of North America*, vol. 103, no. 3, pp. 463–473, 2019.

[2] R. Nooreldeen and H. Bach, "Current and future development in lung cancer diagnosis," *International Journal of Molecular Sciences*, vol. 22, no. 16, p. 8661, 2021.

[3] M. Alexander, S. Y. Kim, and H. Cheng, "Update 2020: management of non-small cell lung cancer," *Lung*, vol. 198, no. 6, pp. 897–907, 2020.

[4] S. Jonna and D. S. Subramaniam, "Molecular diagnostics and targeted therapies in non-small cell lung cancer (NSCLC): an update," *Discovery Medicine*, vol. 27, no. 148, pp. 167–170, 2019.

[5] L. Osmani, F. Askin, E. Gabrielson, and Q. K. Li, "Current WHO guidelines and the critical role of immunohistochemical markers in the subclassification of non-small cell lung carcinoma (NSCLC): moving from targeted therapy to immunotherapy," *Seminars in Cancer Biology*, vol. 52, Part 1, pp. 103–109, 2018.

[6] M. L. Hsu and J. Naidoo, "Principles of immunotherapy in non-small cell lung cancer," *Thoracic Surgery Clinics*, vol. 30, no. 2, pp. 187–198, 2020.

[7] D. C. Hinshaw and L. A. Shevde, "The tumor microenvironment innately modulates cancer progression," *Cancer Research*, vol. 79, no. 18, pp. 4557–4566, 2019.

[8] I. Vitale, G. Manic, L. M. Coussens, G. Kroemer, and L. Galluzzi, "Macrophages and metabolism in the tumor microenvironment," *Cell Metabolism*, vol. 30, no. 1, pp. 36–50, 2019.

[9] M. Locati, G. Curtale, and A. Mantovani, "Diversity, mechanisms, and significance of macrophage plasticity," *Annual Review of Pathology*, vol. 15, no. 1, pp. 123–147, 2020.

[10] J. Lan, L. Sun, F. Xu et al., "M2 macrophage-derived exosomes promote cell migration and invasion in colon cancer," *Cancer Research*, vol. 79, no. 1, pp. 146–158, 2019.

[11] Y. S. Weng, H. Y. Tseng, Y. A. Chen et al., "MCT-1/miR-34a/IL-6/IL-6R signaling axis promotes EMT progression, cancer stemness and M2 macrophage polarization in triple-negative breast cancer," *Molecular Cancer*, vol. 18, no. 1, p. 42, 2019.

[12] X. Wang, G. Luo, K. Zhang et al., "Hypoxic tumor-derived exosomal miR-301a mediates M2 macrophage polarization via PTEN/PI3Kγ to promote pancreatic cancer metastasis," *Cancer Research*, vol. 78, no. 16, pp. 4586–4598, 2018.

[13] B. Chen, M. S. Khodadoust, C. L. Liu, A. M. Newman, and A. A. Alizadeh, "Profiling tumor infiltrating immune cells with CIBERSORT," *Methods in molecular biology (Clifton, NJ)*, vol. 1711, pp. 243–259, 2018.

[14] S. Hänzelmann, R. Castelo, and J. Guinney, "GSVA: gene set variation analysis for microarray and RNA-seq data," *BMC Bioinformatics*, vol. 14, no. 1, p. 7, 2013.

[15] X. Ren, X. Chen, K. Fang et al., "COL5A2 promotes proliferation and invasion in prostate cancer and is one of seven Gleason-related genes that predict recurrence-free survival," *Frontiers in Oncology*, vol. 11, article 583083, 2021.

[16] R. Tibshirani, "The lasso method for variable selection in the Cox model," *Statistics in Medicine*, vol. 16, no. 4, pp. 385–395, 1997.

[17] J. Fu, K. Li, W. Zhang et al., "Large-scale public data reuse to model immunotherapy response and resistance," *Genome Medicine*, vol. 12, no. 1, p. 21, 2020.

[18] W. Yang, J. Soares, P. Greninger et al., "Genomics of Drug Sensitivity in Cancer (GDSC): a resource for therapeutic biomarker discovery in cancer cells," *Nucleic Acids Research*, vol. 41, no. Database issue, pp. D955–D961, 2013.

[19] R. L. Siegel, K. D. Miller, H. E. Fuchs, and A. Jemal, "Cancer statistics, 2022," *CA: a Cancer Journal for Clinicians*, vol. 72, no. 1, pp. 7–33, 2022.

[20] Q. Xie, H. Chu, J. Yi et al., "Identification of a prognostic immune-related signature for small cell lung cancer," *Cancer Medicine*, vol. 10, no. 24, pp. 9115–9128, 2021.

[21] D. B. Doroshow, M. F. Sanmamed, K. Hastings et al., "Immunotherapy in non-small cell lung cancer: facts and hopes," *Clinical Cancer Research: An Official Journal of the American Association for Cancer Research*, vol. 25, no. 15, pp. 4592–4602, 2019.

[22] X. Chen, Y. Wang, X. Qu, F. Bie, Y. Wang, and J. Du, "TRIM58is a prognostic biomarker remodeling the tumor microenvironment inKRAS-driven lung adenocarcinoma," *Future oncology (London, England)*, vol. 17, no. 5, pp. 565–579, 2021.

[23] P. Liu, C. Morrison, L. Wang et al., "Identification of somatic mutations in non-small cell lung carcinomas using whole-exome sequencing," *Carcinogenesis*, vol. 33, no. 7, pp. 1270–1276, 2012.

[24] M. Nie, K. Yao, X. Zhu et al., "Evolutionary metabolic landscape from preoplasia to invasive lung adenocarcinoma," *Nature Communications*, vol. 12, no. 1, p. 6479, 2021.

[25] M. A. Tantawy, S. Shaheen, S. W. Kattan et al., "Cytotoxicity,in silicopredictions and molecular studies for androstane heterocycle compounds revealed potential antitumor agent against lung cancer cells," *Journal of Biomolecular Structure & Dynamics*, vol. 40, no. 10, pp. 4352–4365, 2022.

[26] X. Zeng and D. Ju, "Hedgehog signaling pathway and autophagy in cancer," *International journal of molecular sciences*, vol. 19, no. 8, p. 2279, 2018.

[27] A. M. Skoda, D. Simovic, V. Karin, V. Kardum, S. Vranic, and L. Serman, "The role of the hedgehog signaling pathway in cancer: a comprehensive review," *Bosnian Journal of Basic Medical Sciences*, vol. 18, no. 1, pp. 8–20, 2018.

Research Article

LncRNA LINC02257: A Potential Biomarker for Diagnosis and Prognosis of Colorectal Cancer

Mei Chen, Changbing Li, Qinghua Luo [ID], and Anhui Tan [ID]

Department of Anorectal, The National Hospital Of Enshi Autonomous Prefecture, Enshi, Hubei, China

Correspondence should be addressed to Qinghua Luo; luoqinghuazd@163.com and Anhui Tan; t787856462@163.com

Colorectal cancer (CRC) is the third most common cancer and the second leading cause of cancer mortality worldwide. However, efficient markers for CRC diagnosis are limited. Accumulating evidence reveals that long noncoding RNAs (lncRNAs) are related to the genesis and developments of many tumors. In this study, we aimed to explore the diagnostic and prognostic value of LINC02257 in CRC patients. TCGA datasets were utilized to examine LINC02257 expression in a variety of human malignancies. The Kaplan–Meier method analysis was then used to study the link between LINC02257 expression and patient prognosis. Multivariate assays were applied for the determination of the associations of the variables and patients' survivals. RT-PCR was used to examine the level of LINC02257 expression in 14 pairs of clinical CRC tissues as well as many distinct CRC cell lines. CCK-8 assay was used to assess cell proliferation. We found that the expression of LINC02257 exhibited variable patterns of upregulation or downregulation in the various forms of cancer. In CRC, LINC02257 expression was distinctly increased in CRC specimens compared with normal specimens. The results of ROC curves revealed that the AUC was 0.886 (0.862 to 0.909, 95% CI, $p < 0.001$) in a comparison between CRC specimens and matched normal specimens. Survival studies revealed that high LINC02257 expression was associated with shorter overall survival and disease specific survival. More importantly, multivariate assays confirmed that high expression of LINC02257 was an independent prognostic factor for CRC patients. The results of RT-PCR indicated that LINC02257 expression was distinctly overexpressed in both CRC specimens and cell lines. Functionally, silence of LINC02257 distinctly suppressed the proliferation of CRC cells. In conclusion, our research showed that LINC02257 is an intriguing candidate as a diagnostic and prognostic indicator for patients diagnosed with CRC.

1. Introduction

Colorectal cancer (CRC) belongs to the globally commonest malignancies, with almost 1.35 million new cases and 0.8 million deaths annually [1]. Recent years have shown a trend toward an increased occurrence of this condition, which is consistent with the tremendous shift in dietary composition and lifestyle that has occurred all across the world [2]. The widespread use of surgical resection, which may or may not be accompanied by adjuvant chemotherapy and radiation therapy depending on the clinical stages of tumors, has led to an improvement in the clinical outcome for a significant number of patients with CRC [3, 4]. On the other hand, it has been discovered that some patients who undergo early surgery suffer from distant metastases, in particular liver

metastases, which may ultimately result in the treatment not working [5, 6]. Therefore, it is of the utmost importance to locate sensitive diagnostic and prognostic biomarkers in order to establish the most effective therapy methods for patients suffering from CRC.

The great advancements that have been made in genome and transcriptome sequencing in recent years have allowed for the discovery of a large number of genes that do not code for proteins [7]. These genes make up approximately 75% of the genome. RNAs that are longer than 200 nucleotides and are transcribed from genes that do not code for proteins are referred to as long noncoding RNAs (lncRNAs) [8]. Despite the fact that lncRNAs are unable to code for proteins, which limits their biological function in the growth of cells, there is growing evidence that many lncRNAs have the potential to

affect genetic control, epigenetic regulation, and post-transcriptional regulation [9, 10]. Recent research has shown that a number of lncRNAs are aberrantly expressed in a variety of tumors. These lncRNAs have the potential to play either an oncogenic or an antioncogenic role in the oncogenesis and progression of different types of tumors by participating in a sequence of cellular progressions, such as cellular growth and distant metastasis [11, 12]. In addition, an increasing number of studies suggested the value of using lncRNAs as potential diagnostic and prognostic markers for patients suffering from various forms of cancer, including CRC. Despite this, there were still a significant number of lncRNAs that needed to be identified clinically.

Long intergenic nonprotein coding RNA 2257 (LINC02257) is a newly identified lncRNA which is located on 1q41. To date, the study of LINC02257 on tumors was rarely reported. Its expression and prognostic value were just reported in kidney renal clear cell carcinoma and CRC [13, 14]. However, the studies are limited. The purpose of this study was to investigate the expression pattern, clinical relevance, and potential of LINC02257 in patients with CRC.

2. Patients and Methods

2.1. Data Collection. RNA-seq profiles of 480 cases of colorectal cancer and 41 samples of normal tissue were collected using TCGA database (https://portal.gdc.cancer). In addition to that, we derived demographic information from these samples.

2.1.1. Patients and Tissue Samples. CRC specimens and adjacent normal specimens, which were histopathologically confirmed by two experienced pathologists, were collected from 14 CRC patients who underwent surgery at the First Affiliated Hospital of The National Hospital of Enshi Autonomous Prefecture from July 2020 to June 2021. All cases received no preoperative adjuvant therapies such as radiotherapy and chemotherapy. The follow-up period for all cases was five years. All collected specimens (CRC tissues and normal specimens) were snap-frozen in liquid nitrogen and stored at $-80°C$ immediately after resection for further RT-PCR assays. Written informed consent for the application of biological specimens was obtained from each patient involved in the study, and the ethics committee of our hospital approved this study.

2.1.2. Cell Lines. Five CRC cell lines (HT29, SW480, HCT15, HCT116, and DLD1) and one normal colonic epithelial cell line (FHC) were obtained from the American Type Culture Collection. The standard culture media for all of the cell lines was Dulbecco's modified Eagle's medium (DMEM; Gibco BRL, Grand Island, New York, United States), which contained 10 percent fetal bovine serum (FBS; Gibco BRL). The lipofectamine RNAiMAX reagent from Thermo Fisher Scientific, Waltham, Massachusetts, was used to transfect cells with small interfering RNAs (siRNAs), as outlined in the protocol provided by the manufacturer. GenePharma was responsible for the design and synthesis of both the LINC02257 siRNA (si-LINC02257) and the negative control siRNA (si-NC).

2.1.3. The Real-Time Reverse Transcription Polymerase Chain Reaction (RT-PCR). Total RNA from all samples of 14 CRC patients was isolated using the TRIzol reagent (Invitrogen, Hangzhou, Zhejiang, China). A reaction mixture containing $1 \mu g$ of total RNA was reversely transcribed to cDNA using Synthesis SuperMix (Transgene Biotek, Ltd., Hyderabad, India). Real-time PCR detection of genes was carried out by the use of the SYBR Green Master Mix (Biosystems, Xunwu, Nanjing, China). All reactions were run in triplicate. The LINC02257 level was calculated with the $2^{-\Delta\Delta Ct}$ methods, which was normalized to GAPDH. The expressions of LINC02257 and GAPDH were relative to the fold change of the matched normal specimens, which were defined as 1.0. The primer sequences were presented as follows: LINC02257 $5'$-CTCTAGCCTCTGGCATCACAG-$3'$ (forward) and $5'$-CTCCACTAGGCTCGCCACG$'$(reverse), and GAPDH $5'$-GGTGAAGGTCGGAGT CAACG-$3'$ and $5'$-CAAAGTTGTCATGGATGHACC -$3'$.

2.1.4. Cell Counting Kit-8 (CCK-8). Both DLD1 and SW480 cells were grown in 96-well plates at a density of 4×10^4 cells per well for a period of 24 hours. After that, $10 \mu l$ of a solution from a cell counting kit-8 (CCK-8) manufactured by Dojindo Laboratories, Inc (Pudong, Shanghai, China) was added to the medium, and the cells were then incubated for 2 hours at $37°C$ in an atmosphere containing 5% CO_2. With the use of a Spectrafluor microreader plate, the value of the optical density was determined at a wavelength of 450 nm (Molecular Devices, LLC). These trials were carried out three times in all.

2.2. Statistical Analysis. All statistical data were analyzed by SPSS 18.0 software (SPSS, Chicago, IL, USA). Statistical analyses were carried out by the use of either an analysis of variance (ANOVA) or Student's t-test. Receiver operating characteristic (ROC) curves were established to examine the possible clinical value of LINC02257 expression for CRC diagnosis. The Kaplan–Meier method with the log-rank test for comparisons was used to calculate overall survival (OS) and disease-specific survival (DSS) rates. Univariate and multivariate assays were applied for the determination of the associations of the variables and patients' survivals. A p value <0.05 was considered to be statistically significant.

3. Results

3.1. Pan-Cancer Analysis of LINC02257 Expression Levels. For the purpose of investigating the role that LINC02257 plays in cancer, the expression levels of LINC02257 were evaluated across a wide spectrum of cancers using TCGA datasets. According to the findings, the expression of LINC02257 exhibited variable patterns of upregulation or downregulation in the various forms of cancer (Figure 1(a)). We were able to discover that the expressions of LINC02257

(a)

(b)

(c)
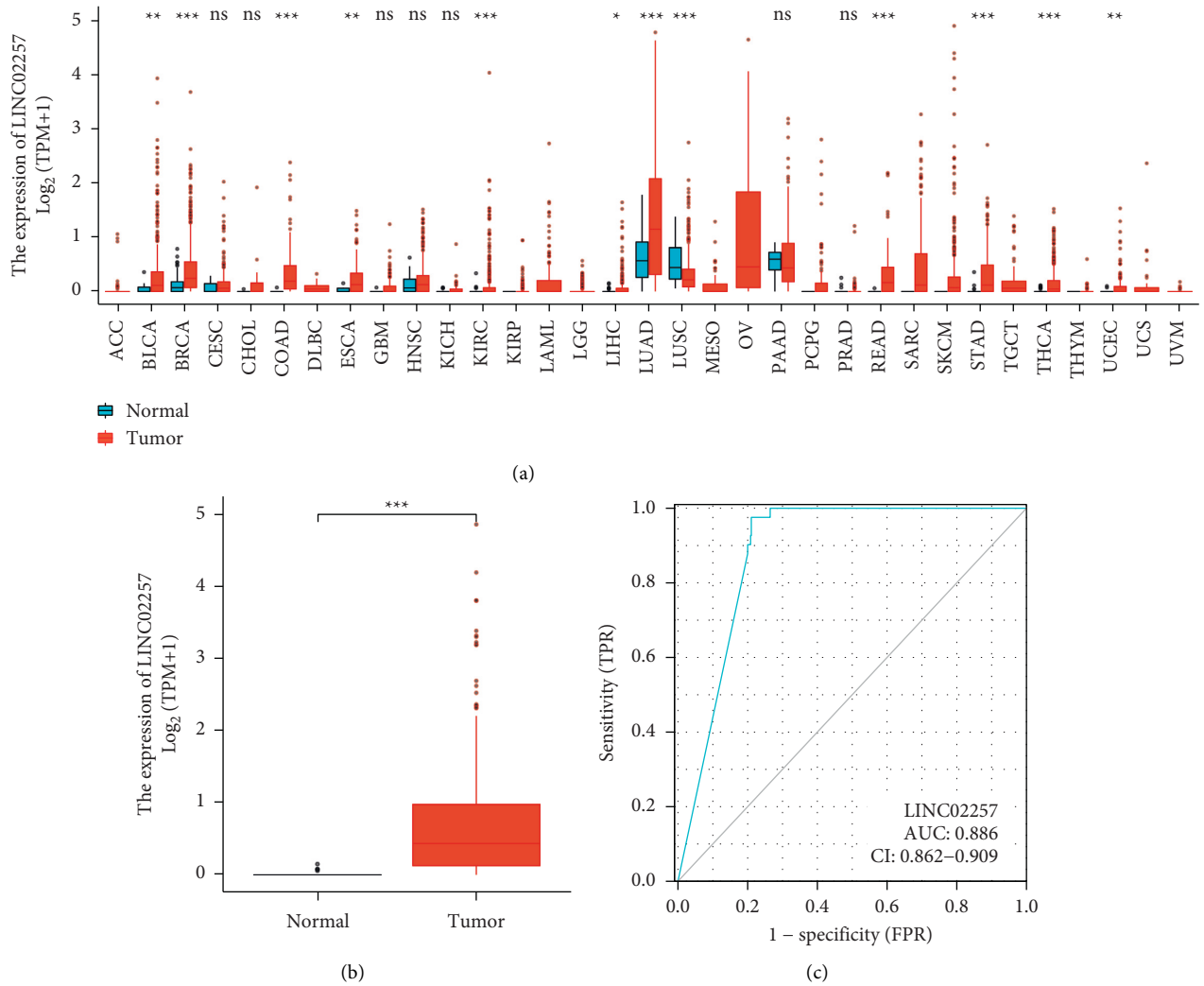
FIGURE 1: Expression of LINC02257 in TCGA cohorts. (a) Differential expressions of LINC02257 between non-tumor and tumor specimens in TCGA datasets. the X axis represents the expression of LINC02257 and the X axis represents the names of tumors. (b) LINC02257 was overexpressed in CRC specimens compared with non-tumor specimens. (c) Receiver operator characteristic curve analysis of LINC02257.

were distinctly increased in the majority of different types of cancers. These findings provide evidence of the inherent changes in the expression of LINC02257 that exist between the various types of tumors. Detailed assessments of the expression of LINC02257 were taken into consideration for further study. Importantly, our group observed that the expressions of LINC02257 were distinctly upregulated in CRC specimens compared with normal specimens (Figure 1(b)). The significant upregulation of LINC02257 in CRC patients encouraged us to further explore its diagnostic value for CRC patients. As shown in Figure 2, the results of ROC curves revealed that the AUC was 0.886 (0.862 to 0.909, 95% CI, $p < 0.001$) in a comparison between CRC specimens and matched normal specimens (Figure 1(c)).

3.2. Association of LINC02257 Expression with Clinicopathological Features of CRC Patients. To explore the clinical effect of LINC02257 on the progression of CRC patients, 478 CRC samples were divided into two subgroups high-group:

$n = 239$ and low-group: $n = 239$ according to the median ratio of relative LINC02257 expressions. The chi-square test suggested that high LINC02257 expression in 239 CRC patients was distinctly associated with the pathologic stage ($p = 0.003$) (Table 1). However, there were no significant associations between LINC02257 expressions and other clinical features.

3.3. Association between LINC02257 Expression and Patient Survival. Then, we explored whether there are any associations between dysregulated expression of LINC02257 and clinical survivals of CRC patients. First, we analyzed the survival data from a cohort (478 CRC patients) from TCGA datasets, finding that patients with high LINC02257 expressions had shorter OS ($p < 0.001$, Figure 2(a)) and DSS ($p < 0.001$, Figure 2(b)) time than those with low LINC02257 expressions. To further determine the prognostic values of LINC02257 expression in CRC patients, we performed univariate and multivariate assays which suggested that high

(a)

(b)
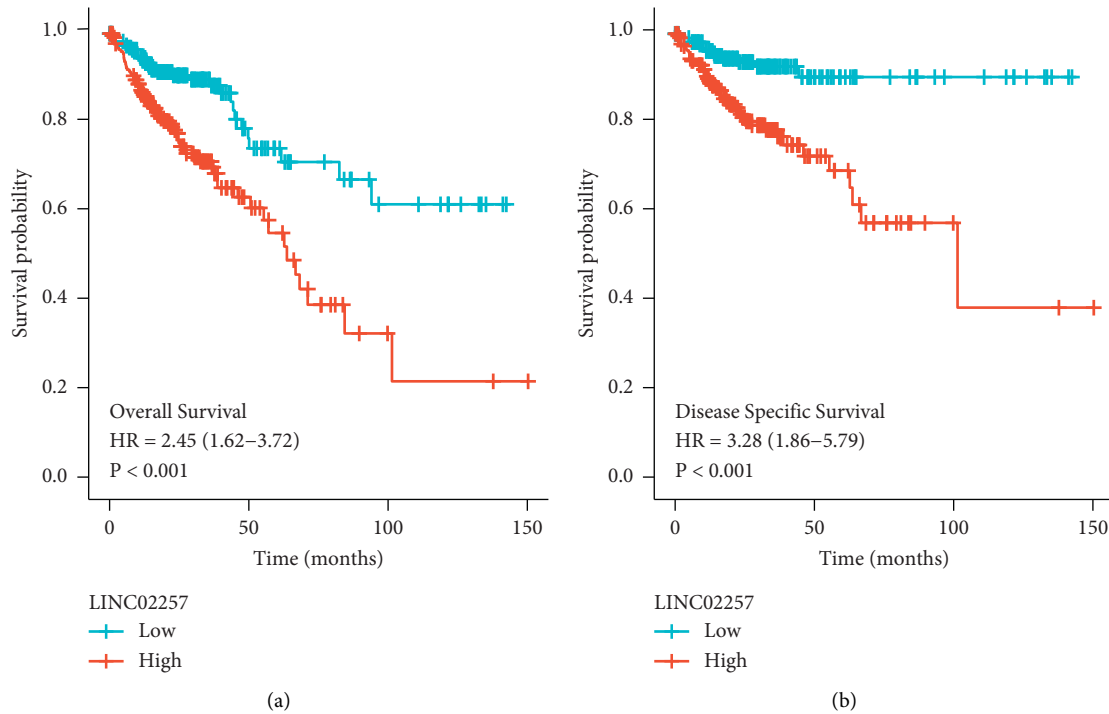
Figure 2: Kaplan-meier methods estimating the overall survivals and disease specific survivals according to the expression of LINC02257 in patients with CRC.

Table 1: Association between LINC02257 and clinicopathological parameters of CRC.

Characteristic	Low expression of LINC02257	High expression of LINC02257	p
n	239	239	
Gender, n (%)			0.927
Female	112 (23.4%)	114 (23.8%)	
Male	127 (26.6%)	125 (26.2%)	
Age, n (%)			0.780
<=65	99 (20.7%)	95 (19.9%)	
>65	140 (29.3%)	144 (30.1%)	
Pathologic stage, n (%)			0.003
Stage I	53 (11.3%)	28 (6%)	
Stage II	95 (20.3%)	92 (19.7%)	
Stage III	60 (12.8%)	73 (15.6%)	
Stage IV	24 (5.1%)	42 (9%)	
Age, median (IQR)	68 (59.5, 76.5)	69 (58, 78)	0.550

expression of LINC02257 was an independent prognostic factor for both OS (HR = 2.13, 95% CI: 1.395–3.280; $p < 0.001$, Table 2) and DSS (HR = 2.574, 95% CI: 1.450–4.569; $p < 0.001$) (Table 3).

3.4. The Upregulation of LINC02257 Expression in CRC and Its Oncogenic Roles. Then, we carried out RT-PCR to examine the levels of LINC02257 in 14 pairs of CRC specimens and non-tumor specimens. As shown in Figure 3(a), we discovered that the levels of LINC02257 was noticeably increased in CRC tissues in comparison to nontumor specimens. Moreover, the results of ROC assays revealed that the AUC was 0.8622 ($p < 0.001$) in a comparison between CRC specimens and matched normal

specimens (Figure 3(b)). Next, LINC02257 expression was detected by qRT-PCR in 5 human colorectal cancer cell lines (Figure 3(c)). Notably, all the cell lines expressed higher levels of LINC02257 versus the FHC, but DLD1 and SW480 cells expressed relatively higher levels of LINC02257 compared with other three cells. Therefore, we chose DLD1 and SW480 for further studies. For the silencing assays, cells were treated with LINC02257 siRNA or scramble siRNA controls. LINC02257 levels were significantly reduced in DLD1 and SW480 after siRNA treatments, compared to controls (Figure 3(d)). The results of further CCK-8 experiments demonstrated that silence of LINC02257 markedly suppressed the growth of DLD1 and SW480 cells (Figures 3(e) and 3(f)).

Table 2: Univariate and multivariate analysis of overall survival in CRC patients.

Characteristics	Total (N)	Univariate analysis		Multivariate analysis	
		Hazard ratio (95% CI)	p value	Hazard ratio (95% CI)	p value
Age	477				
<=65	194	Reference			
>65	283	1.610 (1.052–2.463)	**0.028**	2.114 (1.354–3.299)	**<0.001**
Gender	477				
Female	226	Reference			
Male	251	1.101 (0.746–1.625)	0.627		
Pathologic stage	466				
Stage I & stage II	267	Reference			
Stage III & stage IV	199	2.947 (1.942–4.471)	**<0.001**	3.114 (2.033–4.768)	**<0.001**
LINC02257	477				
Low	238	Reference			
High	239	2.451 (1.617–3.716)	**<0.001**	2.139 (1.395–3.280)	**<0.001**

Table 3: Univariate and multivariate analysis of disease specific survival in CRC patients.

Characteristics	Total (N)	Univariate analysis		Multivariate analysis	
		Hazard ratio (95% CI)	p value	Hazard ratio (95% CI)	p value
Age	461				
<=65	191	Reference			
>65	270	1.165 (0.702–1.933)	0.555		
Gender	461				
Female	220	Reference			
Male	241	1.142 (0.697–1.871)	0.599		
Pathologic stage	451				
Stage I & stage II	259	Reference			
Stage III & stage IV	192	6.085 (3.235–11.447)	**<0.001**	5.533 (2.934–10.432)	**<0.001**
LINC02257	461				
Low	230	Reference			
High	231	3.280 (1.860–5.785)	**<0.001**	2.574 (1.450–4.569)	**0.001**

(a)

(b)

(c)

Figure 3: Continued.

(d)

(e)

(f)
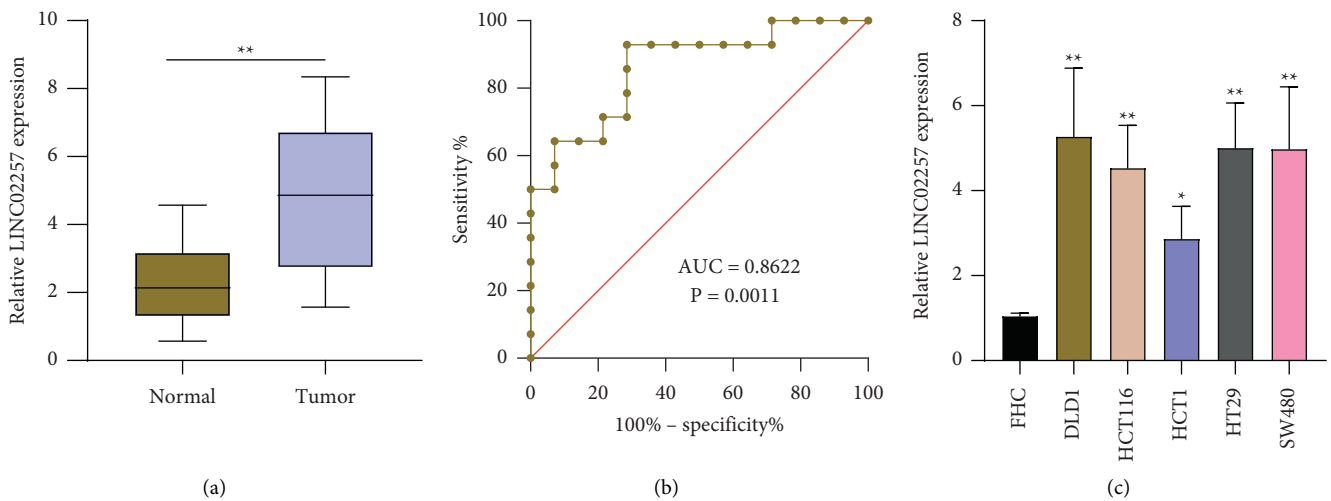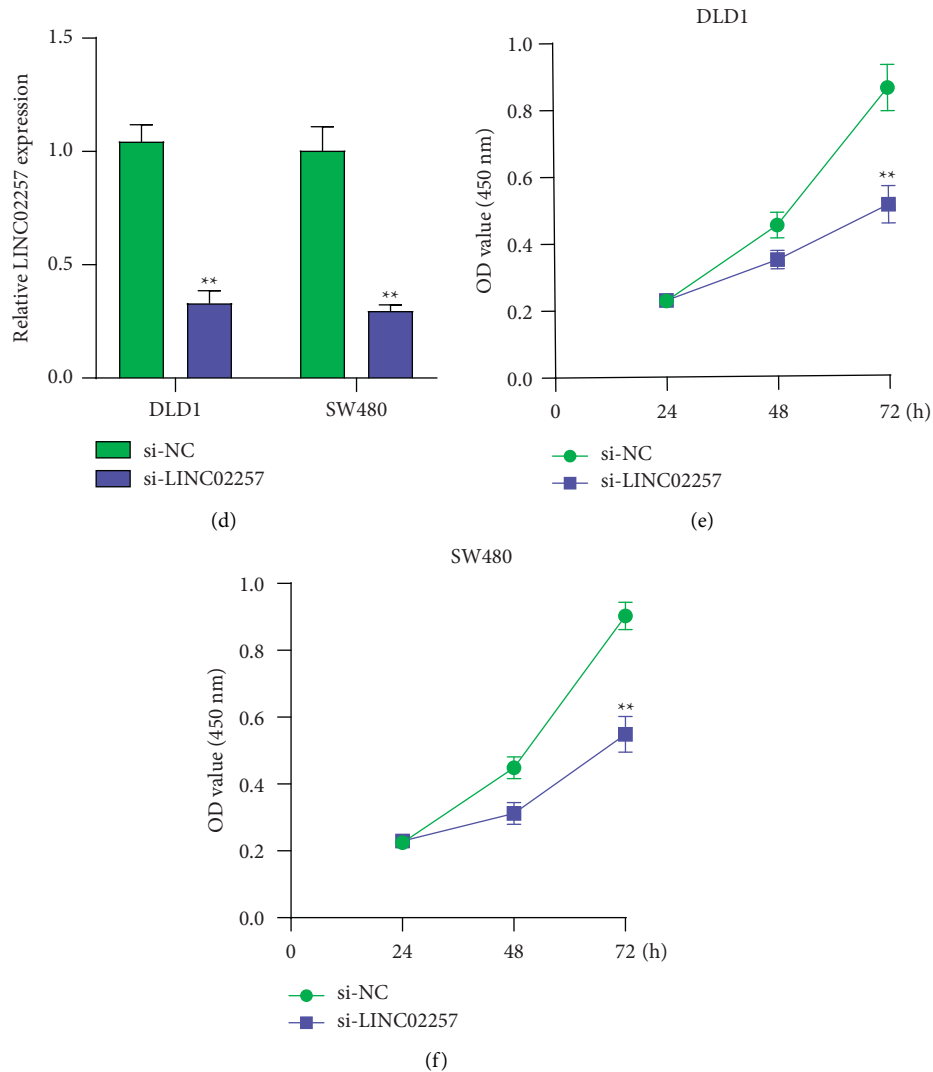
FIGURE 3: The expression of LINC02257 in our cohort and its functional roles. (a) The LINC02257 relative expression levels were determined by qRT-PCR in 14 pairs of CRC tissues and the adjacent non-tumor specimens. (b) The ROC curve analysis for discriminative ability between CRC specimens and normal tissues. (c) LINC02257 expressions were increased in CRC cell lines compared to normal FHC cells. (d) RT-PCR analysis of LINC02257 expression levels following DLD1 and SW480 cell treatment with si-LINC02257.

4. Discussion

The most common cause of death from colorectal cancer is the progression of metastasis, and the liver is the primary organ in which metastatic colonization can be found in more than 65 percent of CRC patients [15]. It is highly important for the reduction in the number of occurrences of metastatic illness to have both an early diagnosis and a treatment plan that is optimized based on the possible prognosis of CRC patients [16, 17]. In recent years, an increasing number of studies have reported that long noncoding RNAs, or lncRNAs, play an important role in the progression of tumors. Furthermore, their abnormal expressions in the cancer specimens and blood of patients suggested that lncRNAs may have the potential to be used as novel biomarkers [18, 19]. Several long noncoding RNAs have been proven to have a positive association with the long-term survivals of colorectal cancer patients and to exhibit clinical significance in differentiating cancer specimens from non-tumor samples.

In this research, our group observed that the expressions of LINC02257 exhibited an increased trend in many types of tumors, which suggested its oncogenic roles in tumor progression. However, there may be some abnormal phenomena. Some lncRNAs are highly expressed in some tumors, but their overexpression deficiency can inhibit tumor proliferation and metastasis, which may be due to the complex mechanisms involved in tumor progression [20, 21]. For LINC02257, we have looked up a lot of literature. Only some studies reported that LINC02257 was highly expressed in some tumors, such as kidney renal clear cell carcinoma and CRC [13, 14]. However, there was no in vivo or in vitro experimental study on its function. Here, we found that LINC02257 expressions were distinctly

increased in CRC, which was consistent with previous findings. In addition, we confirmed that this lncRNA has certain diagnostic significance via ROC assays. Clinical assays confirmed that LINC02257 was an independent poor prognostic factor for both OS and DSS. On the other hand, we firstly studied the potential function of LINC02257 in CRC progression, finding that silence of LINC02257 exhibited a suppressor effect in the proliferation of CRC cells, suggesting it as an oncogene in CRC progression. Our findings first reported that this lncRNA has a carcinogenic effect.

However, there are still some shortcomings in this study. First, it is a retrospective research, and as such, it suffers from the inherent selection bias and reporting bias that plague all retrospective studies. Due to the limited number of patients who participated in our study, additional research including a substantial number of patients is necessary to validate the results of our investigation. Second, our data are restricted to overall patient survival, and it will be of interest to analyze the association of LINC02257 expression with cancer recurrences. Third, in this article, the functional mechanisms are not investigated in great detail. Therefore, to compensate for these shortcomings, additional research ought to be carried out.

5. Conclusion

We identified a novel CRC-related lncRNA, LINC02257, which could be used as a potential marker for CRC patients. To further show the prognostic and diagnostic significance of LINC02257 in patients with CRC, additional in-depth investigations are required.

Data Availability

The data used to support the findings of this study are available from the corresponding author upon request.

Conflicts of Interest

The authors declare that there are no conflicts of interest.

Authors' Contributions

Mei Chen and Changbing Li contributed to this work equally.

References

[1] R. L. Siegel, K. D. Miller, H. E. Fuchs, and A. Jemal, "Cancer Statistics," *Ca - a Cancer Journal for Clinicians 2021*, vol. 71, no. 1, pp. 7–33, 2021.

[2] J. J. DeCosse, G. J. Tsioulias, and J. S. Jacobson, "Colorectal cancer: detection, treatment, and rehabilitation," *Ca - a Cancer Journal for Clinicians*, vol. 44, no. 1, pp. 27–42, 1994.

[3] V. Goh, A. R. Padhani, and S. Rasheed, "Functional imaging of colorectal cancer angiogenesis," *The Lancet Oncology*, vol. 8, no. 3, pp. 245–255, 2007.

[4] J. L. Drewes, F. Housseau, and C. L. Sears, "Sporadic colorectal cancer: microbial contributors to disease prevention, development and therapy," *British Journal of Cancer*, vol. 115, no. 3, pp. 273–280, 2016.

[5] D. Rebello, E. Rebello, M. Custodio, X. Xu, S. Gandhi, and H. K. Roy, "Field carcinogenesis for risk stratification of colorectal cancer," *Advances in Cancer Research*, vol. 151, pp. 305–344, 2021.

[6] I. O. Silla, D. Rueda, Y. Rodríguez, J. L. García, F. de la Cruz Vigo, and J. Perea, "Early-onset colorectal cancer: a separate subset of colorectal cancer," *World Journal of Gastroenterology*, vol. 20, no. 46, pp. 17288–17296, 2014.

[7] J. R. Prensner and A. M. Chinnaiyan, "The emergence of lncRNAs in cancer biology," *Cancer Discovery*, vol. 1, no. 5, pp. 391–407, 2011.

[8] N. Malmuthuge and L. L. Guan, "Noncoding RNAs: regulatory molecules of host-microbiome crosstalk," *Trends in Microbiology*, vol. 29, no. 8, pp. 713–724, 2021.

[9] S. Toden, T. J. Zumwalt, and A. Goel, "Non-coding RNAs and potential therapeutic targeting in cancer," *Biochimica et Biophysica Acta (BBA) - Reviews on Cancer*, vol. 1875, no. 1, Article ID 188491, 2021.

[10] S. C. Su, R. J. Reiter, H. Y. Hsiao, W. H. Chung, and S. F. Yang, "Functional interaction between melatonin signaling and noncoding RNAs," *Trends in Endocrinology and Metabolism*, vol. 29, no. 6, pp. 435–445, 2018.

[11] H. Yan and P. Bu, "Non-coding RNA in cancer," *Essays in Biochemistry*, vol. 65, no. 4, pp. 625–639, 2021.

[12] Y. Ortiz-Pedraza, J. O. Muñoz-Bello, L. Olmedo-Nieva et al., "Non-coding RNAs as key regulators of glutaminolysis in cancer," *International Journal of Molecular Sciences*, vol. 21, no. 8, p. 2872, 2020.

[13] G. Lin, H. Wang, Y. Wu, K. Wang, and G. Li, "Hub long noncoding RNAs with m6A modification for signatures and prognostic values in kidney renal clear cell carcinoma," *Frontiers in Molecular Biosciences*, vol. 8, Article ID 682471, 2021.

[14] X. Wang, J. Zhou, M. Xu et al., "A 15-lncRNA signature predicts survival and functions as a ceRNA in patients with colorectal cancer," *Cancer Management and Research*, vol. 10, pp. 5799–5806, 2018.

[15] Y. N. Peng, M. L. Huang, and C. H. Kao, "Prevalence of depression and anxiety in colorectal cancer patients: a literature review," *International Journal of Environmental Research and Public Health*, vol. 16, no. 3, p. 411, 2019.

[16] C. Kong and T. Fu, "Value of methylation markers in colorectal cancer (Review)," *Oncology Reports*, vol. 46, no. 2, p. 177, 2021.

[17] L. Signorini, S. Delbue, P. Ferrante, and M. Bregni, "Review on the immunotherapy strategies against metastatic colorectal carcinoma," *Immunotherapy*, vol. 8, no. 10, pp. 1245–1261, 2016.

[18] F. Long, Z. Lin, L. Li et al., "Comprehensive landscape and future perspectives of circular RNAs in colorectal cancer," *Molecular Cancer*, vol. 20, no. 1, p. 26, 2021.

[19] Y. Okugawa, W. M. Grady, and A. Goel, "Epigenetic alterations in colorectal cancer: emerging biomarkers," *Gastroenterology*, vol. 149, no. 5, pp. 1204–1225, 2015, e1212.

[20] F. Mirzadeh Azad, I. L. Polignano, V. Proserpio, and S. Oliviero, "Long noncoding RNAs in human stemness and differentiation," *Trends in Cell Biology*, vol. 31, no. 7, pp. 542–555, 2021.

[21] C. M. Arraiano, "Regulatory noncoding RNAs: functions and applications in health and disease," *FEBS Journal*, vol. 288, no. 22, pp. 6308-6309, 2021.

Research Article

Long Noncoding RNA LINC02249 Is a Prognostic Biomarker and Correlates with Immunosuppressive Microenvironment in Skin Cutaneous Melanoma

Maotao Du,[1,2] Liang Han,[1] Pan Shen,[1] Dengyan Wu,[2] and Shenghao Tu [1]

[1]*Department of Integrated Chinese Traditional and Western Medicine, Tongji Hospital, Tongji Medical College,*
 Huazhong University of Science and Technology, Wuhan, China
[2]*Department of Dermatology and Plastic Surgery, The Second Affiliated Hospital of Chongqing Medical University,*
 Chongqing 400010, China

Correspondence should be addressed to Shenghao Tu; bslw2017@sina.com

Skin cutaneous melanoma (SKCM) is one of the most aggressive and life-threatening tumors. It has a high incidence rate, as well as significant metastasis and fatality rates. To successfully treat SKCM and to increase the overall survival rate, early identification and risk stratification are both absolutely necessary. Long noncoding RNAs (lncRNAs) play a significant regulatory role in a variety of cancers. However, the expression and function of many lncRNAs have not been investigated. We evaluated the expression profile of the long noncoding RNA LINC02249 (LINC02249) in pan-cancers by using data on gene expression obtained from TCGA and GTEx. The biological function of LINC02249 was determined by gene ontology (GO) and Kyoto Encyclopedia of Genes and Genomes (KEGG). The prognostic value of LINC02249 expression in SKCM patients was statistically analyzed. Besides, the ssGSEA approach was utilized in order to investigate the degree to which LINC02249 expression is correlated with tumor immune infiltration. In this study, the expression of LINC02249 was found to be abnormally high in a variety of tumors, according to our findings. When compared with nontumor specimens, the level of expression of LINC02249 was shown to be significantly elevated in SKCM samples. GO and KEGG assays revealed LINC02249 may be involved in tumor progression. High expression of LINC02249 was associated with shorter overall survival and disease-specific survival of SKCM patients. More importantly, multivariate methods revealed that LINC02249 expression was an independent prognostic factor for SKCM cases. Using ssGSEA, we found that the expression of LINC02249 was negatively associated with different tumor-infiltrating immune cells, especially aDC, Treg, and macrophages. Overall, our findings suggested that LINC02249 can serve as a novel biomarker to predict the prognosis and immune infiltration in SKCM.

1. Introduction

Skin cutaneous melanoma (SKCM) is a malignant transformation of melanocytes derived from neural crest stem cells [1]. Over the course of the last ten years, the prevalence of SKCM has skyrocketed across the globe [2]. Despite the fact that SKCM only accounts for about 5 percent of all skin tumors, it is responsible for more than 75 percent of deaths that are caused by skin tumors [3, 4]. In addition, the majority of people diagnosed with melanoma experience relapses or do not respond to

therapies because of toxicity, intrinsic drug resistance, and other factors that are not fully understood [5, 6]. Internal heterogeneity is shown by the molecular properties of SKCM; this is the primary factor that prevents customized treatment and is the primary factor in determining drug resistance [7, 8]. The dissatisfied prognosis of SKCM has not changed considerably despite the fact that numerous treatments, including phototherapy, chemotherapy, immunotherapy, local resection, and radiotherapy, have been used in SKCM patients [9]. Besides, early diagnosis of SKCM is still a huge challenge.

Thus, it is of the utmost need to find novel biomarkers that are effective in detecting, diagnosing, and predicting the prognosis of GC.

Long noncoding RNA (lncRNA) is a class of noncoding RNA greater than 200 nucleotides in length [10]. Increasing studies have shown that lncRNAs play key roles in the processes of chromosomal silencing, chromatin epigenetic modification, gene transcription, protein translation, and protein localization [11]. It is important to highlight that abnormal regulation of lncRNAs has been linked to the development and progression in a variety of human cancers [12, 13]. Several lncRNAs, such as lncRNA HCP5, lncRNA TEX41, and lncRNA TTN-AS1, play important roles in the growth of malignant cells in SKCM [14–16]. In addition, there are a growing number of studies that point to the fact that abnormally expressed lncRNAs have been utilized as possible biomarkers for the diagnosis and prognosis of cancer [17, 18]. lncRNA MALAT1, which is a 6.5-kilobase pair long noncoding RNA, has been discovered to be involved in multiple steps in the development of tumors. It also demonstrated diagnostic and prognostic significance in several neoplasms, including melanoma, lung cancer, breast cancer, glioma, and prostate cancer [19–23]. As a whole, the emerging linkages between noncoding RNAs and cancers have heralded the possibility that lncRNAs may serve either as diagnostic biomarkers or therapeutic targets for SKCM.

By exploiting public databases, we find that lncRNA LINC02249, mapped to chromosome 15q13.2, exhibited a dysregulated level in most types of tumors. To date, the potential function of LINC02249 has not been investigated. Our research aimed to clarify the associations between LINC02249 and SKCM using TCGA datasets.

2. Materials and Methods

2.1. Data Download and Preprocessing. TCGA, which acts as a public repository used to analyze high-throughput microarray data, was applied to obtain the gene expression profile as well as the clinical information of SKCM patients. TCGA datasets included 471 SKCM tissues and 1 nontumor tissue. Subsequent processing excluded cases with insufficient or complete information regarding age, overall survival time, and TNM stage. Because the TCGA database does not contain any samples of normal tissue, controls were derived from the genotype-tissue expression (GTEx) database instead. The full names of cancers in TCGA are shown in Table S1.

2.2. Screening of Differentially Expressed Genes (DEGs). Finding DEGs between two groups (high LINC02249 expression group and low LINC02249 expression group), which were characterized by the median expression level of LINC02249, was accomplished by applying the RNA-seq data obtained from the TCGA-SKCM. The "DESeq2" R package was used to screen for DEGS, while the "heatmap" R package was utilized to plot heatmaps in two different cohorts. Significant upregulation of DEGs was defined as having a p value of less than 0.05 and a log FC value more

than 1.5; significant downregulation of DEGS was defined as having a p value of less than 0.05 and a log FC value less than 1.5.

2.3. Kyoto Encyclopedia of Genes and Genomes (KEGG) and Gene Ontology (GO) Pathway Analysis. The GO analysis is broken down into three sections, which are the cellular component, the molecular function, and the biological process. These sections each explain the biological function of a specific gene from their own unique perspective. KEGG is an analysis tool that is used to figure out which biological pathways' particular genes are significantly overrepresented in. After that, we carry out a study of GO and KEGG pathways based on DEGS with low expression versus high expression of LINC02249.

2.4. Estimation of Stromal and Immune Scores. The ESTIMATE technique was used to standardize the expression matrix in order to facilitate accurate estimation of the stromal and immunological scores [24]. A single-sample gene set enrichment analysis was performed, and the results were used to construct stromal and immunological scores. The ESTIMATE score was derived using these scores; thus they should be considered reliable.

2.5. Tumor Infiltration Analysis. The XIANTAO platform (https://www.xiantao.love/) was used to conduct an analysis of the immune infiltration profiles of the tumors. A total of 24 immunological markers were utilized in order to differentiate between the various immunocytes. Using the single-sample generalized estimating equations analysis (ssGSEA) method, we were able to determine the Spearman correlations between immunocyte markers and LINC02249 expression levels.

2.6. Statistical Analysis. All statistical analyses were performed with R software 3.5.3. The unpaired *t*-test was utilized to investigate the possibility of differential expression of LINC02249 in cancer tissues in comparison to nontumor specimens. We used chi-square and *t*-tests to investigate whether or not there was a correlation between the levels of LINC02249 expression and the clinicopathological characteristics. The Kaplan–Meier survival curves were built to analyze survival differences between the high-LINC02249 group and low-LINC02249 expression group. Univariate and multivariate assays were developed in order to assess the HRs of clinical elements. A two-tailed $p < 0.05$ was considered to indicate a statistically significant difference.

3. Results

3.1. LINC02249 Expression Analysis in Pan-Cancer. Firstly, we examined the expression of LINC02249 in TCGA and GTEx pan-cancer datasets. According to the findings, a significant amount of LINC02249 expression was found in five different tumors: GBM, KIRP, LAML, LGG, SKCM, and THYM. In comparison, low LINC02249 expression was

(a)

(b)
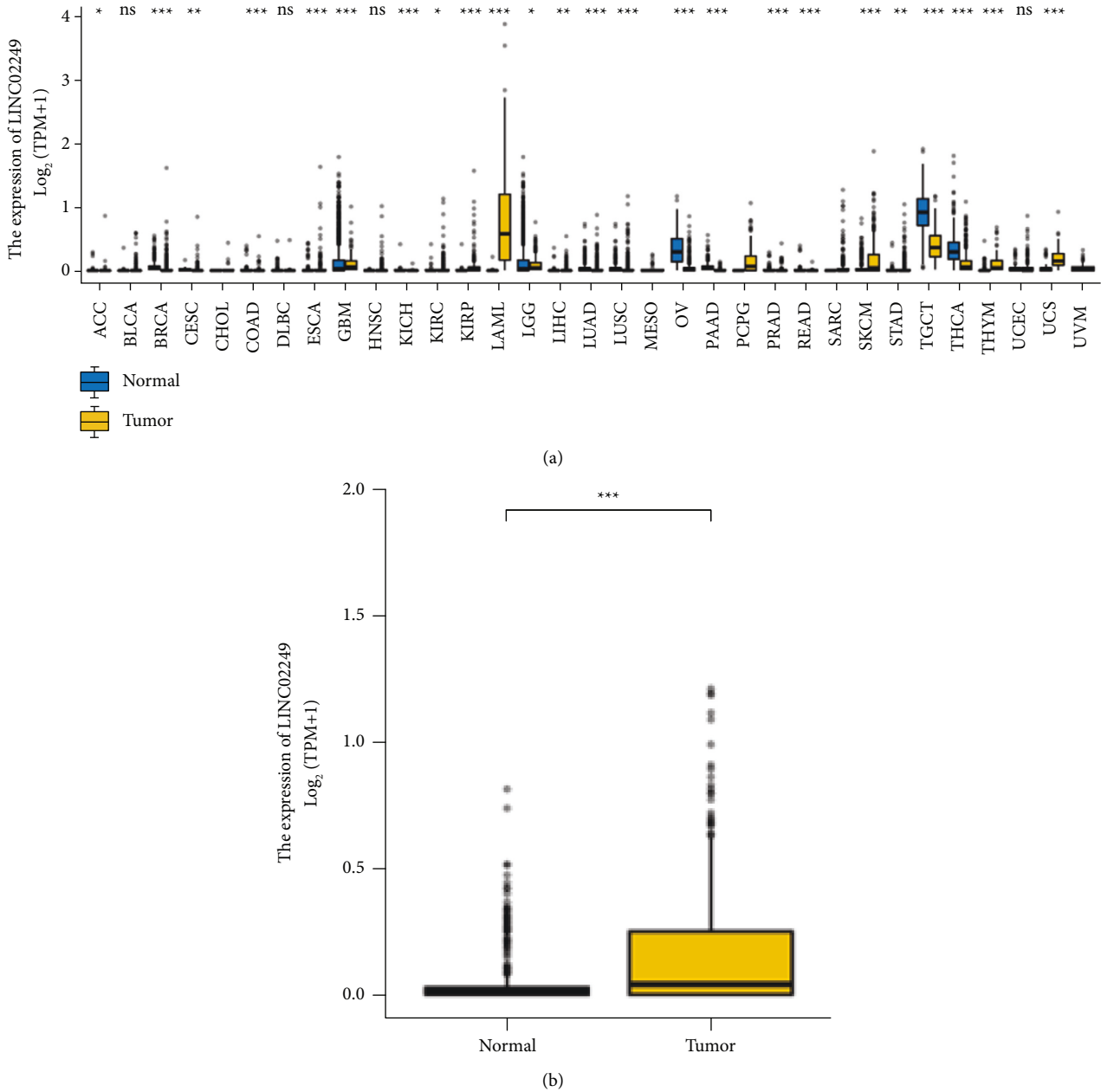
FIGURE 1: Expression assays for LINC02249 in multiple tumors. (a) LINC02249 expression in pan-cancer ($^{*}p < 0.05$; $^{**}p < 0.001$; and $^{***}p < 0.0001$). (b) LINC02249 expression was distinctly increased in SKCM specimens compared with nontumor specimens. $^{***}p < 0.001$.

observed in 18 tumors: ACC, BLCA, CESC, COAD, ESCA, KICH, KIRC, LIHC, LUAD, LUSC, OV, PAAD, PRAD, READ, STAD, TGCT, THCA,and UCEC (Figure 1(a)). Our findings suggested that LINC02249 expression was distinctly increased in most types of tumors, suggesting it as an oncogene in tumors. However, high LINC02249 expression was observed in five tumors, especially in SKCM (Figure 1(b)). Our findings suggested LINC02249 may exhibit a different role based on specific tumor types.

3.2. KEGG and GO Enrichment Analyses of DEGs. We analyzed the DEGs between LINC02249 high and low expression subgroups and identified 135 DEGs. To study the possible effects of DEGs on tumor progression, we carried out GO enrichment analyses, including biological processes (BP), molecular functions (MF), and cellular components (CC). We observed that changes in MF of DEGs were distinctly enriched in the chemokine activity, tubulin binding, histone kinase activity, and microtubule binding.

(a)

(b)
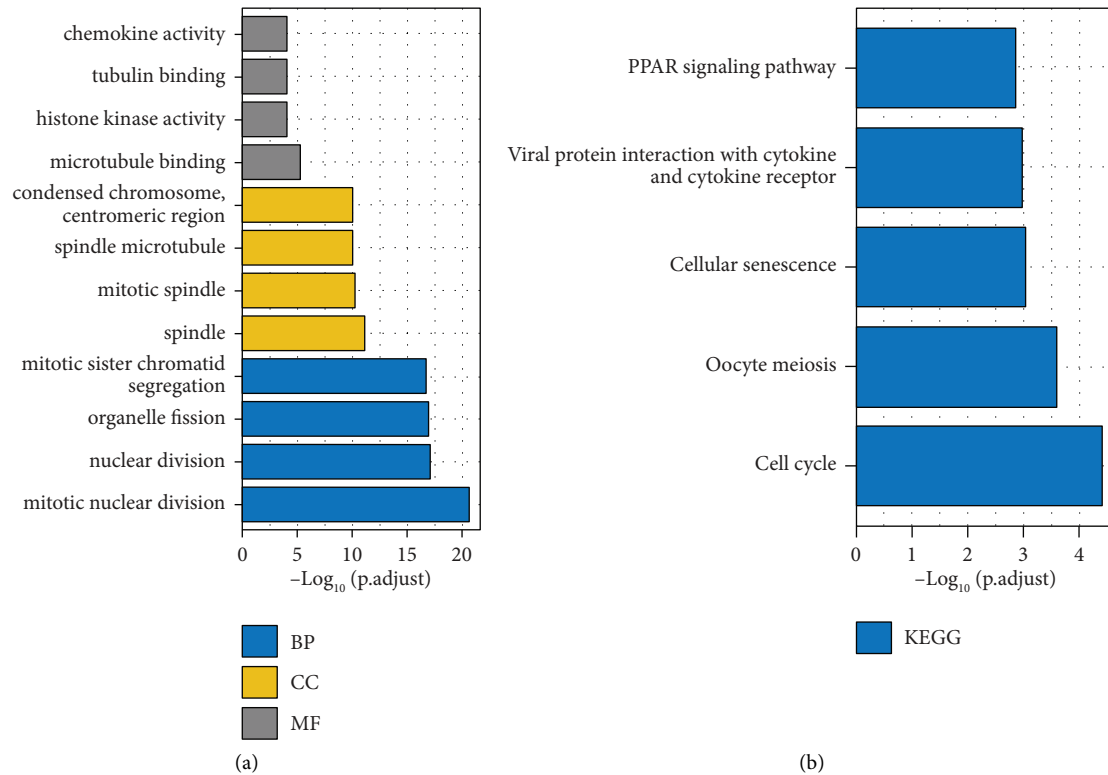
FIGURE 2: GO terms and KEGG pathway enrichment analysis of LINC02249. (a) GO terms and (b) KEGG pathway enrichment analysis of DEGs between the high LINC02249 expression group and low LINC02249 expression group.

For CC, DEGs were largely enriched in microtubule binding, spindle microtubule, mitotic spindle, and spindle. Within the BP category, mitotic sister chromatid segregation, organelle fission, nuclear division, and mitotic nuclear division were predominant (Figure 2(a)). KEGG enrichment analysis showed that PPAR signaling pathway, viral protein interaction with cytokine and cytokine receptor, cellular senescence, oocyte meiosis, and ell cycle were significantly enriched in DEGs (Figure 2(b)).

3.3. The Clinical Significance and Prognostic Value of LINC02249 in SKCM Patients.

We analyzed the relationship between the LINC02249 expression level and the clinico-pathological factors of the SKCM patients in order to elucidate the underlying function of LINC02249 in the development of SKCM. This was done so that we could better understand how LINC02249 contributed to the progression of SKCM. However, there was no significant association with the normal factors (Figure 3 and Table 1). To further investigate the correlation between LINC02249 expression and long-term survivals of SKCM patients, we used Kaplan–Meier survival and log-rank analysis. We found that patients with high LINC02249 expressions showed a shorter overall survival (Figure 4(a)) and disease-specific survival (Figure 4(b)) than those with low LINC02249 expression. Moreover, we performed subgroup analysis. Interestingly, we found that LINC02249 was more suitable for the prediction of the clinical outcomes of female patients than male patients ($p = 0.001$ vs. $p = 0.046$,

Figures 4(c) and 4(d)). On the other hand, we observed it was better that LINC02249 was used to predict the overall survival of SKCM patients with advanced stage (Figures 4(e)–4(g)). Finally, we performed Cox proportional hazards regression analysis to explore the effects of LINC02249 and clinicopathological factors on patient survival. The univariate analysis demonstrated that pathologic stage, age, and LINC02249 expression were significantly associated with overall survival (Table 2) and disease-specific survival (Table 3) of SKCM patients. More importantly, multivariate assays showed that LINC02249 was an independent prognostic factor for overall survival (Table 2) and disease-specific survival (Table 3) of SKCM patients.

3.4. Relationship of Estimate-Stromal-Immune Scores and LINC02249 Expression.

Subsequently, using the estimate package in R, we compared the immunological and stromal scores of each of these individuals. The subsequent step was to collect data from 471 patients who had complete immune and stromal scores. We found the expression of LINC02249 was distinctly negatively associated with stromal scores, immune scores, and estimate scores (Figure 5(a)).

3.5. LINC02249 Expression Correlates with Immune Cell Infiltration in SKCM Tissues.

The degree of immune infiltration into the microenvironment of the tumor was an important component in determining both the effectiveness of anticancer treatment and the final prognosis of the
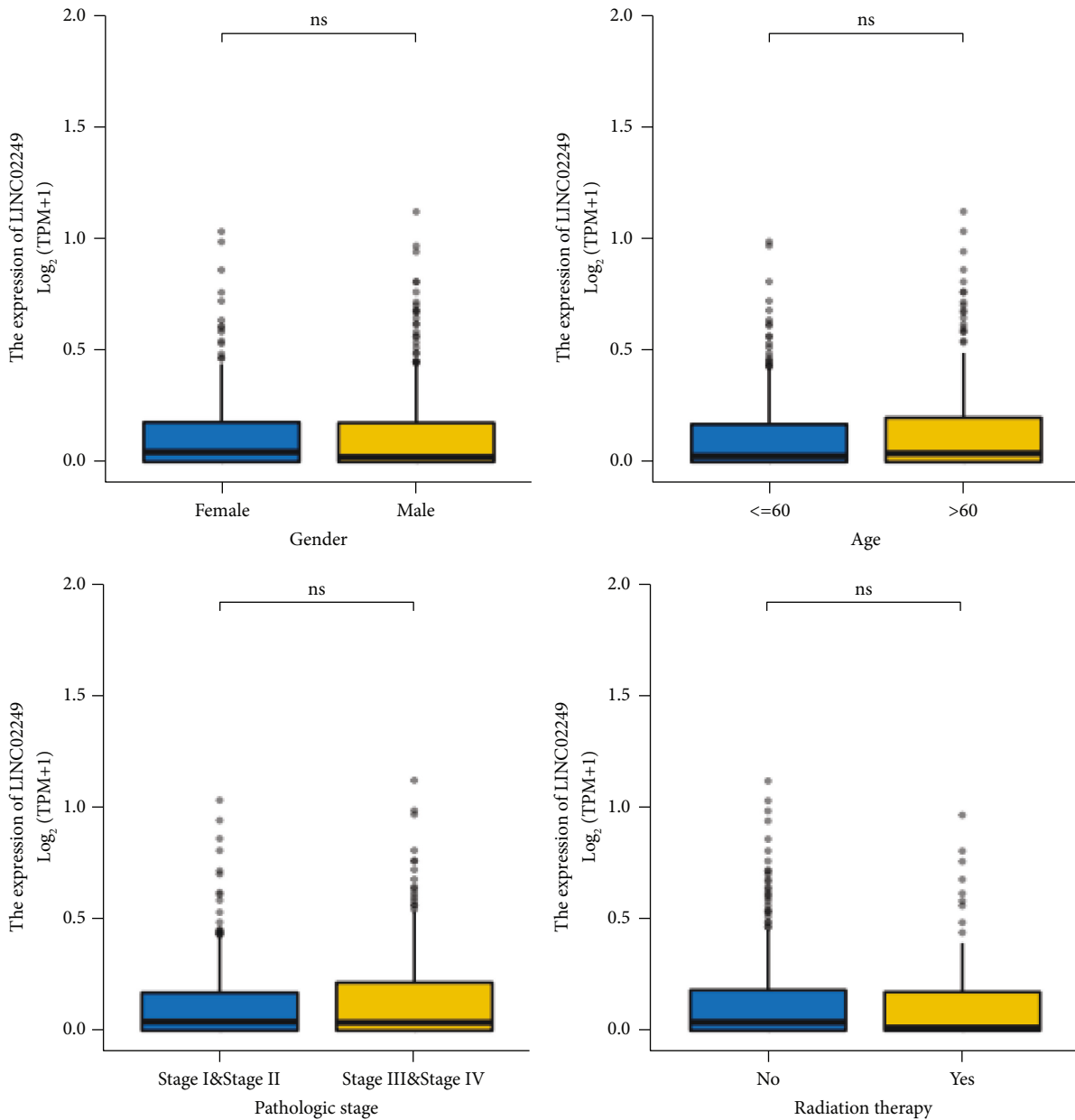
FIGURE 3: The associations between LINC02249 expression and several clinical factors, including gender, age, pathologic stage, and radiation therapy. ns: no statistical significance.

patient. In SKCM tissues, we investigated whether or not there was a link between the expression of LINC02249 and immune infiltration profiles. The findings demonstrated that out of the 24 different types of infiltrating immune cells, 11 of those types displayed a strong inverse correlation with the following: NK CD56bright cells, NK CD56dim cells, DC, B cells, Th1 cells, cytotoxic cells, neutrophils, iDC, T cells, pDC, macrophages, Treg, and aDC cells (Figure 5(b)). In addition, the different expression of 24 types of infiltrating immune cells between LINC02249 high and low expression subgroups was shown in Figure 5(c). According to these findings, an increase in LINC02249 expression might be followed by a decrease in anticancer immune infiltration, which would lead to a poorer prognosis for patient survival.

4. Discussion

SKCM is caused by the change of skin melanocytes into cancerous cells [25]. It is characterized by a high degree of malignancy, a strong invasiveness, and the fact that it can affect people of any age [26, 27]. If it is not actively treated, there is a high risk that it will migrate through the dermis and metastasis. Patients diagnosed with SKCM have a bad prognosis and a high mortality rate as a result [28]. Even though a number of different treatment modalities like targeted therapy, immunotherapy, chemotherapy, and radiotherapy have been utilized to enhance long-term survivals of patients, issues like limited drug sensitivity and drug resistance still need to be taken into consideration

TABLE 1: Association of LINC02249 expression levels with clinical factors in SKCM patients.

Characteristics	Low expression of LINC02249	High expression of LINC02249	p
n	235	236	
Age, n (%)			0.200
≤60	132 (28.5%)	120 (25.9%)	
>60	97 (21%)	114 (24.6%)	
Gender, n (%)			0.063
Female	79 (16.8%)	100 (21.2%)	
Male	156 (33.1%)	136 (28.9%)	
Pathologic stage, n (%)			0.061
Stage I	46 (11.2%)	31 (7.5%)	
Stage II	57 (13.8%)	83 (20.1%)	
Stage III	84 (20.4%)	87 (21.1%)	
Stage IV	11 (2.7%)	13 (3.2%)	
Radiation therapy, n (%)			0.120
No	183 (39.4%)	200 (43.1%)	
Yes	47 (10.1%)	34 (7.3%)	
Age, median (IQR)	57 (47, 68)	60 (48, 73)	0.040

Overall Survival
HR = 1.72 (1.31–2.26)
P < 0.001

LINC02249
Low
High

(a)

Disease Specific Survival
HR = 1.69 (1.27–2.25)
P < 0.001

LINC02249
Low
High

(b)
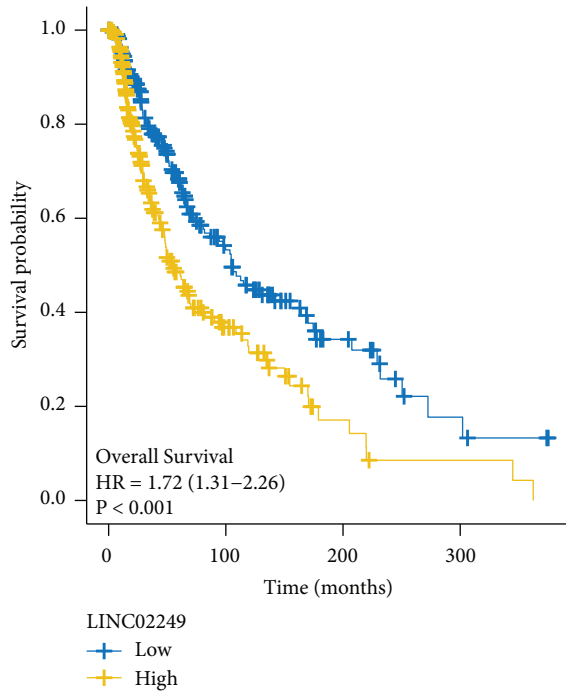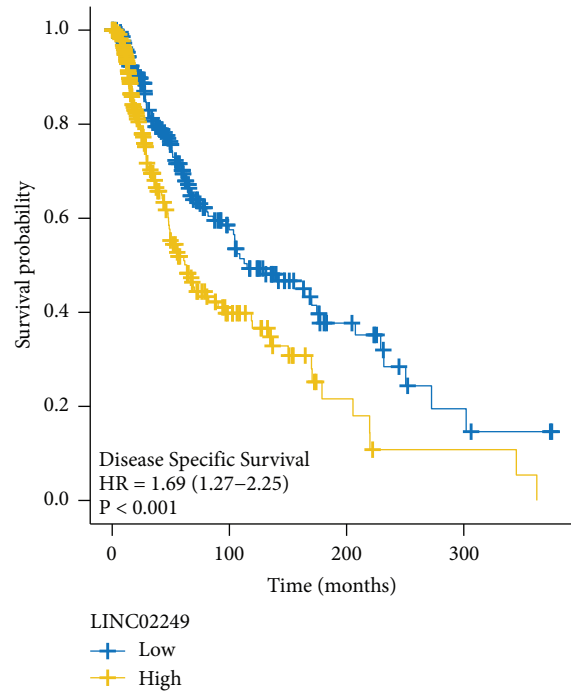
FIGURE 4: Continued.

(c)

(d)

(e)

(f)

FIGURE 4: Continued.

Pathologic stage: Stage IV

Overall Survival
HR = 2.37 (0.61−9.20)
P = 0.211

LINC02249
— Low
— High

(g)
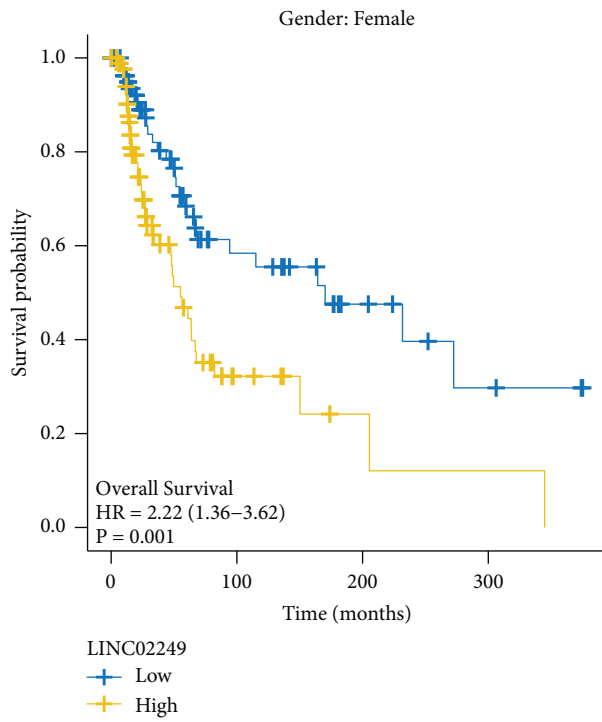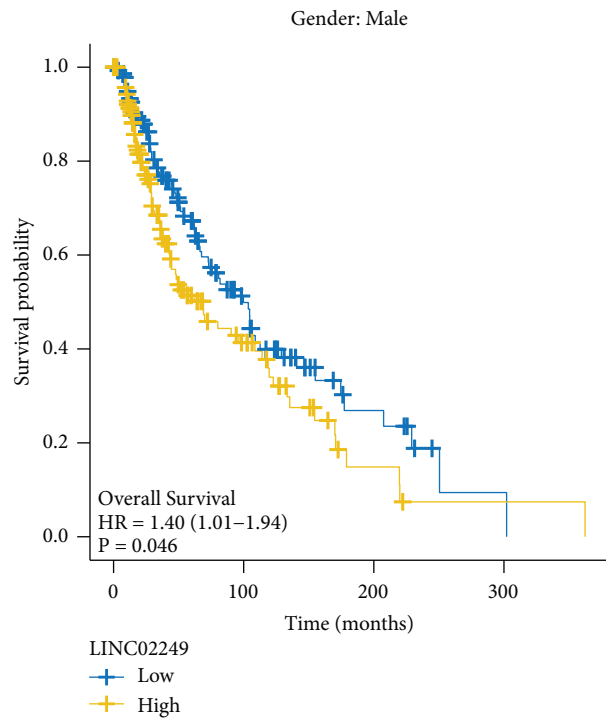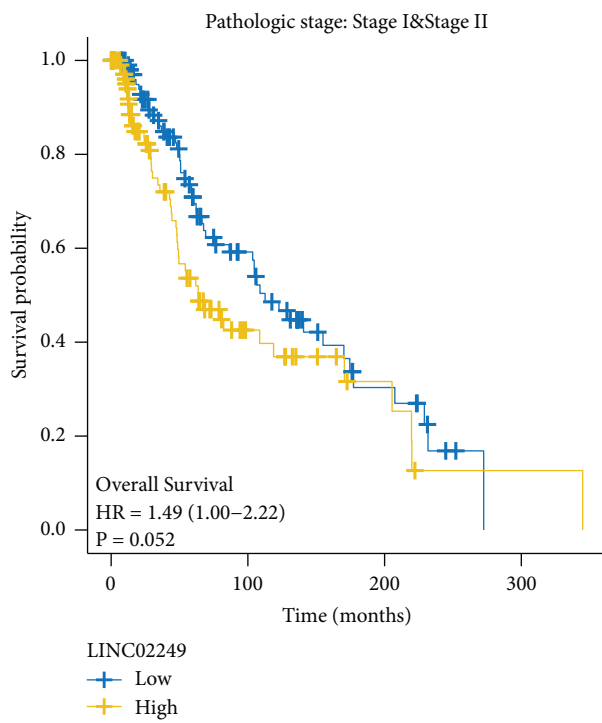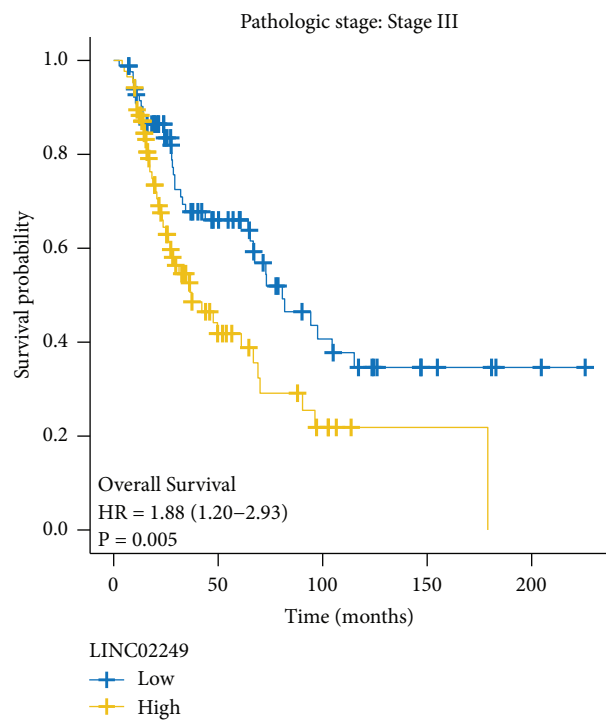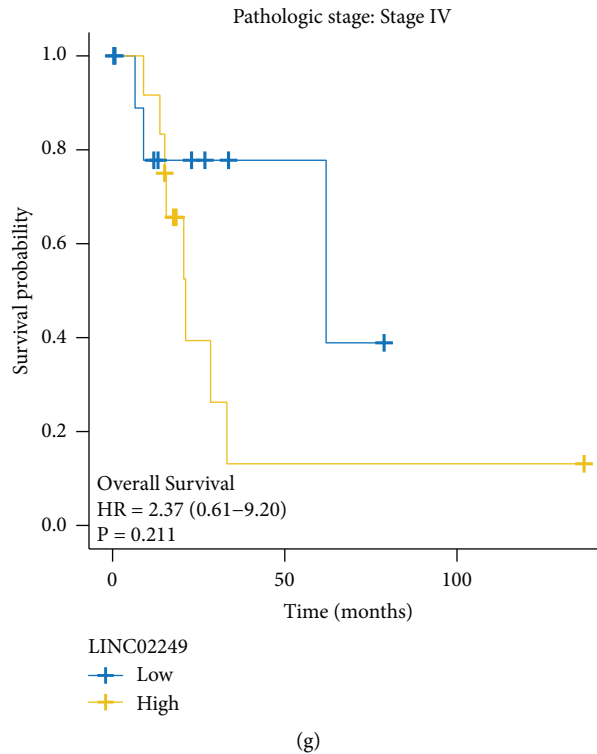
FIGURE 4: Kaplan–Meier survival curves for SKCM patients in TCGA dataset. (a, b) The overall survival and disease-specific survival rates of the high LINC02249 expression group and low LINC02249 expression group. (d–g) Stratified analyses of clinicopathological factors in SKCM: (c) female, (d) male, (e) pathologic stage (I-II), (f) pathologic stage (I-II), and (g) pathologic stage (IV).

TABLE 2: Univariate and multivariate analyses for overall survival in SKCM patients.

Characteristics	Total (N)	Univariate analysis		Multivariate analysis	
		Hazard ratio (95% CI)	p value	Hazard ratio (95% CI)	p value
Pathologic stage	410				
Stage I and Stage II	217	Reference			
Stage III and Stage IV	193	1.617 (1.207–2.165)	**0.001**	1.723 (1.283–2.314)	**<0.001**
Gender	456				
Female	172	Reference			
Male	284	1.172 (0.879–1.563)	0.281		
Age	456				
≤60	246	Reference			
>60	210	1.656 (1.251–2.192)	**<0.001**	1.461 (1.089–1.962)	**0.012**
LINC02249	456				
Low	226	Reference			
High	230	1.724 (1.315–2.260)	**<0.001**	1.693 (1.267–2.263)	**<0.001**

[29, 30]. Therefore, it is of the utmost need to locate additional prognostic biomarkers and possible medications for SKCM.

Over the past few years, an increasing number of studies have indicated that long noncoding RNAs (lncRNAs) may be implicated in the advancement of SKCM. For instance, An et al. reported that AGAP2-AS1 was significantly higher in melanoma than in healthy tissues, and the researchers found that the level of AGAP2-AS1 in cancer tissues was significantly connected to the TNM stage of the patient's

malignancy. Individuals who had a high level of AGAP2-AS1 had a survival duration that was noticeably lower than that of patients who had a low level of AGAP2-AS1, and this was true for both progression-free survival and overall survival [31]. In melanoma, inhibiting the expression of the long noncoding RNA AGAP2-AS1 has the functional effect of reducing carcinogenesis and ferroptosis resistance via the SLC7A11-IGF2BP2 pathway. Shan et al. showed that lncRNA SNHG8 levels were distinctly increased in melanoma specimens, and melanoma cell viability, migration,

TABLE 3: Univariate and multivariate analyses for disease-specific survival in SKCM patients.

Characteristics	Total (N)	Univariate analysis		Multivariate analysis	
		Hazard ratio (95% CI)	p value	Hazard ratio (95% CI)	p value
Pathologic stage	405				
Stage I and Stage II	215	Reference			
Stage III and Stage IV	190	1.536 (1.125–2.096)	**0.007**	1.632 (1.192–2.233)	**0.002**
Gender	450				
Female	172	Reference			
Male	278	1.161 (0.855–1.575)	0.340		
Age	450				
≤60	244	Reference			
>60	206	1.699 (1.258–2.294)	**<0.001**	1.484 (1.085–2.031)	**0.014**
LINC02249	450				
Low	224	Reference			
High	226	1.690 (1.266–2.255)	**<0.001**	1.627 (1.196–2.213)	**0.002**

(a)

(b)
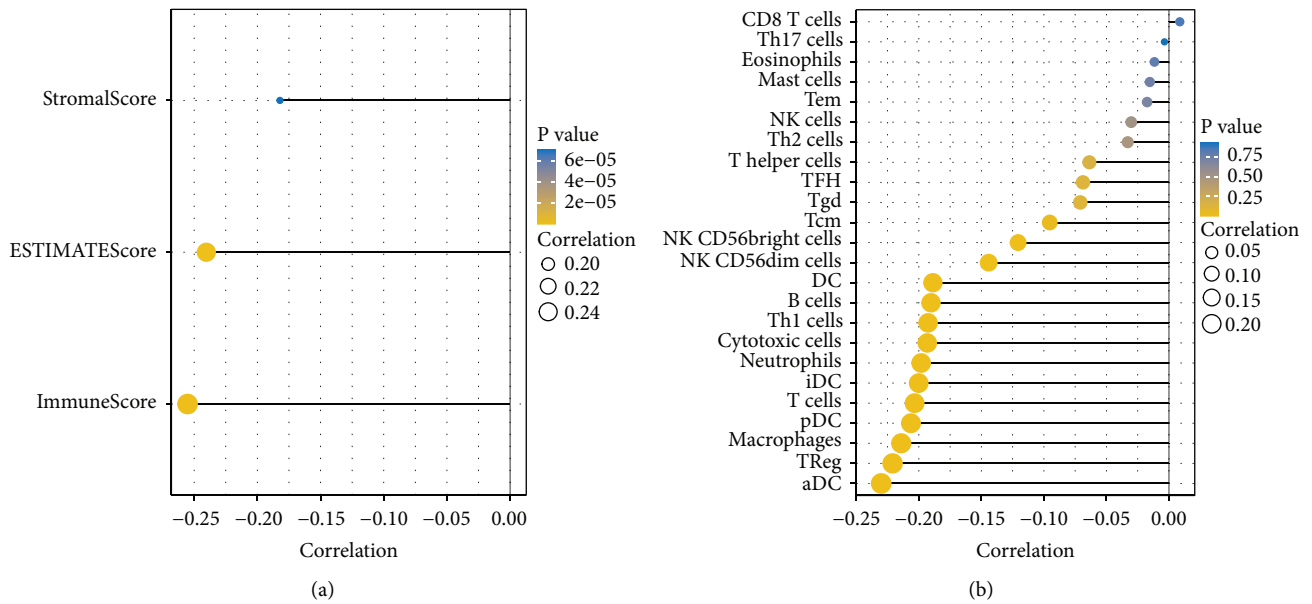
FIGURE 5: Continued.
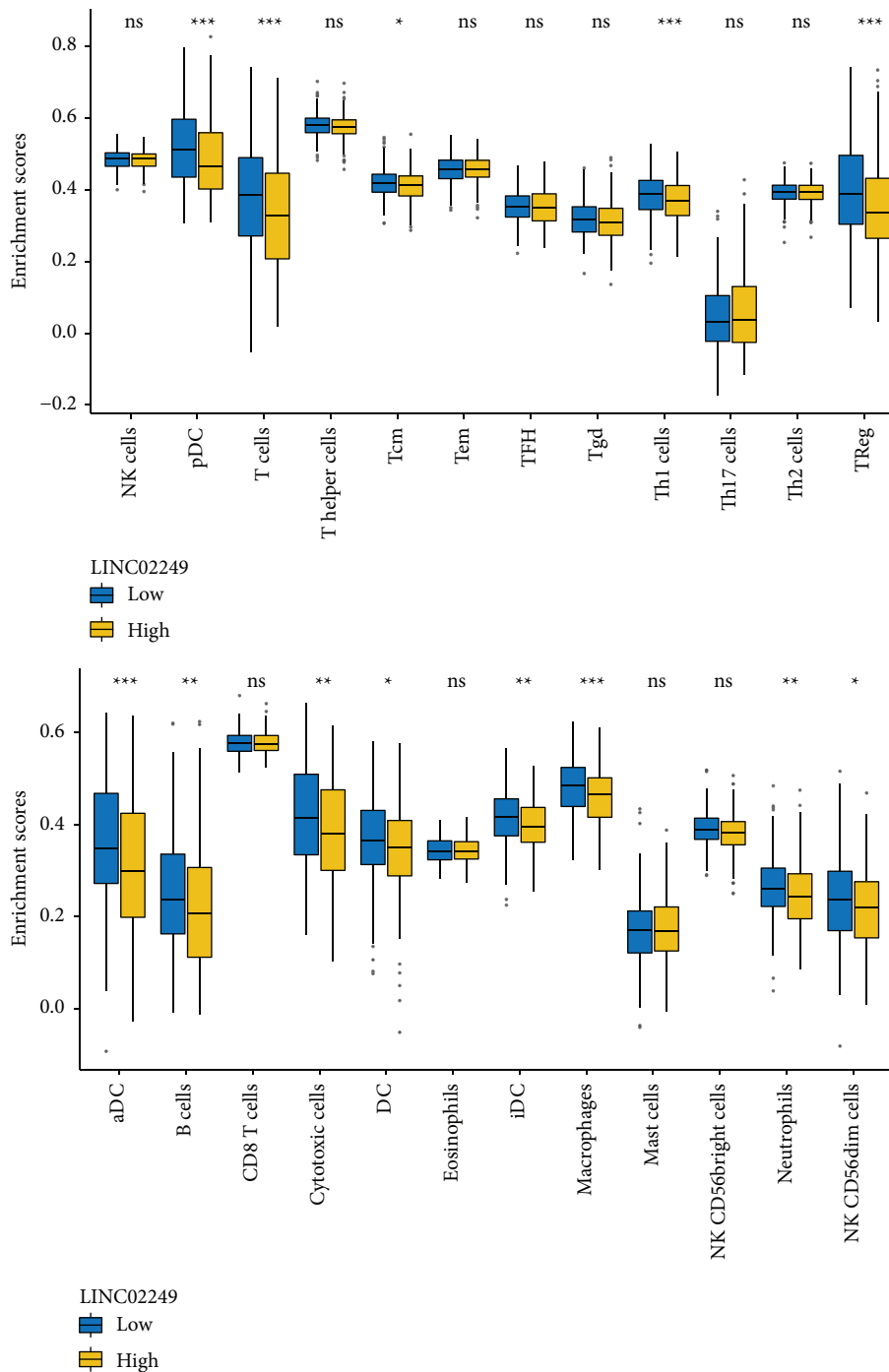
(c)

Figure 5: Immune infiltration analysis of LINC02249. (a) The association between LINC02249 expression and immune and stromal scores by the use of ESTIMATE algorithm. (b, c) In order to measure the difference in immune infiltration between patients with low and high LINC02249 levels, the ssGSEA algorithm was applied.

and invasion were all inhibited by inhibiting the lncRNA SNHG8 pathway, which was mediated by the miRNA-656-3p/SERPINE1 axis [32]. We initially found the differential expression of LINC02249 in SKCM utilizing data on pan-cancer that was freely available to the public in order to acquire a comprehensive grasp of the role that LINC02249 plays in SKCM. We were able to demonstrate that

LINC02249 was differentially expressed in a number of different cancers; in particular, the expression of LINC02249 was found to be considerably elevated in SKCM in comparison to other tumors. According to our findings, the differential expression of LINC02249 might be exclusive to certain tissues, and it served as a tumor promotor in SKCM. Then, KEGG assays confirmed that LINC02249 may play an

important role in the regulation of PPAR signaling pathway, viral protein interaction with cytokine and cytokine receptor, cellular senescence, oocyte meiosis, and cell cycle. Moreover, we analyzed the prognostic value of LINC02249 expression in SKCM patients, finding that high LINC02249 expression was associated with shorter overall survival and disease-specific survival. More importantly, multivariate analysis showed that LINC02249 were an independent prognostic factor for overall survival and disease-specific survival of SKCM patients.

We explored the expression of LINC02249 and the infiltration of immune cells in the tumor tissue because gene alterations may contribute to an abnormal immune microenvironment in malignancies [33, 34]. LINC02249 is a lncRNA that may lead to abnormal immune microenvironments in cancers. Immune evasion and immunosuppression have emerged as critical areas for tumor-targeted therapy in recent years [35, 36]. The development of tumor antigen-specific T cells is a crucial step in the process of antitumor immune surveillance, and macrophages have a part to play at every stage of the progression of tumors, from tumor initiation through tumor spread. It is beyond question that macrophages with an M2-like phenotype might contribute to immunosuppression, tumor development, and angiogenesis [37, 38]. In our study, we found the expression of LINC02249 was distinctly negatively associated with stromal scores, immune scores, and estimate scores. Moreover, we found that the results showed that among 24 types of infiltrating immune cells, 11 types showed a strong negative correlation with NK CD56bright cells, NK CD56dim cells, DC, B cells, Th1 cells, cytotoxic cells, neutrophils, iDC, T cells, pDC, macrophages, Treg, and aDC. Incorrect signal transduction had a significant role in the progression of the tumor. T cell infiltration and its functional pathway is a signaling pathway that has been conserved throughout the evolution. This pathway regulated the immunologic status of the tumor, and as a result, has an effect on the outcome. Our new knowledge of how LINC02249 influenced the immune microenvironment in individuals with SKCM may be beneficial to the development of future medicines that target tumors specifically.

This study had several limitations. First, the information used in our research came from publicly available sources, such as the TCGA datasets. Thus, an evaluation of the reliability of the data was impossible. Second, extensive research must be conducted on the biological roles of LINC02249, and these functions must be clarified through *in vitro* and *in vivo* tests. Particular attention must be paid to the immunological infiltration process.

5. Conclusion

We observed that LINC02249 was significantly expressed in a variety of human cancers (including SKCM), and its upregulation was related with a poor outcome in SKCM. Besides, we discovered that the expression of LINC02249 was connected to the invasion of immune cells. LINC02249 has the potential to function as an independent prognostic biomarker for SKCM. In addition, the research lays the theoretical groundwork for treatment objectives.

Data Availability

The datasets used to support the findings of this study are available from the corresponding author upon reasonable request.

Conflicts of Interest

The authors declare that they have no conflicts of interest.

Supplementary Materials

Table S1: the full names of pan-cancers in TCGA datasets. (*Supplementary Materials*)

References

[1] R. L. Siegel, K. D. Miller, H. E. Fuchs, and A. Jemal, "Cancer statistics, 2021," *CA: A Cancer Journal for Clinicians*, vol. 71, pp. 7–33, 2021.

[2] C. de Martel, D. Georges, F. Bray, J. Ferlay, and G. M. Clifford, "Global burden of cancer attributable to infections in 2018: a worldwide incidence analysis," *Lancet Global Health*, vol. 8, pp. e180–e190, 2020.

[3] H. Gogas, A. M. Eggermont, A. Hauschild et al., "Biomarkers in melanoma," *Annals of Oncology*, vol. 20, no. Suppl 6, pp. vi8–13, 2009.

[4] M. Marzagalli, N. D. Ebelt, and E. R. Manuel, "Unraveling the crosstalk between melanoma and immune cells in the tumor microenvironment," *Seminars in Cancer Biology*, vol. 59, pp. 236–250, 2019.

[5] K. J. Ransohoff, P. D. Jaju, J. Y. Tang, M. Carbone, S. Leachman, and K. Y. Sarin, "Familial skin cancer syndromes: increased melanoma risk," *Journal of the American Academy of Dermatology*, vol. 74, no. 3, pp. 423–434, 2016.

[6] P. Terheyden, A. Krackhardt, and T. Eigentler, "The systemic treatment of melanoma," *Deutsches Arzteblatt International*, vol. 116, no. 29-30, pp. 497–504, 2019.

[7] C. Wohlmuth and I. Wohlmuth-Wieser, "Vulvar melanoma: molecular characteristics, diagnosis, surgical management, and medical treatment," *American Journal of Clinical Dermatology*, vol. 22, no. 5, pp. 639–651, 2021.

[8] A. Slominski, J. Wortsman, A. J. Carlson, L. Y. Matsuoka, C. M. Balch, and M. C. Mihm, "Malignant melanoma," *Archives of Pathology and Laboratory Medicine*, vol. 125, no. 10, pp. 1295–1306, 2001.

[9] E. A. Merkel, L. S. Mohan, K. Shi, E. Panah, B. Zhang, and P. Gerami, "Paediatric melanoma: clinical update, genetic basis, and advances in diagnosis," *The Lancet Child and Adolescent Health*, vol. 3, no. 9, pp. 646–654, 2019.

[10] U. Gowthaman, D. García-Pichardo, Y. Jin, I. Schwarz, and S. Marquardt, "DNA processing in the context of noncoding transcription," *Trends in Biochemical Sciences*, vol. 45, no. 12, pp. 1009–1021, 2020.

[11] A. B. Herman, D. Tsitsipatis, and M. Gorospe, "Integrated lncRNA function upon genomic and epigenomic regulation," *Molecular Cell*, vol. 82, no. 12, pp. 2252–2266, 2022.

[12] C. J. Guo, G. Xu, and L. L. Chen, "Mechanisms of long noncoding RNA nuclear retention," *Trends in Biochemical Sciences*, vol. 45, no. 11, pp. 947–960, 2020.

[13] Y. Zhang, Y. Tao, and Q. Liao, "Long noncoding RNA: a crosslink in biological regulatory network," *Briefings in Bioinformatics*, vol. 19, no. 5, pp. 930–945, 2018.

[14] S. P. Hu, M. X. Ge, L. Gao, M. Jiang, and K. W. Hu, "LncRNA HCP5 as a potential therapeutic target and prognostic biomarker for various cancers: a meta-analysis and bioinformatics analysis," *Cancer Cell International*, vol. 21, no. 1, p. 686, 2021.

[15] Z. Y. Chen, J. Q. Huang, Y. Zhu, Y. S. Chen, and X. F. Yu, "Comprehensive analysis of the immune implication of TEX41 in skin cutaneous melanoma," *Disease Markers*, vol. 2021, pp. 1–11, 2021.

[16] Y. Wang, D. Li, J. Lu et al., "Long noncoding RNA TTN-AS1 facilitates tumorigenesis and metastasis by maintaining TTN expression in skin cutaneous melanoma," *Cell Death and Disease*, vol. 11, no. 8, p. 664, 2020.

[17] M. Huarte, "The emerging role of lncRNAs in cancer," *Nature Medicine*, vol. 21, no. 11, pp. 1253–1261, 2015.

[18] Q. Zheng, Q. Zhang, X. Yu, Y. He, and W. Guo, "FENDRR: a pivotal, cancer-related, long non-coding RNA," *Biomedicine and Pharmacotherapy*, vol. 137, no. 2021, Article ID 111390, 2021.

[19] F. Li, X. Li, L. Qiao, W. Liu, C. Xu, and X. Wang, "MALAT1 regulates miR-34a expression in melanoma cells," *Cell Death and Disease*, vol. 10, no. 6, p. 389, 2019.

[20] J. Jen, Y. A. Tang, Y. H. Lu, C. C. Lin, W. W. Lai, and Y. C. Wang, "Oct4 transcriptionally regulates the expression of long non-coding RNAs NEAT1 and MALAT1 to promote lung cancer progression," *Molecular Cancer*, vol. 16, no. 1, p. 104, 2017.

[21] J. Kim, H. L. Piao, B. J. Kim et al., "Long noncoding RNA MALAT1 suppresses breast cancer metastasis," *Nature Genetics*, vol. 50, no. 12, pp. 1705–1715, 2018.

[22] Y. Z. Chang, R. C. Chai, B. Pang et al., "METTL3 enhances the stability of MALAT1 with the assistance of HuR via m6A modification and activates NF-κB to promote the malignant progression of IDH-wildtype glioma," *Cancer Letters*, vol. 511, pp. 36–46, 2021.

[23] T. Hao, Z. Wang, J. Yang, Y. Zhang, Y. Shang, and J. Sun, "MALAT1 knockdown inhibits prostate cancer progression by regulating miR-140/BIRC6 axis," *Biomedicine and Pharmacotherapy*, vol. 123, Article ID 109666, 2020.

[24] K. Yoshihara, M. Shahmoradgoli, E. Martínez et al., "Inferring tumour purity and stromal and immune cell admixture from expression data," *Nature Communications*, vol. 4, no. 1, p. 2612, 2013.

[25] A. Rajabi-Estarabadi, J. M. Bittar, C. Zheng et al., "Optical coherence tomography imaging of melanoma skin cancer," *Lasers in Medical Science*, vol. 34, no. 2, pp. 411–420, 2019.

[26] Y. A. Chen, J. K. Teer, Z. Eroglu et al., "Translational pathology, genomics and the development of systemic therapies for acral melanoma," *Seminars in Cancer Biology*, vol. 61, pp. 149–157, 2020.

[27] V. C. Ho and A. J. Sober, "Therapy for cutaneous melanoma: an update," *Journal of the American Academy of Dermatology*, vol. 22, no. 2, pp. 159–176, 1990.

[28] K. Kamposioras, G. Pentheroudakis, D. Pectasides, and N. Pavlidis, "Malignant melanoma of unknown primary site. To make the long story short. A systematic review of the literature," *Critical Reviews in Oncology*, vol. 78, no. 2, pp. 112–126, 2011.

[29] V. De Giorgi, A. Saggini, M. Grazzini et al., "Specific challenges in the management of subungual melanoma," *Expert Review of Anticancer Therapy*, vol. 11, no. 5, pp. 749–761, 2011.

[30] G. Stevens and M. J. McKay, "Dispelling the myths surrounding radiotherapy for treatment of cutaneous melanoma," *The Lancet Oncology*, vol. 7, pp. 575–583, 2006.

[31] L. An, J. Huang, S. Ge, X. Zhang, and J. Wang, "lncRNA AGAP2-AS1 facilitates tumorigenesis and ferroptosis resistance through SLC7A11 by IGF2BP2 pathway in melanoma," *Computational and Mathematical Methods in Medicine*, vol. 2022, Article ID 1972516, 8 pages, 2022.

[32] B. Shan, S. Qu, S. Lv, D. Fan, and S. Wang, "YY1-induced long non-coding RNA small nucleolar RNA host gene 8 promotes the tumorigenesis of melanoma via the microRNA-656-3p/SERPINE1 mRNA binding protein 1 axis," *Bioengineered*, vol. 13, no. 3, pp. 4832–4843, 2022.

[33] K. DePeaux and G. M. Delgoffe, "Metabolic barriers to cancer immunotherapy," *Nature Reviews Immunology*, vol. 21, no. 12, pp. 785–797, 2021.

[34] M. McLaughlin, E. C. Patin, M. Pedersen et al., "Inflammatory microenvironment remodelling by tumour cells after radiotherapy," *Nature Reviews Cancer*, vol. 20, no. 4, pp. 203–217, 2020.

[35] A. K. Singh and J. P. McGuirk, "CAR T cells: continuation in a revolution of immunotherapy," *The Lancet Oncology*, vol. 21, no. 3, pp. e168–e178, 2020.

[36] A. Tanaka and S. Sakaguchi, "Regulatory T cells in cancer immunotherapy," *Cell Research*, vol. 27, no. 1, pp. 109–118, 2017.

[37] Y. Zhu, X. An, X. Zhang, Y. Qiao, T. Zheng, and X. Li, "STING: a master regulator in the cancer-immunity cycle," *Molecular Cancer*, vol. 18, no. 1, p. 152, 2019.

[38] K. Okła, D. L. Farber, and W. Zou, "Tissue-resident memory T cells in tumor immunity and immunotherapy," *Journal of Experimental Medicine*, vol. 218, no. 4, Article ID e20201605, 2021.

Hindawi

Research Article

Machine Learning and Novel Biomarkers Associated with Immune Infiltration for the Diagnosis of Esophageal Squamous Cell Carcinoma

Jipeng Zhang,[1] **Nian Zhang,**[2] **Xin Yang,**[3] **Xiangbin Xin,**[1] **Cheng-hui Jia,**[1,4] **Sen Li,**[1,5] **Qiang Lu** [iD][1] **, Tao Jiang** [iD][1] **, and Tao Wang** [iD][1]

[1]*Department of Thoracic Surgery, Tangdu Hospital, The Air Force Military Medical University, Xi'an 710038, Shaanxi, China*
[2]*Department of Anesthesiology, Tangdu Hospital, The Air Force Military Medical University, Xi'an 710038, Shaanxi, China*
[3]*Pathology Department, The Second Affiliated Hospital of Shaan Xi University of Traditional Chinese Medicine, Xi'an 710038, Shaanxi, China*
[4]*Department of Thoracic Surgery, The First Affiliated Hospital of Xi'an Medical College, Xi'an 710000, China*
[5]*Department of Cardio-Thoracic Surgery, Luohe Centre Hospital, Luohe 462000, Henan, China*

Correspondence should be addressed to Qiang Lu; luqiang@fmmu.edu.cn, Tao Jiang; jiangtaochest@163.com, and Tao Wang; tddocwangt@163.com

Esophageal squamous cell carcinoma (ESCC) accounts for the main esophageal cancer type, which is related to advanced stage and poor survivals. Therefore, novel diagnostic biomarkers are critically needed. In the current research, we aimed to screen novel diagnostic biomarkers based on machine learning. The expression profiles were obtained from GEO datasets (GSE20347, GSE38129, and GSE75241) and TCGA datasets. Differentially expressed genes (DEGs) were screened between 47 ESCC and 47 nontumor samples. The LASSO regression model and SVM-RFE analysis were carried out for the identification of potential markers. ROC analysis was carried out to assess discriminatory abilities. The expressions and diagnostic values of the candidates in ESCC were demonstrated in the GSE75241 datasets and TCGA datasets. We also explore the correlations between the critical genes and cancer immune infiltrates using CIBERSORT. In this study, we identified 27 DEGs in ESCC: 5 genes were significantly elevated, and 22 genes were significantly decreased. Based on the results of the SVM-RFE and LASSO regression model, we identified five potential diagnostic biomarkers for ESCC, including GPX3, COL11A1, EREG, MMP1, and MMP12. However, the diagnostic values of only GPX3, MMP1, and MMP12 were confirmed in GSE75241 datasets. Moreover, in TCGA datasets, we further confirmed that GPX3 expression was distinctly decreased in ESCC specimens, while the expression of MMP1 and MMP12 was noticeably increased in ESCC specimens. Immune cell infiltration analysis revealed that the expression of GPX3, MMP1, and MMP12 was associated with several immune, such as T cells CD8, macrophages M2, macrophages M0, and dendritic cells activated. Overall, our findings suggested GPX3, MMP1, and MMP12 as novel diagnostic marker and correlated with immune infiltrates in ESCC patients.

1. Introduction

Esophageal cancer (EC) is one of the most common malignancies worldwide, which is always accompanied by high morbidity and mortality [1]. Esophageal cell squamous carcinoma (ESCC) accounts for over 80% of all cases of EC in China [2]. Surgery, radiation therapy, and chemotherapy

are the only treatment options that are currently available; despite the significant progress that has been made in the treatment of this illness, the patient survival rate within five years is still extremely low [3, 4]. This is due to the fact that the only treatment options that are currently available are those three. Metastatic ESCC patients have a five-year survival rate of fewer than 5% [5]. ESCC often spreads to

the liver, lung, bone, and brain [6]. For the detection of ESCC, they are ineffective because they lack appropriate sensitivity and specificity [7]. Therefore, novel and reliable molecular biomarkers to complement and improve on current ESCC screening strategies are urgently needed.

The investigation of gene expression profiles using microarrays has become a frequent method for locating important hub genes and important pathways [8]. In this day and age of integrated bioinformatics, it is not a problem to get data; rather, the task of normalization appears to be a challenging one. It is possible to perform prognosis studies on cancer patients using microarray techniques in addition to identifying genes associated with various diseases and potential antitumor medication targets [9, 10]. In addition, microarray techniques have an important ability in analyzing the associations between the expression of functional genes and their modulation [11, 12]. In the field of clinical research, they are also responsible for contributing ideas for the diagnosis and treatment of specific disorders. We found that there have been studies exploring the diagnostic genes of many types of tumors, but the application of machine-learning for the identification of novel diagnostic biomarkers for ESCC was rarely reported. In the current study, we performed a joint analysis in multidatabases to explore diagnostic marker genes for ESCC patients.

2. Materials and Methods

2.1. Microarray Data. The microarray dataset GSE20347, GSE38129, and GSE75241 was downloaded from the Gene Expression Omnibus (GEO) database. The GSE20347 dataset included 17 pairs of ESCC and nontumor specimens, whereas the GSE38129 dataset included 30 pairs of ESCC and nontumor specimens. Due to the fact that the GSE38129 datasets share a platform and are important for merging data from a variety of datasets, they have been combined into a metadata cohort for the purpose of doing additional integration analysis. In addition, the combat function contained inside the "SVA" software package in R was utilized in order to eliminate the batch effect. In addition, the validation cohort comprised 15 pairs of ESCC tissues and neighboring normal tissues, which were taken from the GSE75241 datasets.

2.2. Identification of Differentially Expressed Genes (DEGs). The DEG analysis was carried out with the help of the Limma program [13]. In order to evaluate the changes in gene expression, an empirical Bayesian methodology was adopted, and moderated t-tests were utilized. The DEGs are genes that had an adjusted p value that was lower than 0.05 and had an absolute fold change that was higher than 3.

2.3. GO Term and KEGG Pathway Enrichment Analysis. The biological importance of DEGs was investigated using GO term enrichment analysis, which included biological processes, cellular components, and molecular functions. This research was conducted using the "GOstats" program included in Bioconductor. The KEGG pathway enrichment analysis of DEGs was carried out by the "GeneAnswers"

Bioconductor program in order to identify important pathways that are closely associated with the beginning and development of ESCC. In order to reach statistical significance and achieve significant enrichment, a p value of less than 0.05 was required.

2.4. Novel Diagnostic Biomarkers Screening. When doing five-fold cross-validation, a technique known as least absolute shrinkage and selector operation (LASSO) and support vector machine-recursive feature elimination (SVM-RFE) were employed, respectively, to filter the critical genes [14, 15]. Then, in order to filter the essential diagnostic genes, we pooled the results that the LASSO and SVM-RFE algorithms had produced. The genes that were shared by the two methods were incorporated, and the expressions of novel genes were checked for accuracy using the GSE75241 datasets.

2.5. Diagnostic Value of Critical Genes in ESCC. In order to determine whether or not the found biomarkers had any predictive power, we constructed a ROC curve by comparing the levels of mRNA expression in 47 ESCC tumor specimens to 47 nontumor tissues. The value of AUC was used to measure the diagnostic efficiency in distinguishing ESCC specimens from nontumor specimens, and this finding was then verified using the GSE75241 dataset.

2.6. Estimation of Immune Cell Abundance. Based on the reference signature matrix of 547 genes, we employed CIBERSORT to analyze the percentages of various immune cells in tumor and nontumor specimens. When we ran the program with the default LM22 feature matrix at 1000 permutations, we submitted the data of gene expressions generated from the sample mixture file to the CIBERSORT web page (https://cibersort.stanford.edu/). A mixture sample's relative immune cell fraction was estimated using CIBERSORT and can be applied to compare immune cell populations within and across studies.

2.7. Statistical Analysis. All statistical analyses were conducted using R (version 3.6.3, R Core Team, Massachusetts, USA). $p < 0.05$ was considered statistically significant.

3. Results

3.1. Identification of DEGs in ESCC. Extensive retrospective analysis was performed on the GSE20347 and GSE38129 GEO datasets, which contained data on 47 ESCC and 47 nontumor samples. We used the Limma package to remove batch effects before analyzing the metadata DEGs. There were a total of 27 DEGs collected: 5 genes were significantly elevated, and 22 genes were significantly decreased (Figure 1(a)).

3.2. GO and KEGG Pathway Enrichment Analyses of DEGs. Later, we carried out GO assays using the "clusterProfiler" R package and observed that, in the BP group, the DEGs were

(a)

(b)
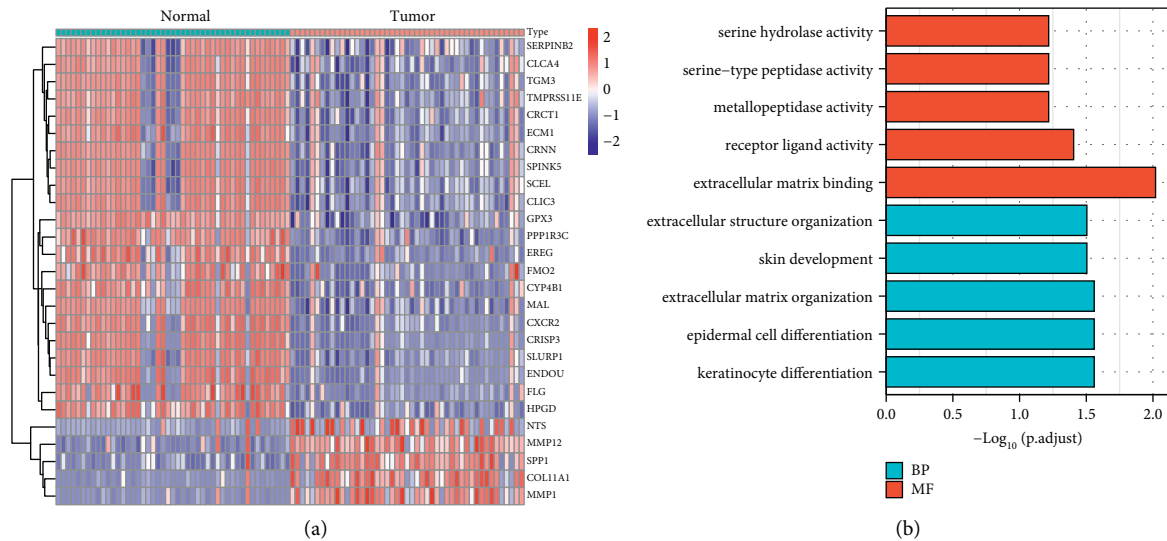
FIGURE 1: Identification of DEGs in ESCC and their enrichment analysis. (a) A total of 139 DEGs were obtained between ESCC specimens and nontumor specimens, which were shown in the heat map. (b) Representative results of GO analyses in TCGA.

mainly involved in extracellular structure organization, skin development, extracellular matrix organization, epidermal cell differentiation, and keratinocyte differentiation. In the MF group, the DEGs were mainly involved in serine hydrolase activity, serine-type peptidase activity, metallopeptidase activity, receptor ligand activity, and extracellular matrix binding (Figure 1(b)). However, the results of KEGG did not show any significant terms.

3.3. Identification and Validation of Diagnostic Feature Biomarkers.
Researchers made use of two distinct algorithms in their search for possible biomarkers. Regression analysis carried out with the LASSO algorithm helped reduce the number of DEGs, which led to the identification of eight biomarkers for ESCC (Figure 2(a)). The SVM-RFE algorithm was used to narrow down the features of the DEGs to a selection of five characteristics (Figure 2(b)). In the end, the four traits that were found to overlap between these two methods, known as GPX3, COL11A1, EREG, MMP1, and MMP12, were chosen (Figure 2(c)). GSE75241 dataset was utilized to check the expressions of five characteristics to obtain more accurate and reliable results. ESCC tissue had significantly higher levels of GPX3, MMP1, and MMP12 expression than normal tissues (Figure 3(a)). However, regarding the levels of expression of COL11A1 and EREG, there was not a discernible difference between the two groups (Figure 3(b)).

3.4. Diagnostic Effectiveness of Novel Biomarkers in ESCC.
The diagnostic abilities of GPX3, MMP1, and MMP12 in discriminating ESCC from nontumor specimens confirmed excellent diagnostic values, with an AUC of 0.939 (95% CI 0.879–0.986) in MMP12, AUC of 0.959 (95% CI 0.916–0.990) in MMP1, AUC of 0.985 (95% CI 0.963–0.100) in GPX3, AUC of 0.962 (95% CI 0.922–0.990), and AUC of 0.924 (95% CI 0.853–0.979) (Figure 4). Moreover, a powerful

discrimination ability was demonstrated in the GSE75241 dataset with an AUC of 0.920 (95% CI 0.791–0.100) in GPX3, AUC of 1.000 (95% CI 1.000–1.000) in MMP12, and AUC of 1.000 (95% CI 1.000–1.000) in MMP1 (Figure 5(a)). However, the AUC for COL11A1 and EREG was 0.556 and 0.707 (Figure 5(b)).

3.5. Pan-Cancer Expression Landscape of GPX3, MMP1, and MMP12 Based on TCGA Datasets.
We conducted pan-cancer assays based on TCGA datasets to investigate the putative roles of GPX3, MMP1, and MMP12 in malignancies. According to our findings, the GPX3 expression is markedly decreased in most cancers (Figure 6(a)), while MMP1 and MMP12 expression was distinctly upregulated in most types of tumors (Figures 6(b) and 6(c)). According to our findings in Figure 7(a), we found that MMP1 and MMP12 expression was markedly elevated in ESCC samples compared to nontumor samples, while the GPX3 expression was decreased (Figures 7(b) and 7(c)). However, the results of paired t-test did not show a distinct difference of GPX3 expressions between ESCC samples and nontumor samples (Figure 7(d)), while the MMP1 and MMP12 expression was also further confirmed by the use of paired t-test (Figures 7(e) and 7(f)).

3.6. Correlation of GPX3, MMP1, and MMP12 Expression with Tumor-Infiltrating Immune Cells (TICs).
The CIBERSORT tool in R programming language was used to conduct additional studies to verify the association between GPX3, MMP1, and MMP12 expression and the TME. Figure S1(a) shows the establishment of 22 types of immune cell profile in ESCC samples and nontumor samples, and the relationship between these TICs was exhibited by the use of heatmap (Figure S1(b)). Subsequently, we compared the proportions of TICs in the ESCC samples with those in the nontumor samples, and we found that differences in B cells naïve,
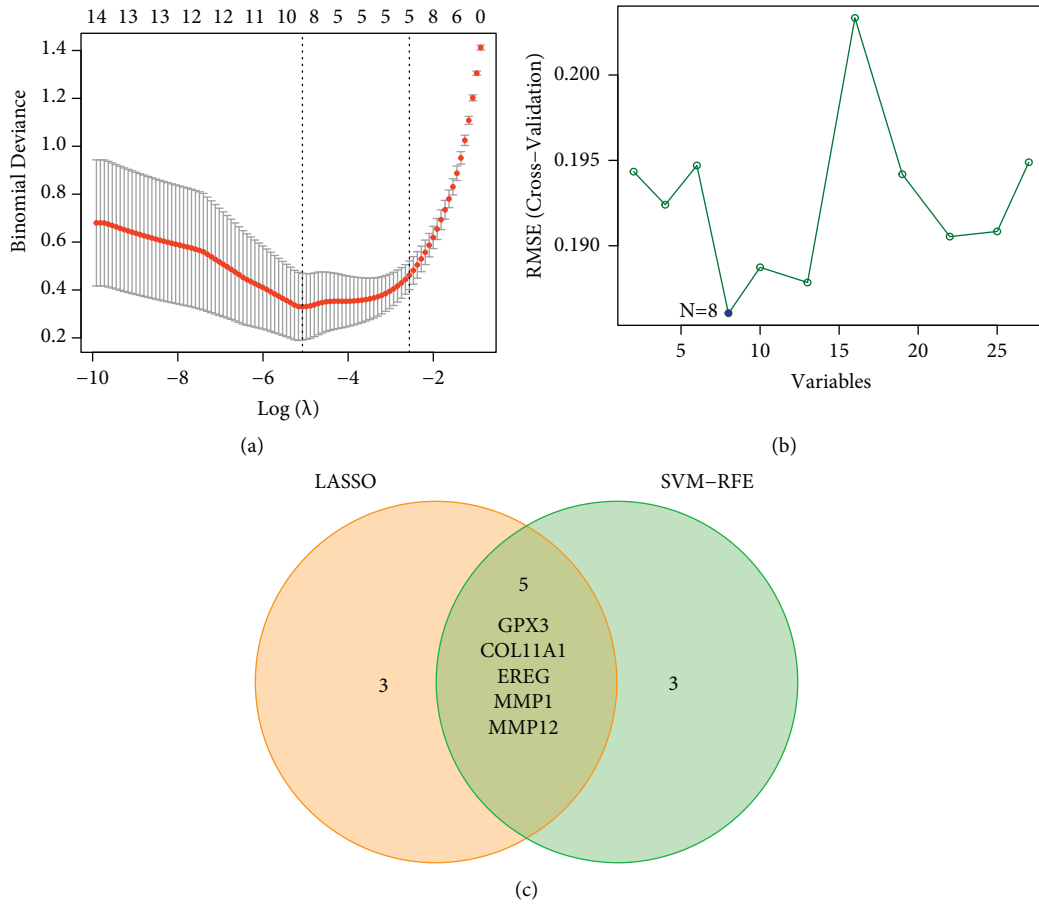
FIGURE 2: Identification of novel diagnostic biomarkers for ESCC diagnosis. (a) Tuning feature selection in the LASSO. (b) A plot of markers selection via the SVM-RFE algorithm. (c) Venn diagram demonstrating five diagnostic markers shared by the LASSO and SVM-RFE algorithms.
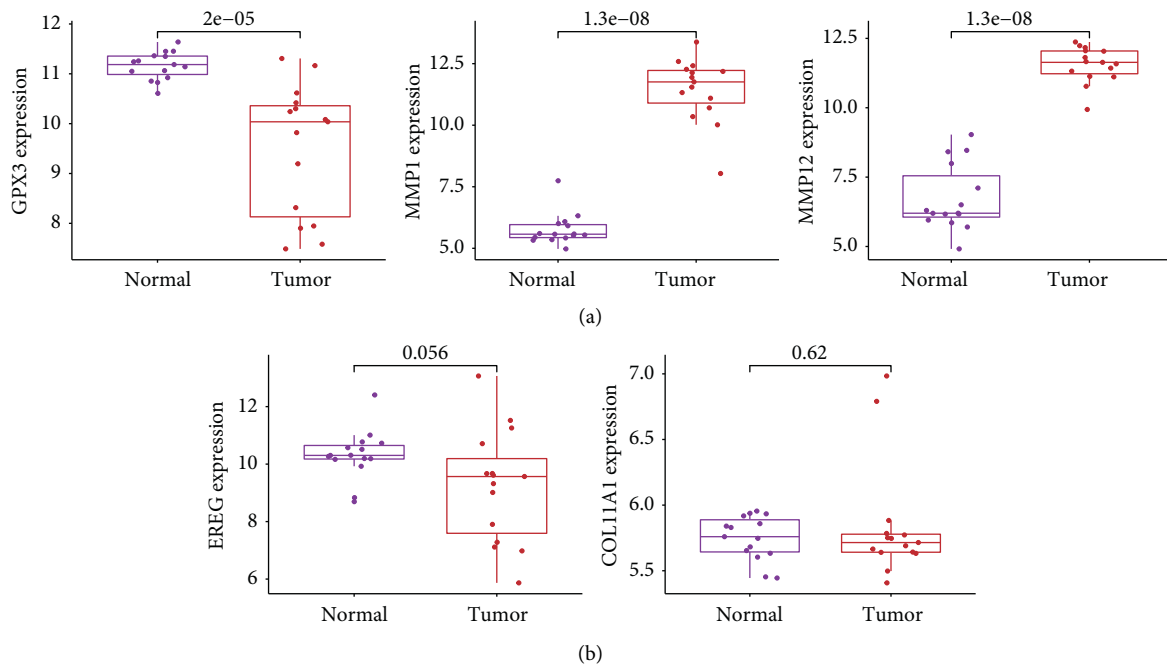
FIGURE 3: The expression of GPX3, COL11A1, EREG, MMP1, and MMP12 in ESCC specimens and nontumor from GSE75241 datasets.
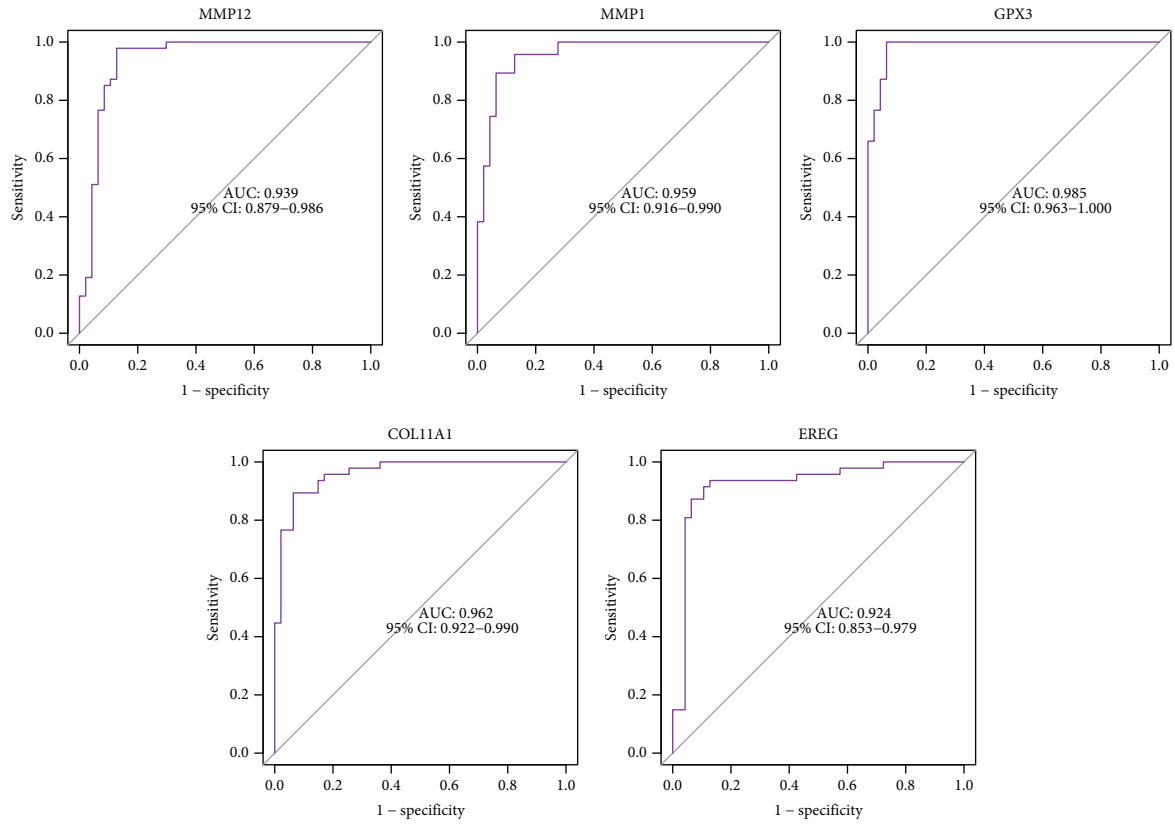
Figure 4: ROC curve of the five diagnostic markers using GSE20347 and GSE38129 datasets.

(a)
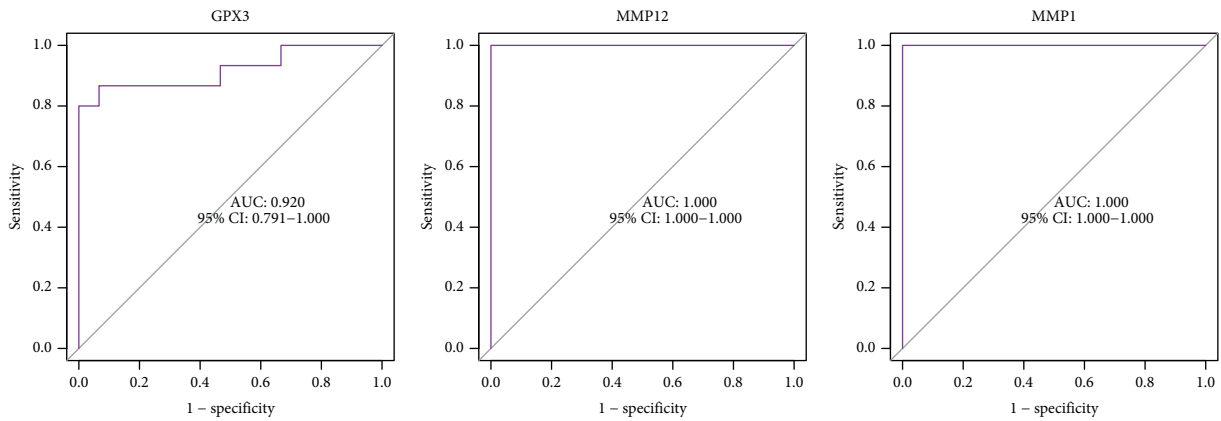
Figure 5: Continued.
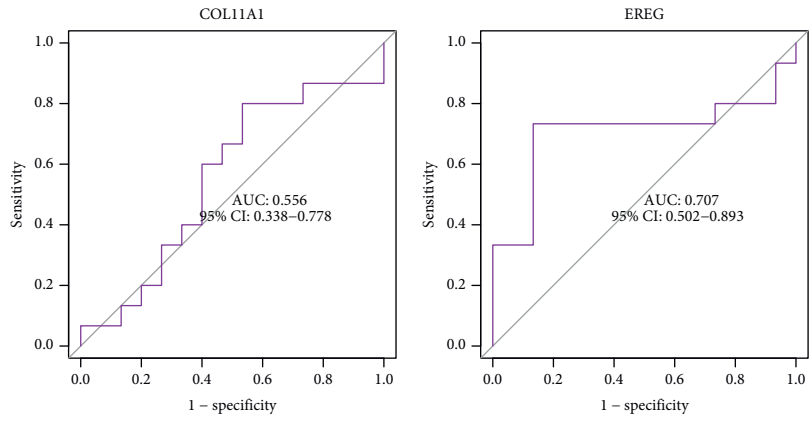
(b)

Figure 5: ROC curve of the five diagnostic markers using GSE75241 datasets.

(a)

(b)

Figure 6: Continued.

(c)
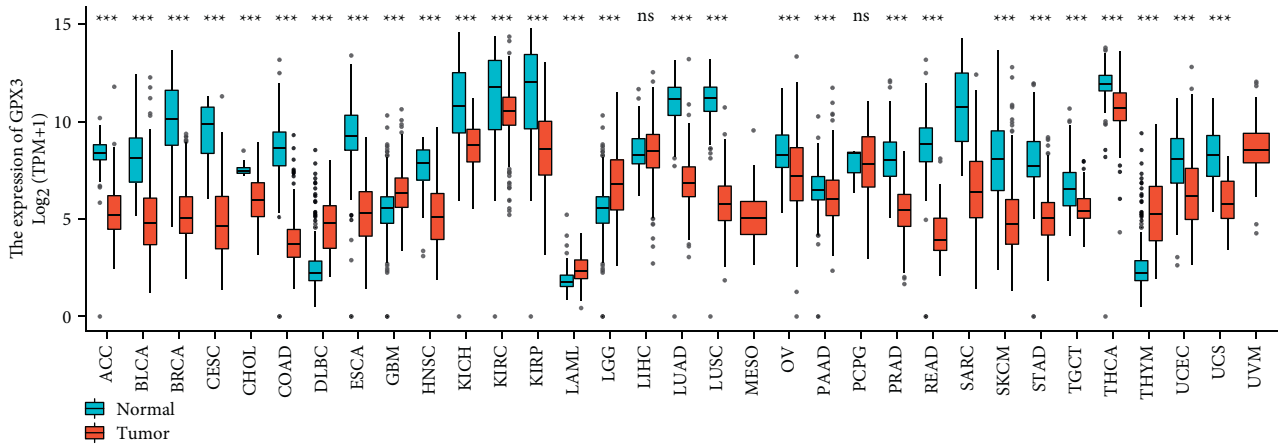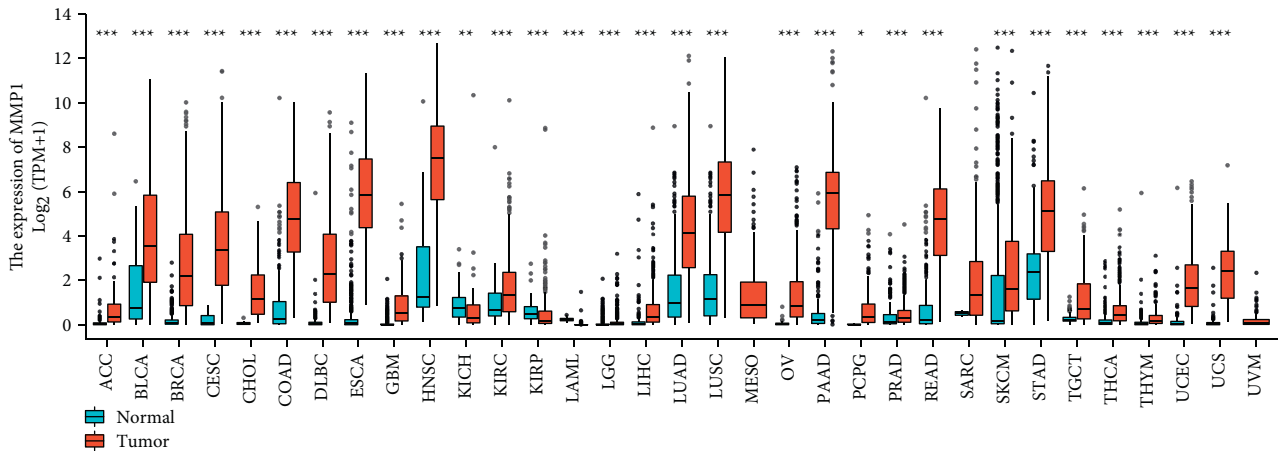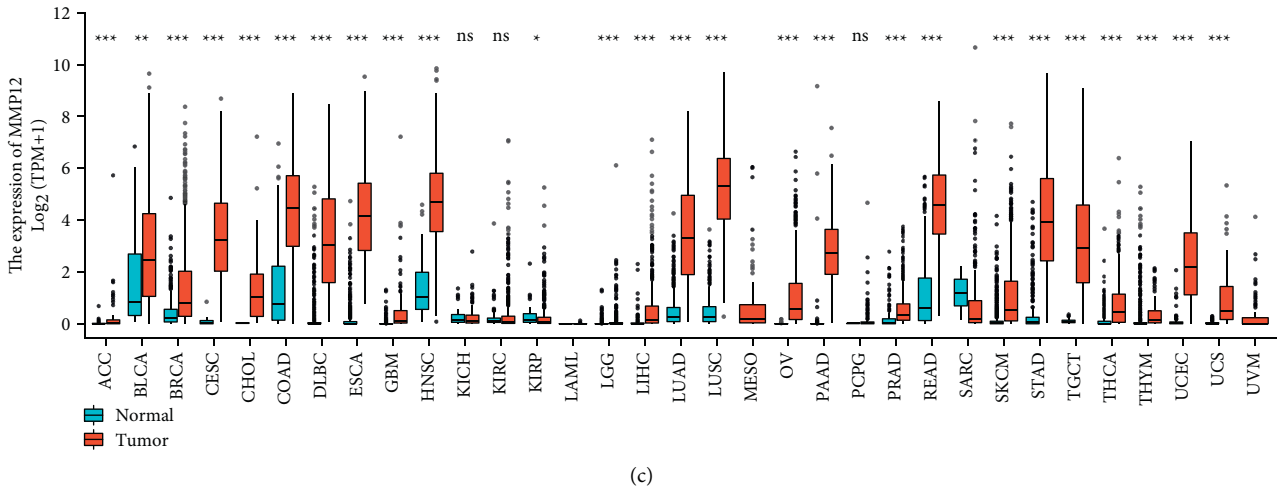
FIGURE 6: The pan-cancer analysis using TCGA datasets.

(a)

(b)

(c)

(d)

(e)

(f)
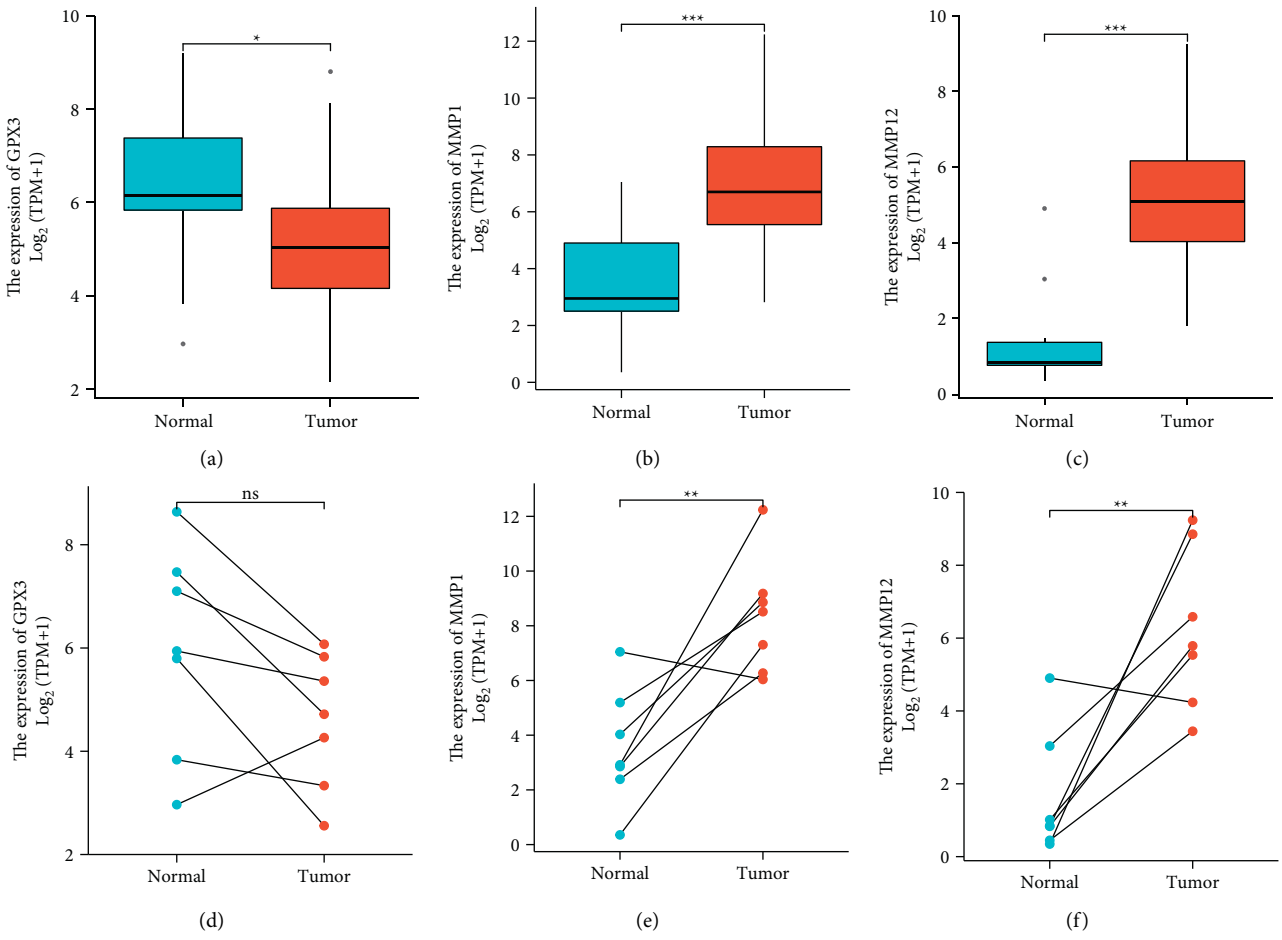
FIGURE 7: The expression of GPX3, MMP1, and MMP12 between ESCC specimens and nontumor specimens from TCGA datasets using (a–c) unpaired t-test and (d, e) paired t-test. $***p < 0.001$, $**p < 0.01$, and $*p < 0.05$.

plasma cells, T cells CD8, T cells CD4 naïve, T cells CD4 memory resting, T cells CD4 memory activated, T cells follicular helper, T cells regulatory (Tregs), monocytes, macrophages M0, macrophages M1, macrophages M2, dendritic cells activated, mast cells resting, and neutrophils were statistically significant (Figure S1(c)). Moreover, we observed that the GPX3 expression was associated with the expression of T cells CD8, mast cells resting, T cells regulatory (Tregs), macrophages M2, T cells CD4 memory resting, monocytes, dendritic cells resting, T cells gamma

delta, neutrophils, T cells CD4 memory activated, B cells naïve, plasma cells, T cells CD4 naïve, macrophages M1, T cells follicular helper, dendritic cells activated, and macrophages M0 (Figure 8(a)). MMP1 expression was associated with the expression of macrophages M0, dendritic cells activated, macrophages M1, T cells CD4 memory activated, neutrophils, plasma cells, T cells CD4 naïve, mast cells resting, T cells CD4 memory resting, monocytes, T cells regulatory (Tregs), and T cells CD8 (Figure 8(b)). MMP12 expressions were related to the expressions of macrophages M0, dendritic cells activated, macrophages M1, T cells CD4 memory activated, neutrophils, T cells CD4 naïve, plasma cells, T cells follicular helper, T cells CD4 memory resting, T cells regulatory (Tregs), monocytes, mast cells resting, and T cells CD8 (Figure 8(c)).

4. Discussion

The most common kind of esophageal cancer found all over the world is ESCC [16]. ESCC ranks as the fourth greatest cause of death from cancer-associated causes in China [17]. Even with the recent advances that have been made in diagnosis and therapy, the outlook for ESCC remains dismal [18, 19]. Patients diagnosed with ESCC have a survival rate of fewer than 30 percent after 5 years. Despite the fact that various biomarkers for ESCC have been discovered, the therapeutic relevance of the majority of them has not been validated [20, 21]. Therefore, there is an immediate need for research into more effective biomarkers for the diagnosis of ESCC.

To the best of our knowledge, this is the first retrospective study that has used GEO databases to look for diagnostic indicators that are associated with immune cell infiltration in patients with ESCC. Two cohorts were drawn from the GEO datasets, and the data were subjected to an integrated analysis. There were 27 DEGs in total: five genes showed distinct increases, whereas 22 genes showed distinct decreases. The results of enrichment analyses revealed that the dysregulated genes were primarily involved in matrix organization, skin development, extracellular, extracellular structure organization, epidermal cell differentiation, and keratinocyte differentiation. In the MF group, the abnormal expressed genes were primarily involved in serine hydrolase activity, serine-type peptidase activity, metallopeptidase activity, receptor ligand activity, and extracellular matrix binding. A total of five diagnostic indicators have been discovered using two machine-learning algorithms, including the following: GPX3, COL11A1, EREG, MMP1, and MMP12. In addition, we used GSE75241 datasets to further demonstrate our findings, and the diagnostic value of GPX3, MMP1, and MMP12 was further confirmed.

The human matrix metalloproteinases (MMPs) family belongs to the metzincin superfamily [22]. Extracellular matrix degradation is aided by MMPs, which catalyze proteolytic processes [23]. Several types of cancers are affected by MMPs in different ways [24, 25]. As of this writing, a total of 24 MMPs have been discovered (MMP1, 2, 3, 4, 5, 7, 8, 9, 10, 11, 12, 13, 14, 15, 16, 17, 18, 19, 20, 21, 23, 23a/23b, 24, 25, 26, 27, and 28). Liu et al. reported that lymph node

metastases, microvessel density, and an advanced TNM stage were all linked to ESCC patients with elevated MMP1 expression. Multivariate and Kaplan–Meier analyses found that MMP1 was a significant independent predictor of overall survival of ESCC patients. In vitro experiments showed that MMP1 overexpression improved cell viability, colony formation, and cell movement capacities. The opposite effect was observed when MMP1 was knocked down in ESCC cells. The PI3K/AKT pathway was activated when MMP1 was expressed ectopically in tumor cells, resulting in tumor development and metastasis [26]. In addition, the prognostic values of MMP12 have been reported in several previous studies [27–29]. In this study, according to the results of GSE20347, GSE38129, GSE75241, and TCGA datasets, we further confirmed that MMP1 and MMP12 expressions were distinctly increased in ESCC specimens compared with nontumor samples. ROC assays also confirmed their diagnostic value in screening ESCC samples from normal samples. Overall, the results from machine-learning, together with previous findings, suggested MMP1 and MMP12 as critical diagnostic and prognostic factors for ESCC. However, research on the role of MMP1 and MMP12 in ESCC progression needed to be conducted in both vitro and animal models.

Glutathione peroxidase (GPX) is an important peroxide that has been demonstrated to be widely involved in nontoxic compounds, the reduction of toxic peroxides into hydroxyl compounds, and the decomposing of enzymes [30, 31]. Growing studies have confirmed that GPX reduces the occurrence and development of tumors [32, 33]. It has been found that the methylation of GPX3, a member of the GPX family of tumor-suppressor genes, increases the risk of breast, live, and cervical cancer substantially [34–36]. In ESCC, GPX3 has been reported to be lowly expressed in ESCC and its overexpression promoted the migration and invasion of ESCC cells via regulating FAK/AKT pathway [37]. Our findings were consistent with previous findings.

The role of the tumor microenvironment (TME) in the development of the tumor was proven by an increasing amount of evidence [38]. The malignant characteristics of cancer, such as immortal proliferation, resistance to apoptosis, and evasion of immune surveillance, are thought to be at least partially caused by cooperative interactions between cancer cells and the cells that sustain them [39, 40]. As a result, the TME exerts a considerable amount of impact over the therapeutic response and clinical outcome in cancer patients. Thus, we evaluated the correlation between GPX3, MMP1, and MMP12 expressions and immune cell infiltration in ESCC. Interesting, we found that the expression of GPX3, MMP1, and MMP12 was distinctly associated with the expressions of many immune cells. Therefore, the positive correlation between the amounts of several immune cells and the expressions of GPX3, MMP1, and MMP12 in ESCC patients suggested that GPX3, MMP1, and MMP12 were responsible for the maintenance of an immune-active condition in TME.

However, our present study has some limitations. Firstly, considering the limited size of the sample, it will be necessary to do extensive clinical tests. Secondly, we fail to evaluate the expression profile of GPX3, MMP1, and MMP12 in the

(a)

(b)

(c)
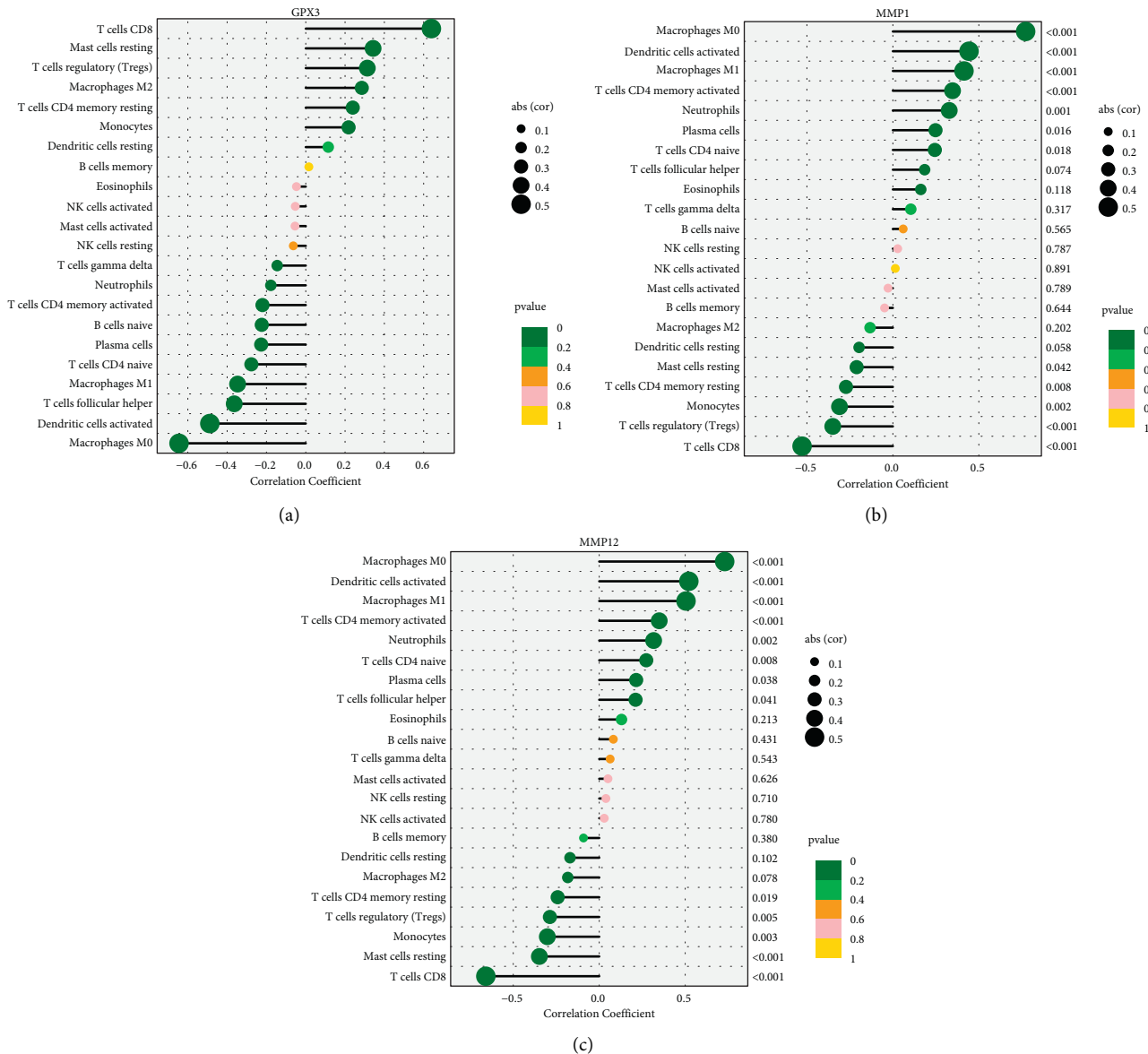
FIGURE 8: Relationships between (a) GPX3, (b) MMP1, (c) MMP12, and infiltrating immune cells in ESCC.

serum/plasma samples in patients with ESCC. Analyzing the biomarkers present in the serum and plasma samples could be an effective way to evaluate the response to treatment in real time. Additionally, the function of GPX3, MMP1, and MMP12 remained largely unclear, and their function and mechanism were worth further exploration by molecular function experiment. We plan to better incorporate more data sets to demonstrate our findings in the next paper. In order to make these more accurate, we intend to obtain tumor specimens in addition to clinical data and demonstrate the accuracy of the results via tests.

5. Conclusion

We identified GPX3, MMP1, and MMP12 as novel diagnostic genes for ESCC. Our research also provided

methods to evaluate those that had a higher potential to benefit from immunotherapy and identified a number of candidate therapeutic targets that could provide a more efficient form of treatments.

Data Availability

The data used to support the findings of this study are included within the article. Additional data can be made available from the corresponding author upon request.

Disclosure

Jipeng Zhang, Nian Zhang, and Xin Yang should be considered as equal co-first authors

Conflicts of Interest

The authors declare that they have no conflicts of interest.

Authors' Contributions

Jipeng Zhang, Nian Zhang, and Xin Yang contributed equally to this work.

Acknowledgments

Supplementary Materials

Figure S1. (a, b) The proportion of the 22 immune cells detected by the CIBERSORT algorithm. (c) The differences in the structure of TIICs between normal tissue and ESCC tissues. (*Supplementary Materials*)

References

[1] H. Sung, J. Ferlay, and R. L. Siegel, "Global cancer statistics 2020: GLOBOCAN estimates of incidence and mortality worldwide for 36 cancers in 185 countries," *CA: A Cancer Journal for Clinicians*, vol. 71, pp. 209–249, 2021.

[2] X. Liu, M. Zhang, and S. Ying, "Genetic alterations in esophageal tissues from squamous dysplasia to carcinoma," *Gastroenterology*, vol. 153, pp. 166–177, 2017.

[3] H. Hirano and K. Kato, "Systemic treatment of advanced esophageal squamous cell carcinoma: chemotherapy, molecular-targeting therapy and immunotherapy," *Japanese Journal of Clinical Oncology*, vol. 49, no. 5, pp. 412–420, 2019.

[4] S. He, J. Xu, X. Liu, and Y. Zhen, "Advances and challenges in the treatment of esophageal cancer," *Acta Pharmaceutica Sinica B*, vol. 11, pp. 3379–3392, 2021.

[5] H. N. Lin, L. Q. Chen, Q. X. Shang, Y. Yuan, and Y. S. Yang, "A meta-analysis on surgery with or without postoperative radiotherapy to treat squamous cell esophageal carcinoma," *International Journal of Surgery*, vol. 80, pp. 184–191, 2020.

[6] S. X. Wang and M. B. Marshall, "Chemoradiation therapy as definitive treatment of esophageal cancer," *Surgical Clinics of North America*, vol. 101, no. 3, pp. 443–451, 2021.

[7] D. C. Codipilly, Y. Qin, S. M. Dawsey et al., "Screening for esophageal squamous cell carcinoma: recent advances," *Gastrointestinal Endoscopy*, vol. 88, no. 3, pp. 413–426, 2018.

[8] Z. Tao, A. Shi, R. Li, Y. Wang, X. Wang, and J. Zhao, "Microarray bioinformatics in cancer- a review," *Journal of B.U.ON, Official journal of the Balkan Union of Oncology*, vol. 22, no. 4, pp. 838–843, 2017.

[9] M. Bednár, "DNA microarray technology and application," *Medical Science Monitor: International Medical Journal of Experimental and Clinical Research*, vol. 6, no. 4, pp. 796–800, 2000.

[10] M. C. Pirrung and E. M. Southern, "The genesis of microarrays," *Biochemistry and Molecular Biology Education*, vol. 42, no. 2, pp. 106–113, 2014.

[11] C. H. Cho, M. Cho, and J. K. Park, "Biomarker barcodes: multiplexed microfluidic immunohistochemistry enables high-throughput analysis of tissue microarray," *Lab on a Chip*, vol. 21, no. 18, pp. 3471–3482, 2021.

[12] A. Sadhu and B. Bhattacharyya, "Common subcluster mining in microarray data for molecular biomarker discovery," *Interdisciplinary Sciences: Computational Life Sciences*, vol. 11, no. 3, pp. 348–359, 2019.

[13] M. E. Ritchie, B. Phipson, D. Wu et al., "Limma powers differential expression analyses for RNA-sequencing and microarray studies," *Nucleic Acids Research*, vol. 43, no. 7, p. e47, 2015.

[14] W. Cai and M. van der Laan, "Nonparametric bootstrap inference for the targeted highly adaptive least absolute shrinkage and selection operator (LASSO) estimator," *International Journal of Biostatistics*, vol. 16, no. 2, 2020.

[15] H. Sanz, C. Valim, E. Vegas, J. M. Oller, and F. Reverter, "SVM-RFE: selection and visualization of the most relevant features through non-linear kernels," *BMC Bioinformatics*, vol. 19, no. 1, p. 432, 2018.

[16] F. L. Huang and S. J. Yu, "Esophageal cancer: risk factors, genetic association, and treatment," *Asian Journal of Surgery*, vol. 41, no. 3, pp. 210–215, 2018.

[17] Y. Lin, Y. Totsuka, Y. He et al., "Epidemiology of esophageal cancer in Japan and China," *Journal of Epidemiology*, vol. 23, no. 4, pp. 233–242, 2013.

[18] J. Yang, X. Liu, S. Cao, X. Dong, S. Rao, and K. Cai, "Understanding esophageal cancer: the challenges and opportunities for the next decade," *Frontiers in Oncology*, vol. 10, Article ID 1727, 2020.

[19] L. Y. Chu, Y. H. Peng, X. F. Weng, J. J. Xie, and Y. W. Xu, "Blood-based biomarkers for early detection of esophageal squamous cell carcinoma," *World Journal of Gastroenterology*, vol. 26, no. 15, pp. 1708–1725, 2020.

[20] Y. Zhao, J. Xu, and Q. Chen, "Analysis of curative effect and prognostic factors of radiotherapy for esophageal cancer based on the CNN," *Journal of healthcare engineering*, vol. 2021, pp. 1–8, 2021.

[21] N. Zhou and W. L. Hofstetter, "Prognostic and therapeutic molecular markers in the clinical management of esophageal cancer," *Expert Review of Molecular Diagnostics*, vol. 20, no. 4, pp. 401–411, 2020.

[22] C. Kapoor, S. Vaidya, V. Wadhwan, G. Kaur, and A. Pathak, "Seesaw of matrix metalloproteinases (MMPs)," *Journal of Cancer Research and Therapeutics*, vol. 12, no. 1, pp. 28–35, 2016.

[23] P. Pittayapruek, J. Meephansan, O. Prapapan, M. Komine, and M. Ohtsuki, "Role of matrix metalloproteinases in photoaging and photocarcinogenesis," *International Journal of Molecular Sciences*, vol. 17, no. 6, p. 868, 2016.

[24] S. Mondal, N. Adhikari, S. Banerjee, S. A. Amin, and T. Jha, "Matrix metalloproteinase-9 (MMP-9) and its inhibitors in cancer: a minireview," *European Journal of Medicinal Chemistry*, vol. 194, Article ID 112260, 2020.

[25] H. Y. Liao, C. M. Da, B. Liao, and H. H. Zhang, "Roles of matrix metalloproteinase-7 (MMP-7) in cancer," *Clinical Biochemistry*, vol. 92, pp. 9–18, 2021.

[26] M. Liu, Y. Hu, M. F. Zhang et al., "MMP1 promotes tumor growth and metastasis in esophageal squamous cell carcinoma," *Cancer Letters*, vol. 377, no. 1, pp. 97–104, 2016.

[27] C. L. Lin, T. H. Ying, S. F. Yang et al., "MTA2 silencing attenuates the metastatic potential of cervical cancer cells by inhibiting AP1-mediated MMP12 expression via the ASK1/MEK3/p38/YB1 axis," *Cell Death and Disease*, vol. 12, no. 5, p. 451, 2021.

[28] F. Klupp, L. Neumann, C. Kahlert et al., "Serum MMP7, MMP10 and MMP12 level as negative prognostic markers in colon cancer patients," *BMC Cancer*, vol. 16, no. 1, p. 494, 2016.

[29] F. Z. Lv, J. L. Wang, Y. Wu, H. F. Chen, and X. Y. Shen, "Knockdown of MMP12 inhibits the growth and invasion of

lung adenocarcinoma cells," *International Journal of Immunopathology and Pharmacology*, vol. 28, no. 1, pp. 77–84, 2015.

[30] N. Sharma, E. J. Shin, D. T. Pham et al., "GPx-1-encoded adenoviral vector attenuates dopaminergic impairments induced by methamphetamine in GPx-1 knockout mice through modulation of NF-κB transcription factor," *Food and Chemical Toxicology*, vol. 154, Article ID 112313, 2021.

[31] E. J. Shin, S. H. Lee, N. Sharma et al., "An adenoviral vector encoded with the GPx-1 gene attenuates memory impairments induced by β-amyloid (1-42) in GPx-1 KO mice via activation of M1 mAChR-mediated signalling," *Free Radical Research*, vol. 55, no. 1, pp. 11–25, 2021.

[32] M. Strycharz-Dudziak, S. Fołtyn, J. Dworzański et al., "Glutathione peroxidase (GPx) and superoxide dismutase (SOD) in oropharyngeal cancer associated with EBV and HPV coinfection," *Viruses*, vol. 12, no. 9, Article ID 1008, 2020.

[33] A. E. Yuzhalin and A. G. Kutikhin, "Inherited variations in the SOD and GPX gene families and cancer risk," *Free Radical Research*, vol. 46, no. 5, pp. 581–599, 2012.

[34] W. Lou, B. Ding, S. Wang, and P. Fu, "Overexpression of GPX3, a potential biomarker for diagnosis and prognosis of breast cancer, inhibits progression of breast cancer cells in vitro," *Cancer Cell International*, vol. 20, no. 1, p. 378, 2020.

[35] X. Qi, K. T. P. Ng, Y. Shao et al., "The clinical significance and potential therapeutic role of GPx3 in tumor recurrence after liver transplantation," *Theranostics*, vol. 6, no. 11, pp. 1934–1946, 2016.

[36] X. Zhang, Z. Zheng, S. Yingji et al., "Downregulation of glutathione peroxidase 3 is associated with lymph node metastasis and prognosis in cervical cancer," *Oncology Reports*, vol. 31, no. 6, pp. 2587–2592, 2014.

[37] X. Zhu, J. Wang, L. Li et al., "GPX3 suppresses tumor migration and invasion via the FAK/AKT pathway in esophageal squamous cell carcinoma," *American Journal of Tourism Research*, vol. 10, no. 6, pp. 1908–1920, 2018.

[38] D. C. Hinshaw and L. A. Shevde, "The tumor microenvironment innately modulates cancer progression," *Cancer Research*, vol. 79, no. 18, pp. 4557–4566, 2019.

[39] J. Kim and J. S. Bae, "Tumor-associated macrophages and neutrophils in tumor microenvironment," *Mediators of Inflammation*, vol. 2016, pp. 1–11, 2016.

[40] M. Jarosz-Biej, R. Smolarczyk, T. Cichoń, and N. Kułach, "Tumor microenvironment as A "game changer" in cancer radiotherapy," *International Journal of Molecular Sciences*, vol. 20, no. 13, Article ID 3212, 2019.

Hindawi

Research Article

The Clinical Value of Long Noncoding RNA DDX11-AS1 as a Biomarker for the Diagnosis and Prognosis of Hepatocellular Carcinoma

Xiaojun Luo, Yang Wang, Xi Zhang ⓘ, and Wenbin Liu ⓘ

Hepatic Biliary and Pancreatic Cancer Center, Chongqing University Cancer Hospital, Chongqing, China

Correspondence should be addressed to Xi Zhang; zhangxi110@cqu.edu.cn and Wenbin Liu; liuwenbin@cqu.edu.cn

Hepatocellular carcinoma (HCC) is a high-mortality malignant tumor with genetic and phenotypic heterogeneity, making predicting clinical outcomes challenging. The purpose of this investigation was to examine the potential usefulness of lncRNA DDX11 antisense RNA 1 (DDX11-AS1) as a biomarker for diagnosis and prognosis in hepatocellular carcinoma (HCC). The TCGA-LIHC datasets were searched for patients' clinical information and RNA-seq data, which were then collected. Relative expression levels of DDX11-AS1 in HCC tissues were determined by qRT-PCR. In order to test the sensitivity and specificity of the DDX11-AS1 receiver, receiver operating characteristic curves were utilized. The association of DDX11-AS1 expression with clinicopathological factors or prognosis was statistically analyzed. We found that the levels of DDX11-AS1 were higher in HCC specimens than in normal specimens. ROC analysis showed that DDX11-AS1 was a useful marker for discriminating HCC tissues from normal nontumor specimens. According to the results of clinical tests, a high level of DDX11-AS1 expressions was significantly related to the pathologic stage ($p = 0.015$) and the histologic grade ($p < 0.001$). Survival studies indicated that patients with higher DDX11-AS1 expression had a significantly poorer overall survival ($p = 0.005$) and progression-free interval ($p = 0.003$) than those with lower DDX11-AS1 expression. Multivariate survival analysis verified that DDX11-AS1 expression level was an independent predictor for HCC patients. Overall, DDX11-AS1 may serve as a tumor promotor during HCC progression, and its high level may be a potential marker for HCC patients.

1. Introduction

Human hepatocellular carcinoma (HCC), which ranks one of the most common and aggressive hepatic illnesses, is the third most widespread cause of cancer-associated mortality around the world, in particular, in East Asia as well as sub-Saharan Africa [1]. The incidence rate has been increasing in China [2]. HCC makes up the larger part of the malignancy of the liver, which often results from the average clinical risk factors [3]. Surgical resection is regarded as the most effective therapy for HCC. However, about 80% of patients were diagnosed with locally advanced or metastasis tumor and were not suitable for hepatectomy [4]. Furthermore, it has been demonstrated that >45% of patients with HCC relapse in the follow-up time after resection [5]. The former research studies demonstrated a great number of HCC-related deregulated genes and signaling pathways; however, the highly complicated molecular mechanisms based on carcinogenesis and progressions are still less explicit [6, 7]. Thus, the identification of better underlying molecular markers for HCC is essential for more accurate early diagnosis and more effective therapeutic strategies.

As genome and transcriptome sequencing technologies are developing and genomics consortiums are being implemented, it has been demonstrated that a large proportion of the genome acts as an example for the transcribing of noncoding RNAs (ncRNAs) [8, 9]. lncRNAs are characterized as noncoding RNA molecules that are orientated with more than 200 nucleotides; they have the potential to play crucially essential roles in chromatin modification, regulation of transcription genes, and post-transcriptional management [10, 11]. More and more

evidence has demonstrated that lncRNAs have been implicated in pathophysiological procedures like gene expression, cell multiplication, apoptosis, as well as tumor genesis [12, 13]. Recent years have witnessed that, as new technological methods are developing, great numbers of lncRNAs have been discovered to express a strong correlation with the dysregulation process of various cancers, which serve as oncogenes or tumor suppressors [14, 15]. Loss-of-function and gain-of-function experiments have led to the discovery of a number of lncRNAs with functional properties. Nonetheless, in spite of the discoveries, there are merely a small number of lncRNAs that have been characterized, and the functions featured by most lncRNAs have not been given characterization and are in need of in-depth investigation.

lncRNA DDX11 antisense RNA 1 (DDX11-AS1), located on 12p11.21, is a newly identified tumor-related lncRNA that has been reported to be dysregulated in several tumors, such as glioma and bladder cancer [16, 17]. In addition, the oncogenic roles of DDX11-AS1 have been demonstrated in gastric cancer and osteosarcoma [18, 19]. However, its expression and function in HCC remain unclear. In this study, we aimed to explore the potential of DDX11-AS1 used as a novel biomarker for HCC patients.

2. Patients and Methods

2.1. Data Sources. The RNA-seq data of 374 liver cancer samples used in the TCGA-LIHC research were obtained from the UCSC Xena website (https://xena.ucsc.edu/), which was also the source of the clinical information. The data were presented in FPKM format. The nontumor specimens in TCGA-LIHC ($n = 50$) and nontumor specimens in GTEx ($n = 110$) were both included in the RNA-seq data. The datasets for both of these types of samples were retrieved from the UCSC Xena data center.

2.1.1. Differential Expression Analysis of DDX11-AS1 in HCC. Differential analysis of DDX11-AS1 was performed on HCC samples and normal samples obtained from TCGA and GTEx. In order to study the differences in the levels of DDX11-AS1 found in normal liver tissues and HCC tissues, Student's *t*-tests were carried out. By analyzing the receiver operating characteristic (ROC) curve and the area under the curve (AUC), researchers were able to determine whether or not DDX11-AS1 has the potential to identify HCC tissues from normal tissues.

2.2. Patients and Specimens. From July 2021 to January 2022, 12 HCC patients who underwent complete resection of the tumor in Chongqing University Cancer Hospital were subsequently enrolled in our study. No patient was given chemotherapy, radiotherapy, or immunotherapy prior to surgery. Two pathologists confirmed the HCC diagnosis. All tissue samples were frozen in liquid nitrogen following the surgical removal and then put into storage at −80°C until further use. Current research obtained approval from the Ethics Committee of Chongqing University Cancer Hospital; every patient had signed the written informed consent.

2.2.1. Real-Time PCR. The extraction of total RNA was attained from tissue samples by applying TRIzol reagent (Invitrogen, China) according to the directions of the manufacturer. RNA was put under reverse transcription into cDNA in virtue of the Prime-Script™ one -step RT-PCR kit (TaKaRa, Kunming, Yunnan, China). The performance of QRT-PCR reactions was conducted in virtue of an ABI7600 System (Applied Biosystems, Pudong, Shanghai, China) and SYBR Green PCR Master Mix (Takara, Hangzhou, Zhejiang, China). The reaction program was 5 min at 95°C, followed by three-step reactions at 95°C/30 s, 60°C/30 s, and 72°C/10 s for 40 cycles. The normalization of transcription levels was made oriented with GAPDH expression. The relative amount of DDX11-AS1 was calculated using the equation $2^{-\Delta\Delta Ct}$. The experiments were implemented with three copies for each case. The PCR primers for DDX11-AS1 or GAPDH are expressed below: lncRNA DDX11-AS1 forward: 5′-CCTCTGCCTACAATACAAAAGTCA-3′; lncRNA DDX11-AS1 reverse: 5′- CAGGGTAAATGTACT TCAGCCAC-3′; GAPDH forward: 5′-CGGTCTCCTCTG ACTTCAA-3′; GAPDH reverse: 5′-GGTGAGGGTCTC TCTCTTC-3′.

2.3. Statistical Analysis. The entire statistical analysis was completed via R program 4.0.2 (R Core Team, Massachusetts, USA) and SPSS13.0 for Windows (SPSS Inc., Chicago, IL, USA). Statistical analyses between the two groups were evaluated in virtue of two-tailed Student's *t*-test or chi-square test. For the purpose of distinguishing HCC specimens from normal nontumor tissues, ROC curves were developed. The probabilities of overall survival (OS) and progression-free interval (PFI) were calculated through the Kaplan–Meier methods, and the comparison was made applying the Log-rank Test. The Cox regression model was used for univariate and multivariate analyses. Two-tailed *p* values lower than 0.05 were regarded to be of statistical significance.

3. Results

3.1. Increased Expression of DDX11-AS1 in HCC Tissues. To investigate whether DDX11-AS1 was a functional lncRNA in HCC progression, our research explored the presentation of DDX11-AS1 in HCC and nontumor specimens from TCGA datasets. As presented in Figure 1(a), DDX11-AS1 expression was increased in HCC tissues in comparison to the nontumor tissues ($p < 0.001$). A similar result was also observed based on TCGA datasets and GTEx data (Figure 1(b)). After that, we investigated whether or not the levels of DDX11-AS1 had any diagnostic value. High DDX11-AS1 expressions yielded an AUC value of 0.967 (95 percent confidence interval: 0.951 to 0.983) for HCC in TCGA datasets, as indicated by the ROC assays (Figure 1(c)). In addition, high DDX11-AS1 expressions had an AUC value of 0.812 (95% CI: 0.775 to 0.850) for HCC in TCGA datasets and GTEx data (Figure 1(d)). According to the
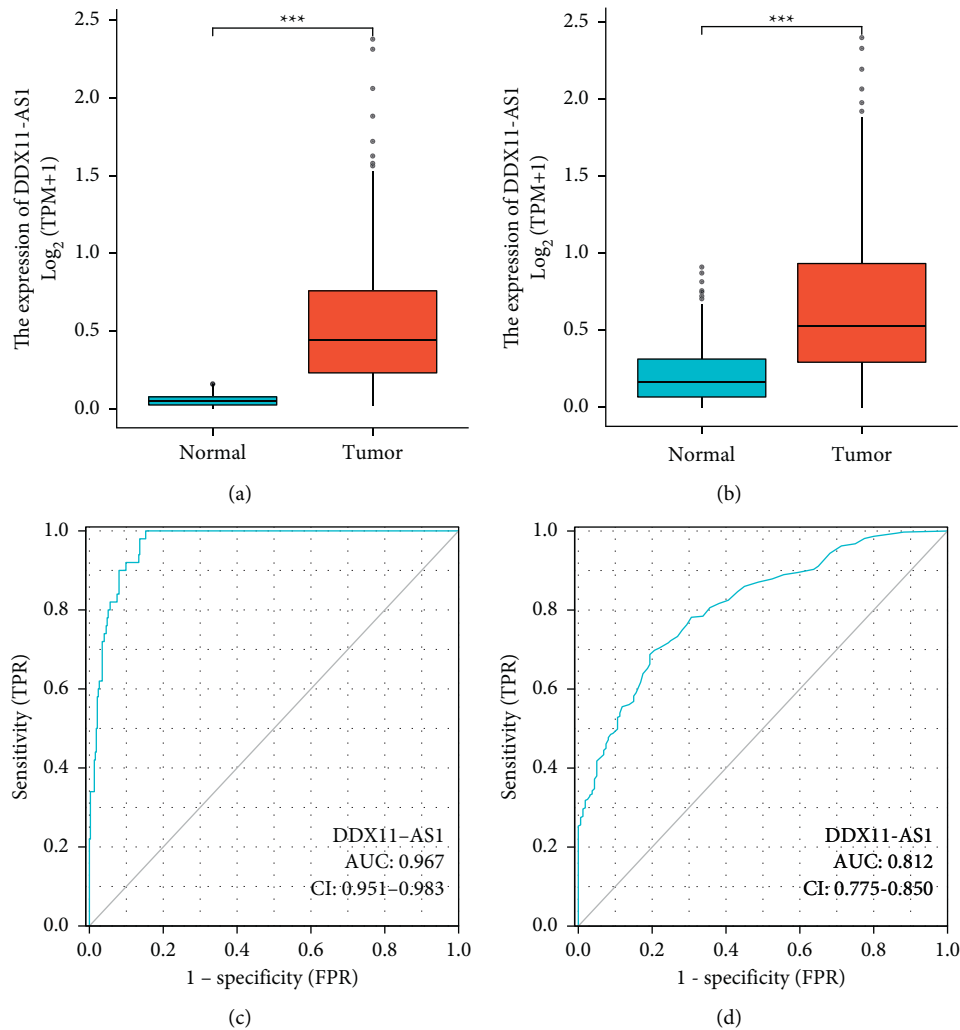
Figure 1: The expression of DDX11-AS1 and its diagnostic value in HCC patients. (a and b) DDX11-AS1 expression was distinctly increased in HCC specimens and nontumor specimens from TCGA datasets and/or GTEx data. (c and d) ROC assays for DDX11-AS1 as a diagnostic marker for HCC patients from TCGA datasets and/or GTEx data.

results of our research, DDX11-AS1 is a functional regulator in HCC.

3.2. DDX11-AS1 Associations with Clinical and Pathological Characteristics.

To assess the clinical relevance harbored by DDX11-AS1 expressions in HCC, the median level of DDX11-AS1 performed the duty of a cutoff point to divide all 374 patients into two groups (high groups: $n = 187$ and low groups: $n = 187$). Subsequently, our group investigated the connection between the presentation of DDX11-AS1 and clinicopathological parameters. Based on Table 1, high expression of DDX11-AS1 was observed to be distinctly relevant to pathologic stage ($p = 0.015$) and histologic grade ($p < 0.001$). Nevertheless, other characteristics did not show any significant difference.

3.3. Prognostic Significance of DDX11-AS1 Expression as a New Marker in HCC.

The Kaplan–Meier assays helped corroborate the link between the expression of DDX11-AS1 and the outcomes of 374 HCC patients. We observed that patients with high expression of DDX11-AS1 had poorer OS ($p = 0.005$, Figure 2(a)) and PFI ($p = 0.002$, Figure 2(b)) compared with those in the low DDX11-AS1 group. In addition, the areas under the time-dependent ROC for OS of the TCGA cohort are 0.711, 0.654, and 0.649 for 1-, 3-, and 5-year survival, respectively (Figure 2(c)). Moreover, the areas under the time-dependent ROC for PFI of the TCGA cohort are 0.667, 0.578, and 0.788 for 1-, 3-, and 5-year survival, respectively (Figure 2(d)). In addition, multivariate analyses were performed to establish whether or not DDX11-AS1 was a factor that was independent in the prognostic prediction of HCC patients. Importantly, the data revealed that high DDX11-AS1 expression can independently predict the clinical outcome of patients regarding OS (HR = 0.578, 95% CI: 0.398–0.838, $p = 0.004$, Table 2) and PFI (HR = 0.615, 95% CI: 0.452–0.837, $p = 0.002$, Table 3).

3.4. The Expression of DDX11-AS1 and Its Diagnostic Value in Our Cohort.

To demonstrate the above results, we collected a total of 12 HCC samples and matched noncancerous tissue

Table 1: Association between DDX11-AS1 expression level and clinical characteristics.

Characteristic	Low expression of DDX11-AS1	High expression of DDX11-AS1	p
N	187	187	
Gender, *n* (%)			0.269
Female	55 (14.7%)	66 (17.6%)	
Male	132 (35.3%)	121 (32.4%)	
Age, *n* (%)			0.196
≤60	82 (22%)	95 (25.5%)	
>60	105 (28.2%)	91 (24.4%)	
Pathologic stage, *n* (%)			0.015
Stage I	97 (27.7%)	76 (21.7%)	
Stage II	35 (10%)	52 (14.9%)	
tage III	35 (10%)	50 (14.3%)	
Stage IV	4 (1.1%)	1 (0.3%)	
Histologic grade, *n* (%)			<0.001
G1	37 (10%)	18 (4.9%)	
G2	104 (28.2%)	74 (20.1%)	
G3	41 (11.1%)	83 (22.5%)	
G4	2 (0.5%)	10 (2.7%)	
Age, median (IQR)	62 (54, 70)	60 (51, 68)	0.056

Overall Survival
HR = 1.65 (1.17–2.34)
P = 0.005

DDX11−AS1
Low
High

(a)

Progress Free Interval
HR = 1.56 (1.16–2.09)
P = 0.003

DDX11−AS1
Low
High

(b)

Figure 2: Continued.

DDX11−AS1
— 1−Year (AUC = 0.711)
— 3−Year (AUC = 0.654)
— 5−Year (AUC = 0.649)

(c)

DDX11−AS1
— 1−Year (AUC = 0.667)
— 3−Year (AUC = 0.578)
— 5−Year (AUC = 0.788)
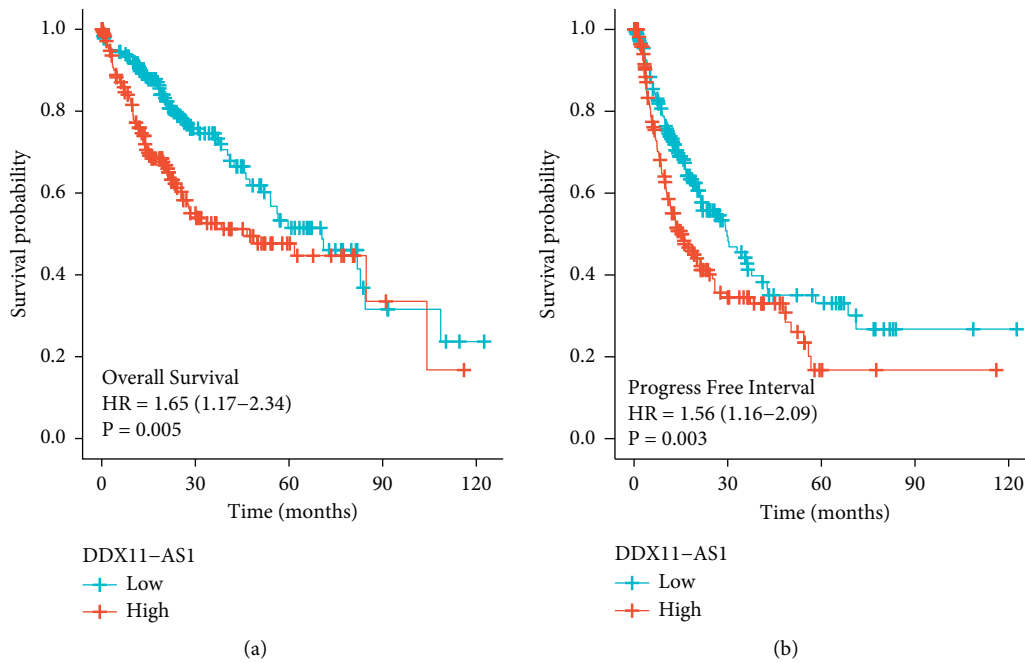
(d)
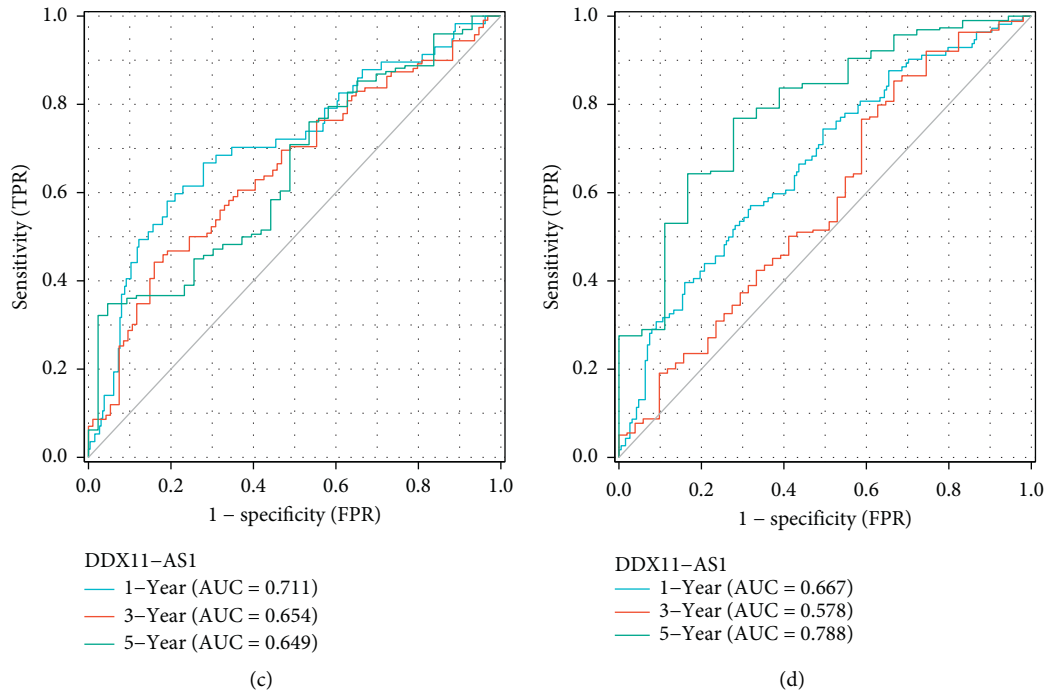
Figure 2: The significance of DDX11-AS1 expression as a predictive factor in patients with HCC. (a and b) Kaplan–Meier curves for OS and PFI and DDX11-AS1 expression in group of 374 HCC patients. (c and d) The AUC for 1-, 2-, and 3-year OS and PFI in TCGA datasets.

Table 2: Univariate and Multivariate analyses of prognostic parameters for overall survival of patients with HCC.

Characteristics	Total (N)	Univariate analysis		Multivariate analysis	
		Hazard ratio (95% CI)	p Value	Hazard ratio (95% CI)	p Value
Gender	373				
Female	121	References			
Male	252	0.793 (0.557–1.130)	0.200		
Age	373				
≤60	177	References			
>60	196	1.205 (0.850–1.708)	0.295		
Histologic grade	368				
G1&G2	233	References			
G3&G4	135	1.091 (0.761–1.564)	0.636		
Pathologic stage	349				
Stage I&Stage II	259	References			
Stage III&Stage IV	90	2.504 (1.727–3.631)	<0.001	2.491 (1.717–3.615)	<0.001
DDX11-AS1	373				
High	186	References			
Low	187	0.604 (0.427–0.856)	0.005	0.578 (0.398–0.838)	0.004

samples. The results of RT-PCR revealed that DDX11-AS1 expression was distinctly increased in HCC specimens compared with nontumor specimens (Figure 3(a)). After that, we investigated whether or not the levels of DDX11-AS1 had any diagnostic value. The ROC tests revealed that high DDX11-AS1 expression had an AUC value of 0.8507 (95 percent confidence interval: 0.6903 to 1.000) for HCC (Figure 3(b)). Our findings were consistent with the results from TCGA datasets.

4. Discussion

HCC features violence, invasion ability, particularly intrahepatically, and likely postresection recurrence [20]. Up to date, the clinical results featured by HCC patients have obtained no benefit from the latest progress of novel diagnostic and therapeutic approaches due to the supremely high recurrence rate and metastasis rate [21, 22]. Recent years have witnessed increasingly growing research studies

Table 3: Univariate and Multivariate analyses of prognostic parameters for progression-free survival of patients with HCC.

Characteristics	Total (N)	Univariate analysis		Multivariate analysis	
		Hazard ratio (95% CI)	p Value	Hazard ratio (95% CI)	p Value
Gender	373				
Female	121	References			
Male	252	0.982 (0.721–1.338)	0.909		
Age	373				
≤60	177	References			
>60	196	0.960 (0.718–1.284)	0.783		
Histologic grade	368				
G1&G2	233	References			
G3&G4	135	1.152 (0.853–1.557)	0.355		
Pathologic stage	349				
Stage I&Stage II	259	References			
Stage III&Stage IV	90	2.201 (1.591–3.046)	<0.001	2.252 (1.625–3.122)	<0.001
DDX11-AS1	373				
High	186	References			
Low	187	0.642 (0.479–0.860)	0.003	0.615 (0.452–0.837)	0.002

(a)

(b)
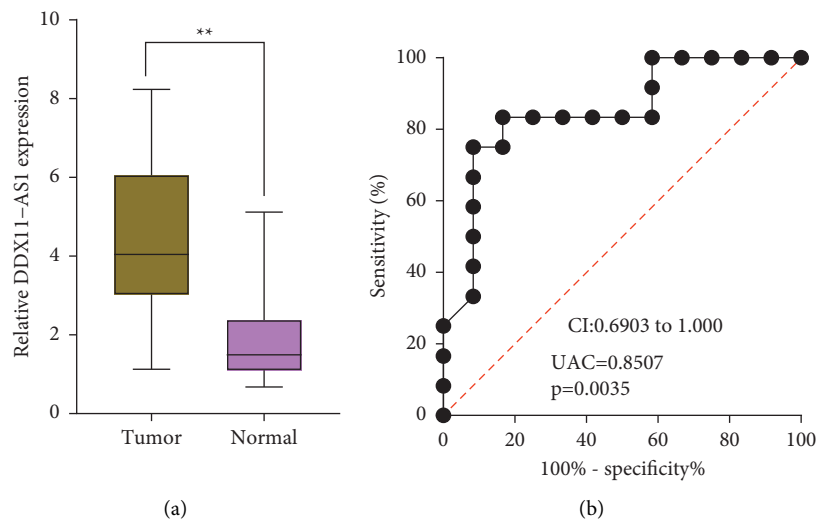
Figure 3: Identification of the expression of DDX11-AS1 in our cohort. (a) Relative expressions of DDX11-AS1 in HCC specimens and adjacent nontumor specimens determined using qRT-PCR. (b) ROC assays for DDX11-AS1 as a diagnostic marker for HCC patients.

which have unveiled the potential of lncRNAs used as novel diagnostic and prognostic markers for HCC patients due to their abnormal levels and the development of the wide detection of lncRNAs in the serum and tissues of tumor patients using high throughput sequencing [23, 24]. In addition, more than one lncRNA has been identified for positive relevance to the clinical outcome of HCC patients, such as lncRNA MCM3AP-AS1, lncRNA CASC9, and lncRNA-PDPK2P [25–27].

lncRNAs represent an emerging group, which may regulate HCC cell proliferation, migration, and apoptosis. For instance, lncRNA F11-AS1 was shown to be highly expressed in HCC and its overexpression suppressed the proliferation, migration and invasion of HCC cells, yet induced apoptosis via modulating NR1I3 through binding to miRNA-211-5p [28]. lncRNA HCG11 was found to be

overexpressed in HCC and promote the proliferation and metastasis of HCC cells via the modulation of miRNA-26a-5p/ATG12 axis [29]. Those discoveries revealed that different lncRNAs might display a different part in HCC. Recently, Zheng et al. reported that the expressions of DDX11-AS1 were shown to be increased in glioma tissues and cells. There was a correlation between high levels of DDX11-AS1 expression and a poor prognostic value. DDX11-AS1 knockdown, from a functional standpoint, inhibited proliferation, migration, and invasion while simultaneously inducing apoptosis through the regulation of the miR-499b-5p/RWDD4 Axis [30]. Chen and his group showed that the expression of DDX11-AS1 was found at an astonishingly high level in bladder cancer and contributed to the aggressiveness of the disease. The proliferation was inhibited when DDX11-AS1 was knocked out through the

mechanism of protecting LAMB3 from downregulation by sponging miRNA-2355-5p [16]. The above results revealed DDX11-AS1 as an oncogenic lncRNA in bladder cancer and glioma. However, the potential effects of DDX11-AS1 in HCC have not been explored.

This thesis first illustrated the distinct up-regulation of DDX11-AS1 expression in HCC specimens in comparison to nontumor specimens in TCGA datasets and our cohort, which was consistent with the expressing trend of DDX11-AS1 in bladder cancer and glioma. Further tests of the diagnostic usefulness of DDX11-AS1 confirmed that high DDX11-AS1 expression in the tumor specimens enabled the classification of HCC patients from normal specimens, suggesting that it is a viable diagnostic biomarker for HCC. Moreover, high DDX11-AS1 expression was observed to be of association with Pathologic stage and Histologic grade. A clinical study with a five-year following-up pointed out that patients who had high DDX11-AS1 expressions displayed a shorter OS and PFI, suggesting that overexpression of DDX11-AS1 may positively influence the clinical progression of HCC. In multivariate assays, increased DDX11-AS1 presentation was demonstrated to be an independent poor prognostic factor for both OS and PFI, indicating that DDX11-AS1 might be a promising biomarker for the diagnosis and prognosis of HCC patients. However, the small sample size of the present study was a limitation, which might likely lead to a not very convincing conclusion. In addition, whether the overexpression or knockdown of DDX11-AS1 may influence the proliferation and metastasis of HCC cells needed to be further studied in vitro and in vivo. In the future, we will collect more HCC specimens to further confirm our findings. Besides, the potential function of DDX11-AS1 will be further studied.

5. Conclusions

Our findings revealed that upregulation of DDX11-AS1 in HCC has an association with aggressive progression with poor prognosis and that DDX11-AS1 may function as a prognostic and diagnostic marker for HCC.

Data Availability

The data used in this research are available from the corresponding author upon reasonable request.

Conflicts of Interest

The authors declare that they have no conflicts of interest.

Authors' Contributions

Xiaojun Luo and Yang Wang contributed equally to this work.

References

[1] R. L. Siegel, K. D. Miller, and A. Jemal, "Cancer statistics, 2019," *CA: A Cancer Journal for Clinicians*, vol. 69, no. 1, pp. 7–34, 2019.

[2] M. Xue, X. Lin, Q. X. Lin et al., "Association between hepatitis B and E virus infection and hepatocellular carcinoma risk," *International Journal of Cancer*, vol. 148, no. 12, pp. 2974–2981, 2021.

[3] A. J. Craig, J. von Felden, T. Garcia-Lezana, S. Sarcognato, and A. Villanueva, "Tumour evolution in hepatocellular carcinoma," *Nature Reviews Gastroenterology & Hepatology*, vol. 17, no. 3, pp. 139–152, 2020.

[4] J. D. Yang and J. K. Heimbach, "New advances in the diagnosis and management of hepatocellular carcinoma," *BMJ*, vol. 371, 2020.

[5] X. Li, C. Li, L. Zhang et al., "The significance of exosomes in the development and treatment of hepatocellular carcinoma," *Molecular Cancer*, vol. 19, 2020.

[6] K. A. McGlynn, J. L. Petrick, and H. B. El-Serag, "Epidemiology of hepatocellular carcinoma," *Hepatology*, vol. 73, pp. 4–13, 2021.

[7] J. C. Nault and A. Villanueva, "Biomarkers for hepatobiliary cancers," *Hepatology*, vol. 73, pp. 115–127, 2021.

[8] M. Matsui and D. R. Corey, "Non-coding RNAs as drug targets," *Nature Reviews Drug Discovery*, vol. 16, no. 3, pp. 167–179, 2017.

[9] M. Esteller, "Non-coding RNAs in human disease," *Nature Reviews Genetics*, vol. 12, pp. 861–874, 2011.

[10] S. J. Johnson and T. A. Cooper, "Overlapping mechanisms of lncRNA and expanded microsatellite RNA," *Wiley Interdiscip Rev RNA*, vol. 12, p. e1634, 2021.

[11] W. X. Peng, P. Koirala, and Y. Y. Mo, "LncRNA-mediated regulation of cell signaling in cancer," *Oncogene*, vol. 36, no. 41, pp. 5661–5667, 2017.

[12] T. Ali and P. Grote, "Beyond the RNA-dependent function of LncRNA genes," *Elife*, vol. 9, Article ID e60583, 2020.

[13] Y. Chi, D. Wang, J. Wang, W. Yu, and J. Yang, "Long noncoding RNA in the pathogenesis of cancers," *Cells*, vol. 8, no. 9, 2019.

[14] Z. Wu, X. Liu, L. Liu et al., "Regulation of lncRNA expression," *Cellular and Molecular Biology Letters*, vol. 19, no. 4, pp. 561–575, 2014.

[15] J. Li, H. Meng, Y. Bai, and K. Wang, "Regulation of lncRNA and its role in cancer metastasis," *Oncology Research Featuring Preclinical and Clinical Cancer Therapeutics*, vol. 23, no. 5, pp. 205–217, 2016.

[16] D. Chen, J. Chen, J. Gao et al., "LncRNA DDX11-AS1 promotes bladder cancer occurrence via protecting LAMB3 from downregulation by sponging miR-2355-5p," *Cancer Biotherapy and Radiopharmaceuticals*, vol. 35, no. 5, pp. 319–328, 2020.

[17] Z. Xiang, Q. Lv, Y. Zhang et al., "Long non-coding RNA DDX11-AS1 promotes the proliferation and migration of glioma cells by combining with HNRNPC," *Molecular Therapy—Nucleic Acids*, vol. 28, pp. 601–612, 2022.

[18] H. Zhang, J. Lin, J. Chen et al., "DDX11-AS1 contributes to osteosarcoma progression via stabilizing DDX11," *Life Sciences*, vol. 254, Article ID 117392, 2020.

[19] Z. Ren, X. Liu, Y. Si, and D. Yang, "Long non-coding RNA DDX11-AS1 facilitates gastric cancer progression by regulating miR-873-5p/SPC18 axis," *Artificial Cells, Nanomedicine, and Biotechnology*, vol. 48, no. 1, pp. 572–583, 2020.

[20] J. S. Lee and S. S. Thorgeirsson, "Comparative and integrative functional genomics of HCC," *Oncogene*, vol. 25, no. 27, pp. 3801–3809, 2006.

[21] H. Zhang, X. Chen, J. Zhang et al., "Long non-coding RNAs in HBV-related hepatocellular carcinoma (Review)," *International Journal of Oncology*, vol. 56, pp. 18–32, 2020.

[22] X. Xu, Y. Tao, L. Shan et al., "The role of MicroRNAs in hepatocellular carcinoma," *Journal of Cancer*, vol. 9, no. 19, pp. 3557–3569, 2018.

[23] T. E. Jabbour, S. M. Lagana, and H. Lee, "Update on hepatocellular carcinoma: pathologists' review," *World Journal of Gastroenterology*, vol. 25, no. 14, pp. 1653–1665, 2019.

[24] N. Tsuchiya, Y. Sawada, I. Endo, K. Saito, Y. Uemura, and T. Nakatsura, "Biomarkers for the early diagnosis of hepatocellular carcinoma," *World Journal of Gastroenterology*, vol. 21, no. 37, pp. 10573–10583, 2015.

[25] Y. Wang, L. Yang, T. Chen et al., "A novel lncRNA MCM3AP-AS1 promotes the growth of hepatocellular carcinoma by targeting miR-194-5p/FOXA1 axis," *Molecular Cancer*, vol. 18, no. 1, p. 28, 2019.

[26] J. Yao, J. Fu, Y. Liu, W. Qu, G. Wang, and Z. Yan, "LncRNA CASC9 promotes proliferation, migration and inhibits apoptosis of hepatocellular carcinoma cells by down-regulating miR-424-5p," *Annals of Hepatology*, vol. 23, no. 2021, Article ID 100297.

[27] W. Pan, W. Li, J. Zhao et al., "lncRNA-PDPK2P promotes hepatocellular carcinoma progression through the PDK1/AKT/Caspase 3 pathway," *Molecular Oncology*, vol. 13, no. 10, pp. 2246–2258, 2019.

[28] Y. Deng, Z. Wei, M. Huang et al., "Long non-coding RNA F11-AS1 inhibits HBV-related hepatocellular carcinoma progression by regulating NR1I3 via binding to microRNA-211-5p," *Journal of Cellular and Molecular Medicine*, vol. 24, no. 2, pp. 1848–1865, 2020.

[29] M. L. Li, Y. Zhang, and L. T. Ma, "LncRNA HCG11 accelerates the progression of hepatocellular carcinoma via miR-26a-5p/ATG12 axis," *European Review for Medical and Pharmacological Sciences*, vol. 23, no. 24, pp. 10708–10720, 2019.

[30] Y. Zheng, J. Xie, X. Xu et al., "LncRNA DDX11-AS1 exerts oncogenic roles in glioma through regulating miR-499b-5p/RWDD4 Axis," *OncoTargets and Therapy*, vol. 14, pp. 157–164, 2021.

Hindawi

Retraction

Retracted: Efficacy Evaluation of Inflammatory Mediators in the Treatment of Multiple Myeloma with Daratumumab

Journal of Oncology

This article has been retracted by Hindawi following an investigation undertaken by the publisher [1]. This investigation has uncovered evidence of one or more of the following indicators of systematic manipulation of the publication process:

(1) Discrepancies in scope

(2) Discrepancies in the description of the research reported

(3) Discrepancies between the availability of data and the research described

(4) Inappropriate citations

(5) Incoherent, meaningless and/or irrelevant content included in the article

(6) Peer-review manipulation

The presence of these indicators undermines our confidence in the integrity of the article's content and we cannot, therefore, vouch for its reliability. Please note that this notice is intended solely to alert readers that the content of this article is unreliable. We have not investigated whether authors were aware of or involved in the systematic manipulation of the publication process.

In addition, our investigation has also shown that one or more of the following human-subject reporting requirements has not been met in this article: ethical approval by an Institutional Review Board (IRB) committee or equivalent, patient/participant consent to participate, and/or agreement to publish patient/participant details (where relevant).

Wiley and Hindawi regrets that the usual quality checks did not identify these issues before publication and have since put additional measures in place to safeguard research integrity.

We wish to credit our own Research Integrity and Research Publishing teams and anonymous and named external researchers and research integrity experts for contributing to this investigation.

The corresponding author, as the representative of all authors, has been given the opportunity to register their agreement or disagreement to this retraction. We have kept a record of any response received.

References

[1] J. Meng, X. Zhao, D. Jiang, C. Liang, X. Ji, and M. Dong, "Efficacy Evaluation of Inflammatory Mediators in the Treatment of Multiple Myeloma with Daratumumab," *Journal of Oncology*, vol. 2022, Article ID 9350211, 6 pages, 2022.

Research Article

Efficacy Evaluation of Inflammatory Mediators in the Treatment of Multiple Myeloma with Daratumumab

Jie Meng,[1] Xiaoyu Zhao,[2] Duanfeng Jiang,[1] Changjiu Liang,[1] Xunxiu Ji,[1] and Min Dong ⬡[1]

[1]*The Second Affiliated Hospital of Hainan Medical University, Haikou 570216, Hainan, China*
[2]*Institute of Microbiology, Heilongjiang Academy of Sciences, Harbin 150010, Heilongjiang, China*

Correspondence should be addressed to Min Dong; mindonghn@hainmc.edu.cn

Objective. This study aimed to investigate the regulatory ability and clinical therapeutic effect of daratumumab on inflammatory mediators in patients with multiple myeloma. *Method.* The Multiple Myeloma Public Genetic Data Array download GSE125361 dataset was collected. The GO analysis and KEGG analysis were performed on the differential genes to elucidate the multiple myeloma cytokine-related gene pathways. Daratumumab is a CD38 monoclonal antibody used to treat multiple myeloma. Patients with newly diagnosed multiple myeloma were treated with monoclonal antibodies containing CD38, and the control group was treated with a regimen without daratumumab. The serum levels of IL-2, IL-4, IL-6, IL-10, TNF-α, and IFN-γ were measured in the two groups before and after treatment and the therapeutic effects of the two groups were compared. *Result.* The KEGG analysis showed that the Th17 cell differentiation, apoptosis, and cytokine-cytokine receptor interaction pathways were differentially expressed in multiple myeloma. The expression levels of serum IL-2, IL-6, IL-10, and TNF-α in patients in the daratumumab group were lower than those in the control group after chemotherapy. The overall effective rate of patients treated with daratumumab after chemotherapy was higher than that of the control group. *Conclusion.* Daratumumab can effectively improve the levels of IL-2, IL-6, IL-10, and TNF-α in patients with multiple myeloma and improve the therapeutic effect.

1. Introduction

Multiple myeloma (MM) is a malignant proliferative disease caused by the abnormal production of B cell monoclonal M protein [1–4]. Clinically, MM is accompanied by complications such as osteolytic injury, repeated infection, and kidney injury [5]. Epidemiological statistics demonstrated that multiple myeloma has a high incidence rate, and it has become the second hematological malignancy after leukemia and lymphoma [6]. Myeloma cells can enter the bone marrow through interactions with stromal cells and osteoblasts, which in turn affect the generation of plasma cells and the differentiation of myeloma cells [7]. The involvement of inflammatory mediators is essential and IL-6 can promote the growth of multiple myeloma cells [8]. Inflammatory pathways such as NF-κB can also promote the growth of multiple myeloma [9]. With the development of pharmacological research, the CD38 monoclonal antibody

for the treatment of multiple myeloma, namely, daratumumab, has made a qualitative leap in the efficacy of multiple myeloma treatment. Daratumumab is a humanized, antiCD38 IgG1 monoclonal antibody that binds to CD38 expressed by tumor cells through complement-dependent cytotoxicity (CDC), antibody-dependent cell-mediated cytotoxicity (ADCC), and antibody-dependent phagocytosis (ADCP), as well as Fcγ receptors and other immune-related mechanisms, to induce tumor cell apoptosis [10]. The current research study on this drug is limited to the complement pathway, antibody-dependent pathway, phagocytosis, and so on. The effect of daratumumab on inflammatory mediators has not been established. The guiding significance of inflammatory mediators in the judgment of clinical efficacy is not yet clear. In this experiment, the method of bioinformatics research will be used to mine inflammatory mediator-related genes in multiple myeloma, and then, the ELISA method will be used to detect

the level of inflammatory mediators in serum, and the clinical treatment effect will be calculated. This study will provide some experience for the clinical treatment of multiple myeloma with daratumumab.

2. Materials and Methods

2.1. Data Collection. The genetic data involved in this study are the GSE125361 chip carried in the public gene chip data platform database on the website of the American National Center for Biotechnology Information, and the chip platform is GPL20844 Agilent-072363 SurePrint G3 Human GE v3 8×60 K Microarray 039494. This version contains mRNA from 45 multiple myeloma samples and 3 control tissue mRNAs.

2.2. Screening of Differential Genes. The analysis of the downloaded data chip was carried out by the R program, which read all the matrix files and then analyzed the multiple myeloma tissue data set and the control group tissue data set with the LIMMA function analysis package to obtain the differentially expressed genes, and then deduplicate the data results. The threshold for filtering was set as $\log2FC \geq 1$ or $\log2FC \leq -1$, absolute value<0.05. Then, the GGPLOT function package was used to load the R program and draw the volcano map.

2.3. Patient Data. A total of 21 patients with multiple myeloma who were admitted to the First District of the Hematology and Cell Therapy Department of the Second Affiliated Hospital of Hainan Medical University between June 2020 and April 2022 were selected. The patients included 9 males and 12 females, aged 51–86 years, with an average age of 67 years. The inclusion criteria for this study were clinical symptoms and auxiliary examinations of the patients. They all met the relevant requirements of the Chinese Guidelines for the Diagnosis and Treatment of Multiple Myeloma. The exclusion criteria were as follows: (1) The patient had a history of infection. (2) The patient is missing, lost to follow-up, or died. (3) The patient's family refused to sign the informed consent. (4) Patients with organ failure. (5) Patients with an impaired liver and kidney function.

2.4. Grouping. Patients were grouped according to whether they were treated with daratumumab. There were 7 males and 7 females in the control group (without daratumumab), aged 51–82 years, with an average age of 68 years. In the experimental group (using daratumumab), there were 2 males and 5 females, aged 52–81 years, with an average age of 65 years. On the basis of the control group, oral administration of daratumumab was added to the experimental group.

2.5. Detection of Serum Cytokines. The nursing staff used a vacuum anticoagulation tube coated with EDTA to collect 5 ml of cubital venous blood for all patients after admission, before chemotherapy, and after each chemotherapy for the

first ten times. After the collection, the samples of the patients were sent to the laboratory for examination. The levels of IL-2, IL-4, IL-6, IL-10, TNF-α, and IFN-γ were measured using commercial ELISA kits (Beyotime, China) according to the manufacturer's instructions.

2.6. Patient Evaluation. The efficacy evaluation indexes of patients involved blood routine, liver function, renal function, serum ions, immunoglobulin, β-microglobulin, bone marrow image, and protein electrophoresis.

2.7. Statistical Analysis. The statistical analysis was performed using SPSS 24.0 software (IBM SPSS Statistics, Chicago, USA). The data were presented as mean ± standard deviation (SD). All data were first tested for homogeneity of variance. After the homogeneity of variance test was satisfied, the T test was used for the measurement data and the chi-squared test was used for the count data. Differences within groups were analyzed by the F test and sequence data by the Wilcox-rank sum test. A two-sided P value less than 0.05 was considered statistically significant.

3. Result

3.1. The Differential Gene Expression of the GSE125361 Dataset. As shown in Figures 1(a) and 1(b), a total of 3553 differential genes, of which 1430 were upregulated and 2123 were downregulated, were identified in the GSE125361 dataset. In the volcano map, the genes with FC differences more than 2 times and statistically significant differences were counted and observed. The GO analysis of upregulated genes revealed biological processes focused on endoplasmic reticulum unfolded protein response, ubiquitin-dependent ERAD pathway, response to endoplasmic reticulum stress, apoptotic processes, negative regulation of viral processes, cellular components involved in membrane components of the receptor complex, components of the endoplasmic reticulum membrane, endoplasmic reticulum membrane, and endoplasmic reticulum. The KEGG-involved pathway includes protein processing in the endoplasmic reticulum, Th17 cell differentiation, apoptosis, and cytokine-cytokine receptor interaction.

3.2. GO and KEGG Analysis of Differential Genes. GO and KEGG signaling pathway enrichment analysis of upregulated genes was performed using David's website online analysis of differential genes, and the specific results are shown in Figure 2. The GO analysis showed that biological processes were concentrated in the endoplasmic reticulum unfolded protein response, ubiquitin-dependent ERAD pathway, response to endoplasmic reticulum stress, apoptosis process, negative regulation of the viral process, cellular components involved in membrane components, receptor complex, components of endoplasmic reticulum membrane, endoplasmic reticulum membrane, and endoplasmic reticulum. The KEGG-involved pathway included protein processing in the endoplasmic reticulum, Th17 cell
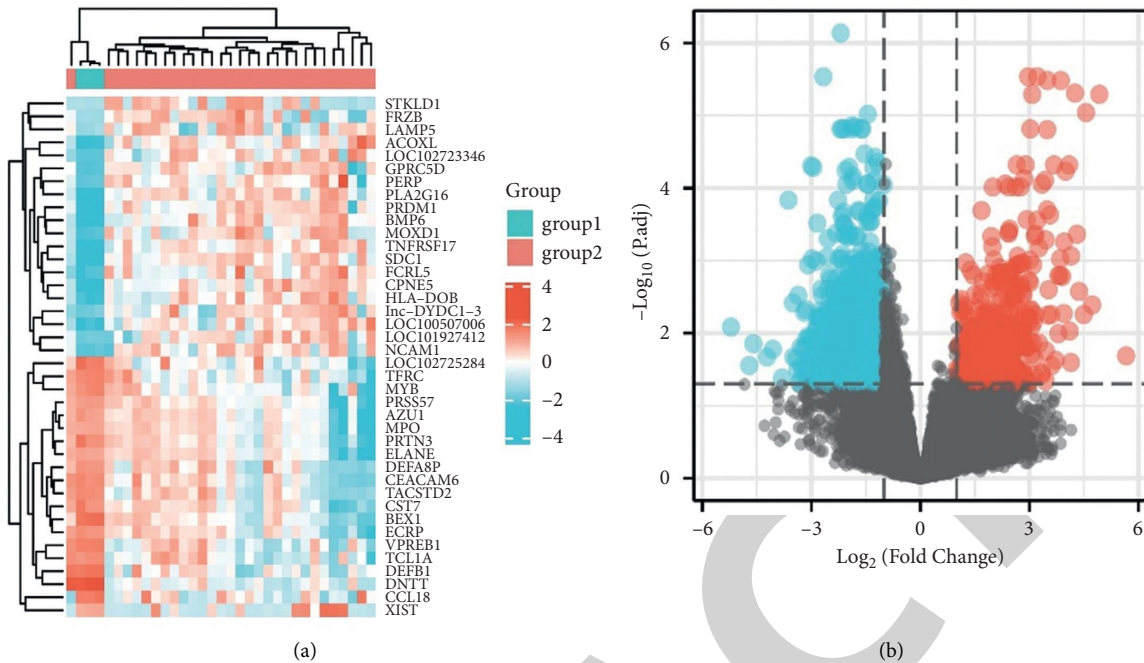
(a)

(b)

FIGURE 1: (a) Expression heat map of the dataset and (b) volcano plots showing differentially expressed genes.

differentiation, apoptosis, and cytokine-cytokine receptor interaction. The genes involved in cytokine-cytokine receptor interactions include TNFRSF17, BMP4, BMP6, BMPR1A, CD40, CCR10, IFNAR2, IL2RB, IL5RA, IL6R, IL6ST, IL12RB1, IL15, IL16, CCL3, CCL24, XCL1, TNFRSF14, TNFRSF10A, IL32, IL27RA, CCL4L2, TNFRSF13B, IL22RA1, EDA2R, ACVR1C, IFNLR1, and BMP8A (see Figure 3).

3.3. Basic Information of Patients in the Two Groups.
The basic data of patients in the two groups are shown in Table 1. The statistical analysis of the basic data of the patients in the daratumumab group compared with the control group showed that the data difference was not statistically significant ($P > 0.05$).

3.4. Serum Levels of Inflammatory Cytokines in the Two Groups of Patients.
The expression levels of serum inflammatory factors in the two groups of patients are shown in Table 2. The serum levels of IL-2, IL-6, IL-10, and TNF-α in patients in the daratumumab group were significantly lower than those in the control group ($P < 0.05$).

3.5. Curative Effect Distribution of Patients in the Two Groups.
The therapeutic effects of the two groups are shown in Table 3. The treatment effect in the daratumumab group was significantly higher than that in the control group ($P < 0.05$).

4. Discussion

Multiple myeloma is the most common malignant plasma cell tumor, and abnormal serum cytokines are the most common phenomena in patients with multiple myeloma. At present, the cause of abnormal serum cytokines is not clear, but it is generally believed that these inflammatory factors are autocrine by tumor cells or secreted by lymphocytes after tumor stimulation. Several growth factors have been shown to promote the growth of multiple myeloma tumors. In this study, the activation of the cytokine-cytokine receptor interaction pathway was found to be an obvious KEGG pathway in differentially expressed genes by selecting microarray data sets from multiple myeloma tissues. TNFRSF17, BMP4, BMP6, BMPR1A, CD40, CCR10, IFNAR2, IL2RB, IL5RA, IL6R, IL6ST, IL12RB1, IL15, IL16, CCL3, CCL24, XCL1, TNFRSF14, TNFRSF10A, IL32, IL27RA, CCL4L2, TNFRSF13B, IL22RA1, EDA2R, ACVR1C, IFNLR1, and BMP8A are genes activated in this pathway. Among them, TNFRSF14 and TNFRSF10A are the code genes of TNF receptor family member proteins, IL6R and IL6ST are the code genes of IL-6 receptor proteins, IL2RB is the code gene of the IL-2 receptor protein family, and IFNLR1 is the code gene of the IL-10 receptor protein. The activation of these genes indicates that the translation level of the receptor protein has increased, and the reason for the upregulation of the receptor is the increase in the number of ligands. IL-6, IL-2, IL-10, and TNF-α play a prominent role in the pathogenesis of multiple myeloma.

IL-6 is an important cytokine for multiple myeloma cell growth [11–14], which can be secreted by bone marrow stromal cells. IL-6R is a transmembrane protein on the cell membrane, and its binding to IL-6 triggers the activation of the Jak-STAT pathway [15], leading to further gene activation. At the same time, IL-6 can also promote cell proliferation directly through the activation of the RAS-MAP pathway [16]. IL-10 promotes cell proliferation by inducing the expression of IL-11 [17]. IL-2 and TNF-α are cytokines
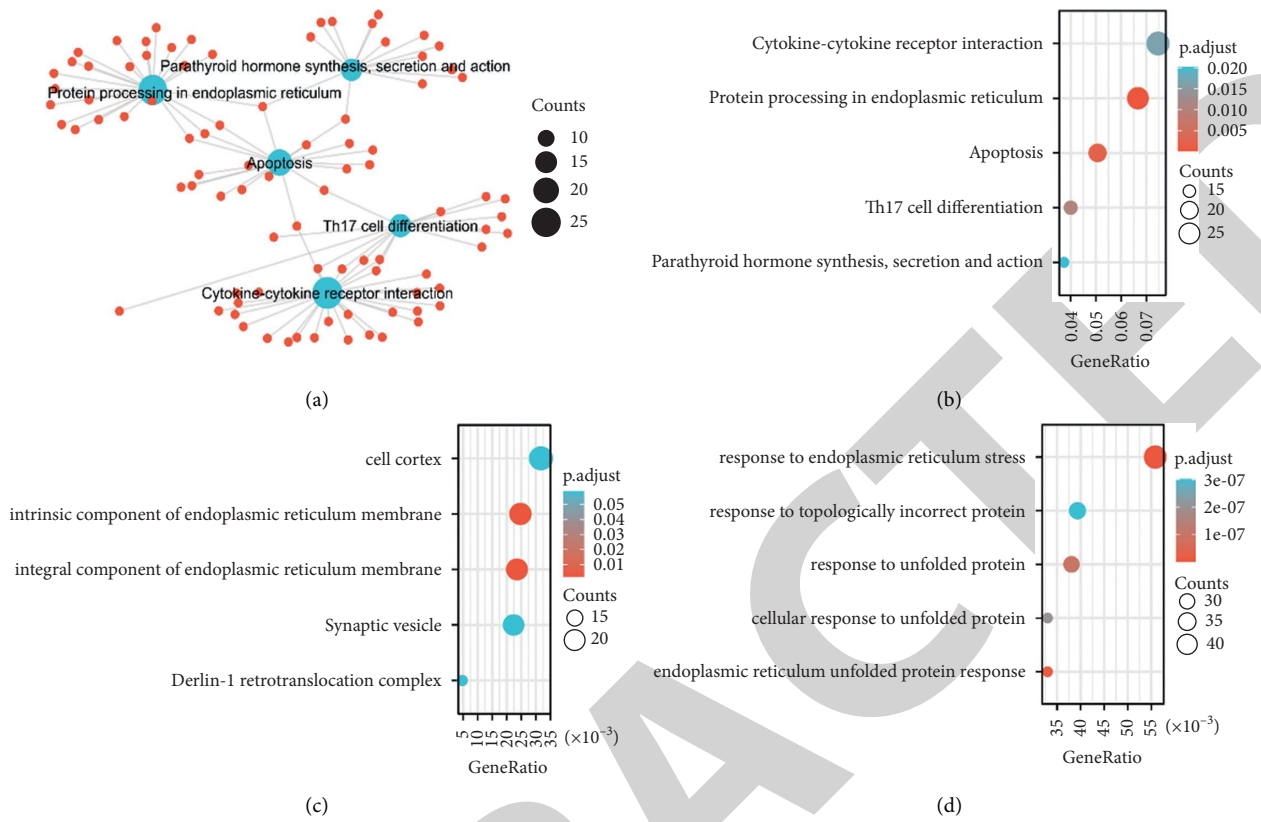
(a)

(b)

(c)

(d)

Figure 2: (a) GO and (b, c, d) KEGG pathway enrichment of dataset.
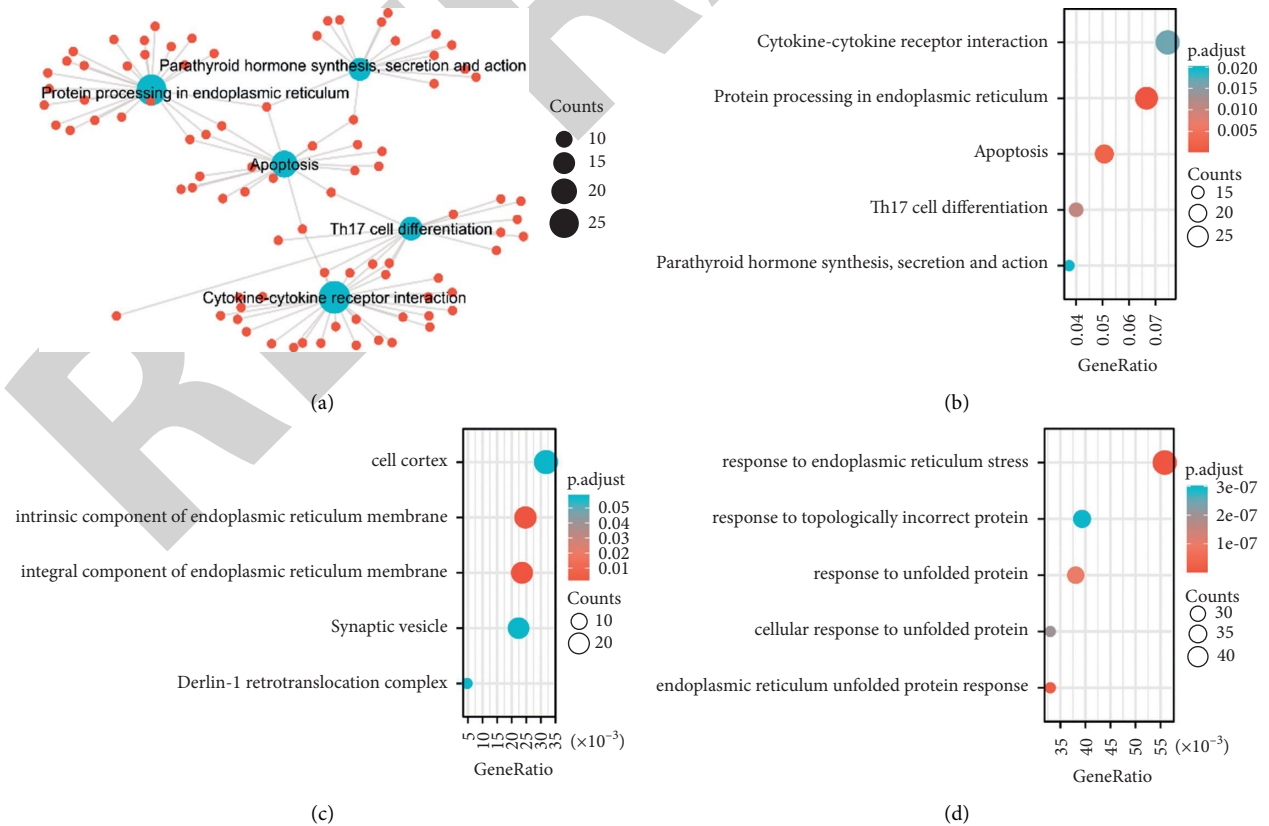

(a)

(b)

(c)

(d)

Figure 3: (a) KEGG. (b) KEGG. (c) BP. and (d) CC.

TABLE 1: Disease characteristics of enrolled patients.

	Experimental group	Control group
Gender	2 : 5	7 : 7
Age	Age 52–81 (average 65)	Age 51–82 (average 68)
DS staging ratio (I : II : III)	0 : 0 : 100%	0 : 0 : 100%
ISS staging ratio (I : II : III)	1 : 4 : 2	1 : 5 : 8
R-ISS staging ratio (I : II : III)	0 : 1 : 6	1 : 6 : 7
SMART staging (standard risk: high risk)	1 : 6	10 : 4

TABLE 2: Serum levels of inflammatory factors in the two groups.

	IL-2	IL-4	IL-6	IL-10	TNF-α	INF-γ
Experimental group (pg/ml)	62.53	0.52	489.34	72.69	3.36	17.12
Control group (pg/ml)	<0.97	0.57	10.58	1.75	<0.85	16.15

TABLE 3: Curative effect of patients in the two groups.

	Complete remission (%)	Very good partial remission. (%)	Partial remission (%)	Ineffective (%)
Experimental group	14.29	42.86	28.57	14.29
Control group	0	33.33	55.56	11.11

that play a protective role in multiple myeloma [18]. TNF-α is an important molecule in the autoimmune stage of the body, which has a certain role in tumor killing and inhibiting tumor growth [19]. IL-2 can induce the production of NK cells and increase the ability to dissolve tumor cells [20]. The data in Table 2 show that the levels of IL-2 and TNF-α are lower in patients treated with daratumumab in this experiment. This may be due to the toxic effects of the drug on multiple myeloma cells, which cause cell damage, and the decrease in cell numbers reduces the body's related mechanism of killing it. The decrease of IL-6 and IL-10 indicates that when daratumumab is used in the treatment of multiple myeloma, its main mechanism of tumor inhibition is related to it. Daratumumab is a monoclonal antibody drug against CD38. This drug can induce cytolytic death through the interaction of cytotoxicity, antibody-dependent cellular cytotoxicity, and antibody-dependent cellular phagocytosis. This drug can also adjust the immune microenvironment of tumors and eliminate the inhibitory ability of TREGS, BREGS, and other cells, to improve the level of inflammatory factors. In this experiment, through the data in Table 3, it can be found that daratumumab is more effective in patients. The reason for this phenomenon is not only that the drug can kill myeloma but also that the drug can increase the secretion level of the myeloma stroma and cytokines. Therefore, improving the cytokines of the tumor microenvironment is an important mechanism to improve the treatment of multiple myeloma.

In conclusion, daratumumab can inhibit the expression levels of IL-6, IL-2, IL-10, and TNF-α in patients with multiple myeloma, thereby inhibiting the growth of multiple myeloma. However, this experiment cannot carry out the verification of related genes due to the limitation of conditions. In future research, we will verify the expression level

of related genes by the RT-qPCR method, in order to expect to obtain more abundant theoretical results.

Data Availability

All the data are within the manuscript.

Conflicts of Interest

The authors declare that they have no conflicts of interest.

Acknowledgments

References

[1] I. Vaxman, E. Muchtar, P. Kapoor et al., "Chemotherapy-based stem cell mobilization in multiple myeloma patients treated with novel agents: the mayo clinic experience," *Journal of Clinical Oncology*, vol. 39, no. 15_suppl, Article ID e20000, 2021.

[2] P. Moreau, M. A. Dimopoulos, J. Mikhael et al., "Isatuximab, carfilzomib, and dexamethasone in relapsed multiple myeloma (IKEMA): a multicentre, open-label, randomised phase 3 trial," *Lancet*, vol. 397, no. 10292, pp. 2361–2371, 2021.

[3] S. Mastaglio, P. Genovese, Z. Magnani et al., "NY-ESO-1 TCR single edited stem and central memory T cells to treat multiple myeloma without graft-versus-host disease," *Blood*, vol. 130, no. 5, pp. 606–618, 2017.

[4] L. H. Wang, X. Y. Yang, K. Mihalic, W. Xiao, D. Li, and W. L. Farrar, "Activation of estrogen receptor blocks

Research Article

Identification of MAN1B1 as a Novel Marker for Bladder Cancer and Its Relationship with Immune Cell Infiltration

Xueping Wang, Bin Chen, Yifang Cao, Yi He, and Wei Chen [ORCID]

Department of Urology, The Affiliated Hospital of Jiaxing University, Jiaxing, Zhejiang, China

Correspondence should be addressed to Wei Chen; chenwjxyy@126.com

Bladder cancer (BC) is a common malignant tumor of the genitourinary system, and there are not enough tumor biomarker tests that are specific, trustworthy, and noninvasive for the diagnosis and prognosis. The purpose of this study is to investigate the clinical relevance, prognostic value, and immunological signature of Mannosidase alpha class 1B member 1(MAN1B1) expressions in BC. The Cancer Genome Atlas (TCGA) and Genotype-Tissue Expression (GTEx) databases provided the raw information that was used to analyze the expression of MAN1B1 in tumor patients. Then, a statistical study was carried out to assess the correlations of MAN1B1 expression with the clinical characteristics and the prognosis of BC. The correlation between MAN1B1 expression and tumor immune infiltration was explored via single-sample gene set enrichment analysis (ssGSEA). In human cancers, MAN1B1 expressions were shown to be generally higher in tumors than in normal specimens. We confirmed that MAN1B1 expression was distinctly increased in BC specimens compared with nontumor specimens. BC specimens with advanced T stage and M stage showed a higher level of MAN1B1. Survival analysis revealed that the overall survival (OS), disease-specific survival (DSS), and progression-free interval (PFI) of patients with high MAN1B1 expressions were distinctly worse than those with low MAN1B1 expressions. Importantly, multivariate analyses only confirmed that MAN1B1 expression was an independent prognostic factor for OS of the patients with BC. Furthermore, we observed that MAN1B1 expression level was significantly correlated with abundance of multiple immune infiltrates including Th2 cells, macrophages, Th1 cells, neutrophils, T helper cells, and NK CD56 bright cells. In conjunction with all of these findings, elevated MAN1B1 expression is associated with a poor prognosis and a higher number of immune cells in BC. MAN1B1 has the potential to act as a biomarker that can evaluate both the patient's prognosis and the degree of immune infiltration in BC.

1. Introduction

Bladder cancer (BC) is the fourth most prevalent cancer in men and the most frequently diagnosed malignancy of the urinary system worldwide [1]. The risk of developing BC increases with age, and there has been a discernible rising trend in the overall incidence of BC over the past several years [2, 3]. Approximately 90 percent of all cases of cancer are classified as transitional cell carcinoma. The majority of bladder cancers are known as nonmuscle-invasive bladder cancers (NMIBCs), which frequently recur and progress into muscle-invasive bladder cancers [4, 5]. MIBCs account for around 30 percent of all cases of BC, and the treatment of choice for these cases is radical cystectomy in conjunction

with pelvic lymph node dissection [6, 7]. In contrast to the majority of other malignancies, the diagnostic procedures, treatment options, and percentage of patients who are still alive after five years have not altered in the past three decades [8, 9]. With a recurrence rate of between 60 and 70 percent, BC continues to be a significant risk to human health all over the world. As a consequence of this, it is necessary to create methods of precise prediction in order to advance clinical diagnosis and therapy.

Mannosidase alpha class 1B member 1(MAN1B1), located on 9q34.3, encodes an enzyme belonging to the glycosyl hydrolase 47 family [10]. This enzyme has a role in N-glycan biosynthesis and belongs to the class I alpha-1,2-mannosidase family [11]. It converts Man9GlcNAc to

Man8GlcNAc isomer B in a very particular manner. MAN1B1 encoded α-1,2-mannosidase α-Mannosidase is known to have an important role in both the modification of protein glycosylation and the hydrolysis of glycoprotein polysaccharides [12, 13]. It is composed of many different classes, including -Mannosidases I, -Mannosidases II, and unclassified -Mannosidase [14]. Evidence indicating alpha-mannosidase has a role in the progression of cancer has been accumulating steadily over the years [15–17]. However, the potential function of MAN1B1 in tumors was rarely reported. In the current investigation, our goals were to investigate the predictive significance of MAN1B1 in BC and to investigate its connection with immune infiltration.

2. Materials and Methods

2.1. Raw Data Acquisition and Processing. The Cancer Genome Atlas (TCGA) research network has profiled and evaluated a massive collection of clinical data on > 10,000 cancer patients representing 33 distinct types of tumors. Downloading clinical data and RNA expression information from the TCGA and Genotype-Tissue Expression (GTEx) databases was accomplished through the usage of the UCSC Xena database (https://xenabrowser.net/datapages/). 33 cancer types were included: OV, PAAD, PRAD, READ, SKCM, STAD, TGCT, THCA, THYM, UCEC, UCS, ACC, BLCA, BRCA, COAD, DLBC, ESCA, GBM, HNSC, KICH, KIRC, KIRP, LAML, LGG, LIHC, LUAD, and LUSC.

2.2. Analysis of MAN1B1 Expression in Cancers. The TCGA and GTEx projects were the sources for the information regarding the abnormal expressions of MAN1B1 between cancer and normal specimens that were matched to the tumor. A tissue bank and data resource known as GTEx (https://gtexportal.org) was established by the National Institutes of Health (NIH) Common Fund. In total, 53 human normal specimens from approximately 1,000 individuals have been analyzed for RNA sequencing, genetic variation and molecular phenotypes. Plotting was done using log2 (TPM + 1) converted expression data, which was our choice for the parameter selection process.

2.3. Cox Regression Analysis and Survival Analysis. In order to investigate the connection between MAN1B1 expressions and patients' overall survival (OS), disease-specific survival (DSS), and progression-free interval (PFI) in bladder urothelial carcinoma(BLCA) patients, a Cox regression analysis was carried out in the R environment. After using the best approach for separating patients into groups with high and low MAN1B1 expression, the Kaplan–Meier methods were applied to produce survival curves for patients. This was done after sorting patients into groups with high or low MAN1B1 expressions. An examination of the survival was carried out with the aid of survival receiver operating characteristics (ROC) and the survival package in R. The log-rank test was applied to analyze the differences between the curves, and a $p < 0.05$ was considered statistically significant.

2.4. Immune Cell Infiltration. Using ssGSEA, the relative degrees of tumor infiltration by 24 different immune cell types were assessed. This allowed us to investigate the expression of genes found in published signature gene lists. The signatures that we used contained a total of 509 genes and included a wide variety of cell types involved in both adaptive and innate immune responses. The Wilcoxon rank sum test and Spearman correlation were utilized in order to investigate whether or not there is a connection between MAN1B1 and the infiltration levels of immune cells, as well as whether or not there is an association between the infiltration levels of immune cells and the various expression groups of MAN1B1.

2.5. Statistical Analysis. All statistical analyses were performed in the R package (V3.6.2). The Wilcoxon test was utilized in order to compare the differences between two groups of data that were not regularly distributed. The relationship between clinical pathologic features and MAN1B1 was analyzed with the Wilcoxon signed-rank sum test and logistic regression. ROC curves were established to evaluate the diagnostic value of MAN1B1 in BC patients. A $p < 0.05$ was considered statistically significant.

3. Results

3.1. MAN1B1 Expression in Pan-Cancer. Based on TCGA datasets, we investigate the level of MAN1B1 expression in each of the many cancer types. Figure 1(a) showed that the levels of MAN1B1 expression in the tumor specimens of ACC, BLCA, BRCA, CESC, CHOL, COAD, DLBC, GBM, HNSC, KICH, KIRC, KIRP, LAML, LGG, LIHC, LUAD, LUSC, SARC, STAD, THYM, UCEC, and UCS are all higher than those in the nontumor tissues. However, the expression of MAN1B1 in the tumor tissues of SKCM and TGCT was significantly lower than that in the normal tissues (Figure 1(a)). The expression of MAN1B1 in BLCA is shown in Figure 1(b). Due to the considerable overexpression of MAN1B1 in BLCA patients, we were motivated to further investigate the diagnostic significance of this gene for BLCA patients. As shown in Figure 1(c), the results of ROC curves revealed that the AUC was 0.793 (0.6999 to 0.888, 95% CI) in a comparison between BLCA specimens and nontumor specimens. In addition, we also performed a paired *t*-test. A similar finding was also observed (Figures 2(a) and 2(b)). Our findings suggest that overexpression of MAN1B1 in malignancies may be a common occurrence.

3.2. Association between Clinicopathological Characteristics and MAN1B1 Expression in BLCA Patients. We evaluated the association between the expression of MAN1B1 and the clinicopathological aspects of BLCA in order to further define the relevance of MAN1B1 in BLCA. This was done in order to better understand the role that MAN1B1 plays in BLCA. On the basis of the median relative MAN1B1 expression value, all of the patients diagnosed with BLCA were separated into two groups. As shown in Table 1, we did not observe a distinct association between MAN1B1 expression

(a)

(b)

(c)
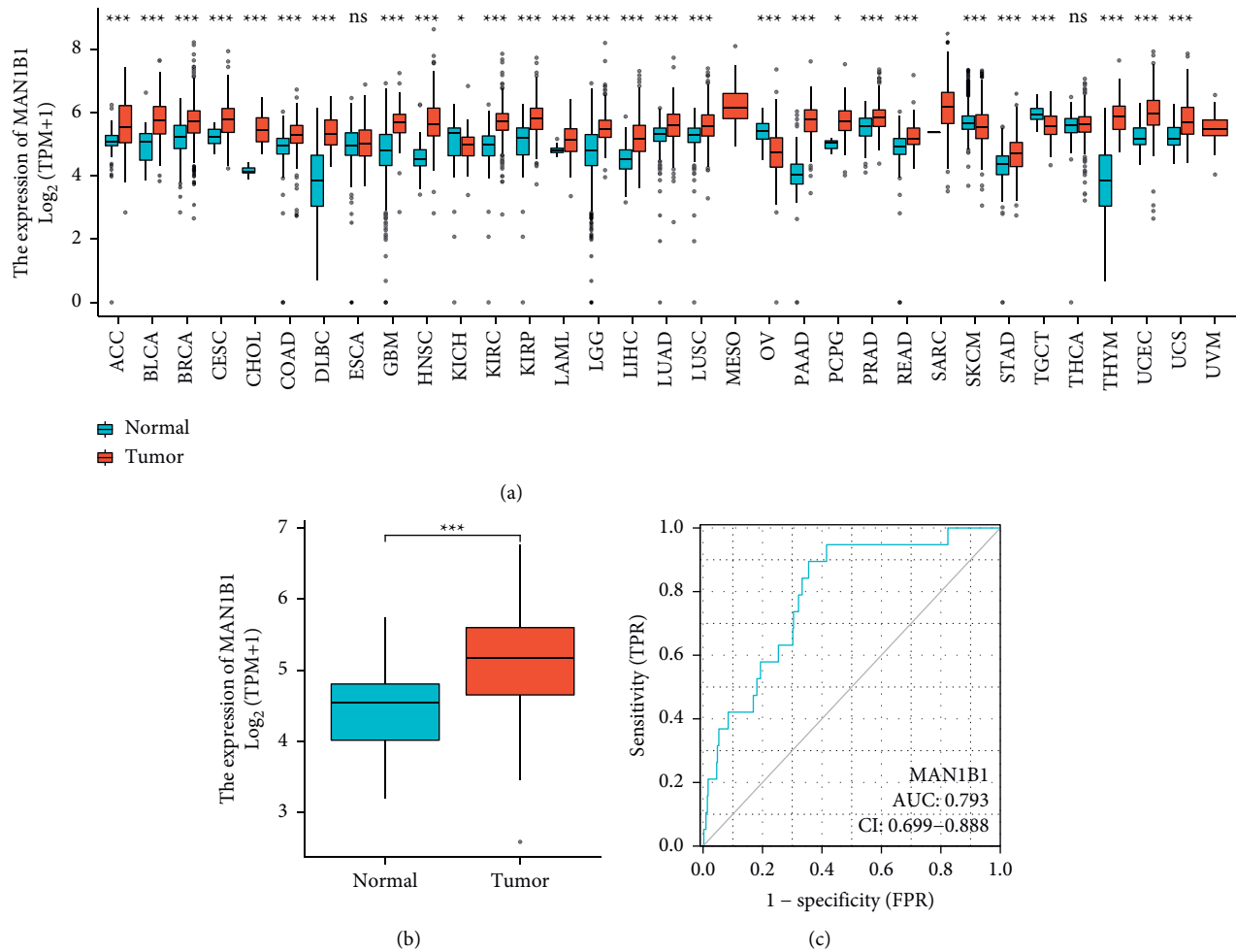
FIGURE 1: TCGA and GTEx databases show MAN1B1 expression in both healthy and cancerous tissues. (a) pan-cancer analysis. (b) MAN1B1 expression was increased in BC specimens compared with nontumor specimens. (c) MAN1B1's ROC in BC. on the X-axis, false-positive rates are measured; on the Y-axis, true-positive rates are measured. $^{*} p < 0.05$, $^{**} p < 0.01$, $^{***} p < 0.001$.

and several clinical factors based on the results of the chi square test. In the T-test, we also did not observe a distinct association between MAN1B1 expression and gender and age (Figures 3(a) and 3(b)). However, we found that BLCA specimens with advanced T stage and M stage showed a higher level of MAN1B1 (Figures 3(c) and 3(d)). The expression of MAN1B1 did not change distinctly in specimens with different N stages (Figure 3(e)). Moreover, we found that the expression of MAN1B1 was distinctly increased in BLCA specimens with high grade or dead status (Figure 3(f) and 3(g)).

3.3. Associations between MAN1B1 Expression and Patient Survival. To explore the relationships between MAN1B1 expressions and survivals of BLCA patients, Kaplan–Meier methods were performed to analyze the differences in OS, DSS, and PFI. As shown in Figure 4, the OS, DSS, and PFI of patients with high MAN1B1 expressions were distinctly worse than those with low MAN1B1 expressions. In univariate analyses, we observed that MAN1B1 expression was associated with OS

(Table 2), DSS (Table 3), and PFI (Table 4) of BLCA patients. However, multivariate analyses only confirmed that MAN1B1 expression (HR = 1.970, 95% CI 1.226–3.167, $p = 0.005$) was an independent prognostic factor for OS of the patients with BLCA (Table 2). The potential prognostic values of MAN1B1 used as an independent prognostic factor for DSS and PFI of BLCA patients were not further confirmed (Tables 3 and 4).

3.4. The Correlation between MAN1B1 Expression and Immune Infiltration. The spearman correlation test was used to investigate the relationship between the expression of MAN1B1 and the amount of immune cell infiltration that was measured using ssGSEA. The abundance of acquired immunocytes, such as T helper cells and NK CD56bright cells, was found to have a negative correlation with the expression of MAN1B1, while the abundance of innate immunocytes, such as Th2 cells, Macrophages, Th1 cells, Neutrophils, NK CD56dim cells, and other such cells, had a positive correlation with the expression of MAN1B1 (Figure 5).

(a)

(b)
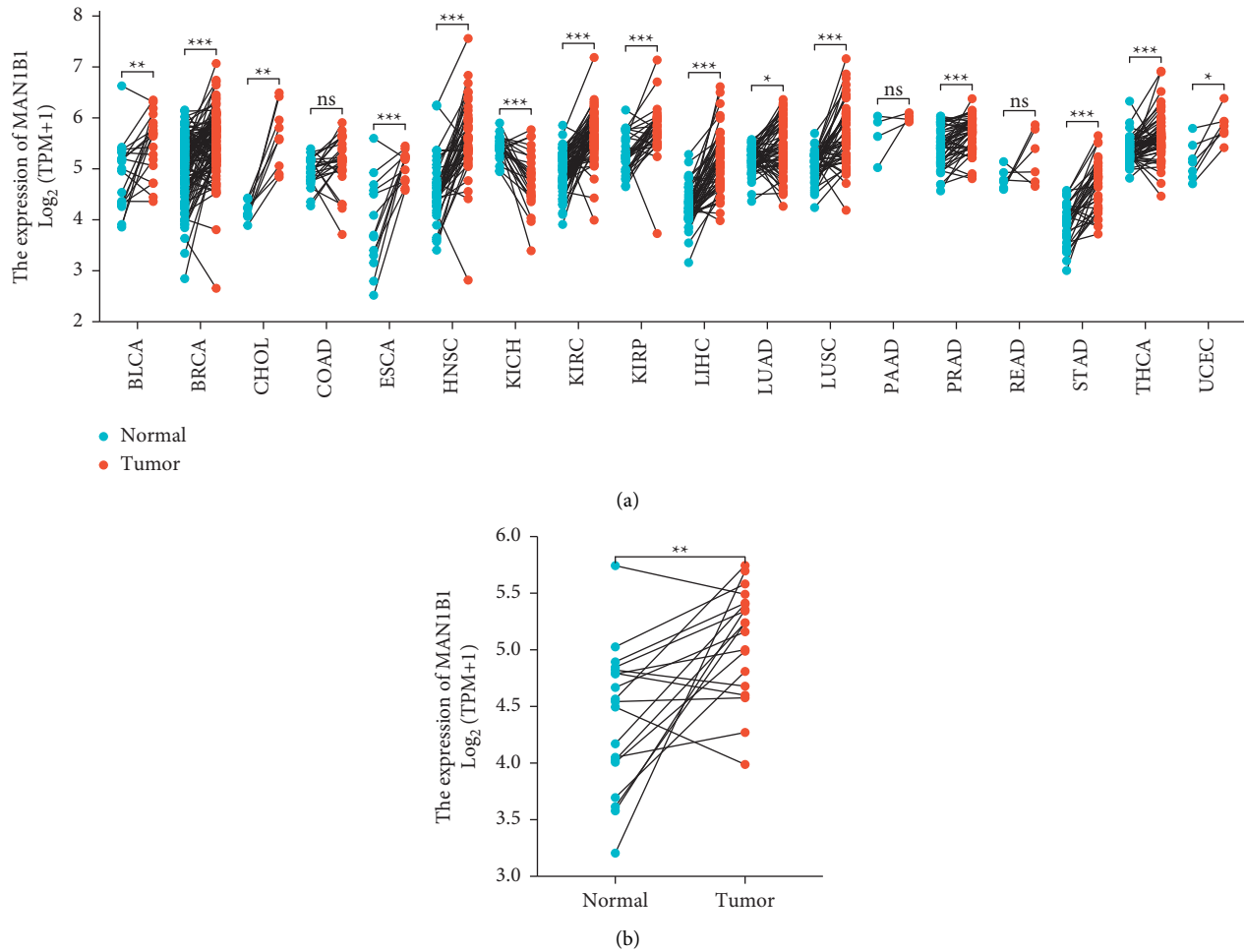
FIGURE 2: TCGA and GTEx databases' unpaired t-tests reveal MAN1B1 expression in healthy and cancerous tissues. (a) pan-cancer analysis. (b) MAN1B1 expression in BC and nontumor specimens. $^{*}p < 0.05$, $^{**}p < 0.01$, $^{***}p < 0.001$.

4. Discussion

A number of cancers, including carcinomas, share a phenomenon known as deregulation of tumor-related genes, which plays a significant part in the progression of cancer via a variety of intricate pathways [18, 19]. Alterations in the expression of a particular gene have been shown to have a strong correlation both with the development of human malignancies and their overall prognosis [20, 21]. Thus, to better understand how BC develops and progresses, finding mRNA molecular profiles related to a patient's prognosis could reveal biological mechanisms at work. It could also lead to the discovery of new therapeutic targets for the disease.

MAN1B1 is a newly identified tumor-related gene. Previous study by Wang et al. reported that the expressions of MAN1B1 were distinctly higher in cancerous specimens than in nontumor samples. In addition, there was a correlation between increased MAN1B1 expression and a bad prognosis in patients with BC. In functional experiments, the suppression of MAN1B1 resulted in a reduction of BC cell proliferation, invasion, and migration [22]. To our best

knowledge, this is the only research about the function of MAN1B1 in tumor. In this study, we first performed a pan-cancer analysis and observed that MAN1B1 expression was distinctly increased in most types of tumors, which was consistent with previous findings in BC. Our data revealed that MAN1B1 may serve as an oncogene in human tumors. Then, we further explored the relationships between MAN1B1 expressions and the prognosis of BC patients. We found that BC specimens with advanced stages showed an increased level. Interestingly, we found that the BC specimen with a dead event also showed an increased level of MAN1B1, suggesting that MAN1B1 may influence the clinical outcome of BC patients. The results of Kaplan–Meier methods confirmed that the OS, DSS, and PFI of patients with high MAN1B1 expression was significantly worse than those with low MAN1B1 expression. More importantly, multivariate analyses only confirmed that MAN1B1 expression were an independent prognostic factor for OS of the patients with BC. Our findings suggest MAN1B1 as a novel diagnostic and prognostic biomarker for BC patients.

Recent research studies have demonstrated that immune cells that infiltrate tumors, known as tumor infiltrating cells

TABLE 1: Correlation between MAN1B1 expression with clinicopathologic features of BLCA.

Characteristic	Low expression of MAN1B1	High expression of MAN1B1	p
n	207	207	
T stage, n (%)			0.121
T1	4 (1.1%)	1 (0.3%)	
T2	65 (17.1%)	54 (14.2%)	
T3	86 (22.6%)	110 (28.9%)	
T4	32 (8.4%)	28 (7.4%)	
N stage, n (%)			0.111
N0	126 (34.1%)	113 (30.5%)	
N1	16 (4.3%)	30 (8.1%)	
N2	42 (11.4%)	35 (9.5%)	
N3	5 (1.4%)	3 (0.8%)	
M stage, n (%)			0.336
M0	129 (60.6%)	73 (34.3%)	
M1	5 (2.3%)	6 (2.8%)	
Gender, n (%)			0.655
Female	52 (12.6%)	57 (13.8%)	
Male	155 (37.4%)	150 (36.2%)	
Age, n (%)			0.921
<=70	118 (28.5%)	116 (28%)	
>70	89 (21.5%)	91 (22%)	
Age, median (IQR)	69 (60, 76)	68 (60, 76)	0.880

(a)

(b)

(c)

(d)

(e)

(f)

FIGURE 3: Continued.

(g)
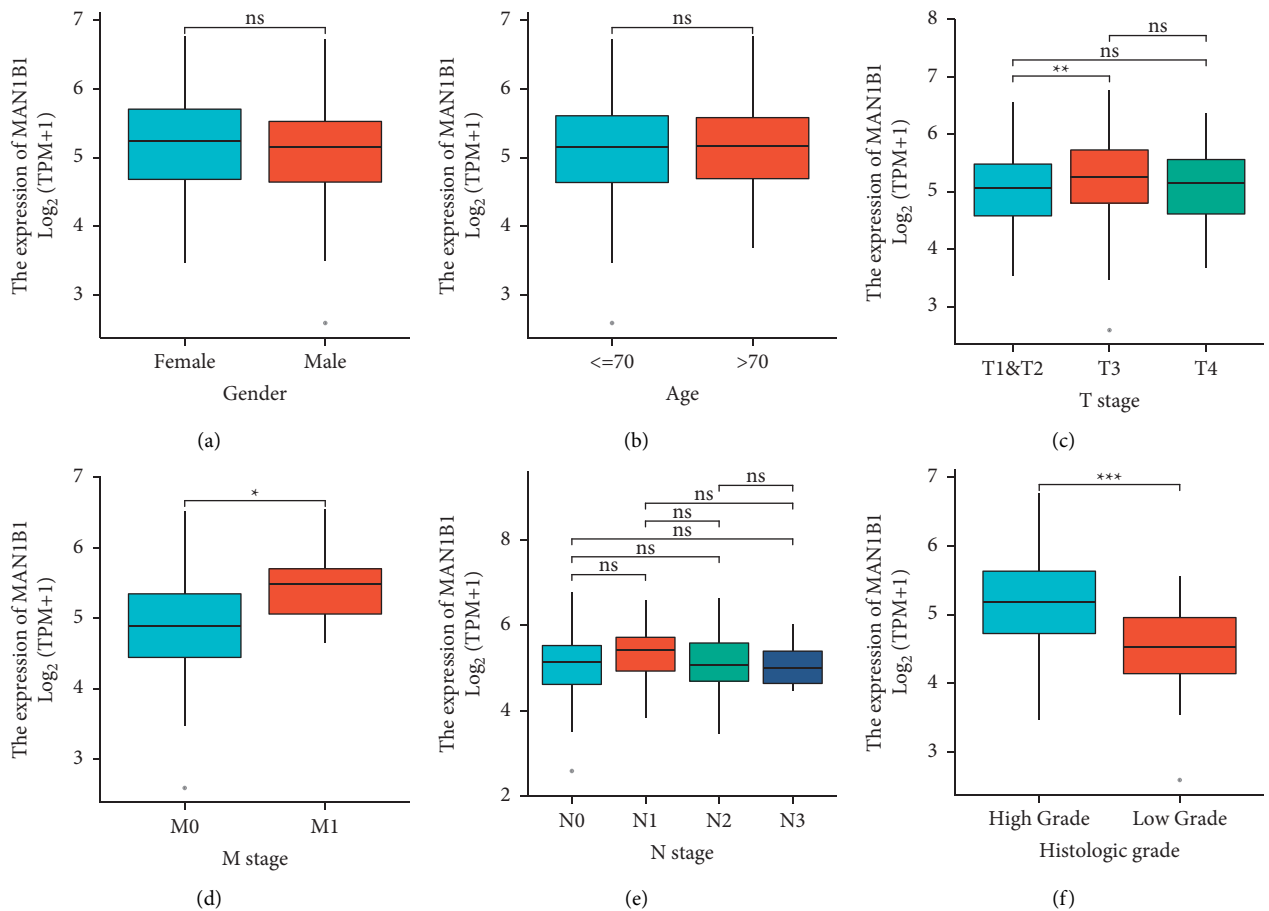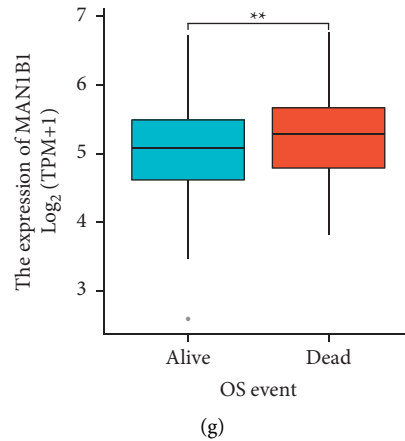
Figure 3: The associations between MAN1B1 expressions and several clinical factors. (a) gender, (b) age, (c) T stage, (d) M stage, (e) N Stage, (f) histologic grade, (g) OS event. $^*p < 0.05$, $^{**}p < 0.01$, $^{***}p < 0.001$.

(a)

(b)

(c)
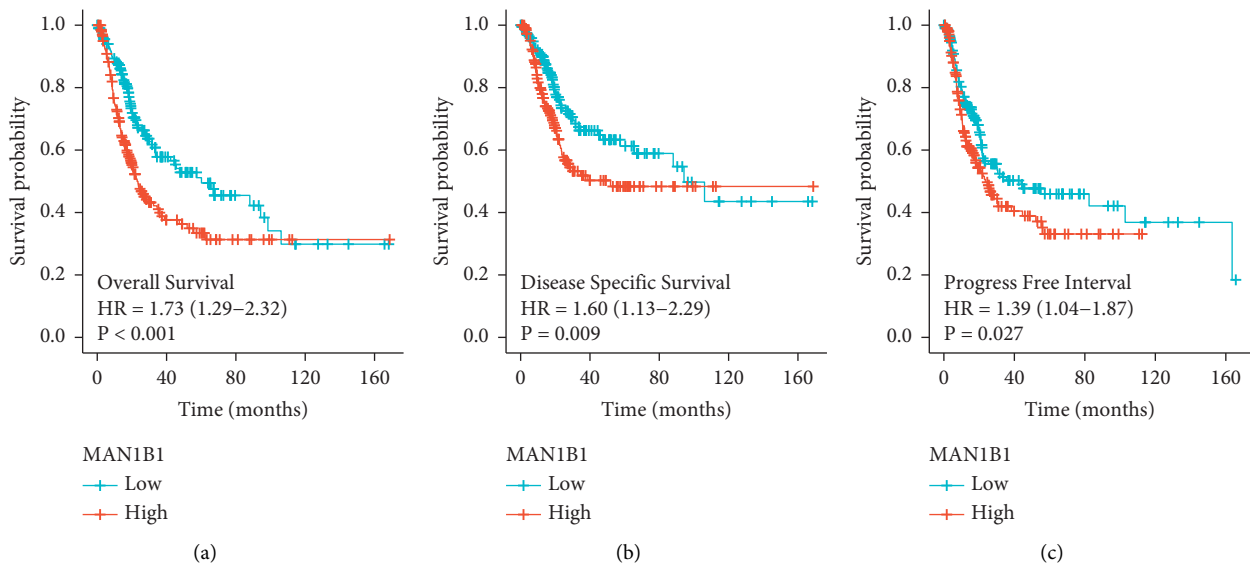
Figure 4: Kaplan–Meier curves estimating the OS, DSS, and PFI rates according to the expressions of MAN1B1 in patients with BC.

(TIICs), may be able to control the process of both the genesis and progression of tumors [23, 24]. In addition to this, TIICs have the capacity to undergo clonal expansion and are enriched preferentially in BC; a poor prognosis has been shown to correspond with an accumulation of TIICs in BC [25]. Then, our results demonstrated that MAN1B1 expression in BC was negatively associated with multiple types of immune cell infiltration. In previous studies, although it has been reported that the functions and prognostic relevance of numerous subtypes of TIICs in multiple forms of cancer are inconsistent, some of the results are still unclear. For example, infiltrating CD8+ T cells are generally considered to be tumor inhibitors that are associated with a positive prognosis in most types of cancer; however, in renal cell carcinoma and prostate cancer, CD8+ T cells are reported to be associated with poor clinical outcomes [26–29]. This is because infiltrating CD8+ T cells are

associated with an increased risk of death. In addition, Hald et al. observed that CD8+ T cells were a predictor of a favorable prognosis in non-small-cell lung cancer [30]; however, the findings of Tian et al., who found that CD8+ T cells serve as a predictor of a less favorable prognosis, were in direct opposition to Hald et al. [31]. In macrophages, natural killer (NK) cells, and dendritic cells, researchers have obtained results that are similarly inconsistent. Due to the specialized roles and prognostic value of TIICs, additional samples and research work that are thoroughly developed are required to confirm the prognostic significance of these cells. In this investigation, we showed that the expression of MAN1B1 was connected with the presence of immune cells in the majority of tumors, which suggests that it may have an effect on the immunological status in BC.

There were several limitations to this study. First, since all of the data used in this study were obtained by

Table 2: Univariate and multivariate analysis of OS in BLCA patients.

Characteristics	Total (N)	Univariate analysis		Multivariate analysis	
		Hazard ratio (95% CI)	p value	Hazard ratio (95% CI)	p value
T stage	379				
T1 & T2	124	Reference			
T3	195	1.997 (1.358–2.939)	**<0.001**	1.975 (1.019–3.826)	**0.044**
T4	60	3.095 (1.934–4.954)	**<0.001**	2.572 (1.154–5.732)	**0.021**
N stage	369				
N0	239	Reference			
N1	46	1.858 (1.199–2.879)	**0.006**	1.634 (0.850–3.142)	0.141
N2 & N3	84	2.581 (1.828–3.646)	**<0.001**	2.176 (1.206–3.928)	**0.010**
M stage	213				
M0	202	Reference			
M1	11	3.136 (1.503–6.544)	**0.002**	1.028 (0.381–2.777)	0.956
MAN1B1	413				
Low	207	Reference			
High	206	1.728 (1.286–2.323)	**<0.001**	1.970 (1.226–3.167)	**0.005**
Age	413				
<=70	233	Reference			
>70	180	1.421 (1.063–1.901)	**0.018**	1.292 (0.804–2.075)	0.289
Gender	413				
Female	109	Reference			
Male	304	0.849 (0.616–1.169)	0.316		

Table 3: Univariate and multivariate analysis of DSS in BLCA patients.

Characteristics	Total (N)	Univariate analysis		Multivariate analysis	
		Hazard ratio (95% CI)	p value	Hazard ratio (95% CI)	p value
T stage	366				
T1 & T2	124	Reference			
T3	184	2.015 (1.262–3.216)	**0.003**	2.058 (0.873–4.853)	0.099
T4	58	3.243 (1.850–5.687)	**<0.001**	2.385 (0.851–6.682)	0.098
N stage	357				
N0	233	Reference			
N1	45	2.775 (1.675–4.599)	**<0.001**	2.259 (1.031–4.950)	**0.042**
N2 & N3	79	3.573 (2.341–5.452)	**<0.001**	2.896 (1.396–6.004)	**0.004**
M stage	208				
M0	197	Reference			
M1	11	4.205 (1.889–9.359)	**<0.001**	1.051 (0.337–3.282)	0.931
MAN1B1	399				
Low	204	Reference			
High	195	1.605 (1.126–2.286)	**0.009**	1.678 (0.915–3.076)	0.094
Age	399				
<=70	226	Reference			
>70	173	1.026 (0.718–1.466)	0.888		
Gender	399				
Female	103	Reference			
Male	296	0.849 (0.576–1.251)	0.408		

downloading them directly from public sources and analyzing them using bioinformatics approaches, the results need to be validated using additional experimental research.

Secondly, in order to investigate the possible connection between MAN1B1 and the cancer-related immune microenvironment in BC, more investigations were needed.

TABLE 4: Univariate and multivariate analysis of PFI in BLCA patients.

| Characteristics	Total (N)	Univariate analysis		Multivariate analysis	
		Hazard ratio (95% CI)	p value	Hazard ratio (95% CI)	p value
T stage	380				
T1 & T2	124	Reference			
T3	196	1.848 (1.261–2.710)	**0.002**	2.354 (1.159–4.780)	**0.018**
T4	60	3.268 (2.043–5.227)	**<0.001**	2.934 (1.255–6.863)	**0.013**
N stage	370				
N0	239	Reference			
N1	46	2.394 (1.548–3.702)	**<0.001**	1.612 (0.824–3.155)	0.163
N2 & N3	85	3.157 (2.212–4.505)	**<0.001**	2.340 (1.274–4.300)	**0.006**
M stage	213				
M0	202	Reference			
M1	11	6.455 (3.117–13.367)	**<0.001**	1.770 (0.642–4.882)	0.270
MAN1B1	414				
Low	207	Reference			
High	207	1.393 (1.038–1.870)	**0.027**	1.478 (0.893–2.446)	0.128
Age	414				
<=70	234	Reference			
>70	180	1.066 (0.792–1.435)	0.673		
Gender	414				
Female	109	Reference			
Male	305	0.891 (0.642–1.235)	0.488		
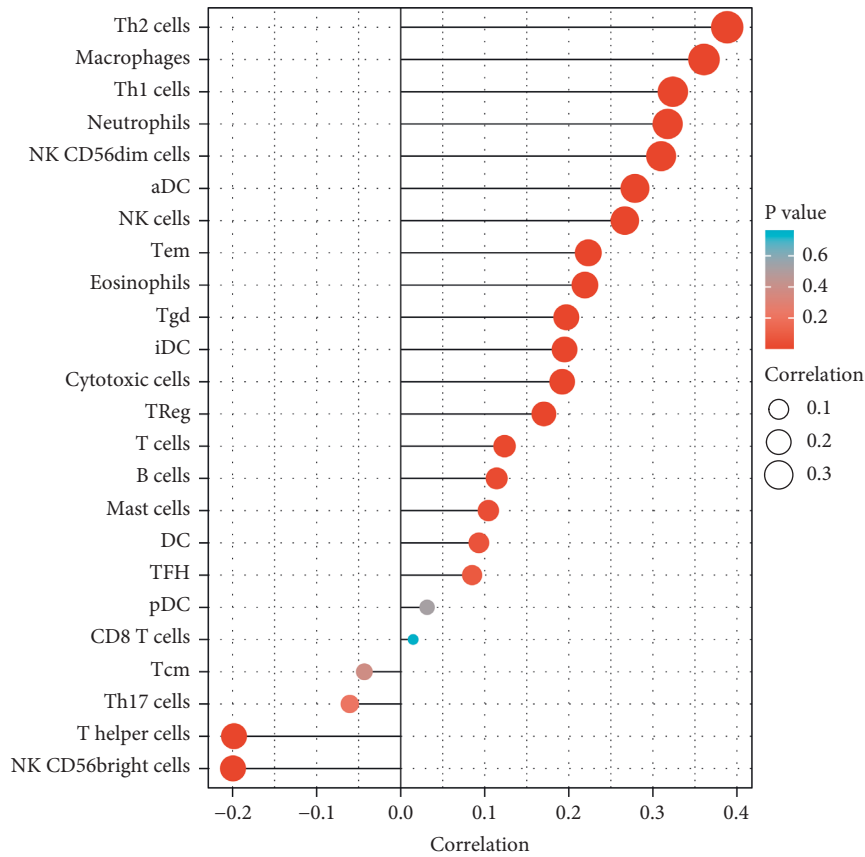
FIGURE 5: Lollipop chart of MAN1B1 expressions in 24 immune cells. The levels of MAN1B1 were associated with the levels of several immune cells.

5. Conclusion

We discovered that MAN1B1 was overexpressed in BC and that its overexpression was significantly connected to a poor prognosis. There was a possibility that MAN1B1 plays a role in the progression of tumors and metastasis. In addition, our results suggest that MAN1B1 probably plays an important part in the polarization of macrophages and the infiltration of immune cells. Thus, it has the potential to be exploited as a prognostic target for BC.

Data Availability

The datasets used and/or analyzed during the current study are available from the corresponding author upon reasonable request.

Conflicts of Interest

The authors declare that there are no conflicts of interest.

Acknowledgments

References

[1] R. L. Siegel, K. D. Miller, and A. Jemal, "Cancer statistics, 2019," *CA: A Cancer Journal for Clinicians*, vol. 69, no. 1, pp. 7–34, 2019.

[2] A. T. Lenis, P. M. Lec, K. Chamie, and M. D. Mshs, "Bladder cancer: a review," *JAMA*, vol. 324, no. 19, pp. 1980–1991, 2020.

[3] J. Dobruch, S. Daneshmand, M. Fisch et al., "Gender and bladder cancer: a collaborative review of etiology, biology, and outcomes," *European Urology*, vol. 69, no. 2, pp. 300–310, 2016.

[4] Z. Kirkali, T. Chan, M. Manoharan et al., "Bladder cancer: epidemiology, staging and grading, and diagnosis," *Urology*, vol. 66, no. 6, pp. 4–34, 2005.

[5] H. Pham, H. Torres, and P. Sharma, "Mental health implications in bladder cancer patients: a review," *Urologic Oncology: Seminars and Original Investigations*, vol. 37, no. 2, pp. 97–107, 2019.

[6] A. Pham and L. K. Ballas, "Trimodality therapy for bladder cancer: modern management and future directions," *Current Opinion in Urology*, vol. 29, no. 3, pp. 210–215, 2019.

[7] C. Alifrangis, U. McGovern, A. Freeman, T. Powles, and M. Linch, "Molecular and histopathology directed therapy for advanced bladder cancer," *Nature Reviews Urology*, vol. 16, no. 8, pp. 465–483, 2019.

[8] L. Tran, J. F. Xiao, N. Agarwal, J. E. Duex, and D. Theodorescu, "Advances in bladder cancer biology and therapy," *Nature Reviews Cancer*, vol. 21, no. 2, pp. 104–121, 2021.

[9] K. C. DeGeorge, H. R. Holt, and S. C. Hodges, "Bladder cancer: diagnosis and treatment," *American Family Physician*, vol. 96, no. 8, pp. 507–514, 2017.

[10] C. S. Kasapkara, A. Olgac, M. Kilic, L. Keldermans, G. Matthijs, and J. Jaeken, "MAN1B1-CDG: novel patients and novel variant," *Journal of Pediatric Endocrinology and Metabolism*, vol. 34, no. 9, pp. 1207–1209, 2021.

[11] N. Okamoto, T. Ohto, T. Enokizono et al., "Siblings with MAN1B1-CDG showing novel biochemical profiles," *Cells*, vol. 10, no. 11, 2021.

[12] S. Iwamoto, Y. Kasahara, Y. Yoshimura et al., "Endo-α-mannosidase-catalyzed transglycosylation," *ChemBioChem*, vol. 18, no. 14, pp. 1376–1378, 2017.

[13] S. Abbondante and E. Pearlman, "Breaching bacterial biofilm with neutrophil α-mannosidase," *Journal of Leukocyte Biology*, vol. 105, no. 6, 2019.

[14] M. R. Ceccarini, M. Codini, C. Conte et al., "Alpha-mannosidosis: therapeutic strategies," *International Journal of Molecular Sciences*, vol. 19, no. 5, 2018.

[15] Z. Y. Lee, J. S. E. Loo, A. Wibowo, M. F. Mohammat, and J. B. Foo, "Targeting cancer via Golgi α-mannosidase II inhibition: how far have we come in developing effective inhibitors?" *Carbohydrate Research*, vol. 508, Article ID 108395, 2021.

[16] P. W. Cheng, S. Davidson, and G. Bhat, "Markers of malignant prostate cancer cells: golgi localization of α-mannosidase 1A at GM130-GRASP65 site and appearance of high mannose N-glycans on cell surface," *Biochemical and Biophysical Research Communications*, vol. 527, no. 2, pp. 406–410, 2020.

[17] F. Hamester, K. Legler, B. Wichert et al., "Prognostic relevance of the golgi mannosidase MAN1A1 in ovarian cancer: impact of N-glycosylation on tumour cell aggregation," *British Journal of Cancer*, vol. 121, no. 11, pp. 944–953, 2019.

[18] S. Mallett, J. J. Deeks, S. Halligan, S. Hopewell, V. Cornelius, and D. G. Altman, "Systematic reviews of diagnostic tests in cancer: review of methods and reporting," *BMJ*, vol. 333, no. 7565, 2006.

[19] A. Lugli, I. Zlobec, M. D. Berger, R. Kirsch, and I. D. Nagtegaal, "Tumour budding in solid cancers," *Nature Reviews Clinical Oncology*, vol. 18, no. 2, pp. 101–115, 2021.

[20] P. S. Steeg, "The blood-tumour barrier in cancer biology and therapy," *Nature Reviews Clinical Oncology*, vol. 18, no. 11, pp. 696–714, 2021.

[21] A. Wong-Rolle, H. K. Wei, C. Zhao, and C. Jin, "Unexpected guests in the tumor microenvironment: microbiome in cancer," *Protein & Cell*, vol. 12, no. 5, pp. 426–435, 2021.

[22] H. F. Wang, J. H. Wu, J. W. Gai et al., "MAN1B1 is associated with poor prognosis and modulates proliferation and apoptosis in bladder cancer," *Gene*, vol. 679, pp. 314–319, 2018.

[23] P. A. Albertsson, P. H. Basse, M. Hokland et al., "NK cells and the tumour microenvironment: implications for NK-cell function and anti-tumour activity," *Trends in Immunology*, vol. 24, no. 11, pp. 603–609, 2003.

[24] E. Sick, A. Jeanne, C. Schneider, S. Dedieu, K. Takeda, and L. Martiny, "CD47 update: a multifaceted actor in the tumour microenvironment of potential therapeutic interest," *British Journal of Pharmacology*, vol. 167, no. 7, pp. 1415–1430, 2012.

[25] C. Ayari, H. LaRue, H. Hovington et al., "Bladder tumor infiltrating mature dendritic cells and macrophages as predictors of response to bacillus Calmette-Guérin immunotherapy," *European Urology*, vol. 55, no. 6, pp. 1386–1396, 2009.

[26] A. Byrne, P. Savas, S. Sant et al., "Tissue-resident memory T cells in breast cancer control and immunotherapy responses," *Nature Reviews Clinical Oncology*, vol. 17, no. 6, pp. 341–348, 2020.

[27] A. M. van der Leun, D. S. Thommen, and T. N. Schumacher, "CD8 (+) T cell states in human cancer: insights from single-cell analysis," *Nature Reviews Cancer*, vol. 20, no. 4, pp. 218–232, 2020.

[28] D. A. Braun, Y. Hou, Z. Bakouny et al., "Interplay of somatic alterations and immune infiltration modulates response to PD-1 blockade in advanced clear cell renal cell carcinoma," *Nature Medicine*, vol. 26, no. 6, pp. 909–918, 2020.

[29] Q. Zhang, X. Yang, M. Pins et al., "Adoptive transfer of tumor-reactive transforming growth factor-beta-insensitive CD8+ T cells: eradication of autologous mouse prostate cancer," *Cancer Research*, vol. 65, no. 5, pp. 1761–1769, 2005.

[30] S. M. Hald, R. M. Bremnes, K. Al-Shibli et al., "CD4/CD8 co-expression shows independent prognostic impact in resected non-small cell lung cancer patients treated with adjuvant radiotherapy," *Lung Cancer*, vol. 80, no. 2, pp. 209–215, 2013.

[31] C. Tian, S. Lu, Q. Fan et al., "Prognostic significance of tumor-infiltrating CD8+ or CD3+ T lymphocytes and interleukin-2 expression in radically resected non-small cell lung cancer," *Chinese Medical Journal*, vol. 128, no. 1, pp. 105–110, 2015.

Research Article

CircFMN2 Boosts Sorafenib Resistance in Hepatocellular Carcinoma Cells via Upregulating CNBP by Restraining Ubiquitination

Chen Fan,[1] Xiaoli Zhu,[2] Qi Zhou,[1] and Weidong Wang [1]

[1]*Department of Intervention, Wuxi People's Hospital, Nanjing Medical University, Wuxi 214023, China*
[2]*Department of Intervention, The First Affiliated Hospital of Soochow University, Suzhou 215006, China*

Correspondence should be addressed to Weidong Wang; wangweidong@njucm.edu.cn

Purpose. Noncoding RNAs exert critical biological effects in hepatocellular carcinoma (HCC). The role of circFMN2, a newly discovered functional RNA in prostate cancer and colorectal cancer, was investigated for the first time in sorafenib-resistance HCC cells. *Methods*. The level of circFMN2 was assessed via quantitative real-time PCR (qRT-PCR). Cell proliferation was detected via CCK-8 and colony formation assay. Cell apoptosis was measured via the TUNEL assay and flow cytometry analysis. A Western blot assay was conducted to detect the CCHC-type zinc finger nucleic acid binding protein (CNBP) level and ubiquitination. RNA pull-down assay and RNA immunoprecipitation were carried out to explore the interaction between circFMN2 and CNBP. *Results*. CircFMN2 was highly expressed in multidrug-resistant (MDR) cells. CircFMN2 overexpression exerted proproliferation effects in sorafenib-treated HCC cells, while depletion of circFMN2 displayed negative effect on sorafenib-treated MDR cells. Moreover, CNBP was verified as the binding protein of circFMN2. CNBP was upregulated in MDR cells, which was achieved by inhibition of ubiquitination by circFMN2. Besides, CNBP overexpression was found to boost sorafenib resistance in HCC cells. *Conclusions*. CircFMN2 is aberrantly expressed in sorafenib-resistant HCC cells and contributes to sorafenib resistance in HCC cells via upregulation of CNBP by restraining ubiquitination.

1. Introduction

Hepatocellular carcinoma (HCC) has been a tremendous health and economic burden globally. Among all kinds of cancers, liver cancer, or HCC, is the second most fatal cancer with a death rate of over 90% and its prevalence is still trending up worldwide [1, 2]. It was disclosed by the World Health Organization in the annual projections that deaths from HCC will be over one million in 2030 [3]. A growing concern is needed for the prevalence of hepatic carcinoma. Although considerable progress has been achieved in the treatment of hepatic carcinoma such as microwave ablation, radiofrequency, liver resection, chemotherapy, and liver transplantation, there are still many intractable obstacles including low diagnosis rate, high postoperative recurrence, drug resistance, and poor survival rates [4–11]. There is a

great need to find the effective therapeutic targets, risk factors for drug resistance, and efficient diagnostic markers.

Due to the inconspicuous symptoms at an early stage, HCC cases are often confirmed at advanced stages, missing the opportunity of surgical treatment or ablation. Hence, a systematic targeted therapy has raised considerable interest. Sorafenib is a first-line FDA-approved systematic targeted therapeutic drug, exerting crucial therapeutically effects on HCC at later stages [12, 13]. In clinical practice, its benefit in survival after sorafenib therapy has been fully validated [14–16]. However, considering the prevalence of HCC, therapeutic breakthroughs on sorafenib resistance and existing treatment efficiency are still concerned.

CircRNAs with a covalently closed circular structure are a class of stable functional molecules and have been confirmed as vital regulators in the diagnosis, treatment, and

drug resistance in HCC. Circ_100395 exerts anticancer effects in HCC via regulating epithelial-mesenchymal transition, apoptosis, and proliferation [17]. Circ_0003418 improves cisplatin chemoresistance via suppression of Wnt/β-catenin pathway in HCC [18]. CircUHRF1 contributes to anti-PD1 therapy resistance via disturbing NK cell function in HCC [19]. CircFoxo3 drives adriamycin resistance via modulating the miR-199a-5p/ABCC1 axis in HCC [20]. The effects of most circRNAs in HCC remain unknown and so far, there are few reports on the circRNAs regulating sorafenib resistance. CircFMN2 is a newly discovered circRNA involved in prostate cancer and colorectal cancer [21, 22], and its functions in sorafenib resistance in HCC remains undefined. CCHC-type zinc finger nucleic acid binding protein (CNBP, also known as ZNF9) is a conserved single-stranded DNA binding protein, which has been shown to participate in the metabolism of HCC cells [23], but if it helps or prohibits the development and growth of HCC is still unclear. In this study, we explored the role of circFMN2 in sorafenib resistance and its underlying mechanism in HCC.

2. Methods

2.1. Cell Culture and Treatment.
HCC cell (BEL-7402) and multidrug-resistant HCC cell (BEL-7402/5-Fu) were purchased from Wuhan Chundo Biotechnology Co. LTD. (Wuhan, China). The BEL-7402 and BEL-7402/5-Fu cells were cultured in Dulbecco's modified eagle medium (DMEM) (Gibico, Rockville, MD, USA) containing 100 μg/ml streptomycin, 100 IU/ml penicillin, and 10% fetal bovine serum (FBS) (Gibico, Rockville, MD, USA) at 37°C in an incubator with 5% CO_2. For the role of circFMN2 and CNBP in sorafenib (SOR) resistance, the cells were treated with sorafenib (6.5 μmol/L) for 24 h.

2.2. Cell Transfection.
After sorafenib treatment, the BEL-7402 cells were transfected with pcDNA3.1-CircFMN2 vector, pcDNA3.1-CNBP vector, and their corresponding negative controls (BlueGene Biotech, Shanghai, China). BEL-7402/5-Fu cells were transfected with siRNA and its negative control (si-circFMN2 5′-AAGAAAGACTTGAA-AGCTGTT-3′; si-circFMN2-NC 5′-GUGAGGCUCUU-GAGCCAGAUGAUUG-3′; BlueGene Biotech, Shanghai, China) using Lipofectamine 3000 (Invitrogen, Carlsbad, CA, USA) on the basis of manufacturer's instructions.

2.3. Quantitative Real-Time Polymerase Chain Reaction (qRT-PCR).
Isolation of total RNAs was conducted using RNAprep Pure cell kit (TianGen Biotech, Beijing, China). HiFiScript complementary deoxyribose nucleic acid (cDNA) Kit (CWBIO, Beijing, China) was used to synthesis cDNA. CircFMN2 primers (forward: 5′- TCAGAAACTCCCCA-AAAACG-3′, reverse: 5′-AGAAGACCCATGGCAATGAT-3′) and other primers were synthesized by BlueGene Biotech, Shanghai, China. Quantitative analysis was carried out in triplicates on StepOne Plus Real-time PCR System (Applied Biosystems, Foster City, CA, USA) using SYBR Green. U6 (forward: 5′-GCTTCGGCAGCACATATACT-AAAAT-3′, reverse: 5′-CGCTTCACGAATTTGCGTGT-CAT-3′) served as an internal reference. The quantitative calculation was done using $2^{-\Delta\Delta Ct}$ methods. Experiments were triplicated.

2.4. Cell Counting Kit-8 (CCK-8) Assay.
The cell viability was measured using CCK-8 (GlpBio, Shanghai, China) in line with the instructions of manufacturer. Briefly, 2×10^3 cells were seeded into each well of the 96-well plate and after sorafenib treatment and transfection, cells in each well were incubated with CCK-8 solution (10 μL) for 2 h. The cell viability was determined by measuring the absorbance at 450 nm. Experiments were triplicated.

2.5. Colony Formation Assay.
The cells after sorafenib treatment and transfection were seeded in six-well plates. Fourteen days later, 4% paraformaldehyde fixation was carried out followed by crystal violet staining. The colonies were counted and observed under a microscope (Olympus, Tokyo, Japan). Experiments were triplicated.

2.6. Flow Cytometry Assay.
The cell apoptosis was evaluated using Annexin V-FITC/PI Apoptosis Detection Kit (YEA-SEN, Shanghai, China) as described in the instructions of the manufacturer. Briefly, the cells after sorafenib treatment and transfection were digested with trypsin followed by centrifugation at 4°C; the cells were resuspended in the binding buffer (100 μL). Then, 5 μL Annexin V-FITC and 10 μL PI staining solution were incubated with the cells away from light at room temperature for fifteen minutes. The analysis of cell apoptosis was carried out using the FACScan flow cytometer (Becton Dickinson, Franklin Lakes, NJ, USA). Experiments were triplicated.

2.7. TUNEL Assay.
The cells apoptosis was measured using Colorimetric TUNEL Apoptosis Assay Kit (Beyotime, Shanghai, China) in accordance with the instructions of the manufacturer. Briefly, the cells after treatment in the study groups were washed with PBS, followed by 4% paraformaldehyde fixation. After rinsing, the cells were incubated with 3% Triton X-100 at room temperature for five minutes followed by a rinse with PBS. Then, the cells were incubated in the PBS containing 0.3% H_2O_2 for twenty minutes. Then, the cells were reacted with biotin-labeled solution which is prepared as described in the instructions for one hour at 37°C. Subsequently, streptavidin-HRP working solution was added into the cells. After diaminobenzidine staining, hematoxylin counterstain, the cell apoptosis was analyzed under a microscope (Olympus, Tokyo, Japan). Experiments were triplicated.

2.8. Western Blot.
The extraction of the total proteins was performed in lysis buffer (50 mM DTT, 0.1% SDS and 1% NP-40) followed by centrifugation at 4°C (10,000 $\times$ g, 15 min). The supernatants were collected and protein was

quantified using bicinchoninic acid (BCA) protein assay kit (Abcam, Cambridge, MA, USA). Then, electrophoresis of proteins (25 μg) was performed on 15% SDS-PAGE followed by transferring to polyvinylidene fluoride membranes (Millipore, Billerica, MA, USA). After 5% skimmed milk blockage, the membranes were reacted with the primary antibodies against CNBP (1 : 100, cat no. ab272676, Abcam, Cambridge, MA, USA) overnight and then incubated with goat anti-rabbit secondary antibody (1 : 5000, cat no. ab216773, Abcam, Cambridge, MA, USA). An Odyssey infrared scanner (Li-Cor) was used for detection of the blots. Experiments were triplicated.

2.9. RNA Pull-Down Assay. The interaction between circFMN2 and CNBP was explored using RNA pull-down kits (Guangzhou Saicheng Biological Technology Co. LTD., Guangzhou, China) according to the instructions of manufacturer. Briefly, the cell lysates were prepared using lysis buffer followed by centrifugation. The probers including biotin-labeled circFMN2, biotin-labeled anti-sense circFMN2, and biotin-labeled circFMN2 fragments were incubated with streptomycin magnetic beads for six hours. Then, the magnetic bead-prober complex was obtained and incubated with the cell lysates overnight. The target protein was eluted and detected via Western blot assay.

2.10. RNA Immunoprecipitation. The interaction of circFMN2 and CNBP was further examined through the RNA immunoprecipitation assay using Imprint® RNA Immunoprecipitation (RIP) Kit (Sigma-Aldrich, St. Louis, MO, USA) in line with the protocol of manufacturer. Briefly, after cell lysis, the supernatants were collected and incubated with a magnetic bead anti-CNBP antibody complex or magnetic bead-IgG complex, respectively. After purification of the immunoprecipitated RNA, the RNA level was quantitatively analyzed via the RT-PCR assay.

2.11. Ubiquitination Assay. The cells were transfected with pcDNA3.1-CircFMN2 vector or its negative control and 5 μmol/ml MG132 was added. Forty-eight hours after transfection, the cells were lysed and the supernatant was collected. Then, immunoprecipitation was performed via using anti-CNBP antibody and IgG. The immunoprecipitated protein was analyzed through Western blot assay via using anti-ubiquitin antibody (Cell Signaling Technology, Danvers, MA, USA).

2.12. Statistical Analysis. Statistical Product and Service Solutions (SPSS) 19.0 (IBM, Armonk, NY, USA) was used for data analysis. Difference between two groups was assessed using independent t tests. A 2-sided p-value under 0.05 suggested a significant difference.

3. Results

3.1. CircFMN2 Was Highly Expressed in Multidrug Resistance (MDR) Cells. In order to examine the underlying role of circFMN2 in BEL-7402 and BEL-7402/5-Fu cells, BEL-7402 and BEL-7402/5-Fu cells were transfected with pcDNA3.1-CircFMN2 vector and si-circFMN2, respectively. As revealed by the results of the PCR assay, the level of circFMN2 was elevated after circFMN2 transfection and decreased by si-circFMN2 transfection in comparison with MDR, suggesting that the overexpression and silencing of circFMN2 were successfully realized (Figure 1(a)). Besides, a significant increase of circFMN2 level was found in MDR group versus control, demonstrating that circFMN2 may act as a crucial player in multidrug-resistant cells. We further examined the effects of circFMN2 on cell proliferation and apoptosis after sorafenib treatment. As shown by the CCK-8 assay (Figure 1(b)) and colony formation assay (Figures 1(c) and 1(d)), circFMN2 overexpression significantly elevated cell viability and colony formation in BEL-7402 cells after sorafenib treatment, verifying the effect of circFMN2 overexpression on sorafenib resistance. Moreover, silencing of circFMN2 decreased cell proliferation in sorafenib treated MDR cells, indicating that knockdown of circFMN2 may be an efficient avenue in improving sorafenib resistance. The impact of circFMN2 on cell apoptosis after sorafenib treatment was assessed by flow cytometry and TUNEL assay. The apoptotic cells indicated by flow cytometry (Figure 1(e)) and TUNEL assay (Figures 1(f) and 1(g)), were increased significantly in sorafenib-treated MDR cells by circFMN2 depletion, further disclosed the effects of circFMN2 depletion on sorafenib resistance in MDR cells. On the other hand, this also indicated that circFMN2 is a crucial sorafenib resistant target in HCC.

3.2. CircFMN2 Elevated the CNBP Level via Restraining Its Ubiquitination Degradation. The downstream mechanism of circFMN2 in sorafenib resistance was further examined. CNBP was predicted as the binding protein of circFMN2 using bioinformatics online tools (StarBase and RNA interactome Database website). The CNBP level was measured via the Western blot assay. CNBP was upregulated by circFMN2 overexpression in BEL-7402 cells in contrast to control (Figures 2(a) and 2(b)), revealing that circFMN2 was an upregulator of CNBP. The level of CNBP was higher in MDR cells than that in BEL-7402 cells, suggesting that CNBP may be another drug resistance factor in MDR cells. The interaction between circFMN2 and CNBP was further validated through RNA-pull down and RNA immunoprecipitation assay, which revealed that the enrichment of CNBP was found in the circFMN2 with positive-sense strand group (Figure 2(c)). Moreover, it was observed that circFMN2 level was enriched in the CNBP immunoprecipitation group, and in contrast, very small amounts of circFMN2 were found in other groups (Figure 2(d)). These findings substantiated the binding of circFMN2 and CNBP. The binding sites of circFMN2 were further explored via deletion-mapping analysis and the results manifested that the CNBP was pulled down by circFMN2 fragments 306–458 nt and 459–612 nt (Figures 2(e) and 2(f)). The regulatory mechanism of circFMN2 on CNBP was also examined via ubiquitination assay. The ubiquitination level
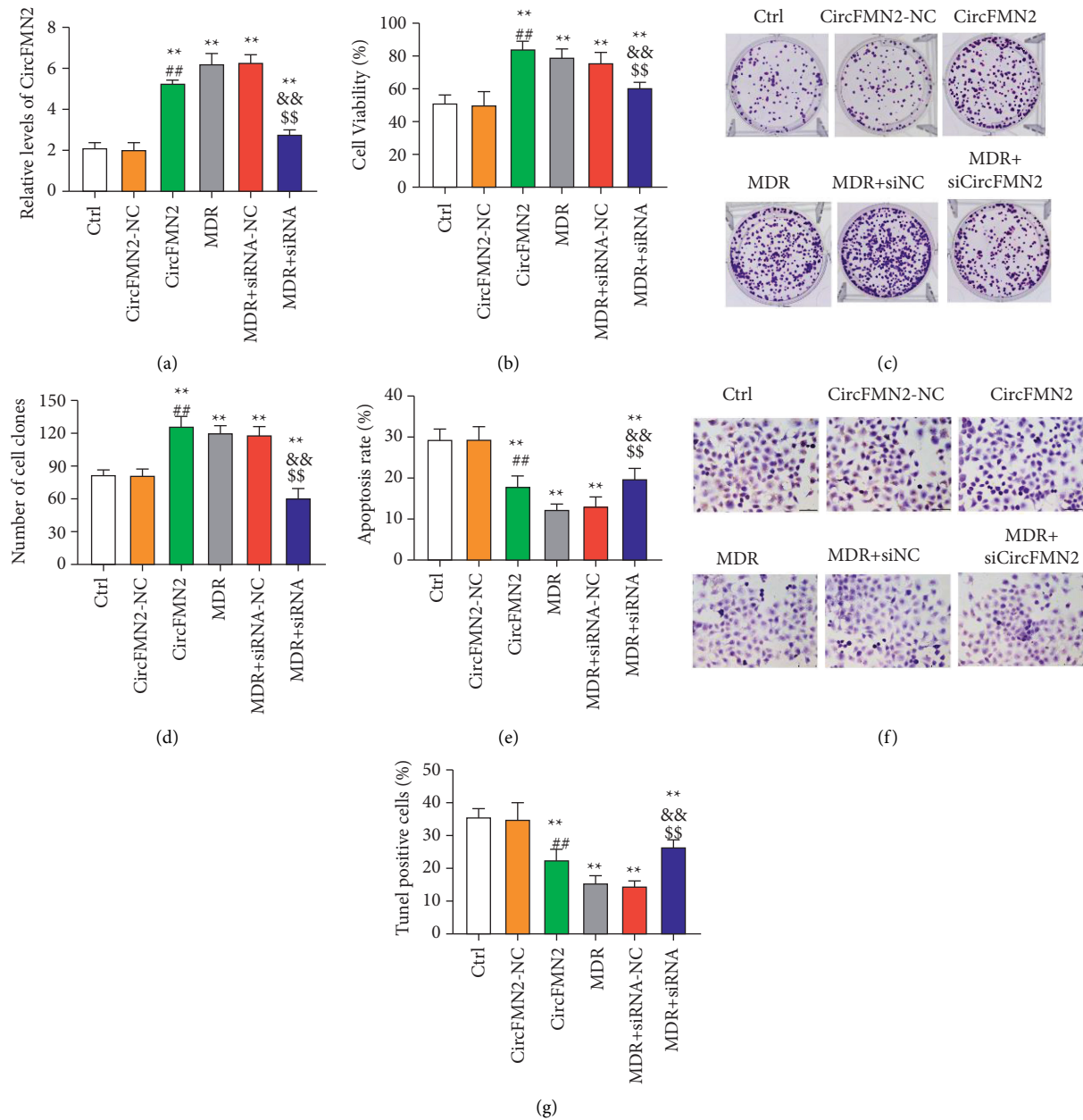
(a)

(b)

(c)

(d)

(e)

(f)

(g)

Figure 1: CircFMN2 was upregulated in MDR cells. The influence of circFMN2 on cell proliferation and apoptosis in multidrug-resistant cells and nonresistant cells. The level of circFMN2 assessed via RT-qPCR (a), cell proliferation measured by CCK-8 assay (b), colony formation ability (c) and (d), and cell apoptosis analyzed by flow cytometry (e) and TUNEL assay (f), (g) in the study groups. $^{***} p < 0.001$, $^{**} p < 0.01$ vs. control group; $^{##}$, $p < 0.01$, $^{###}$, $p < 0.001$ vs. circFMN2-NC group; $^{\&} p < 0.05$, $^{\&\&} p < 0.01$, $^{\&\&\&} p < 0.001$ vs. MDR group; $^{\$}$, $p < 0.05$, $^{\$\$}$, $p < 0.01$, $^{\$\$\$}$, $p < 0.001$ vs. MDR + siRNA-NC group.

of CNBP was decreased transparently by the circFMN2 overexpression (Figure 2(g)), suggesting that circFMN2 overexpression elevates CNBP level via inhibiting its ubiquitination.

3.3. CircFMN2 Boosts Sorafenib Resistance in HCC Cells by Upregulating CNBP. As stated in the aforementioned results, CNBP was upregulated in drug-resistant cells and may exert an underlying role in drug resistance, we therefore further examined the effects of CNBP on

sorafenib efficacy in HCC cells. We found that CNBP was significantly decreased by sorafenib treatment in HCC cells when compared with control cells, and CNBP over-expression reversed this effect (Figures 3(a) and 3(b)). The cell viability and colony formation capacity were all reduced significantly by sorafenib in HCC cells (Figures 3(c)–3(e)). Moreover, the cell apoptosis assessed by flow cytometry and positive cells in TUNEL staining were all increased by sorafenib in HCC cells (Figures 3(f)–3(h)). These results were consistent with the previous findings [24, 25], demonstrating an antiproliferation and
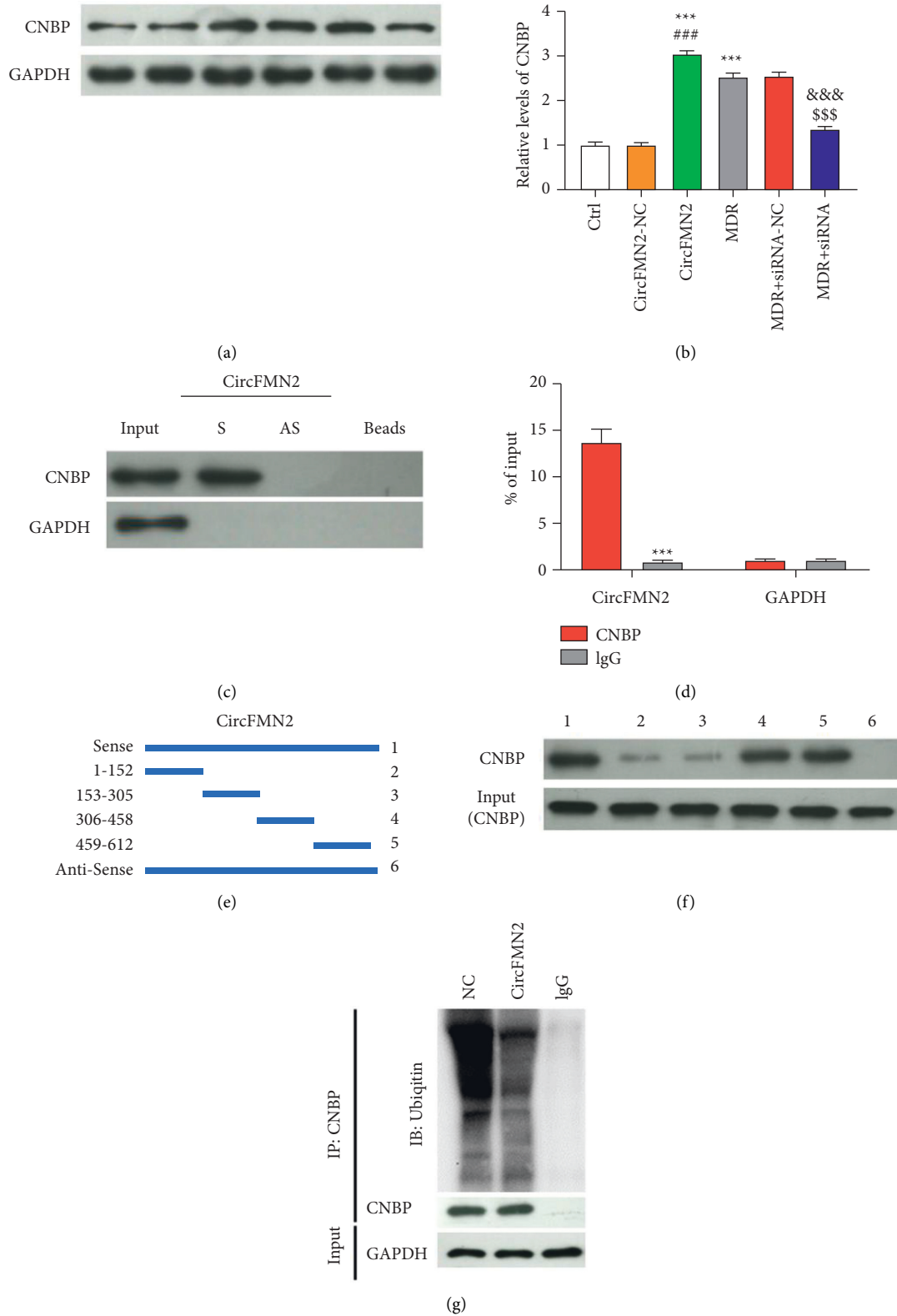
(a)

(b)

(c)

(d)

(e)

(f)

(g)

FIGURE 2: CNBP was confirmed as the binding protein of circFMN2. CNBP level was measured via Western blot (a), (b) lanes in panel A were corresponding to columns in panel B, Western blot analysis of CNBP level after RNA pull-down assay (c), circFMN2 level detected by RT-qPCR following RNA immunoprecipitation assay (d), The deletion fragments, sense strand and anti-sense strand of circFMN2 in deletion-mapping analysis (e), Western analysis of CNBP level following RNA pull-down assay with different circFMN2 constructs in deletion-mapping analysis (f), and ubiquitination level detected by Western blot assay (g). *** $p < 0.001$ vs. control group; ###, $p < 0.001$ vs. circFMN2-NC group; &&&, $p < 0.001$ vs. MDR group; $$$, $p < 0.001$ vs. MDR + siRNA-NC group.
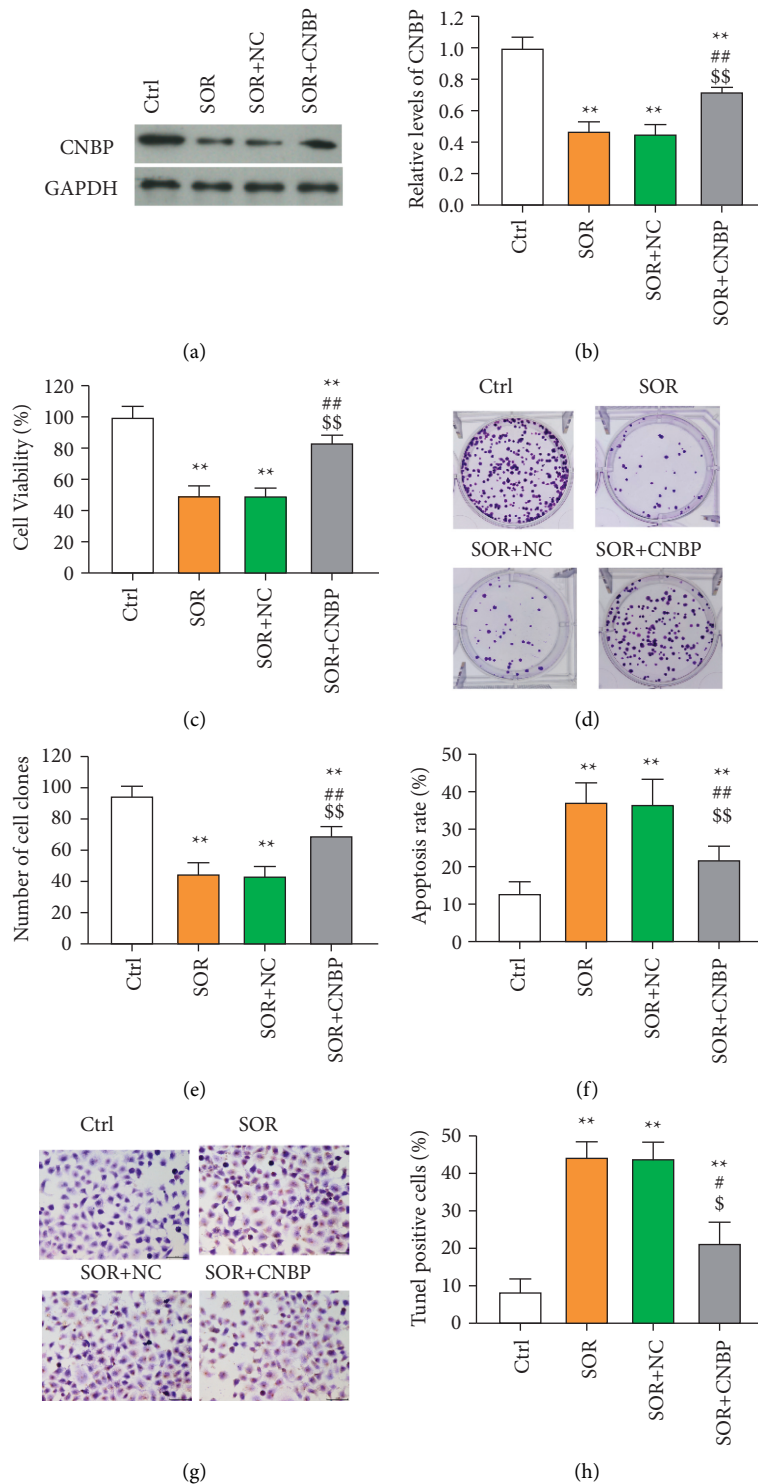
(a)

(b)

(c)

(d)

(e)

(f)

(g)

(h)

FIGURE 3: CNBP was upregulated in MDR cells. The influence of CNBP on cell proliferation and apoptosis in HCC cells. The level of CNBP assessed via Western blot (a) and (b), cell proliferation measured by CCK-8 assay (c); colony formation ability (d) and (e), and cell apoptosis analyzed by flow cytometry (f) and TUNEL assay (g), (h) in the study groups. *** $p < 0.001$ vs. control group; #, $p < 0.05$, ##, $p < 0.01$ and ###, $p < 0.001$ vs. SOR group; $, $p < 0.05$, $$, $p < 0.01$ and $$$, $p < 0.001$ vs. SOR + NC group.

proapoptosis role of sorafenib in HCC. CNBP was high expressed in MDR cells and after CNBP overexpression, the effects of sorafenib on cell apoptosis and proliferation in HCC cells were reversed, supporting that CNBP acts as a

contributor in sorafenib resistance. Besides, it has been confirmed in the aforementioned results that upregulation of CNBP was realized via inhibition of ubiquitination by circFMN2.

4. Discussion

Sorafenib as a first-line anticancer drug, has become a standard treatment of advanced liver cancer, wining a crucial position in HCC therapy [26–28]. The sorafenib therapy has yielded a modest survival benefit in patients with advanced HCC [29, 30]. Nevertheless, sorafenib treatment still confronts tremendous challenges in sorafenib resistance [31]. The sorafenib-resistant mechanism is still not completely unambiguous and its elucidation is imperative. In the present report, we found that circFMN2 facilitates sorafenib resistance via upregulating CNBP through restraining inhibiting ubiquitination.

As revealed by accumulative evidence, aberrant expressed noncoding RNAs has become an essential factor in HCC therapy and sorafenib resistance [32, 33]. A lot of research on treatment of liver cancer and sorafenib resistance are focused on aberrantly expressed miRNA or lncRNA [33–38]. Nevertheless, the reports of circRNA participating in sorafenib resistance are limited. Compared with miRNAs and lncRNAs, circRNAs, owing to its stable circular structure, has more potential to be an excellent treatment target and drug resistant biomarker. In the present study, circFMN2, a newly found circRNA in cancerous cells, was found to be upregulated in MDR HCC cells, implying its underlying role in drug resistance.

Cell proliferation and apoptosis are critical indicators of drug resistance. β-catenin regulated by Nek2 contributes to sorafenib resistance via regulating cell apoptosis and proliferation [39]. Rage participates in sorafenib resistance via modulating proliferation and apoptosis by the AMPK/mTOR pathway [40]. CircFMN2 was reported to exert a carcinogenic effect in colorectal cancer and prostate cancer cells via regulating cell proliferation and apoptosis [22, 23]. In this research study, we found that after circFMN2 overexpression, the cell viability and colony formation capacity were increased and cell apoptosis was reduced in sorafenib treated cells, hinting that circFMN2 is a critical functional molecular in facilitating sorafenib resistance. As circFMN2 is highly expressed in MDR cells, we further conducted experiments into the effects of circFMN2 depletion on cell apoptosis and proliferation in sorafenib treated MDR cells. Surprisingly, circFMN2 depletion displayed mitigative effects on sorafenib resistance via augmenting cell apoptosis and suppressing cell proliferation in multidrug resistance cells. The outcome disclosed that circFMN2 is an underlying sorafenib resistance target; on the other hand, high level of circFMN2 is the crucial inducer of sorafenib resistance.

CircRNAs as critical regulators, commonly work by regulating their downstream miRNA targets, binding proteins, and certain signaling pathways. As reported in the previous literature, circRNA-SORE is found to facilitate sorafenib resistance through β-catenin signaling in liver cancer [41]. CircFN1 augments sorafenib resistance via sponging miR-1205 and modulating the expression of e2f1 in HCC cells [42]. In the present study, we sought to find more drug resistant by exploring the downstream mechanism of circFMN2.

As pinpointed by the bioinformatics tools, CNBP was predicted as the binding protein of circFMN2. CNBP is ubiquitous in various tissues and organs, exerting dual regulator functions at translational and transcriptional levels [43, 44]. In this report, CNBP has been identified as the binding protein via RNA pull-down and RNA immunoprecipitation assay. As further verified by deletion-mapping analysis, CNBP is capable to bind to circFMN2 fragments 306–458 nt and 459–612 nt. Besides, circFMN2 upregulated CNBP by ubiquitination inhibition. Since circFMN2 is an underlying MDR target, we speculated that CNBP as a downstream binding protein may have similar effects. We found that CNBP is also upregulated in MDR cells versus nonresistant cells, which confirmed our speculation. Many studies have shown that CNBP is a vital regulator of cell apoptosis and proliferation [45–47]. Besides, CNBP is also confirmed to act as a crucial regulator of cell biology by modulating oncogene expression in tumor [48].

5. Conclusions

In this research, circFMN2, a drug resistant target was found in HCC cells. We also identified a new sorafenib-resistant mechanism that circFMN2 contributes to sorafenib resistance via upregulation of CNBP through ubiquitination inhibition. The findings of this research provide a new solution for sorafenib resistance and extend our interest in sorafenib resistance in HCC.

Data Availability

The data used to support the findings of this study are available from the corresponding author upon request.

Conflicts of Interest

The authors declare that they have no conflicts of interest.

Acknowledgments

References

[1] C. Mattiuzzi and G. Lippi, "Current cancer epidemiology," *Journal of Epidemiology and Global Health*, vol. 9, no. 4, pp. 217–222, 2019.

[2] "Expression of concern: Long noncoding RNA HAGLROS regulates apoptosis and autophagy in Parkinson's disease via regulating miR-100/ATG10 axis and PI3K/Akt/mTOR pathway activation," *Artificial Cells, Nanomedicine, and Biotechnology*, vol. 48, p. 708, 2020.

[3] A. Villanueva, "Hepatocellular carcinoma," *New England Journal of Medicine*, vol. 380, no. 15, pp. 1450–1462, 2019.

[4] L. Deng, X. Li, Z. Shi, P. Jiang, D. Chen, and L. Ma, "Maternal and perinatal outcome in cases of fulminant viral hepatitis in late pregnancy," *International Journal of Gynecology & Obstetrics*, vol. 119, no. 2, pp. 145–148, 2012.

[5] F. Izzo, V. Granata, R. Grassi et al., "Radiofrequency ablation and microwave ablation in liver tumors: an update," *The Oncologist*, vol. 24, no. 10, pp. e990–1005, 2019.

[6] Y. Yang, L. Deng, X. Li et al., "Evaluation of the prognosis of fulminant viral hepatitis in late pregnancy by the MELD scoring system," *European Journal of Clinical Microbiology & Infectious Diseases*, vol. 31, no. 10, pp. 2673–2678, 2012.

[7] K. Gurusamy, N. Corrigan, J. Croft et al., "Liver resection surgery versus thermal ablation for colorectal liver metastases (LAVA): study protocol for a randomised controlled trial," *Trials*, vol. 19, no. 1, p. 105, 2018.

[8] Y. Yang, L. Deng, X. Li et al., "Analysis of prognosis-associated factors in fulminant viral hepatitis during pregnancy in China," *International Journal of Gynecology & Obstetrics*, vol. 114, no. 3, pp. 242–245, 2011.

[9] B. L. Wang, Q. W. Tan, X. H. Gao, J. Wu, and W. Guo, "Elevated PIVKA-II is associated with early recurrence and poor prognosis in BCLC 0-A hepatocellular carcinomas," *Asian Pacific Journal of Cancer Prevention*, vol. 15, no. 16, pp. 6673–6678, 2014.

[10] X. M. Li, L. Ma, Y. B. Yang, Z. J. Shi, and S. S. Zhou, "Prognostic factors of fulminant hepatitis in pregnancy," *Chinese Medical Journal*, vol. 118, no. 20, pp. 1754–1757, 2005.

[11] G. K. Abou-Alfa, T. Meyer, A. L. Cheng et al., "Cabozantinib in patients with advanced and progressing hepatocellular carcinoma," *New England Journal of Medicine*, vol. 379, no. 1, pp. 54–63, 2018.

[12] Y. J. Zhu, B. Zheng, H. Y. Wang, and L. Chen, "New knowledge of the mechanisms of sorafenib resistance in liver cancer," *Acta Pharmacologica Sinica*, vol. 38, no. 5, pp. 614–622, 2017.

[13] K. Eugen, "Current treatment options for hepatocellular carcinoma," *Klinická Onkologie*, vol. 33, pp. 20–25, 2020.

[14] H. Zhu, B. Ye, Z. Qiao, L. Zeng, and Q. Li, "Hepatectomy combined with sorafenib in patients with intermediate-advanced hepatocellullar carcinoma," *Journal of Buon*, vol. 24, no. 4, pp. 1382–1389, 2019.

[15] Q. Liu and Y. Dai, "Sorafenib combined with transarterial chemoembolization prolongs survival of patients with advanced hepatocellular carcinoma," *Journal of Buon*, vol. 25, no. 2, pp. 945–951, 2020.

[16] L. Xu and W. Fan, "Efficacy of sorafenib combined with radiofrequency ablation in renal cancer and its effects on immunity and inflammation in patients," *Journal of Buon*, vol. 25, no. 1, pp. 514–519, 2020.

[17] Q. Chen, Z. Chen, S. Cao et al., "Role of CircRNAs_100395 in proliferation and metastases of liver cancer," *Medical Science Monitor*, vol. 25, pp. 6181–6192, 2019.

[18] H. Chen, S. Liu, M. Li, P. Huang, and X. Li, "circ_0003418 inhibits tumorigenesis and cisplatin chemoresistance through wnt/β-catenin pathway in hepatocellular carcinoma," *OncoTargets and Therapy*, vol. 12, pp. 9539–9549, 2019.

[19] P. F. Zhang, C. Gao, X. Y. Huang et al., "Cancer cell-derived exosomal circUHRF1 induces natural killer cell exhaustion and may cause resistance to anti-PD1 therapy in hepatocellular carcinoma," *Molecular Cancer*, vol. 19, no. 1, p. 110, 2020.

[20] W. Huang, F. Huang, and C. Feng, "CircFoxo3 promotes adriamycin resistance through regulation of miR-199a-5p/ATP binding cassette subfamily C member 1 Axis in hepatocellular carcinoma," *OncoTargets and Therapy*, vol. 13, pp. 5113–5122, 2020.

[21] G. Shan, B. Shao, Q. Liu et al., "circFMN2 sponges miR-1238 to promote the expression of LIM-homeobox gene 2 in prostate cancer cells," *Molecular Therapy—Nucleic Acids*, vol. 21, pp. 133–146, 2020.

[22] Y. Li, C. Li, R. Xu, Y. Wang, D. Li, and B. Zhang, "A novel circFMN2 promotes tumor proliferation in CRC by regulating the miR-1182/hTERT signaling pathways," *Clinical Science*, vol. 133, no. 24, pp. 2463–2479, 2019.

[23] G.-Z. Jin, Y. Zhang, W. M. Cong et al., "Phosphoglucomutase 1 inhibits hepatocellular carcinoma progression by regulating glucose trafficking," *PLoS Biology*, vol. 16, no. 10, Article ID e2006483, 2018.

[24] P. Y. Zhuang, K. W. Zhang, J. D. Wang et al., "Effect of TALEN-mediated IL-6 knockout on cell proliferation, apoptosis, invasion and anti-cancer therapy in hepatocellular carcinoma (HCC-LM3) cells," *Oncotarget*, vol. 8, no. 44, pp. 77915–77927, 2017.

[25] H. Yu, P. Guo, X. Xie, Y. Wang, and G. Chen, "Ferroptosis, a new form of cell death, and its relationships with tumourous diseases," *Journal of Cellular and Molecular Medicine*, vol. 21, no. 4, pp. 648–657, 2017.

[26] S. Bangaru, J. A. Marrero, and A. G. Singal, "Review article: new therapeutic interventions for advanced hepatocellular carcinoma," *Alimentary Pharmacology & Therapeutics*, vol. 51, no. 1, pp. 78–89, 2020.

[27] M. Bouattour, N. Mehta, A. R. He, E. I. Cohen, and J. C. Nault, "Systemic treatment for advanced hepatocellular carcinoma," *Liver Cancer*, vol. 8, no. 5, pp. 341–358, 2019.

[28] A. Huang, X. R. Yang, W. Y. Chung, A. R. Dennison, and J. Zhou, "Targeted therapy for hepatocellular carcinoma," *Signal Transduction and Targeted Therapy*, vol. 5, no. 1, p. 146, 2020.

[29] J. L. Raoul, J. S. Frenel, J. Raimbourg, and M. Gilabert, "Current options and future possibilities for the systemic treatment of hepatocellular carcinoma," *Hepatic Oncology*, vol. 6, no. 1, p. P11, 2019.

[30] J. Bruix, A. L. Cheng, G. Meinhardt, K. Nakajima, Y. De Sanctis, and J. Llovet, "Prognostic factors and predictors of sorafenib benefit in patients with hepatocellular carcinoma: analysis of two phase III studies," *Journal of Hepatology*, vol. 67, no. 5, pp. 999–1008, 2017.

[31] J. J. Marin, R. I. Macias, M. J. Monte et al., "Molecular bases of drug resistance in hepatocellular carcinoma," *Cancers*, vol. 12, no. 6, p. 1663, 2020.

[32] L. Wei, X. Wang, L. Lv et al., "The emerging role of micro-RNAs and long noncoding RNAs in drug resistance of hepatocellular carcinoma," *Molecular Cancer*, vol. 18, no. 1, p. 147, 2019.

[33] L. J. Lim, S. Y. Wong, F. Huang et al., "Roles and regulation of long noncoding RNAs in hepatocellular carcinoma," *Cancer Research*, vol. 79, no. 20, pp. 5131–5139, 2019.

[34] Y. T. Liu, G. Q. Liu, and J. M. Huang, "FAM225A promotes sorafenib resistance in hepatocarcinoma cells through modulating miR-130a-5p-CCNG1 interaction network," *Bioscience Reports*, vol. 40, Article ID BSR20202054, 2020.

[35] J. Zhang, X. Zhao, X. Ma, Z. Yuan, and M. Hu, "KCNQ1OT1 contributes to sorafenib resistance and programmed death-ligand1mediated immune escape via sponging miR506 in hepatocellular carcinoma cells," *International Journal of Molecular Medicine*, vol. 46, no. 5, pp. 1794–1804, 2020.

[36] L. Ji, Z. Lin, Z. Wan et al., "miR-486-3p mediates hepatocellular carcinoma sorafenib resistance by targeting FGFR4 and EGFR," *Cell Death & Disease*, vol. 11, no. 4, p. 250, 2020.

[37] D. Li, T. Wang, F. F. Sun et al., "MicroRNA-375 represses tumor angiogenesis and reverses resistance to sorafenib in

hepatocarcinoma," *Cancer Gene Therapy*, vol. 28, no. 1-2, pp. 126–140, 2021.

[38] F. Li, F. Wang, C. Zhu, Q. Wei, T. Zhang, and Y. L. Zhou, "miR-221 suppression through nanoparticle-based miRNA delivery system for hepatocellular carcinoma therapy and its diagnosis as a potential biomarker," *International Journal of Nanomedicine*, vol. 13, pp. 2295–2307, 2018.

[39] L. Deng, J. Sun, X. Chen, L. Liu, and D. Wu, "Nek2 augments sorafenib resistance by regulating the ubiquitination and localization of beta-catenin in hepatocellular carcinoma," *Journal of Experimental & Clinical Cancer Research*, vol. 38, no. 1, p. 316, 2019.

[40] J. Li, P. W. Wu, Y. Zhou et al., "Rage induces hepatocellular carcinoma proliferation and sorafenib resistance by modulating autophagy," *Cell Death & Disease*, vol. 9, no. 2, p. 225, 2018.

[41] J. Xu, Z. Wan, M. Tang et al., "N(6)-methyladenosine-modified CircRNA-SORE sustains sorafenib resistance in hepatocellular carcinoma by regulating beta-catenin signaling," *Molecular Cancer*, vol. 19, no. 1, p. 163, 2020.

[42] C. Yang, Z. Dong, H. Hong et al., "circFN1 mediates sorafenib resistance of hepatocellular carcinoma cells by sponging miR-1205 and regulating E2F1 expression," *Molecular Therapy—Nucleic Acids*, vol. 22, pp. 421–433, 2020.

[43] L. Cao, P. Zhang, J. Li, and M. Wu, "LAST, a c-Myc-inducible long noncoding RNA, cooperates with CNBP to promote CCND1 mRNA stability in human cells," *Elife*, vol. 6, Article ID e30433, 2017.

[44] E. Lee, T. A. Lee, J. H. Kim et al., "CNBP acts as a key transcriptional regulator of sustained expression of interleukin-6," *Nucleic Acids Research*, vol. 45, no. 6, pp. 3280–3296, 2017.

[45] N. B. Calcaterra, P. Armas, A. M. J. Weiner, and M. Borgognone, "CNBP: a multifunctional nucleic acid chaperone involved in cell death and proliferation control," *IUBMB Life*, vol. 62, no. 10, pp. 707–714, 2010.

[46] A. M. Weiner, M. L. Allende, T. S. Becker, and N. B. Calcaterra, "CNBP mediates neural crest cell expansion by controlling cell proliferation and cell survival during rostral head development," *Journal of Cellular Biochemistry*, vol. 102, no. 6, pp. 1553–1570, 2007.

[47] P. Armas, T. H. Aguero, M. Borgognone, M. J. Aybar, and N. B. Calcaterra, "Dissecting CNBP, a zinc-finger protein required for neural crest development, in its structural and functional domains," *Journal of Molecular Biology*, vol. 382, no. 4, pp. 1043–1056, 2008.

[48] E. Lee, T. A. Lee, H. J. Yoo, S. Lee, and B. Park, "CNBP controls tumor cell biology by regulating tumor-promoting gene expression," *Molecular Carcinogenesis*, vol. 58, no. 8, pp. 1492–1501, 2019.